Mean-Field Game description of virus propagation

Louis Brémaud

université PARIS-SACLAY

Mean-Field Game description of virus propagation

Etude des propagations épidémiques à l'aide des jeux à champ moyen

Thèse de doctorat de l'université Paris-Saclay

École doctorale n° 564, physique en Île-de-France (PIF)
Spécialité de doctorat: Physique
Graduate School: Physique. Référent: Faculté des sciences d'Orsay

Thèse préparée dans l'unité de recherche **LPTMS** (Université Paris-Saclay, CNRS), sous la direction de **Denis Ullmo**, directeur de recherche, et la co-direction de **Olivier Giraud**, directeur de recherche

Thèse soutenue à Paris-Saclay, le 16 décembre 2024, par

Louis BRÉMAUD

Composition du jury

Membres du jury avec voix délibérative

Alain BARRAT Directeur de recherche, CPT, Marseille	Président
Gabriel TURINICI Professeur des Universités, Laboratoire Ceremade, Université Paris-Dauphine	Rapporteur & Examinateur
Sergio GÓMEZ JIMÉNEZ Associate professor éq. HDR, Département d'ingénérie informatique et mathématiques, Universitè Rovira i Virgili	Rapporteur & Examinateur
Marc BARTHÉLÉMY Directeur de recherche, IPhT, CEA Saclay	Examinateur
Laura DI DOMENICO Docteure, Institute of Social and Preventive Medicine (IPSM), Berne	Examinatrice

THESE DE DOCTORAT

NNT: 2024UPASP179

université PARIS-SACLAY | ÉCOLE DOCTORALE Physique en Île-de-France (PIF)

Titre: Étude des propagations épidémiques à l'aide des jeux à champ moyen
Mots clés: Jeux à champ moyen, SIR, Propagations d'épidémies, Réseaux

Résumé: Cette thèse explore l'intégration du comportement humain dans la modélisation épidémique. La pandémie de Covid-19 a mis en évidence l'importance du facteur humain dans les modèles épidémiques, à la fois par les réponses spontanées des individus face à l'épidémie et par les mesures restrictives mises en place par les autorités. Ces effets créent une boucle de rétroaction qui influence à son tour l'évolution de l'épidémie. Cependant, la plupart des modèles actuels utilisés pour les prévisions épidémiques ne prennent pas en compte ce facteur humain dans la boucle, le traitant plutôt comme un paramètre externe. Dans cette thèse, nous étudions le paradigme des jeux à champ moyen (Mean-Field Games, MFGs), qui offre un cadre prometteur pour intégrer le comportement humain dans les modèles épidémiques. Notre objectif est de progressivement combler l'écart entre cette approche théorique et de potentielles utilisations pratiques. Concrètement, cela consiste en deux étapes: implémenter le cadre des MFG dans des modèles épidémiologiques utilisés aujourd'hui, et évaluer la pertinence d'une éventuelle application pratique: les comportements prédits par le modèle sont-ils cohérents avec ceux attendus ? Quels types de questions pouvons-nous adresser en pratique ? Quels sont les paramètres clés qu'il s'agira d'évaluer correctement ?

La première partie de la thèse applique l'approche MFG à un modèle compartimental SIR accompagné d'une structure sociale, où les individus arbitrent entre le risque lié à l'infection et les coûts associés à la réduction des contacts sociaux. Une fois implémenté, nous simulons numériquement ce modèle avec un jeu de paramètres réalistes afin d'évaluer le comportement que pourrait avoir notre modèle en pratique. Un équilibre de Nash, résultant de l'optimisation égoïste des individus, est établi et résolu numériquement. Il est comparé à l'optimum social, qui correspond à une stratégie optimale où chacun coopère pour minimiser les coûts sociétaux. L'écart entre ces deux scénarios est en partie réduit en résolvant des équilibres de Nash sous contraintes, qui intègrent des interventions gouvernementales. Enfin, nous explorons d'autres stratégies collectives susceptible de mettre fin à une épidémie. Nous montrons que des changements dans la taille de la population ou dans la durée du "jeu" peuvent conduire à des transitions de phase du premier ordre parmi les stratégies optimales du point de vue sociétal. Dans la seconde partie de la thèse, nous appliquons les MFG à des réseaux complexes, où les individus sont classés selon leur nombre de connexions (degré). Nous dérivons d'abord la dynamique des quantités épidémiques macroscopiques sur des réseaux en utilisant l'approximation par paires, puis nous implémentons l'approche MFG. Nous simulons le modèle avec un réseau de contacts réaliste puis nous étudions l'impact de la forme du coût social sur l'équilibre de Nash. Nos résultats révèlent d'importantes variations des comportements individuels selon leur degré ou la forme du coût choisie. Enfin, dans un projet annexe, nous dérivons une solution analytique implicite du modèle SIR sur des réseaux réguliers de degré k quelconque. Dans la limite SIR, nous dérivons une nouvelle formulation de résultats analytiques connus, apportant de nouveaux éclairages.

L'implémentation des MFG apparaît réalisable et flexible dans la plupart des modèles d'épidémiologie utilisés aujourd'hui. Cette approche permet l'émergence de comportement dynamiques réalistes et permet d'adresser de nombreuses questions relatives aux restrictions d'un point de vue quantitatif. Au delà de recherches supplémentaires concernant les coûts associés à l'infection et à la réduction des contacts, la connaissance de la structure sociale et l'horizon temporel choisi semblent être des critères déterminants dans l'établissement de l'équilibre de Nash.

Title: Mean-Field Game description of virus propagation
Keywords: Mean-Field Game, SIR, Epidemic propagation, Networks

Abstract: This thesis explores the integration of human behavior into epidemic modeling. The Covid-19 pandemic has highlighted the importance of the human factor in epidemic models, both through individuals' spontaneous responses to the outbreak and through the restrictive measures imposed by authorities. These effects create a feedback loop that, in turn, influences the evolution of the epidemic. However, most current models used for epidemic forecasting do not account for this human-in-the-loop factor, treating it instead as an external parameter. In this thesis, we study the Mean-Field Game (MFG) paradigm, which provides a promising framework for incorporating human behavior into epidemic models. Our goal is to progressively bridge the gap between this theoretical approach and potential practical applications. This involves two main steps: implementing the MFG framework in currently used epidemic models and assessing the feasibility of practical applications. Do the behaviors predicted by the model align with expected outcomes? What kind of questions can this model help address in practice? What are the key parameters that must be accurately evaluated?

The first part of the thesis applies the MFG approach to a compartmental SIR model with a social structure, where individuals make tradeoffs between the risk of infection and the costs associated with reducing social contacts. After implementing this model, we simulate it numerically using realistic parameters to evaluate the model's potential real-world behavior. A Nash equilibrium, which arises from individuals' selfish optimization, is established and solved numerically. It is then compared with the social optimum, which corresponds to a cooperative strategy aimed at minimizing societal costs. The gap between these two scenarios is partially reduced by solving constrained Nash equilibria, which include government interventions. Finally, we explore other collective strategies to end an epidemic. We show that changes in population size or the duration of the model can lead to first-order phase transitions among optimal strategies from a societal perspective. In the second part of the thesis, we apply the MFG framework to complex networks, where individuals are categorized by their number of connections (degree). We first derive the dynamics of macroscopic epidemic quantities on networks using pairwise approximation, and then we implement the MFG approach. We simulate the model using a realistic contact network and investigate the impact of different social cost structures on Nash equilibria. Our results reveal significant variations in individual behavior depending on their degree or the chosen cost structure. Lastly, as a related project, we derive an implicit analytical solution for the SIR model on regular networks with any degree k. In the SIR limit, we present a novel formulation of previously known analytical results, providing new insights.

The implementation of the MFG framework appears feasible and flexible in most current epidemiological models. This approach allows for the emergence of realistic dynamic behaviors and can address numerous questions regarding restrictions from a quantitative perspective. Beyond further research on the costs associated with infection and contact reduction, knowledge of the social structure and the chosen time horizon seem to be critical factors in establishing the Nash equilibrium.

Remerciements

Cette thèse a été financée par l'École Doctorale Physique en Île-de-France (EDPIF), que je souhaite remercier pour sa confiance, et pour la prolongation qui m'a été accordée à la fin de ma thèse pour me permettre d'achever mes travaux de recherche et mon manuscrit dans de bonnes conditions. Je tiens à remercier sincèrement tous les membres de mon jury, en particulier mes rapporteurs, qui ont accepté de lire mon travail avec un regard critique et de participer à ma soutenance.

Je souhaite remercier les membres de mon comité de suivi, qui m'ont accompagné pendant cette thèse, à savoir Marc Barthélémy et Françoise Cornu, ainsi que Véronique Terras pour son accompagnement au sein de l'école doctorale.

J'ai passé un peu plus de 3 ans au LPTMS, depuis mon stage de master 2 qui a démarré en avril 2020. Je souhaite tout d'abord remercier sincèrement Denis Ullmo, qui m'a donné l'opportunité d'effectuer ce travail de recherche, lequel m'a beaucoup plu au quotidien. J'ai apprécié le cadre de travail qu'il m'a proposé, avec bienveillance, autonomie et confiance, dans une relation davantage d'égal à égal que hiérarchique; ainsi que nos nombreuses discussions au cours de ces 3 années lors des pauses déjeuner. Merci !

Ma thèse a été marquée par un passage compliqué en 2e année. J'ai fait une chute à vélo en septembre 2022, qui m'a conduit à rester un mois et demi en dehors du labo, avec des soins qui se sont ensuite poursuivis pendant un an, suite à plusieurs fractures de la mâchoire et la perte de plusieurs dents. Peu après mon retour au laboratoire, Denis a lui aussi rencontré des soucis de santé qui l'ont éloigné pendant un peu plus de 6 mois. Durant toute cette période, j'ai été particulièrement soutenu, notamment par le directeur du LPTMS, Alberto Rosso, ainsi que par l'équipe du secrétariat et plusieurs autres chercheurs. Merci à vous tous. Je tiens à remercier spécifiquement Olivier Giraud, qui s'est rapidement manifesté pour se proposer de travailler avec moi et m'accompagner pendant ma thèse à partir de janvier 2023, en devenant mon co-directeur.

Cette collaboration m'a permis de me remobiliser pendant cette période, elle a été très enrichissante. En mars 2023, Olivier est parti à Singapour, et notre collaboration s'est donc poursuivie à distance. Malgré cela, Olivier s'est toujours montré disponible et volontaire pour poursuivre le travail de recherche que nous avions entamé. Je le remercie aussi pour l'opportunité qu'il m'a offerte de partir à Singapour pendant 3 semaines en septembre 2023. Je tiens également à remercier le laboratoire qui m'a accueilli, le Majulab de Singapour, sa directrice Alexia Auffèves, ainsi que les différents chercheurs avec qui j'ai pu échanger et passer d'agréables moments là-bas, comme Gabriel ou Maxime. Cette mission a été très enrichissante pour moi, tant sur le plan scientifique, en passant de nombreuses journées avec Olivier à échanger et avancer ensemble, que sur le plan culturel, en découvrant un pays, une culture et des paysages très différents de ceux que l'on connaît en France.

Je remercie particulièrement Denis et Olivier pour leur travail patient, attentif et rigoureux qu'ils ont effectué en acceptant de relire ma thèse.

Au-delà du travail de recherche, le LPTMS m'a permis de pleinement profiter de mon doctorat en me donnant l'opportunité de participer, en plus de mon voyage à Singapour, à des congrès, séminaires, workshops, ainsi qu'à une école d'été en Sicile et une conférence sur les réseaux à Venise. Je tiens à remercier Alberto Rosso pour ces différentes opportunités, ainsi que l'équipe du secrétariat composée de Claudine Le Vaou, Delphine Hannoy, et auparavant Karolina Kolodziej, pour leur excellente gestion et leur façon de faciliter la vie des membres du laboratoire.

Je retiendrai les discussions et échanges que j'ai pu avoir avec des scientifiques inspirants, parmi lesquels Martin Lenz, Guillaume Roux, Nicolas Pavloff, Christophe Texier, ainsi que Satya et Leonardo. Je remercie particulièrement Guillaume pour son implication dans la direction du laboratoire et pour ses réflexions sur la réduction de l'empreinte carbone du LPTMS. J'espère que le travail que nous avions initié avec Stéphane Ouvry et Karolina pourra se poursuivre ! La vie du laboratoire est également portée par de nombreux doctorants et post-doctorants avec qui j'ai eu le plaisir de partager ces années. I want to thank the former students of the lab, such as Felix for our chess games together, as well as Sap, Lara, and Lorenzo among others. I also want to acknowledge the current students and post-docs of the lab: Jules, Benoît, Alice, Lukas, Pietro, Giorgio, Vincent, Andrey, Florent, Marco, Charbel, Romain, and others for their energy and efforts in promoting various activities at the lab (dinners, parties,

journal clubs, aperos, climbing, and, of course, the traditional lunchtime). These activities create a nice atmosphere, particularly for integrating new students into the lab. Je tiens particulièrement à remercier Matteo avec qui j'ai partagé mon bureau pendant ces 3 ans. J'ai beaucoup apprécié nos nombreuses discussions, et j'espère que cette amitié pourra perdurer au-delà de cette thèse.

Enfin, ces 3 années m'ont permis de m'épanouir dans mes projets personnels, notamment en co-fondant un parti politique, Équinoxe. J'ai également pu faire du sport de façon parfois intensive avec les différentes associations du secteur (club de triathlon, de cyclisme et d'échecs d'Orsay).

Bien sûr, je ne peux pas terminer ces remerciements sans évoquer ma famille et mes proches. Je tiens à remercier mes parents pour tout ce qu'ils ont fait pour moi jusqu'à présent, pour leur éternelle bienveillance, pour la curiosité et pour le goût de l'apprentissage qu'ils m'ont transmis. Je sais que je peux toujours compter sur eux ; ils ont été des soutiens importants au moment de mon accident en m'aidant à traverser cette épreuve de la meilleure des façons. Mes frères, et ma famille de façon plus générale, m'ont également apporté un soutien dont je suis reconnaissant. Je souhaite plus particulièrement évoquer mon frère jumeau Vincent avec qui je suis en colocation depuis 2 ans. Je réalise la chance que j'ai de partager la quasi-totalité de mes passions avec lui. Nous avons souvent joué aux échecs, fait du vélo, et travaillé ensemble pour Équinoxe, parmi d'autres passions partagées. Sur le plan plus personnel, je tiens à remercier Yasmine, qui m'a aidé à reprendre confiance et à me rétablir après mon accident. Enfin et surtout, un immense merci à Marianne pour sa gentillesse omniprésente, sa bienveillance envers chacun, son énergie, sa curiosité dans nos discussions, et sa patience pendant la rédaction de mon manuscrit ainsi que les élections. J'ai beaucoup apprécié cette dernière année passée à tes côtés, avec tous les moments que nous avons partagés ensemble. J'espère qu'il y en aura de nombreux autres.

Je souhaite une bonne lecture à celles et ceux qui prendront le temps de lire cette thèse. Pour ceux qui le souhaitent, une synthèse en français est présentée à la fin de la thèse (appendice F) ; elle est plus accessible (sans équations ni notations) et permettra, je l'espère, de comprendre l'essence du travail de recherche que j'ai réalisé avec Denis et Olivier.

Contents

General introduction

Epidemics have posed significant challenges to human societies for millennials. One of the earliest recorded pandemics is Antonine Plague (165-190) which significantly impacted Romanian empire, particularly the Roman army [1]. It has been followed by the Plague of Justinian (541-549), which originated in Constantinople and spread throughout the Byzantine Empire, affecting the Middle East, much of the Mediterranean Basin, and Europe. This plague is estimated to have killed between a quarter and half of Europe's population [2], leading to profound economic, social, and political consequences, including conflicts and a rise in grain prices [3]. Several centuries later, the bubonic plague (1346-1353), caused by the same bacterium and also known as the Black Death, wiped out approximately 50% of Europe's population [4]. Originating in Eastern Europe, it spread across the continent via trade routes. For the first time, authorities implemented measures like social distancing and quarantine to curb the epidemic. The Black Death remains one of the deadliest pandemics in human history, with more than 50 million deaths. More recently, pandemics such as the Spanish Flu (1918-1920) and Covid-19 (2020-present) have claimed tens of millions of lives globally, profoundly impacting human life.

In response to these crises, people have long sought to understand epidemics, though early efforts were largely empirical. For instance, quarantine measures during the Black Death were based on observation rather than scientific understanding. It was not until the discovery of pathogens by Louis Pasteur in the late 19^{th} century that the mechanisms of infectious diseases became clear. Pasteur's pioneering work led to the development of vaccines and treatments against pathogens [5], and he initiated a research field focused on understanding the biological structures of pathogens and viruses [6]. This research made significant progress throughout the 20^{th} century, culminating in the development of highly effective vaccines against viruses [7]. These advancements have been crucial for public health, not only in combating human-transmitted epidemics but also in addressing infectious diseases more broadly. The containment and eradication of numerous deadly infectious diseases during the 20^{th} century can largely be attributed to the development of vaccines and medical treatments [7].

A few decades after Pasteur's groundbreaking discoveries, physicists and mathematicians began to study the propagation of infectious diseases in more detail. This led to the introduction of the famous Susceptible-Infected-Recovered (SIR) model by Kermack and McKendrick in 1927 in their seminal paper [8]. This marked the beginning of a second field of research in combating epidemics —epidemiological modeling— which has significantly enhanced our understanding of epidemic dynamics and the effectiveness of various control measures. While theoretical advancements in this field progressed slowly after Kermack and McKendrick, the late 20th century saw a surge in research due to the advent of computational power and the availability of data sets, enabling more accurate epidemic predictions. Nevertheless, despite its potential to mitigate and anticipate outbreaks, the impact of epidemiological modeling on global health has been significantly less pronounced compared to biological approaches.

Despite the substantial progress in both biology and epidemiological modeling, epidemics continue to pose a major challenge to human societies today. The recent Covid-19 crisis is a stark example, but many other epidemics emerge each year, such as Ebola, var-

ious dengue fevers, cholera, and different types of influenza [9]. The apparent increase in disease outbreaks is likely due to a combination of improved global health monitoring systems, which detect more epidemics than in the past, and societal changes [10]. Indeed, most viruses originate in wildlife, with transmission occurring through animals [11]; and Human-wildlife interactions are increasing for several reasons [10, 12, 13], such as the artificialization of land leading to closer contact between humans and wildlife, and the exploitation of animals. These interactions are expected to grow further due to climate change [14]. Additionally, epidemics are now more likely to spread rapidly across the globe, as human interactions have significantly increased and become faster than ever before. Within countries, the rise in urban populations – which is expected to reach around 60% by 2050 [15] – also contributes to higher interaction rates. Internationally, even geographically distant regions are now connected through air travel, facilitating the spread of infectious diseases. Consequently, both biologists and epidemiological modelers must develop more effective and accurate solutions or predictions in a timely manner to combat future pandemics.

The recent Covid-19 crisis is a perfect illustration of the interplay between biology and epidemiological modeling. At the onset of the epidemic, biologists focused on identifying, sequencing, and understanding the behavior of the pathogen, while epidemiologists and modelers worked to collect data from infected individuals to estimate key characteristics of the virus, such as the reproduction number R_{eff}. They quickly needed to develop models and predictions about the potential extent and impact of a global pandemic, as well as to propose various strategies to mitigate its effects for policymakers. Meanwhile, biologists and physicians explored different medical treatments and, most importantly, worked on developing a vaccine against the virus. Until the vaccine was developed in a record time (just a few months), the world largely relied on the restrictions and guidelines provided by epidemiologists and modelers.

Both fields demonstrated the significant advances made over the past few decades, such as agent-based models in epidemiology and RNA-based vaccines, and showed impressive reactivity and results during the Covid-19 crisis. However, the crisis also revealed significant limitations that persist in the models used. Modeling an epidemic is a complex task involving numerous parameters, each with substantial effects on the model's accuracy. Among these, the reproductive number R_{eff} is the most critical and still carries considerable uncertainty [16, 17]. This parameter represents the average number of individuals an infected person will transmit the virus to during their infectious period. If $R_{\text{eff}} > 1$, the epidemic will grow, while it will decline if $R_{\text{eff}} < 1$. Accurately knowing R_{eff} and predicting its evolution are crucial tasks for modelers. At the onset of an epidemic, R_{eff} is largely determined by biological factors (such as contagiousness and transmission mode), but its evolution is influenced by three main factors:

- The emergence of new variants with different levels of contagiousness.
- Changes in the number of susceptible individuals within the population.
- Changes in contact patterns among individuals due to the epidemic (i.e., individual behavioral responses).

While the first factor is difficult to predict with models [18], the second is relatively well understood through models that simulate population structure. However, there remains a significant gap in modeling the third factor. The individual behavioral response to an epidemic is a major source of uncertainty in current models, which often fail to account

for it beyond the macroscopic constraints that might be imposed by a government.

To address this issue, several recent works [19, 20] investigate a way to integrate the individual behavioral response to the epidemic through a promising route: the Mean-Field Game (MFG) paradigm. This framework relies on the mathematical game theory, in which a mean-field approach is realized. It allows to consider individuals as rational individuals who act for their own interest making a balance between their risk perception of infection, and their cost due to reduction of social contacts. Thus, the individual contact rate become an outcomes of the model that we do not have to guess. Moreover, this approach allows to consider the design of appropriate strategies to mitigate an epidemic, by evaluating their cost on the entire society.

The goal of this thesis is to explore theoretically the complex interplay between human behavior and epidemics dynamics. For that purpose, we use the MFG approach to develop and investigate further the work started by the community, and close the gap between the mathematical framework and practical applications.

Structure of the thesis

The first part corresponding to Chapters 1 and 2 is dedicated to a progressive introduction into the specific topic of this thesis.

Chapters 1 and 2: This part introduces the essential tools for our analysis. Chapter 1 provides an overview of fundamental epidemiological models, with a particular focus on deriving the well-known SIR model. A brief review of the epidemiological models currently studied is also presented. Following this, we explore the importance of incorporating human behavior into these models. In Chapter 2, we introduce the Mean-Field Games paradigm, outlining the key conceptual tools that will be employed throughout our work, and applying these concepts directly to the SIR model.

Then, the three following Chapters 3-4-5 correspond to the three main projects conducted during this thesis.

Chapter 3: This Chapter addresses our first main project. We develop a mean-field game version of an epidemic model that incorporates a social structure. We then explore the potential of this model through a numerical experiment. Initially, we focus on individual optimization, followed by the design and control of Non-Pharmaceutical Interventions (NPIs) adapted to the specific characteristics of the disease.

Chapter 4: In this part, we focus on our second main project: applying MFG to complex networks. We begin by deriving approximated equations for epidemic models on networks using a novel approach. Subsequently, we incorporate the MFG framework and investigate the resulting behavior of individuals within both homogeneous and heterogeneous networks.

Chapter 5: Apart from MFG, we show in our third project that new analytical results can be obtained for random homogeneous networks using the pairwise approximation, leading to meaningful insights.

A final part including a discussion of numerical techniques and a concluding section.

Chapter 6: This Chapter is dedicated to the numerical techniques used all along the thesis, particularly for solving MFG equations.

Chapter 7: Discussion and conclusion of our work, providing a summary of our main results and perspectives for following research.

We then provide several appendices to complete the work presented.

Appendix A provides supplementary details about the choice of parameters used in the numerical experience in Chapter 3.

Appendix B provides supplementary details of our work to complete Chapter 4.

Subsequently, the different works which have been published (or submitted) during this thesis are displayed in their original version.

Appendix C is the letter published in Phys. Rev. E associated with Chapter 3.

Appendix D is the long version of the previous paper. This paper has been published in Phys. Rev. E and is associated with Chapter 3.

Appendix E corresponds to our paper published in Phys. Rev. E on analytical results on random homogeneous networks, associated with Chapter 5.

Appendix F corresponds to a preprint letter submitted in Phys. Rev. E on a Mean-Field Game approach to epidemic propagation on networks, associated with Chapter 4.

Finally **Appendix G** is a French summary of the thesis.

1 - Introduction: human behavior in epidemiological models

This introduction first focuses in Sec. 1.1 on the construction of epidemiological models, particularly the SIR model, providing essential conceptual and mathematical tools for the subsequent work. Next, in Sec. 1.2, we examine the progresses made by theoreticians in the field up to the present day. The most complex epidemiological models currently under study explore various promising directions, ranging from fully microscopic to macroscopic descriptions. These models are used both for practical applications and theoretical research, yet they still exhibit certain limitations, particularly regarding the incorporation of human behavioral responses to epidemics. In Sec. 1.3, we discuss the potential benefits of integrating human behavior as an outcome of these models, and we review various approaches that have been proposed to achieve this integration.

1.1 Basic SIR model

In this section, we begin by building step by step the well-known SIR model (Susceptible - Infected - Recovered). In Sec. 1.1.1, we start with an epistemological discussion on the key features of epidemics that need to be modeled, particularly emphasizing the stochastic nature of epidemics. Then, in Sec. 1.1.2, we introduce the mathematical tools required to handle stochastic processes, through a Markovian description. This groundwork enables us to derive the SIR model in Sec. 1.1.3 from an individual based (and stochastic) perspective, highlighting the various approximations made, which will be important to recognize in order to refine and improve the SIR model in the following sections.

1.1.1 Key parameters

In our work, we focus on transient epidemics that spread through direct contact between individuals over a certain period and eventually dissipate due to factors such as natural immunity or vaccination. In this context, transmission occurs when a susceptible individual comes into direct contact with an infectious person. Other types of epidemics, which reach stable configurations known as endemic phases or spread through more complex interactions (such as waterborne or non-human epidemics) will not be our primary concern here. Our first goal is to identify the key parameters necessary to describe these transient epidemics, aiming at using the minimal number of parameters that can effectively capture most of the dynamics.

Based on the above discussion of the transmission mechanisms, we can see that the state of an individual (specifically their susceptibility to infection) and the transmission dynamics between individuals are essential components of a fundamental model. The simplest approximation is to neglect all the other contributions and adopt a compartmental model where individuals are categorized by their state: s, i, or r, with s for "susceptible", i for "infected" and r for "recovered". These three compartments are well-defined: an individual is classified as "susceptible" if she can be infected by the virus, "infected" when she is contagious and capable of transmitting the disease, and "recovered" when she is immune to the disease and no longer infectious. Once these compartments are established, we need to define the transitions between these states using a minimal set of parameters. Typically, this involves two parameters: one governing the transition from susceptible to infected,

describing the infectious process, and another governing the transition from infected to recovered, describing the recovery process.

Another critical aspect of epidemics is their inherent randomness; it is impossible to predict exactly when and how an individual will become infected. This uncertainty comes from numerous unknown factors, such as the complexity of interactions between susceptible and infected individuals, the conditions of contact (e.g., duration, location), the infectiousness of the infected person, natural immunity, and the viral load received by the susceptible individual. These variables are too complex to be model precisely. Additionally, even the frequency and nature of contacts between individuals are influenced by numerous unpredictable factors. To address this complexity, it is common to treat these parameters probabilistically. This shifts our focus from deterministic processes, where outcomes are precisely known, to stochastic processes, where variables evolve according to probabilistic laws. In the next section, we provide a brief introduction to the mathematical tools used for modeling epidemics within this stochastic framework.

1.1.2 Stochastic processes

Stochastic processes are widely used in statistical physics to model the behavior of complex systems which have many interacting elements. A system is considered stochastic if it comprises a set of dynamic random variables, where these variables follow probabilistic laws rather than deterministic processes. In physics, stochastic processes are often represented through noise, which are random variables with specific probabilistic characteristics, such as a Gaussian white noise. A classic example in physics is the Brownian motion, where the motion of a particle with mass m and velocity v in a fluid is described by the Langevin equation, which includes a Gaussian white noise as a representation of stochastic variability.

Similarly, epidemics involve numerous uncertain events that can be modeled using a stochastic approach. Unlike Brownian motion, which is described by a continuous state variable $x(t)$, epidemics are characterized by discrete states (susceptible, infected, recovered). Moreover, epidemic processes are typically characterized by short-term memory, meaning that the dynamics at time t depends only on the state of each individual at that moment, not on their previous states. Such processes are said to be Markovian.

These Markovian processes are a specific type of stochastic processes characterized by the Markov property, which assumes a short-memory hypothesis [21]. These processes involve a discrete (or occasionally continuous) set of random variables $X(t) = (x_1(t), x_2(t), \ldots, x_N(t))$, indexed by a parameter t that can be either discrete or continuous. Markovian processes are often referred to as Continuous Time Markov Chains (CTMC) or Discrete Time Markov Chains (DTMC) [22], where the chain represents the different states of the system $X(t)$ at each time t. In a DTMC, the state space is discrete, and the process is described by a set of random variables $x_i(t)$ that represent the N elementary components of the system. To illustrate the Markov hypothesis, we consider a DTMC. Let $(X_1, \ldots, X_n)$ a list of consecutive states of the system and $(t_1, \ldots, t_n)$ a set of discrete times. The evolution of the system is given by the joint probability $P(X_{n-1}, t_{n-1}; \ldots; X_1, t_1)$, which represents the probability that $X(t)$ is in state X_1 at t_1, X_2 at t_2, and so forth until X_{n-1} at t_{n-1}.

The dynamics of the process is then described by the conditional probability $P(X_n, t_n \mid X_{n-1}, t_{n-1}; \ldots; X_1, t_1)$. The Markov assumption states that the future state of the system depends only on its most recent state. Therefore, we get

$$P(X_n, t_n \mid X_{n-1}, t_{n-1}; ...; X_1, t_1) = P(X_n, t_n \mid X_{n-1}, t_{n-1}) \ . \tag{1.1}$$

Markov assumption is very useful to express this conditional probability, also known as the transition rate, in a very simple way. For epidemics, this approximation suits particularly well, it is used almost everywhere in the literature of epidemiological models. Nevertheless, some works has recently focused on non-Markovian approaches, which notably allows to consider a time delay for the appearance of symptoms [23, 24].

All along our work, we will consider a CTMC to describe the dynamics of epidemics. With those mathematical tools at hand, we now introduce to build in detail the SIR model.

1.1.3 The basic SIR model as a founding element

In this section, we rebuild the famous SIR model. This derivation has already been performed several times since its introduction by McKendrick and Kermack in 1927 [8] (see [25] for a complete introduction to the subject). However, we find it useful to rederive it here, as it will be the first step towards more complex models. Also we would like to highlight some steps and approximations which will be useful later but are often skipped in the derivations present in the literature.

The SIR model is defined as follows. We consider a fixed population of N individuals. Let $x_k(t) \in \{s, i, r\}$ be the state of individual k at time t. Starting from some initial configuration at $t = 0$, we then assume that the system evolves in a stochastic way, with a dynamics described by a Markovian process (CTMC) where $\{x_k(t)\}$ are stochastic variables. Between times t and $t + dt$, individuals can switch from one state to another with a certain probability, which depends on their contact rate with the rest of the population and of the status of people they meet. In a population composed of N individuals, the probability for a susceptible individual k to have contact with another individual l during the interval $[t, t + dt[$ is $\frac{1}{N}\chi_{kl}(t)dt$, with $\chi_{kl}(t)$ a (possibly time dependent) parameter corresponding to the contact rate between individuals k and l. If individual l is infected, then there is a probability ρ that the disease be transmitted from l to k. Finally, infected individuals have a probability ξdt to recover from their illness during the interval $[t, t+dt[$, after which they are immune to the disease. Note here that we introduce 3 types of parameters even though only 2 are required to set the model. We distinguish explicitly ρ and χ, to ease the derivations regarding the contact rates and in preparation for the models that we will consider later.

We thus obtain the following Markov equations describing our process at the microscopic level for each individual k

$$\begin{cases} \mathcal{P}\left[x_k(t+dt) = i | x_k(t) = s\right] = \rho \sum_{l=1}^{N} \frac{1}{N} \chi_{kl}(t) \delta_{x_l(t),i}\ dt \\ \mathcal{P}\left[x_k(t+dt) = s | x_k(t) = s\right] = 1 - \rho \sum_{l=1}^{N} \frac{1}{N} \chi_{kl}(t) \delta_{x_l(t),i}\ dt \\ \mathcal{P}\left[x_k(t+dt) = r | x_k(t) = i\right] = \xi\ dt\,, \\ \mathcal{P}\left[x_k(t+dt) = i | x_k(t) = i\right] = 1 - \xi\ dt\,, \end{cases} \tag{1.2}$$

with $\mathcal{P}[e]$ the probability of the event e, and $\delta_{a,b}$ the Kronecker symbol, all other transition rates are zero. Figure 1.1 summarizes the process that drives an individual from state s to i to r. We can know compute the evolution of macroscopic quantities of the epidemic. The relative proportions of susceptible, infected and recovered in a population of size N

Figure 1.1: Illustration of the Markov process for the classic SIR model with the transition rates to move from one state to another between time t and $t+dt$. An individual susceptible at t has a probability $\rho\chi(t)I(t)dt$ to become infected (we omit the bracket notation on I). If this individual is already infected at t, she will have a constant probability ξdt to recover from the disease.

can be written as

$$\begin{cases} S(t) = \dfrac{1}{N}\displaystyle\sum_{k=1}^{N} \delta_{x_k(t),s} \\ I(t) = \dfrac{1}{N}\displaystyle\sum_{k=1}^{N} \delta_{x_k(t),i} \\ R(t) = \dfrac{1}{N}\displaystyle\sum_{k=1}^{N} \delta_{x_k(t),r} \quad . \end{cases} \tag{1.3}$$

These quantities are stochastic because $x_k(t)$ is. Let us now consider an individual k which is susceptible at time t (i.e. $\delta_{x_k(t),s} = 1$). To become infected at time $t+dt$, this individual must meet an infected individual l in the time interval $[t, t+dt[$, and this encounter must lead to a transmission of the disease. Thus the proportion of individuals which are susceptible at time t and infected at time $t+dt$ is given, for a given realisation of the Markov process, by

$$S(t+dt) - S(t) = -\frac{1}{N}\sum_{k=1}^{N}\sum_{l=1}^{N} C_{kl}(t)\ \delta_{x_k(t),s}\ \delta_{x_l(t),i}\ , \tag{1.4}$$

with $C_{kl}(t)$ the purely stochastic variable which takes value 1 if k and l met during the interval $[t, t+dt[$ and this encounter leads to k being infected (if k is susceptible and l is infected), and 0 otherwise. This stochastic variable $C_{kl}(t)$ has an average value (over random realizations of the Markov process) which is the product of the probability of contact during dt, $\frac{1}{N}\chi_{kl}(t)dt$, by the transmission rate ρ since both events are independent. At this point, we need to make the assumption that all individuals can be met by k with equal probability (in other words, the population considered from the point of view of k is homogeneous), namely $\chi_{kl}(t) = \chi_k(t)$. One then takes the average over realizations assuming the independence of the two stochastic variables $\delta_{x_k(t),s}$, and $\delta_{x_l(t),i}$ which amounts to assume that the events "individual k is susceptible at t", and "individual l is infected at t" are independent because N is large and the population is homogeneous. One also made a natural independence hypothesis between the stochastic variable $C_{kl}(t)$ and the state variables $x_{k,l}(t)$. The previous approximations lead to

$$\begin{aligned} \frac{d\langle S(t)\rangle}{dt} &= -\frac{1}{N^2}\sum_{k=1}^{N}\sum_{l=1}^{N} \rho\chi_k(t)\langle\delta_{x_k(t),s}\rangle\langle\delta_{x_l(t),i}\rangle \\ &= -\frac{1}{N}\sum_{k=1}^{N} \rho\chi_k(t)\langle\delta_{x_k(t),s}\rangle\langle I(t)\rangle \quad . \end{aligned} \tag{1.5}$$

The next simplification is to assume that the contact rate $\chi_k(t)$ only depends on the state $x_k(t)$ of individual k at t. That means that all individuals with the same status have the same contact rate $\chi_k(t) = \chi_{x_k(t)}(t)$. Denoting by $\chi(t) = \chi_s(t)$ the contact rate of

individuals which are susceptible at t, Eq. (1.5) reduces to

$$\frac{d\langle S(t)\rangle}{dt} = -\rho\chi(t)\langle S(t)\rangle\langle I(t)\rangle \,. \tag{1.6}$$

The other SIR equations in Eq. (1.7) are obtained in the same way.

Noting $\langle S(t)\rangle$, $\langle I(t)\rangle$ and $\langle R(t)\rangle$ the average over realizations of the Markov process, the evolution of the epidemic is governed by this system of equations

$$\begin{aligned}
\langle \dot{S}\rangle &= -\rho\chi(t)\langle S(t)\rangle\langle I(t)\rangle \\
\langle \dot{I}\rangle &= \rho\chi(t)\langle S(t)\rangle\langle I(t)\rangle - \xi\langle I(t)\rangle \\
\langle \dot{R}\rangle &= \xi\langle I(t)\rangle \,.
\end{aligned} \tag{1.7}$$

This system of equations, almost a century old [8], involves only the average quantities $\langle S\rangle$, $\langle I\rangle$, and $\langle R\rangle$, which are determined as solutions of the system. It is also characterized by two "extrinsic" parameters: the recovery rate ξ and the product of the contact rate $\chi(t)$ by the probability ρ of transmitting the disease. The term "extrinsic" here indicates that these parameters are inputs to the model, requiring empirical data for practical application.

According to the central limit theorem, the actual realizations of the Markov process which yield S, I, and R will be distributed according to a Gaussian distribution around the solution given by Eq. (1.7), with a standard deviation for I that scales as $1/\sqrt{N\langle I\rangle}$ (and respectively for S and R). This implies that stochastic effects can significantly impact finite populations, particularly at the beginning or end of epidemics when $\langle I\rangle$ is small, as is well known. However, since our focus is on large populations and the core phase of the epidemic, fluctuations will not play a significant role. Therefore, we will not emphasize them in our analysis. To simplify the notation, we will omit the bracket notation $\langle\,\rangle$ around epidemic quantities in the following sections.

Despite its simplicity, and even in its most basic form where $\chi(t) = \chi$ is constant, there is no known explicit analytical solution for Eq. (1.7), with the solutions only existing in implicit integral form [26]. While numerical solutions can be easily obtained, analytical understanding of the model's equations is often necessary to fully understanding the model (and thereby the underlying phenomena). For instance, several insights can still be extracted from the SIR equations without their analytical solution. In Eq. (1.7), we see that the ratio

$$R_0(t) = \rho\chi(t)/\xi \tag{1.8}$$

must exceed 1 for an epidemic to develop (assuming $S(0) \simeq 1$). This insight led to the main contribution of Kermack and McKendrick, who derived the threshold theorem "$R_0 = 1$" for the onset of epidemics.

In addition to identifying this threshold, this simple model also helps to explain the concept of collective (or herd) immunity. By rewriting the second equation of Eq. (1.7), we obtain $\dot{I}(t) = \xi\,(R_{\text{eff}} - 1)\,I(t)$, where $R_{\text{eff}}(t) = R_0(t)S(t)$. Thus, when $S(t)$ falls below a critical level, specifically when $\rho\chi(t)S(t)/\xi$ drops below 1, or equivalently $S < 1/R_0$, then $\dot{I} < 0$ and the epidemic begins to decrease until it eventually disappears. Note that $R_{\text{eff}}(t)$ can be interpreted as the average number of individuals to which an infected person at time t will transmit the virus: each infected individual has a probability $\xi R_{\text{eff}}(t)dt$ of infecting a susceptible individual during the time interval $[t; t+dt[$, and remains infectious for an average duration of $1/\xi$.

These considerations highlight the clear advantages of simple models, particularly the ability to understand a phenomenon from a physical perspective. However, this simplicity

comes with the drawback of significant oversimplifications of the complex realities of the world. Below, we outline the main approximations of the SIR model, which are important to identify both for recognizing the model's limitations and for identifying potential avenues to refine and improve this model. First, regarding the contact structure: we assume three types of homogeneity. The first one concerns the uniformity of individual's contact rate with others, meaning that the probability of meeting any other individual is the same, expressed as $\chi_{kl}(t) = \chi_k(t)$ being independent of l. The second concerns homogeneity in individuals' contact rates, assuming they are identical, i.e., $\chi_k(t) = \chi(t)$ is independent of k. The third involves homogeneity over time, where $\chi(t) = \chi$ becomes constant.

Second, we consider a very large population. This allows us to neglect the intrinsic fluctuations of epidemic dynamics and assume that the status of two individuals in contact are independent. In reality, correlations may exist, either due to individuals' status or because of specific links (e.g., family members).

Third, all other parameters, such as ρ and ξ, are taken constant, even though they may vary across individuals and time. For instance, individuals may require different viral loads to become infected, or they may engage contacts of varying risk (e.g., wearing masks, avoid physical gestures like handshakes). Recovery rates may also differ between individuals. Furthermore, the emergence of new variants during an epidemic could alter both ρ and ξ.

A final approximation is the consideration of only three compartments (S, I, R). As we will see, additional compartments may be necessary to adequately characterize the state of each individual. However, adding such compartments is straightforward and can be easily implemented.

Since the SIR model, epidemiological modelers have developed various methods to refine the SIR model, leading to the sophisticated models studied nowadays. We discuss some of these advancements in the next section.

1.2 Current epidemiological models

In the previous section, we observed that the SIR model employs several approximations that, while beneficial for theoretical understanding, fall short for practical applications. The natural approach to enhancing this model is to relax (at least partially) some of these approximations. In Sec. 1.2.1, we discuss the balance required to develop models that are both practical and efficient, drawing an analogy with climate science. Then, in Sec. 1.2.2, we introduce the three main families of epidemiological models that researchers have explored for decades: compartmental models, models based on networks, and agent-based models. We present each of these families, providing examples of recent works and highlighting their remaining limitations. We start with compartmental models in Sec. 1.2.3, followed by network-based models in Sec. 1.2.4, and finally, agent-based models in Sec. 1.2.5.

1.2.1 Practical efficiency: a balance between accuracy and complexity

As discussed earlier in the context of the SIR model in Sec. 1.1.3, advancing the modeling process requires introducing new parameters. On the one hand, this is done to enhance accuracy, i.e., reduce the discrepancy observed between theoretical predictions and real-world data. On the other hand, incorporating more parameters can enable the model to address specific questions that cannot be tackled with simpler frameworks. For example, assessing the role of vaccination in mitigating epidemics requires the introduction of an-

other compartment, which cannot be addressed with the basic SIR model alone. However, the inclusion of more parameters also increases the complexity of the model in several ways:

1. **Model calibration:** The practical use of the model will be harder, as fixing the parameters will require larger data sets or specific data which can be very complicated to obtain with precision.

2. **Overfitting risks:** The potential number of free parameters will increase. This increase the risk of overfitting, that is to find particular sets of parameter which will only fit the training set but not pass the validation test.

3. **Interpretability:** The physical understanding of the system become less clear. It will be harder to know what is the exact influence of each parameter when there are competing in a sophisticated and intricated way.

4. **Numerical complexity:** The increasing complexity will lead to more sophisticated systems to solve. This usually leads to the increasing time of numerical computations, which may also be more challenging to realize technically.

All these issues are already present in several fields in physics and complex systems particularly, including epidemics. We provide below an illustrative example of climate science which already faced number of these issues, before turning to epidemiological field.

1.2.1.1 *Analogy with climate science*

In climate physics, highly complex models with thousands of parameters are used. This field, developed through extensive international collaboration, directly confronts the limitations mentioned earlier. Climate physicists contend with a limited number of observations and inherent uncertainties in data, which challenge the model calibration. This calibration may also be affected by the chaotic nature of weather, which could impede advancements in forecasting due to data uncertainties, despite progress in modeling. However, thanks to the vast number of databases available for parameter fitting, overfitting risks are less significant in this field (unlike for instance in biology, where data accessibility is a major issue). At a macroscopic scale, emergent phenomena such as the dynamics of major atmospheric currents influencing global air circulation are not always fully understood, even though models predict them. To address this, climate physicists study these phenomena by focusing on smaller models with fewer parameters, retaining those suspected of causing unexplained phenomena to enhance the interpretability of their model. This approach through fractional models, where phenomena are divided for separate study (e.g., water, atmosphere, ice), is widely used. The field also faces the challenge of increasing computational power required for climate (and especially weather) simulations.

Considering these points, we can understand why climate physicists build their models using grids of a few kilometers square, still far from the molecular scale of atmospheric constituents. As illustrated in Fig. 1.2, a balance between accuracy and complexity is necessary in most complex systems. However, there are often multiple ways to construct such models, and climate physicists have developed numerous formulations that are not always easy to classify. In this context, an effective way to ensure accurate predictions is to verify that multiple models with slightly different assumptions yield predictions within a certain small interval, which then becomes the "confidence in-

terval". The IPCC [27] has employed this approach with a certain success in predicting climate change, despite its complexity.

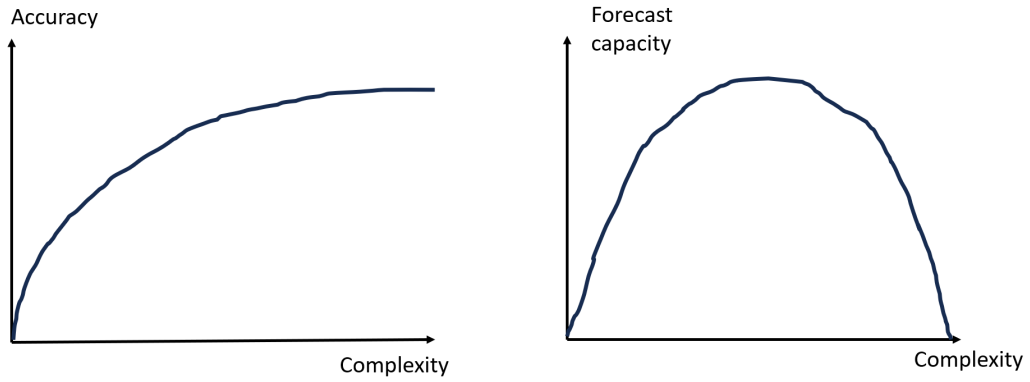

Figure 1.2: *Illustration inspired from [28] of the evolution of "accuracy" and "forecast capacity" of models describing a complex phenomenon in terms of "complexity". Here, "accuracy" refers to a model's ability to provide predictions close to real observations on unknown data sets, while "complexity" typically represents the number of parameters in the model. Accuracy generally increases with complexity, following a concave pattern, as key parameters are considered first. "Forecast capacity" refers to model's practical usability, reflecting its ability to closely match real data sets, together with factors such as ease of use, the amount of required data, simulation time, and the risk of overfitting (which is the main factor considered in [28]).*

1.2.1.2 The case of epidemic modelling

Forecasting epidemics presents similar challenges. For model calibration, the issue often lies in data accessibility and availability, as population testing is frequently required. Even when data are available, they often lack quantitative details. For instance, if an individual tests positive for a disease, we know she is infected at the time of the test, but we do not know when or how she has been infected, nor the duration of her infectiousness. The stochastic effects also considerably affect model calibration, as epidemiologists need to infer reproductive numbers or other critical parameters with a very limited number of data in a short time. Related to this aspect, the risk of overfitting is also relevant in epidemic modeling, as appropriate data sets for parameter estimation are not always available. Additionally, large-scale numerical simulations may sometimes be required, especially for agent-based models. Finally, specific (or fractional) models for particular dynamics such as information spreads, vaccination, are also developed to allow interpretability. These challenges —among others— are areas where epidemiologists can learn from climate physicists [29]. In recent decades, numerous models have emerged as strong candidates for epidemic prediction. During the Covid-19 crisis, epidemiologists began to really compare model forecasts to provide robust guidelines to policymakers [30]. Such direction could be further explored to enhance global predictions. In this thesis, we will rather focus on specific models of spontaneous behavior changes and their possible integration to more global models.

In this section on the practical efficiency of models, we aimed to show that while epidemiological models can be enhanced in various ways, it is crucial for modelers to avoid introducing excessive complexity due to inherent limitations. In the next section, we will explore the most promising directions currently being explored by the epidemiological community.

1.2.2 Epidemiological models family

Epidemiological modeling has grown to become a vast field encompassing a wide range of topics. While it is beyond the scope of this work to provide a comprehensive review of the literature, certain techniques and methods have emerged as particularly effective. These are discussed below along with specific examples.

Epidemiological models can be broadly categorized into three main families:

1. **Compartmental models:** These models, which belong to the same family as the SIR model, employ a "top-down" approach. They begin with broad compartments that may be numerous. Then, the fully homogeneous description of the population is often abandoned for more refined descriptions, by introducing various batches that consider for instance factors like age classes or different living regions. This allows for a mesoscopic-scale description of individuals' characteristics through mean-field equations.

2. **Compartmental models based on explicit networks:** In these models, individuals are represented as nodes within an explicit network, with specific descriptions for each node. To make the system of equations more manageable, mean-field equations are often derived, incorporating the network's structural properties.

3. **Agent-based models:** These models provide a detailed individual-level description of contacts. Each individual has a specific risk of infection, and there are no mean-field equations. Instead, the model relies on the concept of synthetic populations, which are designed to mimic the characteristics of a real population by capturing relevant distributions such as age, employment status, etc.

1.2.3 Compartmental models currently used by health authorities

As discussed in Sec. 1.1.3 concerning the SIR model, compartmental models, first introduced in 1927, have since undergone significant extensions. In these models, individuals are grouped into compartments, and macroscopic parameters describe their average interactions, such as the probabilistic law of infection determined by the transmission rate.

A natural extension of the SIR model is to introduce more than three compartments, allowing for a more structured representation of individuals' status. Indeed, the status of individuals plays a crucial role in epidemic dynamics. For instance, the presence of individuals with natural immunity or a high proportion of vaccinated people can significantly alter the epidemic's trajectory. Common extensions of compartmental models include the SEIR model (E for exposed [31]), the SIRD model (D for deceased [32]), the SIRV model (V for vaccination [33]), the MSIR model (M for maternally derived immunity [34]), and the SIRC model (C for carrier but asymptomatic [35]). Models used by authorities often combine multiple compartments to capture the complexity of real-world epidemics.

Then, the assumptions on the homogeneity of contacts (among individuals and regarding contacts) are the strongest ones as we know now that the contact networks of individuals is far from homogeneity [36]. Thus, such approximations are almost always partially broken in recent epidemiological models where individuals are classified in batches according to their age and sometimes to their living place. Then, the contacts between individuals batches are described by the so called contact matrices [37, 38]. Each entry M_{ij} of a contact matrix M will describe the contact frequency of individuals of batch i with individuals of batch j. These matrices are not always symmetric due to the possible difference of population between batches.

Among the various models currently employed to predict epidemic dynamics, compartmental models remain the most widely used. For a comprehensive review of the models applied to the Covid-19 pandemic, primarily compartmental ones, refer to [39]. One of the most notable models is the spatiotemporal compartmental model developed by Alex Arenas *et al.* [40] for the Covid-19 epidemic in Spain that we present below.

In this study, the authors present a metapopulation compartmental model where individuals are characterized by three key factors: their region of residence (corresponding to towns in Spain), their age group (young, middle-aged, elderly), and their status (with ten possible categories). Within this population, individuals interact according to contact matrices, and mobility matrices are used to model interactions across different regions. Figure 1.3 illustrates this model. Building on this compartmental model, the authors ac-

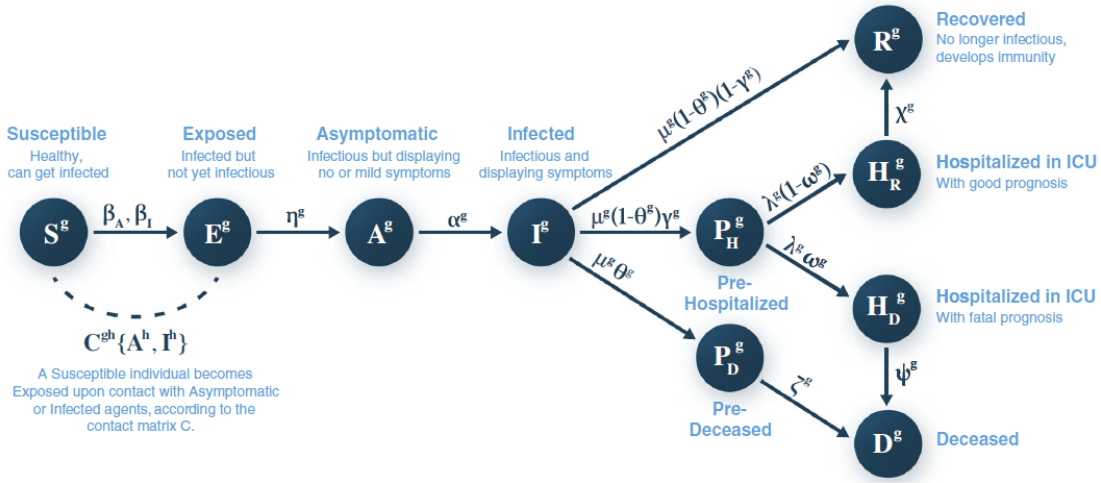

Figure 1.3: Figure extracted from Alex Arenas *et al.* [40]. Compartments of the epidemic model. The acronyms correspond to susceptible (S^g), exposed (E^g), asymptomatic infectious (A^g), symptomatic infectious (I^g), prehospitalized in ICU (P_H^g), predeceased (P_D^g), in ICU before recovery (H_R^g), in ICU before death (H_D^g), deceased (D^g), and recovered (R^g), where g denotes the age stratum for all compartments. The arrows indicate the transition probabilities.

count for population density in each region to estimate the number of contacts between individuals. Additionally, they differentiate between two transmission rates for asymptomatic and symptomatic individuals. On top of that, a model for confinement measures is proposed (cf Laura Di Domenico's PhD thesis [41] for possible ways of implementing restrictions). They introduce a parameter to represent the severity of lockdown, reducing individuals' mobility between regions, which becomes time-dependent. They also incorporate a reduction in contact rates by introducing a social distancing parameter, alongside a reduction in contacts due to the closure of public spaces (limiting contacts to home or work environments).

Another focus of their study is the utilization of Intensive Care Unit (ICU) beds and the duration of ICU stays. From their formalism, the authors derive a probability of infection for individuals. Using a discrete-time Markov chain approach, they describe the model with a system of 10 coupled equations. While this system is highly coupled and analytically unsolvable, it remains numerically tractable. The authors simulated the model for the first wave of the Covid-19 epidemic in Spain, yielding the results shown in Fig. 1.4. These findings, along with other results presented in the paper, demonstrate excellent agreement between the model's predictions and the actual data. This model introduces significant complexity, incorporating tens of independent parameters. It provides a far more

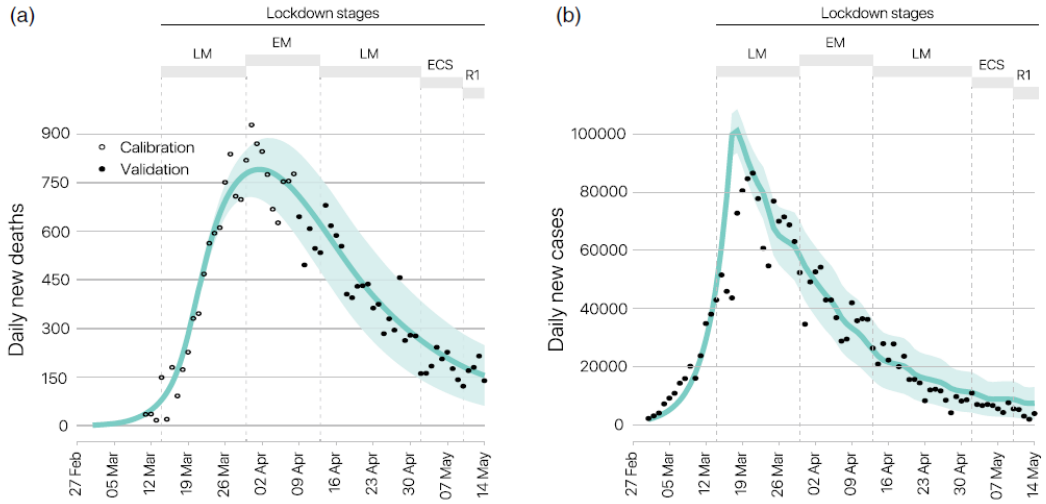

Figure 1.4: Figure extracted from Alex Arenas *et al.* [40]. Model validation and spatiotemporal propagation of Covid-19 across Spain. Top: Solid lines show model predictions for the daily fatalities (a) and the daily number of new symptomatic individuals (b), whereas dots correspond to real data. The shadowed areas represent the 95% prediction interval.

accurate representation of reality compared to the simpler SIR model discussed earlier. However, it requires extensive data to describe individual contacts within the country being modeled. The key advantage of this model is that only 6 parameters are calibrated, while the remaining parameters derived from existing datasets. The small number of fitted parameters suggests that the model's complexity is manageable, as the necessary databases are accessible. Moreover, it implies that the model's predictions are robust, since only a few parameters depend on the optimization process.

Additionally, the optimization procedure converges within a relatively narrow region, indicating that the parameter set fitting the data points closely matches the optimized set. The authors also demonstrate that the model can be used to study the effects of lockdown measures. They derive an approximate formula for the reproduction number $R(t)$ and show how adjusting the three confinement parameters can control the epidemic by ensuring $R(t) \leq 1$.

Despite these impressive results, which represent cutting-edge research in epidemic modeling, there are still limitations. One key issue is the need for the time-dependent evolution of a parameter, $\kappa_0(t)$, which quantifies the severity of confinement, specifically, the fraction of people who is under lockdown at time t. Essentially, the authors calibrate their model up to beginning-April 2020 and validate it from beginning-April to mid-May. However, they rely on data available until mid-May, which corresponds to the validation period. This reliance on future data for $\kappa_0(t)$ limits the model's practical applicability for forecasting subsequent epidemics, as such data will not be immediately available. Epidemiologists often address this challenge by using data from previous epidemics or by estimating trends based on recent patterns. This issue highlights a broader challenge for epidemiologists: predicting or fitting extrinsic time-dependent parameters, a topic discussed further in Sec. 1.3.1.

With respect to social contacts, these sophisticated compartmental models are based on an implicit network that is homogeneous at a "mesoscopic" level (e.g., within age strata in each city). A natural extension is to employ fully heterogeneous networks, which involve explicit contact networks. This field emerged in the late 20^{th} century, and we introduce it

in the following section.

1.2.4 Networks-based models

Network-based epidemic models enable the study of contact connectivity patterns among individuals, through which diseases spread. The structure of such networks has long been recognized as a critical factor in epidemic dynamics [42, 43, 44, 45, 46, 47, 48, 49, 50]. For a comprehensive review on the structure and dynamics of complex networks, reader can refer to [51] while for a review applied to epidemics, see [52].

Beyond epidemic related questions, research in the area of complex networks began in the second half of the 20$^{\text{th}}$ century with two primary focuses:

- Analytical study of network phenomena (e.g. threshold effects such as percolation or avalanches)
- Developing methods to construct realistic networks

Networks were initially explored in physics for their ability to explain the emergence of macroscopic phenomena, such as phase transitions, from microscopic interactions. Percolation theory was introduced in 1957 by mathematicians [53] to study the behavior of networks, particularly the size of the giant component (i.e., the largest connected portion of the network) as edges are removed or nodes are deactivated. This led to the discovery of geometrical phase transitions, a topic still actively researched today [54]. Similarly, the study of avalanches or cascades on networks focuses on sequences of causally linked events. This field, which emerged in the early 2000s, primarily concerns neuronal avalanches in the brain, where neurons activate in cascades [55]. Another key concept in diffusion phenomena on networks are the thresholds for epidemic onsets, which aim to identify the critical value of key parameters that drive the spread of processes across the network. The concept originated in 1943 with the work of Ryan *et al.* [56] and has since been applied to a wide range of topics, including epidemic spreading at the end of the 20$^{\text{th}}$ century [57, 58, 59], and more recently with [60]. Threshold effects have also been studied extensively since 2000, starting with [61] and continuing to recent work such as [62], to assess network robustness to attacks and resilience.

In parallel, researchers have built efficient algorithms to construct artificial but realistic networks. One of the most famous model is the one of Erdős-Rényi introduced in 1960 [63]. In Erdős-Rényi networks, each edge exists with a fixed probability p. These networks, which have been extensively studied, exhibit homogeneous properties with a Poisson degree distribution.

However, many real networks appear to be heterogeneous. A number of them exhibit a power-law degree distribution with "fat tails" that have been observed in contexts such as airline connections [64], the World Wide Web [65], and inter-bank connections [66]. These networks are referred to as "scale-free" networks, as they lack a characteristic scale. In 1999, Albert and Barabási published their seminal work [67], demonstrating how scale-free networks emerge from two simple mechanisms: the continuous addition of nodes and a preferential attachment rule. This rule states that new nodes are more likely to connect to highly connected nodes than to those with low connectivity.

Like Barabási-Albert networks, small-world networks have been observed in numerous real-world systems, including social networks [68], food webs [69], electric power grids [70], and neural networks in the brain [71]. These networks are said "small-world" as they display unique features such as hubs, shortcuts, and clusters (small regions with densely connected nodes). Notably, small-world networks are characterized by the average

path length between any two nodes scaling as logarithm of the number of nodes in the network. Watts and Strogatz introduced their renowned small-world model in 1998 [42], showing how a regular network can be transformed into a random one through a simple rewiring process. This process involves a single parameter p that controls the network's regularity. For intermediate values of p, these networks become "small-world" and exhibit the associated properties.

These models, along with many others, were extensively studied throughout the 2000s, greatly advancing the understanding of network dynamics and structure. Since then, research in complex networks has extended the study of epidemiology on networks and expanded the field into new directions:

- Simulating macroscopic dynamics on networks using refined mean-field equations, rather than focusing solely on the early stages of the dynamics.
- Building, collecting, and inferring real networks from large datasets.

In the early 2000s, several studies focused on deriving mean-field equations to predict and simulate dynamic processes on networks. These dynamics often rely on Markovian processes at the node level, which are stochastic and highly dependent on the network's structure. Various mean-field approximations have been proposed, with varying degrees of consideration for network structure (see [72] for a recent review). These equations also enable the calculation of new epidemic thresholds across different network types. For instance, the epidemic threshold on heterogeneous scale-free networks have been shown to vanish [46], highlighting how the presence of super-spreaders (highly connected individuals) can significantly accelerate disease transmission. A more detailed discussion of these mean-field equations is provided in Chapter 4.

For a long time considered exclusively as a theoretical problem, experimentalists and data scientists investigated the field of complex networks approximately two decades ago. For instance, network inference —constructing complete networks from partial observations— is increasingly studied. To do so, researchers collect data on the precise contact network of, for example, a neighborhood or a school, and then extrapolate to the broader system. For recent work on the subject see [73, 74, 75, 76, 77]. Other studies focus on gathering data from real networks, such as modifications to air transportation during the Covid-19 pandemic [78], or directly analyzing social contact networks, as in [79]. In this paper, the authors used GPS data from a specific application to build the contact network of 468 individuals, on which they simulated and tested different epidemic containment strategies. This work exemplifies the efforts of the contact tracing community, particularly over the last decade.

Despite recent progress, compartmental models on complex networks using mean-field equations are still mainly employed to derive insights and properties of epidemics, rather than to accurately predict epidemic dynamics. However, taking advantage of advancements in network theory and computational capabilities, researchers have developed new methods to model processes at the microscopic scale, leading to the emergence of Agent-Based Models, which we consider now.

1.2.5 Agent-Based Models

Agent-Based Models (ABM) are powerful numerical tools developed over the past few decades, designed to simulate virtual populations at the individual level. In these models, interactions between individuals can take various forms, such as social contacts, economic exchanges, or road traffic. The key idea is to capture the emergent behavior resulting

from complex interactions at the microscopic level. In the context of epidemics, these interactions represent social contacts between individuals occurring in different locations. For a practical introduction to ABM, the reader can refer to [80].

Pioneers of this approach include Eubank *et al.* [36], who introduced a rigorous mathematical framework for ABMs. The authors described a bipartite network structure, where individuals and locations form distinct sets of nodes, as illustrated in Fig. 1.5.

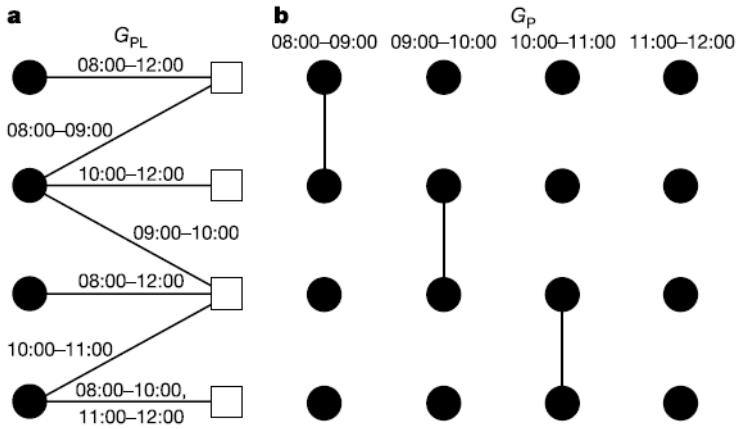

Figure 1.5: Figure extracted from Eubank *et al.* [36]. An example of a small social contact network. **a**, A bipartite graph G_{PL} with two types of vertex representing four people (P) and four locations (L). If person p visited location l, there is an edge in this graph between p and l. Vertices are labelled with appropriate demographic or geographic information, edges with arrival and departure times. **b**, disconnected graph G_p induced by connecting vertices that were separated by exactly two edges in G_{PL}.

Two individuals interact when they are in the same location at the same time. This approach generates a large-scale, dynamic contact graph, replacing the traditional differential equations used in classical epidemic models. The epidemic simulation, called EpiSims, is built upon the Transportation Analysis and Simulation System (TRANSIMS), developed at Los Alamos National Laboratory. TRANSIMS enables the creation of a synthetic population that closely mirrors a real population in terms of age, income, and demographic movement patterns. EpiSims was the first microsimulation tool designed for epidemic modeling at this level of detail.

The authors applied it to a specific case study in Portland, with the bipartite graph consisting of 1.5 million individuals and 180,000 locations. The representative distributions of various network characteristics are shown in Fig. 1.6. The authors simulated the spread of smallpox within this network, which exhibited small-world characteristics due to its high clustering coefficient [36]. They also explored how intervention strategies, such as early detection and targeted vaccination, could mitigate the disease. Since this work, numerous other numerical tools have been developed to implement ABM approaches (see [81] for a review). Notable examples include the Pandemic Simulator (PanSim), which was used for Covid-19 simulations [82], and the model by Ferguson *et al.* [83] (2005-2006), initially designed for influenza pandemics, and later adapted for Covid-19 response by Imperial College [17]. These models simulate millions of individuals to generate a synthetic population for the UK and the US.

This detailed representation allows direct modeling of interventions without additional assumptions. For example, a "stay-at-home" order is straightforward to model: individuals affected by the restriction will stay at home, altering the contact network and the transmission dynamics accordingly. There is no need for extra parameters, like those required in compartmental models. Ferguson *et al.* presented their findings, depicted in Fig. 1.7,

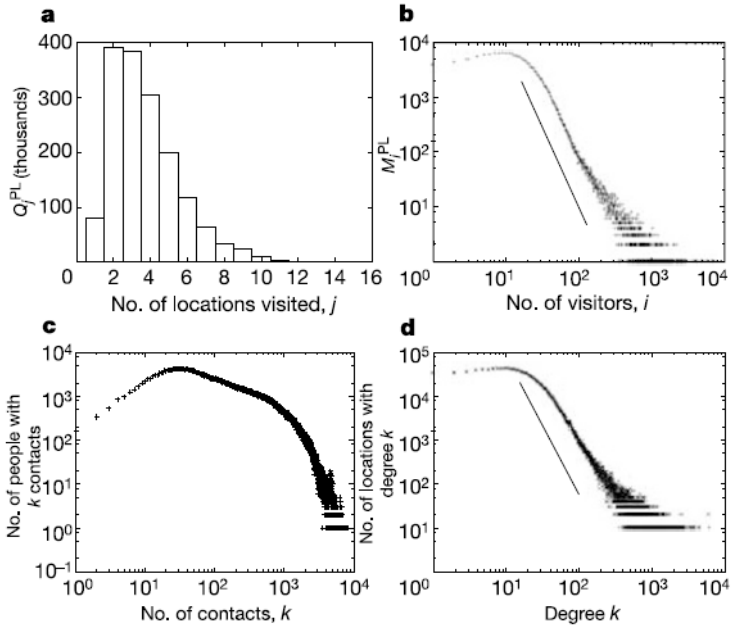

Figure 1.6: Figure extracted from Eubank *et al.* [36]. Degree distributions for the estimated Portland social network. **a**, The number of people Q_j^{PL} who visited j different locations in the bipartite people–locations graph G_{PL}. **b**, The number of locations M_i^{PL} in G_{PL} that are visited by exactly i different people. The slope of the straight-line graph is -2.8. **c**, The number of people who have k neighbours in the static people–contact graph G_P on log–log scale. **d**, The in and out degree distributions of the locations network G_L. The slope of the straight-line graph is -2.8.

which had a profound global impact. Headlines warned that without intervention, the UK could face over 500,000 deaths from the Covid-19 pandemic. The authors demonstrated the potential outcomes of the epidemic under various mitigation scenarios and with different estimates of R_0, which was still uncertain at the time. This work, published on March 14, 2020, directly influenced the policy decisions made few days later. Due to the rapid increase in Covid-19 cases and these alarming predictions, policymakers in several European countries opted to impose lockdown measures [84].

Agent-based modeling holds significant promise, especially in highlighting the role of heterogeneity within a system. However, ABM also presents several challenges. The most immediate issue is the computational power required for such simulations. Despite notable progress in the development of efficient algorithms [85, 86, 87, 88], this remains a substantial obstacle. A second issue arises from the complexity of these models. They typically involve a large number of parameters, many of which are free and must be determined using data that are not always readily available. Moreover, these models can become highly specific to a particular disease or region due to the choices made during their construction. This specificity can make them less tractable for theorists and limit their generalizability, as they often lack analytical results, complicating physical interpretation.

This concludes our review of the various modeling approaches used in epidemiology. The following section will focus on the central topic of this thesis: modeling human behavior within epidemiological frameworks.

		Total deaths			
R_0	On Trigger	Do nothing	CI_HQ_SD	PC_CI_SD	PC_CI_HQ_SD
2	60	410,000	47,000	6,400	5,600
	100	410,000	47,000	9,900	8,300
	200	410,000	46,000	17,000	14,000
	300	410,000	45,000	24,000	21,000
	400	410,000	44,000	30,000	26,000
2.2	60	460,000	62,000	9,700	6,900
	100	460,000	61,000	13,000	10,000
	200	460,000	64,000	23,000	17,000
	300	460,000	65,000	32,000	26,000
	400	460,000	68,000	39,000	31,000
2.4	60	510,000	85,000	12,000	8,700
	100	510,000	87,000	19,000	13,000
	200	510,000	90,000	30,000	24,000
	300	510,000	94,000	43,000	34,000
	400	510,000	98,000	53,000	39,000
2.6	60	550,000	110,000	20,000	12,000
	100	550,000	110,000	26,000	16,000
	200	550,000	120,000	39,000	30,000
	300	550,000	120,000	56,000	40,000
	400	550,000	120,000	71,000	48,000

Figure 1.7: Figure extracted from Ferguson *et al.* [17]. Suppression strategies for GB. Impact of three different policy option (case isolation + home quarantine + social distancing, school/university closure + case isolation + social distancing, and all four interventions) on the total number of deaths seen in a 2-year period. Social distancing and school/university closure are triggered at a national level when weekly numbers of new Covid-19 cases diagnosed in ICUs exceed the thresholds listed under "On trigger" and are suspended when weekly ICU cases drop to 25% of that trigger value. Other policies are assumed to start in late March and remain in place. Peak GB ICU surge capacity is approximately 5000 beds. Results are qualitatively similar for the US.

1.3 Human behavior in epidemiological models

Among the key parameters influencing the virus transmission rate, two primary components can be identified: one coming from biological factors [89] (such as the viral load required for infection, natural immunity, or the specific variant), and the other linked to individual behavior (nature and frequency of contacts, willingness to be vaccinate). In the latter case, a portion of this behavior is influenced by the progression of the epidemic itself, as individuals tend to adjust their actions based on the evolving dynamics. In Sec. 1.3.1, we discuss the significance of this behavioral adaptation in shaping epidemic dynamics, justifying its integration into theoretical models. In Sec. 1.3.2, we examine how this behavioral aspect is incorporated into epidemiological models, ranging from simple models driven by "social forces" to more complex frameworks.

1.3.1 Modeling human behavior is crucial

Human behaviors influencing the course of epidemics are twofold: behaviors consistent across epidemics and those that respond to the epidemic itself. On the one hand, some behaviors relate to mobility patterns [90], such as attending school or taking holidays, as well as the socio-demographic structure of the population [91], which captures the heterogeneous nature of contacts based on factors like living location, age, or occupation. Despite its complexity, this aspect has been extensively studied, and this beyond epidemic prediction. Researchers benefit from the fact that these behaviors are generally stable over time within a population, even though contact patterns may vary (e.g., depending on the

day of the week). This stability enables precise forecasting, as seen in energy consumption predictions by authorities or utility companies [92]. Thus, this first behavioral component is relatively well-understood compared to the second.

On the other hand, behavioral changes induced by epidemic outbreaks can play a critical role in the dynamics of the disease [93, 94]. Beyond government-imposed restrictions, these changes are driven by individuals' perceptions of fear and risk regarding the disease. For instance, some people, feeling vulnerable, may reduce risky behaviors during an outbreak [95, 96]. Additionally, depending on their level of information and risk perception, individuals may choose whether to participate in vaccination programs [97]. The impact of these self-protective actions on epidemic dynamics has received increasing attention recently [98, 99, 100, 101], from both theoretical and empirical perspectives. These actions, referred to as spontaneous behavioral responses in the literature [102], encompass all behavior changes triggered by the epidemic, driven by factors such as individual decision-making, risk perception, beliefs, and access to information.

These behavioral responses can be broadly classified into two subcategories [102]: a first one with reactions to vaccination campaigns and another one with actions aimed at reducing social contacts and transmission risk. We provide here a meaningful example of the different concepts describe above for the Covid-19 pandemic where one can clearly observe the feedback loop between human behavior and epidemic dynamics. Throughout the pandemic, various behavioral changes significantly influenced the spread of the virus. These included imposed restrictions, such as lockdowns, non-spontaneous shifts (e.g., holiday periods [103]), and spontaneous adaptations, notably vaccination campaigns and social distancing measures. The latter two, being directly linked to the epidemic's course and highly dependent on individual choices, remain the least understood aspects. These behavioral shifts, along with other factors like variant emergence, are illustrated in Fig. 1.8, which shows the temporal evolution of R_{eff} during the Covid-19 pandemic in France. The

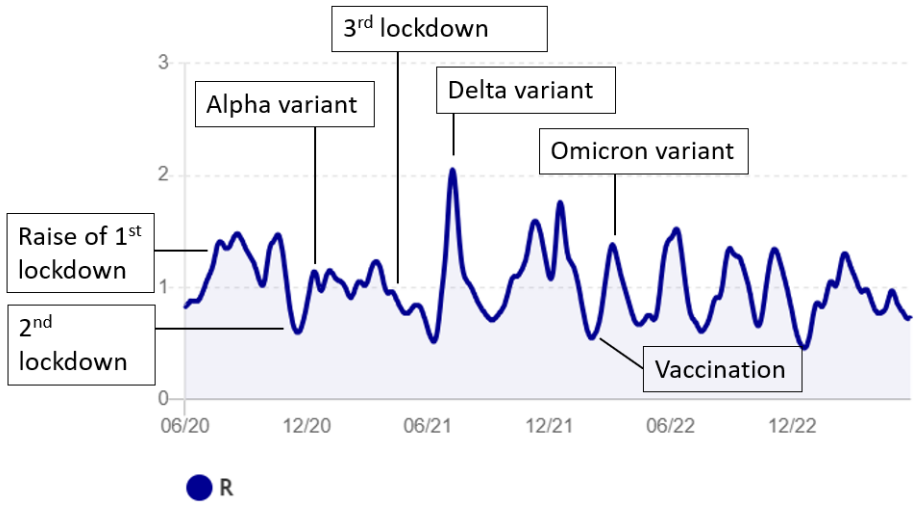

Figure 1.8: Evolution of R_{eff} in France during the Covid-19 pandemic between June 2020 and June 2023. R_{eff} corresponds to the effective reproduction number of the virus, that is, the average number of people to which the virus is transmitted by a sick individual. If $R_{\text{eff}} > 1$, the epidemic grows, and it decreases if $R_{\text{eff}} < 1$. We see that there are significant variations of R_{eff} which range from 0.6 to 2. We marked on the figure some peaks and valleys that have clearly identified origins (Data from "Santé Publique France", author: Guillaume Rozier [`https://covidtracker.fr`].)

figure illustrates that $R_{\text{eff}}(t)$ does not follow a continuously decreasing trend over time, as would be expected if the transmission rate were constant and $R_{\text{eff}} = R_0 S(t)$. This deviation can be partially attributed to spontaneous behavioral changes triggered by the spread of the epidemic, which played a significant role in shaping the dynamics of Covid-19 [104], corroborating earlier studies on the subject. Recently, researchers have attempted to integrate these behavioral dynamics into theoretical models using various approaches, which will be discussed in the next section. While much of the literature focuses on vaccination behavior [105, 102], our focus will be on modeling social distancing adaptations.

Before turning into the modelization of these spontaneous behavioral responses, it is crucial to clearly distinguish between extrinsic and intrinsic parameters in epidemiological models.

- **Extrinsic parameter:** These are parameters that can be time-dependent and are typically fitted using real-world data. In epidemic modeling, biological parameters such as the recovery rate or the transmission rate $\beta(t)$ often fall into this category. Extrinsic parameters are usually considered constant over time because fitting them over varying time intervals can be challenging. However, incorporating time dependence is sometimes necessary, as in [40], which may involve significant guesswork or predictions based on available data. The uncertainty on such parameters mainly depends on the quality and precision of the available databases.
- **Intrinsic parameter:** These are parameters which emerge from the internal dynamics of the model, they depend on extrinsic parameters. Here, the uncertainties sources came both from the extrinsic parameters on which these parameters rely on, and on the modelization itself.

In our context, the goal of modelers is to shift from an extrinsic $\beta(t)$, which is challenging to infer from datasets, to an intrinsic $\beta(t)$ that evolves based on the epidemic's dynamics. This intrinsic $\beta(t)$ would depend on the state of the epidemic itself, while relying on extrinsic but time-independent parameters. This shift aims at simplifying the model by reducing reliance on time-varying external data and instead focusing on parameters that remain constant over time, thus providing a more manageable framework for prediction and control.

1.3.2 The various ways to model human behavior: from social forces to game theory

Early efforts to model the transmission rate as a time-dependent function date back several decades. A straightforward approach is to modify the bilinearity of the incidence rate in S and I (as seen in Eq. (1.7)), and instead assume that the transmission rate β is a function of time, or more specifically, of the epidemic incidence: $\beta = \beta(t) = \beta(I(t))$. In 1978, Vincenzo Capasso *et al.* [106] proposed a model where the contact rate decreases once the number of infected individuals surpasses a certain threshold, using an ad hoc form for $\beta(I(t))$ that decreases as I increases. Although human behavior is not effectively modeled in these approaches, these models can still generate complex dynamics [107].

In the early 2000s, Mark Tanaka *et al.* [108] introduced a model distinguishing between two behavioral types: "careful" and "risky". The proportion of each behavior type evolves in the population based on interactions, with each having its own transmission rate. This approach demonstrated how fear and information could influence the dynamics of an epidemic.

Further research focused on the behavior of infected individuals during an epidemic. In [109], infected individuals were modeled as reducing their contact rates due to sickness.

Similarly, in [110], the authors assumed that symptomatic individuals did not interact with healthy people because they were isolated (e.g., at home, in quarantine, or hospitalized).

Another part of research which began almost two decades ago rather focused the concept of "information epidemics" [111, 112, 113, 114, 115] which can evolve independently from the primary epidemic. This parallel spread has also been studied in the context of complex contagion processes (see [116] for a review), where changes in behavior, such as mask-wearing, spread when a critical fraction of neighbors adopt the behavior [117, 118]. Although these information dynamics may influence some parameters in our future work, we will not address them further in this thesis. Indeed, these models suggest indirect reactions to epidemics which surely play a significant role, but they lack some specific features that can be reached out by direct reactions models.

We present an illustrative example of such models, discussed in [98] by Poletti *et al.* The authors consider an SIR model in which susceptible individuals can adopt one of two exclusive behaviors: b_n ("normal") or b_a ("altered"). Individuals who adopt behavior b_a reduce their contact rate, leading to a lower transmission rate of the disease compared to those with behavior b_n. The population is thus divided into two groups: "normal" individuals, who become infected at a rate $\beta_n I(t)$, and "altered" individuals, who are infected at a rate $\beta_a I(t)$.

The authors introduce S_a and S_n to represent the proportion of "altered" and "normal" susceptible individuals in the population, respectively, with $S = S_a + S_n$. Defining $x = S_n/(S_a + S_n)$ as the fraction of "normal" individuals among the susceptible, the dynamics of the model can be written as follows:

$$\begin{cases} \dot{S}(t) = -\left[\beta_n S(t)x(t) + \beta_a S(t)(1-x(t))\right] I(t) \\ \dot{I}(t) = \left[\beta_n S(t)x(t) + \beta_a S(t)(1-x(t))\right] I(t) - \gamma I(t) \\ \dot{R}(t) = \gamma I(t) \\ \dot{x}(t) = x(t)(1-x(t))(\beta_a - \beta_n) I(t) \quad , \end{cases} \tag{1.9}$$

where the final equation describes the dynamics of the distribution of "normal" individuals among the susceptible population, driven by the fact that $\beta_a < \beta_n$. To account for behavioral adaptation, the authors allow individuals to switch between the two strategies (b_n and b_a) based on the information they receive, their beliefs, and perceived risk.

In this model, individuals face different costs associated with each strategy. The risk of infection is modeled as linear in I, and is higher for "normal" individuals. On the other hand, "altered" individuals incur a cost k due to their reduced contact rates. The authors define the payoffs for each strategy as follows

$$\begin{aligned} p_n(\tau) &= -m_n I(\tau) \\ p_a(\tau) &= -m_a I(\tau) - k \quad , \end{aligned} \tag{1.10}$$

with $m_n > m_a$, which may correspond to the risk of developing symptoms, and where τ represents the time scale at which individuals consider these payoffs, related to t by $\tau = \alpha t$. These payoff are coupled to the system dynamics, their dynamics are influenced through a selection process based on imitation [119]: the authors assume that a fraction of "normal" individuals can choose to become "altered" after comparing the two strategies, at a rate proportional to $\Delta p = p_n(\tau) - p_a(\tau)$ with a proportional factor ρ. Furthermore, an element of irrational behavior is introduced, with a constant random switching rate χ between the two strategies. Thus, the last equation in Eq. (1.9) becomes

$$\epsilon \dot{x}(t) = x(t)(1-x(t))(1-mI(t)) + \mu(1-2x(t)) \quad , \tag{1.11}$$

with $\epsilon = \frac{\alpha}{k\rho}, m = (m_n - m_a)/k + \epsilon(\beta_n - \beta_a), \mu = \frac{\chi}{k\rho}$. The authors then analyse the different mathematical properties of equilibrium solutions than can emerge from Poletti's model [98]. This example of "direct reaction" model illustrates how individuals can adapt their behavior in an explicit way due to the prevalence of infected in the population and the risk associated to the disease. Indeed, it is clear that this risk play a significant role, as adaptive behaviors due to a common cold will be much less important than for a deadly disease.

However, this model of spontaneous change behavior, as the ones presented before, overlook the phenomenon known as the "free rider problem" [102]: the term "free rider" originates from public transportation, where individuals who use a bus without paying are considered free riders. Although the system needs to operate efficiently, there is a collective interest in everyone paying for their tickets. This situation highlights the conflict between individual optimization and collective optimization, which can result in antagonistic behaviors.

In the context of epidemics, collective optimization might require individuals to stay at home. However, if everyone adheres to this, an individual acting solely in her own interest might prefer to go outside, as the risk of infection would be minimal. This illustrates the equilibrium that must be achieved between individual optimization and the collective behavior of the population. To accurately capture this interplay between individual decisions and the collective behavior, game theory provides an appropriate formalism that we will adopt in our work. The mathematical framework is introduced in the next chapter.

As we will discuss, there are several other advantages of a game theoretical approach compared to classical methods:

- Parameters are less "artificial". Previous approaches, such as those by Poletti, required introducing parameters like m_n and m_a, which have not always have clear physical understanding as they are derived from the equations rather than from a fundamental reasoning.

- Game theory is well-suited to account for anticipation, which is particularly important in scenarios where a central authority is responsible for optimizing the response strategy to an epidemic (see Sec. 2.4.2).

This concludes our general introduction on epidemic models and the modeling of spontaneous behavioral changes due to epidemic propagation. In the subsequent sections, we will employ the framework of game theory, specifically Mean-Field Game theory, to model the interactions between the epidemic and the human behavior through the formation of Nash equilibra.

2 - An introduction to Mean-Field Games using the SIR model

In the previous chapter, we examined how human behavior and epidemic dynamics can significantly influence each other. While this coupling can be artificially modeled through additional forces, its underlying mechanism lies in individual optimization. Game theory provides a natural framework to address such problems, where each agent (or player) optimizes their actions within an environment shaped by the optimizations of others. In Sec. 2.1, we introduce the fundamentals of game theory and the key conceptual tools necessary for our analysis. Subsequently, in Sec. 2.2, we discuss the approximations that lead to the Mean-Field Game approach in game theory, which facilitates the modeling of more realistic scenarios and enables the computational feasibility for large-scale games. In Sec. 2.3, we provide an application of this framework to epidemic modeling with the original SIR model, based on the work of Elie *et al.* [19]. This work will serve as a foundational basis for our following analysis. In Sec. 2.4, we explore other domains where mean-field games are currently being applied in epidemic modeling, as well as potential real-world applications of MFG. Finally in Sec. 2.5 we provide an overview of epidemiological models together with the original works of this thesis that will be presented in the subsequent chapters.

2.1 Basics of game theory

The field of game theory was first developed by mathematicians in the early 20th century, notably by John von Neumann and Oskar Morgenstern. Their groundbreaking work, Theory of Games and Economic Behavior (1944) [120], is often regarded as the foundation of the field. Since then, game theory has become a cornerstone in economics [121, 122], leading to several Nobel Prizes, including those awarded to Nash, Selten, and Harsanyi in 1994, followed by Aumann and Schelling in 2005. Over time, the application of game theory has expanded to various fields such as biology [123], pedestrian behavior [124], epidemic modeling [125], traffic modeling [126], and energy consumption [127], among others. These fields, which largely focus on the behavior of individuals or species, have benefited from game theory's ability to provide new insights into phenomena such as anticipation and sub-optimal equilibrium that are otherwise difficult to capture. In this section, we will introduce the fundamentals of game theory, beginning with the concept of the utility function in Sec. 2.1.1, which underpins the theory. We then explore a well-known yet insightful example, the prisoner's dilemma, in Sec. 2.1.2. Following this, we introduce the framework of individual optimization in Sec. 2.1.3. In Sec. 2.1.4, we discuss the different solutions obtainable through game theory, accompanied by an illustrative example. Finally, in Sec. 2.1.5, we provide a brief overview of the diverse modeling opportunities that game theory offers.

2.1.1 Utility as the key idea of game theory

The rationale behind a game theoretical approach can be illustrated through its successful application in economics. The concept of utility originates from the philosophical school of utilitarianism, developed by philosophers like Bentham in the late 18^{th} century. The core idea in game theory is that a rational individual weighs the positive and negative effects of potential actions. This evaluation, termed "utility", is carried out by each agent

independently, often based on personal judgment. For any given choice, the agent will select the option that maximizes her utility. While not all actions are rational, and the accurate assessment of outcomes is crucial even for rational ones, the explicit formulation of utility function makes it a valuable tool for theoreticians, enabling optimization. Consequently, a key objective in formulating such theoretical model is to define the positive and negative impacts of each choice within the game. These impacts may be immediate (e.g. displacement costs) or extend into the future (e.g. rewards at specific stages of the game). Agents' rationality also incorporates this temporal aspect, reflecting anticipation. This leads to an inter temporal utility that agents aim to maximize. However, by convention, utility is often expressed as the opposite of an inter temporal cost function C that agents aim to minimize. Before turning to the formal framework of game theory, we present a simple example to illustrate several underlying mechanisms of games.

2.1.2 A pedagogical example: the prisoner dilemma

The Prisoner's Dilemma is perhaps the most well-known two-player game, originally formulated by Flood, Dresher, and Tucker in 1950 [128]. In its simplest form, the game involves two rational agents, A and B, who are charged with theft. Each agent can either cooperate (neither betrays the other) or betray (betray their partner for personal gain). The outcomes, and thus the utility balance described previously, depend on the choices made by both players. The general structure of the game is illustrated in Fig. 2.1. Consider

	B stays silent	B betrays A
A stays silent	**Both** serve for 1 year	A serves for 3 years, B goes free
A betrays B	A goes free B serves for 3 years,	**Both** serve for 2 years

Figure 2.1: Possible outcomes of the prisoner dilemma. Each agent has two choices: stay silent or betray. The situation is symmetric for A and B, they cannot communicate and have no way to know the choice of the other. They both make their choice in independent rooms where they are auditioned.

the classic non-cooperative scenario where both players aim to minimize their own costs without regard for the other's outcome. Agent A faces two choices: if A remains silent and B also, then A and B will receive a small sentence (serve for 1 year). However, if B betrays A, A will receive a severe sentence. Conversely, if A betrays B, A will receive no sentence if B remains silent, and a moderate sentence if B also betrays. A thus concludes that regardless of B's choice, betraying will always result in a lesser sentence. Since A's choice does not influence B's decision (as the choices are independent), A will rationally choose to betray. Similarly, B reaches the same conclusion and chooses to betray A. The dilemma arises because both players would benefit from mutual cooperation, yet they each have an incentive to betray, leading to a suboptimal outcome for both. This phenomenon is also

employed in police investigations, where suspects are separated to encourage confessions.

A scenario (as this one) where no player can improve their situation by deviating from their chosen strategy to another without change in other strategies is called a Nash equilibrium. A formal definition of a Nash equilibrium is provided in Sec. 2.1.4.

In contrast, we can consider a cooperative game solution, where both players aim to minimize the total cost, defined as the sum of individual costs. In this cooperative setup, the optimal choice is for both players to remain silent, representing the societal optimum.

There is often a significant discrepancy between the societal optimum (resulting from collective optimization) and a Nash equilibrium (resulting from individual optimization). This illustrates the common misconception that "individual optimization will lead to the collective optimum". The Prisoner's Dilemma highlights the principle of individual optimization, foundational to game theory, but many variations of the dilemma has been designed to model additional phenomena. For instance, the work [129] shows that a successful strategy in repeated Prisoner's Dilemma games is to "tit-for-tat", which involves cooperating until the opponent betrays and then mimicking the opponent's previous move.

This concludes our discussion of this canonical example in game theory. We now turn to a more formal description of the game, incorporating various costs and a larger number of players.

2.1.3 Dynamics of games with large number of players

We consider a formal game involving $i = 1, ..., N$ players, where N may be large. The dynamics of the game is formed of two parts. In Sec. 2.1.3.1 we present the first part discussing the dynamics at the system level, considering the whole population of players who have determined strategies. This will fix the environment in which each player will evolve. The second part is discussed in Sec. 2.1.3.2 and concerns the individual optimization, that is, the way players choose their strategies by optimizing their utility in a given environment.

2.1.3.1 System dynamics at the population level

Players are characterized by their state which can be either discrete or continuous. In the continuous case, the status of a given player is defined by her position $\vec{x}_i$, while she controls a variable $a_i(t)$, which influences her position (a is often related to the velocity). Continuous games lead to systems of equations distinct from those in discrete games, they are used to model phenomena such as pedestrian dynamics, continuous stocks, or energy consumption, among others. Notably, in scenarios where a represents velocity and x corresponds to displacement, the total cost C can be interpreted as a physical action, with players acting as particles [130]. The principle of least action for particles is then analogous to the minimization of the cost function, yielding similar equations and productive analogies (see [131] for an analogy with pedestrian games).

Yet, we will rather focus on discrete games in this thesis. Here, players can occupy a finite number of states, denoted as $y_1, ..., y_m$ where m is the number of possible states. Player i in the k^{th} is denoted $x_i = y_k$. We denote by capital letters the number of players in each state k as Y_k. The game unfolds over a time interval $[0, T]$. Due to the complexity of these systems, many parameters are often unknown and are represented by stochastic variables. This stochasticity is often introduced into discrete games by allowing individuals to control a fraction of their transition rates between states, ensuring stochastic dynamics governed by a Markovian process rather than deterministic transitions. A common example of such stochastic process is the individual transition rate to infection in the SIR model: an individual, susceptible at t and controlling her transmission rate $\chi(t)$ will have a probability $\chi(t)I(t)dt$ to become infected at $t+dt$. Thus, her state at $t+dt$ is unknown and stochastic,

it depends on $\chi(t)$ and $I(t)$. Consequently, each player's state $\{x_i\}$ becomes stochastic, and the dynamics of the number of players in each state Y_k is itself a stochastic quantity which emerge from the Markovian process and the choices followed by each individual. This creates a stochastic environment in which agents can performed their optimization to build their optimal strategy.

2.1.3.2 Individual optimization

We now focus on deriving the equations that arise from individual optimization. We take player i as a reference for this discussion. Importantly, player i is assumed to anticipate the strategies of all other players during her optimization. These strategies define the environment in which player i anticipates to evolve, even though the states of other players remain stochastic and are determined by the underlying Markovian process. Naturally, this anticipation is not guaranteed to be valid a priori; we will come back to this issue later. To pursue with the optimization process, we first define the utility function that each agent seeks to maximize. Yet, for consistency with the literature, we will rather define a cost function that agents want to minimize, with an opposite convention. This cost function represents the cost incurred by player i from the current time t until the end of the game at time T. At each time s within the interval $[t, T]$, player i incurs a current cost $c_i(a_i(s), x_i(s), x_{-i}(s))ds$ during the time step ds. This current cost c_i depends on the characteristics of individual i such as her choice at s, $a_i(s)$, and her state $x_i(s)$. It also depends on the state of all other players than i at s, denoted $x_{-i}(s)$ (similarly, their associated strategies over the whole game will be denoted $a_{-i}(.)$). Given that the states x_{-i} (and $x_i(s)$) are stochastic, player i will pay the following stochastic cost

$$C_i(a_i(.), a_{-i}(.), t) = \int_t^T c_i\left(a_i(s), x_i(s), x_{-i}(s)\right) ds \quad , \tag{2.1}$$

which depends on the precise realization of the states $x_i(s), x_{-i}(s)$ in $[t, T]$. We omitted the initial state of each player in the argument of C_i for simplicity, and similarly, to avoid cumbersome notation, we will often omit the control variables of other players than i in the arguments of C_i (similarly for c_i), since i has no influence over them. In certain contexts, a terminal cost at T could be added, but we omit it here as it is not relevant for our subsequent analysis. However, as we shall see in Sec. 3.4, the duration of the game T could have a significant impact on the results, although it is not explicitly mentioned as an argument of C_i.

Player i aims at minimizing C_i. However, since C_i is a stochastic quantity, player i will rather aim to minimize $\mathfrak{C}_i \equiv \langle C_i \rangle$ the average cost over realizations of the Markovian process (from t to T). To achieve this, we define the *value function* of i, denoted U_i, which corresponds to the minimum expected cost that the agent can incur between t and T. This value function is given by

$$U_i(t) = \min_{a_i(.)} \mathbb{E}\left[C_i(a_i(.), t)\right] \equiv \min_{a_i(.)} \left[\mathfrak{C}_i(a_i(.), t)\right] = \mathbb{E}\left[C_i(a_i^*(.), t)\right] \quad , \tag{2.2}$$

where the expectation $\mathbb{E}$ represents the average over the realizations of the Markovian process, that is over players' states $x_{-i}(.)$, and $x_i(.)$, during the time interval $[t, T]$. The strategy $a_i^*(.)$ corresponds to the optimal strategy that player i seeks to determine (for fixed $a_{-i}(.)$). To derive the evolution of U_i, we employ a standard Bellman argument [130]. The minimal possible cost at time t is obtained by summing two quantities: the minimal possible cost at time $t + dt$, and the cost incurred during the interval $[t, t + dt[$ under the optimal strategy at time t. This implies that the optimal strategy from t to T must also be optimal from $t + dt$ to T, considering that the state at $t + dt$ depends on the state at t

and the optimal strategy applied at t. Given an initial state at time t, we then obtain

$$\begin{aligned} U_i(t) &= \min_{a_i(t)} \mathbb{E}\left[U_i(t+dt) + c_i(t, x_i(t))dt\right] \ , \\ a_i^*(t) &= \operatorname*{argmin}_{a_i(t)} \mathbb{E}\left[U_i(t+dt) + c_i(t, x_i(t))dt\right] \ , \end{aligned} \tag{2.3}$$

which is much simpler than Eq. (2.2) as the minimization is performed only with respect to the time t. Note that we add a t dependence to c_i to make explicit that the current cost c_i will depend on the state of the game at t (it depends rigorously on $x_{-i}(t)$). Equation (2.3) can be solved analytically in some cases, and is at least usually solvable numerically. To do so, one typically solves it backward in time. Starting from $U(T) = 0$ – since with no terminal cost, there is no remaining cost at $t = T$ – one can numerically solve the minimization $U_i(T - dt) = \min_{a_i(t)} \mathbb{E}\left[c_i(T - dt)dt\right]$ and then continue this scheme backward. Upon completing the optimization, one obtains $a_i^*(.)$, the optimal strategy for player i. It is important to note that this strategy $a_i^*(.)$ depends on the other strategies $a_{-i}(.)$ through the cost function C_i, leading to a self consistent condition that is described below.

2.1.4 Nash equilibrium and societal optimum

Here, we formally introduce, in Sec. 2.1.4.1, the concept of Nash equilibrium emerging from individual optimization. Then, we outline in Sec. 2.1.4.2, the societal optimum emerging from global optimization, before an illustrative example in Sec. 2.1.4.3.

2.1.4.1 Nash equilibrium

The game is said to be at a Nash equilibrium if the strategy used by each player is optimal for a given set of player's strategies $\{a_j^{\text{Nash}}(.)\}$. Namely, for any player i which follows a strategy $a_i^{\text{Nash}}(.)$ one has

$$\mathfrak{C}_i\left(a_i^{\text{Nash}}(.), a_{-i}^{\text{Nash}}(.), 0\right) = \min_{a_i(.)} \mathfrak{C}_i\left(a_i(.), a_{-i}^{\text{Nash}}(.), 0\right) \ , \tag{2.4}$$

where the minimization is performed on the set of admissible strategies of $a_i(.)$ at time $t = 0$. Indeed, thanks to the Bellman argument previously described, the minimization performed at $t = 0$ will be also correct at any time $t > 0$. Existence and uniqueness conditions of such Nash equilibrium are difficult subjects which have been studied by mathematicians [132]. If the existence can be shown under several hypotheses on the game or on the cost, uniqueness is not always guaranteed. This Nash equilibrium has been first described by Nash in this thesis at the end of the 1940s, and corresponds to an equilibrium resulting from an individual optimization. It is an equilibrium in the sense that any change away from $a_i^{\text{Nash}}(.)$ will lead to a positive extra cost for player i due to Eq. (2.4). Therefore, nobody has interest to change her strategy to another one if nobody else changes, this is the meaning of "equilibrium under individual optimization".

In the prisoner's dilemma described earlier in Sec. 2.1.2, the strategy where each player chooses to betray is a clear example of a Nash equilibrium. In fact, this strategy is even stronger: a player who chooses to betray does not need to adjust her strategy in response to the other player's possible actions, unlike what is required in Eq. (2.4), since betraying is always the optimal choice. Such strategies are known as "dominant" strategies, they always result in a Nash equilibrium, though not all Nash equilibria imply dominant strategies. In cases involving "non-dominant" Nash equilibrium, the convergence of players' strategies to such Nash equilibrium is a complex issue, which we briefly explore in Sec. 2.4.2.

2.1.4.2 Societal optimum

A Nash equilibrium results from individual optimization, but the cost associated with such a strategy is often not the minimal one, either from individual's perspective or from

society as a whole. This raises the possibility for authorities to build a cost function that better represents societal utility. However, defining utility at the societal level is inherently complex, as it is a psychological concept that is difficult to quantify for a collectivity. Should the goal be to maximize the average utility, or ensure that individual utilities stay above a certain threshold ? What metrics should be used to evaluate societal utility ? For instance, one possible approach could be to aim for a Pareto equilibrium [133], defined as a strategy where no individual can change their strategy without negatively affecting someone else's cost.

Yet, the most common and natural approach in the literature [19] is to construct the societal cost as the average of all individual costs:

$$\mathfrak{C}_{\text{glob}}\left(\{a_j(.)\},0\right) = \frac{1}{N}\sum_i \mathfrak{C}_i\left(\{a_j(.)\},0\right) \ . \tag{2.5}$$

With this definition, all individuals are treated equally, simplifying the optimization of social utility by averaging well-defined individual costs. In any case, this societal cost is more aligned with what should be considered in terms of societal utility compared to a Nash equilibrium. The set of player's strategies $\{a_j(.)\}$ which minimizes this cost, denoted $\{a_j^{\text{SO}}(.)\}$, is called societal optimum strategies and must fulfill the following condition

$$\mathfrak{C}_{\text{glob}}\left(\{a_j^{\text{SO}}(.)\},0\right) = \min_{\{a_j(.)\}} \mathfrak{C}_{\text{glob}}\left(\{a_j(.)\},0\right) \ . \tag{2.6}$$

By definition, this cost is lower than the global cost obtained under the Nash equilibrium strategy[1]. Indeed, the inherent competition among individuals often results in a sub-optimal Nash equilibrium, where a societal optimum would be more beneficial for everyone (as illustrated in the neighborhood game example below). However, the societal optimum is often achieved by balancing costs among individuals, where some individuals bear a higher cost (compared to the Nash equilibrium) to benefit a larger group, ultimately minimizing the global cost. This discrepancy between the global costs for Nash and Societal optimum strategies is commonly referred to as the "cost of anarchy" in the literature:

$$\Delta C = \mathfrak{C}_{\text{glob}}\left(\{a_j^{\text{SO}}(.)\},0\right) - \mathfrak{C}_{\text{glob}}\left(\{a_j^{N}(.)\},0\right) \ . \tag{2.7}$$

For an authority aiming at minimizing the societal cost, the objective is to approach the societal optimum as closely as possible. Achieving this optimum is idealistic, as it requires perfect control over the population at all times t, but one can still try to improve the Nash equilibrium. This "unconstrained" Nash equilibrium arises from individual, self-serving optimization in an unrestricted space, meaning that well-designed constraints could yield a "constrained" Nash equilibrium with a global cost closer to the societal optimum. Referring to Eq. (2.7), this approach aims at reducing ΔC by imposing constraints on the control parameters $a_j(.)$ of individuals, leading to a new Nash equilibrium. This raises the question of how to design and implement such collective constraints. We will further investigate this in our study, especially in the context of epidemic modeling in Sec. 3.3.4.

2.1.4.3 A simple illustration: the neighborhood game

We consider a simple game to make the concepts of Nash equilibrium and societal optimum more concrete. This illustration is inspired from Jean-Philippe Bouchaud M2 lecture and Schelling model of segregation [134]. Suppose there are N individuals who must be distributed across four identical neighborhoods in a town. Each neighborhood has a capacity of $\frac{3}{4}N$ individuals (the town has therefore a capacity of $3N$ individuals).

[1] we often assume the uniqueness of the Nash equilibrium for simplicity

When deciding in which neighborhood to settle, each individual considers the following cost, which is identical for everyone:

$$C(\eta) = 3\eta^2 - 2\eta \,, \tag{2.8}$$

where η is the density of the neighborhood in which the individual will settle (namely, η is equal to the total number of individuals in the neighborhood divided by its capacity). The quadratic term in η^2 reflects congestion effects in overly crowded areas, while the term $-\eta$ indicates that individuals prefer to be with friends and neighbors (they do not want to be isolated). The constants 3 and -2 represent the sensitivity to these effects. The cost in Eq. (2.8) can be minimized, achieving a minimum at $\eta = 1/3$ with $C(1/3) = -1/3$. This results in a distribution of $N/4$ individuals per neighborhood, totaling N individuals, which clearly represents the societal optimum of the game, as illustrated in Fig. 2.3. However, the Nash equilibrium in this game is different. We assume that individuals arrive one by one in the city and start by settling in one neighborhood. Once settled, individuals are free to move to any other neighborhood if it appears beneficial to reduce their cost. When the density η reaches $1/3$, it represents the optimal density for those already settled. However, new individuals will prefer to move into this neighborhood rather than an empty one because the associated cost is lower (see Fig. 2.3). Consequently, η increases until it reaches $2/3$ with $C(2/3) = 0$. At this point, it becomes more advantageous for new arrivals to choose another neighborhood and continue the same process. This leads to a Nash equilibrium where neighborhoods have either $\eta = 0$ or $\eta = 2/3$ with $C(0) = C(2/3) = 0$, as shown in Fig. 2.2). It is clear that, in this scenario, any move by any individual will result in a higher cost, thus confirming that we are at a Nash equilibrium.

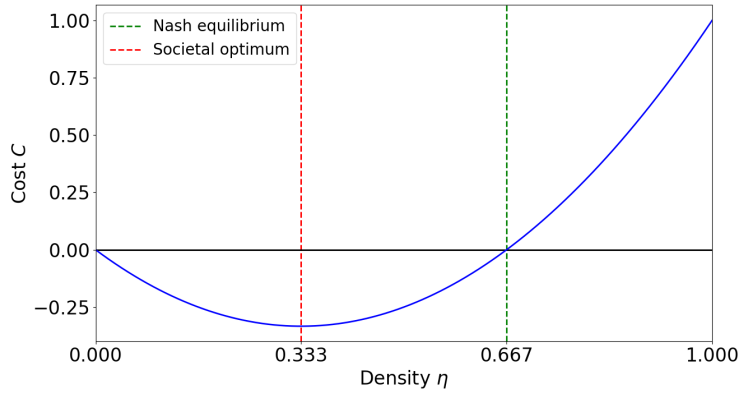

Figure 2.2: Illustration of the evolution of the cost per individual, C, according to the density η of the neighborhood in which the individual want to take place. This cost is zero at $\eta = 0$ and $\eta = 2/3$, and admits a minimum for $\eta = 1/3$ with $C(1/3) = 1/3$.

Regarding the cost, the societal optimum results in a global cost of $-1/3$, whereas the cost at the Nash equilibrium is 0. Therefore, by allowing individuals to act independently, the outcome can be worse for everyone. Specifically, while each individual's cost is 0 at the Nash equilibrium, it is $-1/3$ at the societal optimum. The town authority, concerned with the welfare of its citizens, could implement rules to improve the situation, such as restricting the arrival of new individuals to neighborhoods that are already half occupied. By applying this rule, the Nash equilibrium under these constraints results in a global cost of $-3/16$, which is closer (but still above) the societal optimum cost.

This simple neighborhood game illustrates the concepts of a (free) Nash equilibrium, societal optimum, and Nash equilibrium under constraints in a practical example. From a societal perspective, the game provides insights into phenomena such as segregation, where individuals prefer to settle with similar people, leading to a socially homogeneous

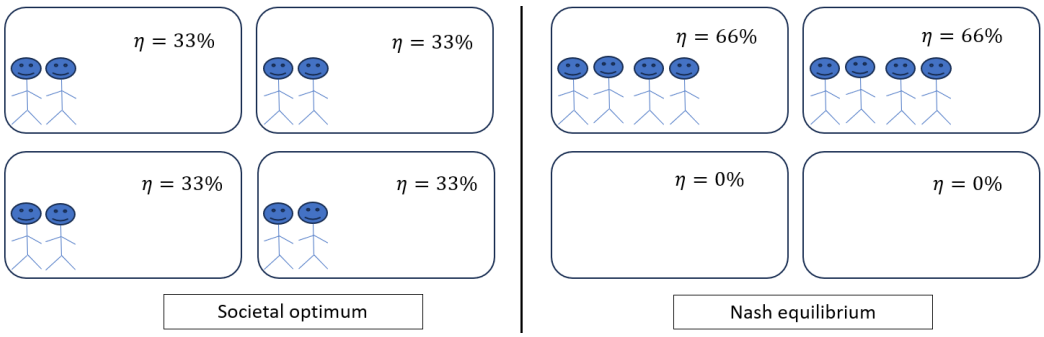

Figure 2.3: Left: illustration of the societal optimum with the four neighborhoods occupied with $\eta = 1/3$. Right: illustration of the Nash equilibrium with the two neighborhoods occupied with $\eta = 2/3$ and two other ones empty. Neighborhoods are fulfilled progressively, the first one starts from $\eta = 0$ to $2/3$, and then the second one, and so forth.

environment that diverges from the initial intent. Reader can refer to the Schelling model for a reference work on the subject [134]. It also demonstrates how implementing simple rules can benefit the entire population.

With the framework of game theory, one must consider every single player to determine their optimal strategy and ultimately achieve the Nash equilibrium. This procedure is often impractical, especially numerically, as the number of players N increases (it becomes impossible with even a few dozen players). To proceed analytically or numerically, several approximations are necessary, leading to the so-called "Mean-field" paradigm. Readers can go directly to Sec. 2.2 to pursue the derivation of the mean-field approach.

2.1.5 Other concepts in game theory

Since its development, game theory has been applied across various fields, leading to the emergence of diverse concepts. We briefly present some of these below:

- **Rationality:** In the games we presented, we considered the agents as perfectly rational, meaning they balance well-known costs. However, we know that human behavior is also influenced by various biases and that cooperative effects can emerge even in non-cooperative situations. Different approaches, such as psychological game theory [135], are therefore investigated to account for these effects.

- **Information:** Related to rationality, information is central in game theory. For each game, it is essential to determine whether players have complete or incomplete access to information. Various methods can represent this lack of information, with one natural approach being to include noise and stochasticity in the quantities to which players have only partial access [136, 137].

- **Evolutionary Games:** This type of games was developed to study evolving populations in biology [123]. It defines a framework where Darwinian competition can occur. These games differ from classical ones as they focus on the evolution of strategies over time to find the most effective ones. Players, such as individuals of different species, experiment with strategies without knowing the utility associated with them. Through repeated games, which could correspond to prey-predator situations in this context, individuals adapt their strategies and attempt to find better ones through random trials.

- **Simultaneous vs iterative games:** As we mentioned with the prisoner dilemma, another type of games are the ones which are iterative. In such contexts, individuals

adapt their strategy at each occurrence of the game, depending on the strategies previously adopted by others [138].

- **Limited anticipation:** Anticipation plays a crucial role in game theory, as it is factored into the utility function, which accounts for future expected costs. However, a well-known bias in human behavior is that present costs (or gains) are perceived as higher than those occurring in the future. This can be modeled in game theory using a discount factor on future costs [139].

2.2 Mean-field Game approach

In the previous section, we discussed that traditional game theory is manageable only for a small number of players. As the number of players increases, the complexity of solving individual optimization equations becomes computationally infeasible. To address this challenge, Lasry and Lions introduced Mean-Field Games (MFG) nearly two decades ago [140, 141, 142], a concept that was independently developed by Huang, Malhamé, and Caines [143]. MFG theory focuses on determining Nash equilibria in populations with a large number of agents. For an in-depth mathematical treatment, readers can refer to [144, 145, 146], while [131, 147] provide an introduction for physicists. MFG has a wide range of applications, including finance [148], economics [149], crowd dynamics [150], and opinion dynamics [151].

In this section, we will explain the mean-field approximation in Sec. 2.2.1. Then, in Sec. 2.2.2, we will demonstrate how the equations from game theory simplify into a system of two equations, which form the mean-field game system.

2.2.1 Mean-field approximation

The mean-field approximation is a well-established concept in physics, used to simplify many-body problems by reducing their dimensionality. The rationale behind this approach is to approximate the total force experienced by any element in the system—resulting from the sum of all microscopic interactions—by an averaged field.

For example, in the case of 1/2 spins on a 2D lattice, the mean field corresponds in the simple case to the average spin across the entire lattice. By averaging the spin-up and spin-down states, we can compute the total magnetization m, which influences the behavior of individual spins. This effective field closely approximates the true field if the fluctuations around the mean are minimal, which generally requires a large number of neighbors per spin and a large overall number of spins. Consequently, the mean-field approximation becomes more accurate as the system's dimensionality increases.

In a similar way, the mean-field approach in game theory allows us to reduce the N optimization equations, derived from individual decisions (analogous to the minimization of free energy in a physical system), to a system of two equations supplemented by a consistency condition that must be satisfied. We pursue now the previously introduced framework describing the game theoretical concepts through the point of view of an individual i in state y_k. Referring back to the cost function for a single agent i, this cost is expressed as in Eq. (2.1)

$$C_i(a_i(.), a_{-i}(.), t) = \int_t^T c_i\left(a_i(s), x_i(s), x_{-i}(s)\right) ds \quad . \tag{2.9}$$

A first approximation that might seem natural in the context of spins is to assume that the Hamiltonian experienced by each particle is the same, as we are dealing with identical particles. However, for individuals in a game-theoretical setting, the cost for each person

would inherently differ, given that individuals have varying sensitivities to different parameters. Thus, the function c_i, which describes the current cost, and consequently the total cost C_i, could vary between individuals. Nevertheless, to proceed further, we often make the approximation that the costs are uniform. Consequently, the strategy of each agent will depend not specifically on the individual i, but rather on the state of i (indexed by k). In cases where individual behaviors are highly diverse, we classify them into distinct categories based on characteristics such as gender, age, or ethnicity.

In the mean-field games framework, we consider scenarios involving a very large number of players, N, where each player interacts with many others. The first step in the mean-field approximation is to assume that individuals are not affected by the precise state of every other individual x_j, but rather by the distribution of individuals across different states, denoted by Y_k. The second step is to disregard fluctuations in Y_k and assume that individuals are only influenced by the mean field, $\langle Y_k \rangle$. We can therefore rewrite the cost function in Eq. (2.1) to reflect this mean-field approach, which now takes the following form, starting from t:

$$C(a_i(.), \{a^k_{\text{col}}(.)\}, t) = \int_t^T c\left(a_i(s), x_i(s), \{\langle Y_k \rangle(s)\}\right) ds \quad . \tag{2.10}$$

In Eq. (2.10), $\{a^k_{\text{col}}(.)\}$ represents the set of strategies followed by individuals in each state k at any time during the game. This strategy is termed "collective" because it is adopted by all individuals except for our reference player i, who is evaluating potential choices for her strategy. Given that $N \to \infty$ and individuals are treated on an equal footing, the strategy chosen by agent i can be considered negligible in its effect on the collective behavior. The current cost c now depends on the average number of individuals in each state k, $\langle Y_k \rangle(s)$, which is deterministic. The only remaining stochastic variable in this cost is the state of the reference individual $x_i(s)$, which may significantly influence her behavior. As a result, the optimization now only concerns the different possible states, and the value function in Eq. (2.2) simplifies to a single equation:

$$U_i(t) = \min_{\{a_i(.)\}} \mathbb{E}_{x_i(.)} \left[C(a_i(.), t) \right] \quad , \tag{2.11}$$

where the expectation is now only over the future states $x_i(\tau > t)$ of the reference individual i. The value function still implicitly depends on the initial state $x_i(t)$, resulting in m distinct value functions instead of N. As before, the full dependencies of C are often omitted to avoid cumbersome notation.

Finally, the Markovian process which was stochastic and dependent of individuals' strategies reduces to a deterministic process depending on the different collective strategies:

$$\dot{\langle Y_k \rangle} = g_k \left(\{\langle Y_k \rangle(s)\}, \{a^k_{\text{col}}(.)\} \right) \quad , k = 1, ..., m \quad , \tag{2.12}$$

where functions g_k correspond to the macroscopic dynamics of each state y_k. This equation is said to be the Kolmogorov equation in the context of MFG. It is also known as the Fokker-Planck equation for continuous systems, driving the dynamics of the latter.

2.2.2 Mean-Field Games equations

Let us summarize the main point discussed above. A MFG can be described as follows:

Let us consider $N \to \infty$ symmetrical agents, optimizing their own cost C in $[0, T]$. Agent's state evolves among m possible states y_k, $k = 1, ..., m$, with $Y_k(t)$ the number of agents in state k at t. Each agent follows a strategy $a_i(.)$, and the collective strategy associated with each state is denoted $a^k_{\text{col}}(.)$. The Nash equilibrium solution of the MFG

is given by any set of strategies $a^k_{\text{col}}(.)$ such that:

$$\dot{\langle Y_k \rangle} = g_k \left(\{ \langle Y_k \rangle(s) \}, \{ a^k_{\text{col}}(.) \} \right) \ , \quad k = 1, ..., m \ , \tag{2.13}$$

with a given set of initial conditions $\{Y_k(0)\}$. This Kolmogorov equation is coupled with the Hamilton-Jacobi-Bellman equation which will be identical for any player i of the game:

$$U_i(t) = \min_{a_i(t)} \mathbb{E} \left[U_i(t + dt) + c(t, x_i(t)) dt \right] = \mathfrak{C}_i(a^*_i(.), t) \ , \tag{2.14}$$

with

$$a^*_i(t) = \underset{a_i(t)}{\text{argmin}} \ \mathbb{E} \left[U_i(t + dt) + c(t, x_i(t)) dt \right] \ , \tag{2.15}$$

To be at equilibrium, the strategy followed by all individuals should be optimal from an individual point of view, otherwise that individual would change her strategy to another one. Thus, this system is completed with the self consistent condition

$$a^*_i(t) = a^k_{\text{col}}(t) \ , \quad \forall t \quad , \tag{2.16}$$

where the individual i is in the state k at t, namely $x_i(t) = y_k$. A solution of this system corresponds to a Nash equilibrium of the game. As for classical games, the existence and uniqueness of a Nash equilibrium is not often guaranteed, we will infer it from our numerical simulations. We describe the numerical techniques used in Chapter 6. In the next section, this MFG framework is illustrated with a founding application to epidemics dynamics.

2.3 Mean-Field Game on the SIR model

Once the framework is established, we can apply the Mean-Field Game approach to epidemic dynamics. As mentioned earlier, this method allows for the modeling of human behavior in response to epidemics, where agents make decisions based on rationality rather than simply adhering to predefined rules.

The application of MFG to epidemic dynamics was first introduced about a decade ago by Reluga *et al.* [99] to model social distancing. Since then, MFG has been used to describe vaccination strategies, which are influenced by individual decision-making. Early contributions in this area include works by Laguzet *et al.* [152] (see also [153, 154]). More recently, in 2020, Elie *et al.* [19] proposed a similar approach to study the impact of individual decisions on distancing and isolation, exploring how these choices affect epidemic dynamics (see [155, 156] for a mathematical perspective). A comprehensive review of recent advances in this field is available in [157]. In this section, we will build upon the framework developed by Elie *et al.* [19] in 2020. We begin by presenting the model in Sec. 2.3.1, followed by the derivation of costs in Sec. 2.3.2. The Hamilton-Jacobi-Bellman equation resulting from individual optimization is derived in Sec. 2.3.3. The outcomes of the game are discussed in Sec. 2.3.4 for the Nash equilibrium and in Sec. 2.3.5 for the societal optimum. A final discussion on the costs is provided in Sec. 2.3.6.

In their paper [19], the authors applied the MFG framework to the simplest epidemic model, the SIR model, which has been discussed in Chapter 1 (see Sec. 1.1.3). Their work primarily focused on the mathematical properties of the game solutions. In this section, we will carefully derive the MFG paradigm they used, using a more physical and extended approach. The notations have been adjusted to align with the forthcoming analysis.

2.3.1 Model presentation

In their paper [19], the authors consider an epidemic spreading over the time interval $[0, T]$ within a large, homogeneous population of N identical individuals. Each individual

exists in one of three possible states at any time t: susceptible, infected, or recovered, denoted respectively as s, i, and r. The Kolmogorov equation (2.12) of the game corresponds to Eq. (1.7), with a contact rate $\bar{\chi}$ that depends on the decisions made by individuals:

$$\begin{aligned} \dot{S} &= -\rho\bar{\chi}(t)S(t)I(t) \\ \dot{I} &= \rho\bar{\chi}(t)S(t)I(t) - \xi I(t) \\ \dot{R} &= \xi I(t)\,. \end{aligned} \tag{2.17}$$

This equation describes the dynamics of the average number of individuals in each state of the game, which depends on the contact rate $\bar{\chi}(t)$. This contact rate is now treated as a variable outcome of the model and represents the strategy chosen by susceptible individuals at time t. At equilibrium, this strategy should be optimal and identical for all individuals. To find this equilibrium, we proceed to the optimization process to derive the Hamilton-Jacobi-Bellman (HJB) equation of the game, preceded by the cost derivation of each individual. The optimization is conducted exclusively for the "susceptible" state, as the authors assume a fully individualistic game where infected and recovered individuals do not have incentive to reduce their contact rate. Indeed, and contrarily with what we will consider in Chapter 3, contacts are not symmetric in this simple SIR model and the infection probability of a susceptible individual will only depend on her contact rate $\chi(t)$.

2.3.2 Cost derivation

Consider a reference individual k. This individual assumes that all other individuals will adopt the same strategy, denoted by $\bar{\chi}(t)$. At time t, individual k estimates the total cost associated with the epidemic as the sum of two components: the cost of the efforts made to avoid infection, and the potential cost of infection if it occurs. This overall cost is dependent on the strategy $\chi_k(t)$ that individual k decides to follow. If individual k becomes infected at some future time $\tau > t$, the total stochastic cost incurred between time t and the end of the optimization period at time T is given by:

$$C\left(\chi_k(.), t, \tau\right) \equiv \mathfrak{r}_\mathrm{I}\mathbf{1}_{\tau<T} + \int_t^{\min(\tau,T)} f\left(\chi_k(s)\right) ds \ . \tag{2.18}$$

This cost depends on $\chi_k(t)$ over the period from t to τ (the infection time) or T (if the individual remains uninfected). It also depends on the collective strategies $\bar{\chi}(t)$ within this interval, but this dependency is implicit through the infection time τ. The first term in Eq. (2.18) represents the infection cost, denoted by a constant $\mathfrak{r}_\mathrm{I}$, which covers expenses related to illness, symptoms, and social isolation (such as quarantine). This cost is incurred immediately upon infection at $t = \tau$, as indicated by the indicator function $\mathbf{1}$. If $\tau > T$, this cost is not incurred and $\tau = +\infty$ is assigned to τ. The second term is the cost associated with reducing social contacts, given by $f(\chi)$. This term measures the psychological and financial costs of limiting social interactions. During each time interval s from t to $\min(\tau, T)$, the agent incurs a cost of $f\left(\chi_k(s)\right) ds$. For $s > \tau$, this cost is zero, as the individual is either infected (with social costs included in $\mathfrak{r}_\mathrm{I}$) or recovered (with no further infections possible in this model). The authors adopt a standard form for this cost function, which is

$$f(\chi(t)) = \frac{\chi_0}{\chi(t)} - 1 \ , \tag{2.19}$$

where $\chi(t)$ ranges within the interval $[\chi_{\min}, \chi_0]$, with $\chi_{\min}$ representing the minimum admissible contact rate (e.g., during a strict lockdown) and χ_0 representing the standard contact rate in the absence of epidemic. From the perspective of agent k at time t, and given that epidemic propagation is a stochastic process, the infection time τ is a random variable with a probability distribution $P_k(\tau)$. This probability distribution also depends

on t, as the agent has obtained information regarding whether she has been infected during the interval $[0, t]$. Consequently, the cost in Eq. (2.18) is also stochastic. At each time t, a rational agent should select her future strategy $\chi_k(s)$ for $s > t$ to minimize the *expected* value of C over the possible realizations of the epidemic,

$$\mathfrak{C}\left(\chi_k(\cdot), \bar{\chi}(\cdot), t\right) \equiv \int_t^\infty d\tau \; P_k(\tau) \; C\left(\chi_k(\cdot), t, \tau\right) \; , \tag{2.20}$$

where $\tau > T$ is interpreted as an absence of infection (allowing us to normalize $\int_t^\infty P_k(\tau)d\tau = 1$, and so $C\left(\chi_k(\cdot), t, \tau > T\right) = \int_t^T f\left(\chi_k(s)\right) ds$).

We now need to determine the probability $P_k(\tau)$ for an agent k who is following a specific strategy $\chi_k(t)$. Let $\phi_k(\tau)$ denote the cumulative probability, which represents the probability that k will be infected before time τ. The probability that the infection time for k falls between τ and $\tau + d\tau$ is given by

$$\phi_k'(\tau)d\tau = P_k(\tau)d\tau = \mathcal{P}\left[x_k(\tau + d\tau) = i | x_k(\tau) = s\right] \times \mathcal{P}\left[x_k(\tau) = s\right] , \tag{2.21}$$

where the probability that k is susceptible at time τ is $\mathcal{P}\left[x_k(\tau) = s\right] = 1 - \phi_k(\tau)$. The probability for k to become infected between τ and $\tau + d\tau$ is given by average version of the Markovian process of SIR model Eq. (1.2), which reads

$$\mathcal{P}\left[x_k(\tau + d\tau) = i \,|\, x_k(\tau) = s\right] = \lambda_k(\tau)d\tau \; , \tag{2.22}$$

with λ_k simply given by

$$\lambda_k(t) \equiv \rho\chi_k(t)I(t) \quad . \tag{2.23}$$

$\lambda_k(t)$ is the force of infection seen by individual k, with ρ the contagiousness per contact, $\chi_k(t)$ her behavior and $I(t)$ the average proportion of infected individuals at t (mean-field approximation). Equation (2.21) thus leads to $\phi_k'(\tau) = \lambda_k(\tau)(1 - \phi_k(\tau))$, which together with $\phi_k(t) = 0$ gives

$$\phi_k(\tau) = 1 - \exp\left(-\int_t^\tau \lambda_k(s)ds\right) \; . \tag{2.24}$$

The average cost (2.20) reads

$$\mathfrak{C}\left(\chi(\cdot), \bar{\chi}(\cdot), t\right) = \int_t^T d\tau \; P_k(\tau)\mathfrak{r}_\mathrm{I} + \int_t^\infty d\tau \; P_k(\tau) \int_t^{\min(\tau,T)} ds \; f\left(\chi_k(s)\right) \; , \tag{2.25}$$

then we develop the second term

$$\begin{aligned} &\int_t^\infty d\tau \; P_k(\tau) \int_t^{\min(\tau,T)} ds \; f\left(\chi_k(s)\right) \\ &= \int_t^T d\tau \; P_k(\tau) \int_t^\tau ds \; f\left(\chi_k(s)\right) + \int_T^\infty d\tau \; P_k(\tau) \int_t^T ds \; f\left(\chi_k(s)\right) \\ &= \int_t^T f\left(\chi_k(s)\right) ds \int_s^T P_k(\tau)d\tau + \int_t^T ds \; f\left(\chi_k(s)\right) \int_T^\infty d\tau \; P_k(\tau) \end{aligned} \tag{2.26}$$

where we invert integrands in the first term using $\int_0^T \left[f(t) \int_0^t g(s)ds\right] dt = \int_0^T \left[g(t) \int_t^T f(s)ds\right] dt$. Equation (2.25) can be therefore written as

$$\mathfrak{C}\left(\chi(\cdot), \bar{\chi}(\cdot), t\right) = \int_t^T ds \; P_k(s)\mathfrak{r}_\mathrm{I} + \int_t^T ds \; f\left(\chi_k(s)\right) \int_s^\infty d\tau \; P_k(\tau) \; . \tag{2.27}$$

We then use $\phi_k'(\tau) = P_k(\tau) = \lambda_k(\tau)(1 - \phi_k(\tau))$ to get [19]

$$\mathfrak{C}\left(\chi(\cdot), \bar{\chi}(\cdot), t\right) = \int_t^T \left[\lambda_k(s) \; \mathfrak{r}_\mathrm{I} + f\left(\chi_k(s)\right)\right] (1 - \phi_k(s))ds \, , \tag{2.28}$$

or in a very explicit way, with Eq. (2.19),

$$\mathfrak{C}\left(\chi_k(\cdot),\bar{\chi}(\cdot),t\right)=\int_t^T\left[\chi_k(s)I(s)\ \mathfrak{r}_{\mathrm{I}}+\frac{\chi_0}{\chi_k(s)}-1\right]\exp\left(-\int_t^u\chi_k(u)I(u)du\right)ds\ . \quad (2.29)$$

In the following, we will often use $\mathfrak{C}\left(\chi_k(\cdot),t\right)$ for simplicity, but the cost still depends implicitly on $\bar{\chi}(\cdot)$ through $I(.)$ which is given by Eq. (2.17).

2.3.3 Hamiton-Jacobi Bellman equation

The expected cost at time t for agent k is a function of her own strategy χ_k and of the infected proportion $I(.)$. The next step is to solve the optimization problem, that is, find the optimal strategy χ^* for a given epidemic $S(.),I(.),R(.)$. Following our previous derivation in this context Eq. (2.3), we introduce the *value function*

$$U_k(t)=\begin{cases}\min\limits_{\chi_k(\cdot)}\mathfrak{C}\left(\chi_k(\cdot),t\right)\ , & k\quad\text{susceptible at } t\\ 0, & k\quad\text{infected (or recovered) at } t.\end{cases} \quad (2.30)$$

This corresponds to the minimal cost that an agent has to pay between t and the end of the game (averaged over random realizations of the game, and assuming that all other players follow some given strategies $\bar{\chi}$). Note that in Eq. (2.28) we assumed that the total cost of infection is paid right after infection, so that individuals do not incur any additional cost at later times. The Markov process of the game is described by the following equations,

$$\begin{cases}\mathcal{P}\left[x_k(t+dt)=i|x_k(t)=s\right]=\lambda_k(t)dt\\ \mathcal{P}\left[x_k(t+dt)=s|x_k(t)=s\right]=1-\lambda_k(t)dt\\ \mathcal{P}\left[x_k(t+dt)=r|x_k(t)=i\right]=\xi\ dt\,.\end{cases} \quad (2.31)$$

We use the standard Bellman argument used in Eq. (2.3) to find the evolution of U. Assuming a status $x_k(t)=s$ at time t, it can be expressed as

$$U_k(t)=\min_{\chi(t)}\mathbb{E}_{x_k(t+dt)}\left[U_k(t+dt)+c(t,\chi_k(t))\right]\ , \quad (2.32)$$

which corresponds to Eq. (2.14), where the expectation is on the status of individual k at $t+dt$ and the current cost $c(t,\chi_k(t))$ corresponds to the integrant of Eq. (2.28). Two situations can occur at $t+dt$ according to the state of the agent k, $x_k(t+dt)$:

- if the agent remains susceptible, that is $x_k(t+dt)=s$, the only cost at t is $c(t,\chi_k(t))=f(\chi_k(t))dt$. Following Eq. (2.30), the quantity $U_k(t+dt)$ involves the average cost $\mathfrak{C}(\chi_k(\cdot),t+dt)$ and is non zero.
- if the agent becomes infected, $x_k(t+dt)=i$, individual k has to bear the cost due to infection in addition to the social cost which will be at first order in dt, and thus $c(t,\chi_k(t))=\mathfrak{r}_{\mathrm{I}}+O(dt)$. In this case, we simply have $U_k(t+dt)=0$ since there is no remaining cost.

Writing explicitly the expectation in Eq. (2.32) and using the probabilities given by Eqs. (2.31) we get

$$U_k(t)=\min_{\chi_k(t)}\left[(\mathfrak{r}_{\mathrm{I}}+O(dt))\lambda_k(t)dt+(1-\lambda_k(t)dt)\left(U_k(t+dt)+f(\chi_k(t))dt\right)\right]\ . \quad (2.33)$$

At first order in dt, this gives the Hamilton-Jacobi-Bellman (HJB) equation of our Mean-Field Game

$$-\frac{dU_k}{dt}=\min_{\chi_k(t)}\left[\lambda_k(t)\left(\mathfrak{r}_{\mathrm{I}}-U_k(t)\right)+f(\chi_k(t))\right]\ , \quad (2.34)$$

and the optimal strategy $\chi_k^*(t)$ at time t is given by

$$\chi_k^*(t) = \underset{\chi_k(t)}{\operatorname{argmin}} \left[\lambda_k(t)\left(\mathfrak{r}_\mathrm{I} - U_k(t)\right) + f(\chi_k(t))\right] \ . \tag{2.35}$$

By taking the particular form for f, Eq. (2.19), one can compute $\chi_k^*(t)$ by setting to zero the derivative of the right hand side of Eq. (2.35) with respect to χ_k, noting that U_k is independent of χ_k. Here, we get an explicit expression of χ_k^*,

$$\chi_k^*(t) = \left(\frac{1}{\chi_0}\left[\mathfrak{r}_\mathrm{I} - U_k(t)\right] I(t)\right)^{-\frac{1}{2}} \ , \tag{2.36}$$

which allows to transform Eq. (2.34) into an explicit equation in U_k which is simple to solve numerically. We now summarize the equations describing our system to solve them and get the Nash equilibrium of the game.

2.3.4 MFG system and Nash equilibrium

Let us first consider the (unconstrained) Nash equilibrium. We have seen that it is described by two sets of differential equations. The first one is the rate equation of the epidemic, Eq. (2.17) (also known as the Kolmogorov equation in this context), which is forward in time, that is, starting from initial conditions $S(0), I(0), R(0)$, populations at later time t are obtained by solving

$$\begin{aligned} \dot{S} &= -\rho\bar{\chi}(t) I(t) S(t) \\ \dot{I} &= \rho\bar{\chi}(t) I(t) S(t) - \xi I(t) \ , \\ \dot{R} &= \xi I(t) \end{aligned} \tag{2.37}$$

The second set of equations corresponds to the Hamilton-Jacobi-Bellman equation (2.34), with one reference individual k, we recall it here for consistency

$$-\frac{dU_k}{dt} = \min_{\chi(t)} \left[\lambda_k(t)\left(\mathfrak{r}_\mathrm{I} - U_k(t)\right) + f(\chi_k(t))\right] \ . \tag{2.38}$$

As only the terminal condition on U is fixed, namely, $U_k(T) = 0$, Eq. (2.38) is backward in time.

At equilibrium, all individuals will follow their own optimal strategy; but as all agents are symmetric, this optimal strategy should be comon for all agents k (who are susceptible at t). Thus we have the additional self-consistency condition

$$\chi_k^*(t) = \bar{\chi}(t) \ . \tag{2.39}$$

Equations (2.37)-(2.38)-(2.39) form the MFG system of the game. Equations (2.39) imposes that if all other agents follow the strategy solution of the MFG system, then deviating from that strategy implies a higher cost. This system of equations couples all epidemic rates $S(.), I(.), R(.)$ and strategy $\bar{\chi}$ via the individual optimal strategies χ_k^*. Indeed, the optimal strategy χ_k^* for a reference individual k is a solution of HJB equation (2.38) and is explicitly given by Eq. (2.36), which depends on the epidemic rate $I(.)$ and therefore on $\bar{\chi}$ through Eq. (2.37). In a mathematical perspective, the self consistent condition (2.39) is a fixed point of the function F: $\bar{\chi} \mapsto \chi_k^*$.

One obtains in this way an initial-terminal value problem (ITVP), which can be solved numerically in different ways; we present some of them in Chapter 6. The authors of [19] used a specific gradient descent on the cost Eq. (2.29) to obtain numerically the Nash equilibrium, but the use of Eq. (2.36) could be more efficient (see Sec. 6.1.1).

In Fig. 2.4, we provide a generic example of what we can obtain by solving the Nash equilibrium of this game (left figure for epidemics dynamics, and right figure for the evolution of $\chi^*(t)$ at the Nash equilibrium).

2.3.5 Societal optimum

In the previous scenario, each agent optimizes their own cost independently, focusing on self-interest. To gauge the impact of these egoistic strategies, it is useful to compare them with the societal optimum strategy introduced in Sec. 3.3.5 that could be enforced by a "benevolent global planner" such as a well-meaning government with complete authority. The goal here is to determine the optimal strategy χ^{SO} that minimizes the total cost for the entire society, defined by Eq. (2.5), averaging over individual costs. Thus, the societal optimum strategy is determined by

$$\chi^{\mathrm{SO}}(\cdot) = \underset{\bar{\chi}(\cdot)}{\operatorname{argmin}} \left[\mathfrak{C}\left(\bar{\chi}(\cdot), \bar{\chi}(\cdot), 0\right)\right] . \tag{2.40}$$

There is already an extensive literature on societal optimization in epidemic models (see, for example, [158, 159, 19, 160, 161, 162, 163, 164, 165, 166]), where the problem typically reduces to a global optimization task (there is no Nash equilibrium resolution here).

In Fig. 2.4, we illustrate an example of the societal optimum strategy for this game (right panel). Both strategies, $\chi^N(.)$ and $\chi^{\mathrm{SO}}(.)$, start and end at the baseline contact rate $\chi_0 = 0.2$. In both cases, efforts are concentrated around the epidemic peak, but the societal optimum involves more prolonged and intense efforts. This "optimal" strategy minimizes the average cost for society when everyone adheres to it. However, from an individual perspective, some agents could deviate and adopt a different strategy to lower their personal costs. Thus, this strategy is effective only in a cooperative context or when imposed by an authority, not in a Nash equilibrium context where individuals optimize selfishly.

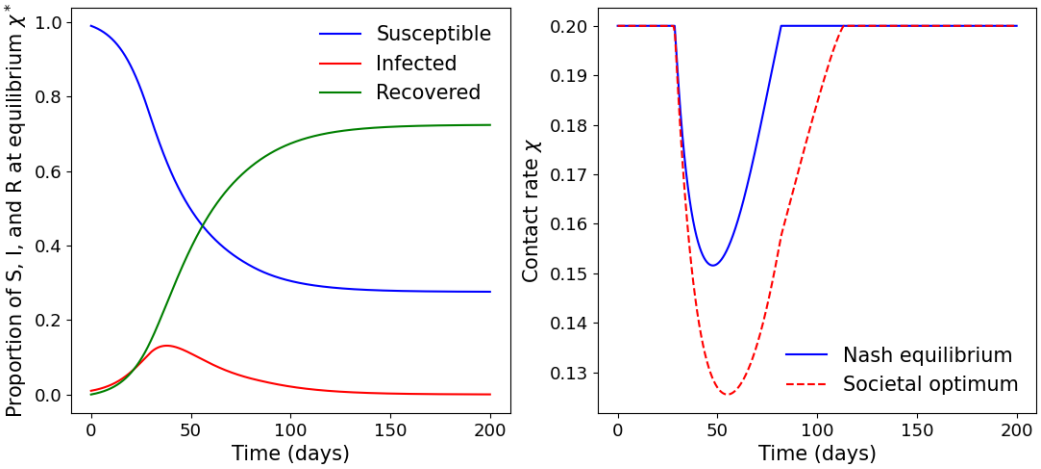

Figure 2.4: Left figure: epidemics dynamics of the MFG system at Nash equilibrium, for $\bar{\chi} = \chi^*$ solution of the system (2.37)-(2.38)-(2.39). Right figure: evolution of $\chi^N(t)$ (blue solid) compare to the evolution of $\chi^{\mathrm{SO}}(t)$ (red dotted). Figure adapted from [19], with the same set of parameters as the ones used by the authors in their numerical experiments.

2.3.6 Discussion about the cost

We briefly discuss here the choice of costs associated with infection and social contact reduction.

In principle, a more generalized infection cost could be considered in Eq. (2.28), which might take the form $\mathcal{I}(I(s))$, as the cost of infection is primarily influenced by the number of infected individuals in the population, particularly through its impact on healthcare capacity. Despite this, the assumption of a constant infection cost $\mathfrak{r}_{\mathrm{I}}$ is not overly restrictive. This cost encompasses various elements (such as symptoms, quarantines, and healthcare

expenses) that may differ among individuals. One could model $\mathfrak{r}_\mathrm{I}$ as a stochastic variable with a distribution $P_{\mathfrak{r}_\mathrm{I}}$, typically Gaussian, centered around a mean value $\langle \mathfrak{r}_\mathrm{I} \rangle$ with a standard deviation σ. However, from an individual's perspective, the focus would still be on the expected value of their cost, leading them to consider the average $\mathfrak{r}_\mathrm{I}$ since there is no inherent correlation with the infection time τ. One scenario where σ could become relevant is in the context of risk aversion, where an individual may react differently (and thus non-linearly) when faced with a high risk (e.g., risk of death) coupled with a low probability.

On the other hand, the cost associated with reducing social contacts can take various forms. The simple choice $f(\chi(t)) = \chi_0/\chi(t) - 1$ reveals several inherent properties of such a cost function:

- **Domain of Definition:** The function f is defined over the interval $[\chi_{\min}, \chi_0]$. To avoid any unrealistic divergence and reflect practical constraints, $\chi_{\min}$ represents the minimum contact rate necessary for individuals to sustain themselves during a strict lockdown.
- **Positivity:** The cost function f is always positive, $f(\chi) \geq 0$ for $\chi \in [\chi_{\min}, \chi_0]$, with $f(\chi_0) = 0$ indicating no incurred cost when no efforts are made to reduce contacts.
- **Monotonicity and Convexity:** The function f is decreasing within $[\chi_{\min}, \chi_0]$ and has a positive second derivative, meaning that as efforts to reduce contacts increase, the marginal cost associated with additional reductions also increases.

The chosen cost form is a simple model that satisfies these natural properties with minimal parameterization.

Determining the effective value of the cost parameters such as $\mathfrak{r}_\mathrm{I}$ and $\chi_{\min}$ and the realistic form of the cost function should be regarded as a whole research program. As discussed in Sec. 2.1.1, these costs often involve non-monetary factors, which must be compared on a common scale. Several approaches have been developed to address this, the most prominent being the QALY (Quality-Adjusted Life Year) and DALY (Disability-Adjusted Life Year) scales [167, 168].

The QALY scale, introduced in 1970 by Joseph S. Pliskin in his doctoral thesis, measures the sanitary impact of health conditions on both the quality and quantity of life lived. It assigns a utility value ranging from 0 (death) to 1 (perfect health) to reflect the impact of a specific health condition, such as an amputation, on an individual's quality of life. This utility is then integrated over the expected life years affected. For example, an amputation might yield a utility of 0.5; over 10 years of expected life, this would result in a QALY of 5, equivalent to 5 years in perfect health. QALY is commonly used to assess the benefits of medical interventions and to guide resource allocation. The potential QALY gain from a medical procedure is compared with its monetary cost to determine the intervention's overall value. The utility values for various health impacts are typically determined through surveys conducted with large populations.

The DALY scale, on the other hand, measures the overall burden of a disease. It combines the years lived with disability (YLD) and the years of life lost (YLL) due to premature death. The total impact of a disease is thus calculated by summing the premature deaths and the years affected by disability, using a weighting factor. This weight varies based on the severity of the disability and the individual's age. For example, individuals between 20 and 30 years old may be more significantly affected by a disability than people younger or older, as their "life potential" is higher at this age. Like QALY, DALY is frequently used

to optimize resource allocation in healthcare settings.

While these measures are well-established, they are insufficient for our purposes, as we seek to compare health-related costs with those arising from reductions of social contacts. In the work of Thunström *et al.* [169], the authors examine the impact of reduced social interactions on the GDP of the USA during the Covid-19 pandemic. This study provides a quantitative framework for comparing the costs of social distancing with the health-related costs of the epidemic, assigning a monetary value to each death. However, it overlooks other important factors, such as psychological costs, which can also be significant. The authors conclude that the restrictions imposed during the Covid-19 pandemic were appropriate when considering both health outcomes and the economic impact on GDP.

We will not discuss further these measures in this thesis, but we have to keep in mind that despite considerable progress in the field, a gap remains, particularly concerning the precise form of cost functions, which should be addressed to enable the practical application of MFG to real-world datasets.

2.4 Applications of MFG

In the previous section, we thoroughly explored the application of Mean-Field Games to epidemics through the modulation of the contact rate $\chi(t)$. However, MFG can be utilized in various other epidemic contexts as well. In Sec. 2.4.1, we outline some of the key applications found in the literature. Then, a crucial aspect to consider is determining the conditions under which Mean-Field Game modeling can accurately represent a real world situation. This discussion on practical applicability is presented in Sec. 2.4.2.

2.4.1 Other applications to epidemics

There are currently two main approaches to applying MFGs to epidemic modeling. For a recent and extensive review on the subject, readers can refer to [157]. The first approach corresponds to the one we have already explored, where $\chi(t)$ serves as the control parameter for individuals. This approach extends beyond the examples presented in this chapter, with several studies focusing on the analysis and design of Non-Pharmaceutical Interventions (NPIs) [20, 170, 155]. These studies differ based on the types of models they rely on and their interpretations and implementations of NPIs.

Another branch of the literature focuses on constructing Stackelberg games [171, 172]. This is a specific type of MFG in which a player, often referred to as the "principal", holds a central and non-negligible role. In the context of epidemics, the principal typically represents a central authority, such as a government, that can impose constraints on individuals to optimize a societal cost. The population, modeled as a mean-field, responds to these constraints by finding their optimal strategies. This interplay influences the principal's decisions, leading to an equilibrium that accounts for the responses of both individuals and the principal to the epidemic.

The second main application of MFGs in epidemic modeling focuses on vaccination behavior. Vaccination, when available, is a key strategy for limiting the spread of epidemics. While authorities may establish vaccination programs, these efforts sometimes fail due to concerns about cost, risk, inefficacy, or side effects of vaccines. As a result, individual perceptions and choices diverge from the authority's approach, with each person making their own vaccination decisions based on perceived risks and costs. These individual decisions, such as whether or not to get vaccinated, significantly impact epidemic dynamics, making the MFG paradigm a promising tool for studying this behavior. This emerging field of

research has been growing rapidly over the past decade, particularly in response to the recent Covid-19 crisis [152, 153, 173, 154].

2.4.2 Practical applications of MFG

Beyond the "technical" requirements such as the assumption of a large number of players and the notion that agents operate in a competitive environment where optimal strategies depend on the behaviors of others, Mean-Field Games typically rely on two fundamental assumptions: perfect information and the mathematical ability to compute the Nash equilibrium.

Taking the example of an MFG applied to the evacuation of a multi-level building by Djehiche and coworkers [174], the assumption of perfect information would require agents to know not only the building's geometry but also the density of other agents in various rooms and levels, much of which would be out of sight. Furthermore, even if this information were available to an agent, it is questionable whether the Nash equilibrium could be computed quickly enough to be useful in a stressful, real-time situation like an evacuation, given that such computations could be quite demanding even for modern computers.

This leads to the plausible concern that, in scenarios like building evacuations, agents might react intuitively based on limited information —- such as their approximate knowledge of the building's layout and whatever they can see -— resulting in behavior that deviates significantly from what an MFG description would predict. In the same way, it is hard to imagine that agents will be able to perform the computation of the Nash equilibrium in a context of epidemics.

At first glance, this analysis suggests that the applicability of MFGs might be extremely limited. However, the range of MFG applications might actually be broader than initially expected, mainly because the strict requirements of perfect knowledge and computability can, to some extent, be relaxed.

In our view, MFGs can be applied in at least the three different following configurations:

- **The pure case:** This is the ideal scenario where agents indeed have sufficient information and possess the operational or numerical capability to compute the Nash equilibrium. One can think to contexts such as energy consumption or financial market where anyone can access to the same global information and to computing capacities.

- **The learned case:** In this situation, agents can anticipate the behavior of others because they have encountered the situation frequently enough to have learned and internalized it, even if they do not perform explicit computations in real-time. This is for example the situation of pedestrian dynamics, or in biological and ecological contexts.

- **The case with a central planner:** Here, although agents may not have the capacity to compute or intuitively guess the Nash equilibrium, they can receive guidance or directives from a trusted central entity (like a government or an emergency management system) that does have the computational ability to determine the optimal strategies. In practical contexts such as global energy consumption, epidemics, or traffic management, it is conceivable that a trusted authority could directly provide a Nash equilibrium (through a specific mobile app for instance), which individuals would be incentived to follow if everyone else does the same. However, a natural question arises regarding the sensitivity of the Nash equilibrium to deviations by individuals who choose not to comply. If the equilibrium is too sensitive to such deviations, it could become ineffective in practice.

These configurations suggest that MFGs could be applicable in a wide array of real-world situations, even when the strict assumptions of perfect information and computational capacity are not fully met.

2.5 A view of epidemiological family

This section conclude this first part of the thesis, dedicated to the introduction of the different tools that will be used on the following, together with the bibliography and previous works that motivated our research. We summarize in Table 2.1 the main models we presented which are represented in the illustration on Fig. 2.5. On this figure, we make an overview of the different epidemiological families, and we indicate in red the different models that will be investigated during this thesis with their location inside the existing works.

N°	Model presented (reference)
M_1	SIR model, Kermack and McKendrick [175]
M_2	Reference compartmental model, Alex Arenas *et al.* [40]
M_3	Heterogeneous networks generation, Barabasi and Watts [67, 42]
M_4	Epidemics on complex networks for Covid-19, Josh A. Firth *et al.* [79]
M_5	Basic Agent-Based Model, Eubank *et al.* [36]
M_6	Agent-Based Model for Covid-19, Ferguson *et al.* [17]
M_7	Adapting transmission rate with $I(t)$, Vincenzo Capasso *et al.* [106]
M_8	Spontaneous behavioural changes, Poletti *et al.* [98]
M_9	A MFG approach to the SIR model, Elie *et al.* [19]
N°	Models studied in this thesis (reference)
M_1'	MFG Approach in a Social Structure model, Bremaud *et al.* [176, 177]
M_2'	MFG on networks [paper under preparation], Bremaud *et al.*
M_3'	Analytical solution of SIR on homogeneous networks, Bremaud *et al.* [178]

Table 2.1: Summary of the 9 main models presented through this introduction. Their associated location in the literature of epidemiological models is illustrated in Fig. 2.5 (black stars). The contributions of this thesis to the literature is summarized by the three works at the bottom of the table. Associated locations in the literature are indicated in Fig. 2.5 (red stars).

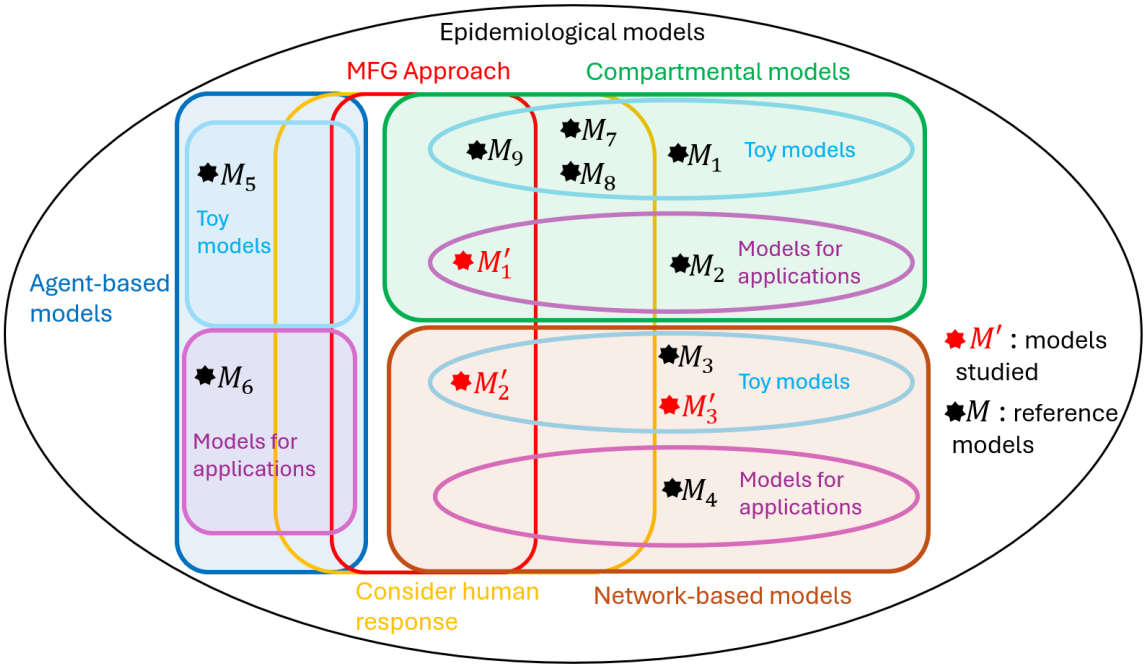

Figure 2.5: Illustration of epidemiological family which split in three categories: **Compartmental models** with a "top to bottom" approach (green box), **Agent-Based models** models with a "bottom to top" approach (blue box), without mean field approximations, and **Network-based models** which often rely on mean field approximations based on the degree of nodes (brown box). For each type of model, a differentiation is made between "Toy models" (blue ellipsis), which correspond to simple models for physicists who develop theoretical tools, while the "Models for applications" (purple ellipsis) are those that are built for practical use (with a more complex structure). Finally, our topic of research (Mean-Field Game approach, red box) is included inside the larger family of models which include theoretically the human response to epidemics (yellow box). Black (Resp. red) stars corresponds to models already present in the literature which have been presented in this thesis (Resp. models or results which have been developed in this thesis). See Table 2.1 for the correspondence between the model index and the associated reference.

3 - MFG Approach to Non-Pharmaceutical Interventions in a Social Structure model of Epidemics

In Section 2.3, we explored how the MFG framework can model individual behavior during epidemics by treating the contact rate $\chi(t)$ as an emergent outcome of the model. This approach developed by Elie *et al.* [19] represents a significant step forward, but its application to more complex models is necessary to be practically relevant. As discussed in Sec. 2.3, the basic SIR model is likely too simplistic to provide meaningful policy guidance.

In this chapter, we demonstrate how MFG models can incorporate a high level of complexity in modeling individuals' differentiated responses to an epidemic. Specifically, these models can account for the social structure within which the epidemic spreads. Moreover, we will illustrate how the MFG approach can address practical issues of significant relevance, such as determining optimal government strategies for the implementation of lockdowns. This aspect of our work aligns with the study of non-pharmaceutical interventions (NPI) strategies to mitigate epidemics through MFG approaches. This Chapter is associated to the works [176, 177] which can be accessed in App. C-D. Thus, some technical details specific to this model which are besides similar to earlier derivations, are not included here; interested readers can refer to App. D for a more comprehensive explanation.

In Sec. 3.1, we introduce the SIR model with an incorporated social structure, which serves as the foundation for our analysis. In Sec. 3.2, we apply the MFG framework to this model, presenting the individual optimization process and the system to solve numerically, to reach the Nash equilibrium of our game. In Sec. 3.3, we make a numerical experience with fictive but realistic data sets, to explore the possibilities of the model. We consider a modified Nash equilibrium under constraints (such as partial lockdowns) imposed by a central authority, and compare this outcome with the societal optimum for our system. In Sec. 3.4, we consider scenarios where the total population size N or the final time T of the epidemic dynamics are finite. We demonstrate that varying these parameters can lead to *first order phase transitions*, where optimal strategies present discontinuous changes, and we discuss the distinct characteristics of the resulting phases. Finally, concluding remarks and further discussion are provided in Sec. 3.5.

3.1 Social structure based modeling of epidemics dynamics

In this section, we begin by outlining the structure of the model, moving from a heterogeneous macroscopic description to a microscopic one in Sec. 3.1.1. Then, in Sec. 3.1.2, we introduce the various variables and parameters involved in our model. Although the model includes numerous parameters, only a subset requires fitting to specific epidemic data, and all are time-independent. Finally, in Sec. 3.1.3, we briefly present the time evolution equations governing the epidemic dynamics in our model.

3.1.1 Social structure and contact rates

We now introduce a SIR model with a social structure, in the spirit of [38]. In this model, rather than taking society as monolithic, we consider a refined description of social contacts. Namely, we introduce three age classes: young, adult and retired, and we assume that individuals have contacts with one another in four different settings: schools, households, community and workplaces; of course a larger number of age classes and settings could easily be implemented. The structure of the population is illustrated in Fig. 3.1. We

assume the total size of the population, N_{tot}, to be large.

In our model, following [38], interactions between individuals depend on two factors: the setting $\gamma \in \{\text{school, workplace, community, household}\}$ in which they meet, and their age class $\alpha \in \{\text{young, adult, retired}\}$. We denote by N_α^{tot} the total number of individuals in class α. We first consider the simple case of a single setting where interactions only depend on age class, which will be labeled by the Greek letters α or β; extension to the case of multiple settings is then straightforward.

A natural assumption, in the spirit of compartmental models, is that behaviour of indi-

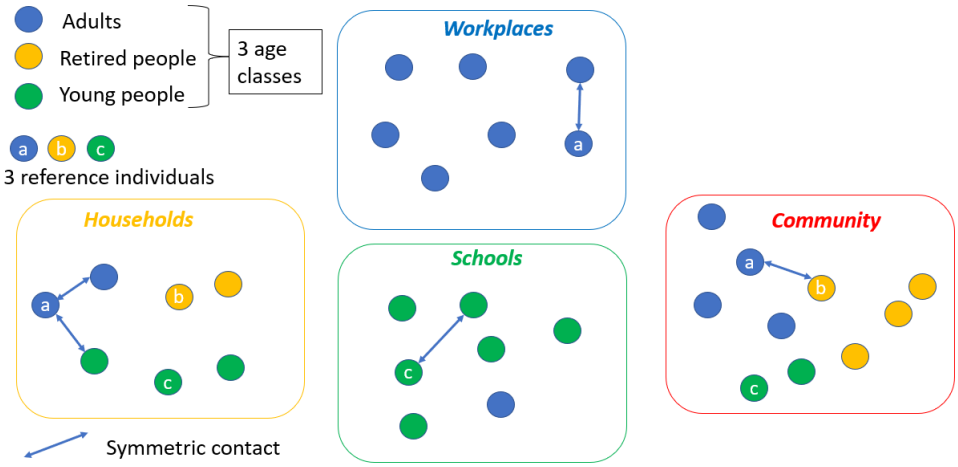

Figure 3.1: Graphical illustration of the social structure we implemented. A reference individual (a, b and c for each age class) will have (symmetric) contacts in each setting, with different type of individuals (more adults at workplaces, more children at school, etc). The precise structure of interactions is detailed in the following section.

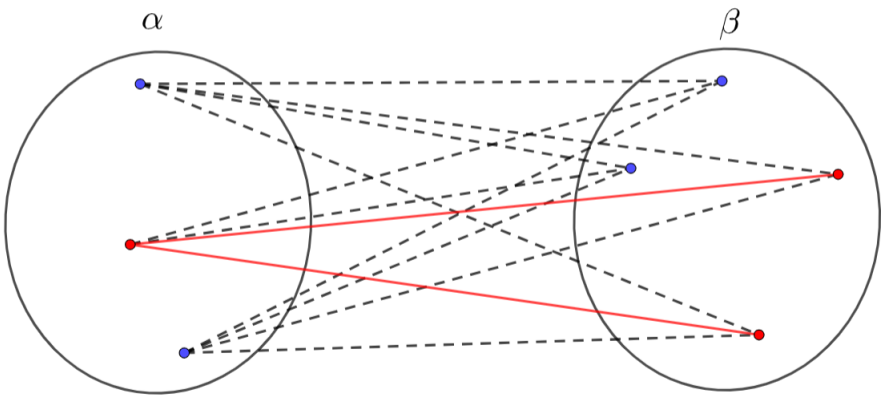

Figure 3.2: Graphical illustration of the interactions in our model. Two age classes α and β are represented, here with $N_\alpha^{\text{tot}} = 3$ individuals of age class α and $N_\beta^{\text{tot}} = 4$ of class β. Each vertex is either "active" (in red) if the corresponding individual is willing to have contact with the other class, or "inactive" (in blue). The $N_\alpha^{\text{tot}} N_\beta^{\text{tot}}$ possible contacts are represented in dashed black lines, and effective contacts between pairs of active individuals are red solid lines. Here we have $w_{\alpha\beta} N_\alpha^{\text{tot}} = 1$ active individual of age class α and $w_{\beta\alpha} N_\beta^{\text{tot}} = 2$ active individuals of age class β, which gives $w_{\alpha\beta} = \frac{1}{3}$ and $w_{\beta\alpha} = \frac{1}{2}$. The probability for a randomly chosen pair to be in contact is $\mathcal{W}_{\alpha\beta} = w_{\alpha\beta} w_{\beta\alpha} = \frac{1}{6}$. The average number of contacts with β for an individual $a \in \alpha$ is $\mathcal{W}_{\alpha\beta} N_\beta^{\text{tot}} = \frac{2}{3}$. Similarly, the average number of contacts with α for an individual $b \in \beta$ is $\mathcal{W}_{\beta\alpha} N_\alpha^{\text{tot}} = \frac{1}{2}$. The total number of contacts between the two classes, corresponding to the number of red links in the graph, is given by $N_\beta^{\text{tot}} N_\alpha^{\text{tot}} \mathcal{W}_{\beta\alpha} = 2$.

viduals toward different age classes is differentiated, but that a given age class is considered homogeneous from the point of view of an individual. That is, an individual $a \in \alpha$ can decide whether she chooses to encounter members of class β or not, but does not decide which individuals she may encounter in that class. In other words, any individual $a \in \alpha$ willing to meet someone from class β will possibly meet all individuals from class β who themselves are willing to meet individuals from class α. At each time, an individual $a \in \alpha$ can decide whether she is open or close to interactions from class β. Let us denote by $w_{\alpha\beta} \in [0,1]$ the fraction of individuals $a \in \alpha$ open to meet people from class β. The willingness $w_{\alpha\beta}$ thus indicates the probability of an individual a taken at random in α to be open to contacts with class β. There are $w_{\alpha\beta}N_\alpha^{\text{tot}}$ individuals $a \in \alpha$ willing to meet people with class β, and $w_{\beta\alpha}N_\beta^{\text{tot}}$ individuals $b \in \beta$ willing to meet people from class α. A contact becomes effective (i.e. occurs with probability dt in the interval $[t, t+dt[$) only if both individuals are willing, and therefore among all $N_\alpha^{\text{tot}}N_\beta^{\text{tot}}$ possible links between α and β, only $w_{\alpha\beta}N_\alpha^{\text{tot}} \times w_{\beta\alpha}N_\beta^{\text{tot}}dt$ are realized during dt. The number of pairs effectively realized can also be expressed as $\mathcal{W}_{\alpha\beta}N_\alpha^{\text{tot}}N_\beta^{\text{tot}}dt$, hence $\mathcal{W}_{\alpha\beta} = w_{\alpha\beta}w_{\beta\alpha}$ (and $\mathcal{W}_{\alpha\beta}$ is a symmetric array, as it should be). Figure 3.2 illustrates the interactions we have introduced here on a simple example.

In "normal times", that is in the absence of epidemic threats, the contact willingness of an individual of class α with class β is a constant $w_{\alpha\beta}^{(0)}$. During an epidemic, however, the agent will adapt her behavior to mitigate the risk of infection, and we assume the contact willingness to take the form

$$w_{\alpha\beta}(t) = n_\alpha(t)w_{\alpha\beta}^{(0)}\,, \tag{3.1}$$

that is, her initial willingness is modulated by a time-dependent coefficient $n_\alpha(t)$ which measures the effort made by agents in the class α to limit their contacts with others. For simplicity we suppose that this effort is independent of β, but a β dependence can easily be implemented to this model and only slightly changes the equations. We additionally assume that $n_\alpha(t) \in [n_{\min}^\alpha, 1]$, with $n_{\min}^\alpha$ the maximum effort that can be expected from an agent in class α. The upper bound 1 corresponds to the natural assumption that the epidemic situation can only reduce the initial willingness.

3.1.2 Asymptomatic individuals

Interactions between individuals may vary with time, but also differ between different age classes and in different settings. As a result, the dynamics of the epidemic will be different in each subcategory. This turns out to be particularly relevant for susceptible agents, and we will go back to this in more details in the next subsection. But the issue could be raised also for infected individuals whose behavior may range from a completely egoistic one, in which they stop limiting their contacts since they are not worried any more about being infected, to being completely altruistic and isolate themselves from the rest of population. To make things more concrete, we assume this latter option, but also assume that a fraction μ of the population is asymptomatic (they do not know if they are infected or not) and hence behave as susceptible, while the other fraction $1-\mu$ is symptomatic and stay home to protect others. This additional status (symptomatic or asymptomatic) is random in the population and is fixed at the beginning of the epidemic. Therefore, the epidemic is only spread by individuals who are both asymptomatic and infected. They represent a fraction $\mu I(t)$ of the population. We summarize our compartmental model in Fig. 3.3.

The parameters defining our SIR model with social structure can thus be divided in two groups. On the one hand we have three "biological" parameters: the probability ρ of transmission of the virus per effective contact between a susceptible and an infected individual, the fraction μ of the infected population which is asymptomatic, and the recovery

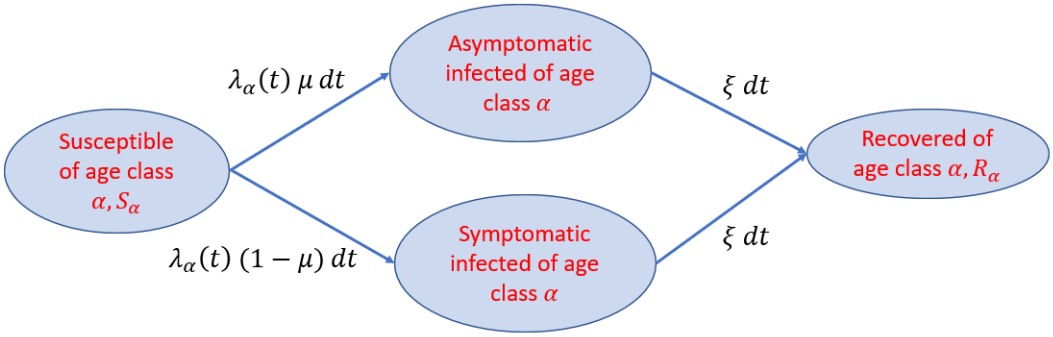

Figure 3.3: Graphical illustration of the particular SIR model we use. An individual infected at time t has a probability μ to be asymptomatic and $1-\mu$ to be symptomatic. The force of infection λ_α is derived in Sec. 3.1.3 and drives the probability of infection $\lambda_\alpha dt$. Then, all individuals have a constant recovery rate ξ to recover from the disease.

Parameter	Definition
ρ	Probability of transmission per contact
μ	Proportion of asymptomatic individuals in the population
ξ	Recovery rate
N_α^{tot}	Number of individuals of age class α
$\mathcal{W}_{\alpha\beta}^{\gamma\,(0)} = w_{\alpha\beta}^{\gamma\,(0)} w_{\beta\alpha}^{\gamma\,(0)}$	Willingness of contacts between two age classes α and β (symmetric in $\alpha \leftrightarrow \beta$) in the setting γ

Table 3.1: Biological parameters and parameters defining the structure of the society. The number of parameters implied by this list is significant, since in particular the array $\mathcal{W}_{\alpha\beta}^{\gamma\,(0)}$ has $3 \times 3 \times 4 = 36$ entries. However the methodology to get these parameters in any specific implementation is relatively well established (see e.g. discussion in App. A).

rate ξ. On the other hand the social structure is defined by the number of individuals N_α^{tot} in the age classe α and by the coefficients $\mathcal{W}_{\alpha\beta}^{\gamma\,(0)} \equiv w_{\alpha\beta}^{\gamma\,(0)} w_{\beta\alpha}^{\gamma\,(0)}$ determining the structure of our society, i.e. the contact rates in the absence of the epidemics. Table 3.1 summarises this information.

For a given epidemic in a given geographic location, determining the parameters of Table 3.1 follows a priori a well defined, though not necessarily straightforward, path, both for the "biologic parameters" (ρ, μ, ξ) typically encountered in traditional SIR-like models [40], but also for the ones associated with the social structure [37]. Much less straightforward is the determination of the time dependence of the "effort parameters" $n_\alpha(t)$ introduced in Eq. (3.1). For the rest of section 3.1, we assume these $n_\alpha(t)$ known, and we will discuss how their dynamics can be computed using the MFG approach in section 3.2.

3.1.3 Time evolution equations

We now derive the time evolution equations of the epidemic quantities for this model. The fraction of susceptible (resp. infected, recovered) individuals in class α is S_α (resp. I_α, R_α), with $S_\alpha + I_\alpha + R_\alpha = 1$. In order to establish the mean-field equations, we single out a reference individual $a \in \alpha$ who is susceptible at time t and has status $x_a(t) = s, i$ or r at subsequent times. We furthermore here lift the hypothesis that all individuals of a given age class behave in exactly the same way, and assume that the reference individual has her own time-dependent strategy $n_a(t)$ and willingness $w_{a\beta}(t) = n_a(t) w^{(0)}_{\alpha\beta}$, with however the understanding that, n_α is the average over susceptible individuals of n_a, which we express as

$$n_\alpha = \frac{1}{S_\alpha N_{\rm tot}} \sum_a n_a \delta_{x_a,s} \ . \tag{3.2}$$

Let $b \in \beta$ be an individual of class β, whose willingness to meet class α is $w_{b\alpha}(t) = n_b(t) w^{(0)}_{\beta\alpha}$. In order for a to be contaminated by b during $[t, t+dt[$, b must be infected *and* asymptomatic, and a and b must meet; contamination then occurs with probability ρ. Distinguishing within the i ="infected" status between i_a ="asymptomatic infected" and i_s ="symptomatic infected", the probability that a become infected by b during $[t, t+dt[$ is therefore

$$P_{ab}(t)dt = \rho n_a(t) n_b(t) \mathcal{W}^{(0)}_{\alpha\beta} \delta_{x_b(t),i_a} dt \ \ , \tag{3.3}$$

where we used the fact that $w^{(0)}_{\alpha\beta} w^{(0)}_{\beta\alpha} = \mathcal{W}^{(0)}_{\alpha\beta}$ (see Table 3.1). Taking the sum over all $b \in \beta$ and all age classes β we get the total probability that an individual a susceptible at time t is infected between t and $t + dt$

$$P_a(t)dt := \mathcal{P}\left[x_a(t+dt) = i \,|\, x_a(t) = s\right] = \sum_\beta \sum_{b\in\beta} P_{ab}(t)dt \ . \tag{3.4}$$

We then follow the same reasoning as in the SIR case (see Eq. (1.4)). Averaging over all individuals $a \in \alpha$ and over realizations of the Markov process, and summing over age classes β, we obtain

$$\frac{dS_\alpha(t)}{dt} = -\rho \sum_\beta \mathcal{W}^{(0)}_{\alpha\beta} \Big(\frac{1}{N^{\rm tot}_\alpha} \sum_{a=1}^{N^{\rm tot}_\alpha} n_a(t) \delta_{x_a(t),s} \Big) \Big(\sum_{b=1}^{N^{\rm tot}_\beta} n_b(t) \mu \delta_{x_b(t),i} \Big) \tag{3.5}$$

$$= -\rho \sum_\beta \mathcal{W}^{(0)}_{\alpha\beta} \left(S_\alpha n_\alpha\right) \left(\mu N^{\rm tot}_\beta I_\beta n_\beta\right) \ . \tag{3.6}$$

To get this last expression, Eq. (3.2) was used, together with the assumption that asymptomatic infected individuals responsible for epidemic spreading behave on average in the same way as susceptible individuals, so that we have also for all age classes

$$n_\beta(t) = \frac{1}{\mu I_\beta N^{\rm tot}_\beta} \sum_{b\in\beta} n_b(t) \delta_{x_b(t),i} \ . \tag{3.7}$$

It should be borne in mind that this approximation would not be valid if a group of agents have higher contact willingness on the whole duration of the epidemic compared to the others.

Equation (3.5) then becomes

$$\frac{dS_\alpha}{dt} = -\lambda_\alpha(t) S_\alpha(t) \,, \qquad \lambda_\alpha(t) \equiv \mu\rho n_\alpha(t) \sum_\beta n_\beta(t) \mathcal{W}^{(0)}_{\alpha\beta} \ N^{\rm tot}_\beta I_\beta(t) \,. \tag{3.8}$$

This equation generalizes in a straightforward way when we include different settings γ in the model. In that case we have

$$\lambda_\alpha(t) \equiv \mu\rho \sum_{\beta=1}^{n_{\rm cl}} N^{\rm tot}_\beta \sum_{\gamma=1}^{n_{\rm set}} n^\gamma_\alpha(t) n^\gamma_\beta(t) \mathcal{W}^{\gamma(0)}_{\alpha\beta} I_\beta(t) \ \ , \tag{3.9}$$

with n_{cl} and n_{set} the number of age classes and settings respectively. Equation (3.8) is the analog of the SIR Eq. (1.6) but in the case of a population with social structure. The two other equations analogous to the system (1.7) are derived in the same way. The system of coupled differential equations for the SIR model with social structure finally reads

$$\begin{aligned} \dot{S}_\alpha &= -\lambda_\alpha(t) S_\alpha(t) \\ \dot{I}_\alpha &= \lambda_\alpha(t) S_\alpha(t) - \xi I_\alpha(t) \\ \dot{R}_\alpha &= \xi\ I_\alpha(t)\,. \end{aligned} \tag{3.10}$$

These equations are the main equations of our SIR model with a social structure, they naturally lead to the averaged epidemic quantities $S(t) \equiv \frac{1}{N_{\text{tot}}} \sum_\alpha N_\alpha^{\text{tot}} S_\alpha(t)$, and respectively for I and R. Once the "interaction strategies" $n_\alpha^\gamma(.)$ are fixed for each age class α and each setting γ, one can solve Eq. (3.10) and obtain the dynamic of the relative proportion of susceptible, infected and recovered in each class. However, for rational agents interaction strategies should depend on the evolution of the epidemic. To address this interplay, we need the machinery of mean-field games, which we now introduce.

3.2 Mean-field game approach

Let's take the individual point of view. In our model, an individual a can choose at each time the value of her own control parameter $n_a^\gamma(t)$, which reflects her desire to have contact with someone in each setting γ. In practice, each agent will adjust her control parameter $n_a^\gamma(t)$ to minimize her foreseeable cost over the epidemic time interval. Hence, $n_a^\gamma(t)$ corresponds to $\chi_k(t)$ of Sec. 2.3, while the global strategy $\bar{\chi}(t)$ will be denoted $n_\alpha^\gamma(t)$ here (one strategy for each age class in each setting). We already derived the Kolmogorov equation of our game Eq. (3.10); we now derive in this section the optimization made by the agents, following in the spirit the work of Elie *et al.* in [19]. Here also, detailed of the computation can be found in App. D.III. We begin with individual optimization in Sec. 3.2.1 with the cost function, before obtaining the Hamilton-Jacobi-Bellman equation in Sec. 3.2.2 and finally describing the Nash equilibrium of our game in Sec. 3.2.3.

3.2.1 Calculation of the expected cost $\mathfrak{C}_a$

We assume here $\mu \ll 1$. As shown in App. D.C, considering a finite μ makes notations slightly heavier without changing qualitatively the dynamics of the epidemics. Therefore in the following sections we shall restrict ourselves to the regime $\mu \ll 1$.

Consider a fixed individual $a \in \alpha$. Individual a can be in one of the three states $s_\alpha, i_\alpha, r_\alpha$, depending of her age class α and on whether she is susceptible, infected or recovered. We denote by $x_a(t)$ the state of a at time t. We do not make a distinction between susceptible and asymptomatic individuals as far as the calculation of the cost function is concerned, since agents know their infected status only when they are infected and symptomatic.

Individual a makes the assumption that all individuals in each age class β will follow the same strategy $n_\beta^\gamma(t)$. If a has no symptoms at time t, she estimates the averaged cost that the epidemic will incur as the sum of two terms: one which is due to the social cost of efforts to avoid infection, denoted f_α and one due to the cost of infection if it happens, denoted $\mathcal{I}_\alpha$. This cost depends on the strategies that a will follow in each of the settings γ. Following the same reasoning as the one in Sec. 2.3.2, we get

$$\mathfrak{C}_a\left(n_a^\gamma(\cdot), \{n_\beta^\gamma(.)\}, t\right) = \int_t^T \left[\lambda_a(s)\ \mathcal{I}_\alpha(I(s)) + f_\alpha\left(n_a^\gamma(s)\right)\right](1 - \phi_a(s))ds\,. \tag{3.11}$$

Here also, we will often use $\mathfrak{C}_a\left(n_a^\gamma, t\right)$ for simplicity, but the cost still depends implicitly on all the $n_\beta^\gamma(\cdot)$. The choice of cost dependencies is discuss in Sec. 3.3.1. Note that the notation $n_a^\gamma(\cdot)$ actually means $(n_a^1(\cdot), ..., n_a^{\mathrm{n_{set}}}(\cdot))$, as quantities involving $n_a^\gamma(\cdot)$ will never depend on a specific γ. Thus, the cost (3.11) is independent of γ.

3.2.2 Hamilton-Jacobi-Bellman equation

The expected cost at time t for agent a is a function of her own strategy n_a and of the epidemic functions $S(.), I(.), R(.)$. The next step is to solve the optimization problem, that is, find the optimal strategy n_a^* for a given epidemic $S(.), I(.), R(.)$. Following the approach that we have already derived in Sec. 2.3.3, we get the Hamilton-Jacobi-Bellman (HJB) equation of our Mean-Field Game

$$-\frac{dU_a(t)}{dt} = \min_{n_a^\gamma(t)} \left[\lambda_a(t)\left(\mathcal{I}_\alpha(I(t)) - U_a(t)\right) + f_\alpha(n_a^\gamma(t))\right] , \tag{3.12}$$

and the optimal strategy $n_\alpha^{\gamma *}(t)$ at time t is given by

$$n_a^{\gamma *}(t) = \operatorname*{argmin}_{n_a^\gamma(t)} \left[\lambda_a(t)\left(\mathcal{I}_\alpha(I(t)) - U_a(t)\right) + f_\alpha(n_a^\gamma(t))\right] , \tag{3.13}$$

with

$$\lambda_a(t) \equiv \mu\rho \sum_{\beta=1}^{n_{\mathrm{cl}}} N_\beta^{\mathrm{tot}} \sum_{\gamma=1}^{n_{\mathrm{set}}} n_a^\gamma(t) n_\beta^\gamma(t) \mathcal{W}_{\alpha\beta}^{\gamma(0)} I_\beta(t) \tag{3.14}$$

In Eq. (3.13), the minimization is on the vector $n_a^\gamma(t)$ as the term to minimize depends on all settings γ (see for instance Eq. (3.14)). However, thanks to the form of f_α we will choose, this minimization will be decoupled for each setting of our model, making the analytical and numerical computations much easier.

3.2.3 Nash equilibrium system

Let us first consider the (unconstrained) Nash equilibrium. We have seen that it is described by two sets of differential equations. The first one is the rate equation of the epidemic, Eq. (3.10) (or Kolmogorov equation), which is forward in time, with starting from initial conditions $S_\alpha(0), I_\alpha(0), R_\alpha(0)$. The second set of equations corresponds to the Hamilton-Jacobi-Bellman equation Eq. (3.12), with one reference individual a for each age class α and the terminal condition on U fixed, namely, $U_a(T) = 0$, Eq. (3.12) is backward in time. At equilibrium, as in the SIR Nash equilibrium presented in Sec. 2.3.4, all individuals will follow their own optimal strategy; but as all agents in a given age class are equivalent, this optimal strategy should be the same for all agents a of age class α. Thus we have the additional self-consistency condition

$$n_a^{\gamma *}(t) = n_\alpha^\gamma(t) . \tag{3.15}$$

This equation imposes that if all other agents follow the strategy solution of the self-consistent system Eqs. (3.10)-(3.12)-(3.15), deviating from that strategy implies a higher cost. The solution of the MFG equations thus corresponds to a Nash equilibrium.

3.3 Numerical experiment

Before we dive into a detailed analysis of the kind of behavior that may emerge within our MFG model, let us summarize briefly the content of the two previous sections. We have first introduced in section 3.1 a SIR model with social structure in which we distinguish three age classes $\alpha \in \{\text{young}, \text{adult}, \text{retired}\}$ and different settings

$\gamma \in \{\text{schools}, \text{household}, \text{communities}, \text{workplace}\}$. In addition to the time dependent variables $n_\alpha^\gamma(t) \in [\mathfrak{n}_{\min}^\gamma, 1]$ corresponding to the effort made by individuals in the setting γ to avoid infection, the model is characterized by three "biological parameters" (the probability ρ of transmission of the disease per contact, the proportion μ of asymptotic individuals in the infected population, and the recover rate ξ), and a set of "social structure parameters" (the number of individuals N_α^{tot} in each age class, and the array $\mathcal{W}_{\alpha\beta}^{\gamma\,(0)}$ specifying the contact rate of the agents in the absence of epidemics); cf Table 3.2.

One remark is in order here. The N_α^{tot} and (the inverse of) $\mathcal{W}_{\alpha\beta}^{\gamma\,(0)}$ are *extensive* quantities: as $N_{\text{tot}} \to \infty$, so does the N_α^{tot}, and the $\mathcal{W}_{\alpha\beta}^{\gamma\,(0)}$ have to go to zero to maintain a finite rate of infection for a given individual. While the formal developments of sections 3.1 and 3.2 were better performed using theses variables, we shall from now on use related *intensive* parameters, which are well-defined in the limit $N_{\text{tot}} \to \infty$ and easier to relate to observable data. We thus introduce $\mathcal{N}_\alpha = N_\alpha^{\text{tot}}/N_{\text{tot}}$, the proportion of agents in age class α, and the array

$$\mathcal{M}_{\alpha\beta}^{\gamma\,(0)} \equiv \mathcal{W}_{\alpha\beta}^{\gamma\,(0)} N_\beta^{\text{tot}}, \tag{3.16}$$

which corresponds to the average number of contacts with β for an individual $a \in \alpha$. The requirement that $\mathcal{W}_{\alpha,\beta}^{\gamma,0}$ is a symmetric matrix implies the constraint $\mathcal{N}_\alpha \mathcal{M}_{\alpha\beta}^{\gamma\,(0)} = \mathcal{N}_\beta \mathcal{M}_{\beta\alpha}^{\gamma\,(0)}$, for all age class pairs (α, β) and all settings γ. We can rewrite the previous equations in terms of these parameters. In particular, $\lambda_\alpha(t)$ become independent of N:

$$\lambda_\alpha(t) \equiv \mu\rho \sum_{\beta=1}^{n_{\text{cl}}} \sum_{\gamma=1}^{n_{\text{set}}} n_\alpha^\gamma(t) n_\beta^\gamma(t) \mathcal{M}_{\alpha\beta}^{\gamma\,(0)} I_\beta(t)\ . \tag{3.17}$$

The theoretical framework of our model is now well established. We will now realize a numerical experiment to explore the full range of its possibilities. In particular, we will examine how our framework can help identify the appropriate types of constraints on individuals to close the gap between societal optimum and Nash equilibrium costs, noting that some constraints may be entirely ineffective. The choice of cost function and parameter values, as detailed in Sec. 3.3.1, are designed to be realistic, meaning that this type of analysis could be applied to actual datasets. However, these choices do not correspond to specific real datasets with precisely fitted parameters, as such work requires specialized tools and data to be conducted reliably and is beyond the scope of this study. We begin with an overview of the epidemic dynamics resulting from the different strategies studied here in Sec. 3.3.2. Subsequently, we describe the different strategies, beginning by the Nash equilibrium in Sec. 3.3.3. It is followed by the Nash equilibrium under constraints in Sec. 3.3.4 and the societal optimum in Sec. 3.3.5. Finally, we compare the costs and the corresponding individual behavior of these different strategies in Sec. 3.3.6.

3.3.1 Cost function and choice of parameters

We turn now to the specific choice of parameters we will use in most of the following to illustrate the properties and operational properties of our MFG model. In practice we need essentially to make a choice, on the one hand for the "social structure" and "biological" parameters of Table 3.1 (or their rescaled version introduced), and on the other hand for the functions $\mathcal{I}_\alpha(I)$ and the $f_\alpha(n_a^\gamma)$ of the cost (3.11), and the associated "cost-function" parameters.

For the former set of parameters, there is a fairly large scientific literature devoted to their evaluation from field data in specific, real-world situations. However, our goal is not to model a particular instance of epidemic dynamics, but rather to illustrate the kinds of questions that can be addressed and the kinds of behaviors that can typically be obtained within our formalism. We have therefore chosen parameter values that we

$\mathcal{M}^S$	$\mathcal{M}^W$	$\mathcal{M}^C$	$\mathcal{M}^H$
$\begin{pmatrix} 100 & 0 & 0 \\ 0 & 0 & 0 \\ 0 & 0 & 0 \end{pmatrix}$	$\begin{pmatrix} 0 & 0 & 0 \\ 0 & 75 & 0 \\ 0 & 0 & 0 \end{pmatrix}$	$\begin{pmatrix} 12.5 & 25 & 12.5 \\ 12.5 & 25 & 12.5 \\ 12.5 & 25 & 12.5 \end{pmatrix}$	$\begin{pmatrix} 15 & 25 & 10 \\ 12.5 & 32.5 & 5 \\ 10 & 10 & 30 \end{pmatrix}$
$\mathcal{N}_\alpha \equiv N_\alpha^{\text{tot}}/N_{\text{tot}}$	$I_\alpha(0)$	(ξ, ρ, μ)	
$(0.25, 0.5, 0.25)$	$(0.01, 0.01, 0.01)$	$(1.2, 0.1, 0.2)$	

Table 3.2: "Social structure" and "biological" parameters used in our simulations. The matrix entries $\mathcal{M}_{\alpha\beta}^{\gamma\,(0)}$ correspond to the average frequency of contacts (per week) between an individual of age class α and someone of age class β in the setting γ. $\mathcal{N}_\alpha = N_\alpha^{\text{tot}}/N_{\text{tot}}$ is the proportion of the population in each age class. $I_\alpha(0)$ are the initial proportion of infected for each age class (we always assume $R_\alpha(0) = 0$). ξ is the recovery rate (per week), ρ the transmission rate per contact, and μ corresponds to the proportion of asymptomatic individuals in the population. Finally, $\alpha = 1, 2, 3$ for age class of young, adults and retired individuals, respectively. The way these parameters have been chosen is discussed in details in App. A.

consider "generic", relying on a number of studies [40, 179, 38, 180, 181, 182] that analyze real epidemiological datasets. This approach makes it possible to evaluate the performance of the model under conditions that closely reflect practical scenarios, and allows us to expect that our model will produce comparable results in realistic applications. The exact way the "social structure" and "biological" parameters were chosen is detailed in App. A, and their values is summarized in Table 3.2.

Turning now to the cost (3.11), we take, for the cost of infection

$$\mathcal{I}_\alpha(I(t)) = \mathfrak{r}_{\text{I},\alpha} \exp\left[\mathfrak{q}_{\text{sat}} \frac{I(t) - \mathfrak{I}_{\text{sat}}}{\mathfrak{I}_{\text{sat}}}\right] . \tag{3.18}$$

This function includes the effect of a possible saturation of health services, and we assume an exponential increase of the strain on human and material resources as the saturation threshold $\mathfrak{I}_{\text{sat}}$ is approached, with a slope $\mathfrak{q}_{\text{sat}}$ corresponding to the impact of saturation on the cost. As $I \ll \mathfrak{I}_{\text{sat}}$, or $\mathfrak{q}_{\text{sat}} \to 0$, $\mathcal{I}_\alpha$ approaches an age-class dependent constant $\mathfrak{r}_{\text{I},\alpha}$ which implements the possibility that retired individual might be put significantly more at risk by the infection that younger ones. In practice we shall write these constants as $\mathfrak{r}_{\text{I},\alpha} = \mathfrak{r}_{\text{I}}\kappa_\alpha$, and keep the age-class dependent part κ_α fixed for all our simulations, while in some instance exploring the changes due to the variations of $\mathfrak{r}_{\text{I}}$.

Turning now to $f_\alpha(n_a^\gamma)$, the cost of modifying social contacts, we choose to follow the same form as Turinici et al. in [19], namely

$$f_\alpha(n_a^\gamma(t)) = \sum_\gamma \left(n_a^\gamma(t)^{-\mathfrak{m}_\gamma} - 1\right) , \tag{3.19}$$

where $\mathfrak{m}_\gamma$ models the degree of "attachment" to the setting γ: for example it is usually easier to reduce contacts at work than inside families. Moreover, f is decreasing with a positive second derivative, meaning that the more one decreases once social contacts, the higher the price to pay.

The set of values chosen in this section for the parameters characterizing the functions $\mathcal{I}_\alpha(I)$ and $f_\alpha(n_a^\gamma)$ is summarized in Table 3.3. Finally the parameter T denotes the time at which agents end their optimization process. This corresponds for instance to the time where herd immunity is reached, or it can depend on other circumstances such as the expected production of a vaccine, the seasonality of the virus, among others. In Sec. 3.3, our simulations are performed on a duration of $T = 40$ weeks to focus on scenarios where

$(\mathfrak{I}_{\rm sat}, \mathfrak{q}_{\rm sat})$	κ_α	$\mathfrak{m}_\gamma$	$\mathfrak{n}^\gamma_{\rm min}$	$(\mathfrak{I}_{\rm d}, \mathfrak{I}_{\rm l}, \mathfrak{s})$	T
(0.1, 0.1)	(1,10,100)	(2,2,1,3)	$\left(\frac{1}{3}, \frac{1}{5}, \frac{1}{5}, \frac{1}{2}\right)$	$(0.12, 4.10^{-4}, 0.35)$	40

Table 3.3: "Cost-function" parameters associated with the function Eq. (3.11) chosen for our simulations. The cost of infection $\mathcal{I}_\alpha$ Eq. (3.18) is characterized on the one hand by its value under "normal circumstances" $\mathfrak{r}_{{\rm I},\alpha} = \mathfrak{r}_{\rm I}\kappa_\alpha$, where we distinguish a common coefficient $\mathfrak{r}_{\rm I}$ that will take different values depending on the simulation, and an age-dependent part κ_α, which we will keep fixed at the value given in this table. On the other hand, $\mathfrak{I}_{\rm sat}$ characterizes the fraction of infected individuals at which the sanitary system starts to malfunction, and $\mathfrak{q}_{\rm sat}$ the speed at which this malfunction sets in. The cost of reducing once social contact is then parameterized by $\mathfrak{n}^\gamma_{\rm min}$, the minimum contact willingness in each setting γ, and $\mathfrak{m}_\gamma$, which weights the cost of contact reduction in each setting. $\mathfrak{I}_{\rm d}, \mathfrak{I}_{\rm l}$ are the thresholds for the best lockdown and $\mathfrak{s}$ its intensity level. T (in weeks) represents the total duration of the optimization, which in this section is consistently much longer than the characteristic timescale of the epidemic.

collective immunity is reached and to avoid short end-time effects. Scenarios for which, due to short end-time, collective immunity is not reached at the end of the optimization period will be studied more specifically in Sec. 3.4. Since the main wave of the epidemic appears in the first 10 weeks, we often present the results on a duration of 15 weeks.

3.3.2 Epidemic dynamics

Solving the MFG equations (3.10)-(3.12)-(3.15) for the set of parameters defined in Tables 3.2-3.3 above yields the dynamics of S, I and R. Technical detail about the numerical implementation is given in Sec. 6.2.2. The corresponding curves are displayed at the second line of Fig. 3.4.

The characteristic features of the Nash equilibrium are better revealed if one compares the corresponding epidemic dynamics with other scenarios. We shall consider the following options, which will be discussed in greater detail in the following subsections. We shall refer to the Nash equilibrium presented in Sec. 3.3.3 as the *unconstrained Nash equilibrium*. By contrast, the second scenario (see Sec. 3.3.4) is a *constrained Nash equilibrium*, where individuals have to deal with global constraints imposed by an authority, for instance a temporary lockdown which limits the agent's strategy freedom, which translates into bounds on n_a. This second scenario divides into two subscenarios, depending on whether these constraints are naive or optimally chosen. A third scenario, discussed in Sec. 3.3.5, is the one of *the societal optimum*, which is the idealistic case where everybody strives to optimize the global cost and chooses their strategy n_a accordingly. We call the "null" scenario *business as usual*: the agents do not adapt their behavior to the epidemics, so that no modification of the contact parameter is done, namely, n_a is fixed to 1.

Solving the MFG equations in these different contexts leads to different dynamics for S, I and R. The dynamics for each of the above scenarios is summarized in Fig. 3.4; the precise description of the scenarios is the object of the following subsections. As Fig. 3.4 shows, there are notable similarities between the different "optimized" scenarios (Nash, constrained Nash and societal optimum) and the business as usual one. For instance, the number of susceptible individuals at the end of the epidemic is $S_\infty \simeq 0.4$ in all cases but for the business as usual scenario, where it is significantly below (first row). This is due to the fact that in all circumstances one needs to reach herd immunity to escape from the disease, and the fact that S_∞ is much below this required value is a clear indication of the

business as usual sub-optimal character. In the same way, for all optimized scenarios there is a significant difference between the height of the infection wave for the different age class, as retired individuals and adults are more impacted by the disease than the youths, and therefore protect themselves. In the business as usual scenario the difference is much less significant, and only due to the relative proportion of contacts in each age class. On the other hand, the constrained Nash equilibrium with "naive" constraints differs from all the others because of the existence of two epidemic waves, which can be understood as originating from an excessive limitation of contacts that prevents the society from reaching herd immunity. Other differences, which are mainly quantitative, also exist between these different scenarios, and will be discussed in more details in section 3.3.6. We now turn to the detailed description of each scenario.

3.3.3 The (unconstrained) Nash equilibrium

Let us first consider the (unconstrained) Nash equilibrium. The two equations (3.10) and (3.12), together with the self consistency condition Eq. (3.15), form a system of equations coupling all epidemic rates $S(.)$, $I(.), R(.)$ and all age-class strategies n_α^γ via the individual optimal strategies $n_a^{\gamma *}$. With the precise form of the costs $\mathcal{I}_\alpha(I(s))$ and $f_\alpha(n_a^\gamma(t))$ chosen in Sec. 3.3.1, $n_a^{\gamma *}$ can be computed explicitly and reads

$$n_a^{\gamma *}(t) = \left(\frac{\mu\rho}{\mathfrak{m}_\gamma} \left[\mathcal{I}_\alpha(I(t)) - U_a(t) \right] \sum_{\beta=1}^{n_{\mathrm{cl}}} n_\beta^\gamma(t) \mathcal{M}_{\alpha\beta}^{\gamma\,(0)} I_\beta(t) \right)^{-\frac{1}{\mathfrak{m}_\gamma + 1}} , \tag{3.20}$$

which depends on the global strategies $n_\beta^\gamma(.)$ explicitly, and implicitly through the epidemic rate $I(.)$. One obtains in this way an initial-terminal value problem (ITVP).

The solutions of the MFG system are displayed in the second row of Fig. 3.4 for the set of epidemics quantities $S_\alpha(.), I_\alpha(.), R_\alpha(.)$, and in Fig. 3.5 for the set of optimal strategies $n_\alpha^\gamma(.)$. For our choice of parameters, young individuals do not modify at all their behaviour, when retired people reach maximal effort for significant amount of time in both community and household settings, and adults do some efforts, but without ever reaching the maximum one.

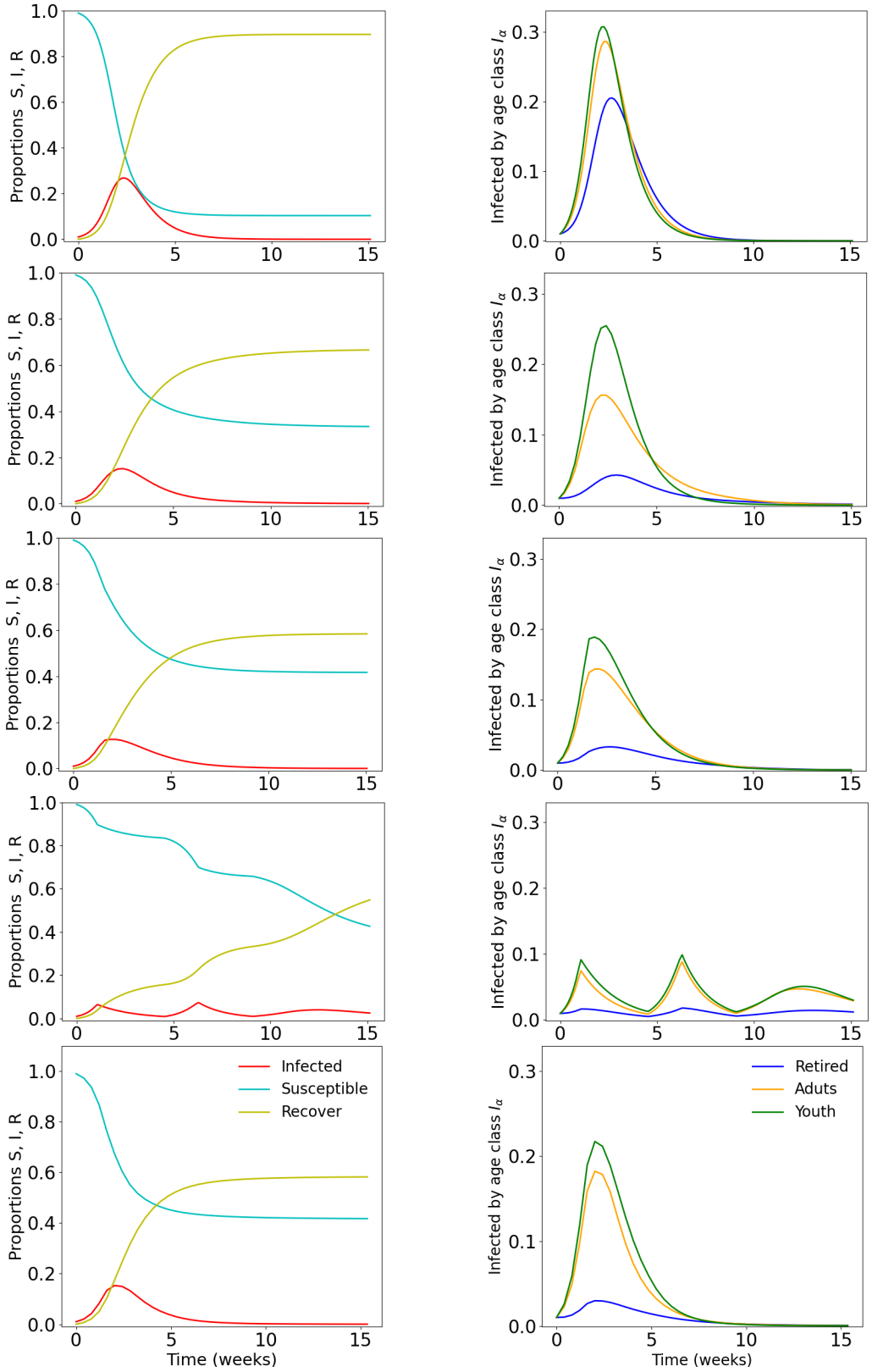

Figure 3.4: Time evolution of the epidemic quantities with $\mathfrak{r}_\mathrm{I} = 1$ and parameters of Tables 3.2-3.3. From top to bottom: Business as usual (no efforts), (unconstrained) Nash equilibrium, Nash equilibrium under optimal constraints, Nash equilibrium with naive constraints, societal optimum. Left: time evolution of the proportion of susceptible S (cyan), infected I (red) and recovered R (yellow) in the population. Right: time evolution of the proportion of infected in each age class I_α, retired people are in blue, adults in orange and youth in green.

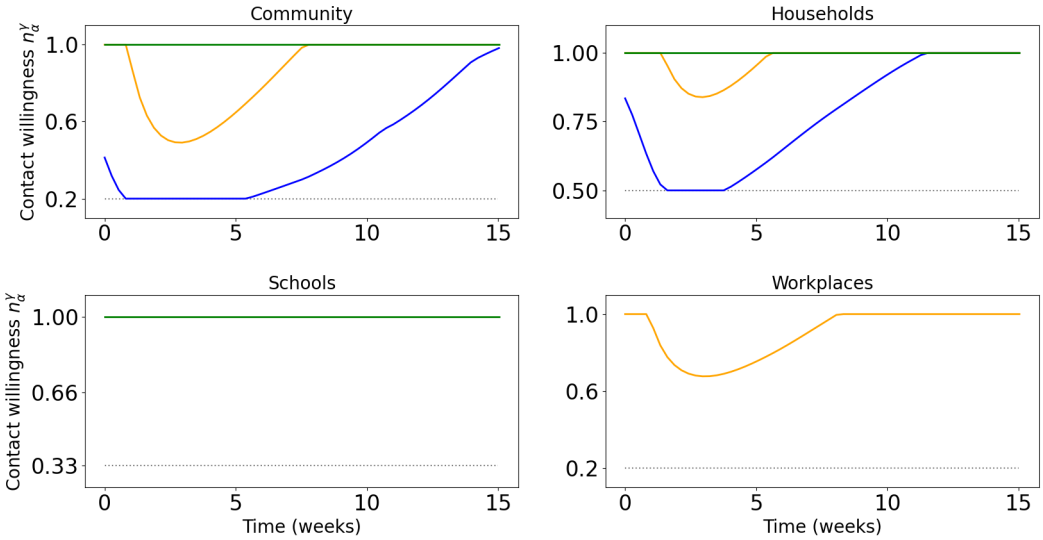

Figure 3.5: Time evolution of the contact willingness $n_\alpha^\gamma(t)$ with $\mathfrak{r}_\mathrm{I} = 1$ at the Nash equilibrium. We plot $n_\alpha^\gamma(t)$ for each type of individual according to their age class (retired people in blue, adults in orange and youth in green) in community (upper left), households (upper right), schools (lower left, for the young) and workplaces (lower right, for the adults). The dotted gray horizontal lines correspond to the minimum contact willingness allowed (maximum effort).

3.3.4 The Nash equilibrium under constraints

In the Nash equilibrium considered above, each agent optimises for herself, and this leads to a global cost for the society,

$$C_\mathrm{glob}\left(\{n_\beta\}\right) \equiv \sum_\alpha \mathcal{N}_\alpha C_\alpha\left(n_a{=}n_\alpha, \{n_\beta\}\right) , \tag{3.21}$$

which is sub-optimal. In Eq. (3.21), $\{n_\beta\}$ is the set of strategies followed by each age class, $n_a = n_\alpha$ means that any given individual a of class α follows the strategy n_α assigned to age class α, and the cost for each age class is weighted by the proportion $\mathcal{N}_\alpha$ of individuals in that class. A question that naturally arises from a public policy point of view is to know whether one could improve the global wellbeing of the population by driving the position of the Nash equilibrium through constraints on the population. This is, in some sense, what has been attempted in many countries during Covid-19 pandemic. The restrictions taken then, however, involved a lot of guesswork, both about the precise decisions to take, and about their potential effects on society (individuals behavioral response, impact on economic, health, etc).

Here we present a possible quantitative approach to study such restriction policies, which aim at reducing the societal cost by constraining the behavior of individuals. Again, we remain here at the level of a "proof of concept", as practical implementations of our formalism would require determining realistic forms of the cost functions and of the constraints, which is clearly beyond the scope of our work.

With the free (i.e. unconstrained) Nash equilibrium, individuals choose their contact willingness $n_\alpha^\gamma(t)$ in the range $[\mathfrak{n}_{\alpha,\min}^\gamma, 1]$, where the maximum 1 correspond to the situation without epidemic. We now add a constraint similar to a partial lockdown, by setting this maximum to $n_{\alpha,l}^\gamma < 1$ when some epidemic level is reached. In that way, everyone is required to make a minimal amount of efforts to preserve the sanitary system and reduce the societal cost (3.21). This "lockdown" is implemented when the proportion of infected $I(t)$ reaches a certain threshold $\mathfrak{I}_\mathrm{d}$, and, as the proportion of infected decreases we assume the lockdown is lifted when $I(t)$ goes below a value $\mathfrak{I}_\mathrm{l} < \mathfrak{I}_\mathrm{d}$ (which is assumed lower than $\mathfrak{I}_\mathrm{d}$

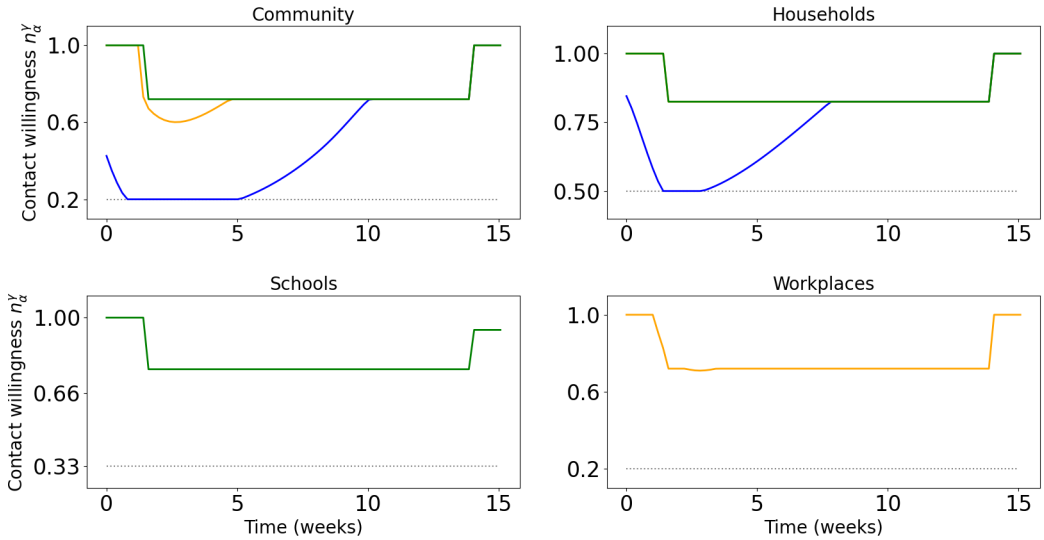

Figure 3.6: Time evolution of the contact willingness $n_\alpha^\gamma(t)$ with $\mathfrak{r}_\mathrm{I} = 1$ for the Nash equilibrium under optimal constraints ($\mathfrak{s} = 0.35, \mathfrak{I}_\mathrm{d} = 0.12, \mathfrak{I}_\mathrm{l} = 4.10^{-4}$). We plot $n_\alpha^\gamma(t)$ for each type of individual according to their age class (retired people in blue, adults in orange and youth in green) in community (upper left), households (upper right), schools (lower left, for the young) and workplaces (lower right, for the adults). The dotted gray horizontal lines correspond to the minimum contact willingness allowed.

to avoid unrealistic oscillations around $\mathfrak{I}_\mathrm{d}$). The lockdown has thus a hysteresis form, and is implemented in the following way (with L a Boolean variable which is 1 if the lockdown is active and 0 otherwise):

$$\begin{cases} \text{if } I(t) < \mathfrak{I}_\mathrm{l} : n_\alpha^\gamma(t) \in [\mathfrak{n}_{\alpha,\min}^\gamma, 1] \quad \& \quad L \mapsto 0 \qquad \text{no constraints} \\ \text{if } I(t) > \mathfrak{I}_\mathrm{d} : n_\alpha^\gamma(t) \in [\mathfrak{n}_{\alpha,\min}^\gamma, n_{\alpha,l}^\gamma] \quad \& \quad L \mapsto 1 \qquad \text{active constraints} \\ \text{if } \mathfrak{I}_\mathrm{l} < I(t) < \mathfrak{I}_\mathrm{d} \text{ and } L = 0 : n_\alpha^\gamma(t) \in [\mathfrak{n}_{\alpha,\min}^\gamma, 1] \quad \text{no constraints} \\ \text{if } \mathfrak{I}_\mathrm{l} < I(t) < \mathfrak{I}_\mathrm{d} \text{ and } L = 1 : n_\alpha^\gamma(t) \in [\mathfrak{n}_{\alpha,\min}^\gamma, n_{\alpha,l}^\gamma] \quad \text{active constraints.} \end{cases} \tag{3.22}$$

In Eq. (3.22), we choose $n_{\alpha,l}^\gamma = \mathfrak{s}\,\mathfrak{n}_{\alpha,\min}^\gamma + (1 - \mathfrak{s})$, with $\mathfrak{s} \in [0, 1]$ a variable measuring the intensity of the lockdown: $\mathfrak{s} = 0$ corresponds to the free situation without any constraint, while $\mathfrak{s} = 1$ corresponds to a strict lockdown with no freedom, as $n_\alpha^\gamma(t)$ is fixed to $\mathfrak{n}_{\alpha,\min}^\gamma$. Therefore, the lockdown is described by a set of three variables $(\mathfrak{s}, \mathfrak{I}_\mathrm{d}, \mathfrak{I}_\mathrm{l})$: the intensity $\mathfrak{s}$, the first threshold $\mathfrak{I}_\mathrm{d}$, and the second threshold $\mathfrak{I}_\mathrm{l}$. The numerical implementation of this set of equations is briefly discussed in Sec. 6.1.3.

In Fig. 3.4 (third row) we show the evolution of the epidemic quantities for the choice of parameters ($\mathfrak{s} = 0.35, \mathfrak{I}_\mathrm{d} = 0.12, \mathfrak{I}_\mathrm{l} = 4.10^{-4}$). As shown in Sec. 3.3.6.3 this choice corresponds to an optimal value in the sense that these parameters minimise the global cost Eq. (3.21) among all possible constraints in the parameter space $(\mathfrak{s}, \mathfrak{I}_\mathrm{d}, \mathfrak{I}_\mathrm{l})$. In Fig. 3.6 we display the corresponding strategies chosen by individuals under these constraints. The constraints are enforced after 2 or 3 weeks into the epidemic, and are raised after almost 14 weeks (over 40 for the total epidemic time) when the proportion of infected is low and there is no risk of any epidemic rebound. The values of the constraints appear as straight lines followed by youth individuals, whose behavior is not dictated by their own "egoistic" optimisation but by the fact they are forced to respect the lockdown as soon as it is imposed. Retired people on the other hand choose most of the time to limit their contact even more than required by the constraints; adults most of the time just follow the lockdown, but sometimes limit their contacts further.

As we shall discuss in section 3.3.6 this optimal lockdown, despite the fact that it depends on only three parameters, can improve on the free Nash equilibrium, in the sense

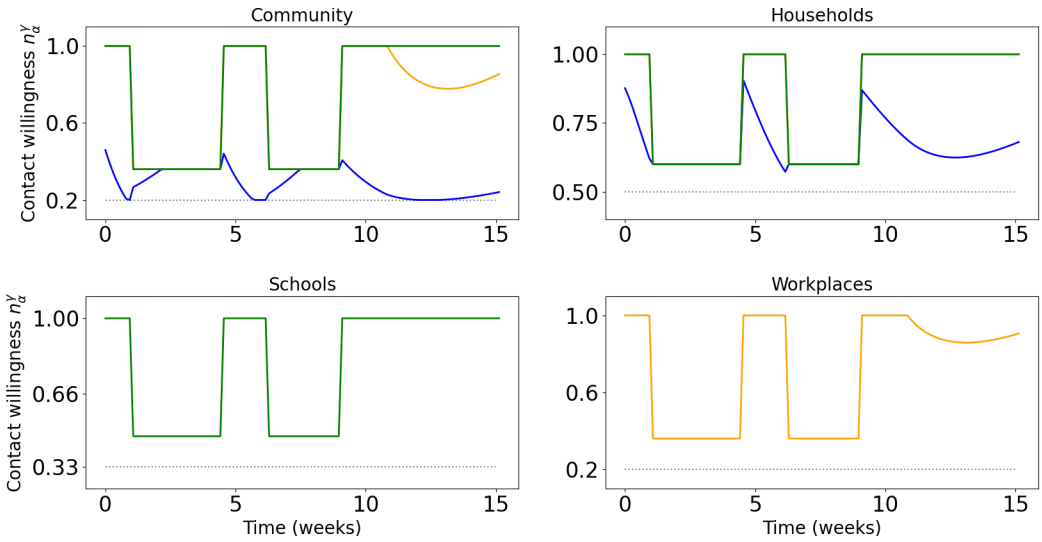

Figure 3.7: Time evolution of the contact willingness $n_\alpha^\gamma(t)$ with $\mathfrak{r}_\mathrm{I} = 1$ for the Nash equilibrium under naive constraints ($\mathfrak{s} = 0.8, \mathfrak{I}_\mathrm{d} = 0.06, \mathfrak{I}_\mathrm{l} = 0.01$). We plot $n_\alpha^\gamma(t)$ for each type of individual according to their age class (retired people in blue, adults in orange and youth in green) in community (upper left), households (upper right), schools (lower left, for the young) and workplaces (lower right, for the adults). The dotted gray horizontal lines correspond to the minimum contact willingness allowed.

that the societal cost Eq. (3.21) is lower. However, public policies executives have to be careful about their choice as it can generate situations which are clearly worse than the free Nash equilibrium. We illustrate this situation in Figs. 3.4 (fourth row) and 3.7 with parameters ($\mathfrak{s} = 0.8, \mathfrak{I}_\mathrm{d} = 0.06, \mathfrak{I}_\mathrm{l} = 0.01$): in that case one imposes a very strong but short lockdown. Since we consider here a long end-time configuration with $T = 40$ weeks, for which collective immunity is required to end the epidemic, this leads to epidemic rebounds and increases significantly the epidemic cost. Indeed, all drastic efforts that are made while the epidemic is low, and before collective immunity is obtained, are essentially useless, and just add to the global cost endured by the population. In what follows we shall thus distinguish Nash under optimal constraints (NOC) and Nash under "naive" (uncarefully chosen) constraints (NNC).

3.3.5 The societal optimum

We recall that the finding the societal optimum of the game is defined as finding the minimum of the global cost Eq. (3.21) which is a possible choice of a societal cost among many others.

In Fig. 3.4 (fifth row) we show the epidemic quantities associated with the societal optimum. This situation is optimal from a society point of view if we look for the global cost only, that is, the addition of all individual costs. However, the total number of infected individuals is not the lowest possible, as infection within the youths does not carry the same cost as within the retired agents. The total amount of infected at the end of the epidemic is still relatively high, because in our framework, one has to reach collective immunity to definitely escape from the disease. Also, the epidemic peak is still at a rather high level, as it is efficient to allow an epidemic spread while keeping the epidemic under control to reach quickly herd immunity. However, the precise distribution of infected proportion in each age class is different from the free Nash equilibrium.

In Fig. 3.8 we show the corresponding optimal contact willingnesses. They do not correspond to individual optimum; rather, there is a cooperation between individuals in different age classes to get an epidemic which will make lower damage with a reasonable

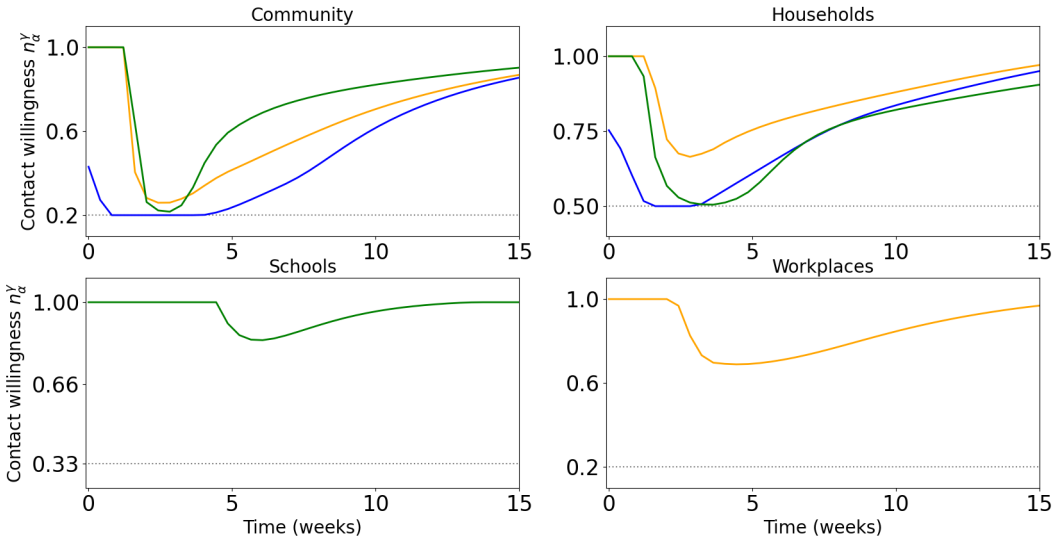

Figure 3.8: Time evolution of the contact willingness $n_\alpha^\gamma(t)$ with $\mathfrak{r}_\mathrm{I} = 1$ for the societal optimum. We plot $n_\alpha^\gamma(t)$ for each type of individual according to their age class (retired people in blue, adults in orange and youth in green) in community (upper left), households (upper right), schools (lower left, for the young) and workplaces (lower right, for the adults). The dotted gray horizontal lines correspond to the minimum contact willingness allowed.

amount of efforts. In the community setting and in households, we observe that all individuals make significant efforts during the epidemic peak to avoid a global infection peak that would saturate the sanitary system: they do it in particular in those two settings to avoid a too strong diffusion to retired people. On the other hand, efforts are done with less intensity in schools and workplaces. Once the epidemic peak is reached, we see that the epidemic continues to spread, in particular in young and adults classes, so that collective immunity can be reached and in this way protect retired people. Thus, the efforts in schools and workplaces are here to smooth sufficiently the epidemic, avoid any rebound, and get a relative collective immunity as fast as possible, making it possible to lift the efforts in communities and households.

3.3.6 Comparison between the different scenarios

In this section, we compare the various scenarios discussed previously. First, in Sec. 3.3.6.1, we assess the societal cost of each scenario in quantitative terms by using the global cost function. Next, in Sec. 3.3.6.2, we analyze the two most effective strategies to understand how the structure of the societal optimum can offer insights into designing optimal constraints. Finally, in Sec. 3.3.6.3, we explore the parameter space of the constraints to intuitively understand the underlying mechanisms driving the system.

3.3.6.1 Comparison of global costs

In order to compare quantitatively the scenarios presented above, we normalize the costs with respect to the total cost of the societal optimum, which we set equal to 100.

In Fig. 3.9 we show, for the choice of parameters given in Tables 3.2-3.3, the global costs obtained with the different kinds of strategies considered above. As expected, the societal optimum (SO) is the best strategy at society level, followed quite closely by the Nash equilibrium under optimal constraints (NOC), which itself is better than the free Nash equilibrium (N). As the imposition of societal-optimal strategies implies a lack of freedom for the individual, as well as a coordination cost which may be significant and which is not included in Eq. (3.21), we argue that the constrained Nash equilibrium presumably forms in practice a good compromise between effectiveness and practicability. One should bear in

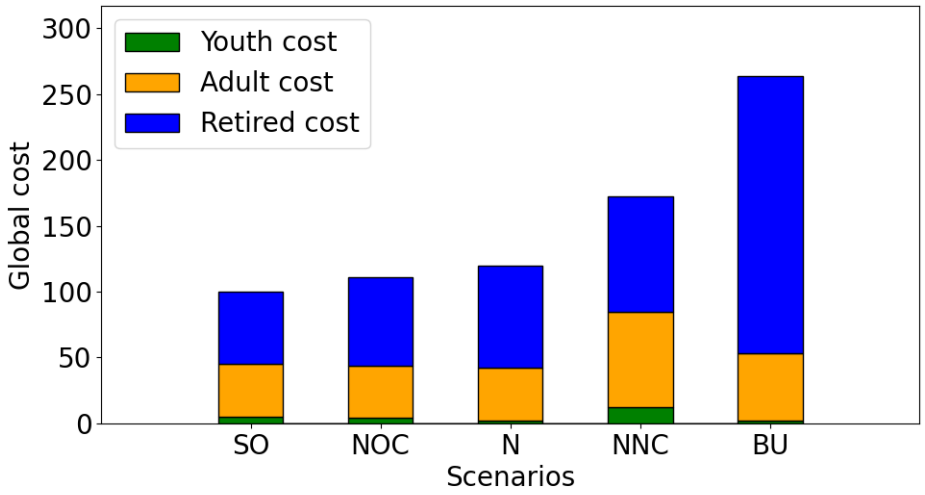

Figure 3.9: Comparison of costs for the different scenarios studied: SO (Societal Optimum), NOC (Nash under Optimal Constraints), N (free Nash equilibrium), NNC (Nash under naive constraints), BU (Business as Usual). The costs are represented on a base of 100 for SO; the color bars represent the total cost of each age class. Thus, the level of each bar comes from the cost per individual multiplied by the proportion $\mathcal{N}_\alpha$ of his age class.

mind, however, that with a naive choice for the constraints, such as for the NNC strategy of Fig. 3.9, one could easily obtain a result worse than for the free Nash equilibrium.

The color bars in Fig. 3.9 illustrate the relative importance of each age class in the total cost paid by the society. This shows that, to reach a global optimum, the key point is to reduce as much as possible the cost for retired people whose contribution is large. This contribution is actually larger than that of adults, despite the latter representing twice as many people as retired individuals in our population choice. Note that, from the point of view of adults or young people, the free Nash equilibrium is the best strategy, as they do not have to make efforts for others. We can also notice that making a wrong choice for the constraints will not lead to the same "extra cost" for everyone. Indeed, for the NNC scenario, the cost for retired people is still relatively low because the epidemic is maintained at a low level, but the cost of social restrictions becomes very high for adults and young individuals. This has to be contrasted with the business as usual scenario where the extra cost is borne almost exclusively by retired people.

3.3.6.2 Comparison of contact willingness for the two best strategies

In Fig. 3.10, we show the comparison between the contact willingness obtained with the societal optimum (dashed line) and the Nash equilibrium under optimal constraints (solid line). We see that for the Nash equilibrium under constraints we get constraints which start at almost the same time as the ones of the societal optimum (after typically 2 weeks); but since it is a Nash equilibrium, these constraints are raised after a long time, around 14 weeks, so that even without individual efforts from adults and youth the epidemic is kept under control. At a global level, these constraints are not too strong compared to the ones of the societal optimum, but since they are less localized, both spatially (in the good settings) and temporally (during the epidemic peak with a progressive release afterwards), they are less effective to protect retired people who suffer from a higher epidemic with a larger total number of infected people at the end of the epidemic.

These two strategies, the societal optimum and the Nash equilibrium under constraints, suggest interesting guidelines for public health executives to mitigate an epidemic through collective immunity. First, quite naturally, sufficiently strong constraints should be imposed at the epidemic peak to avoid saturation of the sanitary system; and the constraints

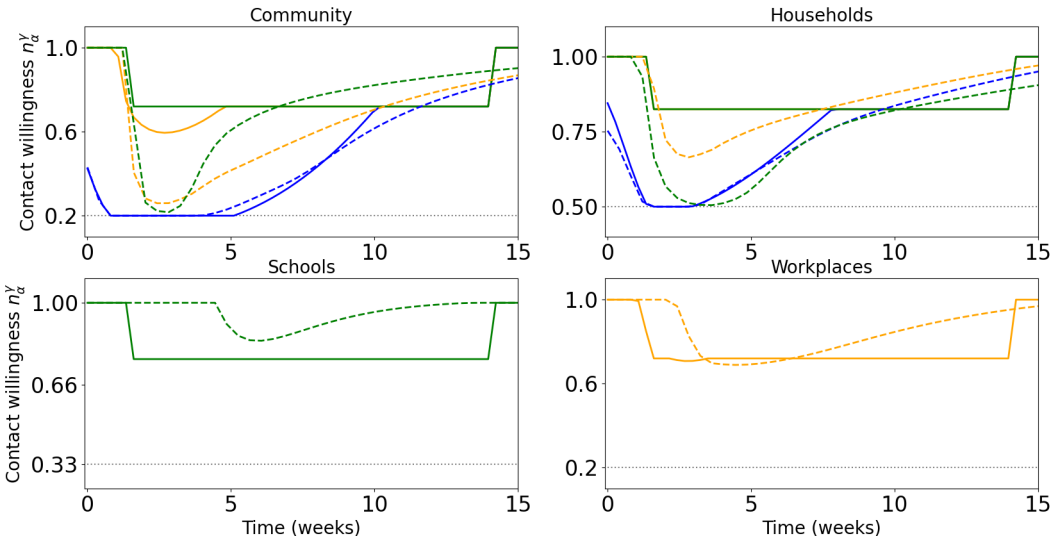

Figure 3.10: Comparison of contact willingness for the Societal Optimum (dashed line) and the Nash equilibrium under optimal constraints (solid line). We plot $n_\alpha^\gamma(t)$ for each type of individual according to their age class (retired people in blue, adults in orange and youth in green) in community (upper left), households (upper right), schools (lower left, for the young) and workplaces (lower right, for the adults). The dotted gray horizontal lines correspond to the minimum contact willingness allowed.

need to protect people at risk, which implies to limit contact both among these people as well as between the rest of the society and these individuals. On the other hand, in a perhaps less intuitive way, constraints on people who are not at risk should be relatively light. Indeed, the epidemic needs to spread on the population, in a controlled way, to reach as fast as possible the collective immunity. After the epidemic peak, one can lift progressively the constraints, until the collective immunity is reached. At this point, the epidemic will be back at a low level and will stay low while the constraints can be completely lifted. The precise characteristics of the constraints, such as their intensity or their timing, will depend on the characteristics of the population and of the disease under consideration. However, strategies that induce epidemic rebound, like the Nash scenario with naive constraints described above, are quite ineffective in such a context, because the time span between the peaks does not help reaching collective immunity and is very costly in terms of constraints on the society.

3.3.6.3 Comparison of global cost for the Nash equilibrium under different constraints

We now study how the global cost for the Nash equilibrium under constraints changes with the three parameters of the constraint; results are displayed in Fig. 3.11. The parameters used in Fig. 3.6 correspond to the minimum found here.

At $\mathfrak{s} = 0$ we recover the free Nash equilibrium, with the same global cost, around $C_{\text{glob}} = 120$. When the intensity $\mathfrak{s}$ is increased, society carries a lower cost than in the free Nash equilibrium, because all individuals are forced to make some efforts. But at a certain intensity, a minimum is reached; the location of this minimum is mainly influenced by $\mathfrak{r}_{\text{I}}$, and corresponds here to the region around $\mathfrak{s} = 0.3-0.4$. In this interval, we find the optimal lockdown configuration that we presented above with $\mathfrak{s} = 0.35, \mathfrak{I}_{\text{d}} = 0.12, \mathfrak{I}_{\text{l}} = 4.10^{-4}$. Among the three parameters $(\mathfrak{s}, \mathfrak{I}_{\text{d}}, \mathfrak{I}_{\text{l}})$ characterizing the partial lockdown, the one which has the most impact on the global cost is $\mathfrak{s}$, as there are no significant variations between the different curves of Fig. 3.11. For $\mathfrak{s} > 0.5$, the constraints become too strong with respect to the epidemic threat for all choices of thresholds, but especially for low $\mathfrak{I}_{\text{d}}$ and

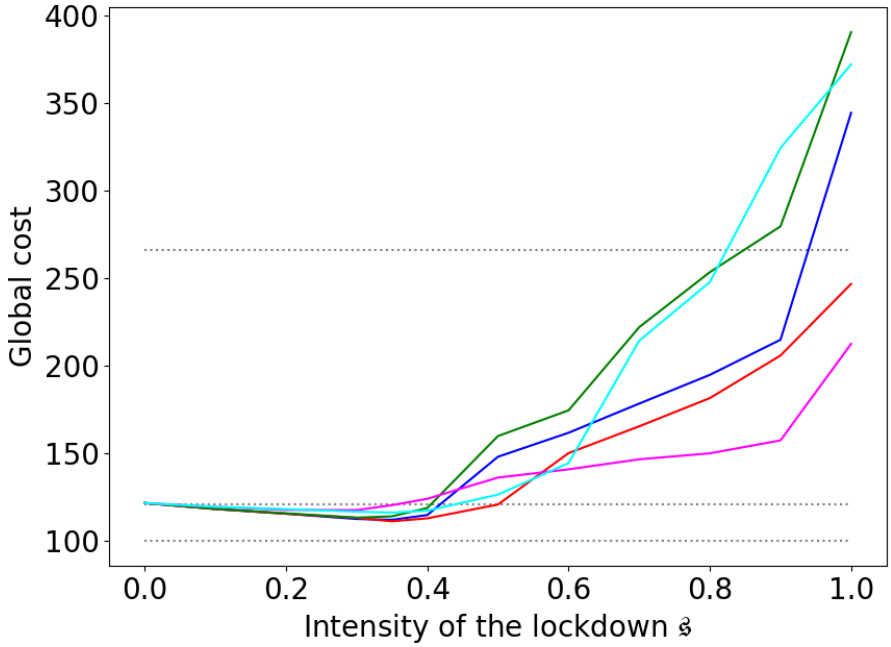

Figure 3.11: Comparison of global cost for different parameters of the constraints. The x-axis correspond to the intensity of the lockdown $\mathfrak{s}$, which could vary from 0 (no constraints) to 1 (maximal constraints). The different curves correspond to different choices for the two threshold parameters $\mathfrak{I}_{\rm d}$ and $\mathfrak{I}_{\rm l}$. We choose $\mathfrak{I}_{\rm d} = (0.12, 0.08, 0.04)$, a too low $\mathfrak{I}_{\rm d}$ will clearly deteriorate the situation as it will impose a duration of the constraints which is too long to reach collective immunity. A higher $\mathfrak{I}_{\rm d}$ is, on the other hand, not effective, as typically the maximum effort with the free Nash equilibrium is around 0.15 for our choice of parameters, and thus the threshold would never be reached. For $\mathfrak{I}_{\rm l}$ we took $\mathfrak{I}_{\rm l} = (1.10^{-2}, 4.10^{-4}, 1.10^{-5})$. $\mathfrak{I}_{\rm l}$ will have a major impact on the duration Δt of constraints, with a log relation of the form $\Delta t \simeq -\log(\mathfrak{I}_{\rm l})$. Increasing $\mathfrak{I}_{\rm l}$ will decrease the extent of lockdowns and conversely. A too high $\mathfrak{I}_{\rm l}$ will lead to epidemic rebounds (the constraints is lifted too early), and a too low $\mathfrak{I}_{\rm l}$ will impose useless extra social cost to the population. Blue curve $(\mathfrak{I}_{\rm d}, \mathfrak{I}_{\rm l}) = (0.08, 4.10^{-4})$, red $(0.12, 4.10^{-4})$, green $(0.04, 4.10^{-4})$, magenta $(0.08, 1.10^{-2})$ and cyan $(0.08, 1.10^{-5})$. Dotted gray horizontal lines from top to bottom correspond respectively to business as usual cost, free Nash equilibrium, and societal optimum.

$\mathfrak{I}_{\rm l}$, because this imposes long constraints which become very costly as $\mathfrak{s}$ increases. When $\mathfrak{s}$ approaches 1 we even reach a point above the business as usual scenario (which had $C_{\rm glob} = 266$), as we enter a regime characterized by a succession of lockdowns followed by epidemic rebounds which are suppressed by the next lockdown before herd immunity can be reached.

3.4 Optimal scenarios to deal with an epidemic from the health authority point of view

Up to this point, we have only considered dynamics with a very long end-time T, and a large number of agents $N_{\rm tot}$, so that the only option to terminate the epidemic is to reach herd immunity. However there are many circumstances (expected production of a vaccine, seasonality of the virus which is expected to disappear in the summer, etc..) where the finiteness of T plays a role, and others (isolated geographic configuration such as islands, strict control of borders, etc..) where the finiteness of $N_{\rm tot}$ does. This opens the way to other possible scenarios, from the point of view of the centralized health authority, to control the epidemics. Our approach allows for the selection of optimal strategies by

providing a quantitative measure: the cost at the societal level. We first describe a threefold approach to controlling an epidemic in Sec. 3.4.1. Then, in Sec. 3.4.2, we develop "template strategies" for each scenario which are designed to approximate the best possible strategies. Finally, we explore the first order phase transition that emerges between these strategies in Sec. 3.4.3.

3.4.1 The threefold way of controlling an epidemic

Based on these considerations, we can identify three possible ways to deal with an epidemic: reaching collective immunity (typically for T, N large), contain the epidemic (for T small), or eradicate the epidemic (for N_{tot} small). We characterize these three ways as follows.

Strategy n°1: reaching collective immunity.

This is the strategy that was implicitly used in the previous sections since we assumed both T and N_{tot} very large. More formally, we consider that collective immunity has been reached at time t if the proportion of infected individuals is a decreasing function of time for $t' > t$ even in the absence of efforts after t. For the basic SIR model Eq. (1.7) with constant χ, let $R_{\text{eff}}(t) = S(t)R_0$ be the effective reproduction number at time t, that is, the average number of secondary infected caused by a single infected agent, with $R_0 = \rho\chi/\xi$ the initial value of R_{eff} when $S = 1$. For this model we have $\dot{I}(t) = \xi I(R_{\text{eff}}(t) - 1)$. In this case, collective immunity is reached as soon as $R_{\text{eff}}(t) < 1$ since S is decreasing. In a similar way, for our compartmental model we introduce

$$R_\alpha(t) = \frac{\mu\rho}{\xi} \sum_{\beta,\gamma} n_\alpha^\gamma(t) n_\beta^\gamma(t) \mathcal{M}_{\alpha\beta}^\gamma S_\beta(t) \ , \tag{3.23}$$

the average number of secondary infected caused by a single infected agent of age class α. We stress that $R_\alpha < 1$ does not imply $\dot{I}_\alpha < 0$, since the number of infected in the age class α involves the R_β of all classes, and some of them may be greater than 1. On the other hand, if *all* the R_α are less than one, the average proportion of infected individuals, $I \equiv \sum_\alpha \mathcal{N}_\alpha I_\alpha$ can be easily shown to be a decreasing function. Indeed, from Eq. (3.10), we have $\dot{I} = \sum_\alpha \mathcal{N}_\alpha S_\alpha \lambda_\alpha - \xi I$, and

$$\sum_\alpha \mathcal{N}_\alpha S_\alpha \lambda_\alpha = \mu\rho \sum_{\beta,\gamma,\alpha} \mathcal{N}_\alpha S_\alpha n_\alpha^\gamma(t) n_\beta^\gamma(t) \mathcal{M}_{\alpha\beta}^\gamma I_\beta = \xi \sum_\beta \mathcal{N}_\beta I_\beta R_\beta \ , \tag{3.24}$$

where we used the sum rule $\mathcal{M}_{\alpha\beta}\mathcal{N}_\alpha = \mathcal{M}_{\beta\alpha}\mathcal{N}_\beta$ enforced by the symmetric nature of contacts. We therefore have

$$\dot{I} = \xi \sum_\alpha \mathcal{N}_\alpha I_\alpha (R_\alpha - 1) \ . \tag{3.25}$$

In the absence of effort, the rates $R_\alpha(t)$ become $R_\alpha^{(0)}(t) = \frac{\mu\rho}{\xi} \sum_{\beta,\gamma} \mathcal{M}_{\alpha\beta}^\gamma S_\beta(t)$, and Eq. (3.25) becomes

$$\dot{I}^{(0)} = \xi \sum_\alpha \mathcal{N}_\alpha I_\alpha (R_\alpha^{(0)} - 1) \ , \tag{3.26}$$

where the superscript denotes the absence of effort. Since the $R_\alpha^{(0)}$ are obviously decreasing functions of time, the constraint that $R_\alpha^{(0)}(t) < 1$ for all age classes α is a sufficient, but not necessary, condition to have reached herd immunity. This constraint is, however, too strong, and is actually not met in our simulations, even when herd immunity is achieved. We thus find more effective to replace it by a heuristic condition obtained by assuming

the I_β to be not very different from the average I (as can be seen for example in Fig. 3.4 towards the end of the epidemics). Using Eq. (3.26), we get $\dot{I}^{(0)} \simeq \xi I(R^{(0)} - 1)$, with

$$R^{(0)} \equiv \sum_\alpha \mathcal{N}_\alpha R_\alpha^{(0)} \ . \tag{3.27}$$

$R^{(0)}$ is also a decreasing function of time, and the heuristic criterion $R^{(0)}(t) < 1$ indicates that herd immunity has been reached at t. This empirical condition does not guarantee mathematically the absence of an epidemic rebound once $R^{(0)}(t) < 1$ (heterogeneous I_α could allow $\dot{I}^{(0)} > 0$). Nevertheless, we will check below numerically that for the cases we considered it does actually correspond to herd immunity [1]. This strategy, where S needs to be low at the end of the epidemics, is often used for moderate epidemics and for epidemics where no other strategy is available.

Strategy n°2: containing the epidemic.

If an external event (e.g. vaccine) is expected to end the epidemic within a relatively short time, another possibility to deal with an epidemic is to contain it during the period of optimization T, keeping the epidemic at a low level, and end at T with a number of susceptible far above the collective immunity threshold. In practice, we are in this phase if $R^{(0)}(T) > 1$. This is the strategy adopted by most countries during the Covid-19 pandemic: hold on and contain the epidemic until a vaccine is available.

Strategy n°3: eradicating the epidemic.

A final possibility is to act on the epidemic sufficiently early and sufficiently intensely, that one will be able to eradicate it before it spreads to the general population. To implement such an idea, we need to assume a finite size $N_{\rm tot}$ of the population, and state that below a certain rate of infected, of order $1/N_{\rm tot}$, the epidemic vanishes or is at least under control so that there is no propagation anymore. Of course in practice, one would need to know precisely who is infected and isulate them from the rest of the population (by keeping them in quarantine at hospital for instance), which would induce an extra cost of coordination which is not taken into account here. Discussing this strategy requires to add one parameter, $I_{\rm thr}$, which corresponds to the threshold at witch we consider that the epidemic vanishes, with a value for $I_{\rm thr}$ of order $1/N_{\rm tot}$. This approach is in practice possible only during the early stages of the epidemic, otherwise it will induce a considerable cost. This strategy has been used many times in China and some insular countries during Covid-19 pandemic, with strong restrictions at the early stages of the epidemic to avoid a massive spreading.

3.4.2 Template strategies

The above scenarios can be classified according to whether $\dot{I}^{(0)}(t) < 0$, $\forall t > T$ (herd immunity), and if this is not the case, whether $I(T) > I_{\rm thr}$ (containment) or $I(T) < I_{\rm thr}$ (eradication). Thus, any set of strategies $n(.) \equiv \{n_\beta^\gamma(.)\}$ (i.e. defined for each age class, in each setting, and all times t) belongs to one and only one of these classes. We can, however, do a little bit more than this formal classification, and introduce for each of these scenarios what we will call a "template strategy", that is, a set of strategies $n(.)$ which provides a good approximation to the optimal one within a given scenario. These "templates" can be defined as follows:

[1] Our criterion is actually better suited to describe herd immunity at the end of the epidemics than, for instance, the one which requires $S < 1/\tilde{R}_0$ with $\tilde{R}_0 = \rho(\rho\mu\mathcal{M}/\xi)$ [38, 183]

- *Reaching collective immunity* $n_{\rm im}$: Our template for the herd immunity scenario is defined as the optimal strategy defined in Sec. 3.3.5 taken in the limit $T \to \infty$ (with $I_{\rm thr} \equiv 0$), namely

$$n_{\rm im}(.) = \underset{n(.)}{\rm argmin} \left[\, C_{\rm glob} \left(n(.), T \longrightarrow \infty \right) \right] \, . \tag{3.28}$$

  Indeed, we can expect that when the best approach is to use herd immunity, there is little end-time effect and the optimal strategy for a finite T will be quite close to the one corresponding to $T \to \infty$. As seen in Fig. 3.12, the global cost associated with $n_{\rm im}$ rises quite significantly at the beginning of the epidemic, as a significant number of agents assume the cost of infection, but once herd immunity is reached this cost flattens out since infection decreases while no effort is required anymore. It can be noted furthermore that $n_{\rm im}$ does not depend much on $\mathfrak{r}_{\rm I}$, as it minimizes the cost due to social contacts (which is independent from $\mathfrak{r}_{\rm I}$), while reaching collective immunity. This leads in first approximation to a constant number of agents who have been infected at the end time T, as the collective immunity threshold is unchanged for any value of $\mathfrak{r}_{\rm I}$. Therefore, the associated final cost of this strategy $n_{\rm im}$ grows with a form $C_{\rm glob}(n_{\rm im}) \simeq F_{\rm tot}(n_{\rm im}) + (S_0 - S_\infty)\mathfrak{r}_{\rm I}$, where $F_{\rm tot}$ is the total amount of efforts made by agents for a strategy $n(.)$, which is (almost) independent of $\mathfrak{r}_{\rm I}$, and the second term grows linearly with $\mathfrak{r}_{\rm I}$.

- *Containing epidemic* $n_{\rm cont}$: We define the reproduction factor R as the $R^{(0)}$ which was introduced in Eq. (3.27), with here arbitrary value for $n(t)$ instead of 1. One can easily claim that a sufficient condition to strictly contain the epidemic in a homogeneous infected population is to keep $R(t) = 1$. With that condition, one will enforce $I(t)$ to stay as the same level or below the initial condition $I(0)$ with a priori the lowest possible cost from the social point of view (keep $R(t) < 1$ will be more expensive). We can therefore define the template strategy of the containment scenario as the one coming from the optimization

$$n_{\rm cont}(t) = \underset{n(.)}{\rm argmin} \left[F_{\rm tot}(n(.)) \text{ such that } R(t) = 1 \quad \forall t \right] \, , \tag{3.29}$$

  where we furthermore assume that for all age classes $S_\alpha(t) \simeq S_\alpha(0) \simeq 1$, so that $n_{\rm cont}$ is actually time independent. Since the social cost only involves current time t, the problem reduces to a simple, local in time, optimization problem, where $n(t)$ becomes a constant n which must respect $R = 1$ and minimize $f(n)$. The result of this optimization, obtained numerically through a gradient descent under constraints, is illustrated in Fig. 3.12. Note that this (constant) strategy $n_{\rm cont}$ is independent of $\mathfrak{r}_{\rm I}$, and the associated global cost $C_{\rm glob}(n_{\rm cont}) \simeq T f(n_{\rm cont})$ is essentially independent of $\mathfrak{r}_{\rm I}$ and grows linearly with T.

- *Eradicate epidemic* $n_{\rm era}$: For this case, it can be shown (see App. D.E) that, for the parameters we consider, the optimal eradication strategy is always obtained by an application of the maximal effort until the time $t_{\rm thr}$ corresponding to the eradication of the epidemics, $I(t_{\rm thr}) \equiv I_{\rm thr}$. This strategy, will be taken as our template eradication strategy. The associated final cost is therefore expected to be of the form $C_{\rm glob}(n_{\rm era}) \simeq T f_{\rm max}$ if $T < t_{\rm thr}$, the cost grows linearly with T , and $C_{\rm glob}(n_{\rm era}) \simeq f_{\rm max} t_{\rm thr}$ if $T > t_{\rm thr}$, where $f_{\rm max}$ denotes the social cost (rate) associated with a maximum amount of efforts and $t_{\rm thr}$ mainly depends on $I_{\rm thr}$.

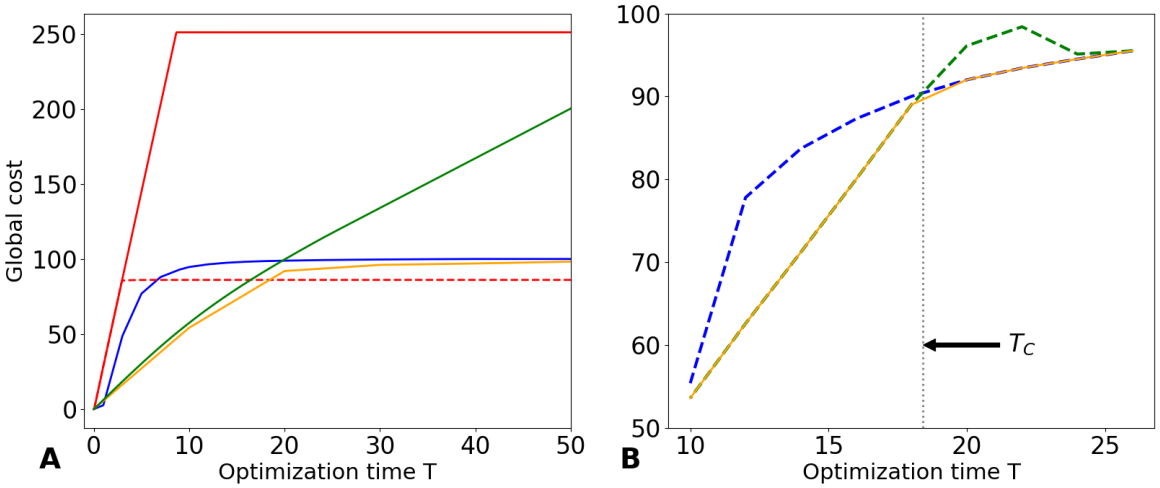

Figure 3.12: **A**. Comparison of the evolution of the global cost $C_{\text{glob}}(n, T)$ for the three template strategies n_{im} (blue line), n_{era} (red lines), n_{cont} (green line) which are well defined for any value of t (from 0 to ∞). For the global cost associated to the eradication strategy n_{era} (in red) we take respectively $I_{\text{thr}} = 1.10^{-5}$ (resp. $I_{\text{thr}} = 1.10^{-3}$) for the solid line (resp. dotted line). Regarding the strategy n_{im}, $T = \infty$ is approximated here by $T = 100$. Finally in orange, we plot the true societal optimum cost at T (with $I_{\text{thr}} = 1.10^{-5}$, solid line parameters). **B**. Evolution of the global cost of the societal optimum (orange solid line) close to the transition time T_c (see text). Dotted blue (resp. green) line: evolution of the global cost with a continuous change of the strategy n for the herd immunity scenario (resp. containment scenario). Details of the computation are explained in the main text.

3.4.3 Phase transition

For these three scenarios, we show on Fig. 3.12A the evolution of the global cost with the optimization time T, for $\mathfrak{r}_{\text{I}} = 1$ and the parameters of Tables 3.2-3.3. As expected, all costs increase with T, but in different ways. In blue, the collective immunity cost grows rapidly at the beginning of the epidemic, so that collective immunity is reached as soon as possible without saturating the sanitary system, after which the cost levels up. For the containment strategy n_{cont} (green), we see that the corresponding cost increases almost perfectly linearly, as the amount of effort due to contact reduction is constant. As $S(0) = 0.99 < 1$, there is in this scenario a small spread of the infection at the beginning of the epidemic (and thus a small additional infection cost), before it vanishes completely. Finally the cost of the eradication strategy (red curve) starts with a strong linear increase (the slope of the curve here is clearly higher than the one of the containment strategy since the maximal effort is applied), and then saturates at a level which depends on the threshold I_{thr}. Figure 3.12A also shows the societal optimum cost (orange curve, $I_{\text{thr}} = 1.10^{-5}$), which always closely follows one of the templates. At low T, it is a bit below the cost of the containment strategy n_{cont}, taking advantages of end-time effects (as illustrated in Fig. 3.13) to slightly reduce the cost. For large T, it follows, again from below, the collective immunity template. For the societal optimum cost, there is a transition around 20 weeks for our choice of parameters, from a "containment" cost to a "collective immunity" cost. For $I_{\text{thr}} = 10^{-3}$ (dotted line in Fig. 3.12), the transition would go from "containement" to "eradication".

This transition between different scenarios' costs strongly suggests that the associated strategies will follow the same pattern, with a transition from the neighborhood of n_{cont} to the neighborhood of n_{im}. To assess this, we compare in Fig. 3.13 the optimal strategy found from the societal optimum approach with the template strategies. We observe that

the small gap between template costs and societal optimum cost which was observed on Fig. 3.12A corresponds to a small difference between the corresponding strategies. For strategy 1 (rows 1-2) we observe a finite-T effect: an additional amount of efforts around 10 to 25 weeks appears to be profitable to limit the number of infected, even though the epidemic is almost over. The structure of the two strategies is nevertheless very similar. Regarding the "containment" strategy (rows 3-4), in each setting the contact willingness of each age class of agents is the same (thereby, only one constant dotted line per setting is plotted) The societal optimum is very close to the strategy n_{cont}, but two effects make it deviate from the idealistic strategy n_{cont}. First, as $S(0)$ is not strictly equal to one (here 0.99), there is some moderate spreading of the epidemics, which induces a small increase of effort from retired people, as well as a small increase of infection cost. Second, there is a clear end-time effect, meaning here that individuals who are not at risk reduce their efforts just before T since epidemic will not have time to propagate massively until T (one can think of a vaccination campaign where individuals will start increasing their contacts before the campaign is completed). Note however that as T gets close, since the epidemic begins to grow, retired individuals protect themselves and actually further limit their contacts. Lastly, for the eradication strategy, the societal optimum is the same as our template strategy n_{era} (see App. D.E for more details).

Figures 3.12A and 3.13 indicate that our template strategies provide an accurate approximation of the societal optimum at small and large T. One question we may ask now is whether the transition we see at $T_c \simeq 20$ from one scenario to another can be understood as a true phase transition, or is rather of a crossover type. To address this question, in Fig. 3.12B we compare the societal optimum near T_c, i.e. the absolute minimum of the global societal cost, with the result of a gradient descent obtained in the following way: starting from above T_c (blue) or below (green), we change T by small steps δT, and use as a starting point for the gradient descent at $T + \delta T$ the result of the calculation at T. What we observe is that doing this procedure, our algorithm finds, for a significant range of T values around T_c a local minimum which follows the herd-immunity template below T_c (dotted blue) or the containment template above T_c (dotted green). This local minimum corresponds either to the true minimum when the blue or green curves match the orange one, and to a metastable state when they do not. Note that both local minima eventually fall to the global minimum (in orange) when they are sufficiently far from T_c, ending in a hysteresis cycle.

There is therefore a discontinuous change of the optimal strategy at T_c, which is the signature of a first-order phase transition. In this analogy with thermodynamics, the cost C_{glob} represents the free energy, and T some macroscopic parameter such as temperature. The Ehrenfest classification, which defines a first-order phase transition as a discontinuity of the first derivative of C_{glob} with respect to T at T_c, is clearly observed in Fig. 3.12B. We expect this phase transition to exist for a large range of parameters of our model, and we have verified its existence numerically on a number of cases. In particular, we have checked that the transition between "containment" phase and "eradication" phase is also first-order.

We end up with three distinct phases for the societal optimum, which exhibit first-order phase transitions between them, and which are well-approximated by template strategies defined above. Since these template strategies provide good approximations of the societal optimum one, we use them in Fig. 3.14 to show the "phase diagram" of the optimal scenarios as a function of the optimization time T and the infection cost $\mathfrak{r}_{\text{I}}$. Of course, the optimal strategy will depend on all the parameters that we have introduced until now, but some of them (matrix of contacts $\mathcal{M}$, capacity of the sanitary system $\mathfrak{q}_{\text{sat}}$, proportion of agents in each age class $\mathcal{N}_\alpha$) may be assumed to be quite similar for different epidemics affecting the

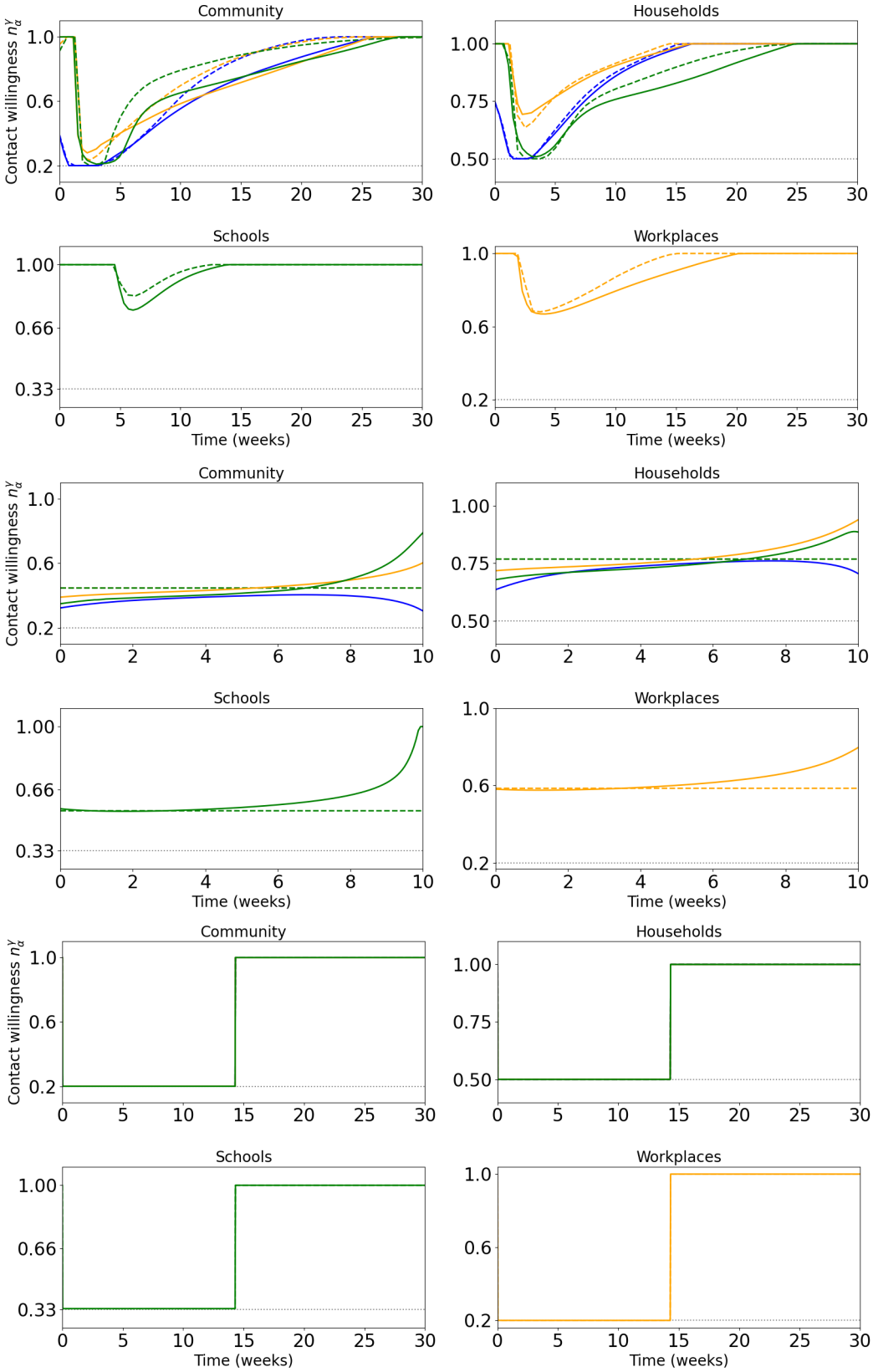

Figure 3.13: Contacts willingness for the three template strategies defined in Sec. 3.4.2 (dotted lines) and the (finite-T) societal optimum for the corresponding parameters (solid lines). Rows 1-2: collective immunity ($T \to \infty$, computed in practice with $T = 100$ and $\mathfrak{r}_\mathrm{I} = 1$, dotted line) and societal optimum (computed with $T = 30, \mathfrak{r}_\mathrm{I} = 1, I_\mathrm{thr} = 0$, solid line). Rows 3-4: contained strategy (dotted) and societal optimum (solid) for $T = 10, \mathfrak{r}_\mathrm{I} = 1$. Rows 5-6: eradication strategy (dotted) and societal optimum (solid) for $T = 30, \mathfrak{r}_\mathrm{I} = 1, I_\mathrm{thr} = 1.10^{-5}$ – the two strategies matches perfectly. Sub-panels and legends are the same as in Fig. 3.5.

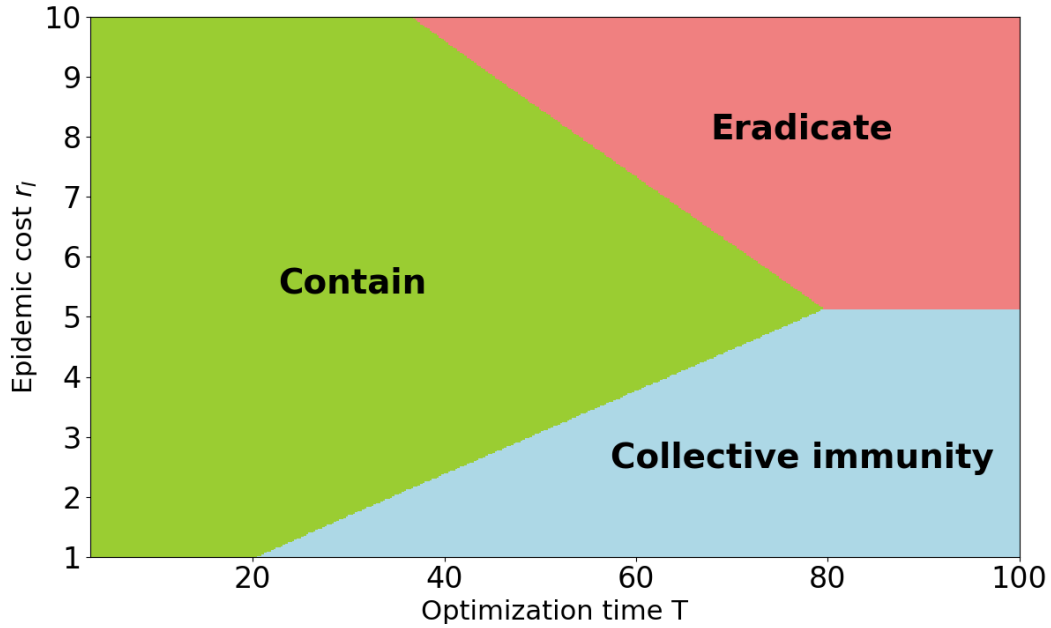

Figure 3.14: Phase diagram showing the best type of strategy to follow among "reach collective immunity" (blue), "contain" (green) and "eradicate" (red) with the parameters of Tables 3.2-3.3 and $I_{\text{thr}} = 1.10^{-7}$ for the eradication strategy (it is more realistic, as it means $N_{\text{tot}} \simeq 10^7$). Change I_{thr} or the initial conditions will naturally change the transition lines (between immunity and eradication areas).

same population, while T and $\mathfrak{r}_{\text{I}}$ depend a lot on the virus under consideration and have a major impact on the best strategy. The three different scenarios appear to be optimal in distinct well-defined areas of the phase diagram. When T is small (below 20 weeks), the containment strategy is optimal whatever $\mathfrak{r}_{\text{I}}$. Then, there is a transient regime, where the optimal strategy can be any of the three scenarios, collective immunity, containment, or eradication according to $\mathfrak{r}_{\text{I}}$. Finally, after $T \simeq 80$ weeks, containing the epidemic is no longer an option, as the linear increase of the cost becomes prohibitive, and the best choice is either to reach collective immunity or to eradicate the epidemic. Since we use template strategies, the first-order phase transitions are represented by linear lines on the graph.

3.5 Discussion

In the present Chapter we developed, following [38], an epidemic model based on the well-known SIR compartmental model supplemented by a social structure. This social structure relies on the idea that contacts are heterogeneous in society, both because individuals socialize in different contexts, and because they react in various ways to the disease (different perception of risk). Therefore, one can divide society into classes of agents which differ by their behavior, by the risk that the disease represents for them, and by the settings in which socialisation takes place. Here we used an age differentiation, but other kinds of classification (e.g. based on the immune status or on the presence of comorbidity) could easily be implemented within the same formalism. In the same way, one can easily add more compartments and more classes or settings to the model, without changing the global framework. The description of social structures obtained in this way is clearly less refined than one that would take into account the heterogeneity of social behaviors at an individual level, but it probably represents a good balance between precision and ease of application when trying to understand the dynamics of an epidemic and take appropriate, targeted action against it.

To this compartmental epidemic model with social structure, we have, following the approach of Elie *et al.*[19], added a Mean-Field Game description of the dynamics: agents may change their individual behavior depending whether they feel at risk of infection or not. After deriving the MFG equations, we computed numerically the Nash equilibrium, where each individual seeks to optimize her own interests. In this paradigm, individuals make a perfectly rational optimization, and are assumed to be able to perform the corresponding calculations which is something that we cannot expect from people in practice, as discussed in Sec. 2.4.2.

As discussed in Sec. 3.3.1, the choice of parameters we used for our simulations does not aim to describe a specific real-world configuration, but nevertheless corresponds to a rather generic situation, and the qualitative behavior we obtained is most likely rather typical of what would be observed in a realistic case. For this set of parameters, the Nash equilibrium obtained within the Mean-Field Game framework reduces significantly the costs associated with the epidemic when compared to the "business as usual" approach where social contacts are kept unchanged. However, there is usually still a gap between the MFG cost and the one that would correspond to the societal optimal policy, which represents the minimal global cost that can be borne by the society. To approach this optimal policy, we introduce the notion of "constrained Nash equilibrium", in which we assume that under some conditions, the central authority can impose some constraints, analog to the partial lockdowns that we have seen during the Covid-19 epidemic, under simple rules which are known to the agents. In our work, we used a simple restrictive policy with three parameters $(\mathfrak{s}, \mathfrak{I}_\mathrm{d}, \mathfrak{I}_\mathrm{l})$ and we optimized this policy (i.e. we find the optimal set $(\mathfrak{s}^*, \mathfrak{I}_\mathrm{d}^*, \mathfrak{I}_\mathrm{l}^*)$) to get the lowest possible societal cost, and in this way close as much as possible the gap between the free Nash equilibrium and the societal optimum (see Figs. 3.6 and 3.9).

In our discussion of the Nash equilibrium and of the "constrained Nash" approach to the societal optimum, we have implicitly limited ourself to a regime of very long optimization time T, and of large population N_tot, for which the societal optimum policy necessary implies in some way to reach herd immunity. In Sec. 3.4, we go back in more details to the analysis of the societal optimum, in particular lifting these constraints on T and N_tot. Depending (mainly) on the values of T, N_tot, and $\mathfrak{r}_\mathrm{I}$, we can identify three *phases* that we label as "reaching collective immunity" (the one implicitly assumed in the previous sections), "containing the epidemic" or "eradicating it" (see Fig. 3.14 showing which scenario is optimal depending on the parameters T and $\mathfrak{r}_\mathrm{I}$). The transition between any two of these phases can by understood as a first-order phase transition, in the sense that the associated strategies present discontinuities and are different from one phase to another. An important consequence of this discontinuity is that it is primordial for an authority to clearly identify the appropriate scenario, as a wrong choice could lead to significant additional costs.

Among these three scenarios, "reaching collective immunity" is the one for which the time dependence of the agent strategies $\{n_\alpha^\gamma(.)\}$ are the more complex, and an authority will probably not be able to impose such exact strategy for all individuals. For this scenario, an approach through a Mean-Field Game paradigm under constraints as the one presented in this work is probably more relevant to approach the societal optimum cost, which would slightly shift the phases boundaries in Fig. 3.14. On the other hand, the "containment strategy" appears to be easier to design for an authority, as it consists in adjusting in real time the constraints, depending on whether the epidemic is growing or not, to follow $R(t) \simeq 1$. Nevertheless, to find the best set of constraints to hold $R(t) \simeq 1$ still involves some complexity, as one should still adapt the strategy to the response of individuals. Advantage of this scenario is that this can be performed "on the fly", and does not really imply any anticipation. Finally, in the "eradication strategy", authority

has to impose the maximum admissible constraints, which is conceptually rather simple. We stress, however, that, contrarily to the "herd immunity" strategy, the societal optimum obtained with strategy "contain" and "eradicate" are very far from any Nash equilibrium, even under "reasonable" constraints. The restrictions imposed with the two latter scenarios lead to epidemics which stay at low levels. In this context, the best individual strategy is to do essentially no effort, as there is almost no risk of infection. The social optimum strategy in this case is thus extremely far from the Nash equilibrium. This emphasizes a profound difference in nature between "herd immunity", where individual optimization is closed to the societal optimum, and the two others where the gap is much more important. This would need to be considered by institutions when they will built collective strategies, as it is presumably very difficult to convince a population to follow on its own will a strategy which is far from a Nash equilibrium, and the required degree of coercion would significantly vary between the two cases.

This concludes our first project which has been the central focus of this thesis. We investigated a complex compartmental model at a mesoscopic scale, with particular attention to the impact of varying infection costs between individuals, differentiated by age class. A natural extension of this work is to further refine the heterogeneity of contacts between individuals by relying on networks based models and exploring the behaviors that would emerge from a MFG analysis, varying the cost associated to social contact reduction. This will be the focus of our second project, presented in the next chapter.

4 - Epidemics spreading on networks through a MFG approach

The previous chapter was dedicated to the implementation of the MFG paradigm in a particular compartmental model with a social structure. The underlying network was implicit, and people were gathered in batches where they interacted between each other in an homogeneous way. This type of epidemiological models corresponds to the first family identified in Fig. 2.5 (in green). In this chapter we turn to the models based on mean-field approaches on networks (network-based models, in brown). Indeed, a game theoretical approach would be probably out of reach numerically on an explicit network without any mean-field approximation (it would correspond to an Agent Based Models). The goal of an explicit network approach is to explore how the structure of the network will influence the course of the epidemic. This structure will be mainly explored through the distribution of the number of neighbors, as well as their correlations between them. We first describe the essential mathematical tools on networks that would be needed for our work in Sec. 4.1, based on degree measures. Then, in Sec. 4.2, we develop the different possible degree-based Mean-Field approximations that can be developed for epidemic spreading on networks, concluding by the degree-based pairwise approximation (PA) system that will be used in the following. In Sec. 4.3, we implement the MFG paradigm on both homogeneous and heterogeneous networks, and we compute the corresponding Nash equilibrium for various forms of the social contact reduction function f leading to significantly different observed behaviors.

4.1 Basic tools for network analysis

In this section, we outline the tools necessary for our analysis. In Sec. 4.1.1, we introduce degree measures on networks, which are central to our analysis, taking a general approach. Since the epidemic spreads through the links of the network, the number of neighbors —or degree— is a key factor influencing the infection probability of each individual. Next, in Sec. 4.1.2, we introduce degree correlations which also play a significant role in epidemic dynamics. Then, in Sec. 4.1.3, we present additional network measures relevant to epidemic dynamics analysis, though they will not be explored further in our work.

4.1.1 Degree distribution

A network can be mathematically described by a set of N nodes (or vertices), which may be connected by links (or edges). The adjacency matrix A allows to represent the connections between nodes, where an entry $A_{ij} = 1$ indicates that nodes i and j are connected, and $A_{ij} = 0$ otherwise. A network is classified as directed if node i can be connected to node j without j being connected to i. Otherwise, it is undirected, and the adjacency matrix is symmetric. In this work, we focus on the latter case.

The degree of a node is the number of neighbors it has, given by $\mathrm{Deg}(i) = \sum_{j\in N} A_{ij}$. The degree distribution $P(k)$, representing the probability that a randomly selected node has degree k, can then be constructed by collecting the degrees of all nodes. This distribution plays a critical role in understanding complex processes on networks, especially for epidemics, it allows for the definition of the network's average degree $\langle k\rangle = \sum_{k=1}^{\infty} kP(k)$ and higher degree moments $\langle k^\mu\rangle = \sum_{k=1}^{\infty} k^\mu P(k)$. A primary distinction in network struc-

ture can be made based on the shape of the degree distribution $P(k)$.

When $P(k)$ is sharply centered around the average degree $\langle k \rangle$, meaning the standard deviation $\sigma = \sqrt{\langle k^2 \rangle - \langle k \rangle^2}$ is small and scales at worst like $\langle k \rangle$ (see Fig. 4.1), the network is said homogeneous. In perfectly homogeneous networks (also called regular), all nodes have the same degree k_0, described by $P(k) = \delta_{k,k_0}$, indicating that every node has exactly k_0 neighbors. Such networks can be generated randomly through several procedures. One of the most well-known homogeneous networks are the Erdös-Rényi (ER) networks, where each link exists with a fixed probability p. These networks exhibit a degree distribution that follows a Poisson law, with the following form: $P(k) = (Np)^k e^{-Np}/(k!)$. ER networks, extensively studied since [63], are particularly useful for exploring general network properties.

On the other hand, if $P(k)$ has a long tail (see Fig. 4.1) or a large standard deviation σ, the network is classified as heterogeneous. A common form of heterogeneous networks in nature [51] is the one which follows a power-law degree distribution, $P(k) \propto k^{-\gamma}$, characterized by a parameter γ. In the thermodynamic limit ($N \to \infty$), such distributions are feasible only for $\gamma > 1$ (to allow the normalization of the distribution). For $2 < \gamma < 3$, we have scale-free networks, where the second moment of the degree distribution is undefined, while the first moment exists. In these networks, fluctuations and correlations can grow arbitrarily large. One well-known method to generate such networks is the Barabási-Albert (BA) preferential attachment model [67], where nodes with a higher degree are more likely to attract new connections. In this model, the probability of a new link attaching to node i is proportional to its degree, $p_i = k_i/(\sum_j k_j)$. Networks of similar degree distribution can

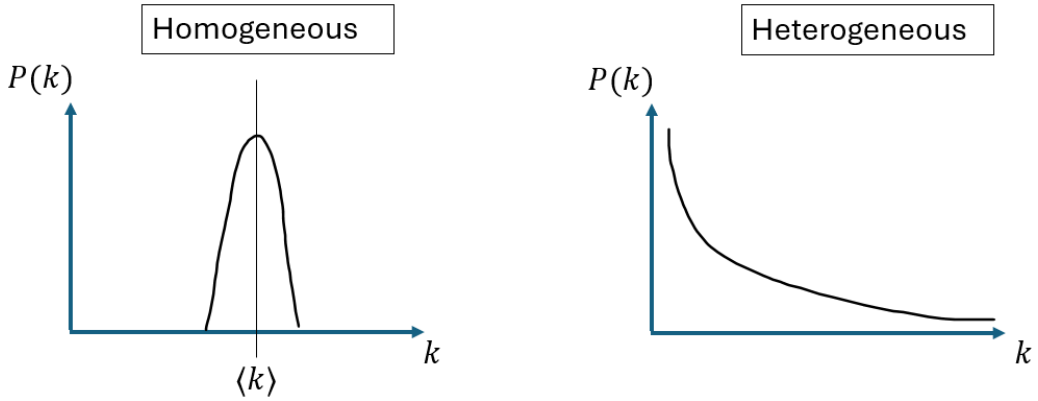

Figure 4.1: Illustration of the different type of networks. Homogeneous networks are peaked around the average degree $\langle k \rangle$ while heterogeneous networks have a large distribution.

nevertheless be significantly different due to the existing correlations inside the network and we need additional quantities to fully characterize them.

4.1.2 Correlations inside the networks

The correlations within a network reflect how the neighborhood structure, or the set of neighbors for a given node, can vary across different nodes. These correlations are often linked to the degrees of the nodes and can be expressed using the conditional probability $P(k'|k)$, which denotes the probability that a randomly selected neighbor of a node with degree k has degree k'. This conditional probability can be formulated as a correlation matrix, $G_{kk'} \equiv P(k'|k)$. This provides all the information about our network, as we will work with Markovian networks which are fully characterized by their degree distribution and their correlation matrix, in the sense that higher moments and higher order correlations inside the network can be written as combination of $P(k)$ and $G_{kk'}$ [184]. Moreover, the

degree correlations is not completely free and must satisfy the detailed degree balance condition

$$P(k)kG_{k'k} = P(k')k'G_{kk'} \quad , \tag{4.1}$$

which symmetrically accounts for the number of edges between nodes of degree k and k'.

Unfortunately, $G_{kk'}$ can be complex and difficult to interpret directly. Therefore, more intuitive metrics, such as the nearest-neighbor degree, denoted by K_{nn}, are often used. The nearest-neighbor degree is defined as $K_{\text{nn}}(k) = \sum_{k'} k'P(k'|k)$ and represents the average degree of the neighbors of nodes with degree k. In uncorrelated networks, $P(k'|k)$ is independent of k, leading to $P(k'|k) = k'P(k')/\langle k\rangle$ which ensures the normalization of the sum over k'.

Discussion on the physical rationale behind $P(k'|k) = k'P(k')/\langle k\rangle$.

Contrarily to what can be expected intuitively, we did not have $P(k)P(k'|k) = P(k')P(k|k') = P(k \cap k')$ as for Bayesian probabilities, as $P(k'|k)$ contains the specific information that the node of degree k' is a neighbor of the node of degree k. Instead, we have the detailed balance condition Eq. (4.1) which counts the number of edges from nodes of degree k to nodes of degree k': a given neighbor of a given node of degree k has a probability $P(k'|k) = G_{kk'}$ to be of degree k'. The node of degree k has therefore $kP(k'|k)$ neighbors of degree k'. We finally add the factor $NP(k)$ (where N is then simplified) to account for the number of nodes of degree k on the network. The right hand side of Eq. (4.1) corresponds to the symmetric reasoning with k' and k instead of k and k'. Taking the sum over k, we get for uncorrelated networks (meaning that $P(k'|k)$ is independent of k):

$$P(k'|k)\langle k\rangle = P(k')k' \sum_k P(k|k') \quad , \tag{4.2}$$

which using the normalization $\sum_k P(k|k') = 1$ leads to the formula we mentioned. This formula is rather not intuitive, as one would expect to get $P(k'|k) = P(k')$ which would also be normalized to 1 and independent of k. Actually, this tells us that even on uncorrelated networks where everyone has the same environment, our neighbors have more neighbors, in average, than us. Indeed, computing explicitly $K_{\text{nn}}(k)$ on uncorrelated networks leads to

$$K_{\text{nn}}(k) = \sum_{k'} k'P(k'|k) = \sum_{k'} \frac{(k')^2 P(k')}{\langle k\rangle} = \frac{\langle k^2\rangle}{\langle k\rangle} \geq \langle k\rangle \quad , \tag{4.3}$$

since the standard deviation should be positive. This equations literally says that the average degree of neighbors of degree k is above $\langle k\rangle$ and independent of k, meaning that we also have $\langle K_{\text{nn}}(k)\rangle \geq \langle k\rangle$. Physically, the fact that neighbors have more neighbors in average is due to the overrepresentation of the neighbors of high degree in the environment of all the nodes, with respect to their representation in the network ($kNP(k)$ edges are starting from them, while they are $NP(k)$ in the network).

In the case of uncorrelated networks, $K_{\text{nn}}(k)$ is therefore constant, meaning that the average degree of a node's neighbors is independent of the node's degree, and the environment appears statistically uniform across the network. The behavior of $K_{\text{nn}}(k)$ as a function of k reveals important information about the degree correlations in the network. Generally, three families of correlations emerge (see Fig. 4.2):

- **Assortative mixing:** Nodes with a high degree k are more likely to connect with other high-degree nodes.

- **Constant:** No degree correlations between nodes.
- **Disassortative mixing:** Nodes with a low degree k are more likely to connect with high-degree nodes.

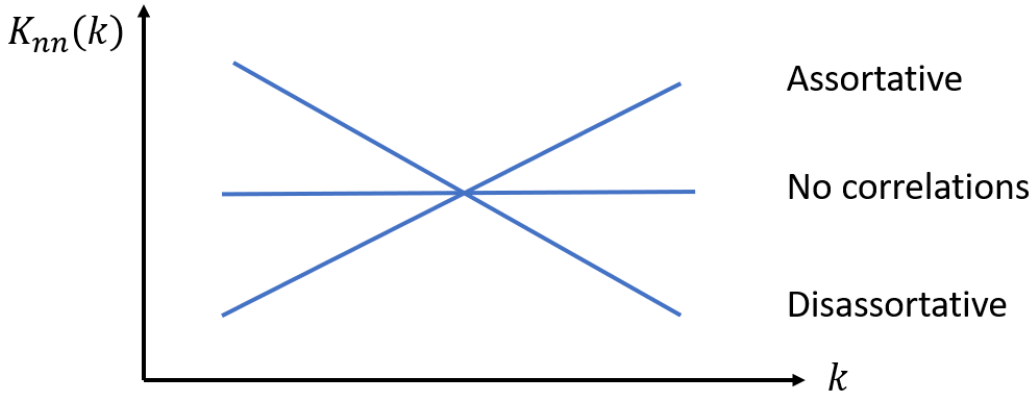

Figure 4.2: Illustration of the different type of correlations inside a network.

Examples of assortative mixing are prevalent in social networks, where individuals with similar attributes (such as age, nationality, or location) are more likely to be connected [185]. Conversely, technological and biological networks often exhibit disassortative mixing [185]. Here, we will nevertheless focus on uncorrelated networks, which already exhibit complex behaviors. This approach allows us to distinguish between phenomena arising from the degree distribution structure $P(k)$ and those potentially caused by $G_{kk'}$.

4.1.3 Other measures on networks

Several additional metrics are commonly employed to model epidemic dynamics on networks, as they provide insights into network structure:

- **Path:** A path denotes the set of links and nodes between a starting node and a final node. In a connected network, there are often several paths between two nodes. The path with the minimum number of links is considered the shortest path. An epidemic will propagate inside the network through these paths.
- **Community:** There exist several formal definitions of a community, which have more or less the same goal: capture the set of nodes such that those nodes are densely connected internally, and poorly connected outside, possibly allowing overlapping between communities. It is a global measure at the scale of the network and a whole topic of research in itself to find the best definition and then the best algorithm that would be able to detect communities in a network. These communities often play central role in the emergence of mesoscopic structure [186]. In epidemics, specific phenomena can occurs in different communities (as different contact rates for epidemics, based on the age, the race or the habits of a certain community)
- **Betweenness centrality:** Betweenness centrality quantifies the importance of a node within a network by counting the number of shortest paths that pass through it. Nodes with high betweenness centrality serve as main intermediaries in the flow of information, often acting as bridges between different communities and occupying central positions in the network. Conversely, nodes with low betweenness centrality reside at the network's periphery. Despite their peripheral location, these nodes can still play a crucial role in complex spreading processes [187, 188], where infection requires a certain proportion of infected neighbors for transmission to occur [189].

- **Clustering coefficient:** Clustering is a local metric that measures how close the neighborhood of a given node is to forming a complete graph, indicating whether the node's neighbors are densely interconnected. In the context of epidemics, clustering plays a significant role at a local level, as it influences correlations within the network [36]. For instance, if a member of your cluster, such as a family member, becomes infected, the high level of interconnectivity increases the likelihood that you will also become infected.

There exists a wide literature to find the pertinent measures on networks for epidemic spreading analysis, reader can refer to [52] for a more thorough development. We will not develop them further in our work, and rather use the degree distribution $P(k)$ and the degree correlation matrix $G_{kk'}$.

4.2 Mean-Field approximations on networks

In this section, we assume that networks are fully described by their degree distribution and their correlation matrix which can be general (Markovian networks). Although some specific features of real social networks may be overlooked, Markovian heterogeneous networks provide a reasonable approximation of real social structures. These networks can be fully controlled and offer a practical framework for implementing the Mean-Field Game paradigm. Before introducing the game, we will first assess the suitability of different Mean-Field approximations in this context in this section.

In the context of epidemics spreading, we would like to compute the macroscopic number of susceptible, infected and recovered individuals on a network. An epidemic will spread through it with a classical Markov description, with for node i

$$\mathcal{P}\left[x_i(t+dt) = i \mid x_i(t) = s\right] = \sum_{j \in V_j} \delta_{x_j(t),i} \lambda dt \quad , \tag{4.4}$$

which denotes the probability for node i to be infected at t, and V_j represents the set of neighbors of node i, while λ is the infection rate. However, this description is microscopic and specific to each node, requiring a vast amount of computational power to be performed numerically without approximations. For practical applications, this model demands detailed knowledge of the network structure, which is often difficult to obtain from real datasets. Additionally, since the model is stochastic, multiple simulations are needed to obtain quantitative results. These kinds of models fall under the category of agent-based models, which are computationally intensive and make the implementation of paradigms like Mean-Field Games challenging, as discussed in Sec. 1.2.5.

To overcome these issues, physicists have developed Mean-Field approaches that reduce the complexity of the system to a reasonable set of equations, allowing for the prediction of average epidemic dynamics within the network. These techniques help to better understand the different types of correlations that occur within the network. A brief overview of these methods is provided in this section.

We first present in Sec. 4.2.1 the Pure Mean-Field approach (PMF), which coincides with the SIR model, we then turn to the Heterogeneous Mean-Field approach (HMF) in Sec. 4.2.2, in which all nodes of the same degree are equivalent. In Sec. 4.2.3, the Quench Mean-Field (QMF) approach is briefly presented, involving the whole adjacency matrix of the network, while in Sec. 4.2.4 the Dynamical Message Passing approach (DMP) is presented, with the cavity state method. Finally in Sec. 4.2.5, the degree Pairwise Approximation approach is presented (PA). This latter approximation will be the one used in

the following, as it accounts for the main correlations in the networks, and reproduces perfectly the numerical simulations of Markovian networks with a reasonable set of equations. A complete introduction to these approximations can be found in [72].

4.2.1 The pure Mean-Field approach

In this very simple case, all the nodes of the network are considered equivalent and the infection probabilities of two nodes are assumed to be the same (nodes are independent). We have at the microscopic level for each node,

$$\mathcal{P}\left[x_i(t+dt) = i \mid x_i(t) = s\right] = \langle k \rangle I \lambda dt \ , \tag{4.5}$$

which therefore gives at the macroscopic level for the probability $I(t)$ of a node to be infected at t:

$$\dot{I} = \langle k \rangle \lambda I S - \gamma I \ , \tag{4.6}$$

which is nothing but the classical SIR equations Eqs. (1.7). This approach has been widely used during the 20$^{\text{th}}$ century. The main advantage of this approach is that the system is reduced to a single equation. However, the only network structure which is considered is $\langle k \rangle$, and no correlation or specificities of nodes are taken into account.

4.2.2 Heterogeneous Mean-Field approach

The next natural step is to consider that nodes of same degree are equivalent, through an heterogeneous Mean-Field approach developed by Pastor-Satorras and Vespignani at the beginning of 2000s [190]. This leads to the formation of degree classes; we will thus denote $I_k(t)$ the fraction of infected nodes of degree k at t. We then compute $\theta_k(t)$ which corresponds to the average probability (over nodes of degree k) that a given neighbor is infected. This quantity is defined by

$$\theta_k(t) = \sum_{k'} k' P(k'|k) I_{k'}(t) \ . \tag{4.7}$$

Then, one makes the assumption that networks are uncorrelated, which leads to a $\theta_k(t)$ independent of k which can be written as

$$\theta(t) = \frac{1}{\langle k \rangle} \sum_k k P(k) I_k(t) \ , \tag{4.8}$$

which, together with

$$\dot{I}_k(t) = \beta k S_k(t) \theta(t) - \gamma I_k(t) \ , \tag{4.9}$$

forms a close system that can be solved numerically easily. The macroscopic number of infected is naturally given by $I = \sum_k P(k) I_k$. This approach has several interesting advantages. It only involves the knowledge of the degree distribution $P(k)$, which is a rather accessible quantity, and it provides a precise epidemic threshold which explicitly depends on the network structure and heterogeneity through $\langle k^2 \rangle$ (the threshold is $\beta_{HMF} = \langle k \rangle / \langle k^2 \rangle$). Hence, for homogeneous networks of high degree, one recovers $1/\langle k \rangle$, but for heterogeneous networks with power-law distribution with $2 < \gamma < 3$, the epidemic threshold vanishes due to the divergence of $\langle k^2 \rangle$, which is one of the main results on epidemic growth on heterogeneous networks.

Nevertheless, as shown on Fig. 4.3, the quantitative comparison on long time scale is still not satisfying. θ is unique to all the nodes, and ignores the intrinsic correlations inside the networks (both regarding degrees and states). We still miss a part of the network topology, and a part of this topology can be captured directly through the adjacency matrix.

4.2.3 Quench Mean-Field approach

Another approach in [72], more radical, is to take directly the adjacency matrix A to capture all the topology of the network. We still do not consider the existing correlations between the states of two neighbors in the network, meaning that the probability for a neighbor j of node i to be infected at t will be $I_j(t)$ (independent of i). This leads to a dynamical evolution of $I_i(t)$ given by

$$\dot{I}_i(t) = \lambda S_i(t) \sum_j^N A_{ij} I_j(t) - \gamma I_i(t) \quad . \tag{4.10}$$

This Quench Mean-Field approach consider the full topology of the network through adjacency matrix A, which can be a drawback for numerical simulations notably, as the precise use of Eq. (4.10) involves one evolution equation for each node, which would become very time consuming for large N. Moreover, Eq. (4.10) still lacks the intrinsic existing correlations between the states of neighboring nodes, which appears to be a crucial element (Fig. 4.3).

4.2.4 Dynamical Message Passing approach

The issue with Eq. (4.10) is that the term I_j, which represents the probability for node j to be infected at t, is overestimated when i is itself susceptible. To take into account the correlation effect that a neighbor j of a susceptible node i is less likely to be infected than usual I_j, Karrer and Newman propose the Dynamical Message Passing approach [191], in which the reference node i is disallowed and cannot be infected. Thus, Eq. (4.10) becomes

$$\dot{I}_i(t) = \lambda S_i(t) \sum_j^N A_{ij} \theta_{j\to i}(t) - \gamma I_i(t) \quad , \tag{4.11}$$

where $\theta_{j\to i}(t)$ is the probability for j to be infected in the absence of node i (from the beginning of the dynamics). Thus, in the extreme case where j has only one neighbor i, it will never infect him while it was possible in Eq. (4.10). Evolution equation of $\theta_{j\to i}(t)$ can be derived in a straightforward way (see [72]). Although DMP approach can be numerically accurate [191], the system (4.11) is still very hard to solve, as it involve $N + 2E$ equations (where E is the number of edges). To simplify this system, Barthelemy *et al.* [46] classify the nodes according to their degree, writing the system

$$\begin{aligned} \dot{I}_k &= \lambda S_k(t) k \theta_k(t) \\ \theta_k(t) &= \sum_{k'} I_{k'} \frac{k'-1}{k'} P(k'|k) \quad , \end{aligned} \tag{4.12}$$

with the factor $(k'-1)/k'$ coming from the fact that the neighbor considered has $k'-1$ neighbors which could have infected him, as the initial node of degree k considered is still susceptible ("cavity mode" [191]). System (4.12) only has $2k_{\max}$ equations, with $k_{\max}$ the maximum degree of the network. It shows better results numerically than the HMF approach (see Fig. 4.3), thanks to the cavity mode technique, but it still fails to be accurate at long time when I significantly increases, because the correlations between two neighbors are more tricky than the one described in Eq. (4.12). This method is however well suited to study the beginning of epidemics [46].

4.2.5 The degree Pairwise Approximation approach

We now turn to the approximation we will adopt in the following. The core idea of the degree Pairwise Approximation approach is to still consider that nodes of the same degree are equivalent, but add their state (s, i, r) into their characterization (and not only the degree). Thus, susceptible nodes of degree k will be equivalent between them, but different from infected nodes of degree k, as their neighbors will have different states due to correlations. Pairwise Approximation has been introduced in [192, 60] through the adjacency matrix, and in [193] with a degree classification. This latter classification is more convenient in practice, as it will considerably reduce the number of equations.

In a slightly different way than in the literature, we introduce the conditional probability for a given node to be of state y and degree k', knowing that this node has a neighbor of state x and degree k. We denote it $G^{xy}_{kk'}$ and we denote the nodes' classes as x_k and $y_{k'}$ respectively. Thus, we consider the state of the node $(x = s, i, r)$ and its degree (k) to compute the probability for one of its neighbors to be infected. The time evolution equation of I_k can therefore be written as

$$\dot{I}_k(t) = \lambda S_k(t) k \sum_{k'} G^{si}_{kk'}(t) - \gamma I_k(t) \ , \tag{4.13}$$

where $G^{si}_{kk'}(t)$ is the correlation matrix between states and degrees, describing the probability to find an infected neighbor of degree k', considering a susceptible node of degree k. The time evolution equation of this quantity can be obtained as follows.

The key idea of our derivation is to examine the evolution of directed edges $x - y$, from a starting node of state x to an arrival node of state y. At time t, there are $NP(k)kx_k(t)G^{xy}_{kk'}(t)$ edges between the classes x_k and $y_{k'}$. This moreover verifies the degree-states detailed balance relation between these two classes

$$NP(k)kx_k(t)G^{xy}_{kk'}(t) = NP(k')k'y_{k'}(t)G^{yx}_{k'k}(t) \ . \tag{4.14}$$

Our edges under consideration have a probability $x_k(t)G^{xy}_{kk'}(t)$ of connecting nodes from class x_k to $y_{k'}$ at t. At time $t + dt$, the probability for each edge to link these two classes becomes $x_k(t + dt)G^{xy}_{kk'}(t + dt)$, to first order in dt. There are two main possibilities based on the situation at time t: either the edge was already linking the two classes x_k and $y_{k'}$ at time t and remains linked at $t + dt$ with some probability, or the edge was not connecting the two classes at time t but establishes a connection at $t + dt$. We break these two possibilities down into five sub-cases (the first three corresponding to the former, and the latter two to the latter):

1. No change for the starting and the arrival node. Contribution: $+x_k(t)G^{xy}_{kk'}(t)$
2. The state of the starting node change from x to $z \neq x$: $-\sum_{z\neq x}\left[x_k(t)G^{xy}_{kk'}(t)T^{kk'}_{(x,y)\to(z,y)}dt\right]$
3. The state of the arrival node change from y to $z \neq y$: $-\sum_{z\neq y}\left[x_k(t)G^{xy}_{kk'}(t)T^{kk'}_{(x,y)\to(x,z)}dt\right]$
4. The state of the starting node change from $z \neq x$ to x: $+\sum_{z\neq x}\left[z_k(t)G^{zy}_{kk'}(t)T^{kk'}_{(z,y)\to(x,y)}dt\right]$
5. The state of the arrival node change from $z \neq y$ to y: $+\sum_{z\neq y}\left[x_k(t)G^{xz}_{kk'}(t)T^{kk'}_{(x,y)\to(x,z)}dt\right]$

where $T^{kk'}_{(x,y)\to(x',y')dt}$ denotes the probability that the states of the starting and ending node changes from (x, y) to (x', y'), with k and k' denoting their respective degrees. We define

similarly $T^k_{x\to x'}$ for the transition probability of one node taken alone or if the state of the other node has no influence on it - like in the recovering process. For the SIR model, we obtain four non-vanishing transition rates:

$$\begin{aligned} T^k_{i\to r} &= \gamma \\ T^k_{s\to i} &= \lambda G^{si}_k k \\ T^{kk'}_{(s,y)\to(i,y)} &\simeq \lambda\Big[\delta_{y,i} + (k-1)G^{si}_k\Big] \end{aligned} \tag{4.15}$$

where we introduce the notation $G^{si}_k = \sum_{k''} G^{si}_{kk''}$. In Eq. (4.15), we use the pairwise approximation for the equation of the form $T^{kk'}_{(s,x)\to(i,x)}$: to close the evolution equation and restrict correlations to pairs (without considering correlations between three, four, or more nodes), we assume that the probability for another neighbor (different than the one already considered of class $y_{k'}$) of the starting susceptible node of degree k to be infected is given by G^{si}_k. This implies that we disregard the information about the state of the neighbor from class $y_{k'}$ when computing this probability (as it should have an influence on G^{si}_k), although we include it with the term $\delta_{y,i}\lambda$ in $T^{kk'}_{(s,x)\to(i,x)}$, which accounts for the contribution of a node whose state is known. Thus, this approximation neglects the impact of triangles and higher-order loops on a node's state, leading to limitations in networks with high clustering. However, in the thermodynamic limit $N \to \infty$ for the Markovian networks studied, this approximation becomes exact, as the number of finite loops becomes negligible. The two other transition rates of the form $T^k_{x\to x'}$ are the usual ones when one knows nothing about the neighbors of the starting node. Summing all the contribution together, we get at time $t + dt$

$$\begin{aligned} \frac{d\left[x_k(t)G^{xy}_{kk'}(t)\right]}{dt} &= x_k(t)\sum_{z\neq y}\left[G^{xz}_{kk'}T^{kk'}_{(x,z)\to(x,y)} - G^{xy}_{kk'}T^{kk'}_{(x,y)\to(x,z)}\right] \\ &+ \sum_{z\neq x}\left[z_k(t)T^{kk'}_{(z,y)\to(x,y)}G^{zy}_{kk'} - x_k(t)T^{kk'}_{(x,y)\to(z,y)}G^{xy}_{kk'}\right], \end{aligned} \tag{4.16}$$

which is the usual equation we found in the literature [194, 195, 196], with usually a compact notation for $x_k(t)G^{xy}_{kk'}(t)$. However, having introduce $G^{xy}_{kk'}$ allows to write $\dot{x}_k(t) = \sum_{z\neq x}\left[z_k T^k_{z\to x} - x_k T^k_{x\to z}\right]$ and then express the evolution of $G^{xy}_{kk'}$ as

$$\begin{aligned} \dot{G}^{xy}_{kk'} =& \sum_{z\neq y}\left[G^{xz}_{kk'}T^{kk'}_{(x,z)\to(x,y)} - G^{xy}_{kk'}T^{kk'}_{(x,y)\to(x,z)}\right] \\ &+ \sum_{z\neq x}\left[\frac{z_k(t)}{x_k(t)}\left(T^{kk'}_{(z,y)\to(x,y)}G^{zy}_{kk'} - T^k_{z\to x}G^{xy}_{kk'}\right) + G^{xy}_{kk'}(T^k_{x\to z} - T^{kk'}_{(x,y)\to(z,y)})\right], \end{aligned} \tag{4.17}$$

which involves the two forms of transition rate we introduced. This equation together with Eq. (4.13) close the system of equations with $3+(3k_{\max})^2$ equations, which is smaller than N or E for large N networks. We adopted a somewhat physical approach, following a single edge, but a more formal approach is proposed in App. B.1, reader may also refer to [195] for a mathematical derivation in the case of homogeneous networks.

The introduction of state correlated matrices $G^{xy}_{kk'}$, instead of the the quantities $x_k G^{xy}_{kk'}$ usually introduced in the literature, allows to easily obtain all marginal probabilities obtained by summing over one or more variables of $G^{xy}_{kk'}$. For instance, $G_k{}^y$ will denote the probability to encounter a neighbor of state y, whatever its degree, knowing that the starting node is of degree k, it can be computed rather naturally as

$$G_k{}^y = \sum_{x,k'} x_k G^{xy}_{kk'} = \sum_x x_k G^{xy}_k \quad . \tag{4.18}$$

With this notation, $G_{kk'}$ naturally denotes the conditional probability $P(k'|k)$ and we get a large number of closure and normalization relations among these different conditional probabilities (See App. B.2). Moreover, as shown in App. B.2, the detailed balance relation Eq. (4.14) remains valid over time, which demonstrates the consistency of the system.

The Pairwise Approximation is the one which accounts for almost all the existing correlations that we know on the network (between degrees and states). We will now test numerically the different approximations we presented to check whether the Pairwise Approximation is accurate or not.

4.2.6 Comparison between the different approaches

In Fig. 4.3 we illustrate the performance of the different approximations to predict the infected curve $I(t)$ of a random heterogeneous (Markovian) network. At each iteration, another network is drawn with the same macroscopic characteristics and another seed of infected is realized at $t = 0$. We have chosen our parameters in order to test the approximations on a random heterogeneous (scale-free) network, they are somewhat arbitrary and other parameter sets will likely lead to the same conclusions (for heterogeneous networks). We observe in Fig. 4.3 that the Pairwise Approximation (red curve) matches perfectly the

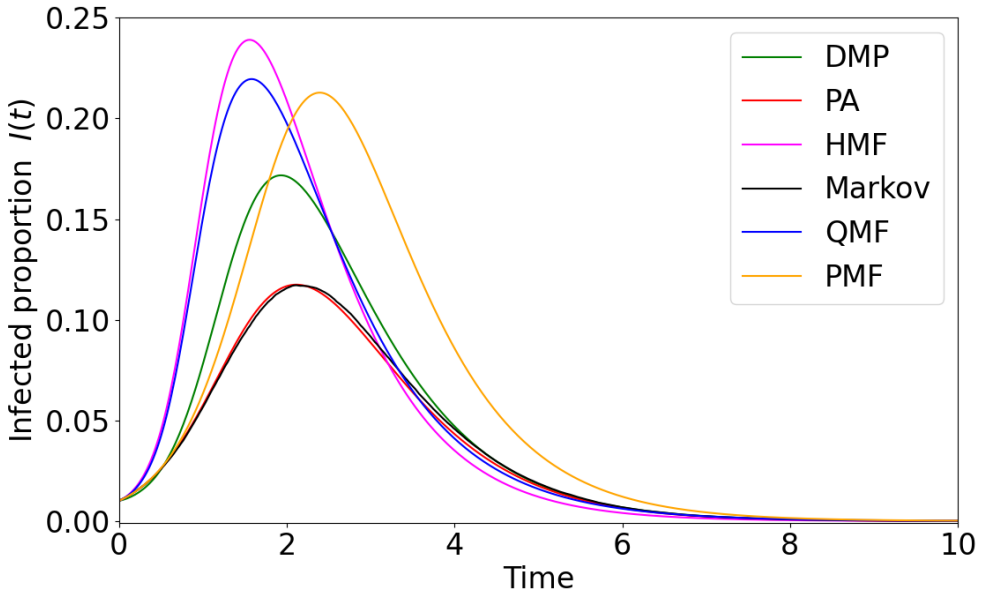

Figure 4.3: Comparison of the different approximations mentioned above with the "true" simulated number of infected nodes in a random heterogeneous network, represented by the average of the Markovian process Eq. (4.4) (black solid line). We took $N = 3000$ nodes averaged over $n_{\text{it}} = 200$ iterations of the Markovian process. PMF, QMF and HMF approaches (respectively orange, blue and purple lines) clearly overestimate the number of infected, as they consider that a neighbor of a susceptible has a probability I to be infected, whereas it is in reality lower due to the state correlations. DMP (green line) provides a better approximation thanks to the cavity method which partially accounts for the state correlation between neighboring nodes. Finally, the Pairwise Approximation (red line) provides a very accurate result. Other parameters: $P(k) \propto k^{-2.5} \in [k_{\min}, k_{\max}]$, $\lambda/\gamma = 2/3$, $I_0 = 0.01$, $k_{\min} = 2$, $k_{\max} = 20$.

average Markovian process (black curve), as it should in the limit n_{it} , $N \to \infty$. Other approximations fail to reproduce the results of the Markovian process but are rather useful in other contexts or at the beginning of epidemics. For instance, the Dynamical Message Passing approach, widely studied, is rather efficient in networks with high level of clustering.

In the following of our work, we will (naturally) continue with the Pairwise Approximation. The numerical complexity of the different approximations we presented here was also a significant stake of this work, we display them in Sec. 6.3.3.

4.3 Mean-Field Games on networks

We are now ready to apply the Mean-Field Games framework to networks. Similarly to Chapter 3, individuals will optimize a control variable related to their contact rate. However, instead of classifying individuals by age, we will categorize them by their number of neighbors (degree). This classification is particularly relevant when considering infection probability, as individuals with a higher number of contacts (i.e., a higher degree) are more susceptible to contracting the disease. In this context, it becomes crucial to assess whether individuals "at risk" due to a high number of contacts will choose to reduce their interactions or accept the associated risk. This decision is reflected on the shape of the social cost function f, particularly its dependence on k. Understanding how $f(k)$ influences behavior will provide insights into the strategies adopted by different individuals according to their degree.

In Sec. 4.3.1, we first introduce an implementation of the MFG paradigm applied to a general heterogeneous network using the pairwise approximation, in the spirit of the MFG approach used in Chapter 3. In Sec. 4.3.2, we analyze the results of the Nash equilibrium on a homogeneous network. Then, we explore the MFG Nash equilibrium in more details for realistic heterogeneous networks in Sec. 4.3.3, considering social cost functions f which can be either increasing or constant with k. Finally, Sec. 4.3.4 is dedicated to a brief discussion of the obtained results. This Section is associated with the paper presented in App. F.

4.3.1 The MFG model on a network

We split the model presentation into three sections: one dedicated to the system dynamics in Sec. 4.3.1.1, another one dedicated to the individual optimization in Sec. 4.3.1.2 and finally a short section dedicated to the choice of parameters in Sec. 4.3.1.3. Before, we briefly precise the network structure on which we will rely.

We will consider a population of N individuals which can be in one of the three possible states ($x = s, i, r$) represented by random Markovian networks. In practice, we will work in this section with uncorrelated networks, but any specific $G_{kk'}$ could be easily implemented. For each edge between two neighbors, there is a probability $\lambda(t)dt$ that an infected individual will infect its (susceptible) neighbor during the time interval $[t, t + dt[$. This probability $\lambda(t)dt$ will therefore correspond to a certain contact probability βdt times the probability ρ to infect someone when a contact occurs. As in the basic SIR model, infected individuals may also recover from the disease during that time interval with a probability denoted γdt here. The dynamics will follow a standard Markovian process and the averaged macroscopic quantities will be computed through the pairwise approximation Eq. (4.13), which is the more appropriate under our hypothesis.

4.3.1.1 System dynamics

To implement a Mean-Field Game, a natural approach, in line with Chapter 3, is to ensure symmetry in the contacts between individuals. In this model, individuals control their contact rate $\lambda(t)$ with their neighbors via a control variable $n(t)$, which they can adjust. The symmetry in the infection rate λ arises from including the actions of both neighbors in an equivalent manner. Following the approach of Chapter 3, we assume

that individuals within the same degree class exhibit identical behavior at equilibrium. This leads to defining individual control coefficients n_k for each degree class. Physically, n_k represents the willingness of individuals with degree k to engage in risky interactions with their neighbors. We will call it the "effort parameter", while the maximum effort corresponds to $n_k(t) = \mathfrak{n}_{\min}$ for a certain value of $\mathfrak{n}_{\min}$ and the minimum effort corresponds to $n_k(t) = 1$. Note that n_k is assumed to be independent of the neighbor's degree k'. While this assumption could overlook some practical circumstances, it simplifies both the analytical and numerical resolution of the model.

Thus, the symmetric contact rate between individuals a and b is given by $\lambda^{(0)} n_a n_b$, where $\lambda^{(0)}$ represents the baseline contact rate in the absence of epidemic. Consequently, the pairwise equation and, more generally, the SIR system for each degree class can be expressed as

$$\begin{aligned}
\dot{S}_k(t) &= -\lambda^{(0)} n_k(t) S_k(t) k \sum_{k'} n_{k'}(t) G^{si}_{kk'}(t) \ , \\
\dot{I}_k(t) &= \lambda^{(0)} n_k(t) S_k(t) k \sum_{k'} n_{k'}(t) G^{si}_{kk'}(t) - \gamma I_k(t) \ , \\
\dot{R}_k(t) &= \gamma I_k(t)
\end{aligned} \tag{4.19}$$

with the dynamics of $G^{si}_{kk'}(t)$ given by the $9k^2_{\max}$ equations given by Eq. (4.17) which are coupled, although some of them are not independent:

$$\begin{aligned}
\dot{G}^{xy}_{kk'} = &\sum_{z \neq y} \left[G^{xz}_{kk'} T^{kk'}_{(x,z)\to(x,y)} - G^{xy}_{kk'} T^{kk'}_{(x,y)\to(x,z)} \right] \\
&+ \sum_{z \neq x} \left[\frac{z_k(t)}{x_k(t)} \left(T^{kk'}_{(z,y)\to(x,y)} G^{zy}_{kk'} - T^{k}_{z\to x} G^{xy}_{kk'} \right) + G^{xy}_{kk'} (T^{k}_{x\to z} - T^{kk'}_{(x,y)\to(z,y)}) \right] ,
\end{aligned} \tag{4.20}$$

with the slightly modified relations with respect to Eq. (4.15):

$$\begin{aligned}
T^{k}_{i\to r} &= \gamma \\
T^{k}_{s\to i} &= \lambda^{(0)} n_k(t)\, k \sum_{k'} n_{k'}(t) G^{si}_{kk'}(t) \\
T^{kk'}_{(s,x)\to(i,x)} &= \lambda^{(0)} n_k(t) \left[n_{k'}(t) \delta_{x,i} + (k-1) \sum_{k''} n_{k''}(t) G^{si}_{kk''}(t) \right] ,
\end{aligned} \tag{4.21}$$

where n_k indicates the collective behavior followed by individuals of degree k, similarly to n_α for individuals of age class α in Chapter 3. This system forms the Kolmogorov system of our MFG. We now turn to the individual optimization.

4.3.1.2 Individual optimization

As in the previously introduced MFG, we assume that individuals of degree k are sensitive to an inter-temporal mean-field cost between the optimization time t and the end of the game at time T. A representative individual a of degree k considers the following averaged cost:

$$\mathfrak{C}\left(n_a(\cdot), \{n_{k'}(\cdot)\}, t\right) = \int_t^T \left[\lambda_a(s)\ \mathfrak{r}_{\mathrm{I}} + f_k\left(n_a(s)\right)\right] (1 - \phi_a(s)) ds \,, \tag{4.22}$$

where $\{n_{k'}(\cdot)\}$ denotes the set of collective strategies of individuals of all the possible degrees k' (including k). This cost has exactly the same form as Eq. (2.28), with the force of infection given by

$$\lambda_a(s) = \lambda^{(0)} n_a(t) k \sum_{k'} n_{k'}(t) G^{si}_{kk'}(t), \tag{4.23}$$

while the probability of being infected at time $s > t$ is given by $\phi_a(s) = 1 - e^{-\int_t^s \lambda_a(u) du}$. Regarding the cost functions, we assume a constant infection cost $\mathfrak{r}_{\mathrm{I}}$, as there is no inherent

natural difference between individuals of varying degrees. However, the social cost is likely to depend on the degree k and will therefore be denoted f_k, it will be specified in the following sections depending to the context.

As in Eq. (2.30), we then introduce the value function to minimize the cost (4.22) from the individual's perspective:

$$U_a(t) = \begin{cases} \min\limits_{n_a(\cdot)} \mathfrak{C}\left(n_a(\cdot), \{n_{k'}(\cdot)\}, t\right) , & a \quad \text{susceptible at } t \\ 0, & a \quad \text{infected (or recovered) at } t. \end{cases} \tag{4.24}$$

This value function corresponds to the minimum cost that individual a can expect to pay between t and the rest of the game, according to her status. A straightforward derivation, following the one of Sec. 2.3.3, leads to

$$-\frac{dU_a}{dt} = \min_{n_a(t)} \left[\lambda_a(t)\left(\mathfrak{r}_\mathrm{I} - U_a(t)\right) + f_k(n_a(t))\right] \quad , \tag{4.25}$$

which together with the final condition $U_a(T) = 0$ provides the HJB equation of our game. Besides, we will compute explicitly the optimal strategy $n_a^*(t)$ for individual a of degree k, susceptible at t, which will depend on the precise shape of f_k.

Finally, the consistency condition to be at a Nash equilibrium is that for any individual a one has

$$n_a^*(t) = n_k(t) \quad , \tag{4.26}$$

with k the degree of individual a. Equations (4.19)-(4.17)-(4.21) (Kolgomorov system) together with Eq. (4.25)(HJB) and Eq. (4.26)(Consistency) form the MFG system of our game whose solution is a Nash equilibrium.

4.3.1.3 Parameters choice for our simulations

To explore the behavior of this MFG system, we implemented and solved it numerically using the gradient descent method (see Sec. 6.1.2) to reach the Nash equilibrium of our game[1], for different parameters of our game. We explore two kinds of networks: perfectly homogeneous and a "realistic" heterogeneous network. On the latter case, we will study the Nash equilibrium for increasing or constant f_k with k. Importantly, we will keep the "biological" parameters of our system constant to be able to compare them, which means that the baseline contact rate $\lambda^{(0)}$ has to be rescaled according to $\langle k \rangle$: $\mu = \gamma/(\lambda^{(0)}\langle k \rangle)$ is fixed to $1/4$. Other parameter used are summarized in Table 4.1. For the social cost function, we chose the specific form

$$f_k^\epsilon(n(t)) = k^\epsilon \left(\frac{1}{n(t)} - 1\right) \quad , \quad \epsilon = 0, 1 \, , \tag{4.27}$$

which allows us to explore different regimes of social dependence to neighbors. Physically, the choice $\epsilon = 1$ implies that a constant social cost of $(\frac{1}{n_a(t)} - 1)$ is assigned to each neighbor, which means that for a fixed fraction of contacts lost, an individual with a higher number of neighbors is more impacted than an individual with fewer neighbors. In the case $\epsilon = 0$ the social cost is the same for all individuals, whatever their degree. This two bounds appear to be the most natural ones that one can think about, the dependency of f with k in practice will probably be for ϵ in $[0, 1]$, regarding the physical meaning associated to ϵ only.

[1] Here also, the Nash equilibrium seems unique

(S_0, I_0, R_0)	μ	$\lambda^{(0)}\langle k\rangle$	$\mathfrak{r}_{\mathrm{I}}$	$\mathfrak{n}_{\min}$
(0.995, 0.005, 0)	1/4	4	50	0.1

Table 4.1: Parameters used in our simulations for MFG on networks. We took a small $\mu = \gamma/(\lambda^{(0)}\langle k\rangle) = 1/4$ to ensure that an epidemic will easily propagate even for epidemics on homogeneous networks of low degree (where the threshold is $(k-2)/k$ as we will see in Chapter 5) and for the low degree region of heterogeneous networks. We keep $\lambda^{(0)}\langle k\rangle = 4$ in all our simulations to be able to compare epidemics between them, for both homogeneous and heterogeneous networks. $\mathfrak{r}_{\mathrm{I}}$ is chosen to be comparable with f_k. Finally, we took an arbitrary $\mathfrak{n}_{\min} = 0.1$ which corresponds to the lower bound of the effort parameter, sufficiently low to not affect the observed behaviors here. The time scale of the results are in days, it may vary according situation studied: we have always chosen the time scales of our simulations to enforce reaching collective immunity and thus compare similar scenarios each time.

4.3.2 Nash equilibrium on homogeneous networks

We first consider the simplest case of homogeneous networks (or regular graphs), where each node has the same number k of neighbors. The Kolmogorov system (4.19)-(4.17)-(4.21) is then significantly simplified (see the system (5.1)-(5.2) for an explicit version). In an homogeneous network of degree k, we are left with a single class of individuals, with $\lambda(t)$ equal to $\lambda^{(0)}n^2(t)$ and $n(t)$ is the effort parameter chosen by individuals of degree k (we drop the index as there is no other k involved). For our specific choice f_k^ϵ we can compute the optimal strategy $n_a^{\epsilon,*}(t)$:

$$n_a^{\epsilon,*}(t) = \left(k^{1-\epsilon}\ \lambda^{(0)} G_k^{si}(t)[\mathfrak{r}_{\mathrm{I}} - U_a(t)]\right)^{-1/2} \quad , \tag{4.28}$$

which allows us to more easily compute the Nash equilibrium of the game numerically (and verify that we have reached the Nash equilibrium). After numerically solving the system of equations discussed above and reaching a Nash equilibrium, we obtain the epidemic rates and associated effort parameters. They are displayed in Fig. 4.4 for the two different possibilities $f_k^{0,1}$. Several observations can be made.

First, we observe in Fig. 4.4 that while individuals reduce their contact rate predominantly during the epidemic peak, their maximal effort occurs slightly after the peak is reached (see, for instance, the case $k = 4$ on the first row), and they maintain their effort well beyond the peak. This suggests that individuals engage in a form of "reverse anticipation". More precisely, it is not the anticipation of the incoming epidemic that motivates their behavior, but the compound effect of the actual (present time) intensity of the epidemic and of the *anticipation of its end*. Indeed, at the onset of the epidemic, the prospect of maintaining a significant effort for the whole duration of the epidemic, while the latter is still growing slowly and individuals anticipate that collective immunity will not be reached anytime soon, appears more costly (with our choice of parameters) than paying the "one time" cost of infection. However, as collective immunity is in sight, shortly before the epidemic peak and for some time after, it becomes advantageous to make efforts to avoid infection, since the epidemic is still severe, and the remaining time before the epidemics is over is reasonably short. It then becomes advantageous for susceptible individuals to make significant efforts, as they have a good chance of avoiding infection forever if they protect themselves for a relatively short period.

While the mechanism described above is rather generic, the precise range and intensity at which it is at play of course depends on the choice of parameters. In particular,

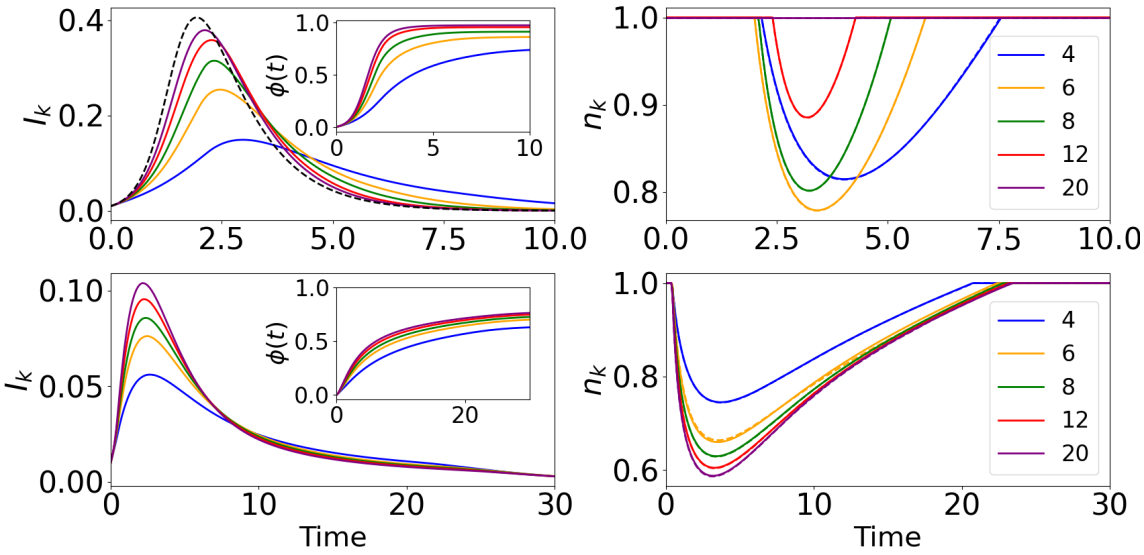

Figure 4.4: Left column: Dynamics of infected individuals, corresponding to the Nash equilibrium, with the parameters of Table 4.1 for different homogeneous networks, with $k = 4$ (blue), 6 (orange), 8 (green), 12 (red), 20 (purple) and classical SIR model (black dashed); the social cost function is f_k^ϵ with $\epsilon = 1$ (top) and $\epsilon = 0$ (bottom). Inset: dynamics of the probability $\phi(t)$ to be infected before t. Right column: Dynamics of the corresponding individual effort parameter, with the same parameters and color code as for the left column. Dashed lines correspond to the best individual response in a population which follow the solid lines strategies. They perfectly match solid lines, meaning that we have reached a Nash equilibrium of our MFG system (it is a check of the self-consistent equation (4.26)).

epidemics on random homogeneous networks progress faster and are more intense as k increases as we shall see in Chapter 5. For constant f_k ($\epsilon = 0$, second row of Fig. 4.4), the ratios between social effort and infection cost remain essentially constant across degrees, and are fairly low for our choice of parameters. This leads to effort patterns that are similar across degrees, with individuals tending to protect themselves by "flattening" the infection curve $\phi(t)$, thereby minimizing their probability of infection. The only difference between classes is that individuals with higher degrees face more intense epidemics, requiring greater and more prolonged effort while maintaining the same overall pattern. On the other hand, when the social cost f_k increases with k ($\epsilon = 1$, first row of Fig. 4.4), this increasing social cost may compete with the one of the infection. As Fig. 4.4 shows, these two factors essentially balance each other around a critical value $k^* \simeq 6$, leading there to a significant intensity of efforts. However, below this threshold, the epidemic is not sufficiently virulent, and above k^* efforts becomes too costly to justify a strong reduction of social contact. As $k \to \infty$, individual behavior converges to the effortless parameter $n(t) = 1$, and the infection curve approaches that of the classical SIR model (see dashed curve in Fig. 4.4).

4.3.3 MFG on heterogeneous networks

In this section, we examine the behavior of the Nash equilibrium on heterogeneous networks in order to apply our MFG framework on a more realistic scenario. The characteristics of the network are as follows: first, we use an uncorrelated network, meaning that $G_{kk'} = P(k')k'/\langle k \rangle$ is independent of k. Although we know that realistic social contact networks tend to be assortative, we were unable to find a satisfactory analytical description

of the associated correlation matrix in the literature. However, any specific correlation matrix can easily be implemented, and the system we derived works for any $G_{kk'}$. Interested reader can refer to the paper in App. F in which we found a way to implement a realistic assortativity.

Regarding the degree distribution, the work of Eubank *et al.* [36] highlights that degree distributions follow a piecewise power-law distribution. For realistic measures, we based the degree distribution on Béraud *et al.* [181], who conducted extensive surveys to infer the French social contact network. Initially in [181], $P(k)$ increases from $k = 1$ or $k = 2$ to a maximum at $k_{\text{peak}} \simeq 5$. Then, as shown in [197], $P(k)$ decreases in two phases, following a power law. We chose the critical degrees and coefficients to align with the observations made by Béraud *et al.* [181]. The average number of contacts per day is given by

$$P(k) \propto \begin{cases} k^{1} & 2 \leq k \leq 5 \\ k^{-1.5} & 5 \leq k \leq 10 \\ k^{-3} & 10 \leq k \leq 100 \end{cases} , \tag{4.29}$$

where the normalization values are set such that branches coincide at boundaries and the distribution is normalized. We then compute the average degree $\langle k \rangle \simeq 9$ and the standard deviation $\sigma \simeq 10$ to verify that it was coherent with the ones given in [181]. This allows us to consider that our degree distribution is rather typical of a real contact networks, although we still not consider the higher level structure of the network (we did not consider degree correlations between two or more neighbors).

In order to perform the numerical simulations in reasonable time scales (see Sec. 6.3.3), we split our distribution $P(k)$ in n_b batches:

$$\mathcal{B}_i = \left[\tilde{k}_i, \tilde{k}_{i+1}\right[\quad , \quad i = 1, ..., n_b \quad , \tag{4.30}$$

where the variables $\tilde{k}_1, ..., \tilde{k}_{n_b+1}$ allow to define the degree boundaries of the batches. They are chosen such that

$$\sum_{k=\tilde{k}_i}^{\tilde{k}_{i+1}-1} P(k) \simeq \frac{1}{n_b} \quad , \tag{4.31}$$

meaning that the proportion of nodes in each batch is approximately identical. Inside each batch, we treat all the degrees k equivalently, using the averaged K_i of the batch $\mathcal{B}_i$ and its associated probability $\tilde{P}(K_i)$:

$$K_i = \sum_{k=\tilde{k}_i}^{\tilde{k}_{i+1}-1} kP(k) \quad , \qquad \tilde{P}(K_i) = \sum_{k=\tilde{k}_i}^{\tilde{k}_{i+1}-1} P(k) \quad . \tag{4.32}$$

Thus, our distribution $P(k)$ of maximum degree $k_{\max}$ is transformed into a distribution $\tilde{P}(K)$ composed of n_b different batches which have degrees K. Similarly, the correlation 100×100 uncorrelated matrix $G_{kk'}$ is transformed into a 5×5 uncorrelated matrix $G_{KK'}$. We summarize in Table 4.2 the choice we made for the batch distribution that we will use throughout our work on heterogeneous networks. We show in App. B.3 that the error associated with this approximation is reasonably small.

Interval $[\tilde{k}_i, \tilde{k}_{i+1}[$	($[2,5[, [5,7[, [7,10[, [10,19[, [19,100]$)
Average K	(3.2, 5.4, 7.8, 12.5, 31.2)
Distribution $\tilde{P}(K)$	(0.26, 0.25, 0.22, 0.20, 0.07)

Table 4.2: Parameters of the batches used to simulate our heterogeneous network of degree distribution $P(k)$ described in Eq. (4.29). We took $n_b = 5$ batches with the following form for each batch: $\mathcal{B}_i = ([\tilde{k}_i, \tilde{k}_{i+1}[, K_i, \tilde{P}(K_i))$.

The dynamics of the epidemics and the associated effort parameters at the Nash equilibrium are obtained by solving Eqs. (4.21)–(4.26). We assume that $G^{xy}_{kk'}(0) = X_k(0)G_{kk'}$, which indicates that there is no correlation between states and degrees at time $t = 0$. The results are displayed in Fig. 4.5 for the two different choices of f^{ϵ}_k. The specific impact of a realistic distribution, together with the interactions between classes (heterogeneity), can be captured. In all cases, we observe that, contrary to what might be expected, the spread, as a function of k, of the total number of infected at T (inset panel) increases compared to the homogeneous case. This is related to the collective immunity that is now achieved at the network level (and not for each degree class as in the homogeneous case). This essentially means that very high-degree individuals cannot really avoid the disease, since they are infected before all other classes. For them, applying a strong social distancing would only delay the infection peak, but would not lead to heard immunity. Then, the epidemic continues to spread in the network even though all high-degree individuals have been infected, since they represent a very small fraction of all nodes. On the other hand, low degree individuals take advantage of this situation and reach a collective immunity with a rate I_k below that required in the homogeneous case. In fact, more than the proportion of infected individuals among high-degree individuals, the average degree of the remaining susceptible nodes decreases rapidly, which helps achieve herd immunity.

Differences in infection rates result in infection curves that strongly depend on the degree. For $\epsilon = 1$ (Fig. 4.5, upper row), interactions between classes tend to synchronize the epidemic peak times which occur in a very narrow period, with differences regarding the intensity of the curves. This results in effort parameters which display similar patterns between degree classes with differences for the intensity only. The "reverse anticipation" effect can clearly be observed here also.

For $\epsilon = 0$ (Fig. 4.5, lower row), two categories emerge: first, very high-degree individuals ($K = 31.2$) has a particular infection curve compare to others, which lead them to an high probability of infection - it is almost impossible for them to avoid the disease. The remaining susceptible individuals of such degree employ a specific strategy with a constant effort to protect themselves once the epidemic peak is behind them (note that the epidemics curves are only display in $[0, 10]$ time to ensure the readability of the curves). The second category regards all other individuals which act in a more homogeneous manner: infections curves and effort parameters display similar patterns among degrees, with low-degree individuals which tend to act less to protect themselves, while benefiting from the collective immunity achieved by others and get a low final infection probability (e.g $\phi(T) < 0.5$ for $K = 3.2$). In this case, we observe a long tail for the decrease of effort parameters because of the infection dynamics which remain non negligible for a long time.

Nevertheless, thanks to high the infection rate of high-degree individuals, this tail is shorter than for homogeneous networks.

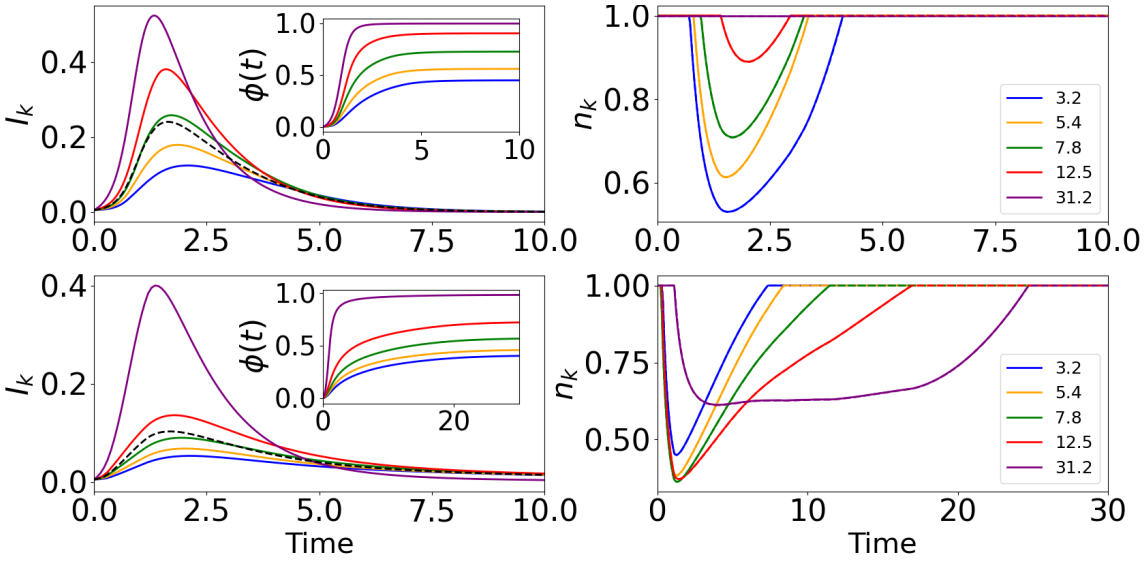

Figure 4.5: Left panels: Dynamics of infected individuals at Nash equilibrium for different batches, with the parameters of Tables 4.1 and 4.2. Inset: dynamics of the probability $\phi(t)$ to be infected before t. Right panels: Dynamics of the corresponding individual effort parameter. Colored solid lines corresponds to the dynamics (for infected and effort parameter) associated with each batch of the network: $K = 3.4$ (blue), 5.4 (orange), 7.8 (green), 12.5 (red), 31.2 (purple). Each row represents a specific choice of f_k^ϵ: $\epsilon = 1, 0$ for the first and second row, respectively. Dashed lines (right panels) correspond to the best individual response in a population which follow the solid lines strategies. They perfectly match solid lines, meaning that we have reached a Nash equilibrium of our MFG system (it is a check of the self-consistent equation (4.26)).

4.3.4 Discussion

In this chapter, we refined our understanding of how the Nash equilibrium, resulting from individual decisions, is influenced by the cost of social contact reduction, f_k, when occurring on networks. This work complements our findings in Chapter 3, where individuals were classified by age, creating differences in their infection costs. Unlike the age classification, which only marginally impacts epidemic dynamics in the absence of an outbreak (as seen in the "Business as Usual" plot in Fig. 3.4), the degree of connectivity plays a significant role in shaping the epidemic dynamics itself. Specifically, an epidemic spreads more rapidly and intensely among individuals with higher connectivity. Thus, there is a balance between this effect and the dependence of f_k on k.

In the first configuration, when f_k increases with k, the two effects act oppositely, resulting in a threshold k^* below which slow epidemic dynamics discourage individuals from exerting effort due to low associated infection risk. Above this threshold, high costs of f_k prompt individuals to accept the risk, as reducing social contacts becomes prohibitively expensive. Thus, the absolute value of efforts are peaked around k^*.

When f_k remains constant with respect to k, the observed differences in dynamics among the batches within the network are solely due to their inherent characteristics and therefore individuals of high-degree, who are more at risk of infection, will tend to act with an higher intensity (see homogeneous case, Fig. 4.4). Interestingly, we observe a specific regime in the heterogeneous case for high-degree individual for which important efforts during the epidemic peak will not be efficient as they are for others, because the epidemic

is already too virulent. Instead, remaining susceptible individuals will do efforts after the epidemic peak to try to avoid infection once the collective immunity is in sight.

Thus, our MFG approach to networks highlights the "reverse anticipation" effect, where individuals adjust their behavior in anticipation of the end of the epidemic - a phenomenon likely to be observed in contexts other than networks. This anticipation can be brief, as in the case of increasing social costs with k, or have a long tail, as in the case of constant social costs, when efforts effectively reduce the probability of infection without being too costly. The introduction of heterogeneity in a realistic network leads to differentiated collective immunity at the node level: low-degree individuals benefit from the fast spreading of the epidemic among high-degree individuals, which reduces the effective connectivity of the remaining susceptible network. Contrary to expectations, heterogeneity reduces costs for low-degree individuals.

It is essential to note that our analysis was conducted using a realistic degree distribution $P(k)$; however, we have not accounted for significant features such as degree correlations, which are characteristic of real-world networks known to be assortative (in contrast to the uncorrelated network considered here). This assortativity is expected to homogenize the network and thus to decrease the discrepancy between degree classes, as the network will be more homogeneous from the point of view of individuals. To be concrete, links between low and high degree nodes will be less present whereas they was helping low degree to avoid infection.

The insights derived from this study should be viewed at a general viewpoint: a precise characterization of individuals, whether by age or degree, is crucial for understanding their behaviors, as these factors influence how they are affected by the epidemic and their sensitivity to associated costs.

This achieves our second project of this thesis, which, chronologically, was the third to be undertaken. In our progression toward developing MFG on networks, we became particularly interested in the Pairwise Approximation discussed in this chapter. The investigation of this approximation on random homogeneous networks led us to an unexpected but productive avenue for discovering new analytical solutions. This third project, which leaves the MFG approach, is presented in the following chapter.

5 - Analytical results on random homogeneous networks

In our way to implement the Mean-Field Games paradigm on networks, we first derived and concentrated on the degree pairwise approximation Eq. (4.13). After checking that the numerical results were according with the numerical simulations, we investigated the analytical resolution of such system, before any MFG implementation. Indeed, despite their success, most of network models so far lack one important feature which is the existence of analytical solutions for the models' equations. The importance and usefulness of these analytical results should not be underrated, as they provide a much deeper understanding of the mechanisms at work than can be achieved numerically. Moreover, they constitute a benchmark for more complex models where no analytical solution is available. Our goal here is to provide such analytical results in the case of random homogeneous networks, which are characterized by their constant connectivity k (also called regular networks). For any given value of k we obtain analytic expressions analogous to (and in some circumstances stronger than) the ones existing for the SIR model Eq. (1.7); when $k = 2$ or 3 we obtain simple explicit expressions, while in the limit $k \to \infty$ we recover the basic SIR, leading to some new physical insight as well as some useful approximations of this well-known model. This chapter is organized as follows. In Sec. 5.1, we derive the (implicit) analytical solution of the SIR model on random homogeneous networks. We then study the impact of our results on the epidemic threshold, and the case of a small number of neighbors, which provides more explicit expressions. In Sec. 5.2, we focus on the limiting case $k \to \infty$ to derive the exact solution of the SIR model. We then derive some significant approximations with simpler expressions, and finally study the consequences of our results on the epidemic's peak time. Finally, concluding remarks are gathered in Sec. 5.3.

This work corresponds to the third and last original project of this thesis. This chapter follows, for a large part, the paper we published on this subject [178]. Reader can refer to this paper for a more comprehensive and detailed presentation, including the appendices.

5.1 Analytics results for homogeneous networks

In this section, we first present the SIR equations for the degree pairwise approximation on a random homogeneous network that we aim to solve analytically in Sec. 5.1.1. We then derive the general analytical expression of this system in Sec. 5.1.2. Subsequently, we analyse these results, first regarding the mathematical consequences, with the derivation of the epidemic threshold in Sec. 5.1.3, and second through the small neighbors case in Sec. 5.1.4 where explicit expressions are available.

5.1.1 Presentation of the system to solve

In the case of random homogeneous networks of degree k, the degree pairwise approximation Eq. (4.13) straightforwardly reduces to

$$\dot{S} = -\lambda k G^{si} S \tag{5.1a}$$

$$\dot{I} = \lambda k G^{si} S - \gamma I \tag{5.1b}$$

$$\dot{R} = \gamma I \ , \tag{5.1c}$$

with $S(t) + I(t) + R(t) = 1$. Here $G^{si}(t)$ corresponds to the probability that a neighbor of a given susceptible individual is itself infected; thus $kG^{si}(t)$ is the average number of

infected individuals in the neighborhood of a susceptible individual. The time dependence of these two-point correlators is given by (see Eq. (4.17))

$$[S\dot{G}^{ss}] = -2SG^{ss}(k-1)G^{si}\lambda \tag{5.2a}$$

$$[S\dot{G}^{si}] = SG^{ss}(k-1)G^{si}\lambda - SG^{si}\left[(k-1)G^{si}+1\right]\lambda - \gamma SG^{si} \tag{5.2b}$$

$$[S\dot{G}^{sr}] = \gamma SG^{si} - SG^{sr}(k-1)G^{si}\lambda\,. \tag{5.2c}$$

In the case of homogeneous networks with a large number of nodes $N \to \infty$, as we consider here, the fraction of loops with arbitrary finite size vanishes [198, 199, 200]. Therefore the correlations beyond two-point ones can be neglected and the degree pairwise approximation becomes exact in this limit [201]. Equations (5.1)-(5.2) form what we will call the "SIR-k model" in the following. In Fig. 5.1 (left inset), we demonstrate the accuracy of our approximation by comparing a numerical solution of Eqs. (5.1)-(5.2) with a Markovian evolution of a population according to the same dynamics. The parameters of our problem are S_0 the initial proportion of susceptible agents, k the number of neighbors, $\beta = \lambda k$ the contagiousness and γ the recovery rate, which leads to a dimensionless quantity $\mu = \gamma/\beta$ driving the epidemic, while β only changes the time scale (see for example [202]).

5.1.2 General analytical expression

From Eqs (5.1)-(5.2), we can obtain an ordinary differential equation involving only $S(t)$. Inserting $G^{si} = -\dot{S}/(\beta S)$, which we get from Eq. (5.1a), into Eq. (5.2a), we have

$$\frac{[S\dot{G}^{ss}]}{SG^{ss}} = 2\frac{k-1}{k}\frac{\dot{S}}{S}\,. \tag{5.3}$$

At $t = 0$, $S(0) = S_0 = G^{ss}(0)$ if we assume that there are no correlations at time 0 (i.e. the neighborhood of infected and susceptible individuals is the same). Then Eq. (5.3) can be integrated as $G^{ss} = S_0^{\frac{2}{k}} S^{1-\frac{2}{k}}$. Using Eq. (5.1a) and this expression for G^{ss}, Eq. (5.2b) yields

$$\ddot{S} = \lambda S_0^{\frac{2}{k}} S^{1-\frac{2}{k}}(k-1)\dot{S} + \frac{k-1}{k}\frac{\dot{S}}{S} - (\gamma+\lambda)\dot{S}. \tag{5.4}$$

This is a second-order differential equation in S that we need to integrate twice. A first integration is obtained by dividing Eq. (5.4) by $\dot{S}$ and introducing $\varphi(S) = \dot{S}$, which verifies

$$\frac{d\varphi(S)}{dS} = \lambda S_0^{\frac{2}{k}} S^{1-\frac{2}{k}}(k-1) + \frac{k-1}{k}\frac{\varphi(S)}{S} - (\gamma+\lambda)\,. \tag{5.5}$$

Equation (5.5) can be integrated as an equation in the variable S to give

$$\varphi(S) = kS_0^{2/k}\lambda S^{2(1-\frac{1}{k})} - k(\lambda+\gamma)S + C_1 S^{1-\frac{1}{k}}\,, \tag{5.6}$$

where C_1 is given by the initial conditions: $C_1 = \dot{S}(0)S_0^{-1+1/k} - \lambda k S_0^{1+1/k} + k(\lambda+\gamma)S_0^{1/k}$. Using $\dot{S}(0) = -\lambda k S_0(1-S_0)$, this constant reduces to $C_1 = k\gamma S_0^{1/k}$. Changing to the variable $z \equiv (S/S_0)^{\frac{1}{k}}$, and using $\mu = \gamma/\beta$, we obtain

$$\dot{z} = \lambda P(z)\,, \qquad P(z) = S_0 z^{k-1} - (k\mu+1)z + k\mu\,. \tag{5.7}$$

Separating the variables z and t and using the partial fraction decomposition of $1/P(z)$ in terms of the roots z_j $(j = 0, \cdots, k-2)$ of $P(z)$, the integral of Eq. (5.7) becomes

$$\int_1^z \frac{dz'}{P(z')} = \sum_{j=0}^{k-2}\int_1^z \frac{A_j}{z'-z_j}dz' = \lambda t\,, \tag{5.8}$$

with

$$A_j = \frac{1}{P'(z_j)} = \frac{1}{\prod_{l\neq j}(z_j - z_l)} \,. \tag{5.9}$$

Equation (5.8) readily gives an explicit expression for t as a function of S as

$$t(S) = \frac{1}{\lambda}\sum_{j=0}^{k-2} A_j \log\left(\frac{(S/S_0)^{1/k} - z_j}{1 - z_j}\right) \,. \tag{5.10}$$

Note that the complex roots z_j are pairwise complex conjugate so that the whole sum is real, as it should. One then gets a parametric solution for the number of infected individuals under the form $(t(S), I(S))$ by integrating Eq. (5.1b). Indeed, since $S(t)$ is monotonous, Eq. (5.1b) can be rewritten

$$\frac{dI}{dS} = -1 - \gamma I \frac{dt}{dS} \,, \tag{5.11}$$

which upon integration yields

$$I(S) = \left(1 - S_0 - \int_{S_0}^{S} e^{\gamma t(s')} ds'\right) e^{-\gamma t(S)} \,. \tag{5.12}$$

The maximum of I corresponds to the value of S where $dI/dS = 0$, that is,

$$I(S)\frac{dt}{dS} = -\frac{1}{\gamma} \,, \tag{5.13}$$

with $t(S)$ explicitly given by Eq. (5.10), while the calculation of $I(S)$ involves a single numerical integral over S.

We checked, for many different values of the parameters (S_0, μ, k), that the analytical solution Eq. (5.10) perfectly reproduces the numerical resolution of Eqs. (5.1)-(5.2), and we illustrate it for one example in Fig. 5.1. Note that a similar approach allows to address the SI model, which corresponds to the limit $\mu \to 0$; in that case we get

$$S(t) = S_0^{-\frac{2}{k-2}} \left(\frac{1 - S_0}{S_0} e^{\lambda(k-2)t} + 1\right)^{-\frac{k}{k-2}} \,, \tag{5.14}$$

which in the limit $k \to \infty$ coincides with the known solution of the SI model [203].

5.1.3 Epidemic threshold

We now comment on the consequences of Eq. (5.10). Polynomials such as $P(z)$ in Eq. (5.7) have a long history, dating back to Lambert [204, 205] and Euler [206]. In particular, one can explicitly express all the roots z_j as infinite series (see [207, 208]). As illustrated in Fig. 5.2A, for $k > 2$ there are two real positive roots, $z_0 \in [0, 1]$ and $z_1 \in [1, \infty[$. Since $S/S_0 \in [0, 1]$, the only possible divergence of t in Eq. (5.10) corresponds to the root z_0, and we thus get that $S_\infty \equiv \lim_{t\to\infty} S(t) = S_0 z_0^k$. A useful quantity for public agencies in charge of controlling the epidemic (see [209] for the basic SIR model) is the fraction of the population which will be infected during the course of the epidemic; it can be expressed as $\mathcal{I}_{\text{tot}}^{(k)} = S_0 - S_\infty = S_0(1 - z_0^k)$. The second positive real root z_1 can then be interpreted as the non-physical limit to which S would tend if one follows the SIR-k equations for negative times, $S_{-\infty} \equiv \lim_{t\to-\infty} S(t) = S_0 z_1^k > 1$. As illustrated in Fig. 5.2C, the associated quantity $z(t) = (S(t)/S_0)^{1/k}$ decreases from 1 to z_0 for $t \in [0, +\infty[$, and from z_1 to 1 for the non-physical part $t \in]-\infty, 0]$.

Whatever the value of μ and k, $P(1) = S_0 - 1$. Thus, as illustrated in Fig. 5.2D, $z = 1$ cannot be a root of $P(z)$ for $S_0 < 1$, but always is for $S_0 = 1$. In this latter case, two situations can occur. The first one would be that $z_1 = 1$ and $z_0 < 1$, in which case an

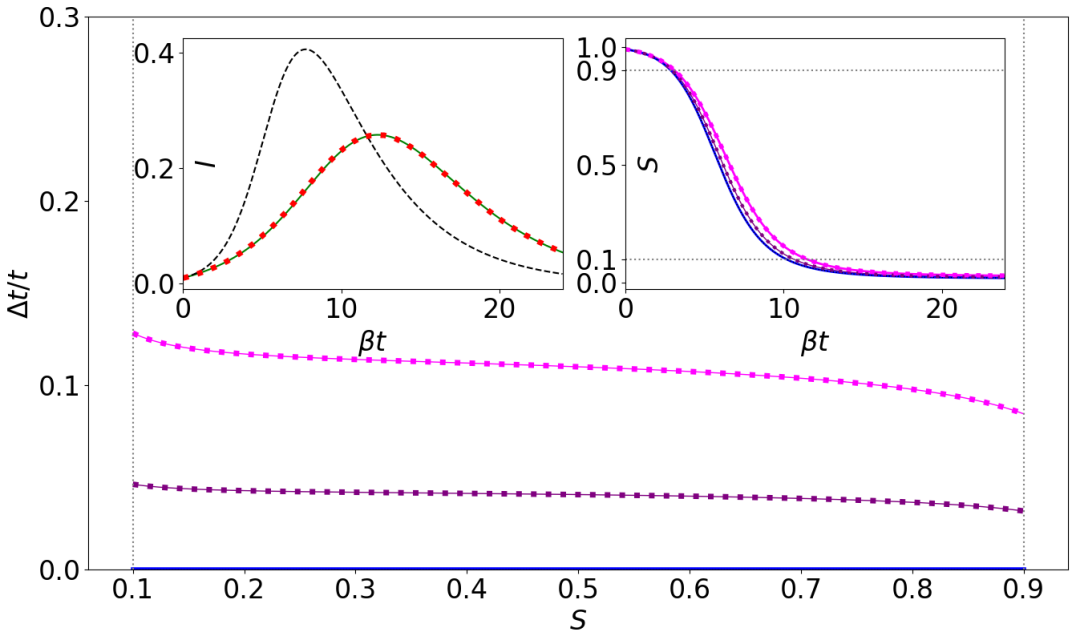

Figure 5.1: Main panel: Time delay $\Delta t = t(S) - t_{\rm SIR}(S)$ with $t_{\rm SIR}$ obtained by numerically solving Eq. (1.7). Solid thick dark blue: analytical expression Eq. (5.25), corresponding to the limit case SIR-∞, yielding 0 as expected. Purple ($k = 50$) and magenta ($k = 20$) plots: numerical resolution of the SIR-k model Eq. (5.1) (solid lines) and corresponding analytical solution Eq. (5.10) (dots). Right inset: proportion of susceptible $S(t)$ for the same configurations. The gray horizontal dotted lines indicate the range of S values taken for the main panel. Left inset: proportion of infected $I(t)$ for $k = 5$. Red dotted line: numerical resolution of the SIR-5 model Eqs. (5.1)-(5.2); green solid line: average over 100 realizations of the Markovian process of an epidemic on a large homogeneous network of degree $k = 5$, with $N = 3000$ nodes (with random initial infected nodes); black dashed line: basic SIR model with $\beta = \lambda k$. Parameters are $\mu = 0.25$, $S_0 = 0.99$.

epidemic starting with $S_0 = 1$ (i.e. with an infinitesimal fraction of infected individuals) will eventually propagate into the network and infect a finite fraction of the population. Introducing the time t_0 corresponding to the constant term in Eq. (5.10), namely

$$t_0 = -\frac{1}{\lambda}\sum_{j=0}^{k-2} A_j \log|z_j - 1| \underset{S_0\to 1}{\sim} \frac{\log(1-S_0)}{\lambda(2+k(\mu-1))}\,, \tag{5.15}$$

we see that $\lim_{S_0\to 1} t_0 = \infty$. This expresses the fact that the beginning of the epidemic takes an infinite amount of time as the initial proportion of infected individuals goes to zero. The other possibility, $z_0 = 1$ and $z_1 \geq 1$, corresponds to $S_\infty = 1$: an epidemic starting with $S_0 = 1$ does not propagate. The value μ_k^* of the parameter μ corresponding to the transition between these two regimes is the threshold beyond which, for $S_0 = 1$, the epidemic does not spread. At the threshold, $z = 1$ is a double root of $P(z)$ and thus $\mu_k^* = (k-2)/k$[1]. As $k \to \infty$ we get $\mu_k^* \to 1$, which coincides with the result of Kermack and McKendrick [175] for the original SIR model.

5.1.4 Small number of neighbors

It is possible to invert the expression Eq. (5.10) for $k = 2$ and 3. Consider first the case $k = 2$. A random network of size N then corresponds to a set of disconnected loops

[1]This expression for the threshold can also be derived from the results in section III.C of [50]

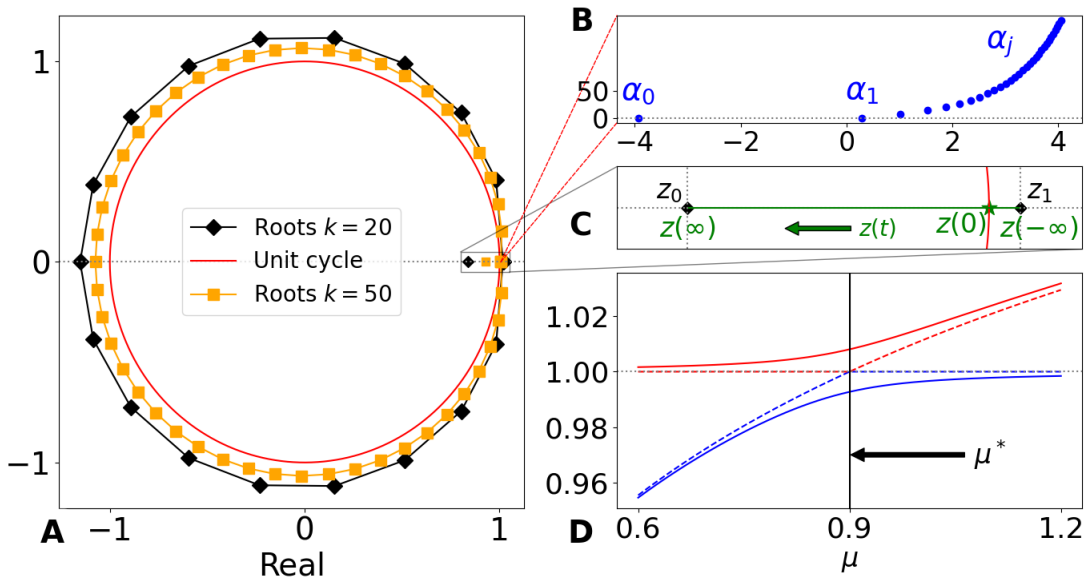

Figure 5.2: **A**. Orange squares (resp. black diamonds): location, in the complex plane, of the roots of the polynomial $P(z)$ Eq. (5.7) for $k = 50$ (resp. $k = 20$) with $S_0 = 0.8$ and $\mu = 0.25$ **B** Blow-up showing, in the complex plane, the limit as $k \to \infty$ of the α_j defined by $z_j = 1 + \alpha_j/k$. The complex z_j (and thus the complex α_j) come in conjugate pairs. **C** Zoom on the complex plane close to 1 with $z(t) = (S(t)/S_0)^{1/k}$ traveling the green line from $z_1 = z(-\infty)$ to $z_0 = z(\infty)$ and passing through $z(0) = 1$. **D** Blue line (resp. red line): illustration, for $k = 20$, of the variation with μ of the roots $z_0(\mu)$ (resp. $z_1(\mu)$) for $S_0 = 0.99$ (solid line) and $S_0 = 1$ (dashed line). The value μ_k^* such that $z_0(\mu_k^*) = z_1(\mu_k^*) = 1$ is the epidemic threshold.

of different sizes. In the $N \to \infty$ limit, however, all but a negligible proportion of agents would belong to a large loop, and the average quantities we consider here, for example in Eqs. (5.1)–(5.2), behave in the same way within a random network or within a single connected loop. Furthermore, there is only one root $z_0 = 2\mu/(I_0 + 2\mu)$, with $I_0 = 1 - S_0$ the initial fraction of infected individuals. We can therefore write Eq. (5.10) as

$$t(S) = \frac{1}{\lambda} A_0 \log\left(\frac{(S/S_0)^{1/2} - z_0}{1 - z_0}\right) , \tag{5.16}$$

with $A_0 = -1/(I_0 + 2\mu) < 0$. Inverting Eq. (5.16) we get

$$S(t) = S_0 \left[1 + \frac{I_0\left(e^{-t/\tau} - 1\right)}{I_0 + 2\mu}\right]^2 , \ \tau = \frac{1}{\lambda(2\mu + I_0)} . \tag{5.17}$$

$S(t)$ thus follows an exponential decay with rate τ and converges to $S_\infty = S_0 z_0^2$, as expected. We get $\mathcal{I}_{\text{tot}}^{(2)} = S_0\left(1 - (1 - I_0/(2\mu))^{-2}\right)$, which varies from S_0 for strong epidemic $I_0/\mu \gg 1$ to 0 with $I_0/\mu \ll 1$. In particular $\lim_{S_0 \to 1} \mathcal{I}_{\text{tot}}^{(2)} = 0$ for any positive value of μ, which can also be seen from the fact that $\mu_2^* = (k-2)/k = 0$. This is unique to the $k = 2$ case because of its essentially 1d geometry, which implies that the number of infected agents caused by a single "patient zero" is necessarily finite.

For the case $k = 3$, we get $P(z) = S_0 z^2 - (3\mu + 1)z + 3\mu$, which has two (real positive) roots

$$z_{0,1} = \frac{1}{2S_0}\left[(3\mu + 1) \pm \sqrt{(3\mu + 1)^2 - 12\mu S_0}\right] , \tag{5.18}$$

yielding

$$t(S) = \frac{A_0}{\lambda} \log \left[\frac{\left((S/S_0)^{1/3} - z_0\right)(1 - z_1)}{\left((S/S_0)^{1/3} - z_1\right)(1 - z_0)} \right] , \tag{5.19}$$

where we have used that $A_1 = -A_0 = 1/(z_1 - z_0)$. We can invert Eq. (5.19) to get

$$S(t) = S_0 \left(\frac{z_0 - z_1 B e^{\lambda(z_0 - z_1)t}}{1 - B e^{\lambda(z_0 - z_1)t}} \right)^3 , \quad B = \frac{1 - z_0}{1 - z_1} . \tag{5.20}$$

As expected, this expression verifies that $S(0) = S_0$ and $S_\infty = S_0 z_0^3$. The explicit expression for $\mathcal{I}_{\text{tot}}^{(3)}$ is $S_0 - \frac{1}{8S_0^2}\left[(3\mu+1) + \sqrt{(3\mu+1)^2 - 12\mu S_0}\right]^3$. For $S_0 = 1$, the roots simplify to $z_0 = \min(1, 3\mu)$, $z_1 = \max(1, 3\mu)$, and we recover $\mu_3^* = \frac{1}{3}$; for $\mu < \mu_3^*$, $\mathcal{I}_{\text{tot}}^{(3)} = 1 - (3\mu)^3$, while for $\mu \geq \mu_3^*$ the epidemic does not propagate as $S_\infty = 1$.

Finally, we consider the case $k = 4$, but limiting ourselves for simplicity to the limit $S_0 \to 1$ and the regime $\mu < \mu_4^* = 1/2$. In that case $P(z)$ has three roots, which, introducing $\kappa = \sqrt{1/4 + 4\mu}$, can be written as $z_0 = \kappa - \frac{1}{2}, z_1 = 1, z_2 = -\kappa - \frac{1}{2}$ with furthermore $A_0 = [\kappa(2\kappa+3)]^{-1}, A_1 = [2 - 4\mu]^{-1}, A_2 = [\kappa(2\kappa - 3)]^{-1}$. The epidemics propagates only if $z_0 < 1$, that is if $\mu < \mu_4^* = 1/2$, in which case, scaling out the time t_0 introduced in Eq. (5.15), the dynamics is described by

$$t - t_0 = \frac{1}{\kappa\lambda} \sum_{\epsilon = \pm 1} \left(\frac{1}{2\kappa + 3\epsilon} \log \left| \frac{S^{1/k} + \epsilon\kappa + \frac{1}{2}}{S^{1/k} - 1} \right| \right) , \tag{5.21}$$

and $\mathcal{I}_{\text{tot}}^{(4)} = (-16\mu^2 - 8\mu + 1/2) + (1 + 8\mu)\sqrt{4\mu + 1/4}$ (which is indeed such that $\mathcal{I}_{\text{tot}}^{(4)}(\mu_4^*) = 0$).

This expression illustrates how the complexity of the solution for $t(S)$ grows with increasing k. The case $k = 4$ is the first instance where the solution becomes non-invertible, and we observe how quickly the expressions for the roots z_j and $\mathcal{I}_{\text{tot}}^{(k)}$ become complicated. However, the large k limit remains somewhat manageable, as it converges to the well-known SIR model. The corresponding results are presented below.

5.2 Large-k limit of the SIR-k model

Another interesting limit of the SIR-k model is $k \to \infty$, through which we recover the original SIR model, but with a new point of view. In Sec. 5.2.1 we derive a new formulation of an analytical exact expression of $t(S)$ for the basic SIR model. Then, in Sec. 5.2.2, we present useful approximations for $t(S)$: a first one in the regime of μ close to 1, which appears to be valid broadly with a great accuracy. The second one regards explicit expressions of the analytical formulation for three different regimes of μ: $\mu \to 0$, intermediate μ and $\mu \to 1$. These expressions are less precise than the previous approximation but they come with direct dependencies of $t(S)$. From these approximations, explicit expressions of the epidemic peak time are derived and investigated in Sec. 5.2.3 for the three different regimes of μ.

5.2.1 Exact expression

As illustrated in Fig. 5.2A, z_0 and z_1 converge to 1 (from below and from above respectively) and all the other roots converge to the unit circle in the complex plane. This can be understood from their series expansion in [207, 208]. Using that z_j is a root of $P(z)$ we can write the factor A_j defined in Eq. (5.9) as

$$A_j = \left[(k-1)k\mu \frac{z_j - 1}{z_j} - k(\mu - 1) - 2 \right]^{-1} . \tag{5.22}$$

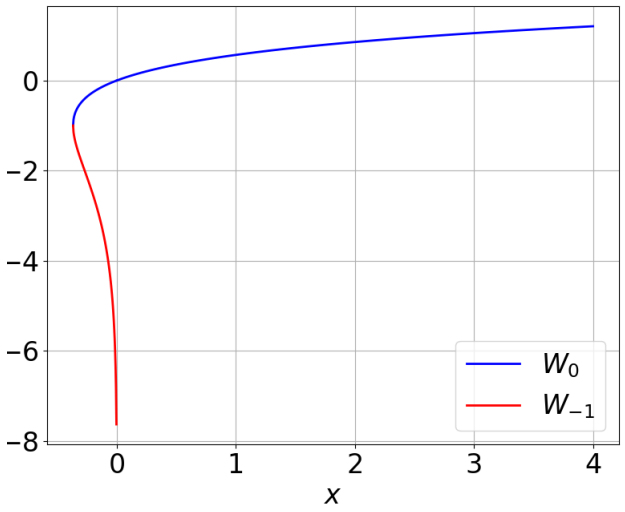

Figure 5.3: Two real branches (0 in blue and -1 in red) of the Lambert W function, related to Euler T function with the relation $W_j(z) = -T_j(-z)$. The two branches coincide at their left boundary in $z = 1/e$ with $W_0(-1/e) = W_{-1}(-1/e) = -1$. In our context, this point corresponds to the coincidence of the two roots $z_0 = z_1 = 1$ when $\mu = 1$ and $S_0 = 1$.

For most roots of $P(z)$, $z_j - 1 = O(k^0)$ (we refer to them as "far from one") and thus $A_j = O(k^{-2})$. It is only for the roots close to one, and more precisely such that $z_j - 1 = O(k^{-1})$, that $A_j = O(k^{-1})$. In the same way, the logarithm factors are $O(k^{-1})$ for the roots far from one and $O(k^0)$ for the roots close to one. In Eq. (5.10), noting that $\lambda^{-1} = k\beta^{-1}$, we see that the sum over roots far from one involves $O(k)$ terms of order $O(k^{-2})$ and has therefore a negligible $O(k^{-1})$ contribution, whereas each root close to one has an $O(k^0)$ contribution. We can thus write all relevant roots as $z_j = 1 + \alpha_j/k$ where α_j reaches a constant value as $k \to \infty$. Writing that z_j is a root of $P(z)$ thus reads

$$S_0 \left(1 + \frac{\alpha_j}{k}\right)^{k-1} = k\mu \left[\left(1 + \frac{1}{k\mu}\right)\left(1 + \frac{\alpha_j}{k}\right) - 1\right] \tag{5.23}$$

which, taking the limit $k \to \infty$ on both sides (with α_j now corresponding to that limit), gives $\exp(\alpha_j) = (\mu/S_0)\,(1/\mu + \alpha_j)$. Defining now $\gamma_j = \alpha_j + 1/\mu$ and $\chi = (S_0/\mu)e^{-1/\mu}$, we get

$$\chi = \gamma_j \exp(-\gamma_j)\ . \tag{5.24}$$

Equation (5.24) can be rewritten in terms of the Euler T function (see [205] for mathematical details) as $\gamma_j = T(\chi)$. The T function has two real branches T_0 and T_{-1} which correspond to the two positive real roots of $P(z)$ (the shape of T is illustrated in Fig. 5.3)), and an infinite number of complex branches corresponding to the complex numbers γ_j. In particular we get for the first root $\lim_{k\to\infty} S_\infty = \mu T_0(\chi)$, which is equivalent to the well-known self-consistent equation $S_\infty = 1 + \mu \ln(S_\infty/S_0)$ given for instance in [34]. Taking the large-k limit in Eq. (5.22) and Eq. (5.10), together with $\beta = \lambda k$ and the expression of the relevant $z_j = 1 + \frac{\alpha_j}{k}$, leads to

$$\begin{aligned} \beta\, t(S) &= \frac{1}{\mu} \sum_{j=-\infty}^{\infty} \frac{1}{\alpha_j + 1/\mu - 1} \log\left(1 + \frac{\log(S_0/S)}{\alpha_j}\right)\ , \\ \alpha_j &= T_{-j}(\chi) - 1/\mu\ , \end{aligned} \tag{5.25}$$

where the complex quantities α_j are pairwise complex conjugate (T_{-2} is conjugate with T_1, T_{-3} with T_2, etc) so that the whole sum is real. In Fig. 5.1 we check the accuracy of this expression.

5.2.2 Approximate expression for $t(S)$

An implicit analytical solution $t(S)$ for the SIR model is known in the literature and takes the form of an integral (see for instance [26]). Our formula Eq. (5.25) is an alternative expression for $t(S)$ and comes with interesting new insights, as it depends on quantities α_j which have an explicit expression. In Fig. 5.2B we show the first terms of the sequence. We see that $\alpha_0 < 0$ and $\alpha_1 > 0$ are indeed the two unique real values, while the subsequent α_j are purely complex; the latter are well approximated by $\alpha_j \simeq 2\pi i j$ for large (possibly negative) j as the roots z_j converge to the unit circle $\exp\left(\frac{2\pi i j}{k-2}\right)$. Therefore, for m sufficiently large, the contributions of the terms $j \geq m$ of Eq. (5.25) can be approximated by

$$\frac{2}{\mu}\,\mathrm{Re}\left[\sum_{j=m}^{\infty}\frac{\log\left(1-\frac{1}{\alpha_j}\log(S/S_0)\right)}{\alpha_j+1/\mu-1}\right] \simeq -\frac{2\log\left(S/S_0\right)}{(2\pi)^2\mu}\int_m^{\infty}\frac{1}{\alpha_j^2}dj \simeq \frac{2\log\left(S/S_0\right)}{(2\pi)^2\mu}\frac{1}{m}\,, \tag{5.26}$$

in which we use that $\alpha_j + 1/\mu - 1 \simeq \alpha_j$ which is valid as long as $2\pi j \gg 1/\mu$, and which becomes quickly negligible as m increases if μ is not too small.

Further understanding of the qualitative behaviour of the sum Eq. (5.25) can be obtained noting that the effective reproduction number $R_{\text{eff}} = S/\mu$ has to be larger than 1 for the epidemic to propagate. One can therefore assume $\mu \in [0,1]$ and S_0 in the interval $[\mu, 1]$. Thus, for μ not too far from 1 and using $\delta\mu = (1-\mu)$ as a small parameter, we can in any case assume $\delta S_0 = (1-S_0) < \delta\mu$. In practice, however, we think of the initial time $t = 0$ as a situation where most agents are susceptible, only a very small fraction is infected , and nobody has recovered yet. In most concrete case, and for essentially all the illustration we shall consider below $\delta S_0 \ll \delta\mu$, and we shall assume that at worse $\delta S_0 = O(\delta\mu^2)$. In that case one can show (App. E.A3) that at all times $\delta S = (1-S) = O(\delta\mu)$, implying also that $\log(S_0/S) = O(\delta\mu)$.

Noting (cf App. E.A) that at $\alpha_0(\mu{=}1) = \alpha_1(\mu{=}1) = 0$, when for $j \geq 2$ $\alpha_j^0 := \alpha_j(\mu{=}1) \neq 0$, this means that the contribution of the two first terms $j = 0, 1$ are $O(\delta\mu^0)$, when all the higher j contributions are $O(\delta\mu)$. We thus have

$$\beta t(S) = \frac{1}{\mu}\left[\sum_{j=0,1}\frac{\log\left(1+\frac{1}{\alpha_j}\log(S_0/S)\right)}{\alpha_j+1/\mu-1} - 2\mathcal{K}^{(0)}\log(S_0/S) + O(\delta\mu^2)\right]\,, \tag{5.27}$$

with $\mathcal{K}^{(0)} := \mathrm{Re}(\sum_{j=2}^{\infty}(\alpha_j^0)^{-2}) \simeq -0.028$ a, fairly small, pure number. As illustrated on Fig. 5.4, the approximation Eq. (5.27) is actually very accurate on a significant portion of the range $[0,1]$, and this range can be even further extended by computing the $O(\delta\mu^2)$ correction to Eq. (5.27) (cf App. E.A).

5.2.3 Epidemic peak time

As mentioned earlier, an important quantity in the context of an epidemics breakout is the epidemic peak time, which, using the fact that, for SIR, the epidemic peak $dI/dt = 0$ implies $S = \mu$, can be obtained as $t_{\text{peak}} = t(S = \mu)$, and for which even a leading order approximation is presumably useful.

For μ sufficiently close to 1 this can be obtained starting from Eq. (5.27), neglecting the $-2\mathcal{K}^{(0)}\log(S_0/S)$ correction, and evaluating α_0 and α_1 to leading order in $\delta\mu$. This calculation is performed in App. E.B. From this we get

$$\beta t_{\text{peak}} \simeq \frac{1}{p}\left[\log\left(1-\frac{\log(S_0/\mu)}{\delta\mu-p}\right) - \log\left(1-\frac{\log(S_0/\mu)}{\delta\mu+p}\right)\right] \tag{5.28}$$

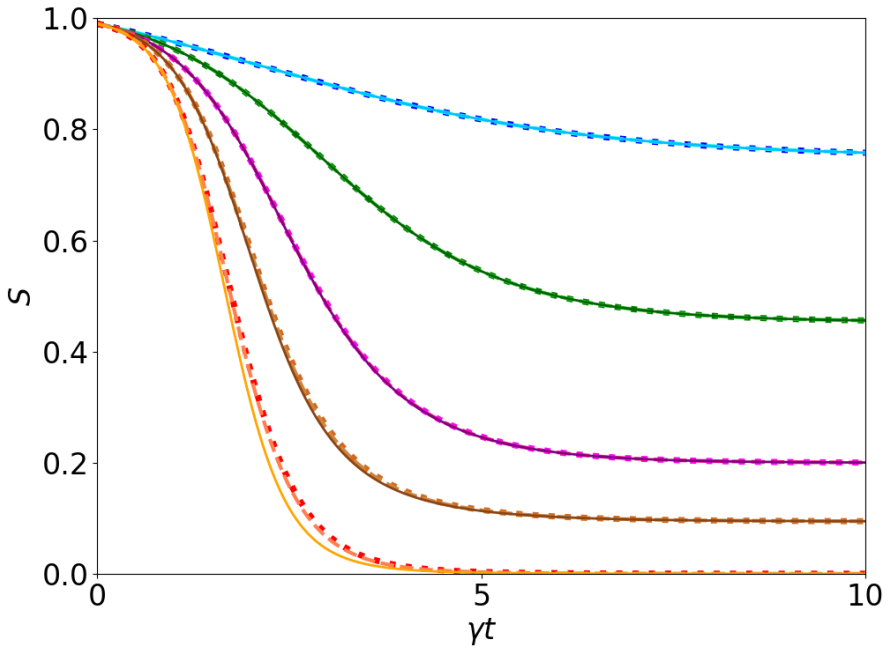

Figure 5.4: Comparison of exact S (solid lines) with approximation Eq. (5.27) at first and second order in $\delta\mu = (1-\mu)$ (dotted and dashed lines respectively). $S_0 = 0.99$ is fixed and μ evolve from 0.1 to 0.9: ($\mu = 0.1$, red), ($\mu = 0.3$, brown), ($\mu = 0.5$, magenta), ($\mu = 0.7$, green), ($\mu = 0.9$, blue). Although Eq. (5.27) is formally an expansion near $\mu = 1$, we see that its validity extends in practice in the whole range of μ, excepted the neighborhood of 0.

with $p = \sqrt{2\delta S_0 + \delta\mu^2}$, valid for $\delta\mu = (1-\mu)$ small ($\delta S_0 = (1-S_0) < \delta\mu$, and possibly $\ll \delta\mu$).

For μ a bit further away from 1, where this approximation starts to degrade, it turns out that a better approximation of t_{peak} can be obtained following the same approach but using the $\mu \to 0$ expansion of α_0 and α_1. We get (see App. E.B2)

$$\beta t_{\text{peak}} \simeq \frac{1}{\mu}\left[\frac{\log\left(1-\frac{\log(\mu/S_0)}{\chi+\chi^2-1/\mu}\right)}{\chi+\chi^2-1} + \frac{\log\left(1-\frac{\log(\mu/S_0)}{(1-S_0)/(S_0-\mu)}\right)}{(1-S_0)/(S_0-\mu)+1/\mu-1}\right], \qquad \chi = (S_0/\mu)e^{-1/\mu}. \tag{5.29}$$

An expansion for $\mu \ll 1$ can finally be obtained from the integral form of $t(S)$ given in [26]), and leads to (cf App. E.B1)

$$\beta t_{\text{peak}} \simeq \log\left(\frac{S_0}{1-S_0}\right) - \log\mu - \mu\left(1+\log(1-S_0) - \frac{1}{2}\log^2\frac{S_0}{\mu} - \text{Li}_2(S_0)\right) \tag{5.30}$$

with Li_n the polylogarithm function.

In Fig. 5.5, we compare the predictions Eqs. (5.28)-(5.29)-(5.30) with the exact βt_{peak}, demonstrating that, with $S_0 \geq 0.999$, the full range of $\mu \in [0,1]$ is covered with these three regimes.

Eqs. (5.28)-(5.29)-(5.30), corresponding respectively to large, intermediate and small μ, provide explicit expressions and physical indications of how one can delay the epidemic peak in practice. Let us assume that the parameter γ which characterises the rate of recovery from the illness is given by biological factors, and thus fixed, but that the transmission rate β can be modified by non-pharmaceutical interventions such as wearing masks or limiting contact between people. We thus assume that μ can be modified, but that this is done with $\beta\mu = \gamma$ constant.

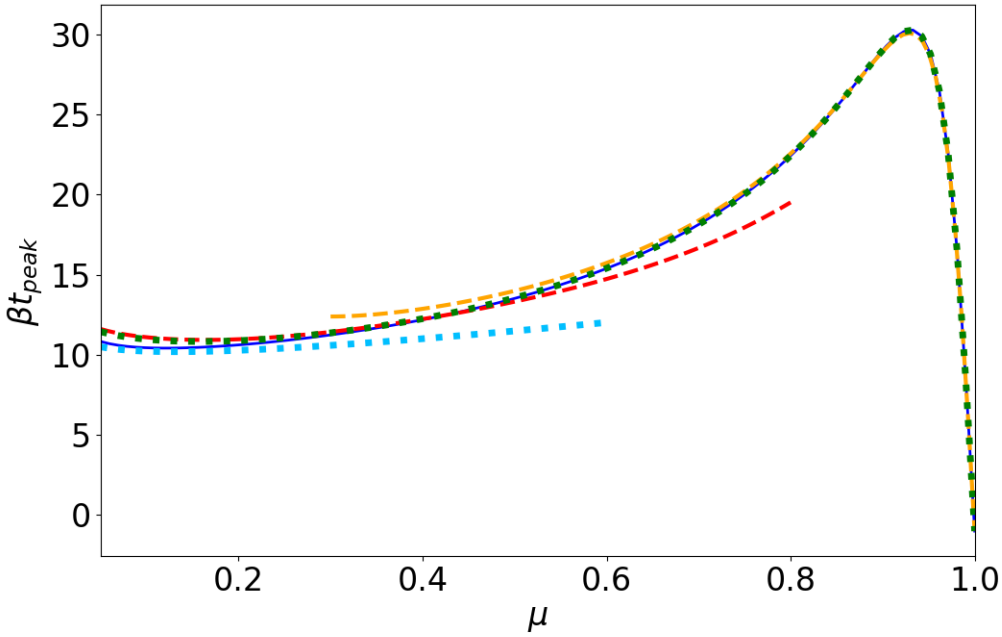

Figure 5.5: Comparison of the exact $\beta t_{\text{peak}}(\mu)$ (blue solid line) with different approximations, for a fixed $S_0 = 0.999$ and $\mu \in [0.05, 1]$. Cyan dotted line: approx. (5.30) which works at small μ. Red dashed line: approx. (5.29) which is valid rather for small and intermediate μ. Orange dashed line: approx. (5.28) for μ close to 1 and also for intermediate μ. Dotted green line: approximation obtained from Eq. (5.27) with $S = \mu$, which match the exact $t_{\text{peak}}(\mu)$ extremely well except for very small μ's. The regimes of validity of the different approximations improve as $S_0 \to 1$, and would somewhat degrade as δS_0 increases.

First, we see in Fig. 5.5 that the curve $\beta t_{\text{peak}}(\mu)$ is rather flat in the range $\mu \in [0.05, 0.5]$, implying that t_{peak} is essentially proportional to $1/\beta$ for $\mu < 0.5$. Then, different kinds of corrections appear in the different regimes. The most useful formula is presumably Eq. (5.29), which provides a compact and explicit analytical result (with only 2 terms), in a regime which corresponds to most of the practical use ($2 \leq R_0 \leq 5$).

As a practical example, starting with $S_0 = 0.99$ and applying restrictive measures to change $\mu = 0.25$ to $\mu = 0.5$ (which means changing R_0 from 4 to 2) would allow to reduce t_{peak} by a factor 2.25 according to Eq. (5.29), while the exact reduction factor is 2.18, with very similar amplitudes. For $S_0 = 0.9$, this factor is only of 1.61 according to Eq. (5.29), while the exact value is 1.57. We therefore have an precise indication about t_{peak} from a very simple expression, which does not require any knowledge of the Lambert function, and does not involve the computation of an integral. This makes it possible to analyse qualitatively why early detection of the epidemic is important, as restrictive measures to delay the peak will be significantly less efficient for an epidemic which has already spread significantly in the population.

5.3 Discussion

In this chapter, we investigated the Pairwise Approximation on random homogeneous networks of degree k, referred to as the SIR-k model. This study serves as a complementary work on complex networks, offering valuable insights into the dynamics of epidemics in these types of networks.

More precisely, we have derived Eqs. (5.1)-(5.2) for the SIR-k model, and obtained an exact implicit expression of $t(S)$ (5.10), valid for arbitrary k, as a finite sum over the roots

z_j of the polynomial $P(z)$ Eq. (5.7).

It turns out that the main qualitative properties of the epidemic dynamics are governed by its two positive real roots (z_0, z_1). In particular the proportion of agents infected during the total duration of the epidemic is given by $\mathcal{I}_{\text{tot}}^{(k)} = S_0(1 - z_0^k)$, for which we have an explicit formula both for small and very large k. Taking $S_0 = 1$, i.e. assuming a negligibly small initial proportion of infected agents (for easier reading), we got $\mathcal{I}_{\text{tot}}^{(3)} = 1 - (3\mu)^3$ for $k = 3$, while for the SIR model limit we obtained $\mathcal{I}_{\text{tot}}^{(\infty)} = 1 - \mu T_0(\chi) \simeq 1 - \mu\chi = 1 - e^{-1/\mu}$. Thus, for small μ (contagious diseases), the larger k, the more virulent the epidemic, as $\mathcal{I}_{\text{tot}}^{(\infty)}$ will converge faster to 0 with $\mu \to 0$ than $\mathcal{I}_{\text{tot}}^{(k)}$.

The values of the real roots, (z_0, z_1), also affect the threshold value of μ for which, even for an infinitely small initial proportion of infected individuals, an epidemic starts to propagate and affects a finite proportion of the agents. This threshold is given by the condition $z_0(\mu_k^*) = z_1(\mu_k^*) = 1$, leading to $\mu_k^* = (k-2)/k$. This value is lower than its counterpart for the basic SIR model $\mu_{\text{SIR}}^* = \mu_\infty^* = 1$, which indicates that the propagation of epidemics is more difficult in the SIR-k model than in the basic SIR one, in agreement with the final epidemic size which is also lower for the SIR-k model. This contrasts with heterogeneous networks, where an epidemic spreads more easily compared to the SIR model. In all these cases, we compare the relative speed of the epidemic on networks keeping the parameter constant $\mu = \gamma/(\langle k \rangle \lambda)$ constant.

In the cases $k = 2$ and $k = 3$ we got exact explicit expressions for $S(t)$. In the limit $k \to \infty$ we obtained new exact expressions for the original SIR model, which provides a new point a view, together with useful approximate results for this well known problem. In particular Eq. (5.27) and Fig. 5.4 demonstrate that for all values of μ except near 0, keeping only the contributions of the real α_j's, i.e. $j = 0, 1$, provides an excellent approximation of $t(S)$. Further approximation for the epidemic peak time Eqs. (5.28)–(5.29)–(5.30) are shown in Fig. 5.5 to work extremely well numerically.

The SIR-k model on homogeneous networks presumably provides a good balance between increase of complexity and increase of effectiveness. It is characterized by only three parameters (S_0, μ, k) which, compared with the basic SIR, only adds the parameter k corresponding to the average number of possible contacts of individuals, a relatively accessible quantity in practice.

Our results pave the way for the analytical study of more realistic social networks, such as heterogeneous networks with the small-world property [42, 67].

This concludes the third and final project of this thesis. We will now move on to a more transverse chapter focused on the numerical techniques developed throughout this work.

6 - Numerical techniques

Throughout our work, we relied heavily on numerical simulations to compute and solve the different Nash equilibria we encountered, as well as the societal optima and more generally to compute epidemics dynamics. All the codes and simulations have been realized in Python language. We employed mainly the following Python libraries:

- First regarding system resolutions, we essentially applied Runge-Kutta methods. At first, this method was implemented manually but for more complex systems we operated the efficient methods of the library *scipy.integrate*, and particularly *solve_ivp* with Runge-Kutta 5(4) method or Radau method.
- Second regarding networks, we used the library *networkX* which is powerful to create a network and then access all quantities of interest such as the adjacency matrix, the neighbors of each node, etc, see [210] for an introduction. For Network generation, we adopted the *random_degree_sequence_graph* method which create a random network from a given sequence of nodes and their degrees. The algorithm makes a certain number of fixed tries to create the network, it links randomly the nodes of the given sequence to build the network successively until the end of the sequence. The algorithm may fail at the end of the network when the remaining links to make cannot fulfill the constraints of the sequence. Reader may refer to [211] for a complete description of this implementation of the Configuration Model.

In this chapter, we outline the different specific methods we employed, as well as different promising techniques. In Sec. 6.1 we focus on the methods we applied to reach Nash equilibra. Next, in Sec. 6.2, we introduce the techniques for solving the societal optimum of the game, which differs from the Nash equilibrium as it requires global minimization across all strategies. In Sec. 6.3, we provide an overview of the numerical complexity of the algorithms we utilized. In Sec. 6.4, we discuss two other promising methods to reach the societal optimum or a Nash equilibrium: the Pontryagin Maximum Principle and Genetic Algorithms respectively. Finally, Sec. 6.5 corresponds to a short discussion.

6.1 Reaching a Nash equilibrium

We will outline the different approaches for the simplest MFG model presented in Sec. 2.3, although these methods have been applied in this thesis to the more complex models discussed in Chapters 3-4.

Let us start by the problem of reaching a Nash equilibrium. It is a solution of a specific system, we recall it below for clarity in the context of the MFG presented in Sec. 2.3. First the Kolmogorov equation with initial conditions $S(0), I(0), R(0)$,

$$\begin{aligned} \dot{S} &= -\bar{\chi}(t) I(t) S(t) \\ \dot{I} &= \bar{\chi}(t) I(t) S(t) - \xi I(t) \ , \\ \dot{R} &= \xi I(t) \end{aligned} \tag{6.1}$$

and then the Hamilton-Jacobi-Bellman equation, with one reference individual a,

$$-\frac{dU_a}{dt} = \min_{\chi_a(t)} \left[\lambda_a(t) \left(\mathfrak{r}_{\mathrm{I}} - U_a(t) \right) + f(\chi_a(t)) \right] \quad , \quad \lambda_a(t) = q \chi_a(t) I(t) \ , \tag{6.2}$$

with only the terminal condition on U fixed, namely, $U_a(T) = 0$. Finally, the self consistent condition needs to be satisfy:

$$\chi_a^*(t) = \bar{\chi}(t) \, . \tag{6.3}$$

Even though this MFG is specific, any MFG will present the same two kind of equations, which together form an Initial Terminal Value Problem, making it impossible to solve with classical solvers of differential equations which require only initial or final conditions.

We tackle this problem with first a natural approach to solve the Nash equilibrium presented in Sec. 6.1.1, based on an inductive sequence. Then, in Sec. 6.1.2, we present a more reliable but slower approach in cases where the first method does not converge, relying on the equivalent definition of the Nash equilibrium on the cost. In Sec. 6.1.3, we finally show how we modified this second method to solve a Nash equilibrium under (evolving) constraints.

6.1.1 Inductive sequence

The first method is likely the most intuitive. The idea is to iterate a scheme until stable and consistent solutions for χ and $\bar{\chi}$ are obtained. The rationale is as follows:

We begin by initializing a global strategy $\bar{\chi}^{(0)}(.)$ (where brackets (.) indicate that this strategy is defined over the entire time horizon). This strategy is typically $\chi^{(0)}(t) = \chi^0$ the business as usual configuration. Using this initial strategy, we compute the associated epidemic quantities $(S^{(0)}(.), I^{(0)}(.), R^{(0)}(.))$ through Eq. (6.1), given the initial conditions of the system. Next, we solve backward the Hamilton-Jacobi-Bellman (HJB) Eq. (6.2) to determine the optimal individual response, $\chi^{*(0)}$, to that epidemic dynamics.

In some cases, the solution for χ^* can be computed explicitly, for example, by using expressions like Eq. (3.20), which allow us to solve Eq. (6.2) directly without further computation. When no explicit solution is available, a standard minimization procedure is used (see Sec. 6.4.2 for a concrete example).

Once $\chi^{*(0)}$ is obtained, it represents the optimal response for all individuals, as each agent is optimizing the same cost function. The global strategy is then updated by setting $\bar{\chi}^{(1)} = \chi^{*(0)}$ (consistent condition). This process is repeated iteratively until the Nash equilibrium condition is met, namely $\bar{\chi}^{(k)} \simeq \chi^{*(k)}$ for sufficiently large k. The global scheme is summarized in Fig. 6.1.

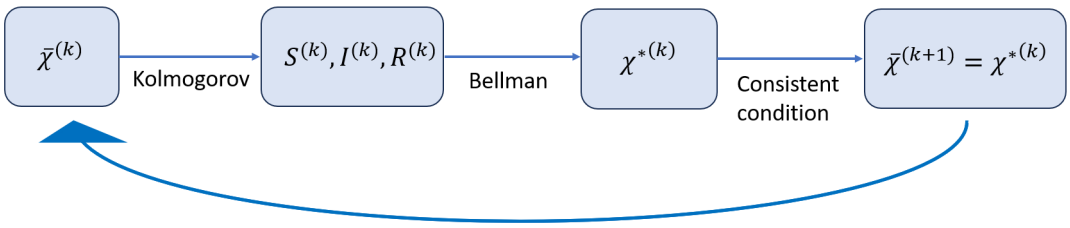

Figure 6.1: Global scheme used for the inductive sequence.

Each step of the process is numerically straightforward, as it essentially involves classical partial differential equations. The sequence described by Fig. 6.1 represents an inductive process $\bar{\chi}^{(k+1)} = F(\bar{\chi}^{(k)})$, where the functional F is defined such that $F(\bar{\chi}^{(k)}) = \chi^{*(k)}$. However, this inductive sequence does not always guarantee convergence to a fixed point of F. The Picard-Banach fixed-point theorem provides sufficient conditions for convergence. It states that every contractive mapping on a complete metric space has a unique fixed point. Furthermore, the theorem ensures that any inductive sequence of the form described will converge geometrically to this fixed point [212]. However, if F is not a contractive mapping, the sequence may fail to converge. In case of convergence, advantages of this

method are twofold: convergence is both fast (geometric) and certain (we always reach the Nash equilibrium). Figure 6.2 illustrates how the iterative process converges to the fixed point, representing the Nash equilibrium. However, when the slope of F is too steep or

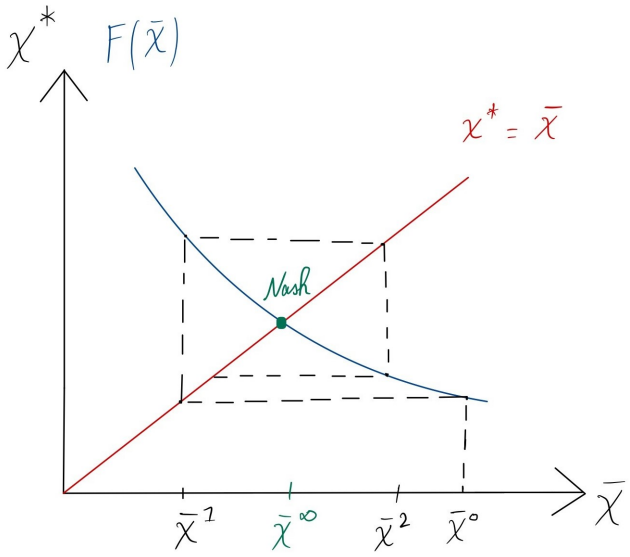

Figure 6.2: Illustration of the inductive sequence we use. We start with $\bar{\chi}^{(0)}$ and we then follow the scheme of the inductive sequence with $\bar{\chi}^{(1)} = F(\bar{\chi}^{(0)})$, $\bar{\chi}^{(2)}$, etc. The blue curve corresponds to the function F, while the red curve is the one where $\bar{\chi} = \chi^*$ which is therefore the line where Nash equilibrium can occur. The green mark is the fixed point of F and corresponds to the Nash equilibrium of the game (unique here). This drawing illustrates that any other $\bar{\chi}$ different from the fix point will lead to an optimal individual response χ^* different from $\bar{\chi}$.

in presence of discontinuities, the method may fail to converge to the Nash equilibrium, necessitating the use of alternative approaches. Besides its efficiency with its geometric convergence, this method has an additional advantage: it allows us to verify whether we have reached a Nash equilibrium by confirming that the system has reached a fixed point of F.

To ensure the uniqueness of the equilibrium, one can run this algorithm with different initial starting points and check that the final fixed point remains consistent across all runs. This provides further confidence that the Nash equilibrium is indeed unique in the system. We turn now to the second method to deal with the cases, actually numerous, where the first method does not converge.

6.1.2 Gradient descent

We present in Sec. 6.1.2.1 the general rationale for this second method based on a gradient descent, for a general control parameter χ. Then, in Sec. 6.1.2.2, we demonstrate the application of this scheme and detail the computations for the specific case of the MFG model introduced in Chapter 3.

6.1.2.1 Presentation of the gradient descent method

This method, as employed in [19], converges to a Nash equilibrium more gradually but with greater robustness. From a cost optimization perspective, a Nash equilibrium corresponds to a strategy χ^N such that, when $\bar{\chi} = \chi^N$, the cost function achieves a minimum $C(\chi^N, \chi^N) = \min_\chi C(\chi, \chi^N)$ with respect to the first variable χ, representing individual behavior. This formulation reflects that any strategy other than χ^N is suboptimal for

the individual, making χ^N the Nash strategy of the game. This definition inspired the following procedure:

$$\chi^{(k+1)}(t) = \chi^{(k)}(t) - h \cdot \nabla_1 C \left(\chi^{(k)}(.), \bar{\chi}^{(k)}(.), t \right) \Big|_{\chi^{(k)}(.)=\bar{\chi}^{(k)}(.)} , \tag{6.4}$$

where we compute the derivatives of the cost C for individual and collective strategies that are identical, which are along the red curve on Fig. 6.2. The gradient is on the first variable of C, the individual parameter χ, and should be interpreted as follows: $\nabla_1 C \left(\chi^{(k)}(.), \bar{\chi}^{(k)}(.), t \right)$ corresponds to the change of the total cost C (over the game) upon a small change of $\chi^{(k)}$ at t. Mathematically, it is defined through the functional derivative of C with respect to its first variable χ, in the direction h (with h a time dependent function, usually a Dirac delta). This functional derivative is denoted $D_h C$ and is defined as

$$D_h C \left(\chi, \bar{\chi} \right) \equiv \lim_{\epsilon \longrightarrow 0} \frac{1}{\epsilon} (C(\chi + \epsilon h, \bar{\chi})), \tag{6.5}$$

where we insist on the fact that the cost C we compute here and in all this section is the global cost of the game, starting at $t = 0$. Indeed, the Nash equilibrium is computed from the cost starting at $t = 0$ thanks to the Bellman property (the optimal strategy at $t = 0$ will also be optimal later for any t). Using the definition of the gradient, this functional derivative can be reexpressed as

$$D_h C \left(\chi, \bar{\chi} \right) = \int_0^T h(t) \cdot \nabla_1 C \left(\chi, \bar{\chi}, t \right) dt , \tag{6.6}$$

which leads to the intuitive formula

$$D_{\delta(t-t_0)} C \left(\chi, \bar{\chi} \right) = \nabla_1 C \left(\chi, \bar{\chi}, t_0 \right) = \frac{\delta C \left(\chi, \bar{\chi} \right)}{\delta \chi(t_0)} \quad . \tag{6.7}$$

Thus, the time t in the gradient denotes the time at which we take the gradient, and not the starting time of the optimization (as it was for the same notation with C). We keep the notation $\nabla_1 C$ in the following, as it allows to denote a vector notation when χ is a vector to, changing the classical product $h(t) \cdot \nabla_1 C$ into a scalar product. This scalar product is the same as the one in Eq. (6.4), where h is the step of the gradient descent, usually taken constant over time (but with possibly a vector form). Coming back to the scheme Eq. (6.4). When the latter converges, that is when $\nabla_1 C \left(\chi^{(k)}(.), \bar{\chi}^{(k)}(.), t \right) = 0$ for all t; then we are, at least, at a local minimum of the red curve along the individual variable of C (horizontal axis). However, it is not sufficient to completely claim that we reach a Nash equilibrium, as it requires to be at a global minimum along the individual variable of C. For that purpose, we compute $F(\chi^N)$ and check that $F(\chi^N) = \chi^N$, meaning that we are at a Nash equilibrium of the game. Whatever the method this last step of verification, when it is possible and not too time consuming, should be used.

The scheme follows the pattern illustrated on Fig. 6.3. We provide an explicit example below in Sec. 6.1.2.2 that will may make the gradient descent clearer.

6.1.2.2 Gradient descent for the SIR model with a social structure

In this MFG, we perform the gradient descent on the variable $n_a(.)$ of the cost $\mathfrak{C}_a$ at $t = 0$ (see Eq. (2.28)) to reach the Nash equilibrium. We use the scheme Eq. (6.4)for each age class α with representative individual a

$$n_a^{(k+1)}(t) = n_a^{(k)}(t) - h \cdot \nabla_1 \mathfrak{C}_a \left(n_a^{(k)}(.), \{ n_\beta^{(k)}(.) \}, t \right) \Big|_{n_a^{(k)}(.)=n_\alpha^{(k)}(.)} , \tag{6.8}$$

where ∇_1 means that the gradient is taken on $n_a^{(k)}(.)$ and h is the step of the gradient descent, that we usually took independent of t. The dot in Eq. (6.4) indicates a scalar

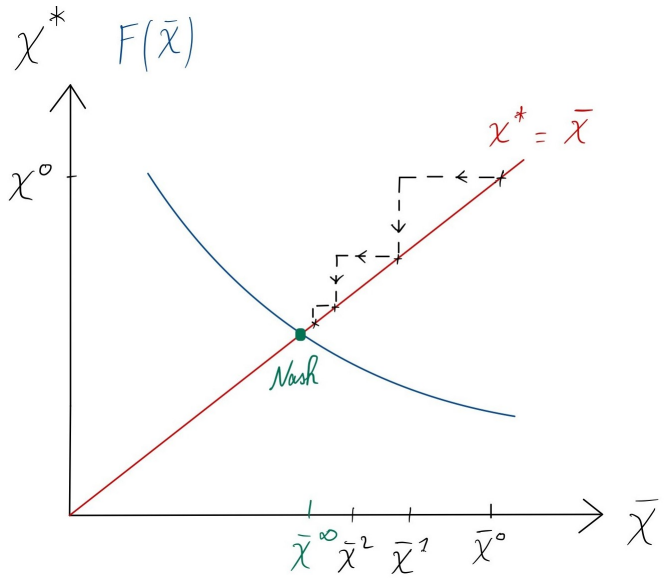

Figure 6.3: Illustration of the gradient descent scheme. The gradient descent follows the red curve. When the Nash equilibrium is reached, the scheme is stopped by definition. However, it can also be stopped in a point of the red line which presents a local minimum along the vertical axis χ.

product, as h and ∇_1 are vectors indexed by γ. In practice, h is usually chosen such that the first steps of the descent are pointing toward a unique direction. This scheme gives $\nabla_1 \mathfrak{C}_a \left(n_a^{(k)}(.), \{n_\beta^{(k)}(.)\}, t \right) = 0$ when we reach the equilibrium.

In order to make the numerical computation of the gradient $\nabla_1 \mathfrak{C}_a$ less heavy and more efficient, we first perform a few analytical steps. To avoid heavy notations, the cost at $t = 0$ will be denoted as $\mathfrak{C}_a \left(n_a, n_\beta \right)$. We have

$$\mathfrak{C}_a \left(n_a, n_\beta \right) \equiv \mathfrak{C}_a \left(n_a^\gamma(\cdot), \{n_\beta^\gamma(.)\}, 0 \right) = \int_0^T \left(f_\alpha \left(n_a^\gamma(s) \right) + \lambda_a(s) \, \mathcal{I}_\alpha(I(s)) \right) (1 - \phi_a(s)) ds \; . \tag{6.9}$$

The functional derivative of $\mathfrak{C}_a$ with respect to its first variable n_a, in the direction h can be written as

$$D_h \mathfrak{C}_a \left(n_a, n_\beta \right) = \int_0^T h(t) \cdot \nabla_1 \mathfrak{C}_a \left(n_a, n_\beta, t \right) dt \; , \tag{6.10}$$

which explicitly written gives $h(t) \cdot \nabla_1 \mathfrak{C}_a = \sum_\gamma h^\gamma(t) \, \frac{\delta \mathfrak{C}_a}{\delta n_a^\gamma(t)}$ with $\frac{\delta \mathfrak{C}_a}{\delta n_a^\gamma(t)}$ the functional derivative of the total cost $\mathfrak{C}_a$ with respect to $n_a^\gamma(t)$. Since $1 - \phi_a(s) = \exp\left(- \int_0^s \lambda_a(u) du \right)$, the cost (6.9) depends on n_a through the terms $f_\alpha(n_a)$ and λ_a via Eq. (3.14); with λ_a is linear in n_a. Using Eq. (6.5) we have at first order $\lambda_a(n_a + \epsilon h) = \lambda_a(n_a) + \epsilon h \cdot \frac{d\lambda_a}{dn_a}(t)$ with $\frac{d\lambda_a}{dn_a}(t)$ a vector indexed by γ, of components

$$\frac{d\lambda_a}{dn_a^\gamma}(t) \equiv \mu \rho \sum_{\beta=1}^{n_{\rm cl}} n_\beta^\gamma(t) \mathcal{M}_{\alpha\beta}^{\gamma(0)} I_\beta(t) \; . \tag{6.11}$$

We then use the integral form Eq. (6.9) to expand Eq. (6.5) to lowest order in ϵ. One of the terms involves a double integral; in order to put $D_h \mathfrak{C}_a \left(n_a, n_\beta \right)$ under the form Eq. (6.10), we invert integrants and change variables, namely $\int_0^T \left[f(t) \int_0^t g(s) ds \right] dt = \int_0^T \left[g(t) \int_t^T f(s) ds \right] dt$. Once the expression is of the form Eq. (6.10) we can read off the

value of the gradient $\nabla_1 \mathfrak{C}_a\left(n_a, n_\beta\right)$:

$$\nabla_1 \mathfrak{C}_a(n_a, n_\beta, t) = \left[\frac{df_\alpha}{dn_a}(n_a(t)) + \frac{d\lambda_a}{dn_a}(t)\mathcal{I}_\alpha(I(t))\right](1-\phi_a(t)) \\ - \frac{d\lambda_a}{dn_a}(t)\int_t^T \left(f_\alpha\left(n_a(s)\right) + \lambda_a(s)\mathcal{I}_\alpha(I(s))\right)(1-\phi_a(s))ds\ , \quad (6.12)$$

with $\frac{df_\alpha}{dn_a}$ the derivative of f_α with respect to the variable $n_a^\gamma(t)$ (with a vector notation). The straights d used here indicates usual derivatives, as f and λ are functions (and not functional) of $n_a^\gamma(t)$. The gradient Eq. (6.12) is then computed numerically in order to follow the scheme Eq. (6.8).

6.1.3 Gradient descent under constraints

Here, we focus on the case of a Nash equilibrium under constraints, similar to those discussed in Sec. 3.3.4. More generally, we consider situations where the control parameter $\chi_i(.)$ of player i evolves within a dynamic interval $[f_{\min}(\chi_{-i}(.)), f_{\max}(\chi_{-i}(.))]$, where $\chi_{-i}(.)$ represents the set of strategies for all players except player i. This differs from the usual constant interval $[\chi_{\min}, \chi_{\max}]$. In a standard gradient descent scheme, these constraints are enforced at each step by adjusting the control parameter to the nearest boundary whenever it exceeds the allowed range. The interval may become time-dependent and reliant on other players' strategies, taking the form $[f_{\min}(\chi_{-i}(.)), f_{\max}(\chi_{-i}(.))]$, as seen, for example, in lockdown strategies that depend on I (and therefore on $\chi_{-i}(.)$). Additionally, the functions f governing the temporal evolution of the constraints often exhibit discontinuities, which complicates numerical resolution.

Furthermore, the strategy $\chi_{-i}(.)$ evolves iteratively throughout the algorithm, at each step and regardless of the method employed (either inductive sequence or gradient descent). As a result, instead of progressing smoothly through the scheme Eq. (6.4), the control parameter $\chi_{-i}(.)$ may sometimes follow the imposed constraints, causing $\chi_{-i}(.)$ to shift abruptly from one step to another in response to the discontinuities in f when new constraints are enforced. These sudden changes can disrupt the convergence of the gradient method, potentially leading to limit cycles that prevent full convergence.

To overcome this challenge, we choose for the numerical simulations of Sec. 3.3.4 to "freeze" the constraints at a certain step k and proceed with the gradient descent as outlined in method 6.1.2.2. After a few iterations, the constraints are recalculated, and the process continues until convergence is achieved.

In practice, we observed that the algorithm may be long to converge in presence of constraints and is sometimes trapped in some little loops, whereas it was reasonable and simpler for the free Nash equilibrium. To accelerate the algorithm and increase its convergence probability, we implemented a dynamic step size h which can be adjusted at each iteration but remains independent of t. The general idea is to select values of h that ensure the gradient descent converges reasonably fast, while avoiding steps that are too large and could lead to undesired regions or limit cycles. To achieve this, we employed two strategies, illustrated here in the context of χ:

- **Step counting in the descent direction:** we track the number of consecutive steps where the cost function $C\left(\chi^{(k)}(.), \bar{\chi}^{(k)}(.), t\right)$ decreases, i.e., $C\left(\chi^{(k+1)}(.), \bar{\chi}^{(k+1)}(.), t\right) \leq C\left(\chi^{(k)}(.), \bar{\chi}^{(k)}(.), t\right)$. After a set number of consecutive decreasing steps (e.g., 5), we double the step size h, assuming the slope of C is relatively "smooth" in that region. Conversely, if $C\left(\chi^{(k+1)}(.), \bar{\chi}^{(k+1)}(.), t\right)$ increases, we reduce h by half.

- **Slope ratio calculation:** we calculate the ratio between the expected slope and the actual observed change over two steps as follows:

$$r = \frac{D_{\delta\chi} C\left(\chi^{(k)}, \bar{\chi}^{(k)}\right)}{C\left(\chi^{(k+1)}, \bar{\chi}^{(k+1)}\right) - C\left(\chi^{(k)}, \bar{\chi}^{(k)}\right)} \quad .$$

  Here, the numerator represents the expected cost variation in the linear regime, involving $\delta\chi(t) = \chi^{(k+1)}(t) - \chi^{(k)}(t) = h(t)\nabla_1 C\left(\chi^{(k)}, \bar{\chi}^{(k)}, t\right)$. The denominator represents the actual change in the cost between steps k and $k+1$. After a certain number of consecutive decreasing steps (e.g., 5) such that r is sufficiently close to 1 (e.g $1.25 \geq r \geq 0.75$), we double the step size h, since the linear approximation regime is valid. Conversely, if r is outsides these bounds, we reduce h by half as the linear approximation is no longer valid. This second strategy allows to avoid too high steps in regions where the cost C varies a lot.

Despite these strategies, the process can be time-consuming and does not always guarantee convergence, as it depends on the choice of constraints and the specific Mean-Field Game model. Furthermore, convergence is influenced by algorithmic parameters such as the total number of steps, the number of steps with frozen constraints, and the step size h.

However, a significant advantage of working with Nash equilibrium is that we can always compute the functional F to verify whether the solution corresponds to a Nash equilibrium. For Nash equilibrium with evolving constraints, more robust approaches such as Markov Chain Monte Carlo (MCMC) methods [213] or machine learning algorithms [214] may offer improved efficiency and should be further investigated.

6.2 Reaching the societal optimum

The social optimum presents a fundamentally different challenge compared to finding a Nash equilibrium. The problem can be framed in a straightforward way, using a generic control parameter χ (which may be a vector): find χ^{SO} such that

$$C_{\text{glob}}(\chi^{SO}, t) \;=\; \min_{\chi} C_{\text{glob}}(\chi, t) \quad . \tag{6.13}$$

This means that, regardless of the chosen global cost function C_{glob}, the problem reduces to finding the global minimum of a functional depending on a control parameter $\chi(.)$. Any method capable of finding the zero of a functional can, in principle, be employed to reach the societal optimum. In Sec. 6.2.1, we outline the general gradient descent method used, and in Sec. 6.2.2, we illustrate its application with the gradient descent we applied in Sec. 3.3.5.

6.2.1 Gradient descent

The method mimics the gradient descent of the Nash equilibrium. The scheme Eq. (6.4) becomes

$$\chi^{(k+1)}(t) = \chi^{(k)}(t) - h \cdot \nabla C_{\text{glob}}\left(\chi^{(k)}, t\right) \quad . \tag{6.14}$$

This method is generally more robust than in the Nash equilibrium case, as it avoids the loops and cycles associated with reaching a Nash equilibrium, given that we are targeting a global minimum. However, computing the gradient ∇C_{glob} can be numerically expensive. This is because the variable now represents the behavior of all individuals, and the complex macroscopic quantities that emerge from this collective behavior must be derived.

In most cases, an analytical expression of ∇C_{glob} is preferable as it will be faster than a brute-force approach, where ∇C_{glob} is computed entirely numerically. As we will see

below, the brute-force method requires recalculating the entire game at every time step t, which can significantly increase computational time.

6.2.2 Application to the societal optimum for the SIR model with a social structure

We can approach the optimal strategy in various ways. In this work, we choose to perform a gradient descent on the global cost C_{glob}, although the Pontryagin maximum principle would be also a viable method, at it will be discussed in Sec. 6.4.1. Our goal is to optimize individual behavior to minimize the overall cost borne by the population, expressed as

$$C_{\text{glob}}(\{n_\beta^\gamma(.)\}) = \sum_\alpha N_\alpha C_\alpha(\{n_\beta^\gamma(.)\}) \ , \tag{6.15}$$

where the cost depends on all the functional $\{n_\beta^\gamma\}$ in an equal footing. For simplicity, we will denote this global strategy over all classes and setting n. To minimize this global cost, we apply the same gradient descent scheme as outlined in Eq. (6.14). We must compute the gradient $\nabla C_{\text{glob}}(n,t)$, which only depends on the collective strategies n and the time t at which the gradient is evaluated. For each age class α, we calculate the gradient

$$D_h C_\alpha(n) \equiv \int_0^T h(t) \cdot \nabla C_\alpha(n,t) dt \ , \tag{6.16}$$

to identify $\nabla C_\alpha(n,t)$ as in Sec. 6.1.1, with ∇ now acting on the global strategy n and having components along both γ and β (as does h). Additional terms emerge due to the fact that quantities such as the proportion of infected individuals $I(.)$ now depend n (whereas it was independent of the individual strategy studied before).

Below, we outline the key steps involved in the calculation. The first step is deriving the functional derivative of the gradient $D_h C_\alpha(n,t)$. Starting from the expression of C_α in Eq. (2.28), we get

$$D_h C_\alpha(n,t) = D_h \left[\int_t^T \left(f_\alpha\left(n_\alpha(s)\right) + \lambda_\alpha(s)\ \mathcal{I}_\alpha(I(s))\right)(1-\phi_\alpha(s)) ds \right] \ . \tag{6.17}$$

Thus, we need to compute each functional derivative of the terms appearing in Eq. (6.17), which give

$$D_h \lambda_\alpha(t) = \lim_{\epsilon \longrightarrow 0} \frac{1}{\epsilon} \left[\sum_\gamma \sum_\beta \rho \mathcal{M}_{\alpha\beta}^\gamma (n_\alpha^\gamma(t) + \epsilon h_\alpha^\gamma(t))(n_\beta^\gamma(t) + \epsilon h_\beta^\gamma(t)) \left(I_\beta(t) + \epsilon D_h I_\beta(t)\right) \right] \tag{6.18}$$

$$D_h \phi_\alpha(t) = (1-\phi_\alpha(t)) \int_0^t D_h \lambda_\alpha(s) ds \tag{6.19}$$

$$D_h I_\beta(t) = \int_0^t \frac{\delta I_\beta(t)}{\delta n(s)} \cdot h(s) ds \tag{6.20}$$

$$D_h f_\alpha(n_\alpha(t)) = d_n f_\alpha(n_\alpha(t)) \cdot h(t) \tag{6.21}$$

$$D_h \mathcal{I}_\alpha(I(t)) = \frac{\kappa_\alpha \mathfrak{r}_\text{I} \mathfrak{q}_\text{sat}}{\mathfrak{I}_\text{sat}} D_h I(t) \exp\left[\mathfrak{q}_\text{sat} \frac{I(t) - \mathfrak{I}_\text{sat}}{\mathfrak{I}_\text{sat}} \right] \ , \tag{6.22}$$

where the dots in Eqs. (6.18)-(6.20)-(6.21) indicate that h and n are indexed by β and γ and indices are summed over. In Eq. (6.20), $\delta I_\beta(t)/\delta n(s)$ indicates the functional derivative of $I_\beta(t)$ with respect to the collective behavior $n(s)$. This "time delayed" derivative is the crucial term of the gradient for the societal optimum, one can perform a linearization of Eqs. (3.10) to propagate linearly the elementary deformation of I_β from time s to time t to avoid several numerical computation of the whole epidemic. This linearization can be performed as follows.

Linearization method to compute $\delta I_\beta(t)/\delta n(s)$.

We illustrate this approach on the SIR model; the generalization to the present model is straightforward. We start from an epidemic given by some contact rate χ (same individual and collective strategies for the societal optimum), and we aim to compute the variation of I at time t_0 for a small variation of χ at time $s \leq t_0$. We will denote this slightly modified strategy $\tilde{\chi} \equiv \chi(t) + \epsilon\delta(t-s)\chi_0$ with ϵ small enough to stay in the linear regime, with δ the Dirac function. We introduce

$$\mathbf{X}(t) = \begin{pmatrix} S_0(t) \\ I_0(t) \end{pmatrix}$$

which is a time dependent vector representing the state of the epidemic with the contact rate $\chi(.)$. The variation of this vector $\mathbf{X}$ upon a change of χ from χ to $\tilde{\chi}$ is denoted by $\tilde{\mathbf{X}}$ with $\delta\mathbf{X} = \tilde{\mathbf{X}} - \mathbf{X}$. From $t = 0$ to $t = s$, $\delta\mathbf{X} = 0$, as χ and $\tilde{\chi}$ are identical. Then, at $t = s$, $\dot{\mathbf{X}}$ and $\dot{\tilde{X}}$ are explicitly different because $\chi(s) \neq \tilde{\chi}(s)$, which leads to a kick $\delta\dot{\mathbf{X}}$ at $t = s$, given by

$$\delta\dot{\mathbf{X}}(s) = \epsilon\chi_0 M(s) \ , \tag{6.23}$$

where we used the monodromy matrix M of the fundamental function G (with respect to χ) representing the SIR system: $\dot{\mathbf{X}}(t) = G\mathbf{X}$. $M(t)$ is therefore given by

$$M(t) = \begin{pmatrix} -I_0(t) & -S_0(t) \\ I_0(t) & S_0(t) - \gamma \ . \end{pmatrix} \tag{6.24}$$

Then, $\tilde{\mathbf{X}}(t)$ associated to the strategy $\tilde{\chi}$ is propagated for any time $t > s$ by

$$\delta\dot{\mathbf{X}}(u) = \chi(u)M(u) \cdot \delta\mathbf{X}(u) \ , \quad \forall u \in [s, t_0] \ . \tag{6.25}$$

The value $\delta\mathbf{X}(t)$, computed in $t = t_0$ is equal to

$$\delta\mathbf{X}(t_0) = \delta\mathbf{X}(s) + \int_s^{t_0} \chi(u)M(u) \cdot \delta\mathbf{X}(u)du \ , \tag{6.26}$$

where we used a Dyson series as $M(t)$ is a time dependent matrix which did not commute with itself at two different times. We then perform this last step numerically to obtain the second line of the vector $\delta\mathbf{X}(t_0)$ that we divide by ϵ to get $\delta I_0(t_0)/\delta\chi(s)$.

As in Sec. 6.1.1 above, we use these expressions to explicitly compute Eq. (6.17) and put it under the form Eq. (6.16), which gives the expression of $\nabla C_\alpha(n,t)$. We can then perform the gradient descent scheme Eq. (6.14) numerically and efficiently without several computations of the whole epidemic at each time t.

6.3 Numerical Complexity

After deriving the methods used for our numerical analysis, we present a brief overview of the complexity of the various algorithms. Our goal is not to offer a rigorous mathematical treatment of numerical complexity but rather to provide practical insights into how these algorithms behave and converge in real implementations. In Sec. 6.3.1, we present the complexity associated with the Nash equilibra we solved for the MFG model presented in Chapter 3, while in Sec. 6.3.2 corresponds to the societal optimum complexity. Finally in Sec. 6.3.3 we rather focus on Chapter 4 and the numerical complexity associated to the different methods.

6.3.1 Complexity of the Nash equilibrium methods

For the inductive sequence method, the convergence toward the Nash equilibrium was rather fast: it converges geometrically in a few number of steps, typically below 50. At each step, the algorithm has to solve backward the HJB equation which is explicit in U (the minimization has been performed numerically), and has to solve the SIR equations at each step. The total time of the algorithm is given by

$$T_{\text{ind seq}} \sim O(n_{\text{step}}\ n_{\text{cl}}\ n_{\text{set}}\ n_P)\ , \tag{6.27}$$

where the product $n_{\text{cl}}\ n_{\text{set}}$ corresponds to the total number of control parameter in our MFG (and will be contracted as n_d for the dimensionality of the control parameters), n_P is the number of discretization points of the interval $[0, T]$ while n_{step} is the number of steps of the algorithm. The convergence (or not) of the algorithm was reached after typically $10s$ on a classical recent computer.

For the gradient descent method, the convergence toward the Nash equilibrium was slower but still reasonable: at each step of the gradient descent, we had to compute the gradient of the cost with respect to each control parameter. The complexity was therefore of the form

$$T_{\text{grad}} \sim O(n_d^2\ n_P^2)\ , \tag{6.28}$$

as computing the gradient at each time t for each control parameter requires to compute an integral from t to T which also involves n_d terms (cf Eq. (6.12)). While the computation of the epidemic is linear in $n_d n_P$, we get for the total algorithm

$$T_{\text{grad Nash}} \sim O(n_{\text{step}}\ n_d^2\ n_P^2)\ . \tag{6.29}$$

with n_{step} typically between 100 and 300 if h was chosen appropriately (typically between 0.05 and 0.5). This led to a convergence time in practice of about few minutes (lower than 10 minutes). The gradient involved in the MFG resolution in Chapter 4 was about the same order of magnitude, slightly slower due to the computation time of the epidemic on heterogeneous networks which involves more than n_P steps (see Sec. 6.3.3).

6.3.2 Complexity of the Societal Optimum

The convergence toward the Societal Optimum was clearly longer: at each step of the gradient descent, we had to compute the gradient of the cost with respect to each control parameter, but its complexity was given by the computation of Eq. (6.17) which involves several subcalculations. The worse being Eq. (6.19) which involves three integrals with respect to time in total, the total complexity scales like

$$T_{\text{grad SO}} \sim O(n_{\text{step}}\ n_d^3\ n_P^3)\ . \tag{6.30}$$

with n_{step} typically between 100 and 300 if h was chosen appropriately (typically between 0.05 and 0.5) and depending of the convergence precision we required. This led to a convergence time in practice of about a few hours on our lab cluster. We usually took $n_P \sim 100$ (while $n_d = 12$), justifying why, with $T = 40$, we could observe discretization effects on some simulations (as in Fig. 3.8).

6.3.3 Complexity of the approximations on networks

The different approximations presented in Sec. 4.2 were associated with different computation times which may have an impact on whether we decide to use them in practice or not. The quantities involved in the computation are the following: the number of points

discretizing the time n_P, the number of nodes n_{nodes} and iterations n_{it} when direct computation on stochastic networks was required, and k_{cl} which is the number of degree classes, typically equal to $k_{\max}$ without further approximation. In the order of the approximations we presented in Sec. 4.2 we got:

The Pure Mean-Field approach

$$T_{\text{PMF}} \sim O(n_P) \ , \tag{6.31}$$

as it is directly the SIR model, which is extremely fast to solve (with n_P steps of time).

Heterogeneous Mean-Field approach

$$T_{\text{HMF}} \sim O(k_{\text{cl}}\ n_P) \ , \tag{6.32}$$

as it is the SIR model with k_{cl} classes, one for each degree. This method is still very fast to solve.

Quench Mean-Field approach

$$T_{\text{QMF}} \sim O(n_{\text{nodes}}\ n_{\text{it}}\ n_P) \ , \tag{6.33}$$

as it used the adjacency matrix and required to compute the infection probability of each node of the network. The factor n_{it} came from the average over many different networks.

Dynamical Message Passing approach

$$T_{\text{DMP}} \sim O(k_{\text{cl}}^2\ n_P) \ , \tag{6.34}$$

similarly to the HMF approach, with a quadratic dependence k_{cl} since we compute now θ_k for each degree class, with θ_k which also involves the k_{cl} terms coming from infection rates of each class.

Degree Pairwise Approximation approach

$$T_{\text{PA}} \sim O(k_{\text{cl}}^4\ n_P) \ , \tag{6.35}$$

since the computation involves a system of k_{cl}^2 equations, with a complexity for each time step scaling like k_{cl}^2 (see Eq. (4.13) and Eq. (4.17)).

Markovian simulation

$$T_{\text{Markov}} \sim O(n_{\text{nodes}}\ n_{\text{it}}^2\ n_P) \ , \tag{6.36}$$

since the computation now involves the stochasticity inherent to the epidemic, which leads to n_{it} iterations to make an average for each network with different initial seeds.

In practice, we were mainly limited by the computation of the Markovian simulation and the Quench Mean-Field approach for the realization of Fig. 4.3. However, once we turn to the Nash equilibrium with the Pairwise Approximation, the behavior in k_{cl}^4 was clearly limiting, at is was almost impossible to go beyond 25 to 30 classes. To address this issue, we decided to batch the nodes of similar degree class together, to end up with a limited number of batches, even for highly heterogeneous degree which have $k_{\max} \simeq 100$ (we took 5 batches in our simulations).

6.4 Other numerical techniques

Although we worked mainly with the methods detailed in the previous sections, we also explored and briefly tested two additional techniques, without full implementation, that appear promising. These are presented in this section. We first introduce the Maximum Pontryagin Principle in Sec. 6.4.1, which serves as an efficient method to achieve the societal optimum [160]. Then, in Sec. 6.4.2, we outline an alternative approach for reaching the Nash equilibrium using genetic algorithms.

6.4.1 Maximum Pontryagin principle

The Pontryagin Maximum Principle originates from optimal control and can be employed to minimize a physical action under constraints [215]. In Sec. 6.4.1.1, we present the general formalism to provide a brief overview of the principle's foundation. Readers interested in its application to epidemic models can refer directly to Sec. 6.4.1.2.

6.4.1.1 General description

We consider a classical dynamical system described by a state variable $q(.)$ which is determined by a control parameter $u(.)$. The goal of the problem is to find an optimal control $u^*(.)$ minimizing a cost functional S which can be seen as the classical action (in the Euler-Lagrange sense) of our system. We make the optimization between time $t = 0$ and $t = T$ fixed. We consider that the system must fulfill the general constraint $\dot{q} = f(q, u, t)$. Using a Lagrangian multiplier, the action can be written as follows

$$S[u(.)] = \int_0^T \left(\mathcal{L}(q(t), u(t), t) - \lambda(t)\left[f(q(t), u(t), t) - \dot{q}\right]\right) dt \ , \tag{6.37}$$

for any real function $\lambda(t)$ since we consider cases which fulfill the constraint $\dot{q} = f(q(t), u(t), t)$.

Next, we introduce a small variation in the control parameter, $\tilde{u}(t) = u(t) + \delta u(t)$, which leads to a corresponding variation in the trajectory, $\tilde{q}(t) = q(t) + \delta q(t)$. By imposing that the variation in the action, δS, must be zero at the optimum —regardless of the values of $(\delta u(t), \delta q(t))$— we obtain the Euler-Lagrange equations under the general constraint

$$\begin{cases} \mathcal{L}_q(q(t), u(t)) - \lambda(t) f_q(q(t), u(t), t) - \dot{\lambda}(t) = 0 \\ \\ \mathcal{L}_u(q(t), u(t)) - \lambda(t) f_u(q(t), u(t), t) = 0 \ , \\ \\ \lambda(T) = 0 \end{cases} \tag{6.38}$$

where we denote $\frac{\partial \mathcal{L}}{\partial q}$ as $\mathcal{L}_q$ and similarly for u. Moving to the Hamiltonian formalism, which is more suitable for dealing with constraints, we construct a control Hamiltonian as

$$\mathcal{H}(\lambda, u, q, t) = \lambda f(q, u, t) - \mathcal{L}(q, u, t) \ . \tag{6.39}$$

This allows to rewrite Euler-Lagrange equations Eq. (6.38)

$$\begin{cases} \dot{\lambda} = -\dfrac{\partial \mathcal{H}}{\partial q} \\ \dfrac{\partial \mathcal{H}}{\partial u} = 0 \ , \end{cases} \tag{6.40}$$

which together with the constraint $\frac{\partial \mathcal{H}}{\partial \lambda} = \dot{q}$ gives

$$\frac{dq}{dt} = \frac{\partial \mathcal{H}}{\partial \lambda} \ , \ \frac{d\lambda}{dt} = -\frac{\partial \mathcal{H}}{\partial q} \ , \ \frac{\partial \mathcal{H}}{\partial u} = 0 \ . \tag{6.41}$$

In this context, λ serves a role analogous to p in the standard Hamiltonian equations. Here, the constraint is seen as an additional equation independent of the two other, the system becomes free and its resolution is ensured thanks to the presence of three distinct variables (including λ). The quantity λ is referred to as the costate of the system and can be physically interpreted as representing the sensitivity of the cost functional to changes in the state of the system at time t. Additionally, we employ the Legendre condition, which is described below.

The Legendre condition: Euler-Lagrange equations were derived from the stationarity condition on the action S: $\delta S = 0$, which is a condition on the first variation of S to be zero. We can go further to impose a minimum on the action, and thus impose the second variation of S to be positive. It follows the second order necessary condition for a minimum, found by Legendre [215]:

$$\frac{\partial^2 \mathcal{L}}{\partial \dot{q}^2}(q(t), \dot{q}(t), t) \geq 0 \tag{6.42}$$

which in our notation, with a variable u instead of $\dot{q}$ and the optimal control parameter $u^*(t)$ associated with $q(t)$ at the minimum:

$$\frac{\partial^2 \mathcal{L}}{\partial u^2}(q(t), u^*(t), t) \geq 0 \tag{6.43}$$

Thus, we get in addition to $\frac{\partial \mathcal{H}}{\partial u} = 0$:

$$\frac{\partial^2 \mathcal{H}}{\partial u^2}(q(t), u^*(t), p(t), t) \leq 0 \quad \forall t \ , \tag{6.44}$$

which means that a supplementary condition (after the EL equations) for a minimum of S is that $\mathcal{H}(q(t), u(t), p(t), t)$ as a function of u must have a maximum in $u^*(t)$ at each t. Weierstrass showed [215] that this maximum is in fact a global one over all admissible u, his derivation works for a general constraint $\dot{q} = f(q, u, t)$.

Pontryagin Principle: we put together the latest statements to get a necessary condition for a maximum.

If $u^*(.)$ and the associated $q^*(.)$ is are solution of the minimization of Eq. (6.37) with a general constraint $\dot{q} = f(q, u, t)$, then, there exists a function $p(.)$ such that (for all t):

$$\begin{aligned}
\dot{q}(t) &= \frac{\partial \mathcal{H}}{\partial p}(q(t), u^*(t), p(t), t) \\
\dot{p}(t) &= -\frac{\partial \mathcal{H}}{\partial q}(q(t), u^*(t), p(t), t) \\
\mathcal{H}(q(t), u^*(t), p(t), t) &= \max_u \mathcal{H}(q(t), u, p(t), t)
\end{aligned} \tag{6.45}$$

This is the Maximum Pontryagin Principle. Note that another convention for H would lead to the minimum Pontryagin Principle. We applied below this principle to the simple SIR model.

6.4.1.2 Application to the MFG version of the SIR model

We consider the simplest MFG version of the SIR model (considered in Sec. 2.3)

$$\begin{cases}
\dot{S} = -\bar{\chi}(t) S(t) I(t) \\
\dot{I} = (\bar{\chi}(t) S(t) - \xi) I(t) \ , \\
\dot{R} = \xi I(t)
\end{cases} \tag{6.46}$$

with $\bar{\chi}$ the strategy followed by all individuals. The total cost over the game is Eq. (2.29)

$$C(\chi, \bar{\chi}) = \int_0^T \left[\mathfrak{r}_{\mathrm{I}} \chi(t) I(t) + g(\chi(t))\right] (1 - \phi(t)) dt \ , \tag{6.47}$$

with $\phi(t) = 1 - \exp\left(-\int_0^t \chi(s) I(s) ds\right)$ and where $\mathfrak{r}_{\mathrm{I}}$ is the cost of infection and g the cost due to social contact reduction (denoted g for convenience). Here we aim to solve the societal optimum, that is we consider that all individuals behave in the same way, which implies $\bar{\chi} = \chi$ and a central planner minimize $C(\chi, \chi)$ over $\chi(.)$. Therefore, the problem is the following:

Find $\chi^*(.)$ with $(S(0), I(0)) = (S_0, I_0)$, such that

$$\begin{cases} \dot{S} = -\chi^* S I \\ \dot{I} = \chi^* S I - \xi I \ , \end{cases} \tag{6.48}$$

and

$$C[\chi^*(.)] = \min_{\chi(.)} C[\chi(.)] \quad . \tag{6.49}$$

We clearly have an equivalent problem as the one presented in Sec. 6.4.1.1 with $q = (S, I)$ a 2-vector (R is simply $1 - S - I$), the action S Eq. (6.37) corresponds to the cost C Eq. (6.47), and the constraint $\dot{q} = f(q, u, t)$ are the rate equations (6.48). Finally the control parameter u is χ and the Lagrangian is $\mathcal{L} = \left[\mathfrak{r}_{\mathrm{I}} \chi(t) I(t) + g(\chi(t))\right] (1 - \phi(t))$ which depends on $S(t), I(t), \chi(t)$.

Thus, we can introduce the control Hamiltonian for our problem by using the formalism used before Eq. (6.39):

$$\mathcal{H}(S, I, \chi, \lambda, t) = \lambda f(S, I, \chi, t) - \left[\mathfrak{r}_{\mathrm{I}} \chi I + g(\chi)\right] (1 - \phi) \tag{6.50}$$

where $f(S, I, \chi, t) = (-\chi I S, \chi I S - \gamma I)$ and we denote by λ_S, λ_I the components of $\lambda = (\lambda_S, \lambda_I)$.

Therefore, the **Maximum Pontryagin Principle** states that if $\chi^*(.)$ (and associated (S, I, R)) is a solution of the minimization of Eq. (6.49) together with the constraints Eq. (6.48), then there exist a couple (λ_S, λ_I) such that $\lambda_S(T) = 0$; $\lambda_I(T) = 0$ and for all t:

$$\begin{cases} \dot{S} = \dfrac{\partial \mathcal{H}}{\partial \lambda_S}(S, I, \chi^*, \lambda_S, \lambda_I, t) = -\chi^* I S \\ \dot{I} = \dfrac{\partial \mathcal{H}}{\partial \lambda_I}(S, I, \chi^*, \lambda_S, \lambda_I, t) = \chi^* I S - \gamma I \\ -\dot{\lambda_S} = \dfrac{\partial \mathcal{H}}{\partial S} = \lambda_I \chi^* I - \lambda_S \chi^* I - g - \mathfrak{r}_{\mathrm{I}} \chi^* I \\ -\dot{\lambda_I} = \dfrac{\partial \mathcal{H}}{\partial I} = \lambda_I (\chi^* S - \gamma) - \lambda_S \chi^* S - \mathfrak{r}_{\mathrm{I}} \chi^* S \\ \mathcal{H}(S, I, \chi^*, \lambda_S, \lambda_I, t) \ = \ \max\limits_{\chi(.)} \mathcal{H}(S, I, \chi, \lambda_S, \lambda_I, t) \end{cases} \tag{6.51}$$

The last equation contains the stationarity condition for $\mathcal{H}$:

$$\frac{\partial \mathcal{H}}{\partial \chi} = \lambda_I I S - \lambda_S I S + \mathfrak{r}_{\mathrm{I}} I S + g'(\chi^*) S = 0 \ . \tag{6.52}$$

Therefore, one can compute $\frac{\partial \mathcal{H}}{\partial \chi}$ and apply the following simple scheme:

$$\chi^{(k+1)}(t) = \chi^{(k)}(t) - h\frac{\partial \mathcal{H}}{\partial \chi}(t) \,, \tag{6.53}$$

which is actually much simpler than the scheme applied in Sec. 6.2.1, as it did not require the knowledge of the societal gradient (6.17) which may be complicated to compute. The addition of λ_S and λ_I allows to skip this computation, but it also required a certain preliminary work. This method has been applied successfully and efficiently by Elie *et al.* in [19] to compute the societal optimum of their game.

6.4.2 Genetic algorithm

Here, we explore genetic algorithms as an alternative route to solve the Nash equilibrium of a MFG. We first introduce the theoretical framework in Sec. 6.4.2.1 and we present an application to a vaccination MFG in Sec. 6.4.2.2.

6.4.2.1 Theoretical framework

Genetic algorithms (GAs) are a class of optimization algorithms, we summarize here the key concepts from [216]. GAs aim to solve optimization problems by identifying $\vec{x}_{opt}$ such that $Q(\vec{x}_{opt}) = \max_{\vec{x}}(Q(\vec{x}))$, where Q is the quality or "fitness" function. This approach can be particularly useful in Mean-Field Games where the Bellman equation is not explicitly derivable, that is when the optimal strategy (e.g. Eq. (3.20)) cannot be determined analytically. A first objective of GAs applied to MFG is to perform the Bellman minimization (2.3), that is solve general the problem $\chi^* = \min_{\chi(.)} C(\chi, \bar{\chi})$ for some collective behavior $\bar{\chi}$. Thus, Q represents the cost function up to a negative sign.

Genetic algorithms, and evolutionary computing more generally, are based on the principle of natural selection. The process follows these steps:

- Define the quality function $Q(\vec{x})$ to be maximized.
- Specify the search space, which may be either the parameter space of $\vec{x}$ or a representation of $\vec{x}$.
- Initialize with a random distribution of individuals, where each individual represents a "candidate" $\vec{x}$ to maximize Q.
- Apply a "natural" selection process: individuals with higher fitness (best Q values) are more likely to survive. These survivors are referred to as "parents".
- Generate offspring from the parents by combining their characteristics (crossover). Additionally, introduce mutations by randomly altering certain parameters in the offspring to ensure diversity and enhance space exploration.
- Repeat the process with the new generation to iteratively approach $\vec{x}_{opt}$.

The generality of this algorithm allows flexibility in choosing the number of parents, offspring, and initial candidates. The process for generating offspring (how parental traits are combined) and the mutation operator (which traits are changed and to what extent) must also be defined. These factors directly affect the algorithm's efficiency, and the parameters must be tailored to the specific problem. For instance, in a large search space, a greater number of offspring relative to parents may be required for adequate exploration (it is common, though not mandatory, to work with a fixed number of individuals per generation for simplicity).

The algorithm can terminate after a fixed number of iterations (generations), when it is sufficiently close to the optimum of Q (if known), or via other stopping criteria.

Another promising route of these algorithms is to reach directly the Nash equilibrium of the game. The main idea would be here to represent the players of our game by a large set of different individual strategies. Then, compare their respective costs and define the global strategy as the average over individual costs. Finally define a selection mechanism, inspired by natural selection, that allows to select the best strategies and then generate a new generation. When the Nash equilibrium would be reached, the best individual strategy of players would be to follow the global strategy. This would lead to the convergence of individual's strategies to the same Nash strategy.

During this thesis, we have applied the first objective of such Genetic Algorithms, that is we developed a GA to perform directly the minimization (2.3) on a specific MFG in Sec. 6.4.2.2 that we present below.

6.4.2.2 Application to the SIR model with vaccination

As an application, we propose to recover the results of Laguzet *et al.* [152] with a genetic algorithm. In brief, authors of [152] implement a MFG paradigm to model the vaccination behavior of individuals in a SIRV model. They introduce a cost function J which integrates two terms: one constant cost due to vaccination, and one infection cost which depend on epidemic dynamics. The best individual vaccination rate, modeled as $\lambda^*(t)$ can be found analytically and ends with a "bang-bang" solution: the vaccination rate is maximum at a certain interval, before the epidemic peak: $\lambda^*(t) \propto 1/S(t) \ \in [t_1^*, t_2^*]$ and is zero elsewhere. The values of (t_1^*, t_2^*) can be found analytically. Then, the game converge until a Nash equilibrium toward some values (t_1^N, t_2^N).

The goal of our GA here is to find the optimized λ^* for a given epidemic S, I, R. We describe the general scheme of the GA applied to our problem:

- Our quality function is $Q(\lambda) = -J(\lambda, u)$. We want maximize it for a certain global strategy u.
- Our search space is: $\mathbb{S} = \{0 \leq \lambda(t) \leq \frac{u_{\max}}{S(t)} \ , \ 0 \leq t \leq T\}$ which corresponds to the space of all possible individual strategies. After discretization of time, we obtain a huge space with nP dimensions (nP is the number of discretization points)
- Our initial candidates are taken randomly. We take 200 candidates per generation.
- Selection procedure: as a first guess, we select simply the candidates with the best quality function. We choose 10 to 50 parents. (and so 190 to 150 offspring).
- Offspring procedure: we choose two parents A and B randomly and for each t, $\lambda(t)_{\text{off}} = \frac{\lambda_A(t)+\lambda_B(t)}{2} + \epsilon \frac{u_{max}}{S(t)} \cdot \text{random}(-1, 1)$ for some small factor ϵ. We define in this way both the offspring procedure and the mutation operator.
- We end up the process after a certain fix number of generations.

Because $\mathbb{S}$ is large with nP dimensions (we actually took nP = 4000 in our numerical simulations), the quality function $Q(\lambda)$ of initial candidates $\lambda(t)$ randomly chosen is rather bad, worse than "do nothing": $\lambda(t) = 0 \ \forall t$. It grows very slowly at each generation because a significant part of $\mathbb{S}$ is flat and is far from the peak of Q. Indeed, it corresponds to the

region of the space where $\lambda(t)$ is completely uncorrelated, whereas it has to be to find the maximum of Q. To solve this issue, we propose to first take $\lambda(t) = C = \text{Cst}$ on $[0, T]$ and make an optimization on this C. When the best C is find, we divide the interval into two smaller intervals $[0, \frac{T}{2}]$ and $[\frac{T}{2}, T]$ and we take $\lambda(t) = \text{Cst}$ on each one. For the first offspring generation with "two intervals", we make mutations on each interval to get new candidates with different values on $[0, \frac{T}{2}]$ and on $[\frac{T}{2}, T]$. This method works because the search space is considerably diminished (only one dimension for the first step, then two, etc). When the algorithm converges with two intervals, we cut each interval in two equals parts and we repeat the procedure. We define a threshold in order to know if we reached the maximum of Q at a certain number of intervals: we go further and split in two each interval when the quality function do not evolve during few generations. For instance, we considered that we have reached the maximum for 8 intervals configuration when the maximum of Q among the candidates does not evolve for 3 generations. Then, we move to the 16 intervals configuration and so forth.

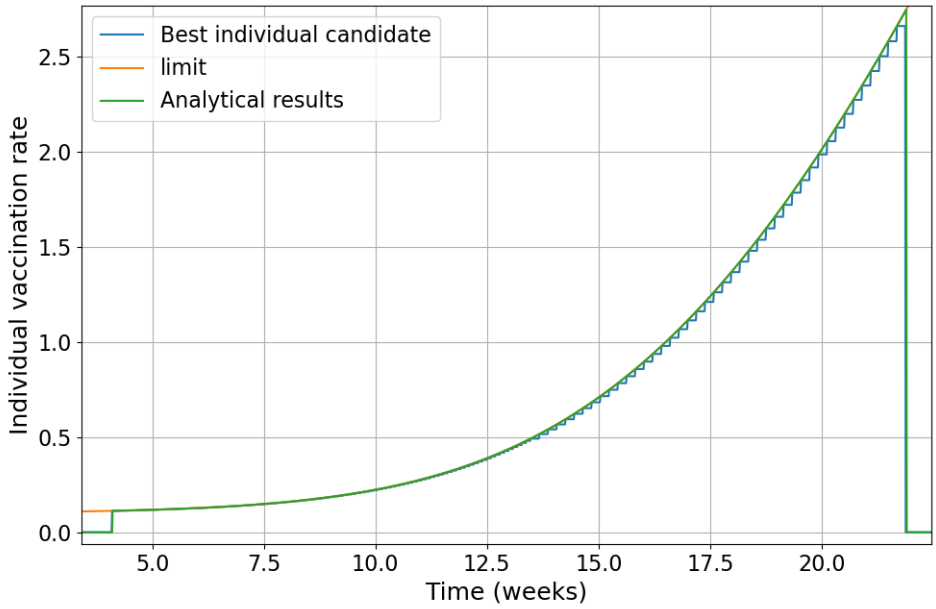

Figure 6.4: Results of the genetic algorithm after 200 generations (512 intervals). The limit in orange is $\lambda_{\max}(t) = \frac{u_{\max}}{S(t)}$. In green are the analytical expected result and in blue the best candidate found by the GA.

We test our algorithm with the same parameters as the ones in [152] and we found the results presented on Fig. 6.4. On Fig. 6.4, we can see that we recover perfectly the expected results. Our algorithm is thus able to compute $F(u) = \lambda^*$ and thus to make the "Bellman arrow" of Fig. 6.1. Then, we can use the inductive sequence to find the Nash equilibrium of our problem (if the latter method converges).

6.5 Discussion

The numerical work of this thesis represented a significant part to implement and test effectively the models developed. The methods that we used to reach the Nash equilibrium or the societal optimum in the different MFG we explored are not optimized or exhaustive. As mentioned in this section, several other techniques already exist and ask to be applied, while other are still under development such as the numerical resolution of the Nash equilibrium through Machine learning approaches [217].

Among the different simulations we performed, the resolution of the Nash equilibrium is probably the one which is the less understood and standardized today in the literature. The Genetic Algorithms introduced in the previous section offer a promising approach to solving the Nash equilibrium by exploring the solution space more broadly. Additionally, the proposed framework is flexible enough to accommodate a wide variety of MFGs with different cost landscapes. This type of algorithm can potentially avoid the formation of loops that may occur with traditional methods, as the transitions between generations tend to be relatively smooth. However, challenges may arise regarding the algorithm's effective convergence within a reasonable time frame, as well as issues related to space discretization that may lead to other complications.

There is still a lack of a general algorithm which would be effective and efficient to find the Nash equilibrium for whole classes of Mean-Field Games.

7 - Conclusion

Modelling human spontaneous behavioral response is crucial if one wants to provide reliable guidelines to policymakers who have to design restrictive measures against an epidemic. As we have seen, a major limitation of current epidemiological models is their failure to incorporate human behavior dynamically, often resulting in overestimated disease impact predictions [17]. While these models now account for restrictions imposed by authorities, they treat human response as an extrinsic factor, overlooking its influence on disease transmission.

Over the past two decades, researchers have explored various models to incorporate behavioral responses as intrinsic parameters. A promising approach is the Mean-Field Games paradigm, which offers several advantages. Notably, it captures the "free rider" effect observed in epidemics, where individuals are less incentivized to act when others do not act. Additionally, the game theoretical framework models individuals as rational agents (or at least partially rational), leading to more realistic and physically grounded emerging behaviors. Pioneer work by Elie *et al.* [19] has introduced MFG into simple models, they have been followed by other works recently [157].

The long-term goal of our work is to progressively bridge the gap between such theoretical models (epidemiological models based on a MFG paradigm) and their practical applications, ultimately evaluating the potential for real-world implementation. To achieve this, two main steps are important: first, incorporating the theoretical framework into models already in use for practical purposes; second, assessing the framework's capabilities using realistic datasets. This work has several objectives:

- **Theoretical advancements:** First on a theoretical viewpoint, determining the difficulties that can occur during the implementation, derivation or the numerical implementation of the model, that may not have been anticipated a priori.
- **Physical understanding:** Second and on a more practical viewpoint, understanding which realistic behaviors the model can capture effectively, while also recognizing the dynamics and effects that remain beyond its scope.
- **Key parameters:** Third, recognizing the key parameters driving the theoretical model, analyzing the associated model sensitivity to determine which ones are essential to obtain from data.
- **Range of possibilities:** Fourth, assessing the potential value for real applications based on the questions the model can effectively address.

From this analysis, we aim to provide data scientists with guidelines for the use of Mean-Field Games in practice, from the parameters that should be extracted from data, along with the range of questions of interest that can be addressed, paving the way for real-world applications.

In this thesis, we developed the two mentioned steps (theoretical implementation and assessing the framework's capabilities) on two different sort of models. In a first part, we implemented in Chapter 3 a MFG approach on a compartmental model with a social structure. This model showed that MFG frameworks can incorporate a reasonable level of complexity, including age-differentiated behavior, while remaining tractable theoretically.

Then, based on realistic (but not real) parameters, we conducted a numerical experiment of our model through realistic datasets. In a second part, we were interested in Chapter 4 to the implementation of a MFG approach inside a Network-based model. Using the pairwise approximation, we developed a MFG model on top of the network structure to study the resulting Nash equilibrium on both homogeneous and heterogeneous networks. We explored the impact of the shape of the social cost f on the Nash equilibrium.

Finally, in a third part in Chapter 5 and as a benchmark for more complicated cases, we left the MFG approach and to focus on the pairwise approximation on regular networks. We solved analytically the SIR-k model (SIR model on regular networks of degree k), namely we got an explicit form for $t(S)$ as a finite sum that we then studied extensively. The $k \to \infty$ limit of our model lead us to derive another formulation for the classical SIR model where an integral form of $t(S)$ is known. The formula we derived Eq. (5.25) allowed us to extract useful approximations, especially for the epidemic peak time. We refer the reader to the more complete conclusion presented in Sec. 5.3 for this part.

Coming back to the MFG models we explored, we got several conclusions regarding our objectives:

Theoretical advancements: On the theoretical side, our work builds upon the contributions by Elie et al.[19], by implementing the Mean-Field Game framework within epidemiological models that can be utilized by authorities. Introducing structures in the population (e.g., age or degree classes, different settings) slightly complicates the equations and derivations, but does not fundamentally alter their nature. During the modeling process, several choices must be made that will significantly impact the cost function, such as the specific nature of interactions between individuals and the corresponding control parameters. In particular, modelers should ensure that their MFG model is symmetric between individuals if they assume symmetric contact patterns. On the numerical side, the gradient descent method proposed in [19] seems appropriate for a variety of scenarios. However, solving the functional equation $F(\bar{\chi}) = \chi^*$ is essential to verify that the system is indeed at a Nash equilibrium. While the Bellman equation provided a straightforward solution in the cases we explored, other minimization techniques (such as Genetic Algorithms) might be required in more complex scenarios. The choice of the number of agent types and control parameters should be made carefully, as the numerical complexity of solving the Nash equilibrium scales at least as $O(n_{\text{cl}}\, n_{\text{set}})$ (and $O(n_{\text{cl}}^4)$ on networks), where n_{cl} is the number of agent classes and n_{set} the number of dynamic control parameters per agent type. Thus, determining the right batching process —i.e., the number and type of classes— becomes a crucial modeling step. However, future numerical advancements could help overcome this limitation, allowing for larger sets of control parameters. Such batching approaches could also be useful for Agent-Based Model implementations.

Physical understanding: The behaviors observed in our numerical simulations were consistent with our physical understanding of the situation: individuals who perceive a high risk of infection —either due to a high probability of infection or the significant consequences of infection— tend to reduce their contact rate. This reduction in contact rates depends on their sensitivity to the cost of contact reduction. The patterns of effort were typically centered around the epidemic peak, displaying smooth U-shaped curves. Additionally, several effects unique to the MFG approach were observed:

- *Cost of Anarchy and the "Free Rider Effect":* The free rider effect, which results in a divergence between individual optimization and societal optimum, presents an opportunity for designing targeted measures based on individual types (e.g., cate-

gorized by age or degree). For high-risk epidemics, the cost of anarchy increases, along with the potential positive impact of external interventions. For lower-risk epidemics, the gap between individual and societal optimization narrows, reducing the margin for imposing constraints. This provides a possible quantitative approach for an intuitive result.

- *Anticipation:* A key feature of the Nash equilibrium in MFG-based epidemic models is the anticipatory behavior of individuals. In typical scenarios where herd immunity is achieved, individuals tend to focus their efforts around the peak of the epidemic when infection probability is high rather than taking preventive measures early. However, the anticipation appears through the cross-anticipation between different groups which plays a significant role. For instance, individuals such as retires or those with lower connectivity adjust their behavior based on their expectations of how others will act. They benefit from the herd immunity achieved in other groups (such as young individuals or those with high connectivity), allowing them to go through the epidemic without experiencing high infection rates within their own group and finally get a better protection for themselves than in absence of the other groups. Furthermore, we observed a "reverse-anticipation" effect among individuals who have minimal efforts to make. These individuals concentrate their efforts slightly after the epidemic peak, once herd immunity has been achieved, capitalizing on the residual high infection level as the epidemic approaches its end. More intricate anticipatory patterns also emerge when individuals implement containment strategies to achieve the Nash equilibrium, strategically avoiding the attainment of herd immunity before the end of their optimization period at time T.

Key parameters: Here we focus on the "cost function" parameters, while other parameters related to social structure or biological factors are well-established in the literature. At the macroscopic level, authorities must carefully select the time horizon T for the epidemic's end, as this choice will lead to different collective strategies: eradication, containment, or achieving herd immunity. However, our work does not provide a specific procedure for setting T, as it likely requires estimations based on factors such as vaccine availability or the seasonality of the virus. The next key parameter is $\mathfrak{r}_{\mathrm{I}}$, which allows for a comparison between the costs of infection and those of social contact reduction. Regarding cost functions, while the cost of infection can be kept constant or based on relatively well-known quantities (e.g., ICU bed availability), the cost of social contact reduction needs to be determined prior to using the model, as it strongly influences the results (see Sec. 4.3). Other quantities, such as $\mathfrak{m}_\gamma$ or $\mathfrak{n}$, are secondary for most applications but would still need to be calibrated for full model integration.

Range of possibilities: Below are the three key questions we have identified to address for the practical implementation of our work:

- *Free Nash equilibrium guided by an authority:* In practice, the Nash equilibrium derived from the MFG framework cannot be expected to be naturally adopted by individual agents. Unlike fields such as Pedestrian Dynamics, where individuals can intuitively anticipate others' behavior, this is not the case here (although similar behaviors may emerge, such as people anticipating their purchases, leading to shortages). However, this Nash equilibrium could be communicated by a trusted health authority, which could provide each individual with the optimal behavior to follow for self-protection, potentially through a mobile application. This mechanism could be loosely compared to road speed limits, where speeds were originally suggested to

help drivers avoid excessive risk, and later formalized into mandatory limits.

- *Design of Non Pharmaceutical Interventions (NPIs):* As discussed earlier, the MFG framework and its resulting Nash equilibrium offer a promising approach for designing NPIs. It allows for consideration of the cost of anarchy, with NPIs aiming to bring the population closer to the societal optimum. For instance, an authority could precisely evaluate the cost of anarchy and decide to implement NPIs when it exceeds a certain threshold, ensuring efficient intervention (also accounting for coordination costs). This provides a more nuanced strategy compared to simply using the "business as usual" scenario as a reference, which can lead to misleading conclusions. Moreover, this framework allows interventions to be designed to different groups, and calculating the societal optimum could serve as a quantitative guideline for designing effective NPIs. Additionally, the chosen collective strategy (eradicating, containing or reaching herd immunity) can be quantitatively realized and refined based on the Nash equilibrium, offering a clearer and more realistic strategies for herd immunity and containment.

- *Get better predictions for epidemic modelling:* By both informing individuals about the Nash equilibrium and designing effective NPIs with anticipated impacts, this work can lead to better predictions of epidemic dynamics. For example, revisiting the work of Ferguson *et al.* [17] on Covid-19, the various scenarios presented could be further refined, affecting epidemic dynamics (through R_0), the range of outcomes, and associated costs. Previously, costs were presented mainly in terms of expected deaths, but non-lethal yet disabling diseases could have severe long-term consequences that are important to consider. Ultimately, this approach could help reduce discrepancies between observed epidemics and predicted outcomes, both in terms of disease spread and associated societal costs.

Research perspectives

We stress out that the three possible routes for applications of MFG to epidemics (namely provide Nash equilibrium to individuals, design NPIs, and get better predictions) still need to be explored and further work is needed before practical applications. In particular, the precise shape of each cost (and the possible costs that we did not use) need to be further investigated. For that purpose, an interdisciplinary work, at the frontier with social and health sciences is required. A promising direction is to follow the way in which QALY and DALY measures have been developed, as they use notions such as utility of a medical condition. Of course, even with such work, uncertainty sources will probably remain important, as the complexity of human behaviors cannot be encapsulated in such simple cost functions. However, it improves on the present status where this question is only addressed is a qualitative way. We point out that this ambition of understanding collective behavior at a macroscopic scale has already been developed in several fields successfully, such as road traffic prediction, protest predictions, or energy consumption.

Beyond this call for practical applications, theoretical ways can be further explored to enhance our comprehension of these Mean-Field Games. First, including a discount factor inside the MFG framework could allow to cut the anticipation time of individuals which may lead to interesting effects, to clearly identity which behaviors are due to anticipation. This discount factor could also close the gap between a realistic individual response and the one provided by the Nash equilibrium studied here, which was reached with a complete information and anticipation for individuals. Other alternative models that may rather

focus on the spontaneous behavior directly, that are closer to the Poletti model's [98], but keeping a "free rider effect", could also be investigated to get fruitful insights. On another perspective, the idea of Stackelberg games with corresponds to a $N + 1$ game between individuals and an authority treated apart seems promising, notably to study the impact and the equilibrium that can be formed between the rules imposed by the authorities and the ones that individuals accept to follow.

I sincerely hope that the work made during my thesis will arouse new works and ideas in the direction of human response modelization in epidemiological models.

A - Choice of parameters in Chapter 3

We reproduce below the set of parameters used in the Tables 3.2-3.3 of Chapter 3 for an easier reading of the parameters choice explanation.

The values of the "social structure" and "biological" parameters in Table A.1 do not represent any particular real-life case, but are chosen to be representative of realistic situations, and therefore in the range typically found in the literature [40, 179, 38, 180, 181, 182]. We take $\xi = 1.2$ week^{-1}, not too far from the values $\xi = 7/6.5 = 1.1$ week^{-1} from [179], $\xi = 7/6.6 = 1.05$ week^{-1} from [182] and $\xi = 7/4 = 1.75$ week^{-1} from [40]. The contagiousness ρ is assumed to be 0.1, similar to the value mentioned in [40] for the Covid-19, where it is slightly lower (about 0.08). Regarding μ, we choose $\mu = 0.2$, of the same order of magnitude as in [182]. Similarly, for the proportion of individuals in the population, the distribution $(25\%, 50\%, 25\%)$ is closed to the one in [182], where it is 22% if you gather the proportion of children and teenagers, 57% for adults, and 21% for seniors. The contact matrices $\mathcal{M}^{\gamma}_{\alpha\beta}$ are inspired by [38] for their shape: almost all contacts in schools are between children, an similarly inside workplaces for adults. In the community, all individuals have the same probability of meeting other individuals, while in households the structure is a bit more complex, with a strong child-adult link and senior-senior contacts. The absolute value of contacts is then normalized so that the average total number of contacts is close to the values presented in [40]. Finally, to ensure the consistency of our choices, we check that all these collected quantities give a reproductive number $\tilde{R}_0 = 2.9$ with the method described in [38, 183] for calculating $\tilde{R}_0$ at the beginning of epidemics in heterogeneous populations. This value is consistent with the literature for viruses such as Covid-19 [16]. The choice of initial conditions $(I_\alpha(t=0))$ is taken uniform among age classes, and since we do not consider stochastic effects at the beginning of epidemics, we take a value of 1% which has little effect on the simulation as long as it is small enough.

The values of the "cost function" parameters in Table A.2 were chosen in a somewhat more arbitrary way with however the following reasoning. The parameters $(\mathfrak{I}_{\text{sat}}, \mathfrak{q}_{\text{sat}})$, which govern the infection dynamics, were selected to ensure that $\mathfrak{I}_{\text{sat}}$ aligns with realistic

$\mathcal{M}^S$	$\mathcal{M}^W$	$\mathcal{M}^C$	$\mathcal{M}^H$
$\begin{pmatrix} 100 & 0 & 0 \\ 0 & 0 & 0 \\ 0 & 0 & 0 \end{pmatrix}$	$\begin{pmatrix} 0 & 0 & 0 \\ 0 & 75 & 0 \\ 0 & 0 & 0 \end{pmatrix}$	$\begin{pmatrix} 12.5 & 25 & 12.5 \\ 12.5 & 25 & 12.5 \\ 12.5 & 25 & 12.5 \end{pmatrix}$	$\begin{pmatrix} 15 & 25 & 10 \\ 12.5 & 32.5 & 5 \\ 10 & 10 & 30 \end{pmatrix}$
$\mathcal{N}_\alpha \equiv N^{\text{tot}}_\alpha / N_{\text{tot}}$	$I_\alpha(0)$	(ξ, ρ, μ)	
$(0.25, 0.5, 0.25)$	$(0.01, 0.01, 0.01)$	$(1.2, 0.1, 0.2)$	

Table A.1: "Social structure" and "biological" parameters used in our simulations. The matrix entries $\mathcal{M}^{\gamma\,(0)}_{\alpha\beta}$ correspond to the average frequency of contacts (per week) between an individual of age class α and someone of age class β in the setting γ. $\mathcal{N}_\alpha = N^{\text{tot}}_\alpha / N_{\text{tot}}$ is the proportion of the population in each age class. $I_\alpha(0)$ are the initial proportion of infected for each age class (we always assume $R_\alpha(0) = 0$). ξ is the recovery rate (per week), ρ the transmission rate per contact, and μ corresponds to the proportion of asymptomatic individuals in the population. Finally, $\alpha = 1, 2, 3$ for age class of young, adults and retired individuals, respectively.

$(\mathfrak{I}_{\text{sat}}, \mathfrak{q}_{\text{sat}})$	κ_α	$\mathfrak{m}_\gamma$	$\mathfrak{n}^\gamma_{\min}$	$(\mathfrak{I}_{\text{d}}, \mathfrak{I}_{\text{l}}, \mathfrak{s})$	T
(0.1, 0.1)	(1,10,100)	(2,2,1,3)	$\left(\frac{1}{3}, \frac{1}{5}, \frac{1}{5}, \frac{1}{2}\right)$	$(0.12, 4.10^{-4}, 0.35)$	40

Table A.2: "Cost-function" parameters associated with the function Eq. (3.11) chosen for our simulations. The cost of infection $\mathcal{I}_\alpha$ Eq. (3.18) is characterized on the one hand by its value under "normal circumstances" $\mathfrak{r}_{\text{I},\alpha} = \mathfrak{r}_{\text{I}}\kappa_\alpha$, where we distinguish a common coefficient $\mathfrak{r}_{\text{I}}$ that will take different values depending on the simulation, and an age-dependent part κ_α, which we will keep fixed at the value given in this table. On the other hand, $\mathfrak{I}_{\text{sat}}$ characterizes the fraction of infected individuals at which the sanitary system starts to malfunction, and $\mathfrak{q}_{\text{sat}}$ the speed at which this malfunction sets in. The cost of reducing once social contact is then parameterized by $\mathfrak{n}^\gamma_{\min}$, the minimum contact willingness in each setting γ, and $\mathfrak{m}_\gamma$, which weights the cost of contact reduction in each setting. $\mathfrak{I}_{\text{d}}, \mathfrak{I}_{\text{l}}$ are the thresholds for the best lockdown and $\mathfrak{s}$ its intensity level. T (in weeks) represents the total duration of the optimization, which in this section is consistently much longer than the characteristic timescale of the epidemic.

estimates from the literature. For instance, the probability of requiring critical care in an ICU due to Covid-19 is estimated at around 0.1% to 1% of the population [17, 40]. In a country like the UK, with a population of approximately 50 million and around 5,000 ICU beds [17], this leads to a saturation threshold of $\mathfrak{I}_{\text{sat}} \simeq 0.1$ at most, to $\mathfrak{I}_{\text{sat}} \simeq 0.01$. Thus, the choice of $\mathfrak{I}_{\text{sat}} = 0.1$ was reasonable, though it represents an upper bound for diseases like Covid-19 and a lower bound for less severe diseases. The epidemic peak observed in the "Business as usual" scenario, reaching 0.2, further motivated this choice.

The parameter $\mathfrak{q}_{\text{sat}}$ was chosen in a more arbitrary manner. A value of $\mathfrak{q}_{\text{sat}} = 1$ led to abrupt and unrealistic behavior changes, while $\mathfrak{q}_{\text{sat}} = 0.01$ produced more significant and physically meaningful effects in the simulations. The parameter κ_α was set based on ICU and mortality probabilities reported in [17, 40]. In [40], there is roughly a factor of 10 between ICU probabilities for different age groups, similar to the classification in Laura Di Domenico's PhD thesis [41], while [17] uses broader age classes.

Parameters $\mathfrak{m}_\gamma$ were chosen more intuitively to explore their impact on individuals' behavior under different settings and the resulting interactions. For example, the weights for school and work were both set to a power of 2 to account for contact reduction, while community contact reduction was assigned a lower weight of 1 and household contacts a higher weight of 3. Similarly, the minimum number of admissible contacts $\mathfrak{n}^\gamma_{\min}$ was chosen based on the relative costs of contact reduction.

We note that these two parameters are not strictly necessary to implement the MFG framework but were useful in exploring the theoretical possibilities of the model while remaining reasonably realistic. The values of $(\mathfrak{I}_{\text{d}}, \mathfrak{I}_{\text{l}}, \mathfrak{s})$ were not predetermined, but resulted from the optimization process within the model's constraints. Finally, before investigating other scenarios, the value of $T = 40$ was chosen so that all simulated epidemics reached herd immunity. The infection cost $\mathfrak{r}_{\text{I}} = 1$ was initially selected to ensure a competitive balance between the different terms of the cost function, but this value was modified in some simulations to test different scenarios.

B - Complements on the Pairwise Approximation

In this appendix we propose complements on the Chapter 4, we first propose an alternative and more formal derivation of the Pairwise Approximation in Sec. B.1. Then, in Sec. B.2, we explain how the notation $G^{xy}_{kk'}$ we introduced can lead to intuitive and useful quantities and we check that the degree-state balance condition is satisfied over time. Finally, in Sec. B.3 we provide a verification that our batching procedure used in Sec. 4.3.3 was still numerically accurate, compared to the averaged Markovian simulation over the associated heterogeneous network.

B.1 Alternative derivation of $G^{xy}_{kk'}$ dynamics with a more formal approach

We derive below a more formal derivation of the Pairwise Approximation. One first remark is that there are two sources of randomness here:

1. The Poisson processes, associated with infection or recovery, are defined by rates.
2. The randomness associated with the network.

B.1.1 Notations

- Vertices will be labeled by Greek letters $(\alpha, \beta, \cdots)$, and the adjacency matrix will be noted $A_{\alpha\beta}$ (equal to one if there is a edge between α and β, zero otherwise).
- The class of a vertex α at time t will be denoted by $c_t(\alpha) = x \in \{s, i, r\}$.
- We will use $\backslash mathbb$ for sets. For instance $\mathbb{V}_\alpha = \{\beta \,/\, A_{\alpha\beta} = 1\}$ is the set of all neighbors of α. The degree d_α of α is $\#\mathbb{V}_\alpha$, where $\#\mathbb{E}$ the cardinal of set $\mathbb{E}$.

For instance

$$\mathbb{D}_k = \{\alpha \,/\, d_\alpha = k\} \qquad \text{(set of vertices of degree } k\text{)}$$
$$\mathbb{TD}_k = \{(\alpha, \beta) \,/\, \alpha \in \mathbb{D}_k \;\&\; \beta \in \mathbb{V}_\alpha\} \qquad \text{(tangent fiber of vertices of degree } k\text{)}$$
$$\mathbb{E}_{kk'} = \{(\alpha, \beta) \,/\, \alpha \in \mathbb{D}_k \;\&\; \beta \in \mathbb{D}_{k'} \;\&\; A_{\alpha\beta} = 1\} \qquad \text{(set of edges between vertices of degree } k \text{ and } k'\text{)}$$

and in the same way

$$\mathbb{X}_k = \{\alpha \,/\, \alpha \in \mathbb{D}_k \;\&\; c_t(\alpha) = x\} \qquad \text{(vertices of degree } k \text{ and class } x \quad (x \in \{s, i, r\})$$

We have $N_k = \#\mathbb{D}_k$ and we define $X_k \equiv \#\mathbb{X}_k / N_k$ $(x \in \{s, i, r\})$ (we note that if $\mathbb{TD}^x_k = \{(\alpha, \beta) \,/\, \alpha \in \mathbb{D}_k \;\&\; c_t(\alpha) = x \;\&\; \beta \in \mathbb{V}_\alpha\}$, then we just have $\#\mathbb{TD}^x_k = k\,\#\mathbb{X}_k = kN_kX_k$).

B.1.1.1 Correlation matrix

We introduce the correlation matrix as

$$\mathbb{G}^{kk'}_{xy} \equiv \{(\alpha, \beta) \in \mathbb{E}_{kk'} \,/\, c_t(\alpha, \beta) = (x, y)\} \tag{B.1}$$
$$G^{kk'}_{xy} \equiv \frac{\#\mathbb{G}^{kk'}_{xy}}{\#\mathbb{TD}^x_k} = \frac{\#\mathbb{G}^{kk'}_{xy}}{kN_kX_k}\,. \tag{B.2}$$

NB: $(\#\mathbb{G}^{kk'}_{xy}) = (\#\mathbb{G}^{k'k}_{yx})$, and thus we recover the detailed balance condition $kN_kX_kG^{kk'}_{xy} = k'N_{k'}Y_{k'}G^{k'k}_{yx}$.

B.1.1.2 Bare rates

Consider a fixed edge (α, β), the rate of transformation of the class of the vertices $c(\alpha, \beta)$ into something else are given by the bare rates

$$\Lambda_{xy}^{x'y'} \text{ such that } P\left[c_{t+dt}(\alpha,\beta)=(x',y') \;/\; c_t(\alpha,\beta)=(x,y)\right] = \Lambda_{xy}^{x'y'}dt \;, \tag{B.3}$$

$$\Lambda_{x}^{x'} \text{ such that } P\left[c_{t+dt}(\alpha)=x' \;/\; c_t(\alpha)=x\right] = \Lambda_{x}^{x'}dt \;. \tag{B.4}$$

In our case

$$\Lambda_{xy}^{x'y'} = \lambda q[\delta_{xs}\delta_{yi} + \delta_{xi}\delta_{ys}]\delta_{x'i}\delta_{y'i} \;, \tag{B.5}$$

$$\Lambda_{x}^{x'} = \xi\delta_{xi}\delta_{yr} \;. \tag{B.6}$$

B.1.1.3 Dressed rates

The point of all the above is to think about sets than directly about probabilities. So again we introduce the sets

$$\mathbb{T}^{kk'}_{(x,y;t)\mapsto(x',y';t+dt)} \equiv \left\{(\alpha,\beta)\in\mathbb{E}_{kk'} \;/\; c_t(\alpha,\beta)=(x,y)\,\&\,c_{t+dt}(\alpha,\beta)=(x',y')\right\} \tag{B.7}$$

and we define the dressed rates $T^{kk'}_{(x,y)\mapsto(x',y')}$ as

$$\left(\#\mathbb{T}^{kk'}_{(x,y;t)\mapsto(x',y';t+dt)}\right) = \left(\#\mathbb{G}^{kk'}_{xy}\right) T^{kk'}_{(x,y)\mapsto(x',y')}dt \;. \tag{B.8}$$

Then, once the vertices (α, β) are specified, one simply uses the bare rates (once the class of two neighbors are fixed, the Poisson process of infection or recovery is completely independent from the statistics of the network), and thus

- If $(x\neq x')$ and $(y\neq y')$

$$\left(\#\mathbb{T}^{kk'}_{(x,y;t)\mapsto(x',y';t+dt)}\right) = \left(\#\mathbb{G}^{kk'}_{xy}\right)\Lambda_{xy}^{x'y'}dt \tag{B.9}$$

- If $(x\neq x')$ and $(y=y')$

$$\left(\#\mathbb{T}^{kk'}_{(x,y;t)\mapsto(x',y;t+dt)}\right) = \left(\#\mathbb{G}^{kk'}_{xy}\right)\left[\Lambda_{xy}^{x'y} + \Lambda_{x}^{x'}\right]dt + \sum_{k''zz'}\left(\#\mathbb{G}^{kk'k''}_{xyz}\right)\Lambda_{xz}^{x'z'}dt \tag{B.10}$$

- If $(x=x')$ and $(y\neq y')$

$$\left(\#\mathbb{T}^{kk'}_{(x,y;t)\mapsto(x,y';t+dt)}\right) = \left(\#\mathbb{G}^{kk'}_{xy}\right)\left[\Lambda_{xy}^{xy'} + \Lambda_{y}^{y'}\right]dt + \sum_{k''zz'}\left(\#\mathbb{G}^{k'kk''}_{xyz}\right)\Lambda_{yz}^{y'z'}dt \;, \tag{B.11}$$

with

$$\mathbb{G}^{kk'k''}_{xyz} = \{(\alpha,\beta,\gamma)\in\mathbb{W}^{k\to k''}_{k\to k'} \;/\; c_t(\alpha,\beta,\gamma)=(x,y,z)\} \;, \tag{B.12}$$

$$\mathbb{W}^{k\to k''}_{k\to k'} = \{(\alpha;\beta,\gamma)\in D_k\times D_{k'}\times D_{k''} \;/\; (\beta,\gamma)\in V_\alpha^2\} \qquad \text{(set of wedges of degrees } k,\, k',k'') \;, \tag{B.13}$$

and where the last term in Eq. (B.10) comes from the vertices other that β to which α is connected, and for Eq. (B.11) from the vertices other α that to which β is connected. From the definition Eq. (B.8) of the dressed rate and Eqs. (B.10)-(B.11), we get

$$T^{kk'}_{(x,y)\mapsto(x',y')} = \Lambda_{xy}^{x'y'} + \delta_{yy'}\left[\Lambda_{x}^{x'} + \sum_{k''zz'}\frac{\left(\#\mathbb{G}^{kk'k''}_{xyz}\right)}{\left(\#\mathbb{G}^{kk'}_{xy}\right)}\Lambda_{xz}^{x'z'}\right] + \delta_{xx'}\left[\Lambda_{y}^{y'} + \sum_{k''zz'}\frac{\left(\#\mathbb{G}^{k'kk''}_{yxz}\right)}{\left(\#\mathbb{G}^{k'k}_{yx}\right)}\Lambda_{yz}^{y'z'}\right] \;. \tag{B.14}$$

In our case, we get for instance

$$T^{kk'}_{(si)\mapsto(ii)} = \lambda q\left(1 + \sum_{k''}\frac{\left(\#\mathbb{G}^{kk'k''}_{sii}\right)}{\left(\#\mathbb{G}^{kk'}_{si}\right)}\right) \;. \tag{B.15}$$

B.1.2 The Pairwise Approximation

As always, we need the $\left(\#\mathbb{G}^{kk'}_{xy}\right)$ to compute the evolution of the $\left(\#\mathbb{G}^{k}_{x}\right) \equiv \left(\#\mathbb{X}^{k}\right)$, but we need the $\left(\#\mathbb{G}^{kk'k''}_{xyz}\right)$ to compute the evolution of the $\left(\#\mathbb{G}^{kk'}_{xy}\right)$. We can move forward if we assume that the three-body correlations are negligible (which presumably make sens if loops are rare). We define

$$\mathbb{G}^{kk'k''}_{xyz} = \{(\alpha,\beta,\gamma) \ / \ \alpha \in \mathbb{D}_k \ \& \ (\alpha,\beta) \in \mathbb{G}^{kk'}_{xy} \ \& \ (\alpha,\gamma \neq \beta) \in \mathbb{G}^{kk''}_{xz}\} \ , \tag{B.16}$$

which, assuming no correlation beyond the two body ones (Pairwise Approximation), leads to write

$$\left(\#\mathbb{G}^{kk'k''}_{xyz}\right) = \underbrace{N_k X_k}_{\#\text{ of } \alpha\in\mathbb{D}_k} \ \underbrace{k}_{\#\text{ of } \beta} \ \overbrace{G^{kk'}_{xy}}^{\text{conditional proba}} \ \underbrace{(k-1)}_{\#\text{ of } \gamma} \ \overbrace{G^{kk''}_{xz}}^{\text{conditional proba}} \ , \tag{B.17}$$

which, with Eq. (B.2) (ie $\#\mathbb{G}^{kk'}_{xy} = G^{kk'}_{xy} k N_k X_k = k' N_{k'} X_{k'} G^{k'k}_{yx}$) gives

$$T^{kk'}_{(x,y)\mapsto(x',y')} = \Lambda^{x'y'}_{xy} + \delta_{yy'}\left[\Lambda^{x'}_{x} + \sum_{k''zz'}(k-1)G^{kk''}_{xz}\Lambda^{x'z'}_{xz}\right] + \delta_{xx'}\left[\Lambda^{y'}_{y} + \sum_{k''zz'}(k'-1)G^{k'k''}_{yz}\Lambda^{y'z'}_{yz}\right] . \tag{B.18}$$

In our case, we get for instance

$$T^{kk'}_{(si)\mapsto(ii)} = \lambda q\left(1 + (k-1)\sum_{k''} G^{kk''}_{si}\right) \ , \tag{B.19}$$

which corresponds to Eq. (4.15).

B.1.3 Getting to Eq. (4.16)

Once the dressed rate are settled, we can write:

$$\int_t^{t+dt} (\#\dot{\mathbb{G}}^{kk'}_{xy})dt = -\sum_{x'y'}\left(\#\mathbb{T}^{kk'}_{(x,y;t)\mapsto(x',y';t+dt)}\right) + \sum_{x'y'}\left(\#\mathbb{T}^{kk'}_{(x',y';t)\mapsto(x,y;t+dt)}\right)$$

and thus, removing the constant factor kN_k which appears in all terms

$$(X_k \dot{G}^{kk'}_{xy}) = -X_k\, G^{kk'}_{xy} \sum_{x'y'} T^{kk'}_{(x,y)\mapsto(x',y')} + \sum_{x'y'} X'_k\, G^{kk'}_{x'y'}\, T^{kk'}_{(x',y')\mapsto(x,y)} \ , \tag{B.20}$$

which is nothing but Eq. (4.16) with slightly more general notations.

B.2 Normalization rules for $G^{xy}_{kk'}$

In our point of view, the interest of introducing $G^{xy}_{kk'}$ resides also in all the correlations that can be accessed through it. This for point correlation matrix (two for states and two other for degrees) allows to write in a very intuitive way three, two and one point correlations. To remove the right hand side point, one only has to sum over the degree or the state, while for the left hand side point one must add a weighting factor. The way of reading these quantities is always the same: it is the probability for a neighbor of a vertex characterized by the two left points (which can be empty) of the matrix (for instance a

vertex of degree k and state x) to have be characterized by the two right point of the matrix. Thus, three point correlations are given by

$$\begin{aligned} G_k^{xy} &= \sum_{k'} G_{kk'}^{xy} = P(\text{neighbor of state y} \mid \text{k of state x}) \\ G^{xy}_{\ k'} &= \sum_{k} k x_k P(k) G_{kk'}^{xy} = P(k' \text{ of state y} \mid \text{vertex of state x}) \ , \end{aligned} \tag{B.21}$$

and the scheme continue for the two points correlations, with for instance (among the 6 possibilities):

$$\begin{aligned} G^{xy} &= \sum_{k,k'} k x_k P(k) G_{kk'}^{xy} = P(\text{vertex of state x} \mid \text{vertex of state y}) \\ G^{x}_{\ k'} &= \sum_{k,y} k x_k P(k) G_{kk'}^{xy} = P(k' \mid \text{vertex of state x}) \ . \end{aligned} \tag{B.22}$$

Continuing this process, we can get the two and one point correlations which are sometimes normalized, together with the normalization which mush be satisfied. The time independent relations are given by

$$\begin{aligned} G_k &= \sum_{k'} G_{kk'} = 1 \\ P(k) k G_{kk'} &= P(k') k' G_{k'k} \ , \end{aligned} \tag{B.23}$$

while other are time dependent:

$$\begin{aligned} &\sum_{y} G_k^{xy} = \sum_{k'} G_{kk'}^{x} = G_k^x = 1 \\ &\sum_{x} x_k = 1 \\ &x_k P(k) k G_{kk'}^{xy} = y_{k'} P(k') k' G_{k'k}^{yx} \ . \end{aligned} \tag{B.24}$$

All these relations should be satisfied at each time t. Using the expression $\dot{G}_{kk'}^{xy}$ that we derived Eq. (4.17), together with these expressions at t, one can check that they remain valid at time $t+dt$, confirming the consistency of the system. Besides, other normalization relations are satisfied:

$$G_{kk'}^{x} = G_{kk'} \tag{B.25}$$

$$G^{\ y}_{kk'} = y_{k'} G_{kk'} \ , \tag{B.26}$$

where the first equation indicates that knowing the state of a starting vertex has no influence on the probability to find a neighbor of degree k', as the networks we considered are completely fixed over time. The second equations indicates that knowing only the degree of a starting vertex will not bring any information about the state of the neighbor y, and therefore the two probabilities (be of degree k' and be of state y) must be independent.

B.3 Validation of our batching procedure on the Pairwise Approximation

In Fig. B.1, we demonstrate that the pairwise approximation, combined with the batching procedure applied in Sec. 4.3.3, provides a highly accurate representation of the network dynamics we aimed to reproduce. The small discrepancies observed do not significantly affect the general observations or the conclusions drawn regarding the Nash equilibrium on such networks.

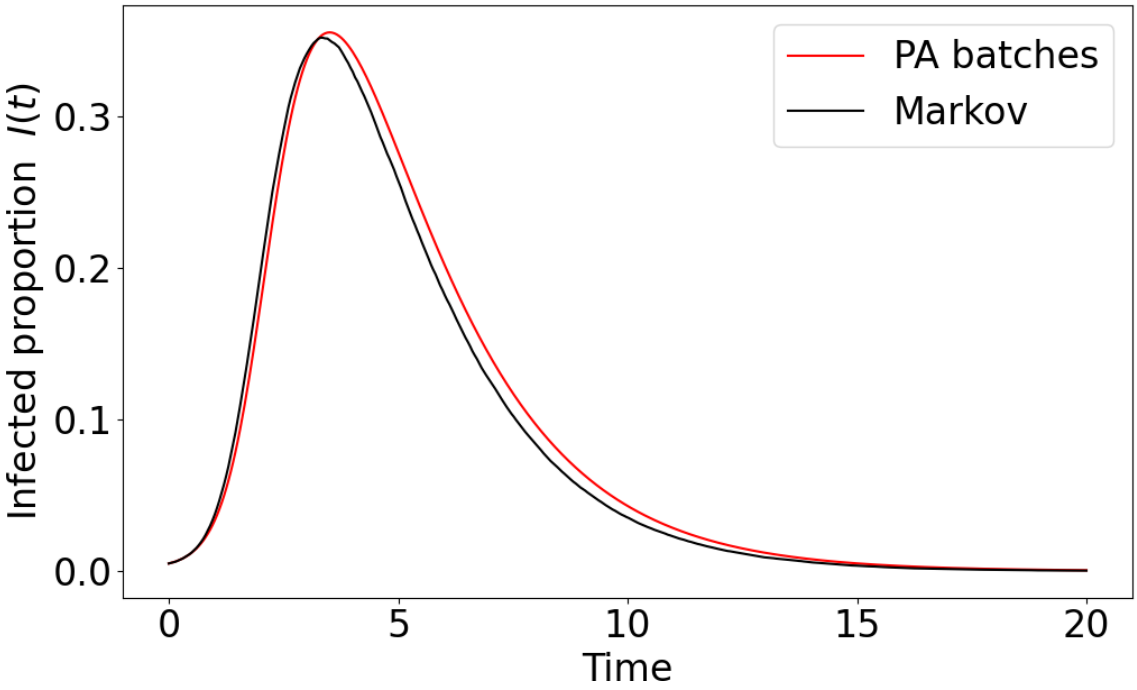

Figure B.1: Evolution of total infected proportion over time on an heterogeneous network. Red line: Pairwise Approximation Eq. (4.13) applied on the heterogeneous network of Sec. 4.3.3, together with the batching procedure describe in the section. Black line: average Markov process over $n_{it} = 10$ iterations, with $N = 15000$ nodes (to allow for the presence of degrees around $k_{\max} \simeq 100$)

C - Social structure description of epidemic propagation with a MFG paradigm

Letter

Social structure description of epidemic propagation with a mean-field game paradigm

Louis Bremaud and Denis Ullmo
Université Paris-Saclay, CNRS, LPTMS, 91405, Orsay, France

(Received 4 July 2022; accepted 14 November 2022; published 5 December 2022)

As emphasized by the recent pandemic crisis, the design of coherent policies against epidemic propagation is of major importance and required to model both epidemic quantities and individuals behavior because the latter has a strong influence on the former. To address this issue, we consider the spread of infectious diseases through a mean field game version of a SIR compartmental model with social structure, in which individuals are grouped by their age class and interact together in different settings. In our game theoretical approach, individuals can choose to limit their contacts if the epidemic is too virulent, but this effort comes with a social cost. We further compare the Nash equilibrium obtained in this way with the societal optimum that would be obtained if a benevolent central planner could decide on the strategy of each individual, as well as to the more realistic situation where an approximation of this optimum is reached through social policies such as lockdown.

DOI: 10.1103/PhysRevE.106.L062301

As Covid-19 has made rather explicit in the last few years, possessing good prediction tools for the dynamics of virus infections is mandatory if one wishes to design public policies making it possible to effectively mitigate the negative impact of an epidemic. Since the early twentieth century, many models have been proposed to address this issue, one of the simplest being the SIR (Susceptible-Infected-Recovered) compartment model [1] and its variations [2], which has been recently refined to take into account the structure of social contacts [3,4] or spatial/geographic aspects of the dynamics [5,6].

For virus epidemics like Covid-19, with very fast dynamics, one important difficulty met by epidemiologists can already be illustrated on the SIR model. Noting S, I, and R the relative proportion of agents in the three possible states (respectively "Susceptible", "Infected", and "Recovered"), the time dependence of these "state variables" follow the set of equations

$$\begin{aligned} \dot{S} &= -\chi S(t) I(t), \\ \dot{I} &= (\chi S(t) - \xi) I(t), \\ \dot{R} &= \xi I(t), \end{aligned} \tag{1}$$

which are characterized by two "*extrinsic*" parameters, (that is, external parameters fixed outside of the model), the recovery rate ξ, and the contact rate χ.

Given the height of the stakes posed by the control of the Covid-19 epidemics in the last couple of years, both from a public health and economic point of view, major efforts have been invested by the epidemiologist community to extract these parameters, or their counterpart in more complex models, from the actual data observed on the field. However, if ξ is mainly fixed by biological considerations, and thus can be considered as essentially constant in time, the contact rate χ on the other hand depends a lot on the agent's behavior (i.e., whether they actually meet or not) which has a dynamic of its own. This dynamic is furthermore coupled to the dynamics of the epidemic itself since people will limit or increase their contacts depending on whether or not they feel at risk from the epidemic. This implies that it is essentially impossible to fit the time dependence of χ on past data. In models used to advise public policies, this time dependence is thus either simply ignored, or involves a lot of guesswork, leading to predictions that can be trusted only for a rather short amount of time (see nevertheless [7,8]). To avoid such a situation, it is necessary to introduce models whose *extrinsic* parameters have no time dependence (on the time scale of the epidemic), and which can therefore be fitted in a reliable way on field data. In other words, it is necessary to make *intrinsic* the dynamics of parameters such as χ (i.e., to make them internal parameters computed within the model). To achieve this, a game theoretical approach is required, and the one that we will follow here is provided by mean field game (MFG) theory.

Introduced by Lasry and Lions a decade ago [9–11] and independently by Huang, Malhamé, and Caines [12], mean field games (MFG) focus on the derivation of a Nash equilibrium within a population containing a larger number of individuals. Reader can look at [13–15] for a complete mathematical description, and to [16,17] for an introduction designed for physicists. Applications of MFG, include finance [18], economics [19], and opinion dynamics [20] among others. The introduction of MFG models to describe epidemic dynamics has been pioneered by Turinici *et al.* to describe vaccination strategies [21] or the dynamics of the parameter $\chi(t)$ in the simple SIR model [22].

The simple toy models addressed in [22] are, however, presumably still too schematic to be relevant from a practical, public policy point of view. The goals of this Letter are to show that a good degree of complexity can be included in these MFG models, and in particular that we can implement a description of the social structure of society in which the

epidemics develop. Furthermore, we shall see that with our mean field game approach, question of direct practical importance, such as defining the best government strategy with respect to confinement and deconfinement policies, can be addressed.

We therefore consider a SIR model with a structure of social contacts proposed in [3,4] to get a more detailed description of the society at a mesoscopic scale. Following [3], we make a differentiation between individuals according to their age. Here we choose to introduce three age classes: "young," "adult," and "retired" people but a more refined description could easily be implemented. Furthermore, we split the society in four main settings where individuals have contacts with others: the schools, the households, the community, and the workplaces. Thus the dynamics of the epidemic may differ for different age classes and the interactions between individuals (of the same class or not) may differ in different settings.

To model the interactions, following [3], we introduce the parameters $M^{\gamma}_{\alpha\beta}$ which measure the average frequency of contacts with someone of age class β for an individual of age class α in the setting γ. To enforce the sum rule imposed by the fact that a contact between two agents involves both of them in a symmetric way, we make a slight variation here with respect to [3] and set $M^{\gamma}_{\alpha\beta} = W^{\gamma}_{\alpha\beta} \cdot K_{\beta}$ where $W^{\gamma}_{\alpha\beta}$ is a symmetric matrix and K_{β} is the proportion of individuals of age class β in the population. Physically, $W^{\gamma}_{\alpha\beta}$ can be seen as the "willingness of contact" between an individual of age class α and another of age class β in the setting γ. We assume here that this symmetric matrix is built as $W^{\gamma}_{\alpha\beta} = w^{\gamma}_{\alpha\beta} \cdot w^{\gamma}_{\beta\alpha,}$ where $w^{\gamma}_{\alpha\beta}$ is the "willingness" of an individual of age class α to have contact with someone of age class β (in the setting γ).

In our game theoretical approach, we assume that individuals of age class α control their "willingness of contact" with other individuals in each setting. We therefore write $w^{\gamma}_{\alpha\beta} = w^{\gamma(0)}_{\alpha\beta} n^{\gamma}_{\alpha}(t)$, where $w^{\gamma(0)}_{\alpha\beta}$ denotes this "willingness" in the absence of epidemic (similarly for $W^{\gamma(0)}_{\alpha\beta}$ and $M^{\gamma(0)}_{\alpha\beta}$), and $n^{\gamma}_{\alpha}(t) \in [n^{\gamma}_{\alpha,\min}, 1]$ is a time dependent coefficient measuring the effort made by the individual to limit contact because of the epidemic situation, and which is assumed to vary between a value $n^{\gamma}_{\alpha,\min}$ representing the maximum effort that can be expected from the agent and one corresponding to the base willingness in the absence of effort. Notice that, for simplicity, we use n^{γ}_{α} instead of $n^{\gamma}_{\alpha\beta}$, that is individuals do not change their behavior according to the age class of the contact β but only according to the setting γ (a β dependence of n could easily be implemented to this model and only slightly change the equations).

Indexing by α the proportion of susceptible/infected/recovered people of age class α, and denoting by q the probability of transmission (of the virus) per effective contact (between a susceptible and an infected), the SIR equations (with $n = 3$ age classes) read [3]

$$\begin{aligned} \dot{S}_{\alpha} &= -\bar{\lambda}_{\alpha}(t) S_{\alpha}(t), \\ \dot{I}_{\alpha} &= +\bar{\lambda}_{\alpha}(t) S_{\alpha}(t) - \xi I_{\alpha}(t), \\ \dot{R}_{\alpha} &= \xi I_{\alpha}(t), \end{aligned} \tag{2}$$

where the "force of infection" $\bar{\lambda}_{\alpha}(t)$ corresponds to q time, the average number of infected people met by a susceptible agent of age class α during dt, and is written as

$$\bar{\lambda}_{\alpha}(t) \equiv q\left[\sum_{\beta=1}^{n}\sum_{\gamma} \bar{n}^{\gamma}_{\alpha}(t)\, \bar{n}^{\gamma}_{\beta}(t)\, M^{\gamma(0)}_{\alpha\beta}\, I_{\beta}(t)\right], \tag{3}$$

with $\bar{n}^{\gamma}_{\alpha}$ the average value of n^{γ}_{α} over agents in the age class α. In the following, we will denote λ (without bar above) when we focus on the force of infection seen by a reference individual, $\lambda_{\alpha}(t) \equiv q[\sum_{\beta=1}^{n}\sum_{\gamma} n^{\gamma}_{\alpha}(t)\bar{n}^{\gamma}_{\beta}(t)M^{\gamma(0)}_{\alpha\beta}I_{\beta}(t)]$.

In our mean field game version of this model, the state variable of an agent k_{α} of age class α is her status $x_{k_{\alpha}} \in \{s_{\alpha} = \text{susceptible}, i_{\alpha} = \text{infected}, r_{\alpha} = \text{recovered}\}$. The control parameters of individuals of age class α are the contact willingness $n^{\gamma}_{\alpha}(t)$, and each individual k_{α} which is susceptible at time t (i.e., $x_{k_{\alpha}} = s_{\alpha}$) will adjust the contact willingness to minimize an inter-temporal cost that we take of the form

$$\begin{aligned} C_{\alpha}(\{n^{\gamma}_{\alpha}(\cdot)\}, t) \equiv \int_{t}^{T} &\left[\lambda_{\alpha}(s)\tilde{r}_{I,\alpha}(I(s)) + f_{\alpha}\left(\left\{n^{\gamma}_{\alpha}(s)\right\}\right)\right] \\ &\times \left(1 - \phi^{I}_{\alpha}(s)\right) ds. \end{aligned} \tag{4}$$

In this equation

$$\tilde{r}_{I,\alpha}(I(s)) = r_{I,\alpha} + g_{\alpha}(I(s)) \tag{5}$$

is the total cost of infection, which includes a base cost $r_{I,\alpha}$ (which we assume increases with the age class α, modeling that we suffer more from infection when we are older), and an additional cost $g_{\alpha}(I(s))$ which models the saturation of the sanitary system. $f_{\alpha}(\{n^{\gamma}_{\alpha}(s)\})$ measures the cost (both psychological and financial) associated with the limitation of social contacts (we assume this cost to be decreasing, with a positive second derivative), and $\phi^{I}_{\alpha}(t)$ is the probability for our reference individual of age class α to be infected before t, so that an infection for this individual happens between t and $t + dt$ with a probability $(1 - \phi^{I}_{\alpha}(t))\lambda_{\alpha}(t)dt$. Note that in principle one should also specifically model the behavior of infected people, as this could vary from a completely egoistic approach where they stop making any effort to a very altruistic one where infected people completely isolate from the rest of population. In epidemics like Covid-19, however, most of the transmission is due to a small part of the infected people not aware of their infectious status. Our model corresponds to the limit where this proportion is extremely small, and for which q, the probability of transmission of the virus, integrates this probability.

To solve this optimization problem, we follow a standard approach in this context [15], and introduce the *value function*

$$U_{\alpha}(t) = \min_{\{n^{\gamma}_{\alpha}(\cdot)\}} C_{\alpha}\left(\left\{n^{\gamma}_{\alpha}(\cdot)\right\}, t\right), \tag{6}$$

which is thus the minimal price (in stochastic average) that a susceptible agent (at t) can pay between t and the end of the game. Using the Bellman equation, which states that, for any intermediate time t_i, the optimal path between t and T can be constructed as the concatenation of optimal paths between t and t_i and between t_i and T followed by an optimization of the state of the system *at* t_i we get the Hamilton-Jacobi-Bellman

equation of our mean field game

$$-\frac{dU_\alpha(t)}{dt} = \min_{\{n_\alpha^\gamma(t)\}}\left[\lambda_\alpha(t)(\tilde{r}_{I,\alpha}(I(t)) - U_\alpha(t)) + f_\alpha\left(\{n_\alpha^\gamma(t)\}\right)\right]. \tag{7}$$

Then, the optimal strategy $n_\alpha^{\gamma *}(t)$ is expressed as

$$\{n_\alpha^{\gamma *}(t)\} = \underset{\{n_\alpha^\gamma(t)\}}{\operatorname{argmin}}\left[\lambda_\alpha(t)(\tilde{r}_{I,\alpha}(I(t)) - U_\alpha(t)) + f_\alpha\left(\{n_\alpha^\gamma(t)\}\right)\right]. \tag{8}$$

We stress, however, that in Eq. (4), the dynamic of the infection Eqs. (2) and (3) at time t, is fixed by the strategies $\bar{n}_\alpha^\gamma(s < t)$, followed (on average) by the total population of agents, which is *a priori* distinct from the one $n_\alpha^{\gamma *}$ followed by the individual optimizing the cost Eq. (4). In all rigor, this cost should be written as $C_\alpha(\{\bar{n}_\alpha^\gamma\}, \{n_\alpha^\gamma\}, t)$, and the situation for which for all settings γ and all age classes α one has

$$n_\alpha^{\gamma *} = \bar{n}_\alpha^\gamma \tag{9}$$

corresponds to a Nash equilibrium, in the sense that an individual agent has no interest in deviating to another strategy if this strategy is followed by the rest of the agents. 'solving" our mean field game therefore amounts to: (i) Solve the rate equations (2) assuming the general population strategy $\{\bar{n}_\alpha^\gamma\}$ given. This in particular will determine epidemic quantities such as $I_\alpha(t)$, from which $\lambda_\alpha(s)$ and $\phi_\alpha^I(t) = 1 - e^{\int_0^t \lambda_\alpha(s)ds}$ can be derived, making it possible to compute the cost Eq.(4) for a given individual strategy $\{n_\alpha^\gamma(t)\}$; (ii) Solve the optimization problem for $\{n_\alpha^\gamma(t)\}$ defined by the cost Eq. (4) and deduce from it $\{n_\alpha^{\gamma *}\}$, the optimal $\{n_\alpha^\gamma\}$ for a given individual; and (iii) Impose the self consistent equation (9) that defines the Nash equilibrium of our MFG. In practice, this third step (iii) can be realized in different ways, either using a recursive sequence until (9) is fulfilled or using a gradient descent, slowly moving the general population strategy to reach the same fixed point where $n_\alpha^{\gamma *} = \bar{n}_\alpha^\gamma$. We use both methods in our numerical simulations.

Since the time dependence of the $\{n_\alpha^\gamma\}$ is now an outcome of the description, our MFG model defined by the dynamics Eqs. (2) and (3) and the cost function Eq. (4) clearly meet the criterion that all the extrinsic parameters characterizing it are time independent, and could in principle be fitted on field data. The actual extraction of these parameters is, of course, well beyond the scope of this work, and in the following, we illustrate the behavior of our MFG for a "reasonable choice" of this parametrization (these quantities are rather generic, and the observed behaviors are *a priori* typical, which was checked by running many simulations with different parameters).

As mentioned above, we consider four settings (S = schools, W = workplaces, C = community, and H = households) and three age classes (y = youth, a = adult, and r = retired). For the cost of infection Eq. (5) we take

$$\tilde{r}_{I,\alpha}(I(t)) = \kappa_\alpha\left[r_I\left(\exp\left[\alpha_{\text{sat}}\frac{I(t) - I_{\text{sat}}}{I_{\text{sat}}}\right]\right)\right], \tag{10}$$

where the factors κ_α account for the fact that older agents are more impacted by the infection, while r_I and α_{sat} are both constant modeling, respectively, the usual cost of infection and the impact of saturation on the cost. The additional cost is exponential with a threshold when we reach the saturation at $I = I_{\text{sat}}$. Finally, for the cost of the contact willingness

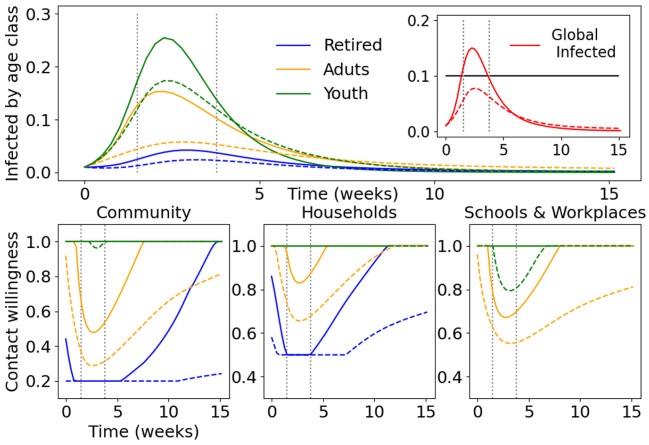

FIG. 1. Evolution of the epidemic quantities and contact willingness with $r_I = 1$ (solid line) and $r_I = 5$ (dashed line). Upper panel: evolution of proportion of infected by age class. Lower panel (left to right): evolution of contact willingness of individuals according to their age class in community, households, schools (for the young), and workplaces (for the adults).

reduction $f_\alpha(\{n_\alpha^\gamma\})$ we take a form inspired from [22]

$$f_\alpha(\{n_\alpha^\gamma(t)\}) = \sum_\gamma\left[\left(\frac{1}{n_\alpha^\gamma(t)}\right)^{\mu_\gamma} - 1\right], \tag{11}$$

where μ_γ models variability of the "attachment" to the setting γ, as it is for example easier to reduce contacts at work rather than inside families.

Figure 1 shows the dynamics of the epidemic together with the choices made by individuals for their contact willingness for both a relatively moderate cost for the infection ($r_I = 1$) and a much stronger one ($r_I = 5$), with the choice of parameters given in Table I. The simulations have been obtained using a gradient descent on the variable $\{n_\alpha^\gamma\}$ of the cost C to reach the Nash equilibrium. In the case $r_I = 1$, we see in this figure that there are significant efforts made by individuals when $I(t)$ exceed the threshold I_{sat}. More precisely, retired people significantly reduce their contacts because the cost associated with the infection is for them very high and this reduction is done, in particular in the community setting, because this is the easiest place to reduce one's contacts. On the other hand, young people, who take no significant risk with the disease, barely modify their behavior, while the adults are in an intermediate situation. For $r_I = 5$, the cost of infection is sufficiently high so that one does not reach the saturation I_{sat}, the epidemic is lower and slower.

In the previous equilibrium analysis, each agent performs a personal, eventually egoistic, optimization. A "benevolent global planner", i.e., a well meaning government with full empowerment, would, on the other hand, attempt to reach a "societal optimum" [22–24], i.e., to optimize the global cost of the entire society, which would amount to solve :

$$\min_{\{\bar{n}^\gamma\}} C_{\text{glob}}\left(\{\bar{n}_\alpha^\gamma\}\right) \equiv \min_{\{\bar{n}^\gamma\}} \sum_\alpha\left[K_\alpha \times C_\alpha\left(\{\bar{n}_\alpha^\gamma\}, \{\bar{n}_\alpha^\gamma\}\right)\right]. \tag{12}$$

The difference between this new minimization and the Nash equilibrium discussed above is referred to as "the cost of

TABLE I. Table of parameters used in our simulations. The matrix entries $M^{\gamma}_{\alpha\beta}$ correspond to the average frequency of contacts (per week) between an individual of age class α and someone of age class β in the setting γ. κ_α is the coefficient appearing in $\tilde{r}_{I,\alpha}$. K_α is the proportion of the population in each age class. $n^{\gamma}_{\min}$ is the minimum contact willingness in each setting γ, while μ_γ weighs the cost of contact reduction in each setting. $(S_\alpha(0), I_\alpha(0))$ are the initial conditions for each age class. ξ is the recovery rate (per week), q the transmission rate per contact. I_l, I_d are the thresholds for the optimal lockdown and σ its level.

M^S	M^W	M^C	M^H	κ_α	K_α	n^{γ}_{min}	μ_γ
$\begin{pmatrix}100&0&0\\0&0&0\\0&0&0\end{pmatrix}$	$\begin{pmatrix}0&0&0\\0&75&0\\0&0&0\end{pmatrix}$	$\begin{pmatrix}12.5&25&12.5\\12.5&25&12.5\\12.5&25&12.5\end{pmatrix}$	$\begin{pmatrix}15&25&10\\12.5&32.5&5\\10&10&30\end{pmatrix}$	(1,10,100)	(0.25, 0.5, 0.25)	$(\frac{1}{3}, \frac{1}{5}, \frac{1}{5}, \frac{1}{2})$	(2,2,1,3)
$S_\alpha(0)$	$I_\alpha(0)$	(I_{sat}, α_{sat})	ξ	q	I_l	I_d	σ
(0.99, 0.99, 0.99)	(0.01, 0.01, 0.01)	(0.01,0.01)	1.2	0.02	0.1	4×10^{-4}	0.39

anarchy", because there is no cooperation between individuals in the Nash equilibrium contrary to the societal optimum case. We compute it with a gradient descent on the cost C_{glob}, and we plot the dynamics on Fig. 2.

In practice however, it is largely impossible for a government to control the detailed behavior of each individual, especially in democratic countries, and even if this was technically feasible, it would involve an important coordination cost that would have to be included in the epidemic cost Eq. (4). Government will therefore use median mode of actions, such as lockdown, to approach the societal optimum at a reasonable coordination (and democratic) cost. We now address the question of how the lockdown policy can be used to approach as well as possible the societal optimum.

We therefore assume that above a certain threshold of infection, I_l, a global planner imposes a reduction of the maximum contact willingness $n^{\gamma}_{\alpha l}$, that we assume of the form $n^{\gamma}_{\alpha l} = \sigma n^{\gamma}_{\alpha,\min} + (1-\sigma)$, $(\sigma \in [0,1])$ in each setting for each individual. As the proportion of infected decreases we assume the lockdown is lifted when $I(t)$ goes below a value $I_d < I_l$, which is assumed lower than I_l to avoid unrealistic oscillations around I_l. For a given value of the thresholds and of the

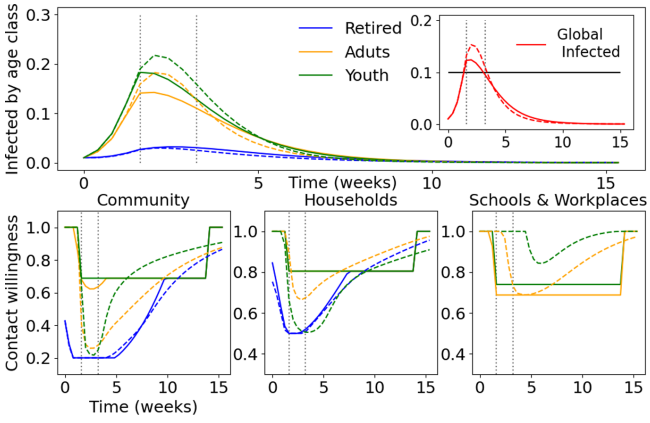

FIG. 2. Evolution of the epidemic quantities and contact willingness for the societal optimum (dashed line) and the optimal lockdown policy (solid line). Upper panel: evolution of proportion of infected by age class (main panel) and on average (inset). Lower panel (left to right): evolution of contacts willingness of individuals according to their age class in community, households, schools, and workplaces.

$n^{\gamma}_{\alpha l}$ we can compute the Nash equilibrium as in our original approach, and we can then perform a gradient descent on these parameters (σ, I_d, I_l) to reach their optimal value, i.e., the optimal lockdown policy.

We show in Fig. 2 the numerical simulation for the societal optimum and for the optimal lockdown policy, with the same parameters as Fig. 1 and $r_I = 1$, giving for the optimal lockdown policy $I_l = 0.1 = I_{sat}$, $I_d = 4 \times 10^{-4}$, and $\sigma = 0.39$. For the societal optimum the cooperation appears clearly: at the epidemic peak there is a mutual action of all individuals to simultaneously limit their contacts, especially in the community and households where adults and young people make efforts in order to limit the number of infected retired people, even if the efforts in households are costly. On the other hand, less efforts are made in schools or in workplaces because this affects retired people less. These combinations of efforts lead to a very low cost for the entire society.

For the Nash equilibrium under optimal constraints, we see in Fig. 2 that adults and young people essentially follow the constraints imposed by the lockdown in each setting (this is the straight solid lines). On the other hand, to achieve better protection for themselves, retired people go beyond the lockdown in the community and households, actually following a strategy very similar to the one of the societal optimum. This lockdown has a strong effect on the epidemic but lacks the coordination of the optimum societal case. This leads to a number of infected adults and young which is lower than the "*societal optimum*" while it is higher for retired people.

To conclude, it might be useful to introduce a "figure of merite" of a given policy $\mathcal{P}$

$$M(\mathcal{P}) = \frac{C_{\text{glob}}(\mathcal{P}) - C_{\text{glob}}(\text{societal optima})}{C_{\text{glob}}(\text{business as usual}) - C_{\text{glob}}(\text{societal optima})}, \tag{13}$$

which is thus such that $M(\mathcal{P})$ is zero if $\mathcal{P}$ is the societal optima and one if $\mathcal{P}$ is the "business as usual" strategy for which no adjustment is made to the contact between agents. From our simulations with $r_I = 1$, for which $C_{\text{glob}}(\text{business as usual}) = 266$ and $C_{\text{glob}}(\text{societal optima}) = 101$, we get $M(\mathcal{P}) = 0.12$ for the unconstrained Nash equilibrium and 0.06 for the optimal lockdown policy. However, nonoptimal lockdown policies are, most of the time, less effective than the unconstrained Nash, and can typically have a M which ranges from values of the order of (or in the best case scenario slightly

below) the unconstrained Nash value (when the thresholds are such that they do not affect the epidemics dynamics much) to values of order one, or even slightly higher.

Although these numbers apply obviously only to the specific model and to the specific set of parameters we have used as an illustration here, we have no doubt that the qualitative features observed are very general in nature. Namely, the Nash equilibrium is already a very significant improvement with respect to the "business as usual approach", and if, on the one hand, an optimized lockdown strategy can further close the gap toward the societal optimum, sub-optimal lockdown strategies can actually "degrade" the situation with respect to the basic Nash equilibrium.

As a final remark, we stress that it should not be assumed, and we certainly do not imply here, that the Nash equilibrium is the "natural outcome" of the epidemic process that would be reached in the absence of any public policy. Indeed, our model assumes that the agents possess both perfect information and the technical resources to compute the Nash equilibrium, which we cannot expect them to have in practice. On the other hand, gathering this information and developing the technical tools to compute the Nash equilibrium appears like a reachable goal for a centralized public agency. If enough trust is built between the government and the individual agents, making that information public can be enough to coordinate the ensemble of agents around the Nash equilibrium. This, as well as the optimization of lockdown or similar policies improving on the basic Nash equilibrium requires developing the necessary conceptual tools. We hope this work provides a useful step in that direction.

[1] William O. Kermack, A. G. McKendrick, and G. T. Walker, A contribution to the mathematical theory of epidemics, Proc. R. Soc. London A **115**, 700 (1927).

[2] H. W. Hethcote, The mathematics of infectious diseases, SIAM **42**, 599 (2000).

[3] L. Fumanelli, M. Ajelli, P. Manfredi, A. Vespignani, and S. Merler, Inferring the structure of social contacts from demographic data in the analysis of infectious diseases spread, PLoS Comput. Biol. **8**, e1002673 (2012).

[4] D. Mistry, M. Litvinova, A. P. y Piontti, M. Chinazzi, L. Fumanelli, M. F. C. Gomes, S. A. Haque, Q.-H. Liu, K. Mu, X. Xiong, M. E. Halloran, I. M. Longini Jr., S. Merler, M. Ajelli, and A. Vespignani, Inferring high-resolution human mixing patterns for disease modeling, Nat. Commun. **12**, 323 (2021).

[5] S. Merler, M. Ajelli, A. Pugliese, and N. M. Ferguson, Determinants of the spatiotemporal dynamics of the 2009 h1n1 pandemic in europe: Implications for real-time modelling, PLoS Comput. Biol. **7**, e1002205 (2011).

[6] S. Eubank, H. Guclu, V. S. A. Kumar *et al.*, Modelling disease outbreaks in realistic urban social networks, Nature (London) **429**, 180 (2004).

[7] N. M. Ferguson, D. Laydon, G. Nedjati-Gilani *et al.*, Impact of non-pharmaceutical interventions (NPIs) to reduce covid-19 mortality and healthcare demand, Imperial College London (2020), https://www.imperial.ac.uk/media/imperial-college/medicine/sph/ide/gida-fellowships/Imperial-College-COVID19-NPI-modelling-16-03-2020.pdf.

[8] R. Dutta, S. N. Gomes, D. Kalise, and L. Pacchiardi, Using mobility data in the design of optimal lockdown strategies for the covid-19 pandemic, PLoS Comput. Biol. **17**, e1009236 (2021).

[9] J.-M. Lasry and P.-L. Lions, Mean field games. 1–the stationary case, Comptes Rendus Mathematique **343**, 619 (2006).

[10] J.-M. Lasry and P.-L. Lions, Mean field games. 2–finite horizon and optimal control, Comptes Rendus Mathematique **343**, 679 (2006).

[11] J.-M. Lasry and P.-L. Lions, Mean field games, Jpn. J. Math. **2**, 229 (2007).

[12] M. Huang, R. Malhame, and P. Caines, Large population stochastic dynamic games: Closed-loop mckean-vlasov systems and the nash certainty equivalence principle, Commun. Inf. Syst. **6**, 115 (2006).

[13] P. E. Caines, M. Huang, and R. P. Malhame, in *Mean Field Games*, edited by T. Başar and G. Zaccour, Handbook of Dynamic Game Theory (Springer, Cham, 2018), pp. 345–372.

[14] R. Carmona and F. Delarue, *Probabilistic Theory of Mean Field Games with Applications I* (Springer, 2018).

[15] D. A. Gomes, J. Mohr, and R. R. Souza, Continuous time finite state mean field games, Appl. Math. Optim. **68**, 99 (2013).

[16] I. Swiecicki, T. Gobron, and D. Ullmo, Schrödinger Approach to Mean Field Games, Phys. Rev. Lett. **116**, 128701 (2016).

[17] D. Ullmo, I. Swiecicki, and T. Gobron, Quadratic mean field games, Phys. Rep. **799**, 1 (2019).

[18] O. Gueant, J.-M. Lasry, and P.-L. Lions, *Mean Field Games and Applications, Paris-Princeton Lectures on Mathematical Finance 2010* (Springer, Berlin Heidelberg, 2011), pp. 205–266.

[19] P. Chan and R. Sircar, Bertrand and cournot mean field games, Appl. Math. Optim **71**, 533 (2015).

[20] D. Bauso, R. Pesenti, and M. Tolotti, Opinion dynamics and stubbornness via multi-population mean-field games, J. Optim. Theory Appl. **170**, 266 (2016).

[21] L. Laguzet, G. Turinici, and G. Yahiaoui, Equilibrium in an individual - societal SIR vaccination model in presence of discounting and finite vaccination capacity, in *New Trends in Differential Equations, Control Theory and Optimization*, edited by Viorel Barbu, Catalin Lefter, and Ioan I. Vrabie (World Scientific Publishing Co, 2016), pp. 201–214.

[22] R. Elie, E. Hubert, and G. Turnici, Contact rate epidemic control of covid-19 : An equilibrium view, Mathematical Modelling of Natural Phenomena **15**, 35 (2020).

[23] R. Morton and K. H. Wickwire, On the optimal control of a deterministic epidemic, Adv. Appl. Probab. **6**, 622 (1974).

[24] K. H. Wickwire, Optimal isolation policies for deterministic and stochastic epidemics, Math. Biosci. **26**, 325 (1975).

D - Mean-Field Game Approach to Non-Pharmaceutical Interventions in a Social Structure model of Epidemics

Mean-field-game approach to nonpharmaceutical interventions in a social-structure model of epidemics

Louis Bremaud [1,*] Olivier Giraud [1,2,3] and Denis Ullmo [1]
[1] *Université Paris-Saclay, CNRS, LPTMS, 91405 Orsay, France*
[2] *MajuLab, CNRS-UCA-SU-NUS-NTU International Joint Research Unit, Singapore*
[3] *Centre for Quantum Technologies, National University of Singapore, Singapore*

(Received 26 April 2024; accepted 7 November 2024; published 2 December 2024)

The design of coherent and efficient policies to address infectious diseases and their consequences requires modeling not only epidemics dynamics but also individual behaviors, as the latter has a strong influence on the former. In our work, we provide a theoretical model for this problem, taking into account the social structure of a population. This model is based on a mean-field-game version of a SIR compartmental model, in which individuals are grouped by their age class and interact together in different settings. This social heterogeneity allows us to reproduce realistic situations while remaining usable in practice. In our game theoretical approach, individuals can choose to limit their contacts by making a trade-off between the risks incurred by infection and the cost of being confined. The aggregation of all these individual choices and optimizations forms a Nash equilibrium through a system of coupled equations that we derive and solve numerically. The global cost born by the population within this scenario is then compared to its societal optimum counterpart (i.e., the cost associated with the optimal set of strategies from the point of view of the society as a whole), and we investigate how the gap between these two costs can be partially bridged within a *constrained Nash equilibrium* for which a governmental institution would, under specific conditions, impose "partial lockdowns" such as the ones that were imposed during the COVID-19 pandemic. Finally, we consider the consequences of the finiteness of the population size N_{tot}, or of a time T at which an external event (e.g., a vaccine) would end the epidemic, and show that the variation of these parameters could lead to *first-order phase transitions* in the choice of optimal strategies. In this paper, all the strategies considered to mitigate epidemics correspond to nonpharmaceutical interventions, and we provide here a theoretical framework within which guidelines for public policies depending on the characteristics of an epidemic and on the cost of restrictions on the society could be assessed.

DOI: 10.1103/PhysRevE.110.064301

I. INTRODUCTION

As our history with COVID-19 has made rather explicit, modeling as precisely as possible the dynamics of epidemics is crucial if one wishes to design public policies able to mitigate effectively their negative impact. One major difficulty encountered toward this goal is that, most often, the parameters one would naturally choose to build such models have significant, and sometimes very fast, variations. This is illustrated, for instance, by the graph plotted in Fig. 1, which shows the time dependence of R_{eff}, the average number of people to which the virus is transmitted by a sick individual, for the COVID-19 pandemic in France.

The figure reveals that there are huge variations of R_{eff} over time. Some of them can easily be associated with known events (lockdown, new variant, etc.) but some other remain unexplained. Indeed, R_{eff} is impacted by many phenomena, such as natural immunity, vaccination, but also by behavioral changes that have important consequences on the spreading of the disease. While data such as immunity or vaccination rate are taken into account in even the most basic models, this is not the case for the evolution of social interactions.

However, these modifications of social behavior, either under governmental influence or because people change their individual habits, significantly affect epidemics dynamics. These individual or collective strategies against the virus sometimes prevented a health disaster [1] by significantly decreasing the total number of infected people and the time at which the peak occurs [1,2]. As a counterpart, they had significant worldwide negative impact, for the economy [3], or in terms of health (as medical acts had to be postponed), time, money, social interactions, psychological pressure [4] (domestic violence, depression), etc., which in turn could increase the stress on the sanitary system [2]. In such a context, any policy or any individual decision must consider the trade-off between the cost of reducing social interaction and the cost of the epidemic; see, for instance, Refs. [5–7], where realistic impacts and constraints on the quarantine and isolation strategies have been considered, and Refs. [8,9] where the individual behavioral response to isolation policy has been investigated. This individual response is of course greatly influenced by cultural habits together with social, economic, religious needs of the population.

In models currently used to describe the propagation of epidemics, social interactions are often described by constant parameters, or at best by time-dependent parameters which are *extrinsic*, in the sense that their time evolution is not predicted

*Contact author: louis.bremaud@hotmail.fr

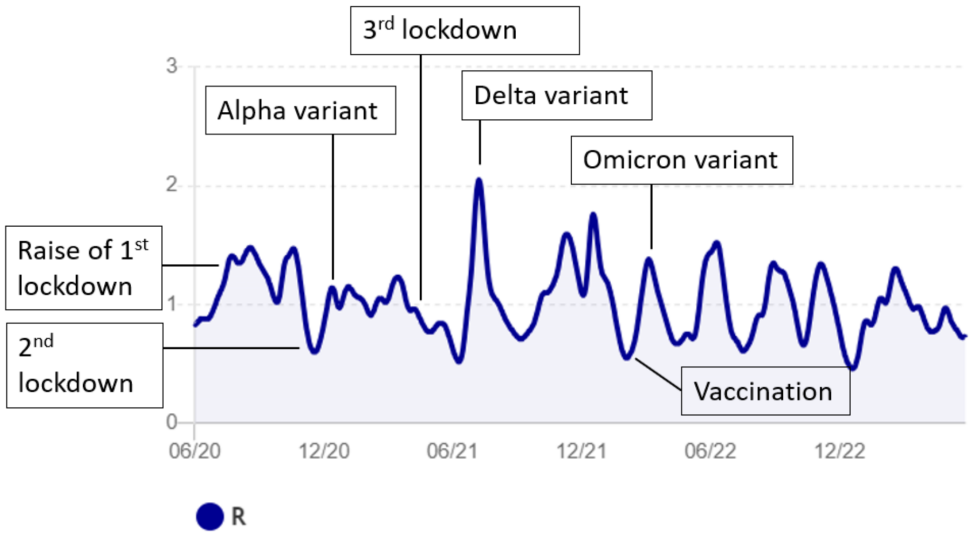

FIG. 1. Evolution of R_{eff} in France during the COVID-19 pandemic between June 2020 and June 2023. R_{eff} corresponds to the effective reproduction number of the virus, that is, the average number of people to which the virus is transmitted by a sick individual. If $R_{\text{eff}} > 1$, then the epidemic grows, and it decreases if $R_{\text{eff}} < 1$. We see that there are very significant variations of R_{eff} which range from 0.6 to 2. We marked on the figure some peaks and valleys that have clearly identified origins (data from "Santé Publique France," by Guillaume Rozier [10].)

by the model itself, but ideally obtained from epidemic data [1,11]. However, given the amplitude and timescale of these variations, and in spite of the large amounts of data used, exploiting these data involves a lot of guesswork and lead to predictions [12,13] which could be inaccurate, especially on long timescales.

To overcome these difficulties, one needs to introduce models for which the *extrinsic* parameters have no time dependence (at least on the timescale of the epidemic), and which can therefore be fitted in a reliable way on field data. However, all time-dependent parameters, and in particular the ones modeling social interactions, should be *intrinsic*, in the sense that their dynamics should be predicted by the model. This naturally calls for a game theoretical approach (for a review, see Ref. [14]). Here we will follow an approach known as mean-field-game theory.

Introduced by Lasry and Lions almost two decades ago [15–17] and independently by Huang, Malhamé and Caines [18], mean-field games (MFG) focus on the derivation of a Nash equilibrium within a population containing a large number of individuals. Readers may refer to Refs. [19–21] for a complete mathematical description, and to Refs. [22,23] for an introduction aimed at physicists. Applications of MFG include finance [24], economics [25], crowd modeling [26], and opinion dynamics [27], among many others.

The introduction of MFG models to describe epidemics dynamics has been first used a decade ago by Reluga *et al.* [28] about social distancing. Mean-field games have been then used to describe vaccination rates, which appears to be an extrinsic parameter with a dynamics mainly influenced by individuals choices. Pioneers on this matter are Laguzet *et al.* [29] (see also Refs. [29–31]). Recently, a similar approach has been proposed by Elie *et al.* in Ref. [32] to study the impact of individual decisions regarding distancing and isolation, that is, to study human impact on the dynamics of the epidemic (see Refs. [33,34] for a mathematical perspective). An extensive review of recent progresses in this new field can be found in Ref. [35].

The significant advances made in Ref. [32] establish how the mean-field-game concepts can be implemented to describe the dynamics of social distancing in a simple epidemic model. The goal of this paper is to go one step further toward the implementation of MFG in realistic situation by demonstrating that enough degree of complexity can be introduced within a MFG framework to address questions of practical importance for public institutions, in the context of what is refereed to, in the literature, as the nonpharmaceutical interventions (NPI) strategies.

To achieve this goal, this paper is divided in two rather distinct parts. In the first part, Secs. II and III, we introduce at a rather general level the class of models we are interested in, describe the corresponding mathematical framework, and derive the associated dynamical equations. More specifically, Sec. II introduces the SIR model with a social structure on which we base our discussion and Sec. III implements the corresponding MFG paradigm, that is, presents the individual optimization scheme and its consequences at the society scale and formulates the corresponding Nash equilibrium. The central results of this part are Eqs. (2.11) and (2.12) and Eqs. (3.14)–(3.16), and its main content is summarized in the header of Sec. IV, so that readers less interested in the mathematical formalism can go directly to this section.

We then turn, in Secs. IV and V, to the second part of the paper, where we illustrate on a particular example the kind of problematic that can be addressed, and the kind of questions that can be asked, within our formalism. We stress that our goal here is not to analyze a specific epidemics in a specific geographic location, as, on the one hand, the idiosyncrasies of any specific real case would obscure our main message, and since, on the other hand, the specification of the parameters of our model based on real data is clearly beyond the scope of this work. Rather, we will consider a particular

implementation/set of parameters which can be considered as rather typical (we will argue why). In Sec. IV we will discuss, on that example, how the Nash equilibrium differ from, on the one hand, a "business as usual" approach where the agents do not modify their behavior during the epidemics, and, on the other hand, a "societal optima" where each individual is assumed to follow a completely altruistic behavior, focusing in particular on how these different scenario may affect in a rather different way the different age classes. We shall also address in that section the effectiveness of possible lockdowns, and the risk they represent. In Sec. V, we then broaden the discussion and consider the various strategies that public institutions can put in place to mitigate an epidemics through nonpharmaceutical interventions and show in particular the existence of a first-order phase transition as some parameters, such as the duration of the epidemics or the risk due to an infection, are varied. Finally, concluding remarks are assembled in Sec. VI. Some mathematical and numerical details, as well as a more general exploration of the parameter space of our model, are gathered in the Appendix.

II. SOCIAL-STRUCTURE MODELING OF THE EPIDEMICS DYNAMICS

In this section, we introduce and analyze in detail the dynamics of the SIR model with social structure which forms the basis of this work. We start by reviewing briefly the plain-vanilla SIR model.

A. SIR model

Since the early 20th Century, many models have been proposed to model epidemic dynamics, one of the simplest being the susceptible-infected-recovered (SIR) compartment model [36] and its variations [37]. Recently, this model has been refined to take into account the structure of social contacts [38,39], as well as spatial or geographic aspects of the dynamics [40,41].

The SIR model is defined as follows. Individuals can be in three possible states $x = s, i$, or r, with $s =$ "susceptible," $i =$ "infected," and $r =$ "recovered." Starting from some initial configuration at $t = 0$, one then assumes that the evolution of the system is Markovian. Between times t and $t + dt$, individuals can switch from one state to another with a certain probability, which depends on their contact rate with the rest of the population and of the status of people they meet. In a population composed of N_{tot} individuals, the probability for an individual k to have contact with another individual l during the interval $[t, t + dt[$ is $\frac{1}{N_{\text{tot}}}\chi(t)dt$, with $\chi(t)$ a (possibly time-dependent) given parameter corresponding to the total contact rate of the individual k. We make the assumption that all individuals can be met by k with equal probability (in other words, the population considered from the point of view of k is homogeneous). If individual l is infected and k susceptible, then there is a probability ρ that the disease be transmitted from l to k upon contact. Last, infected individuals have a probability ξdt to recover from their illness during the interval $[t, t + dt[$, after which they are immune to the disease.

Noting $S(t)$, $I(t)$, and $R(t)$, respectively, the relative proportion of susceptible, infected, and recovered individuals at time t [thus $S(t) + I(t) + R(t) = 1$], the evolution of the epidemic is governed by the system of equations [36]

$$\begin{aligned} \dot{S} &= -\rho\chi(t)S(t)I(t), \\ \dot{I} &= \rho\chi(t)S(t)I(t) - \xi I(t), \\ \dot{R} &= \xi I(t). \end{aligned} \tag{2.1}$$

This system of equations is almost a century old [36]; we derive it for completeness in Appendix A to prepare for the slightly more involved situation that we are going to consider in this paper. Let us highlight here the two main underlying hypotheses of the derivation of Eq. (2.1): (i) the total contact rate of individual k, $\chi(t)$, is independent on the individual k; and (ii) N_{tot} is large enough to consider the states of two randomly chosen individuals k and l as independent. We shall keep both these hypotheses to derive dynamical equations for our model introduced in Sec. II B; while hypothesis (ii) is rather harmless in practice where N_{tot} is large, hypothesis (i) is an important assumption which can be discussed in practice.

Figure 2 summarizes the process that drives an individual from state s to i to r. The system of equations (2.1) only involves average quantities S, I, and R, which are determined as solutions of the system. Furthermore, it is characterized by two extrinsic parameters, the recovery rate ξ and the product of the contact rate $\chi(t)$ by the probability ρ of transmitting the disease, which must be obtained from observation data [13]. For virus epidemics like COVID-19, with a very fast dynamics, this is a challenging task. Major efforts have been invested by the epidemiologist community to extract these parameters, or their counterpart in more complex models, from the actual data observed on the field. While ξ is mainly fixed by biological considerations, and considered constant in time in the present model, the contact rate $\chi(t)$, however, depends a lot on the agent's behavior, that is, how social they are (or are allowed to be); that behavior may vary strongly with time, and in a way that may depend on the dynamics of the epidemic itself. A consequence of this retroaction is that it is essentially impossible to fit the time dependence of $\chi(t)$ on past data. In models used to advise public policies, this time dependence is thus either simply ignored, or involves a lot of guesswork [12], leading to predictions that can be trusted only for a rather short amount of time [13] (see, nevertheless, Refs. [1,42]).

What we discussed above is the simplest version of the SIR model. A number of variations can be found in the literature, that aim to gain in precision. The most common ones are the SIRD model (D for deceased [43]), SIRV (V for vaccination [44]), MSIR (M for maternally derived immunity [37]), SIRC (C for carrier but asymptomatic [45]), or SEIR models (E for exposed class [46]), to name a few—see Ref. [37] for a more detailed literature on the subject of compartmental models. However, there are two essential limitations of these models: they assume that the population is entirely uniform, and they take parameters such as the contact rates as extrinsic.

Let us expand slightly on these two issues. The first limitation is that these models assume a homogeneous population: all individuals are expected to act in the same way, have the same contact rate with all other individuals (in a given compartment), and behave similarly with respect to the epidemic. Of course, this is not true, and social heterogeneity has an

FIG. 2. Illustration of the Markov process for the classic SIR model with the transition rates to move from one state to another between time t and $t + dt$. An individual susceptible at t has a probability $\rho\chi(t)I(t)dt$ to become infected. If this individual is already infected at t, then she will have a constant probability ξdt to recover from the disease.

important impact on epidemics modeling. As an example, epidemics inside schools have a different and faster dynamics than can be expected from the SIR model, because children have a lot of contacts with each other and they live together during a long part of the day. To address this issue, SIR models with a structure of social contacts were proposed in Refs. [38] and [39] to get a more detailed description of the society at a mesoscopic scale. We will address that limitation by introducing a refined model in Sec. II B. The second limitation of SIR models, already discussed in the introduction, is that the contact rates are extrinsic parameters, fixed at the beginning of the dynamical process. A more realistic approach is to consider that people change their behavior as the epidemic unfolds, so that contact rates should be updated according to the dynamics of the epidemic. We shall circumvent this issue by taking a MFG approach to our model with a social structure in Sec. III, where contact rates will become intrinsic parameters, co-evolving with the epidemic.

B. SIR model with social structure

1. *Social structure and contact rates*

We now introduce a SIR model with a social structure, in the spirit of Ref. [38]. In this model, rather than taking society as monolithic, we consider a refined description of social contacts. Namely, we introduce three age classes: young, adult and retired, and we assume that individuals have contacts with one another in four different settings: schools, households, community and workplaces; of course a larger number of age classes and settings could easily be implemented. The structure of the population is illustrated in Fig. 3. We assume the total size of the population, N_{tot}, to be large.

In our model, following Ref. [38], interactions between individuals depend on two factors: the setting $\gamma \in \{\text{school, workplace, community, household}\}$ in which they meet, and their age class $\alpha \in \{\text{young, adult, retired}\}$. We denote by N_α^{tot} the total number of individuals in class α. We first consider the simple case of a single setting where interactions only depend on age class, which will be labeled by the Greek letters α or β; extension to the case of multiple settings is then straightforward.

For two given age classes α and β we define $\mathcal{W}_{\alpha\beta}dt$ as the probability for a pair of individuals $a \in \alpha$, $b \in \beta$ drawn at random to be in contact during a time interval dt. This means that among all possible $N_\alpha^{\text{tot}}N_\beta^{\text{tot}}$ pairs, only $\mathcal{W}_{\alpha\beta}N_\alpha^{\text{tot}}N_\beta^{\text{tot}}dt$ encounters occur during dt. This is illustrated by the graph of Fig. 4; it is similar to Erdös-Renyi graphs, where each potential edge is realized with some probability. In the present case, all potential edges between vertices from one class to the other are realized with some probability that depends on the two classes they connect. A given individual $a \in \alpha$ encounters on average a number $\mathcal{W}_{\alpha\beta}N_\beta^{\text{tot}}dt$ of individuals of class β during dt.

A natural assumption, in the spirit of compartmental models, is that behavior of individuals toward different age classes is differentiated, but that a given age class is considered homogeneous from the point of view of an individual. That is, an individual $a \in \alpha$ can decide whether she chooses to encounter members of class β or not, but does not decide which individuals she may encounter in that class. In other words, any individual $a \in \alpha$ willing to meet someone from

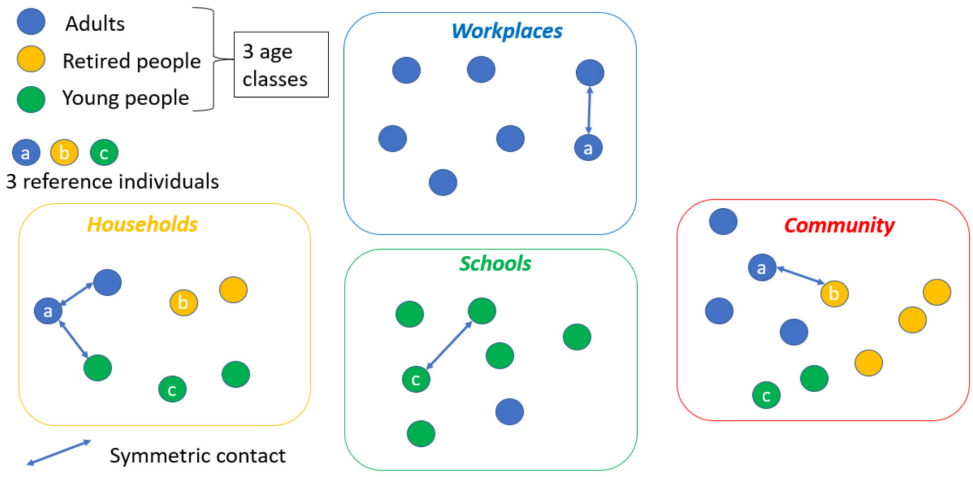

FIG. 3. Graphical illustration of the social structure we implemented. A reference individual (a, b, and c for each age class) will have (symmetric) contacts in each setting, with different type of individuals (more adults at workplaces, more children at school, etc.). The precise structure of interactions is detailed in the following section.

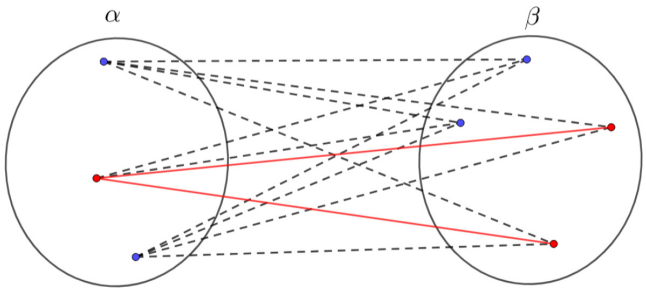

FIG. 4. Graphical illustration of the interactions in our model. Two age classes α and β are represented, here with $N_\alpha^{\rm tot} = 3$ individuals of age class α and $N_\beta^{\rm tot} = 4$ of class β. Each vertex is either "active" (in red) if the corresponding individual is willing to have contact with the other class, or "inactive" (in blue). The $N_\alpha^{\rm tot} N_\beta^{\rm tot}$ possible contacts are represented in dashed black lines, and effective contacts between pairs of active individuals are red solid lines. Here we have $w_{\alpha\beta} N_\alpha^{\rm tot} = 1$ active individual of age class α and $w_{\beta\alpha} N_\beta^{\rm tot} = 2$ active individuals of age class β, which gives $w_{\alpha\beta} = \frac{1}{3}$ and $w_{\beta\alpha} = \frac{1}{2}$. The probability for a randomly chosen pair to be in contact is $\mathcal{W}_{\alpha\beta} = w_{\alpha\beta} w_{\beta\alpha} = \frac{1}{6}$. The average number of contacts with β for an individual $a \in \alpha$ is $\mathcal{W}_{\alpha\beta} N_\beta^{\rm tot} = \frac{2}{3}$. Similarly, the average number of contacts with α for an individual $b \in \beta$ is $\mathcal{W}_{\beta\alpha} N_\alpha^{\rm tot} = \frac{1}{2}$. The total number of contacts between the two classes, corresponding to the number of red links in the graph, is given by $N_\beta^{\rm tot} N_\alpha^{\rm tot} \mathcal{W}_{\beta\alpha} = 2$.

class β will possibly meet all individuals from class β who themselves are willing to meet individuals from class α. At each time, an individual $a \in \alpha$ can decide whether she is open or close to interactions with class β. Let us denote by $w_{\alpha\beta} \in [0, 1]$ the fraction of individuals $a \in \alpha$ open to meet people from class β. The willingness $w_{\alpha\beta}$ thus indicates the probability of an individual a taken at random in α to be open to contacts with class β. There are $w_{\alpha\beta} N_\alpha^{\rm tot}$ individuals $a \in \alpha$ willing to meet people with class β, and $w_{\beta\alpha} N_\beta^{\rm tot}$ individuals $b \in \beta$ willing to meet people from class α. A contact becomes effective (i.e., occurs with probability dt in the interval $[t, t + dt[$) only if both individuals are willing, and therefore among all $N_\alpha^{\rm tot} N_\beta^{\rm tot}$ possible links between α and β, only $w_{\alpha\beta} N_\alpha^{\rm tot} \times w_{\beta\alpha} N_\beta^{\rm tot} dt$ are realized during dt. As mentioned above, the number of pairs effectively realized can also be expressed as $\mathcal{W}_{\alpha\beta} N_\alpha^{\rm tot} N_\beta^{\rm tot} dt$, hence $\mathcal{W}_{\alpha\beta} = w_{\alpha\beta} w_{\beta\alpha}$ (and $\mathcal{W}_{\alpha\beta}$ is a symmetric array, as it should be).

In "normal times," that is in the absence of epidemic threats, the contact willingness of an individual of class α with class β is a constant $w_{\alpha\beta}^{(0)}$. During an epidemics, however, the agent will adapt her behavior to mitigate the risk of infection, and we assume the contact willingness to take the form

$$w_{\alpha\beta}(t) = n_\alpha(t) w_{\alpha\beta}^{(0)}, \tag{2.2}$$

that is, her initial willingness is modulated by a time-dependent coefficient $n_\alpha(t)$ which measures the effort made by agents in the class α to limit their contacts with others. For simplicity we suppose that this effort is independent of β, but a β dependence can easily be implemented to this model and only slightly changes the equations. We additionally assume that $n_\alpha(t) \in [n_{\alpha,\min}, 1]$, with $n_{\alpha,\min}$ the maximum effort that can be expected from an agent in class α; the upper bound 1 corresponds to the natural assumption that the epidemic situation can only reduce the initial willingness.

TABLE I. Biological parameters and parameters defining the structure of the society. The number of parameters implied by this list is significant, since in particular the array $\mathcal{W}_{\alpha\beta}^{\gamma\,(0)}$ has $3\times3\times4 = 36$ entries. However, the methodology to get these parameters in any specific implementation is relatively well established (see, e.g., discussion in Appendix B).

Parameter	Definition
ρ	Probability of transmission per contact
μ	Proportion of asymptomatic individuals in the population
ξ	Recovery rate
$N_\alpha^{\rm tot}$	Number of individuals of age class α
$\mathcal{W}_{\alpha\beta}^{\gamma\,(0)} = w_{\alpha\beta}^{\gamma\,(0)} w_{\beta\alpha}^{\gamma\,(0)}$	Willingness of contacts between two age classes α and β (symmetric in $\alpha \leftrightarrow \beta$)

2. *Asymptomatic individuals*

Interactions between individuals may vary with time, but also differ between different age classes and in different settings. As a result, the dynamics of the epidemic will be different in each subcategory. This turns out to be particularly relevant for susceptible agents, and we will go back to this in more details in the next subsection. But the issue could be raised also for infected individuals whose behavior may range from a completely egoistic one, in which they stop limiting their contacts since they are not worried any more about being infected, to being completely altruistic and isolate themselves from the rest of population. To make things more concrete, we assume this latter option, but also assume that a fraction μ of the population is asymptomatic (they do not know if they are infected or not) and hence behave as susceptible, while the other fraction $1 - \mu$ is symptomatic and stay home to protect others. This additional status (symptomatic or asymptomatic) is random in the population and is fixed at the beginning of the epidemic. Therefore, the epidemic is only spread by individuals who are both asymptomatic and infected. They represent a fraction $\mu I(t)$ of the population. We summarize our model in Fig. 5.

The parameters defining our SIR model with social structure can thus be divided in two groups. On the one hand, we have three "biological" parameters: the probability ρ of transmission of the virus per effective contact between a susceptible and an infected individual, the fraction μ of the infected population which is asymptomatic, and the recovery rate ξ. On the other hand, the social structure is defined by the number of individuals $N_\alpha^{\rm tot}$ in the age classe α and by the coefficients $\mathcal{W}_{\alpha\beta}^{\gamma\,(0)} \equiv w_{\alpha\beta}^{\gamma\,(0)} w_{\beta\alpha}^{\gamma\,(0)}$ determining the structure of our society, i.e., the contact rates in the absence of the epidemics. Table I summarizes this information.

For a given epidemic in a given geographic location, determining the parameters of Table I follows *a priori* a well-defined, though not necessarily straightforward, path, both for the "biologic parameters" (ρ, μ, ξ) typically encountered in traditional SIR-like models [47], but also for the ones associated with the social structure [39]. Much less straightforward

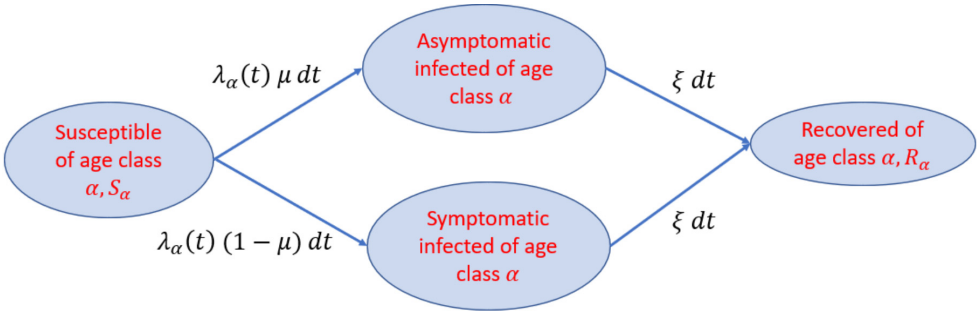

FIG. 5. Graphical illustration of the particular SIR model we use. An individual infected at time t has a probability μ to be asymptomatic and $1-\mu$ to be symptomatic. The force of infection λ_α is derived in Sec. II B 3 and drives the probability of infection $\lambda_\alpha dt$. Then, all individuals have a constant recovery rate ξ to recover from the disease.

is the determination of the time dependence of the "effort parameters" $n_\alpha(t)$ introduced in Eq. (2.2). For the rest of Sec. II B, we assume these $n_\alpha(t)$ known, and we will discuss how their dynamics can be analyzed in Sec. III.

3. Time evolution equations

We now derive the time evolution equations of the epidemic quantities for this model. The fraction of susceptible (respectively, infected, recovered) individuals in class α is S_α (respectively, I_α, R_α), with $S_\alpha + I_\alpha + R_\alpha = 1$. To establish the mean-field equations, we single out a reference individual $a \in \alpha$ who is susceptible at time t and has status $x_a(t) = s, i$ or r at subsequent times. We furthermore here lift the hypothesis that all individuals of a given age class behave in exactly the same way, and we assume that the reference individual has her own time-dependent strategy $n_a(t)$ and willingness $w_{a\beta}(t) = n_a(t) w^{(0)}_{\alpha\beta}$, with, however, the understanding that n_α is the average over susceptible individuals of n_a, which we express as

$$n_\alpha = \frac{1}{S_\alpha N_{\rm tot}} \sum_a n_a \delta_{x_a,s}. \tag{2.3}$$

Let $b \in \beta$ be an individual of class β, whose willingness to meet class α is $w_{b\alpha}(t) = n_b(t) w^{(0)}_{\beta\alpha}$. For a to be contaminated by b during $[t, t+dt[$, b must be infected *and* asymptomatic, and a and b must meet; contamination then occurs with probability ρ. Distinguishing within the $i =$ "infected" status between $i_a =$ "asymptomatic infected" and $i_s =$ "symptomatic infected", the probability that a become infected by b during $[t, t+dt[$ is therefore

$$P_{ab}(t)dt = \rho n_a(t) n_b(t) \mathcal{W}^{(0)}_{\alpha\beta} \delta_{x_b(t),i_a} dt, \tag{2.4}$$

where we used the fact that $w^{(0)}_{\alpha\beta} w^{(0)}_{\beta\alpha} = \mathcal{W}^{(0)}_{\alpha\beta}$ (see Table I). Taking the sum over all $b \in \beta$ and all age classes β we get the total probability that an individual a susceptible at time t is infected between t and $t+dt$

$$P_a(t)dt := \mathcal{P}[x_a(t+dt) = i \,|\, x_a(t) = s] = \sum_\beta \sum_{b\in\beta} P_{ab}(t)dt, \tag{2.5}$$

with $\mathcal{P}[e]$ the probability of the event e.

We then follow the same reasoning as in the SIR case [see Eq. (A3)]. Averaging over all individuals $a \in \alpha$ and over realizations of the Markov process, and summing over age classes β, we obtain

$$\frac{dS_\alpha(t)}{dt} = -\frac{1}{N^{\rm tot}_\alpha} \sum_{a=1}^{N^{\rm tot}_\alpha} \delta_{x_a(t),s} P_a(t) \tag{2.6}$$

$$= -\rho \sum_\beta \mathcal{W}^{(0)}_{\alpha\beta} \left(\frac{1}{N^{\rm tot}_\alpha} \sum_{a=1}^{N^{\rm tot}_\alpha} n_a(t) \delta_{x_a(t),s} \right) \times \left(\sum_{b=1}^{N^{\rm tot}_\beta} n_b(t) \mu \delta_{x_b(t),i} \right) \tag{2.7}$$

$$= -\rho \sum_\beta \mathcal{W}^{(0)}_{\alpha\beta} (S_\alpha n_\alpha) \left(\mu N^{\rm tot}_\beta I_\beta n_\beta \right). \tag{2.8}$$

To get this last expression, Eq. (2.3) was used, together with the assumption that asymptomatic infected individuals responsible for contamination behave on average in the same way as susceptible individuals, so that we have also for all age classes

$$n_\beta(t) = \frac{1}{\mu I_\beta N^{\rm tot}_\beta} \sum_{b\in\beta} n_b(t) \delta_{x_b(t),i_a}. \tag{2.9}$$

Equation (2.8) can then be written as

$$\frac{dS_\alpha}{dt} = -\lambda_\alpha(t) S_\alpha(t), \tag{2.10}$$

where, performing the straightforward generalization to include different settings γ,

$$\lambda_\alpha(t) \equiv \mu\rho \sum_{\beta=1}^{n_{\rm cl}} N^{\rm tot}_\beta \sum_{\gamma=1}^{n_{\rm set}} n^\gamma_\alpha(t) n^\gamma_\beta(t) \mathcal{W}^{\gamma(0)}_{\alpha\beta} I_\beta(t), \tag{2.11}$$

with $n_{\rm cl}$ and $n_{\rm set}$, respectively, the number of classes and settings in the social structure. Equation (2.10) is the analog of the SIR Eq. (A5) but in the case of a population with social structure. The two other equations analogous to the system (2.1) are derived in the same way. The system of coupled differential equations for the SIR model with social structure finally reads

$$\begin{aligned} \dot{S}_\alpha &= -\lambda_\alpha(t) S_\alpha(t), \\ \dot{I}_\alpha &= \lambda_\alpha(t) S_\alpha(t) - \xi I_\alpha(t), \\ \dot{R}_\alpha &= \xi\, I_\alpha(t). \end{aligned} \tag{2.12}$$

These equations are the main equations of our SIR model with a social structure. Once the "interaction strategies" $n_\alpha^\gamma(.)$ are fixed for each age class α and each setting γ, one can solve Eq. (2.12) and obtain the dynamic of the relative proportion of susceptible, infected and recovered in each class. However, for rational agents interaction strategies should depend on the evolution of the epidemic. To address this interplay, we need the machinery of mean-field games, which we now introduce.

III. MEAN-FIELD-GAME APPROACH: INDIVIDUAL OPTIMIZATION

To address the dynamics of the willingness $w_{\alpha\beta}^\gamma(t)$ requires a game theoretical approach, which implies a control parameter that the agents can choose a will, and a cost function that they try to optimize. In our model, the control parameter defining the "strategy" of a given agent a is quite naturally the function $n_a^\gamma(t)$, which reflects her desire to have contact with someone in each setting γ.

Turning now to the cost function, consider a fixed individual $a \in \alpha$. If a has no symptoms at time t, then she estimates the cost she will incur because of the the epidemic as the sum of two terms: one due to the cost of infection if it happens, and one associated with the cost of efforts to avoid the infection. If a becomes infected at some time $\tau > t$, then the total cost paid between t and the end of the optimization process at T is

$$C_a\left(n_a^\gamma(\cdot), \left\{n_\beta^\gamma(.)\right\}, t, \tau\right) \equiv \mathcal{I}_\alpha(I(\tau))\mathbb{1}_{\tau<T} + \int_t^{\min(\tau,T)} f_\alpha\left(n_a^\gamma(t')\right)dt'. \tag{3.1}$$

This cost is an explicit function of τ the time of infection, and of the strategies $n_a^\gamma(\cdot)$ of a in each setting and at each time between t and $\min(\tau, T)$. It also depends implicitly, through the (average) proportion of infected at time τ, $I(\tau) \equiv \frac{1}{N_{\text{tot}}}\sum_\alpha N_\alpha^{\text{tot}} I_\alpha(\tau)$, on all the strategies $\{n_\beta^\gamma(.)\}$ for all age classes β (including α) and settings γ in the same time interval. The first term in Eq. (3.1) is the total cost of infection $\mathcal{I}_\alpha(I(\tau))$ paid by the agent once she is infected. This cost can include financial cost, as the loss of income incurred by not working, the costs of medical treatment or hospitalization, but also moral and psychological costs associated with the pain of going through the illness, permanent health damage, or death. We assume that this cost of infection depends on the age class and on the (average) proportion $I(\tau)$ of infected, reflecting the pressure on the sanitary system. In the second term, $f_\alpha(n_a^\gamma(s))$ measures the cost (both psychological and financial) associated with the limitation of social contacts (incurred, for instance, by the inability of doing business); this cost can be different according to the age class of the individual, and depends on the behavior of the individual only. At each time s between t and τ (the time of infection) or T (if the agent is never infected) the agent will pay a cost $f_\alpha(n_a^\gamma(s))ds$; for $s > \tau$ we have $f_\alpha = 0$, as the individual is either infected (in which case the social cost is included in the term $\mathcal{I}_\alpha$) or recovered (as there is no possible new infection in our model).

We now derive the optimization made by the agents, following in the spirit the work of Turinici *et al.* in Ref. [32].

A. Calculation of the expected cost $\mathfrak{C}_a$

We assume here $\mu \ll 1$. As shown in Appendix C, considering a finite μ makes notations slightly heavier without changing qualitatively the dynamics of the epidemics. Therefore in the rest of the paper we shall restrict ourselves to the regime $\mu \ll 1$.

In that case, almost all infected individuals are symptomatic, and thus individuals with no symptoms can estimate their future cost neglecting the probability that they might be infected. Note however that contamination still occurs via the few infected asymptomatic individuals.

Consider a fixed individual $a \in \alpha$, who incurs the cost Eq. (3.1) as a function of the time of infection τ and of her strategy (for all setups γ and all times t) $n_\alpha^\gamma(t)$. From the perspective of agent a at time t, and since the epidemic propagation is a stochastic process, the time of infection τ is a random variable that changes from one realization of the epidemic to the other. We denote

$$\widetilde{P}_a(\tau)d\tau = \mathcal{P}[x_a(\tau + d\tau) = i \;\&\; x_a(\tau) = s] \tag{3.2}$$

as the probability that the individual a is infected during the time interval $[\tau, \tau + d\tau[$. Note this probability is a *functional* of $n_a^\gamma(t')$, $t' \in [t, \tau]$, and of the strategies $\{n_\beta^\gamma(t')\}$, $t' \in [t, \tau]$ since these latter will determine the $I_\beta(\tau)$, and thus the probability that an individual met at time τ is or not infected. $\widetilde{P}_a$ is also a function of t since the agent has acquired information about whether or not she has been infected in the interval $[0, t]$. The cost in Eq. (3.1) is thus also a stochastic variable, and at each time t, a rational agent should choose her future strategies in each setting $n_a^\gamma(t'), t' > t$, as the ones that minimize the *average* value of C_a over random realizations,

$$\mathfrak{C}_a\left(n_a^\gamma(\cdot), \left\{n_\beta^\gamma(.)\right\}, t\right) \equiv \int_t^\infty d\tau\, \widetilde{P}_a(\tau)\, C_a\left(n_a^\gamma(\cdot), \left\{n_\beta^\gamma(.)\right\}, t, \tau\right), \tag{3.3}$$

where formally we understand $\tau > T$ as an absence of infection (so that we can normalize $\int_t^\infty \widetilde{P}_a(\tau)d\tau = 1$, and $C_a(n_a^\gamma(\cdot), \{n_\beta^\gamma(.)\}, t, \tau > T) = \int_t^T f_\alpha(n_a^\gamma(t'))dt'$).

We now need to evaluate the probability $\widetilde{P}_a(\tau)$ for an agent a who is assumed to follow a specific strategy $n_a^\gamma(\cdot)$. Let $\phi_a(\tau)$ be the corresponding cumulative probability, that is, the probability for a to be infected before time τ (the probability that a is susceptible at some arbitrary time t is is thus $\mathcal{P}[x_a(t) = s_\alpha] = 1 - \phi_a(t)$). The probability that the infection time for a is between τ and $\tau + d\tau$ is

$$\phi_a'(\tau)d\tau = \widetilde{P}_a(\tau)d\tau = \mathcal{P}[x_a(\tau + d\tau) = i_\alpha | x_a(\tau) = s_\alpha] \times \mathcal{P}[x_a(\tau) = s_\alpha], \tag{3.4}$$

where the first term of the right-hand side is obtained from Eqs. (2.5) and (2.9), giving

$$\mathcal{P}[x_a(\tau + d\tau) = i_\alpha \,|\, x_a(\tau) = s_\alpha] = \lambda_a(\tau)d\tau, \tag{3.5}$$

with

$$\lambda_a(t) \equiv \mu\rho \sum_{\beta=1}^{n_{\text{cl}}} N_\beta^{\text{tot}} \sum_{\gamma=1}^{n_{\text{set}}} n_a^\gamma(t) n_\beta^\gamma(t) \mathcal{W}_{\alpha\beta}^{\gamma(0)} I_\beta(t) \tag{3.6}$$

as the force of infection seen by individual a. This individual force of infection differs from the collective one Eq. (2.11)

only by the replacement of the collective behavior n_α^γ by the individual strategy n_a^γ (for all settings γ). Equation (3.4) thus leads to $\phi_a'(\tau) = \lambda_a(\tau)(1-\phi_a(\tau))$, which together with $\phi_a(t) = 0$ gives

$$\phi_a(\tau) = 1 - \exp\left(-\int_t^\tau \lambda_a(s)ds\right). \tag{3.7}$$

The average cost (3.3) then reads

$$\begin{aligned}\mathfrak{C}_a\big(n_a^\gamma(\cdot), \{n_\beta^\gamma(.)\}, t\big) &= \int_t^T d\tau\, \widetilde{P}_a(\tau)\mathcal{I}_\alpha(I(\tau)) \\ &\quad + \int_t^\infty d\tau\, \widetilde{P}_a(\tau)\int_t^{\min(\tau,T)} ds\, f_\alpha\big(n_a^\gamma(s)\big) \\ &= \int_t^T dt'\, \widetilde{P}_a(t')\mathcal{I}_\alpha(I(t')) \\ &\quad + \int_t^T dt'\, f_\alpha\big(n_a^\gamma(t')\big)\int_{t'}^\infty d\tau\, \widetilde{P}_a(\tau).\end{aligned} \tag{3.8}$$

We then use the fact that $\phi_a'(\tau) = \widetilde{P}_a(\tau) = \lambda_a(\tau)(1-\phi_a(\tau))$ to get

$$\begin{aligned}&\mathfrak{C}_a\big(n_a^\gamma(\cdot), \{n_\beta^\gamma(.)\}, t\big) \\ &= \int_t^T \big[\lambda_a(s)\,\mathcal{I}_\alpha(I(s)) + f_\alpha\big(n_a^\gamma(s)\big)\big](1-\phi_a(s))ds.\end{aligned} \tag{3.9}$$

In the following, we will often use $\mathfrak{C}_a(n_a^\gamma, t)$ for simplicity, but the cost still depends implicitly on all the $n_\beta^\gamma(\cdot)$.

B. Hamilton-Jacobi-Bellman equations

The expected cost at time t for agent a is a function of her own strategy n_a and of the epidemic functions $S(.), I(.), R(.)$. The next step is to solve the optimization problem, that is, find the optimal strategy n_a^* for a given epidemic $S(.), I(.), R(.)$. Following a standard approach in this context [20], we introduce the *value function*

$$U_a(t) = \begin{cases} \min\limits_{n_a^\gamma(\cdot)} \mathfrak{C}_a\big(n_a^\gamma(\cdot), t\big), & a \text{ susceptible at } t, \\ 0, & a \text{ infected at } t. \end{cases} \tag{3.10}$$

This corresponds to the minimal cost that an agent has to pay between t and the end of the game (averaged over random realizations of the game, and assuming that all other players follow some given strategies n_β^γ). Note that in Eq. (3.1) we assumed that the total cost of infection is paid right after infection, so that individuals do not incur any additional cost at later times. The Markov process of the game is described by the following equations, illustrated in Fig. 5:

$$\begin{aligned}&\widetilde{P}_a(x_a(t+dt) = i_\alpha | x_a(t) = s_\alpha) = \lambda_a(t)dt, \\ &\widetilde{P}_a(x_a(t+dt) = s_\alpha | x_a(t) = s_\alpha) = 1 - \lambda_a(t)dt, \\ &\widetilde{P}_a(x_a(t+dt) = r_\alpha | x_a(t) = i_\alpha) = \xi\, dt.\end{aligned} \tag{3.11}$$

We use a standard Bellman argument to find the evolution of U_a: the lowest possible cost at time t is given by adding two quantities: the lowest possible cost at time $t+dt$, and the cost incurred in the interval $[t, t+dt[$ associated with the optimal strategy at t. Assuming a status $x_a(t) = s_\alpha$ at time t, this can be expressed as

$$U_a(t) = \min_{n_a^\gamma(t)} \mathbb{E}_{x_a(t+dt)}[U_a(t+dt) + c_a(t)], \tag{3.12}$$

with $c_a(t)$ the cost paid in the interval $[t, t+dt[$. At time $t+dt$, the agent either is still susceptible, or becomes infected. If $x_a(t+dt) = s_\alpha$, then the only cost at t is $c_a(t) = f_\alpha(n_a^\gamma(t))dt$, whereas if $x_a(t+dt) = i_\alpha$ then a has to bear the costs due to infection, and thus $c_a(t) = \mathcal{I}_\alpha(I(t))$. Following Eq. (3.10), if a is susceptible at $t+dt$, then the quantity $U_a(t+dt)$ involves the average cost $C_a(n_a^\gamma(\cdot), t+dt)$, which is an average over all random realizations of the epidemic at times $t' > t+dt$; if a is infected at $t+dt$, then $U_a(t+dt) = 0$. The expectation value in Eq. (3.12) is therefore taken over random realizations of the status $x_a(t+dt)$.

Writing explicitly the expectation in Eq. (3.12) and using the probabilities given by Eq. (3.11) we get

$$\begin{aligned}U_a(t) = \min_{n_a^\gamma(t)}\big[&\mathcal{I}_\alpha(I(t))\lambda_a(t)dt + (1-\lambda_a(t)dt)\big(U_a(t+dt) \\ &+ f_\alpha\big(n_a^\gamma(t)\big)dt\big)\big].\end{aligned} \tag{3.13}$$

At first order in dt, this gives the Hamilton-Jacobi-Bellman (HJB) equation of our mean-field game

$$-\frac{dU_a(t)}{dt} = \min_{n_a^\gamma(t)}\big[\lambda_a(t)(\mathcal{I}_\alpha(I(t)) - U_a(t)) + f_\alpha\big(n_a^\gamma(t)\big)\big], \tag{3.14}$$

and the optimal strategy $n_\alpha^{\gamma *}(t)$ at time t is given by

$$n_a^{\gamma *}(t) = \operatorname*{argmin}_{n_a^\gamma(t)}\big[\lambda_a(t)(\mathcal{I}_\alpha(I(t)) - U_a(t)) + f_\alpha\big(n_a^\gamma(t)\big)\big], \tag{3.15}$$

where the optimization is now performed for a given, *fixed*, time. By taking a particular form for f_α, one can compute $n_a^{\gamma *}(t)$ by setting to zero the derivative of the right-hand side with respect to n. Thus, for a given epidemic, we can obtain the optimal individual behavior backward in time by solving HJB Eq. (3.14). More details will be given in Sec. IV D.

C. Nash equilibrium

The outcome of Secs. II B and III B can now be summarized as follows. Assuming the global (or average) strategies $n_\alpha^\gamma(\cdot)$ known, the time evolution of the epidemics variables $S_\alpha(t), I_\alpha(t), R_\alpha(t)$ are derived from Eqs. (2.11) and (2.12). From the knowledge of these epidemic variables, an individuals a of age class α can perform an individual optimization leading to the optimal strategy $n_a^{\gamma *}(t)$ given by Eq. (3.15).

A (symmetric) Nash equilibrium corresponds to the situation in which this individual optimization actually coincides with the global strategy of class α, which leads to the self-consistent equation

$$n_a^{\gamma *}(\cdot) = n_\alpha^\gamma(\cdot) \tag{3.16}$$

for all age classes α and all settings γ. Under this self-consistent condition an agent can indeed assume that the other individuals will follow the strategies $n_\alpha^\gamma(\cdot)$ as this will indeed correspond for them to an individual optimum, as it does for her. "Solving" our mean-field game will therefore amount to

solve the (forward) rate equations Eqs. (2.11) and (2.12) together with the (backward) HJB equation Eq. (3.14) and with the self-consistent (Nash equilibrium) condition Eq. (3.16).

IV. EPIDEMICS DYNAMICS

In Secs. II and III we described the formalism of our MFG theory of SIR-models with social structure; in the present section we implement the corresponding equations, discuss the resulting epidemics dynamics and analyze the different types of optimal strategies. We shall choose a particular setting to best illustrate what kind of problems can be addressed and what kind of questions can be asked within this framework. Once again, we stress that we do not aim at describing a specific epidemic breakout in a given geographic area with parameters extracted from real data: this would clearly be beyond the reach of this work. Our choice in the present section is to consider a rather "typical" configuration and discuss the kind of information that could be extracted from our model, and how it could be used by public institutions; a more thorough exploration of the model's parameter space will be performed in Appendix G. We start by giving a brief summary of our MFG formalism in Sec. IV A. In Sec. IV B we introduce the specific form of the cost function and the choice of parameters that we will discuss, and in Sec. IV C we introduce different scenarios, corresponding to different choices or constraints on the contact willingness, and summarize the results obtained from solving the equations. These different scenarios are defined in more detail in the subsequent subsections: unconstrained Nash equilibrium in Sec. IV D, Nash equilibrium with constraints (e.g., partial lockdown imposed by a centralized authority) in Sec. IV E, societal optimum (where a global planner controls perfectly the behavior of each agent to minimize the total costs borne by the society) in Sec. IV F. Finally, in Sec. IV G 1 we compare the different scenarios.

A. Summary of Secs. II and III

Before we dive into a detailed analysis of the kind of behavior that may emerge within our MFG model, let us summarize briefly the content of the two previous sections. We have first introduced in Sec. II B a SIR model with social structure in which we distinguish three age classes $\alpha \in \{\text{young, adult, retired}\}$ and different settings $\gamma \in \{\text{schools, household, communities, workplace}\}$. In addition to the time-dependent variables $n_\alpha^\gamma(t) \in [\mathrm{n}_{\min}^\gamma, 1]$ corresponding to the effort made by individuals in the setting γ to avoid infection, the model is characterized by three "biological parameters" (the probability ρ of transmission of the disease per contact, the proportion μ of asymptotic individuals in the infected population, and the recover rate ξ), and a set of "social-structure parameters" (the number of individuals N_α^{tot} in each age class, and the array $\mathcal{W}_{\alpha\beta}^{\gamma\,(0)}$ specifying the contact rate of the agents in the absence of epidemics); cf Table I.

One remark is in order here. The N_α^{tot} and (the inverse of) $\mathcal{W}_{\alpha\beta}^{\gamma\,(0)}$ are *extensive* quantities: as $N_{\mathrm{tot}} \to \infty$, so does the N_α^{tot}, and the $\mathcal{W}_{\alpha\beta}^{\gamma\,(0)}$ have to go to zero to maintain a finite rate of infection for a given individual. While the formal developments of Secs. II and III were better performed using theses variables, we shall from now on use related *intensive* parameters, which are well-defined in the limit $N_{\mathrm{tot}} \to \infty$ and easier to relate to observable data. We thus introduce $\mathcal{N}_\alpha = N_\alpha^{\mathrm{tot}}/N_{\mathrm{tot}}$, the proportion of agents in age class α, and the array

$$\mathcal{M}_{\alpha\beta}^{\gamma\,(0)} := \mathcal{W}_{\alpha\beta}^{\gamma\,(0)} N_\beta^{\mathrm{tot}}, \tag{4.1}$$

which corresponds to the average number of contacts with β for an individual $a \in \alpha$. The requirement that $\mathcal{W}_{\alpha\beta}^{\gamma\,(0)}$ is a symmetric matrix implies the constraint $\mathcal{N}_\alpha \mathcal{M}_{\alpha\beta}^{\gamma\,(0)} = \mathcal{N}_\beta \mathcal{M}_{\beta\alpha}^{\gamma\,(0)}$, for all age class pairs (α, β) and all settings γ.

In terms of these parameters, the dynamics of the epidemic variables given by Eqs. (2.11) and (2.12) takes the form

$$\begin{aligned} \dot{S}_\alpha &= -\lambda_\alpha(t) S_\alpha(t), \\ \dot{I}_\alpha &= \lambda_\alpha(t) S_\alpha(t) - \xi I_\alpha(t), \\ \dot{R}_\alpha &= \xi\, I_\alpha(t). \end{aligned} \tag{4.2}$$

$$\lambda_\alpha(t) \equiv \mu\rho \sum_{\beta=1}^{n_{\mathrm{cl}}} \sum_{\gamma=1}^{n_{\mathrm{set}}} n_\alpha^\gamma(t) n_\beta^\gamma(t) \mathcal{M}_{\alpha\beta}^{\gamma\,(0)} I_\beta(t). \tag{4.3}$$

Within our mean-field-game approach, the dynamics of the variables $n_\alpha^\gamma(\cdot)$ is determined by an optimization of the intertemporal cost Eq. (3.1) which is characterized, for each age class α, by two functions. The first one $\mathcal{I}_\alpha(I)$ measures the damage caused by infection, and has a dependence in the total proportion of infected individual $I = \sum_\alpha \mathcal{N}_\alpha I_\alpha$ to include the consequence of the saturation of the sanitary systems once the epidemics goes beyond a certain level. The second one $f_\alpha(n_a^\gamma)$ measure the instantaneous cost for an individual a of class α due to the limitation of her contact, and depends one the "effort" n_a^γ made in each setting γ. Using Bellman linear programming, the optimal effort is given by Eq. (3.15),

$$n_a^{\gamma *}(t) = \underset{n_a^\gamma(t)}{\operatorname{argmin}} \left[\lambda_a(t)(\mathcal{I}_\alpha(I(t)) - U_a(t)) + f_\alpha\left(n_a^\gamma(t)\right)\right], \tag{4.4}$$

where the *individual force of infection* λ_a Eq. (3.6) is the analog of the global one λ_α Eq. (4.3) with the substitution $n_\alpha^\gamma \leftrightarrow n_a^\gamma$, and in which appears the *value function* $U_a(t)$, Eq. (3.10) determined by the HJB equation (3.14),

$$-\frac{dU_a(t)}{dt} = \min_{n_a^\gamma(t)} \left[\lambda_a(t)(\mathcal{I}_\alpha(I(t)) - U_a(t)) + f_\alpha\left(n_a^\gamma(t)\right)\right]. \tag{4.5}$$

Finally, homogeneity of the population among each class leads to the additional requirement that one reaches a *Nash equilibrium*, i.e., that the optimal strategy of an individual a of class α corresponds to the global choice made on average by the class α lead to the self-consistent condition Eq. (3.16),

$$n_a^{\gamma *}(\cdot) = n_\alpha^\gamma(\cdot). \tag{4.6}$$

Equations (4.2)–(4.6) form the system of equations that need to solve to find the Nash equilibrium of our MFG problem.

B. Cost function and choice of the parameters

We turn now to the specific choice of parameters we will use in most of the following to illustrate the properties and

TABLE II. "Social-structure" and "biological" parameters used in our simulations. The matrix entries $\mathcal{M}_{\alpha\beta}^{\gamma(0)}$ correspond to the average frequency of contacts (per week) between an individual of age class α and someone of age class β in the setting γ. $\mathcal{N}_\alpha = N_\alpha^{\rm tot}/N_{\rm tot}$ is the proportion of the population in each age class. $I_\alpha(0)$ are the initial proportion of infected for each age class [we always assume $R_\alpha(0) = 0$]. ξ is the recovery rate (per week), ρ the transmission rate per contact, and μ corresponds to the proportion of asymptomatic individuals in the population. Finally, $\alpha = 1, 2, 3$ for age class of young, adults, and retired individuals, respectively. The way these parameters have been chosen is discussed in detail in Appendix B.

$\mathcal{W}^S$	$\mathcal{W}^W$	$\mathcal{W}^C$	$\mathcal{W}^H$
$\begin{pmatrix} 100 & 0 & 0 \\ 0 & 0 & 0 \\ 0 & 0 & 0 \end{pmatrix}$	$\begin{pmatrix} 0 & 0 & 0 \\ 0 & 75 & 0 \\ 0 & 0 & 0 \end{pmatrix}$	$\begin{pmatrix} 12.5 & 25 & 12.5 \\ 12.5 & 25 & 12.5 \\ 12.5 & 25 & 12.5 \end{pmatrix}$	$\begin{pmatrix} 15 & 25 & 10 \\ 12.5 & 32.5 & 5 \\ 10 & 10 & 30 \end{pmatrix}$
$\mathcal{N}_\alpha := N_\alpha^{\rm tot}/N_{\rm tot}$	$I_\alpha(0)$	(ξ, ρ, μ)	
$(0.25, 0.5, 0.25)$	$(0.01, 0.01, 0.01)$	$(1.2, 0.1, 0.2)$	

operational properties of our MFG model. In practice we need essentially to make a choice, on the one hand, for the "social-structure" and "biological" parameters of Table I (or their rescaled version introduced in Sec. IV A), and, on the other hand, for the functions $\mathcal{I}_\alpha(I)$ and the $f_\alpha(n_a^\gamma)$ of the cost (3.1), and the associated "cost-function" parameters.

For the former set of parameters, there is a fairly large scientific literature devoted to their evaluation from field data in specific, real-world situations. However, as noted above, our goal is not to model a particular instance of epidemic dynamics, but rather to illustrate the kinds of questions that can be addressed and the kinds of behaviors that can typically be obtained within our formalism. We have therefore chosen parameter values that we consider "generic," relying on a number of studies [1,38,47–50] that analyze real epidemiological datasets. This approach makes it possible to evaluate the performance of the model under conditions that closely reflect practical scenarios, and allows us to expect that our model will produce comparable results in realistic applications. The exact way the "social-structure" and "biological" parameters were chosen is detailed in Appendix B, and their values is summarized in Table II.

Turning now to the cost (3.1), we take, for the cost of infection,

$$\mathcal{I}_\alpha(I(t)) = \mathfrak{r}_{\mathrm{I},\alpha} \exp\left[\mathfrak{q}_{\rm sat} \frac{I(t) - \mathfrak{I}_{\rm sat}}{\mathfrak{I}_{\rm sat}}\right]. \tag{4.7}$$

This function includes the effect of a possible saturation of health services, and we assume an exponential increase of the strain on human and material resources as the saturation threshold $\mathfrak{I}_{\rm sat}$ is approached, with a slope $\mathfrak{q}_{\rm sat}$ corresponding to the impact of saturation on the cost. As $I \ll \mathfrak{I}_{\rm sat}$, or $\mathfrak{q}_{\rm sat} \to 0$, $\mathcal{I}_\alpha$ approaches an (age-class-dependent) constant $\mathfrak{r}_{\mathrm{I},\alpha}$ which implements the possibility that retired individual might be put significantly more at risk by the infection that younger ones. In practice we shall write these constants as $\mathfrak{r}_{\mathrm{I},\alpha} = \mathfrak{r}_{\mathrm{I}}\kappa_\alpha$, and keep the age-class-dependent part κ_α fixed for all our simulations, while in some instance exploring the changes due to the variations of $\mathfrak{r}_{\mathrm{I}}$.

Turning now to $f_\alpha(n_a^\gamma)$, the cost of modifying social contacts, we choose to follow the same form as Turinici *et al.* in Ref. [32], namely,

$$f_\alpha\big(n_a^\gamma(t)\big) = \sum_\gamma \big(n_a^\gamma(t)^{-\mathfrak{m}_\gamma} - 1\big), \tag{4.8}$$

where $\mathfrak{m}_\gamma$ models the degree of "attachment" to the setting γ: for example it is usually easier to reduce contacts at work than inside families. Moreover, f is decreasing with a positive second derivative, meaning that the more one decreases once social contacts, the higher the price to pay.

The set of values chosen in this section for the parameters characterizing the functions $\mathcal{I}_\alpha(I)$ and $f_\alpha(n_a^\gamma)$ is summarized in Table III. Finally, the parameter T denotes the time at which agents end their optimization process. This corresponds, for instance, to the time where herd immunity is reached, or it can depend on other circumstances such as the expected production of a vaccine, the seasonality of the virus, among others. In Sec. IV C, our simulations are performed on a duration of $T = 40$ weeks to focus on scenarios where collective immunity is reached and to avoid short end-time effects. Scenarios for which, due to short end-time, collective immunity is not reached at the end of the optimization period will be studied more specifically in Sec. V B. Since the main wave of the epidemic appears in the first 10 weeks, we often present the results on a duration of 15 weeks.

C. Epidemics dynamics

Solving the MFG equations of Sec. IV A for the set of parameters defined in Tables II and III yields the dynamics of S, I, and R. Technical detail about the numerical

TABLE III. "Cost-function" parameters associated with the function Eq. (3.1) chosen for our simulations. The cost of infection $\mathcal{I}_\alpha$ Eq. (4.7) is characterized, on the one hand, by its value under "normal circumstances" $\mathfrak{r}_{\mathrm{I},\alpha} = \mathfrak{r}_{\mathrm{I}}\kappa_\alpha$, where we distinguish a common coefficient $\mathfrak{r}_{\mathrm{I}}$ that will take different values depending on the simulation, and an age-dependent part κ_α, which we will keep fixed at the value given in this table. On the other hand, $\mathfrak{I}_{\rm sat}$ characterizes the fraction of infected individuals at which the sanitary system starts to malfunction, and $\mathfrak{q}_{\rm sat}$ the speed at which this malfunction sets in. The cost of reducing once social contact is then parameterized by $\mathfrak{n}_{\rm min}^\gamma$, the minimum contact willingness in each setting γ, and $\mathfrak{m}_\gamma$, which weights the cost of contact reduction in each setting. $\mathfrak{I}_{\rm d}$, $\mathfrak{I}_{\rm l}$ are the thresholds for the best lockdown and $\mathfrak{s}$ its intensity level.

$(\mathfrak{I}_{\rm sat}, \mathfrak{q}_{\rm sat})$	κ_α	$\mathfrak{m}_\gamma$	$\mathfrak{n}_{\rm min}^\gamma$	$(\mathfrak{I}_{\rm d}, \mathfrak{I}_{\rm l}, \mathfrak{s})$
$(0.1, 0.1)$	(1,10,100)	(2,2,1,3)	$\left(\frac{1}{3}, \frac{1}{5}, \frac{1}{5}, \frac{1}{2}\right)$	$(0.12, 4.10^{-4}, 0.35)$

implementation is given in Appendix D. The corresponding curves are displayed at the second line of Fig. 6.

The characteristic features of the Nash equilibrium are better revealed if one compares the corresponding epidemic dynamics with other scenarios. We shall consider the following options, which will be discussed in greater detail in the following subsections. We shall refer to the Nash equilibrium presented in Sec. IV D as the *unconstrained Nash equilibrium*. By contrast, the second scenario (see Sec. IV E) is a *"constrained" Nash equilibrium*, where individuals have to deal with global constraints imposed by an authority, for instance, a temporary lockdown which limits the agent's strategy freedom, which translates into bounds on n_a. This second scenario divides into two subscenarios, depending on whether these constraints are naive or optimally chosen. A third scenario, discussed in Sec. IV F, is that of a *the societal optimum*, which is the idealistic case where everybody strives to optimize the global cost and chooses their strategy n_a accordingly. We call the "null" scenario *business as usual*: the agents do not adapt their behavior to the epidemics, so that no modification of the contact parameter is done, namely, n_a is fixed to 1. In each of these cases, the epidemic dynamics is driven by Eqs. (4.2)–(4.6), but with different $\{n_\alpha^\gamma(.)\}$, and thus different forces of infection $\{\lambda_\alpha\}$.

Solving the MFG equations in these different contexts leads to different dynamics for S, I, and R. The dynamics for each of the above scenarios is summarized in Fig. 6; the precise description of the scenarios is the object of the following subsections. As Fig. 6 shows, there are notable similarities between the different "optimized" scenarios (Nash, constrained Nash and societal optimum) and the business as usual one. For instance, the number of susceptible individuals at the end of the epidemic is $S_\infty \simeq 0.4$ in all cases but for the business as usual scenario, where it is significantly below (first row). This is due to the fact that in all circumstances one needs to reach herd immunity to escape from the disease, and the fact that S_∞ is much below this required value is a clear indication of the business as usual suboptimal character. In the same way, for all optimized scenarios there is a significant difference between the height of the infection wave for the different age class, as retired individuals and adults are more impacted by the disease than the youths, and therefore protect themselves. In the business as usual scenario the difference is much less significant, and only due to the relative proportion of contacts in each age class. However, the constrained Nash equilibrium with "naive" constraints differs from all the others because of the existence of two epidemic waves, which can be understood as originating from an excessive limitation of contacts that prevents the society from reaching herd immunity. Other differences, which are mainly quantitative, also exist between these different scenarios, and will be discussed in more details in Sec. IV G. We now turn to the detailed description of each scenario.

D. (Unconstrained) Nash equilibrium

Let us first consider the (unconstrained) Nash equilibrium. We have seen that it is described by two sets of differential equations. The first one is the rate equation of the epidemic, Eq. (4.2) (also known as the Kolmogorov equation in this context), which is forward in time, that is, starting from initial conditions $S_\alpha(0), I_\alpha(0), R_\alpha(0)$, populations at later time t in age class α are obtained by solving Eq. (4.2) with $\lambda_\alpha(t)$ given by Eq. (4.3). The second set of equations corresponds to the Hamilton-Jacobi-Bellman equation (4.5), with one reference individual a for each age class α. As only the terminal condition on U is fixed, namely, $U_a(T) = 0$, Eq. (4.5) is backward in time. At equilibrium, all individuals will follow their own optimal strategy; but as all agents in a given age class are equivalent, this optimal strategy should be the same for all agents a of age class α. Thus we have the additional self-consistency condition Eq. (4.6), which imposes that if all other agents follow the strategy solution of the self-consistent system Eqs. (4.2), (4.5), and (4.6), deviating from that strategy implies a higher cost. The solution of the MFG equation thus corresponds to a Nash equilibrium.

The two equations (4.2) and (4.5), together with the self-consistency condition (4.6), form a system of equations coupling all epidemic rates $S(.)$, $I(.), R(.)$ and all age-class strategies n_α^γ via the individual optimal strategies $n_a^{\gamma *}$. Indeed, the epidemic rates in Eq. (4.2) depend on $\lambda_\alpha(t)$ given in Eq. (4.3), which depend on the global strategies n_β^γ. In turn, the optimal strategy $n_a^{\gamma *}$ for a reference individual a is a solution of HJB equation (4.5). With the precise form of the costs $\mathcal{I}_\alpha(I(s))$ and $f_\alpha(n_a^\gamma(t))$ chosen in Sec. IV B, it can be computed explicitly and reads

$$n_a^{\gamma *}(t) = \left(\frac{\mu\rho}{\mathfrak{m}_\gamma} [\mathcal{I}_\alpha(I(t)) - U_a(t)] \sum_{\beta=1}^{n_{\rm cl}} n_\beta^\gamma(t) \mathcal{M}_{\alpha\beta}^{\gamma(0)} I_\beta(t) \right)^{-\frac{1}{\mathfrak{m}_\gamma + 1}}, \tag{4.9}$$

which depends on the global strategies $n_\beta^\gamma(.)$ explicitly, and implicitly through the epidemic rate $I(.)$. One obtains in this way an initial-terminal value problem, which can be solved numerically in different ways; we present some of them briefly in Appendix D 1.

The solutions of the MFG system (4.2)–(4.6) are displayed in the second row of Fig. 6 for the set of epidemics quantities $S_\alpha(.), I_\alpha(.), R_\alpha(.)$, and in Fig. 7 for the set of optimal strategies $n_\alpha^\gamma(.)$. For our choice of parameters, young individuals do not modify at all their behavior, when retired people reach maximal effort for significant amount of time in both community and household settings, and adults do some efforts, but without ever reaching the maximum one.

E. Nash equilibrium under constraints

In the Nash equilibrium considered above, each agent optimises for herself, and the resulting Nash equilibrium can lead to a global cost for the society,

$$C_{\rm glob}(\{n_\beta\}) \equiv \sum_\alpha \mathcal{N}_\alpha C_\alpha(n_a = n_\alpha, \{n_\beta\}), \tag{4.10}$$

which is suboptimal. In Eq. (4.10), $\{n_\beta\}$ is the set of strategies followed by each age class, $n_a = n_\alpha$ means that any given individual a of class α follows the strategy n_α assigned to age class α, and the cost for each age class is weighted by the proportion $\mathcal{N}_\alpha$ of individuals in that class. A question that naturally arises from a public policy point of view is to

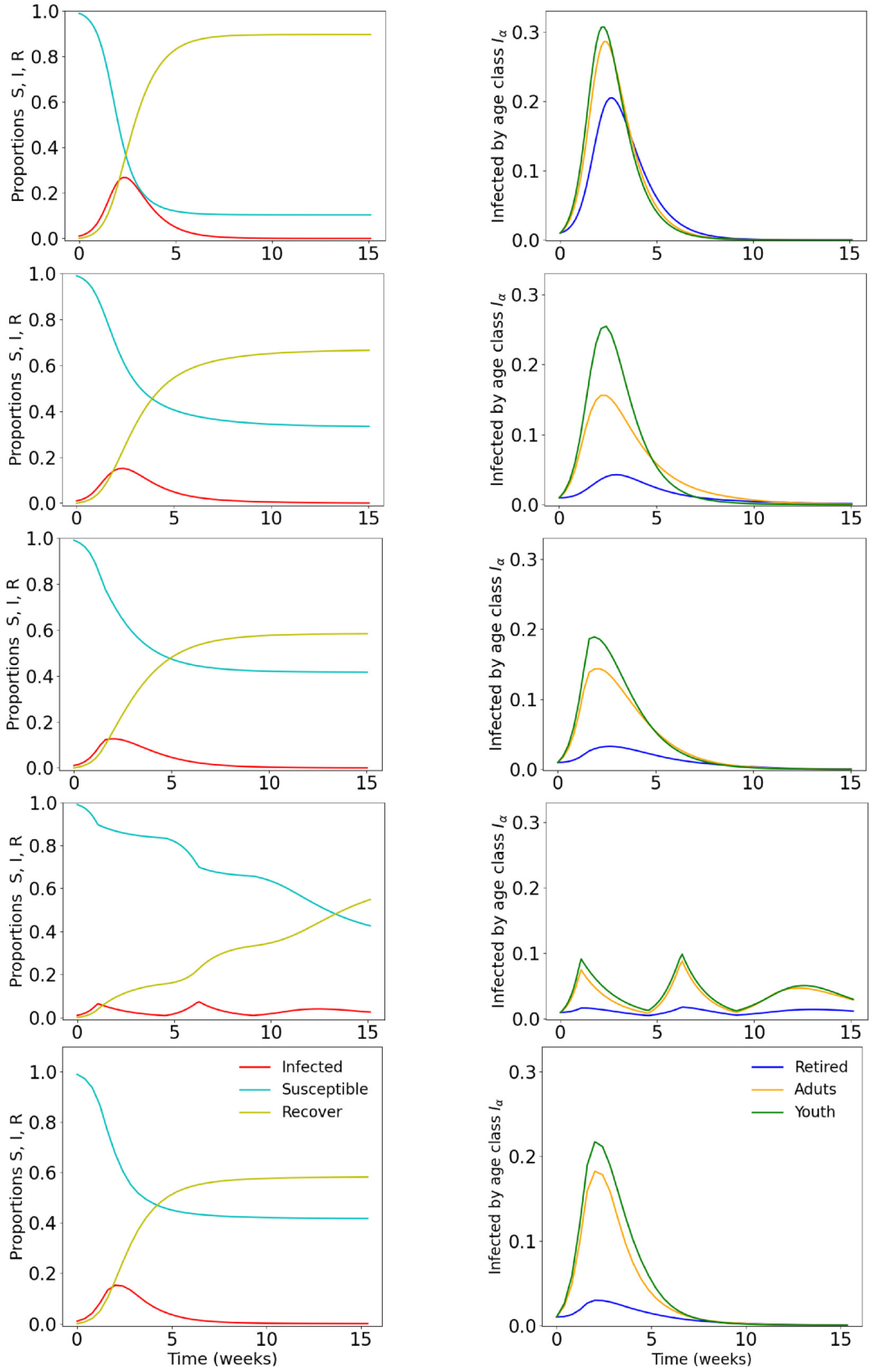

FIG. 6. Time evolution of the epidemic quantities with $\tau_I = 1$ and parameters of Tables II and III. From top to bottom: Business as usual (no efforts), (unconstrained) Nash equilibrium, Nash equilibrium under optimal constraints, Nash equilibrium with naive constraints, societal optimum. Left: Time evolution of the proportion of susceptible S (cyan), infected I (red), and recovered R (yellow) in the population. Right: Time evolution of the proportion of infected in each age class I_α, retired people are in blue, adults in orange, and youth in green.

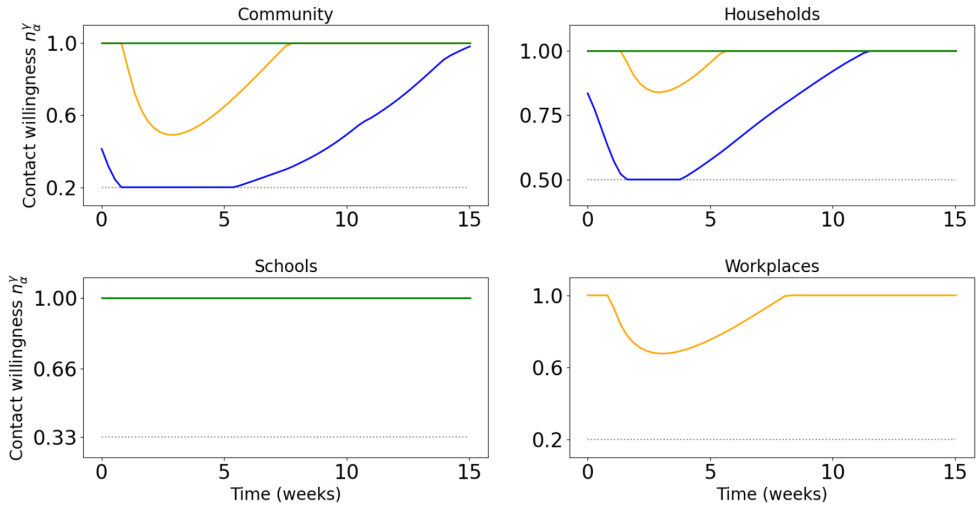

FIG. 7. Time evolution of the contact willingness $n_\alpha^\gamma(t)$ with $\mathfrak{r}_\mathrm{I} = 1$ at the Nash equilibrium. We plot $n_\alpha^\gamma(t)$ for each type of individual according to their age class (retired people in blue, adults in orange and youth in green) in community (upper left), households (upper right), schools (lower left, for the young) and workplaces (lower right, for the adults). The dotted gray horizontal lines correspond to the minimum contact willingness allowed (maximum effort).

know whether one could improve the global wellbeing of the population by driving the position of the Nash equilibrium through constraints on the population. This is, in some sense, what has been attempted in many countries during COVID-19 pandemic. The restrictions taken then, however, involved a lot of guesswork, both about the precise decisions to take, and about their potential effects on society (individuals behavioral response, impact on economic, health, etc.).

Here we present a possible quantitative approach to study such restriction policies, which aim at reducing the societal cost by constraining the behavior of individuals. Again, we remain here at the level of a "proof of concept," as practical implementations of our formalism would require determining realistic forms of the cost functions and of the constraints, which is clearly beyond the scope of our work.

With the free (i.e., unconstrained) Nash equilibrium, individuals choose their contact willingness $n_\alpha^\gamma(t)$ in the range $[\mathfrak{n}_{\alpha,\min}^\gamma, 1]$, where the maximum 1 correspond to the situation without epidemic. We now add a constraint similar to a partial lockdown, by setting this maximum to $n_{\alpha,l}^\gamma < 1$ when some epidemic level is reached. In that way, everyone is required to make a minimal amount of efforts to preserve the sanitary system and reduce the societal cost (4.10). This "lockdown" is implemented when the proportion of infected $I(t)$ reaches a certain threshold $\mathfrak{I}_\mathrm{d}$, and, as the proportion of infected decreases we assume the lockdown is lifted when $I(t)$ goes below a value $\mathfrak{I}_\mathrm{l} < \mathfrak{I}_\mathrm{d}$ (which is assumed lower than $\mathfrak{I}_\mathrm{d}$ to avoid unrealistic oscillations around $\mathfrak{I}_\mathrm{d}$). The lockdown has thus a hysteresis form, and is implemented in the following way (with L a Boolean variable which is 1 if the lockdown is active and 0 otherwise):

$$\begin{aligned}
&\text{if } I(t) < \mathfrak{I}_\mathrm{l} : n_\alpha^\gamma(t) \in \left[\mathfrak{n}_{\alpha,\min}^\gamma, 1\right] \quad \& \quad L \mapsto 0 \qquad \text{no constraints,}\\
&\text{if } I(t) > \mathfrak{I}_\mathrm{d} : n_\alpha^\gamma(t) \in \left[\mathfrak{n}_{\alpha,\min}^\gamma, n_{\alpha,l}^\gamma\right] \quad \& \quad L \mapsto 1 \qquad \text{active constraints,}\\
&\text{if } \mathfrak{I}_\mathrm{l} < I(t) < \mathfrak{I}_\mathrm{d} \text{ and } L = 0 : n_\alpha^\gamma(t) \in \left[\mathfrak{n}_{\alpha,\min}^\gamma, 1\right] \qquad \text{no constraints,}\\
&\text{if } \mathfrak{I}_\mathrm{l} < I(t) < \mathfrak{I}_\mathrm{d} \text{ and } L = 1 : n_\alpha^\gamma(t) \in \left[\mathfrak{n}_{\alpha,\min}^\gamma, n_{\alpha,l}^\gamma\right] \qquad \text{active constraints.}
\end{aligned} \tag{4.11}$$

In Eq. (4.11), we choose $n_{\alpha,l}^\gamma = \mathfrak{s}\,\mathfrak{n}_{\alpha,\min}^\gamma + (1-\mathfrak{s})$, with $\mathfrak{s} \in [0,1]$ a variable measuring the intensity of the lockdown: $\mathfrak{s} = 0$ corresponds to the free situation without any constraint, while $\mathfrak{s} = 1$ corresponds to a strict lockdown with no freedom, as $n_\alpha^\gamma(t)$ is fixed to $\mathfrak{n}_{\alpha,\min}^\gamma$. Therefore, the lockdown is described by a set of three variables $(\mathfrak{s}, \mathfrak{I}_\mathrm{d}, \mathfrak{I}_\mathrm{l})$: the intensity $\mathfrak{s}$, the first threshold $\mathfrak{I}_\mathrm{d}$, and the second threshold $\mathfrak{I}_\mathrm{l}$. The numerical implementation of this set of equations is briefly discussed in Appendix D 2.

In Fig. 6 (third row) we show the evolution of the epidemic quantities for the choice of parameters ($\mathfrak{s} = 0.35, \mathfrak{I}_\mathrm{d} = 0.12, \mathfrak{I}_\mathrm{l} = 4.10^{-4}$). As shown in Appendix E this choice corresponds to an optimal value in the sense that these parameters minimise the global cost Eq. (4.10) among all possible constraints in the parameter space $(\mathfrak{s}, \mathfrak{I}_\mathrm{d}, \mathfrak{I}_\mathrm{l})$. In Fig. 8 we display the corresponding strategies chosen by individuals under these constraints. The constraints are enforced after 2 or 3 weeks into the epidemic, and are raised after almost 14 weeks (over 40 for the total epidemic time) when the proportion of infected is low and there is no risk of any epidemic rebound. The values of the constraints appear as straight lines followed by youth individuals, whose behavior is not dictated by their own

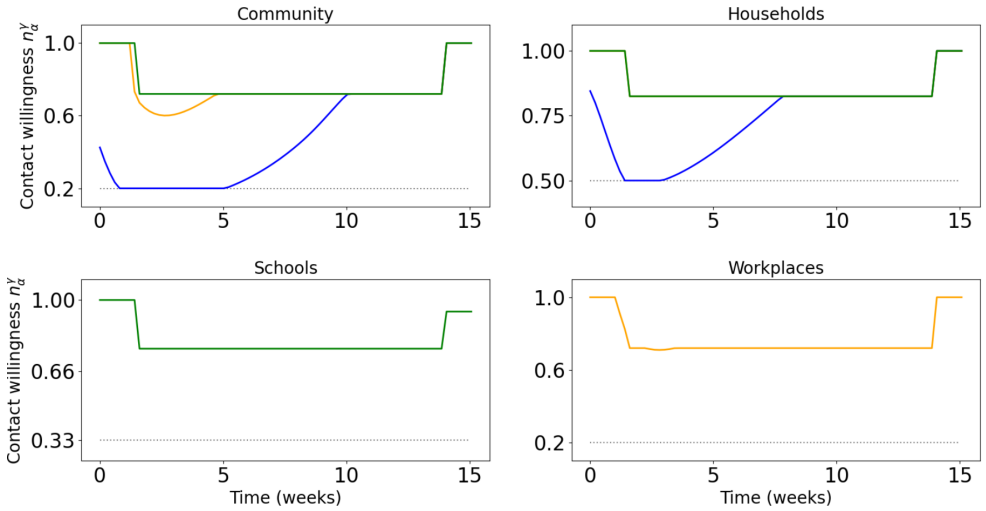

FIG. 8. Time evolution of the contact willingness $n_\alpha^\gamma(t)$ with $\mathfrak{r}_\mathrm{I} = 1$ for the Nash equilibrium under optimal constraints ($\mathfrak{s} = 0.35$, $\mathfrak{I}_\mathrm{d} = 0.12$, $\mathfrak{I}_\mathrm{l} = 4.10^{-4}$). We plot $n_\alpha^\gamma(t)$ for each type of individual according to their age class (retired people in blue, adults in orange and youth in green) in community (upper left), households (upper right), schools (lower left, for the young) and workplaces (lower right, for the adults). The dotted gray horizontal lines correspond to the minimum contact willingness allowed.

"egoistic" optimisation but by the fact they are forced to respect the lockdown as soon as it is imposed. Retired people, however, choose most of the time to limit their contact even more than required by the constraints; adults most of the time just follow the lockdown, but sometimes limit their contacts further.

As we shall discuss in Sec. IV G this optimal lockdown, despite the fact that it depends on only three parameters, can improve on the free Nash equilibrium, in the sense that the societal cost Eq. (4.10) is lower. However, public policies executives have to be careful about their choice as it can generate situations which are clearly worse than the free Nash equilibrium. We illustrate this situation in Figs. 6 (fourth row) and 9 with parameters ($\mathfrak{s} = 0.8$, $\mathfrak{I}_\mathrm{d} = 0.06$, $\mathfrak{I}_\mathrm{l} = 0.01$): in that case one imposes a very strong but short lockdown. Since we consider here a long end-time configuration with $T = 40$ weeks, for which collective immunity is required to end the epidemic, this leads to epidemic rebounds and increases significantly the epidemic cost. Indeed, all drastic efforts that are made while the epidemic is low, and before collective immunity is obtained, are essentially useless, and just add to the global cost endured by the population. In what follows we shall thus distinguish Nash under optimal constraints (NOC) and Nash under "naive" (uncarefully chosen) constraints (NNC).

F. Societal optimum

In the previous two scenarios, each agent performs a personal, possibly constrained, but essentially egoistic,

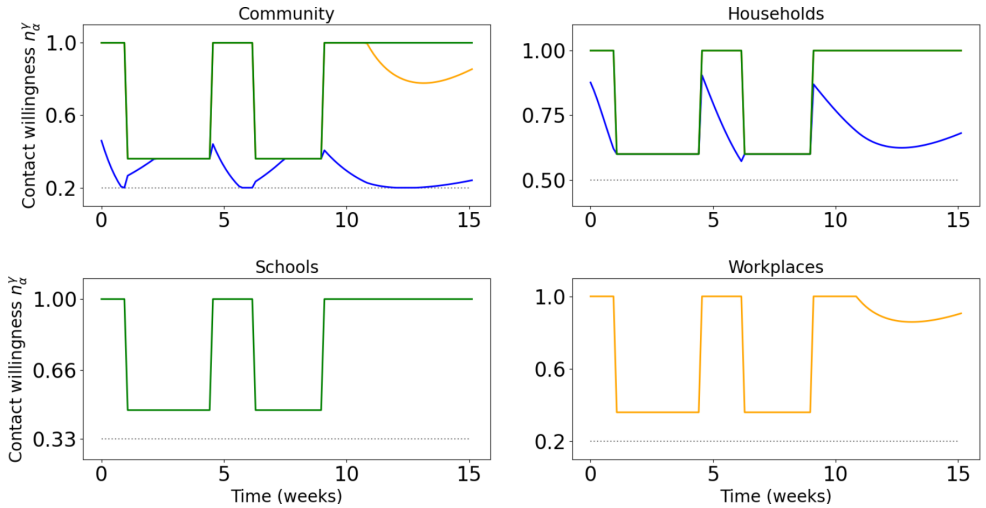

FIG. 9. Time evolution of the contact willingness $n_\alpha^\gamma(t)$ with $\mathfrak{r}_\mathrm{I} = 1$ for the Nash equilibrium under naive constraints ($\mathfrak{s} = 0.8$, $\mathfrak{I}_\mathrm{d} = 0.06$, $\mathfrak{I}_\mathrm{l} = 0.01$). We plot $n_\alpha^\gamma(t)$ for each type of individual according to their age class (retired people in blue, adults in orange and youth in green) in community (upper left), households (upper right), schools (lower left, for the young), and workplaces (lower right, for the adults). The dotted gray horizontal lines correspond to the minimum contact willingness allowed.

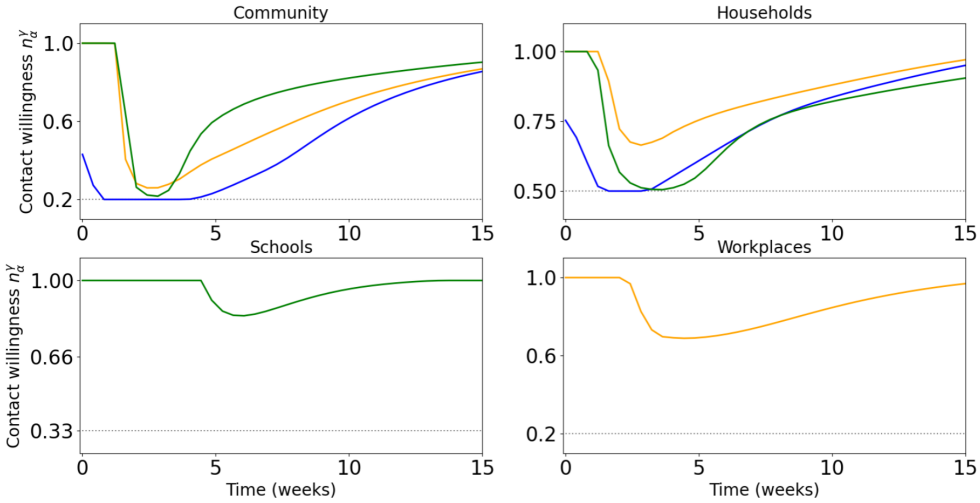

FIG. 10. Time evolution of the contact willingness $n_\alpha^\gamma(t)$ with $\mathfrak{r}_1 = 1$ for the societal optimum. We plot $n_\alpha^\gamma(t)$ for each type of individual according to their age class (retired people in blue, adults in orange and youth in green) in community (upper left), households (upper right), schools (lower left, for the young), and workplaces (lower right, for the adults). The dotted gray horizontal lines correspond to the minimum contact willingness allowed.

optimization. To set the scale of what is the cost associated with these egoistic approaches, it may be useful to compare them with the "societal optimum" that could be imposed by a "benevolent global planner," i.e., a well-meaning government with full empowerment. Considering the global cost, seen at the society level, as the addition of all individual costs, this amounts to finding the minima of the cost Eq. (4.10). There is already a rich literature on topics related to societal optimization (see, for example, Refs. [6,7,32,51–57]) on various types of models, as this problem is reduced to a single global optimization. The difference between this minimization and the Nash equilibrium discussed above is referred to as "the cost of anarchy": while there is no cooperation between individuals in the Nash equilibrium, the societal optimum case corresponds to "the best" (from a societal cost point of view) that one can obtain for C_{glob} among all possible strategies.

The numerical construction of this societal optimum is briefly discussed in Appendix D 3. In Fig. 6 (fifth row) we show the epidemic quantities associated with the societal optimum. However, the total number of infected individuals is not the lowest possible, as infection within the youths does not carry the same cost as within the retired agents. The total amount of infected at the end of the epidemic is still relatively high, because in our framework, one has to reach collective immunity to definitely escape from the disease. Also, the epidemic peak is still at a rather high level, as it is efficient to allow an epidemic spread while keeping the epidemic under control to reach quickly herd immunity. However, the precise distribution of infected proportion in each age class is different from the free Nash equilibrium.

In Fig. 10 we show the corresponding optimal contact willingnesses. They do not correspond to individual optimum; rather, there is a cooperation between individuals in different age classes to get an epidemic which will make lower damage with a reasonable amount of efforts. In the community setting and in households, we observe that all individuals make significant efforts during the epidemic peak to avoid a global infection peak that would saturate the sanitary system: they do it in particular in those two settings to avoid a too strong diffusion to retired people. However, efforts are done with less intensity in schools and workplaces. Once the epidemic peak is reached, we see that the epidemic continues to spread, in particular in young and adults classes, so that collective immunity can be reached and in this way protect retired people. Thus, the efforts in schools and workplaces are here to smooth sufficiently the epidemic, avoid any rebound, and get a relative collective immunity as fast as possible, making it possible to lift the efforts in communities and households.

G. Comparison between the different scenarios

1. Comparison of global costs

To compare quantitatively the scenarios presented above, we normalize the costs with respect to the total cost of the societal optimum, which we set equal to 100.

In Fig. 11 we show, for the choice of parameters given in Tables II and III, the global costs obtained with the different kinds of scenarios considered above. As expected, the societal optimum (SO) is the best strategy at society level, followed quite closely by the NOC, which itself is better than the free Nash equilibrium (N). As the imposition of societal-optimal scenarios implies a lack of freedom for the individual, as well as a coordination cost which may be significant and which is not included in Eq. (4.10), we argue that the constrained Nash equilibrium presumably forms in practice a good compromise between effectiveness and practicability. One should bear in mind, however, that with a naive choice for the constraints, such as for the NNC strategy of Fig. 11, one could easily obtain a result worse than for the free Nash equilibrium.

The color bars in Fig. 11 illustrate the relative importance of each age class in the total cost paid by the society. This shows that, to reach a global optimum, the key point is to reduce as much as possible the cost for retired people whose contribution is large. This contribution is actually larger than

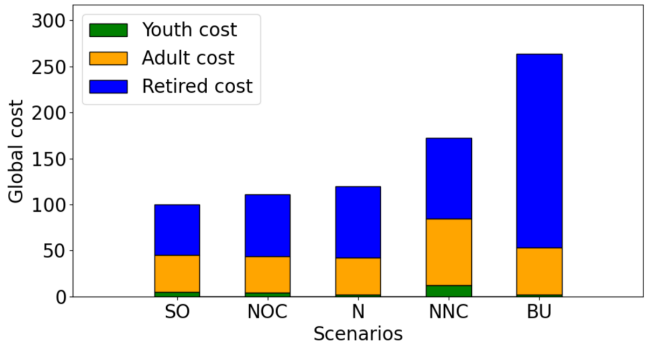

FIG. 11. Comparison of costs for the different scenarios studied: SO (societal optimum), NOC (Nash under optimal constraints), N (free Nash equilibrium), NNC (Nash under naive constraints), BU (business as usual). The costs are represented on a base of 100 for SO; the color bars represent the total cost of each age class. Thus, the level of each bar comes from the cost per individual multiplied by the proportion $\mathcal{N}_\alpha$ of his age class.

that of adults, despite the latter representing twice as many people as retired individuals in our population choice. Note that, from the point of view of adults or young people, the free Nash equilibrium is the best strategy, as they do not have to make efforts for others. We can also notice that making a wrong choice for the constraints will not lead to the same "extra cost" for everyone. Indeed, for the NNC scenario, the cost for retired people is still relatively low because the epidemic is maintained at a low level, but the cost of social restrictions becomes very high for adults and young individuals. This has to be contrasted with the business as usual scenario where the extra cost is borne almost exclusively by retired people.

2. Comparison of contact willingness for the two best scenarios

In Fig. 12, we show the comparison between the contact willingness obtained with the societal optimum (dashed line) and the Nash equilibrium under optimal constraints (solid line). We see that for the Nash equilibrium under constraints we get constraints which start at almost the same time as the ones of the societal optimum (after typically 2 weeks); but since it is a Nash equilibrium, these constraints are raised after a long time, around 14 weeks, so that even without individual efforts from adults and youth the epidemic is kept under control. At a global level, these constraints are not too strong compared to the ones of the societal optimum, but since they are less localized, both spatially (in the good settings) and temporally (during the epidemic peak with a progressive release afterwards), they are less effective to protect retired people who suffer from a higher epidemic with a larger total number of infected people at the end of the epidemic.

These two scenarios, the societal optimum and the Nash equilibrium under constraints, suggest interesting guidelines for public health executives to mitigate an epidemic through collective immunity. First, quite naturally, sufficiently strong constraints should be imposed at the epidemic peak to avoid saturation of the sanitary system; and the constraints need to protect people at risk, which implies to limit contact both among these people as well as between the rest of the society and these individuals. However, in a perhaps less intuitive way, constraints on people who are not at risk should be relatively light. Indeed, the epidemic needs to spread on the population, in a controlled way, to reach as fast as possible the collective immunity. After the epidemic peak, one can lift progressively the constraints, until the collective immunity is reached. At this point, the epidemic will be back at a low level and will stay low while the constraints can be completely lifted. The precise characteristics of the constraints, such as their intensity or their timing, will depend on the characteristics of the population and of the disease under consideration. However, scenarios that induce epidemic rebound, like the Nash scenario with naive constraints described above, are quite ineffective in such a context, because the time span between the peaks does not help reaching collective

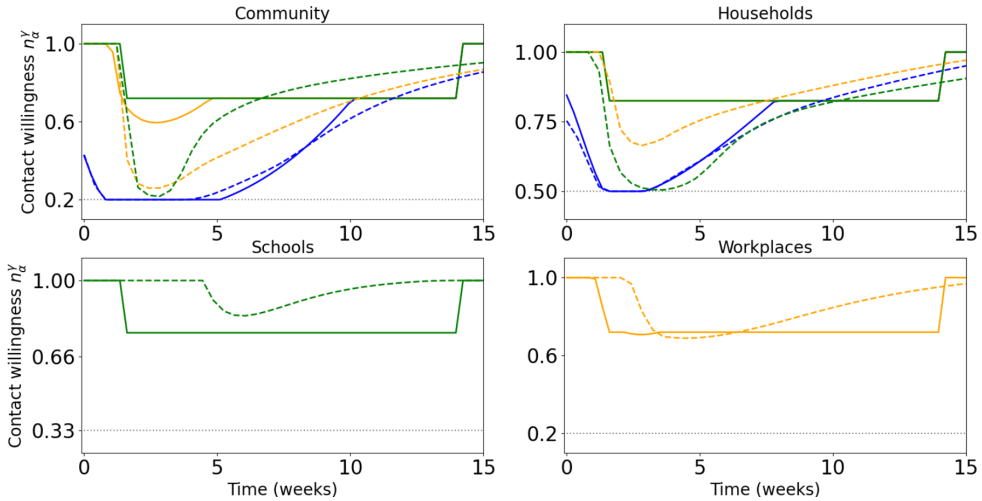

FIG. 12. Comparison of contact willingness for the societal optimum (dashed line) and the Nash equilibrium under optimal constraints (solid line). We plot $n_\alpha^\gamma(t)$ for each type of individual according to their age class (retired people in blue, adults in orange and youth in green) in community (upper left), households (upper right), schools (lower left, for the young) and workplaces (lower right, for the adults). The dotted gray horizontal lines correspond to the minimum contact willingness allowed.

immunity and is very costly in terms of constraints on the society.

V. OPTIMAL STRATEGIES FOR DEALING WITH AN EPIDEMIC FROM THE HEALTH AUTHORITY POINT OF VIEW

Up to this point, we have only considered dynamics with a very long end-time T, and a large number of agents $N_{\rm tot}$, so that the only option to terminate the epidemic is to reach herd immunity. However there are many circumstances (expected production of a vaccine, seasonality of the virus which is expected to disappear in the summer, etc.) where the finiteness of T plays a role, and others (isolated geographic configuration such as islands, strict control of borders, etc.) where the finiteness of $N_{\rm tot}$ does. This opens the way to other possible strategies, from the point of view of the centralized health authority, to control the epidemics. We review them in this section.

A. Threefold way of controlling an epidemic

Based on these considerations, we can identify three possible ways to deal with an epidemic: reach collective immunity (typically for T, N large), contain the epidemic (for T small), or eradicate the epidemic (for $N_{\rm tot}$ small). We characterize these three ways as follows.

1. Strategy No. 1: Reach collective immunity

This is the strategy that was implicitly used in the previous sections since we assumed both T and $N_{\rm tot}$ very large. More formally, we consider that collective immunity has been reached at time t if the proportion of infected individuals is a decreasing function of time for $t' > t$ even in the absence of efforts after t. For the basic SIR model Eq. (2.1) with constant χ, let $R_{\rm eff}(t) = S(t)R_0$ be the effective reproduction number at time t, that is, the average number of secondary infected caused by a single infected agent, with $R_0 = \rho\chi/\xi$ the initial value of $R_{\rm eff}$ when $S = 1$. For this model we have $\dot I(t) = \xi I(R_{\rm eff}(t) - 1)$. In this case, collective immunity is reached as soon as $R_{\rm eff}(t) < 1$ since S is decreasing. In a similar way, for our compartmental model we introduce

$$R_\alpha(t) = \frac{\mu\rho}{\xi}\sum_{\beta,\gamma} n_\alpha^\gamma(t) n_\beta^\gamma(t) \mathcal{M}_{\alpha\beta}^\gamma S_\beta(t), \tag{5.1}$$

the average number of secondary infected caused by a single infected agent of age class α. We stress that $R_\alpha < 1$ does not imply $\dot I_\alpha < 0$, since the number of infected in the age class α involves the R_β of all classes, and some of them may be greater than 1. However, if *all* the R_α are less than one, then the average proportion of infected individuals, $I \equiv \sum_\alpha \mathcal{N}_\alpha I_\alpha$ can be easily shown to be a decreasing function. Indeed, from Eq. (2.12), we have $\dot I = \sum_\alpha \mathcal{N}_\alpha S_\alpha \lambda_\alpha - \xi I$, and

$$\begin{aligned}\sum_\alpha \mathcal{N}_\alpha S_\alpha \lambda_\alpha &= \mu\rho \sum_{\beta,\gamma,\alpha} \mathcal{N}_\alpha S_\alpha n_\alpha^\gamma(t) n_\beta^\gamma(t) \mathcal{M}_{\alpha\beta}^\gamma I_\beta \\ &= \xi \sum_\beta \mathcal{N}_\beta I_\beta R_\beta,\end{aligned} \tag{5.2}$$

where we used the sum rule $\mathcal{M}_{\alpha\beta}\mathcal{N}_\alpha = \mathcal{M}_{\beta\alpha}\mathcal{N}_\beta$ enforced by the symmetric nature of contacts. We therefore have

$$\dot I = \xi \sum_\alpha \mathcal{N}_\alpha I_\alpha (R_\alpha - 1). \tag{5.3}$$

In the absence of effort, the rates $R_\alpha(t)$ become $R_\alpha^{(0)}(t) = \frac{\mu\rho}{\xi}\sum_{\beta,\gamma}\mathcal{M}_{\alpha\beta}^\gamma S_\beta(t)$, and Eq. (5.3) becomes

$$\dot I^{(0)} = \xi \sum_\alpha \mathcal{N}_\alpha I_\alpha \big(R_\alpha^{(0)} - 1\big), \tag{5.4}$$

where the superscript denotes the absence of effort. Since the $R_\alpha^{(0)}$ are obviously decreasing functions of time, the constraint that $R_\alpha^{(0)}(t) < 1$ for all age classes α is a sufficient, but not necessary, condition to have reached herd immunity. This constraint is, however, too strong, and is actually not met in our simulations, even when herd immunity is achieved. We thus find more effective to replace it by a heuristic condition obtained by assuming the I_β to be not very different from the average I (as can be seen for example in Fig. 6 towards the end of the epidemics). Using Eq. (5.4), we get $\dot I^{(0)} \simeq \xi I(R^{(0)} - 1)$, with

$$R^{(0)} \equiv \sum_\alpha \mathcal{N}_\alpha R_\alpha^{(0)}. \tag{5.5}$$

$R^{(0)}$ is also a decreasing function of time, and the heuristic criterion $R^{(0)}(t) < 1$ indicates that herd immunity has been reached at t. This empirical condition does not guarantee mathematically the absence of an epidemic rebound once $R^{(0)}(t) < 1$ (heterogeneous I_α could allow $\dot I^{(0)} > 0$). Nevertheless, we will check below numerically that for the cases we considered it does actually correspond to herd immunity [58]. This strategy, where S needs to be low at the end of the epidemics, is often used for moderate epidemics and for epidemics where no other strategy is available.

2. Strategy No. 2: Contain the epidemic

If an external event (e.g., vaccine) is expected to end the epidemic within a relatively short time, then another possibility to deal with an epidemic is to contain it during the period of optimization T, keeping the epidemic at a low level, and end at T with a number of susceptible far above the collective immunity threshold. In practice, we are in this phase if $R^{(0)}(T) > 1$. This is the strategy adopted by most countries during the COVID-19 pandemic: hold on and contain the epidemic until a vaccine is available.

3. Strategy No. 3: Eradicate the epidemic

A final possibility is to act on the epidemic sufficiently early and sufficiently intensely, that one will be able to eradicate it before it spreads to the general population. To implement such an idea, we need to assume a finite size $N_{\rm tot}$ of the population, and state that below a certain rate of infected, of order $1/N_{\rm tot}$, the epidemic vanishes or is at least under control so that there is no propagation anymore. Of course in practice, one would need to know precisely who is infected and insulate them from the rest of the population (by keeping them in quarantine at hospital, for instance), which would induce an extra cost of coordination which is not taken into account here. Discussing this strategy requires to add

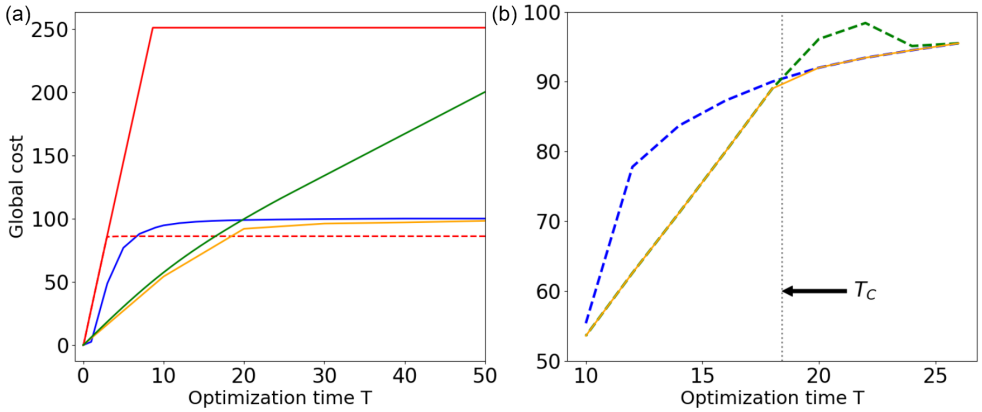

FIG. 13. (a) Comparison of the evolution of the global cost $C_{\rm glob}(n, T)$ for the three template strategies $n_{\rm im}$ (blue line), $n_{\rm era}$ (red lines), $n_{\rm cont}$ (green line) which are well defined for any value of t (from 0 to ∞). For the global cost associated to the eradication strategy $n_{\rm era}$ (in red) we take, respectively, $I_{\rm thr} = 1.10^{-5}$ (respectively, $I_{\rm thr} = 1.10^{-3}$) for the solid line (respectively, dotted line). Regarding the strategy $n_{\rm im}$, $T = \infty$ is approximated here by $T = 100$. Finally, in orange, we plot the true societal optimum cost at T (with $I_{\rm thr} = 1.10^{-5}$, solid line parameters). (b) Evolution of the global cost of the societal optimum (orange solid line) close to the transition time T_c (see text). Dotted blue (respectively, green) line: evolution of the global cost with a continuous change of the strategy n for the herd immunity scenario (respectively, containment scenario). Details of the computation are explained in the main text.

one parameter, $I_{\rm thr}$, which corresponds to the threshold at witch we consider that the epidemic vanishes, with a value for $I_{\rm thr}$ of order $1/N_{\rm tot}$. This approach is in practice possible only during the early stages of the epidemic, otherwise it will induce a considerable cost. This strategy has been used many times in China and some insular countries during COVID-19 pandemic, with strong restrictions at the early stages of the epidemic to avoid a massive spreading.

B. Template strategies

The above scenarios can be classified according to whether $\dot{I}^{(0)}(t) < 0$, $\forall t > T$ (herd immunity), and if this is not the case, whether $I(T) > I_{\rm thr}$ (containment) or $I(T) < I_{\rm thr}$ (eradication). Thus, any set of strategies $n(.) \equiv \{n_\beta^\gamma(.)\}$ (i.e., defined for each age class, in each setting, and all times t) belongs to one and only one of these classes. We can, however, do a little bit more than this formal classification, and introduce for each of these scenarios what we will call a "template strategy," that is, a set of strategies $n(.)$ which provides a good approximation to the optimal one within a given scenario. These "templates" can be defined as follows:

(1) *Reach collective immunity* $n_{\rm im}$: Our template for the herd immunity scenario is defined as the optimal strategy defined in Sec. IV F taken in the limit $T \to \infty$ (with $I_{\rm thr} \equiv 0$), namely,

$$n_{\rm im}(.) = \underset{n(.)}{\rm argmin}[C_{\rm glob}(n(.), T \longrightarrow \infty)]. \qquad (5.6)$$

Indeed, we can expect that when the best approach is to use herd immunity, there is little end-time effect and the optimal strategy for a finite T will be quite close to the one corresponding to $T \to \infty$. As seen in Fig. 13, the global cost associated with $n_{\rm im}$ rises quite significantly at the beginning of the epidemic, as a significant number of agents assume the cost of infection, but once herd immunity is reached this cost flattens out since infection decreases while no effort is required anymore. It can be noted furthermore that $n_{\rm im}$ does not depend much on $\mathfrak{r}_{\rm I}$, as it minimizes the cost due to social contacts (which is independent from $\mathfrak{r}_{\rm I}$), while reaching collective immunity. This leads in first approximation to a constant number of agents who have been infected at the end time T, as the collective immunity threshold is unchanged for any value of $\mathfrak{r}_{\rm I}$. Therefore, the associated final cost of this strategy $n_{\rm im}$ grows with a form $C_{\rm glob}(n_{\rm im}) \simeq F_{\rm tot}(n_{\rm im}) + (S_0 - S_\infty)\mathfrak{r}_{\rm I}$, where $F_{\rm tot}$ is the total amount of efforts made by agents for a strategy $n(.)$, which is (almost) independent of $\mathfrak{r}_{\rm I}$, and the second term grows linearly with $\mathfrak{r}_{\rm I}$.

(2) *Contain epidemic* $n_{\rm cont}$: We define the reproduction factor R as the $R^{(0)}$ which was introduced in Eq. (5.5), with here arbitrary value for $n(t)$ instead of 1. One can easily claim that a sufficient condition to strictly contain the epidemic in a homogeneous infected population is to keep $R(t) = 1$. With that condition, one will enforce $I(t)$ to stay as the same level or below the initial condition $I(0)$ with *a priori* the lowest possible cost from the social point of view [to keep $R(t) < 1$ will be more expensive]. We can therefore define the template strategy of the containment scenario as the one coming from the optimization

$$n_{\rm cont}(t) = \underset{n(.)}{\rm argmin}[F_{\rm tot}(n(.)) \text{ such that } R(t) = 1] \quad \forall t, \quad (5.7)$$

where we furthermore assume that for all age classes $S_\alpha(t) \simeq S_\alpha(0) \simeq 1$, so that $n_{\rm cont}$ is actually time-independent. Since the social cost only involves current time t, the problem reduces to a simple, local in time, optimization problem, where $n(t)$ becomes a constant n which must respect $R = 1$ and minimize $f(n)$. The result of this optimization, obtained numerically through a gradient descent under constraints, is illustrated in Fig. 13. Note that this (constant) strategy $n_{\rm cont}$ is independent of $\mathfrak{r}_{\rm I}$, and the associated global cost $C_{\rm glob}(n_{\rm cont}) \simeq T f(n_{\rm cont})$ is essentially independent of $\mathfrak{r}_{\rm I}$ and grows linearly with T.

(3) *Eradicate epidemic* $n_{\rm era}$: For this case, it can be shown (see Appendix F) that, for the parameters we consider, the optimal eradication strategy is always obtained by an

application of the maximal effort until the time $t_{\rm thr}$ corresponding to the eradication of the epidemics, $I(t_{\rm thr}) \equiv I_{\rm thr}$. This strategy, will be taken as our template eradication strategy. The associated final cost is therefore expected to be of the form $C_{\rm glob}(n_{\rm era}) \simeq T f_{\rm max}$ if $T < t_{\rm thr}$, the cost grows linearly with T, and $C_{\rm glob}(n_{\rm era}) \simeq f_{\rm max} t_{\rm thr}$ if $T > t_{\rm thr}$, where $f_{\rm max}$ denotes the social cost (rate) associated with a maximum amount of efforts and $t_{\rm thr}$ mainly depends on $I_{\rm thr}$.

C. Phase transition

For these three scenarios, we show on Fig. 13(a) the evolution of the global cost with the optimization time T, for $\mathfrak{r}_{\rm I} = 1$ and the parameters of Tables II and III. As expected, all costs increase with T, but in different ways. In blue, the collective immunity cost grows rapidly at the beginning of the epidemic, so that collective immunity is reached as soon as possible without saturating the sanitary system, after which the cost levels up. For the containment strategy $n_{\rm cont}$ (green), we see that the corresponding cost increases almost perfectly linearly, as the amount of effort due to contact reduction is constant. As $S(0) = 0.99 < 1$, there is in this scenario a small spread of the infection at the beginning of the epidemic (and thus a small additional infection cost), before it vanishes completely. Finally, the cost of the eradication strategy (red curve) starts with a strong linear increase (the slope of the curve here is clearly higher than the one of the containment strategy since the maximal effort is applied), and then saturates at a level which depends on the threshold $I_{\rm thr}$. Figure 13(a) also shows the societal optimum cost (orange curve), which always closely follows one of the templates. At low T, it is a bit below the cost of the containment strategy $n_{\rm cont}$, taking advantages of end-time effects (as illustrated in Fig. 14) to slightly reduce the cost. For large T, it follows, again from below, the collective immunity template. For the societal optimum cost, there is a transition around 20 weeks for our choice of parameters, from a "containment" cost to a "collective immunity" cost. For $I_{\rm thr} = 10^{-3}$ (dotted line in Fig. 13), the transition would go from "containement" to "eradication".

This transition between different scenarios' costs strongly suggests that the associated strategies will follow the same pattern, with a transition form the neighborhood of $n_{\rm cont}$ to the neighborhood of $n_{\rm im}$. To assess this, we compare in Fig. 14 the optimal strategy found from the societal optimum scenario with the template strategies. We observe that the small gap between template costs and societal optimum cost which was observed on Fig. 13(a) corresponds to a small difference between the corresponding strategies. For strategy 1 (rows 1 and 2) we observe a finite-T effect: an additional amount of efforts around 10 to 25 weeks appears to be profitable to limit the number of infected, even though the epidemic is almost over. The structure of the two strategies is nevertheless very similar. Regarding the "containment" strategy (rows 3 and 4), in each setting the contact willingness of each age class of agents is the same (thereby, only one constant dotted line per setting is plotted). The societal optimum is very close to the strategy $n_{\rm cont}$, but two effects make it deviate from the idealistic strategy $n_{\rm cont}$. First, as $S(0)$ is not strictly equal to one (here 0.99), there is some moderate spreading of the epidemics, which induces a small increase of effort from retired people, as well as a small increase of infection cost. Second, there is a clear end-time effect, meaning here that individuals who are not at risk reduce their efforts just before T since epidemic will not have time to propagate massively until T (one can think of a vaccination campaign where individuals will start increasing their contacts before the campaign is completed). Note however that as T gets close, since the epidemic begins to grow, retired individuals protect themselves and actually further limit their contacts. Last, for the eradication strategy, the societal optimum is the same as our template strategy $n_{\rm era}$ (see Appendix F for more details).

Figures 13(a) and 14 indicate that our template strategies provide an accurate approximation of the societal optimum at small and large T. One question we may ask now is whether the transition we see at $T_c \simeq 20$ from one scenario to another can be understood as a true phase transition, or is rather of a crossover type. To address this question, in Fig. 13(b) we compare the societal optimum near T_c, i.e., the absolute minimum of the global societal cost, with the result of a gradient descent obtained in the following way: starting from above T_c (blue) or below (green), we change T by small steps δT, and use as a starting point for the gradient descent at $T + \delta T$ the result of the calculation at T. What we observe is that doing this procedure, our algorithm finds, for a significant range of T values around T_c a local minimum which follows the herd-immunity template below T_c (dotted blue) or the containment template above T_c (dotted green). This local minimum corresponds either to the true minimum when the blue or green curves match the orange one, and to a metastable state when they do not. Note that both local minima eventually fall to the global minimum (in orange) when they are sufficiently far from T_c, ending in a hysteresis cycle.

There is therefore a discontinuous change of the optimal strategy at T_c, which is the signature of a first-order phase transition. In this analogy with thermodynamics, the cost $C_{\rm glob}$ represents the free energy, and T some macroscopic parameter such as temperature. The Ehrenfest classification, which defines a first-order phase transition as a discontinuity of the first derivative of $C_{\rm glob}$ with respect to T at T_c, is clearly observed in Fig. 13(b). We expect this phase transition to exist for a large range of parameters of our model, and we have verified its existence numerically on a number of cases. In particular, we have checked that the transition between "containment" phase and "eradication" phase is also first-order.

We therefore end up with three distinct phases for the societal optimum, which exhibit first-order phase transitions between them, and which are well-approximated by template strategies defined above. Since these template strategies provide good approximations of the societal optimum one, we use them in Fig. 15 to show the "phase diagram" of the optimal scenarios as a function of the optimization time T and the infection cost $\mathfrak{r}_{\rm I}$. Of course, the optimal strategy will depend on all the parameters that we have introduced until now, but some of them (matrix of contacts $\mathcal{M}$, capacity of the sanitary system $\mathfrak{q}_{\rm sat}$, proportion of agents in each age class $\mathcal{N}_\alpha$) may be assumed to be quite similar for different epidemics affecting the same population, while T and $\mathfrak{r}_{\rm I}$ depend a lot on the virus under consideration and have a major impact on the best strategy. The three different scenarios appear to be optimal in distinct well-defined areas of the phase diagram. When T

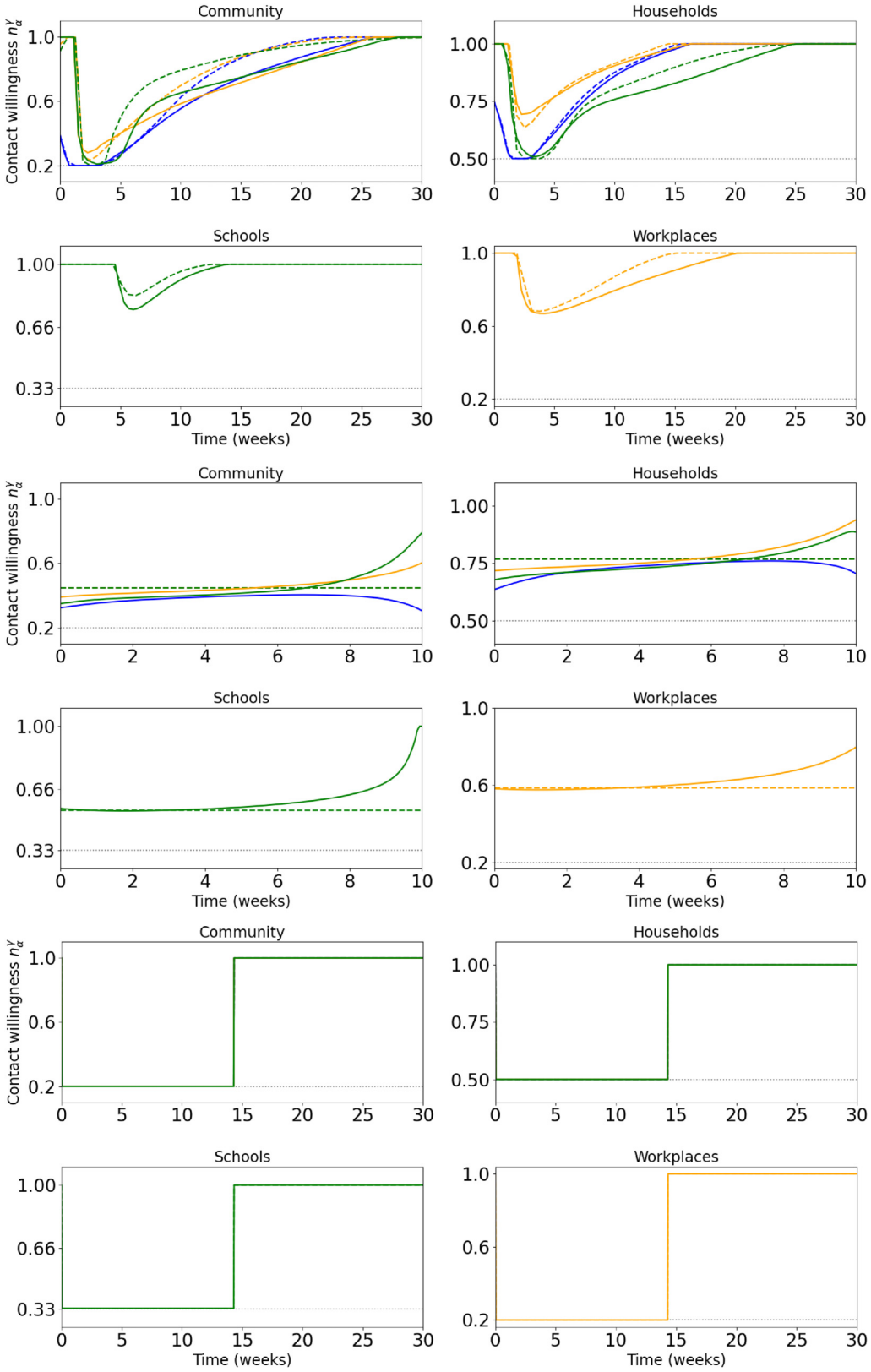

FIG. 14. Contacts willingness for the three template strategies defined in Sec. V (dotted lines) and the (finite-T) societal optimum for the corresponding parameters (solid lines). Rows 1 and 2: collective immunity ($T \to \infty$, computed in practice with $T = 100$ and $\tau_I = 1$, dotted line) and societal optimum (computed with $T = 30$, $\tau_I = 1$, $I_{thr} = 0$, solid line). Rows 3 and 4: contained strategy (dotted) and societal optimum (solid) for $T = 10$, $\tau_I = 1$. Rows 5 and 6: eradication strategy (dotted) and societal optimum (solid) for $T = 30$, $\tau_I = 1$, $I_{thr} = 1.10^{-5}$—the two strategies match perfectly. Subpanels and legends are the same as in Fig. 7.

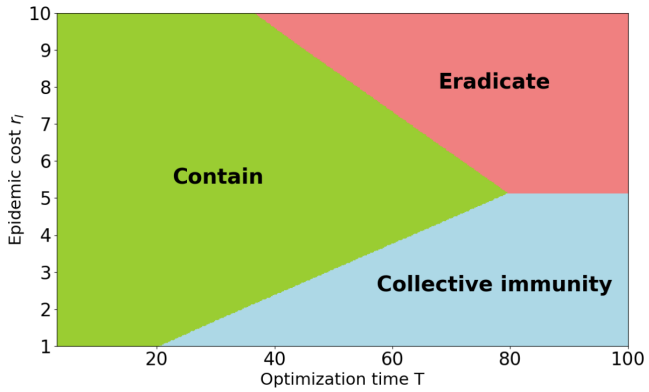

FIG. 15. Phase diagram showing the best type of strategy to follow among "reach collective immunity" (blue), "contain" (green), and "eradicate" (red) with the parameters of Tables II and III and $I_{\rm thr} = 1.10^{-7}$ for the eradication strategy (it is more realistic, as it means $N_{\rm tot} \simeq 10^7$). Change $I_{\rm thr}$ or the initial conditions will naturally change the transition lines (between immunity and eradication areas).

is small (below 20 weeks), the containment strategy is optimal whatever $\mathfrak{r}_{\rm I}$. Then, there is a transient regime, where the optimal strategy can be any of the three scenarios, collective immunity, containment, or eradication according to $\mathfrak{r}_{\rm I}$. Finally, after $T \simeq 80$ weeks, containing the epidemic is no longer an option, as the linear increase of the cost becomes prohibitive, and the best choice is either to reach collective immunity or to eradicate the epidemic. Since we use template strategies, the first-order phase transitions are represented by linear lines on the graph.

VI. CONCLUSION

In the present work we developed, following Ref. [38], an epidemic model based on the well-known SIR compartmental model supplemented by a social structure. This social structure relies on the idea that contacts are heterogeneous in society, both because individuals socialize in different contexts, and because they react in various ways to the disease (different perception of risk). Therefore, one can divide society into classes of agents which differ by their behavior, by the risk that the disease represents for them, and by the settings in which socialisation takes place. Here we used an age differentiation, but other kinds of classification (e.g., based on the immune status or on the presence of comorbidity) could easily be implemented within the same formalism. In the same way, one can easily add more compartments and more classes or settings to the model, without changing the global framework. The description of social structures obtained in this way is clearly less refined than one that would take into account the heterogeneity of social behaviors at an individual level, but it probably represents a good balance between precision and ease of application when trying to understand the dynamics of an epidemic and take appropriate, targeted action against it.

To this compartmental epidemic model with social structure, we have, following the approach of Turinici *et al.* [32], added a mean-field-game description of the dynamics: Agents may change their individual behavior depending whether they feel at risk of infection or not. After deriving the mean-field-game equations, we computed numerically the Nash equilibrium, where each individual seeks to optimize his or her own interests. In this paradigm, individuals make a perfectly rational optimization, and are assumed to be able to performed the corresponding calculations which is something that we cannot expect from people in practice. The assumption here is thus rather than some central authority will solve the system (4.2)–(4.5) and provide to individuals their "best individual behavior" n_α^γ which will be followed by agents if they sufficiently trust the institution.

As discussed in Sec. IV B, the choice of parameters we used for our simulations does not aim to describe a specific real-world configuration, but nevertheless corresponds to a rather generic situation, and the qualitative behavior we obtained is most likely rather typical of what would be observed in a realistic case. For this set of parameters, the Nash equilibrium obtained within the mean-field-game framework reduces significantly the costs associated with the epidemic when compared to the "business as usual" approach where social contacts are kept unchanged. However, there is usually still a gap between the MFG cost and the one that would correspond to the societal optimal policy, which represents the minimal global cost that can be borne by the society. To approach this optimal policy, we introduce the notion of "constrained Nash equilibrium," in which we assume that under some conditions, the central authority can impose some constraints, analog to the partial lockdowns that we have seen during the COVID-19 epidemic, under simple rules which are known to the agents. In our work, we used a simple restrictive policy with three parameters $(\mathfrak{s}, \mathfrak{I}_{\rm d}, \mathfrak{I}_{\rm l})$ and we optimized this policy (i.e., we find the optimal set $[\mathfrak{s}^*, \mathfrak{I}_{\rm d}^*, I_d^*]$) to get the lowest possible societal cost, and in this way close as much as possible the gap between the free Nash equilibrium and the societal optimum (see Figs. 8 and 11).

In our discussion of the Nash equilibrium and of the "constrained Nash" approach to the societal optimum, we have implicitly limited ourself to a regime of very long optimization time T, and of large population $N_{\rm tot}$, for which the societal optimum policy necessary implies in some way to reach herd immunity. In Sec. V, we go back in more details to the analysis of the societal optimum, in particular lifting these constraints on T and $N_{\rm tot}$. Depending (mainly) on the values of T, $N_{\rm tot}$, and $\mathfrak{r}_{\rm I}$, we can identify three *phases* that we label as "reach collective immunity" (the one implicitly assumed in the previous sections), "contain the epidemic" or "eradicate it" (see Fig. 15 showing which scenario is optimal depending on the parameters T and $\mathfrak{r}_{\rm I}$). The transition between any two of these phases can by understood as a first-order phase transition, in the sense that the associated strategies present discontinuities and are different from one phase to another. An important consequence of this discontinuity is that it is primordial for an authority to clearly identify the appropriate scenario, as a wrong choice could lead to significant additional costs.

Among these three scenarios, "reach collective immunity" is the one for which the time dependence of the agent strategies $\{n_\alpha^\gamma(.)\}$ are the more complex, and an authority will probably not be able to impose such exact strategy for all individuals. For this scenario, an approach through a mean-field-game paradigm under constraints as the one presented in this work is probably more relevant to approach the societal optimum cost, which would slightly shift the phases

boundaries in Fig. 15. However, the "containment strategy" appears to be easier to design for an authority, as it consists in adjusting in real time the constraints, depending on whether the epidemic is growing or not, to follow $R(t) \simeq 1$. Nevertheless, to find the best set of constraints to hold $R(t) \simeq 1$ still involves some complexity, as one should still adapt the strategy to the response of individuals. Advantage of this scenario is that this can be performed "on the fly," and does not really imply any anticipation. Finally, in the "eradication strategy," authority has to impose the maximum admissible constraints, which is conceptually rather simple. We stress, however, that, contrarily to the "herd immunity" strategy, the societal optimum obtained with strategy "contain" and "eradicate" are very far from any Nash equilibrium, even under "reasonable" constraints. The restrictions imposed with the two latters scenarios lead to epidemics which stay at low levels. In this context, the best individual strategy is to do essentially no effort, as there is almost no risk of infection. The social optimum strategy in this case is thus extremely far from the Nash equilibrium. This emphasizes a profound difference in nature between "herd immunity," where individual optimization is closed to the societal optimum, and the two others where the gap is much more important. This would need to be considered by institutions when they will built collective strategies, as it is presumably very difficult to convince a population to follow on its own will a strategy which is far from a Nash equilibrium, and the required degree of coercion would significantly vary between the two cases.

The aim of this paper is to contribute to the construction of a theoretical framework on which authorities can rely to build appropriate policies against future epidemics. In particular, it showed that a relatively simple epidemic model including a differentiated behavior of rational agents can describe a number of different scenarios and is versatile to describe the outcome of various political choices. Our work emphasized both the challenge of this task and the extensive research which remains to be done. Indeed, our model still involves a number of parameters. While some of them (as the matrix $\mathcal{M}$) are known or could be relatively easily extracted from field data, some others (as τ_I or the shape of f) are harder to apprehend, although they are crucial if one wants to use such type of models in an appropriate way. The model can be furthermore made more accurate with the addition of some extra cost such as the one associated with coordination in the case of restrictive policies. The question of evaluating quantities such as the risk induced by a possible epidemic is of course not specific to our model, and is is actually one major task of epidemiologists. Here however we hope to provide a more formal framework from which possible course of action can be decided from that information.

From a theoretical perspective, further research could also be performed to improve the framework. First, one may want to integrate the spatio-temporal character of the dynamics taking into account heterogeneity of populations and regions around the world. Second, one could include, in the impact of constraints on individuals behavior, the feedback of the latter with respect to the imposed constraints. This is referred as Stackelberg games [59], which involve a set of agents (small players) and a principal player corresponding to authorities. This sort of games should reveal the importance of getting the agreement of the population or not, depending of the choice of constraints. Third, we did not incorporate explicitly in our model the possible presence of a vaccine. Vaccination campaign also involve individuals behaviors and could be studied from a mean-field game point of view [29]. It can be added to the model but will rather concern another part of the epidemic, once vaccine is available, to optimize the vaccination campaign. A final active research domain is to infer accurately epidemic quantities with limited data sets, which it is almost always the case at the beginning of epidemics where limited number of tests are available.

Even without these improvements, the theoretical framework presented here should already be sufficiently flexible and realistic to be helpful in practice, as one could replace f or the generalized infection cost $\mathcal{I}_\alpha$ by the precise forms that would be obtained by field data, and then pursue the same analysis. We hope that authorities and institutions in charge of design policies against epidemics could use our work to improve accuracy of epidemics prediction as well as the efficiency of nonpharmaceutical interventions.

ACKNOWLEDGMENT

Louis Bremaud thanks the Centre for Quantum Technologies and the National University of Singapore for their hospitality.

APPENDIX A: DERIVATION OF THE SIR EQUATIONS

To prepare for the somewhat more involved discussion of Sec. II B, and to make the underlying hypotheses more explicit, we provide here a brief formal derivation of the SIR equations (2.1).

Let $x_k(t) \in \{s, i, r\}$ be the state of individual k at time t. The relative proportions of susceptible, infected, and recovered in a population of size N_{tot} can be written as

$$\begin{aligned} S(t) &= \frac{1}{N_{\text{tot}}} \sum_{k=1}^{N_{\text{tot}}} \delta_{x_k(t),s}, \\ I(t) &= \frac{1}{N_{\text{tot}}} \sum_{k=1}^{N_{\text{tot}}} \delta_{x_k(t),i}, \\ R(t) &= \frac{1}{N_{\text{tot}}} \sum_{k=1}^{N_{\text{tot}}} \delta_{x_k(t),r}, \end{aligned} \tag{A1}$$

with $\delta_{a,b}$ as the Kronecker symbol.

Furthermore, an important property of the SIR model associated with the homogeneity of the population (all agents are connected with every other agent with a uniform probability) is that, in the $N_{\text{tot}} \to \infty$ limit, the system is *ergodic*, in the sense that averages over realizations of the Markov process and averages over individuals should correspond, i.e.,

$$(\forall k) \quad \lim_{N_{\text{tot}}\to\infty} \langle f_k \rangle = \lim_{N_{\text{tot}}\to\infty} \frac{1}{N_{\text{tot}}} \sum_{k'=1}^{N_{\text{tot}}} f_{k'} \tag{A2}$$

(where $\langle f_k \rangle$ is the average over Markov realisations of the quantity f associated with a given individual k, and where the right-hand side is taken for an arbitrary (but single) real-

isation of this Markov process). Note that for this ergodicity to apply, not only $N_{\rm tot}$ should be large, but also the number of agents within each class and in particular the number of infected $N_{\rm tot}I$, so that at the very beginning of the epidemic nonergodic behavior may exist if $I_0 < 1/N_{\rm tot}$. In the $N_{\rm tot} \to \infty$ limit that we consider here, however, we may and will write $(\langle S\rangle, \langle I\rangle, \langle R\rangle) = (S, I, R)$.

Let us consider an individual k which is susceptible at time t (i.e., $\delta_{x_k(t),s} = 1$). To become infected at time $t + dt$, this individual must meet an infected individual l in the time interval $[t, t + dt[$, and this encounter must lead to a transmission of the disease. Thus the proportion of individuals which are susceptible at time t and infected at time $t + dt$ is given, for a given realisation of the Markov process, by

$$S(t + dt) - S(t) = -\frac{1}{N_{\rm tot}} \sum_{k=1}^{N_{\rm tot}} \sum_{l=1}^{N_{\rm tot}} C_{kl}(t)\, \delta_{x_k(t),s} \delta_{x_l(t),i}, \quad \text{(A3)}$$

with $C_{kl}(t)$ the stochastic variable which take value 1 if k and l met during the interval $[t, t + dt[$ with a possible infection for k (if k is susceptible and l is infected), and 0 otherwise. This stochastic variable has an average value (over random realizations of the Markov process) which is the product of the probability of contact during dt, $\frac{1}{N_{\rm tot}}\chi(t)dt$, by the transmission rate ρ since both events are independent. Note that since the population is assumed homogeneous, the probability of contact as well as the transmission rate are constant across the population (although the stochastic variables C_{kl} are not).

We then take the average over realizations assuming the independence of the three stochastic variables $\delta_{x_k(t),s}$, $\delta_{x_l(t),i}$, and C_{kl}, which amounts to assume that the events "individual k is susceptible at t," "individual l is infected at t," and "the pair of individuals (l, k) meet," are independent because $N_{\rm tot}$ is large and the population is homogeneous. We get

$$\begin{aligned} \frac{d\langle S(t)\rangle}{dt} &= -\frac{1}{N_{\rm tot}^2} \sum_{k=1}^{N_{\rm tot}} \sum_{l=1}^{N_{\rm tot}} \rho\chi(t) \langle \delta_{x_k(t),s}\rangle \langle \delta_{x_l(t),i}\rangle \\ &= -\rho\chi(t)\langle S(t)\rangle\langle I(t)\rangle. \end{aligned} \quad \text{(A4)}$$

Using the identification between ensemble and population average, Eq. (A4) reduces to

$$\frac{dS(t)}{dt} = -\rho\chi(t) S(t) I(t). \quad \text{(A5)}$$

The other SIR equations in Eq. (2.1) are obtained in the same way.

APPENDIX B: PARAMETERS OF THE MODEL

The values of the "social-structure" and "biological" parameters in Table II do not represent any particular real-life case, but are chosen to be representative of realistic situations, and therefore in the range typically found in the literature [1,38,47–50]. We take $\xi = 1.2$ week^{-1}, not too far from the values $\xi = 7/6.5 = 1.1$ week^{-1} from Ref. [1], $\xi = 7/6.6 = 1.05$ week^{-1} from Ref. [50] and $\xi = 7/4 = 1.75$ week^{-1} from Ref. [47]. The contagiousness ρ is assumed to be 0.1, similar to the value mentioned in Ref. [47] for the COVID-19, where it is slightly lower (about 0.08). Regarding μ, we choose $\mu = 0.2$, of the same order of magnitude as in Ref. [50]. Similarly, for the proportion of individuals in the population, the distribution (25%, 50%, 25%) is closed to the one in Ref. [50], where it is 22% if you gather the proportion of children and teenagers, 57% for adults, and 21% for seniors. The contact matrices $\mathcal{M}^{\gamma}_{\alpha\beta}$ are inspired by Ref. [38] for their shape: Almost all contacts in schools are between children, an similarly inside workplaces for adults. In the community, all individuals have the same probability of meeting other individuals, while in households the structure is a bit more complex, with a strong child-adult link and senior-senior contacts. The absolute value of contacts is then normalized so that the average total number of contacts is close to the values presented in Ref. [47]. Finally, to ensure the consistency of our choices, we check that all these collected quantities give a reproductive number $\tilde{R}_0 = 2.9$ with the method described in Refs. [38,60] for calculating $\tilde{R}_0$ at the beginning of epidemics in heterogeneous populations. This value is consistent with the literature for viruses such as COVID-19 [13]. The choice of initial conditions ($I_\alpha(t = 0)$) is taken uniform among age classes, and since we do not consider stochastic effects at the beginning of epidemics, we take a value of 1% which has little effect on the simulation as long as it is small enough.

APPENDIX C: ARBITRARY ASYMPTOMATICITY

In this Appendix, we generalize the discussion of Sec. III A to arbitrary values of the asymptomaticity parameter $\mu \in [0, 1]$. In that case the equations change only slightly. As before, only asymptomatic infected individuals participate to the propagation of the disease. Asymptomatic individuals ignore their status, and if infected feel no harm; as a consequence, they will not change their behavior upon contamination at time τ (thus the integral in Eq. (3.1) will extend up to T), nor bear the health costs [thus the second term in Eq. (3.1) will be zero for them]. The cost for asymptomatic individuals thus reads

$$C_a\big(n^\gamma_a(\cdot), \{n^\gamma_\beta(\cdot)\}, t, \tau\big) \equiv \int_t^T f_\alpha\big(n^\gamma_a(t')\big)dt'. \quad \text{(C1)}$$

Since the agent ignores whether she is asymptomatic or not, the average cost she anticipates is with probability $(1 - \mu)$ the estimated cost (3.9) and with probability μ the cost (C1) (which is independent of τ); therefore,

$$\begin{aligned} \mathfrak{C}^\mu_a\big(n^\gamma_a(\cdot), t\big) &= (1-\mu)\int_t^T \big(f_\alpha\big(n^\gamma_a(t')\big) + \lambda_a(t')\,\mathcal{I}_\alpha(I(t'))\big) \\ &\quad \times (1 - \phi_a(t'))dt' + \mu\int_t^T f_\alpha\big(n^\gamma_a(t')\big)dt' \\ &= \int_t^T \big[(1-\mu)\lambda_a(t')\mathcal{I}_\alpha(I(t'))(1-\phi_a(t')) \\ &\quad + f_\alpha\big(n^\gamma_a(t')\big)(1 - (1-\mu)\phi_a(t'))\big]dt'. \end{aligned} \quad \text{(C2)}$$

The term $(1 - \mu)\phi_a(t')$ can be interpreted as the probability for an individual of age class α to be infected and symptomatic before t', since the two events "have been infected before t'" and "be symptomatic" are independent. In the limit of $\mu \ll 1$, we recover the cost derived before in Eq. (3.9); note that to allow an epidemic growth in this limit we assume that $\mu\rho$ and thus λ_a are of the same order in μ as ξ (the recovery rate), that is, of order 0 in μ.

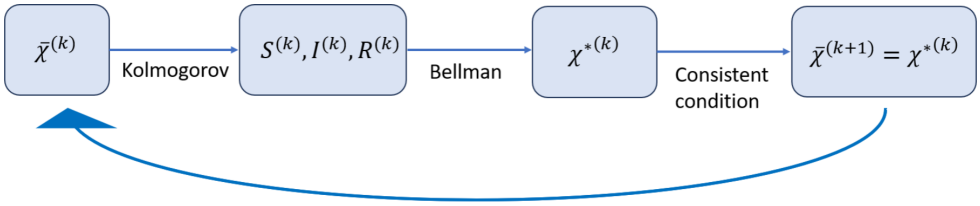

FIG. 16. Global scheme used for the inductive sequence.

APPENDIX D: NUMERICAL IMPLEMENTATION

1. Numerical resolution of the Nash equilibrium

We describe here two numerical methods we have implemented to reach the Nash equilibrium: an inductive sequence method and a gradient descent. Again, we omit the superscript γ to lighten the notations.

a. First method: Inductive sequence

The first method is the most natural one. The idea is the following. We start with an initial global strategy $n_\alpha^{(0)}(.)$ (the brackets (.) indicate that this initial strategy is given at all times), and we compute the associated epidemic quantities $(S^{(0)}(.), I^{(0)}(.), R^{(0)}(.))$ with Eq. (4.2) for these given initial conditions. Then, using Eq. (4.9), we compute the best individual response to this epidemics dynamics, $n_a^{*(0)}$. Since the latter should be followed by all individuals, we obtain a new global strategy $n_\alpha^{(1)} = n_a^{*(0)}$. We repeat the process until we reach the Nash equilibrium condition $n_\alpha^{(k)} \simeq n_a^{*(k)}$ for a sufficiently large k.

To summarize, the global scheme of this method is the following, performed simultaneously for all age classes α: Each step is quite straightforward numerically since we only deal with classical partial differential equations. Figure 16 corresponds to an inductive sequence $n_\alpha^{(k+1)} = F(n_\alpha^{(k)})$ where the functional F is defined as $F(n_\alpha^{(k)}) = n_\alpha^{*(k)}$. However, this inductive sequence will not always converge to a fixed point of F, which is why we consider a second approach below.

In practice, we discretized the interval $[0, T]$ with $T = 40$ weeks using ∼150 time steps; typically the number of iterations to reach the fixed points is ∼10.

b. Second method: Gradient descent

To deal with cases where the inductive sequence does not converge, we use a gradient descent on the variable $n_a(.)$ of the cost $\mathfrak{C}_a$ [see Eq. (3.9)] to reach the Nash equilibrium. We use the following scheme for each age class α with representative individual a

$$n_a^{(k+1)}(t) = n_a^{(k)}(t) - h \cdot \nabla_1 \mathfrak{C}_a\big(n_a^{(k)}(.), \{n_\beta^{(k)}(.)\}, t\big)\big|_{n_a^{(k)}(.)=n_\alpha^{(k)}(.)}, \tag{D1}$$

where ∇_1 means that the gradient is taken on $n_a^{(k)}(.)$. The dot in Eq. (D1) indicates a scalar product, h and ∇_1 are vectors indexed by γ. This scheme gives $\nabla_1 \mathfrak{C}_a(n_a^{(k)}(.), \{n_\beta^{(k)}(.)\}, t) = 0$ when we reach the equilibrium. That is, we are at a local minimum of the cost $\mathfrak{C}_a$ with respect to the first variable $n_a(.)$. We can then check numerically that we are indeed at the true Nash equilibrium, that is, at a global minimum for the variable $n_a(.)$ (for each age class α), by checking that $F(n_{\text{Nash}}) = n_{\text{Nash}}$ for a given Nash candidate n_{Nash}.

To make the numerical computation of the gradient $\nabla_1 \mathfrak{C}_a$ less heavy and more efficient, we first perform a few analytical steps. To avoid heavy notations, the cost at $t = 0$ will be denoted as $\mathfrak{C}_a(n_a, n_\beta)$. We have

$$\begin{aligned}\mathfrak{C}_a(n_a, n_\beta) &\equiv \mathfrak{C}_a\big(n_a^\gamma(\cdot), \{n_\beta^\gamma(.)\}, 0\big) \\ &= \int_0^T \big(f_\alpha\big(n_a^\gamma(s)\big) + \lambda_a(s)\, \mathcal{I}_\alpha(I(s))\big)(1 - \phi_a(s))ds.\end{aligned} \tag{D2}$$

To compute the gradient of the cost with respect to the first variable, we introduce the functional derivative of $\mathfrak{C}_a$ with respect to its first variable n_a, in the direction h (with h a function, usually a Dirac delta). By definition,

$$D_h \mathfrak{C}_a(n_a, n_\beta) \equiv \lim_{\epsilon \longrightarrow 0} \frac{1}{\epsilon}(\mathfrak{C}_a(n_a + \epsilon h, n_\beta) - \mathfrak{C}_a(n_a, n_\beta)). \tag{D3}$$

Using the definition of the gradient, this functional derivative can be reexpressed as

$$D_h \mathfrak{C}_a(n_a, n_\beta) = \int_0^T h(t) \cdot \nabla_1 \mathfrak{C}_a(n_a, n_\beta, t))dt. \tag{D4}$$

which explicitly written gives $h(t) \cdot \nabla_1 \mathfrak{C}_a = \sum_\gamma h^\gamma(t)\, \frac{\delta \mathfrak{C}_a}{\delta n_a^\gamma(t)}$ with $\frac{\delta \mathfrak{C}_a}{\delta n_a^\gamma(t)}$ the functional derivative of the total cost $\mathfrak{C}_a$ with respect to $n_a^\gamma(t)$. Since $1 - \phi_a(s) = \exp(-\int_0^s \lambda_a(u)du)$, the cost (D2) depends on n_a through the terms $f_\alpha(n_a)$ and λ_a via (3.6); with λ_a is linear in n_a. Using Eq. (D3) we have at first order $\lambda_a(n_a + \epsilon h) = \lambda_a(n_a) + \epsilon h \cdot \frac{d\lambda_a}{dn_a}(t)$ with $\frac{d\lambda_a}{dn_a}(t)$ a vector indexed by γ, of components

$$\frac{d\lambda_a}{dn_a^\gamma}(t) \equiv \mu\rho \sum_{\beta=1}^{n_{\text{cl}}} n_\beta^\gamma(t) \mathcal{M}_{\alpha\beta}^{\gamma(0)} I_\beta(t). \tag{D5}$$

We then use the integral form (D2) to expand Eq. (D3) to lowest order in ϵ. One of the terms involves a double integral; to put $D_h \mathfrak{C}_a(n_a, n_\beta)$ under the form (D4), we invert integrants and change variables, namely $\int_0^T [f(t) \int_0^t g(s)ds]dt = \int_0^T [g(t) \int_t^T f(s)ds]dt$. Once the expression is of the form (D4) we can read off the value of the gradient $\nabla_1 \mathfrak{C}_a(n_a, n_\beta)$:

$$\begin{aligned}\nabla_1 \mathfrak{C}_a(n_a, n_\beta, t) = &\left[\frac{df_\alpha}{dn_a}(n_a(t)) + \frac{d\lambda_a}{dn_a}(t) \mathcal{I}_\alpha(I(t))\right](1 - \phi_a(t)) \\ &- \frac{d\lambda_a}{dn_a}(t) \int_t^T (f_\alpha(n_a(s)) + \lambda_a(s) \mathcal{I}_\alpha(I(s))) \\ &\times (1 - \phi_a(s))ds,\end{aligned} \tag{D6}$$

with $\frac{df_\alpha}{dn_a}$ the derivative of f_α with respect to the variable $n_a^\gamma(t)$ (with a vector notation). The straights d used here indicates usual derivatives, as f and λ are functions (and not functional) of $n_a^\gamma(t)$. The gradient (D6) is then computed numerically to follow the scheme (D1).

2. Numerical resolution of the constrained Nash equilibrium

For the constrained Nash equilibrium, the strategies $n_a^k(t)$ in Eq. (D1) additionally must fulfill constraints such as Eq. (4.11). Since these constraints are active or not depending on the value of $I(t)$, at each step k one must check that the strategies respect the constraints defined by the values of the epidemic rate at step k. Each step of the gradient descent therefore comprises two parts. In the first part, we perform the same gradient descent as the one described for the Nash equilibrium Appendix D 1 b, but now we check that the new strategies $\{n_a^{k+1}(.)\}$ respect the constraints defined by the $I(.)$ from step k; if they do not, we enforce them by correcting accordingly the $\{n_a^{k+1}(.)\}$. In the second part, we compute the new epidemic rates and find the corresponding new constraints.

An issue appears when we approach the Nash equilibrium. The variation of the constraints and of the strategy $\{n_a^{k+1}(.)\}$ can form some cycles which impede convergence. To bypass this difficulty, we choose to freeze the constraints at some step k and continue the gradient descent process as in the method Appendix D 1 b; after some steps, we recompute the constraints and we continue the process until the convergence.

3. Numerical resolution of the societal optimum

We can reach the optimal strategy through different ways. Here we choose to make a gradient descent on the cost $\mathfrak{C}_{\text{glob}}$, but one can also use the Pontryagin maximum principle [51]. We optimize the behavior of individuals to minimize the total cost paid by the population

$$\mathfrak{C}_{\text{glob}}\big(\{n_\beta^\gamma(.)\}\big) = \sum_\alpha \mathcal{N}_\alpha \mathfrak{C}_\alpha(\{n_\beta(.)\}), \tag{D7}$$

where the cost depends on all the functional $\{n_\beta^\gamma\}$ in an equal footing. For simplicity, we will denote this global strategy over all classes and setting n. To do this minimization, we will follow the same scheme as described in Eq. (D1). We thus have to compute $\nabla\mathfrak{C}_{\text{glob}}(n,t)$, which only involves all the collective strategies n and the time t at which the gradient is evaluated. For each age class α, we calculate the gradient

$$D_h\mathfrak{C}_\alpha(n) \equiv \int_0^T h(t)\cdot\nabla\mathfrak{C}_\alpha(n,t)dt, \tag{D8}$$

to identify $\nabla\mathfrak{C}_\alpha(n,t)$ as in Appendix D 1 b, with ∇ is now on the global strategy n and having components along γ and β (as does h). New terms appear because quantities such as the proportion of infected individuals $I(.)$ now depend on all n_β. Below, we outline the key steps involved in the calculation. The first step is deriving the functional derivative of the gradient $D_h\mathfrak{C}_\alpha(n,t)$. Starting from the expression of $\mathfrak{C}_\alpha$ in Eq. (3.9), we get

$$D_h\mathfrak{C}_\alpha(n_\beta,t) = D_h\left[\int_t^T \big(f_\alpha(n_\alpha(s)) + \lambda_\alpha(s)\,\mathcal{I}_\alpha(I(s))\big)(1-\phi_\alpha(s))ds\right]. \tag{D9}$$

Thus, we need to compute each functional derivative of the terms appearing in Eq. (D9), which gives

$$D_h\lambda_\alpha(t) = \lim_{\epsilon\longrightarrow 0}\frac{1}{\epsilon}\Bigg[\sum_\gamma\sum_\beta \rho\mathcal{M}_{\alpha\beta}^\gamma\big(n_\alpha^\gamma(t)+\epsilon h_\alpha^\gamma(t)\big)\big(n_\beta^\gamma(t) + \epsilon h_\beta^\gamma(t)\big)(I_\beta(t)+\epsilon D_hI_\beta(t))\Bigg], \tag{D10}$$

$$D_h\phi_\alpha(t) = (1-\phi_\alpha(t))\int_0^t D_h\lambda_\alpha(s)ds, \tag{D11}$$

$$D_hI_\beta(t) = \int_0^t \frac{\delta I_\beta(t)}{\delta n(s)}\cdot h(s)ds, \tag{D12}$$

$$D_hf_\alpha(n_\alpha(t)) = d_nf_\alpha(n_\alpha(t))\cdot h(t), \tag{D13}$$

$$D_h\mathcal{I}_\alpha(I(t)) = \frac{\kappa_\alpha\mathfrak{r}_\text{I}\mathfrak{q}_{\text{sat}}}{\mathfrak{I}_{\text{sat}}}D_hI(t)\exp\left[\mathfrak{q}_{\text{sat}}\frac{I(t)-\mathfrak{I}_{\text{sat}}}{\mathfrak{I}_{\text{sat}}}\right], \tag{D14}$$

where the dots in Eqs. (D10), (D12), and (D13) indicate that h and n are indexed by β and γ and indices are summed over. In Eq. (D12), $\delta I_\beta(t)/\delta n(s)$ indicates the functional derivative of $I_\beta(t)$ with respect to the collective behavior $n(s)$. This "time delayed" derivative is the crucial term of the gradient for the societal optimum, one can perform a linearization of Eqs. (2.12) to propagate linearly the elementary deformation of I_β from time s to time t to avoid several numerical computation of the whole epidemic. As in Appendix D 1 above, we use these expressions to compute explicitly Eq. (D9) and put it under the form Eq. (D8), which gives the expression of $\nabla\mathfrak{C}_\alpha(n,t)$. We can then perform the gradient descent scheme Eq. (D1) numerically and efficiently without several computations of the whole epidemic at each time t.

APPENDIX E: COMPARISON OF GLOBAL COST FOR THE NASH EQUILIBRIUM UNDER DIFFERENT CONSTRAINTS

In this Appendix, we study how the global cost for the Nash equilibrium under constraints changes with the three parameters of the constraint; results are displayed in Fig. 17. The parameters used in Fig. 8 correspond to the minimum found here.

At $\mathfrak{s}=0$ we recover the free Nash equilibrium, with the same global cost, around $C_{\text{glob}}=120$. When the intensity $\mathfrak{s}$ is increased, society carries a lower cost than in the free Nash equilibrium, because all individuals are forced to make some efforts. But at a certain intensity, a minimum is reached; the location of this minimum is mainly influenced by $\mathfrak{r}_\text{I}$, and corresponds here to the region around $\mathfrak{s}=0.3$–0.4. In this interval, we find the optimal lockdown configuration that we presented above with $\mathfrak{s}=0.35$, $\mathfrak{I}_\text{d}=0.12$, $\mathfrak{I}_\text{l}=4.10^{-4}$. Among the three parameters $(\mathfrak{s},\mathfrak{I}_\text{d},\mathfrak{I}_\text{l})$ characterizing the partial lockdown, the one which has the most impact on the global cost is $\mathfrak{s}$, as there are no significant variations between the

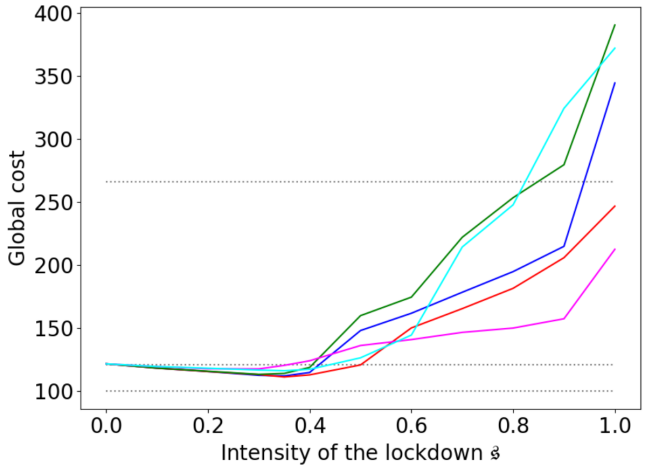

FIG. 17. Comparison of global cost for different parameters of the constraints. The x axis corresponds to the intensity of the lockdown $\mathfrak{s}$, which could vary from 0 (no constraints) to 1 (maximal constraints). The different curves correspond to different choices for the two threshold parameters $\mathfrak{I}_d$ and $\mathfrak{I}_l$. We choose $\mathfrak{I}_d = (0.12, 0.08, 0.04)$, a too low $\mathfrak{I}_d$ will clearly deteriorate the situation as it will impose a duration of the constraints which is too long to reach collective immunity. A higher $\mathfrak{I}_d$ is, however, not effective, as typically the maximum effort with the free Nash equilibrium is around 0.15 for our choice of parameters, and thus the threshold would never be reached. For $\mathfrak{I}_l$ we took $\mathfrak{I}_l = (1.10^{-2}, 4.10^{-4}, 1.10^{-5})$. $\mathfrak{I}_l$ will have a major impact on the duration Δt of constraints, with a log relation of the form $\Delta t \simeq -\log(\mathfrak{I}_l)$. Increasing $\mathfrak{I}_l$ will decrease the extent of lockdowns and conversely. A too high $\mathfrak{I}_l$ will lead to epidemic rebounds (the constraints is lifted too early), and a too low $\mathfrak{I}_l$ will impose useless extra social cost to the population. Blue curve $(\mathfrak{I}_d, \mathfrak{I}_l) = (0.08, 4.10^{-4})$, red $(0.12, 4.10^{-4})$, green $(0.04, 4.10^{-4})$, magenta $(0.08, 1.10^{-2})$, and cyan $(0.08, 1.10^{-5})$. Dotted gray horizontal lines from top to bottom correspond, respectively, to business as usual cost, free Nash equilibrium, and societal optimum.

different curves of Fig. 17. For $\mathfrak{s} > 0.5$, the constraints become too strong with respect to the epidemic threat for all choices of thresholds, but especially for low $\mathfrak{I}_d$ and $\mathfrak{I}_l$, because this imposes long constraints which become very costly as $\mathfrak{s}$ increases. When $\mathfrak{s}$ approaches 1 we even reach a point above the business as usual scenario (which had $C_{glob} = 266$), as we enter a regime characterized by a succession of lockdowns followed by epidemic rebounds which are suppressed by the next lockdown before herd immunity can be reached.

APPENDIX F: ERADICATION STRATEGY

In this Appendix, we show that the optimal eradication strategy is to hold the maximum amount of efforts in the interval $[0, t_{thr}]$ until the eradication of the epidemic when $I(t_{thr}) = I_{thr}$, and then completely release the efforts. This strategy is sometimes referred in the literature as a bang-bang strategy [35]. To show that this strategy is optimal, we have to show that any small reduction of efforts δn made during δt in the interval $[0, t_{thr}]$ will increase t_{thr} so that the total cost paid by individuals will be higher. Without loss of generality, we consider that time 0 corresponds to the time at which we start the efforts. We refer to this slightly different strategy as the deviating strategy, and the associated epidemic is denoted $\tilde{I}$. However, t_{thr} will increase by a time $\delta\tau$, as the time at which epidemic vanish will be greater. We are left with a competition between two costs: $d_n f(n_{min})\delta t\delta n$ which is the (negative) cost caused by the reduction of efforts (this is a gain from the individual point of view), and $\delta\tau f(n_{min})$ which is the extra (positive) cost that individuals will pay to eradicate the epidemic. To compare these costs, we need to evaluate $\delta\tau$ in terms of δt and δn.

At t_{thr}, one has $I(t_{thr}) = 0$. For the deviating strategy, one has $\tilde{I}(t_{thr} + \delta\tau) = 0$, where $\tilde{I}(t) \equiv I(t) + \delta I(t)$, with $\delta I(t)$ the small difference amount of infected between the two strategies. We get

$$\begin{aligned} &(I + \delta I)(t_{thr} + \delta\tau) = I(t_{thr}), \\ &\dot{I}(t_{thr})\delta\tau + \delta I(t_{thr}) = 0, \\ &\delta\tau = -\frac{\delta I(t_{thr})}{\dot{I}(t_{thr})}, \end{aligned} \tag{F1}$$

which allows us to evaluate $\delta\tau$. Indeed, at time t_{thr} we have $\dot{I}(t_{thr}) \simeq -\xi I_{thr}$, as the number of new infected is completely negligible at this point. *A priori*, since there is a little spread of the epidemic in the population we will have $\delta I(t_{thr}) > \delta I(0)\exp(-\xi t_{thr})$, and close to this value if $I(0)$ is small enough. Therefore, we get $\delta\tau > \frac{\delta I(0)}{\xi I_{thr}}\exp(-\xi t_{thr})$. At this stage, we need to give an order of magnitude for t_{thr}. We use that $I(t_{thr}) \simeq I(0)\exp(-\xi t_{thr}) = I_{thr}$ and thus $\delta\tau > \frac{\delta I(0)}{\xi I(0)}$. One can then easily show that $\delta I(0) \propto \delta n\delta t$ where the proportionality coefficient can by written in a formal way as $\frac{\partial\lambda}{\partial n}(n_{min})S(0)$ where we omit age class notations (generalization is straightforward). Finally, we get the extra cost δC paid by individuals,

$$\begin{aligned} \delta C &= d_n f(n_{min})\delta t\delta n + \delta\tau f(n_{min}) \\ &> \delta t\delta n\left[d_n f(n_{min}) + f(n_{min})\frac{\partial\lambda}{\partial n}(n_{min})S(0)\right] > 0. \end{aligned} \tag{F2}$$

For any positive $\delta t, \delta n$, one can check that $[d_n f(n_{min}) + f(n_{min})\frac{\partial\lambda}{\partial n}(n_{min})S(0)] > 0$, where $\frac{\partial\lambda}{\partial n} \propto I(0)$ with $I(0) \geqslant I_{thr}$. The extra cost paid by individuals for the deviating strategy is always positive, it is therefore worse than the initial one. The initial strategy presented at the beginning of this Appendix is the optimal one in this sense. One can also argue that this local minimum is the true minimum among all eradicating strategies, as the above reasoning will be *a priori* true for higher values of n, considering the shape of f.

APPENDIX G: EXPLORATION OF THE PARAMETER SPACE

We present below the Nash equilibrium results (first for epidemic quantities in Fig. 18 and then for contact willingness in Fig 19) where we change at each time one of the parameters presented in Tables II and III. We see in Fig. 18 that the general behaviors observed with the original set of parameters (unicity of the peak, reach collective immunity) are quite robust to many different changes. As expected, contacts between classes allow an epidemic spreading even in classes where no one is infected at $t = 0$ (first row). Then,

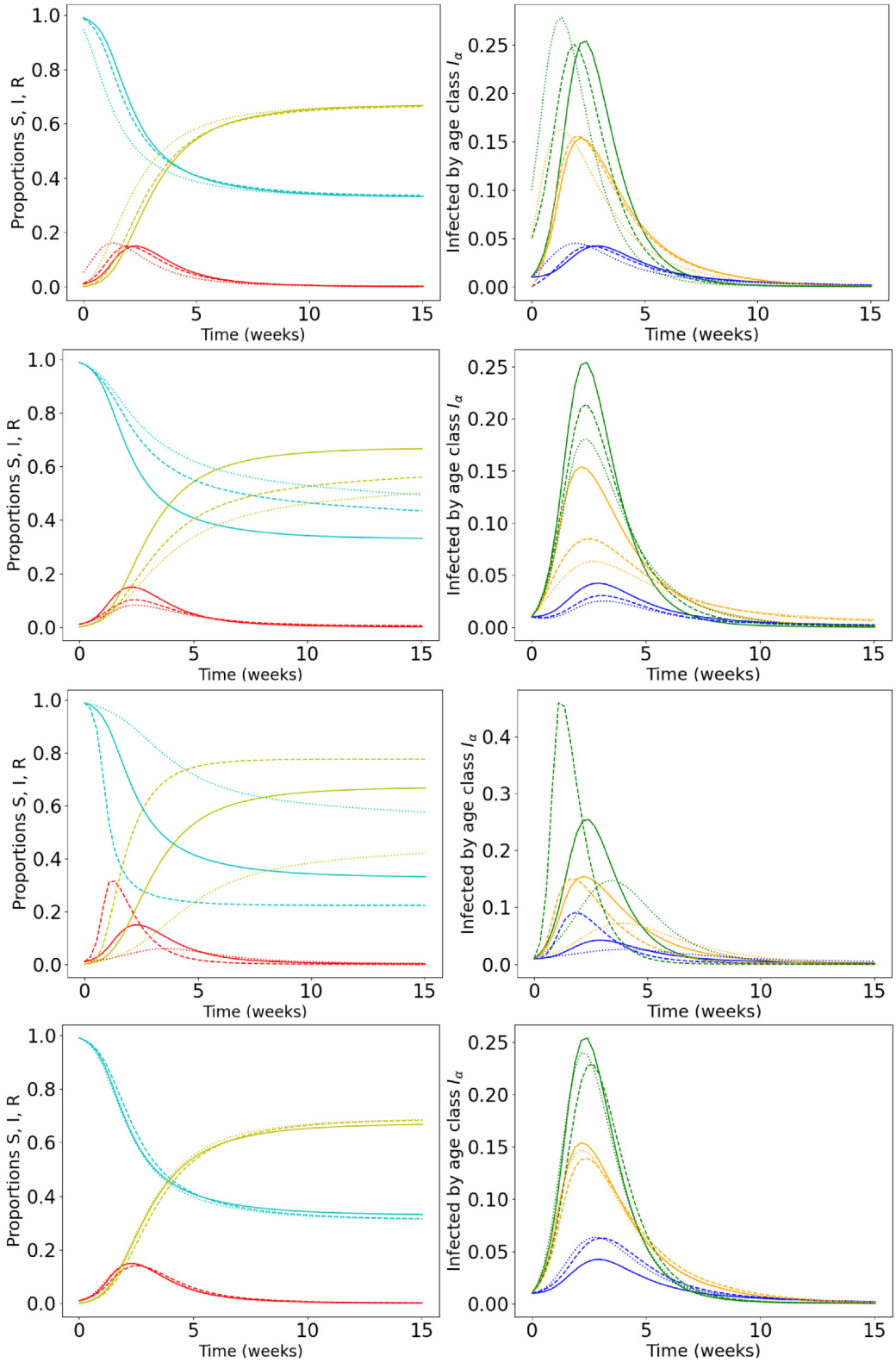

FIG. 18. Comparison of Nash equilibrium epidemics for the set of parameters of Tables II and III with one (arbitrary but realistic) parameter change for each row (solid lines correspond to baseline parameters). Color legend is the same as in Fig. 6. First row: initial conditions change with $(S_0(0), S_1(0), S_2(0)) = (0.99, 0.99, 0.99)$ for solid line, dashed $(0.95, 1, 1)$ and dotted $(0.9, 0.95, 0.99)$. In each case, $I_\alpha(0) = 1 - S_\alpha(0)$ and $R_\alpha(0) = 0$. Second row: three different τ_I with $\tau_I = 1$ (solid), $\tau_I = 3$ (dashed), and $\tau_I = 5$ (dotted). Third row: three different proportions in the population, $(\mathcal{N}_0, \mathcal{N}_1, \mathcal{N}_2) = (0.25, 0.5, 0.25)$ for solid line, $(0.6, 0.2, 0.2)$ for dashed lines, and $(0.2, 0.2, 0.6)$ for dotted lines. Fourth row: three different matrices $\mathcal{M}_1$(solid), $\mathcal{M}_2$(dashed), and $\mathcal{M}_3$(dotted) defined in Table IV.

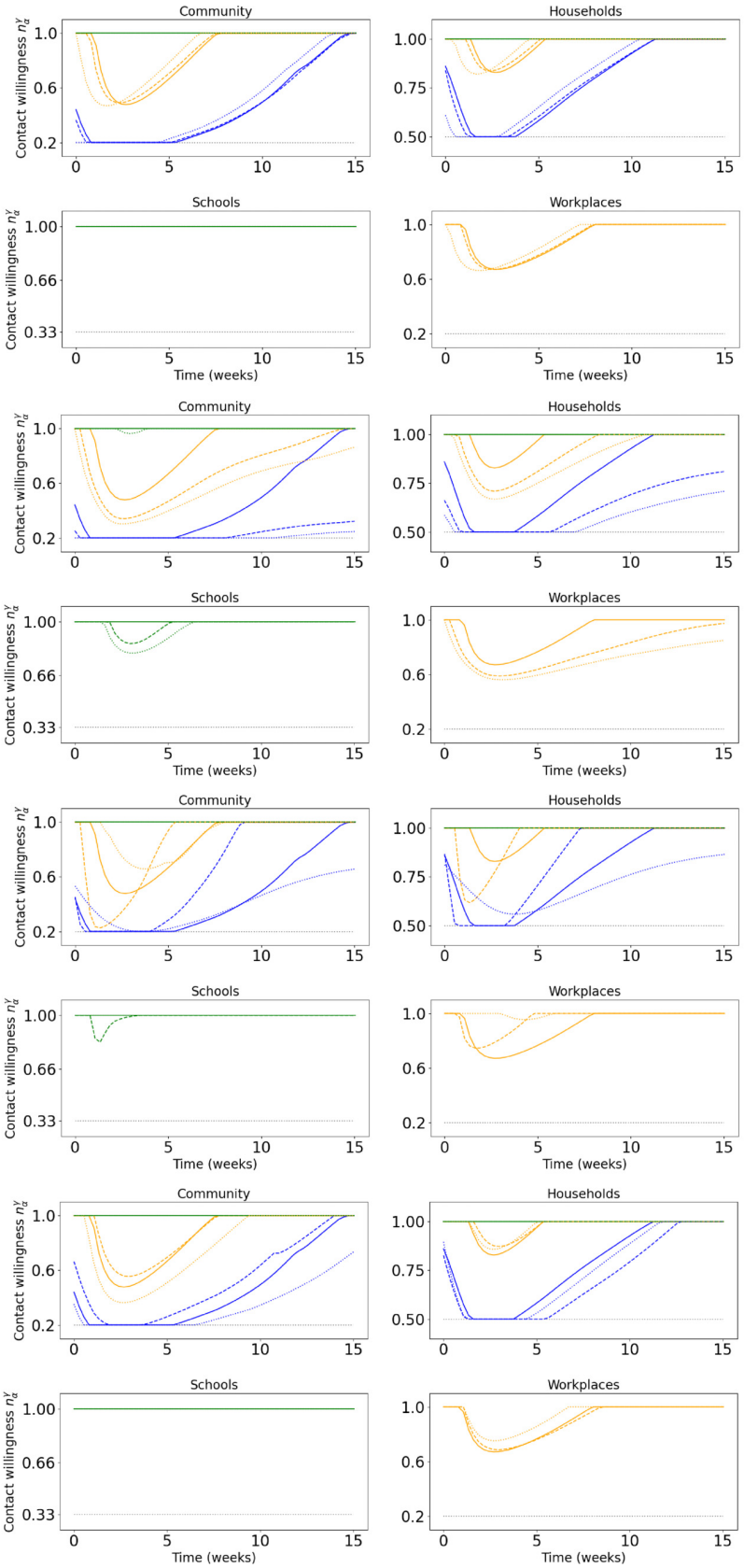

FIG. 19. Comparison of Nash equilibrium contact willingness for the different set of parameters used in Fig. 18 and the same legend for solid, dashed, and dotted lines. We keep the legend of Fig. 7 regarding colors.

TABLE IV. Table of matrices $\mathcal{M}_1$, $\mathcal{M}_2$, and $\mathcal{M}_3$ (given with the form $\mathcal{M}^\gamma$) used for the fourth row of Fig. 18. The first one corresponds to the one we took in our previous simulations (Tables II and III), while the two others are chosen to explore two behaviors: Matrix $\mathcal{M}_2$ corresponds to a society with important heterogeneous contacts, especially in households; while matrix $\mathcal{M}_3$ is a society which is more homogeneous with a lot of contacts in community. Matrix elements are contact rates (per week) in our model.

$\mathcal{M}_1^S$	$\mathcal{M}_1^W$	$\mathcal{M}_1^C$	$\mathcal{M}_1^H$
$\begin{pmatrix} 100 & 0 & 0 \\ 0 & 0 & 0 \\ 0 & 0 & 0 \end{pmatrix}$	$\begin{pmatrix} 0 & 0 & 0 \\ 0 & 75 & 0 \\ 0 & 0 & 0 \end{pmatrix}$	$\begin{pmatrix} 12.5 & 25 & 12.5 \\ 12.5 & 25 & 12.5 \\ 12.5 & 25 & 12.5 \end{pmatrix}$	$\begin{pmatrix} 15 & 25 & 10 \\ 12.5 & 32.5 & 5 \\ 10 & 10 & 30 \end{pmatrix}$
$\mathcal{M}_2^S$	$\mathcal{M}_2^W$	$\mathcal{M}_2^C$	$\mathcal{M}_2^H$
$\begin{pmatrix} 100 & 0 & 0 \\ 0 & 0 & 0 \\ 0 & 0 & 0 \end{pmatrix}$	$\begin{pmatrix} 0 & 0 & 0 \\ 0 & 75 & 0 \\ 0 & 0 & 0 \end{pmatrix}$	$\begin{pmatrix} 12.5 & 15 & 5 \\ 7.5 & 25 & 5 \\ 5 & 10 & 12.5 \end{pmatrix}$	$\begin{pmatrix} 12.5 & 15 & 20 \\ 7.5 & 30 & 17.5 \\ 20 & 35 & 12.5 \end{pmatrix}$
$\mathcal{M}_3^S$	$\mathcal{M}_3^W$	$\mathcal{M}_3^C$	$\mathcal{M}_3^H$
$\begin{pmatrix} 75 & 0 & 0 \\ 0 & 0 & 0 \\ 0 & 0 & 0 \end{pmatrix}$	$\begin{pmatrix} 0 & 0 & 0 \\ 0 & 50 & 0 \\ 0 & 0 & 0 \end{pmatrix}$	$\begin{pmatrix} 25 & 50 & 25 \\ 25 & 50 & 25 \\ 25 & 50 & 25 \end{pmatrix}$	$\begin{pmatrix} 12.5 & 25 & 12.5 \\ 12.5 & 25 & 12.5 \\ 12.5 & 25 & 12.5 \end{pmatrix}$

in second row regarding different τ_I, we see that epidemic peak occurs at a lower level as τ_I increases, since individuals do more efforts to protect themselves. In third row, we see that the different proportion of age classes in the population will have a huge impact on the epidemic. Indeed, it will affect both the matrix of effective contacts (which are higher between young people) and the risk due to infection (which is lower for young). Hence, the observed behavior results in a high and quick epidemic for a young population, while it is significantly lower and slower for an old population. Finally, in the fourth row, the precise matrix of contacts $\mathcal{M}$ affects the epidemic in each class, but in a relatively moderate way regarding the global evolution of infected proportion in the population.

[1] N. Ferguson, D. Laydon, G. Nedjati Gilani, N. Imai, K. Ainslie, M. Baguelin, S. Bhatia, A. Boonyasiri, Z. Cucunuba Perez, G. Cuomo-Dannenburg *et al.*, Report 9: Impact of non-pharmaceutical interventions (NPIs) to reduce COVID-19 mortality and healthcare demand, *Technical Report* (Imperial College, London, UK, 2020).

[2] D. K. Miles, M. Stedman, and A. H. Heald, "Stay at Home, Protect the National Health Service, Save Lives": A cost benefit analysis of the lockdown in the United Kingdom, Int. J. Clin. Pract. **75**, e13674 (2021).

[3] A. A. Toda, Susceptible-infected-recovered (SIR) dynamics of COVID-19 and economic impact, arXiv:2003.11221.

[4] J. D. Osofsky, H. J. Osofsky, and L. Y. Mamon, Psychological and social impact of COVID-19, Psychol. Trauma: Theory, Res., Practice, Policy **12**, 468 (2020).

[5] Q. D. Nguyen and M. Prokopenko, A general framework for optimising cost-effectiveness of pandemic response under partial intervention measures, Sci. Rep. **12**, 19482 (2022).

[6] R. Morton and K. H. Wickwire, On the optimal control of a deterministic epidemic, Adv. Appl. Probab. **6**, 622 (1974).

[7] K. H. Wickwire, Optimal isolation policies for deterministic and stochastic epidemics, Math. Biosci. **26**, 325 (1975).

[8] F. D. Sahneh, F. N. Chowdhury, and C. M. Scoglio, On the existence of a threshold for preventive behavioral responses to suppress epidemic spreading, Sci. Rep. **2**, 632 (2012).

[9] A. Rizzo, M. Frasca, and M. Porfiri, Effect of individual behavior on epidemic spreading in activity-driven networks, Phys. Rev. E **90**, 042801 (2014).

[10] https://covidtracker.fr

[11] L. Wynants, B. Van Calster, G. S. Collins, R. D. Riley, G. Heinze, E. Schuit, E. Albu, B. Arshi, V. Bellou, M. M. Bonten *et al.*, Prediction models for diagnosis and prognosis of COVID-19: Systematic review and critical appraisal, BMJ **369**, m1328 (2020).

[12] H. Salje, C. Tran Kiem, N. Lefrancq, N. Courtejoie, P. Bosetti, J. Paireau, A. Andronico, N. Hozé, J. Richet, C.-L. Dubost *et al.*, Estimating the burden of SARS-CoV-2 in France, Science **369**, 208 (2020).

[13] J. Guan, Y. Wei, Y. Zhao, and F. Chen, Modeling the transmission dynamics of COVID-19 epidemic: A systematic review, J. Biomed. Res. **34**, 422 (2020).

[14] Y. Huang and Q. Zhu, Game-theoretic frameworks for epidemic spreading and human decision-making: A review, Dyn. Games Appl. **12**, 7 (2022).

[15] J.-M. Lasry and P.-L. Lions, Mean field games, Jpn. J. Math. **2**, 229 (2007).

[16] J.-M. Lasry and P.-L. Lions, Jeux à champ moyen. II—Horizon fini et contrôle optimal, C. R. Math. **343**, 679 (2006).

[17] J.-M. Lasry and P.-L. Lions, Jeux à champ moyen. I—Le cas stationnaire, C. R. Math. **343**, 619 (2006).

[18] M. Huang, R. Malhame, and P. Caines, Large population stochastic dynamic games: Closed-loop McKean-Vlasov systems and the Nash certainty equivalence principle, Commun. Inf. Syst. **6**, 115 (2006).

[19] P. E. Caines, Mean field games, in *Encyclopedia of Systems and Control* (Springer, Berlin, 2021).

[20] D. A. Gomes, J. Mohr, and R. R. Souza, Continuous time finite state mean field games, Appl. Math. Optim. **68**, 99 (2013).

[21] R. Carmona, F. Delarue *et al.*, *Probabilistic Theory of Mean Field Games with Applications I–II* (Springer, Berlin, 2018).
[22] D. Ullmo, I. Swiecicki, and T. Gobron, Quadratic mean field games, Phys. Rep. **799**, 1 (2019).
[23] I. Swiecicki, T. Gobron, and D. Ullmo, Schrödinger approach to mean field games, Phys. Rev. Lett. **116**, 128701 (2016).
[24] A. Cousin, S. Crépey, O. Guéant, D. Hobson, M. Jeanblanc, J.-M. Lasry, J.-P. Laurent, P.-L. Lions, P. Tankov, O. Guéant *et al.*, Mean field games and applications, Paris-Princeton Lect. Math. Fin. **2010**, 24 (2011).
[25] P. Chan and R. Sircar, Bertrand and Cournot mean field games, Appl. Math. Optim. **71**, 533 (2015).
[26] T. Bonnemain, M. Butano, T. Bonnet, I. Echeverría-Huarte, A. Seguin, A. Nicolas, C. Appert-Rolland, and D. Ullmo, Pedestrians in static crowds are not grains, but game players, Phys. Rev. E **107**, 024612 (2023).
[27] D. Bauso, R. Pesenti, and M. Tolotti, Opinion dynamics and stubbornness via multi-population mean-field games, J. Optim. Theory Appl. **170**, 266 (2016).
[28] T. C. Reluga, Game theory of social distancing in response to an epidemic, PLoS Comput. Biol. **6**, e1000793 (2010).
[29] L. Laguzet, G. Turinici, and G. Yahiaoui, Equilibrium in an individual-societal SIR vaccination model in presence of discounting and finite vaccination capacity, in *New Trends in Differential Equations, Control Theory and Optimization: Proceedings of the 8th Congress of Romanian Mathematicians* (World Scientific, Singapore, 2016).
[30] E. Hubert and G. Turinici, Nash-MFG equilibrium in a SIR model with time dependent newborn vaccination, Ric. Mat. **67**, 227 (2018).
[31] F. Salvarani and G. Turinici, Optimal individual strategies for influenza vaccines with imperfect efficacy and durability of protection, Math. Biosci. Eng. **15**, 629 (2018).
[32] R. Elie, E. Hubert, and G. Turinici, Contact rate epidemic control of COVID-19: An equilibrium view, Math. Modell. Nat. Phenom. **15**, 35 (2020).
[33] S. Y. Olmez, S. Aggarwal, J. W. Kim, E. Miehling, T. Başar, M. West, and P. G. Mehta, Modeling presymptomatic spread in epidemics via mean-field games, in *Proceedings of the American Control Conference (ACC)* (IEEE, Piscataway, NJ, 2022).
[34] S. Y. Olmez, S. Aggarwal, J. W. Kim, E. Miehling, T. Başar, M. West, and P. G. Mehta, How does a rational agent act in an epidemic?, in *Proceedings of the IEEE 61st Conference on Decision and Control (CDC)* (IEEE, Piscataway, NJ, 2022).
[35] A. Roy, C. Singh, and Y. Narahari, Recent advances in modeling and control of epidemics using a mean field approach, Sādhanā **48**, 207 (2023).
[36] W. O. Kermack and A. G. McKendrick, A contribution to the mathematical theory of epidemics, Proc. R. Soc. London, Ser. A **115**, 772 (1927).
[37] H. W. Hethcote, The mathematics of infectious diseases, SIAM Rev. **42**, 599 (2000).
[38] L. Fumanelli, M. Ajelli, P. Manfredi, A. Vespignani, and S. Merler, Inferring the structure of social contacts from demographic data in the analysis of infectious diseases spread, PLoS Comput. Biol. **8**, e1002673 (2012).
[39] D. Mistry, M. Litvinova, A. Pastore y Piontti, M. Chinazzi, L. Fumanelli, M. F. Gomes, S. A. Haque, Q.-H. Liu, K. Mu, X. Xiong *et al.*, Inferring high-resolution human mixing patterns for disease modeling, Nat. Commun. **12**, 323 (2021).
[40] S. Merler, M. Ajelli, A. Pugliese, and N. M. Ferguson, Determinants of the spatiotemporal dynamics of the 2009 H1N1 pandemic in Europe: Implications for real-time modelling, PLoS Comput. Biol. **7**, e1002205 (2011).
[41] S. Eubank, H. Guclu, V. Anil Kumar, M. V. Marathe, A. Srinivasan, Z. Toroczkai, and N. Wang, Modelling disease outbreaks in realistic urban social networks, Nature (London) **429**, 180 (2004).
[42] R. Dutta, S. N. Gomes, D. Kalise, and L. Pacchiardi, Using mobility data in the design of optimal lockdown strategies for the COVID-19 pandemic, PLoS Comput. Biol. **17**, e1009236 (2021).
[43] D. Sen and D. Sen, Use of a modified SIRD model to analyze COVID-19 data, Ind. Eng. Chem. Res. **60**, 4251 (2021).
[44] S. Gao, Z. Teng, J. J. Nieto, A. Torres *et al.*, Analysis of an SIR epidemic model with pulse vaccination and distributed time delay, Biomed Res. Int. **2017**, 064870 (2007).
[45] H. Li and S. Guo, Dynamics of a SIRC epidemiological model, Electron. J. Differ. Equations **2017**, 1 (2017).
[46] M. Y. Li, H. L. Smith, and L. Wang, Global dynamics of an SEIR epidemic model with vertical transmission, SIAM J. Appl. Math. **62**, 58 (2001).
[47] A. Arenas, W. Cota, J. Gómez-Gardeñes, S. Gómez, C. Granell, J. T. Matamalas, D. Soriano-Paños, and B. Steinegger, Modeling the spatiotemporal epidemic spreading of COVID-19 and the impact of mobility and social distancing interventions, Phys. Rev. X **10**, 041055 (2020).
[48] S. Y. Del Valle, J. M. Hyman, H. W. Hethcote, and S. G. Eubank, Mixing patterns between age groups in social networks, Soc. Netw. **29**, 539 (2007).
[49] G. Béraud, S. Kazmercziak, P. Beutels, D. Levy-Bruhl, X. Lenne, N. Mielcarek, Y. Yazdanpanah, P.-Y. Boëlle, N. Hens, and B. Dervaux, The french connection: The first large population-based contact survey in france relevant for the spread of infectious diseases, PLoS ONE **10**, e0133203 (2015).
[50] L. Di Domenico, G. Pullano, C. E. Sabbatini, P.-Y. Boëlle, and V. Colizza, Impact of lockdown on COVID-19 epidemic in île-de-france and possible exit strategies, BMC Med. **18**, 240 (2020).
[51] J. Tchuenche, S. Khamis, F. Agusto, and S. Mpeshe, Optimal control and sensitivity analysis of an influenza model with treatment and vaccination, Acta Biotheor. **59**, 1 (2011).
[52] D. Bertsekas, *Dynamic Programming and Optimal Control: Volume I* (Athena Scientific, Nashua, NH, 2012), Vol. 4.
[53] A. Abakuks, An optimal isolation policy for an epidemic, J. Appl. Probab. **10**, 247 (1973).
[54] A. Abakuks, Optimal immunisation policies for epidemics, Adv. Appl. Probab. **6**, 494 (1974).
[55] M. Kantner and T. Koprucki, Beyond just "flattening the curve": Optimal control of epidemics with purely nonpharmaceutical interventions, J. Math. Ind. **10**, 23 (2020).
[56] T. Kruse and P. Strack, Optimal control of an epidemic through social distancing, SSRN (2020), http://dx.doi.org/10.2139/ssrn.3581295.
[57] M. Khouzani, S. Sarkar, and E. Altman, Optimal control of epidemic evolution, in *Proceedings of the IEEE INFOCOM* (IEEE, Piscataway, NJ, 2011).
[58] Our criterion is actually better suited to describe herd immunity at the end of the epidemics than, for instance, the one which requires $S < 1/\tilde{R}_0$ with $\tilde{R}_0 = \rho(\rho\mu\mathcal{M}/\xi)$ [38,60].

[59] A. Aurell, R. Carmona, G. Dayanikli, and M. Lauriere, Optimal incentives to mitigate epidemics: A Stackelberg mean field game approach, SIAM J. Control Optim. **60**, S294 (2022).

[60] O. Diekmann, J. A. P. Heesterbeek, and J. A. J. Metz, On the definition and the computation of the basic reproduction ratio R0 in models for infectious diseases in heterogeneous populations, J. Math. Biol. **28**, 365 (1990).

E - Analytical solution of SIR models on homogeneous networks

Analytical solution of susceptible-infected-recovered models on homogeneous networks

Louis Bremaud,[1] Olivier Giraud,[1,2,3] and Denis Ullmo[1]
[1]*Université Paris-Saclay, CNRS, LPTMS, 91405 Orsay, France*
[2]*MajuLab, CNRS-UCA-SU-NUS-NTU International Joint Research Laboratory, 117543 Singapore, Singapore*
[3]*Centre for Quantum Technologies, National University of Singapore, 117543 Singapore, Singapore*

(Received 15 December 2023; accepted 18 September 2024; published 17 October 2024)

The ability to actually implement epidemic models is a crucial stake for public institutions, as they may be overtaken by the increasing complexity of current models and sometimes tend to revert to less elaborate models such as the susceptible-infected-recovered (SIR) model. In our work, we study a simple epidemic propagation model, called SIR-k, which is based on a homogeneous network of degree k, where each individual has the same number k of neighbors. This model represents a refined version of the basic SIR which assumes a completely homogeneous population. We show that nevertheless, analytical expressions, simpler and richer than the ones existing for the SIR model, can be derived for this SIR-k model. In particular, we obtain an exact implicit analytical solution for any k, from which quantities such as the epidemic threshold or the total number of agents infected during the epidemic can be obtained. We furthermore obtain simple exact explicit solutions for small ks, and in the large k limit we find a new formulation of the analytical solution of the basic SIR model, which comes with new insights.

DOI: 10.1103/PhysRevE.110.044307

I. INTRODUCTION

Understanding the dynamics of epidemics is of primary importance to allow public policies to mitigate their negative impact [1,2]. Models of epidemic propagation have therefore been introduced as early as one century ago, in 1927, in particular, the seminal paper of Kermack and McKendrick [3]. In this paper, they introduce the susceptible-infected-recovered (SIR) model, which, despite its simplicity, is still a basis of work in many studies [4–6]. This model divides a population into susceptible, infected, and recovered individuals, and two parameters characterize the evolution: the transmission rate β and the recovery rate γ. In the simplest version of the model, β and γ are assumed to be constant on the epidemic time scale. The time evolution of the fractions (S, I, R) of susceptible, infected, and recovered agents is then given [5,7] by

$$\begin{aligned} \dot{S} &= -\beta SI, \\ \dot{I} &= \beta SI - \gamma I, \\ \dot{R} &= \gamma I. \end{aligned} \tag{1}$$

This system of differential equations was studied in detail during the past century [5,7,8]; in particular, explicit solutions describing the beginning of epidemics [3], and complete implicit solutions [9–11], have been derived.

Even though the basic SIR model has been successful, it can be considered too simplistic. This is why more accurate variants [12–16] and a number of more complex models [7,17–20] have since been introduced. Among these models, compartment models on networks provide a good balance between simplicity, physical understanding, and improved accuracy [16,21–28]. This approach benefited both from the wealth of activity in network theory in the past two decades and from the increased availability of large amounts of data [29] about contact networks (see [30,31] for a complete review on the subject). This has resulted in a steady increase of papers published on the subject of epidemics on networks since the year 2000 [32].

Despite their success in extending the basic SIR model, these network models so far lack one important feature, which is the existence of analytical solutions for the models' equations. The importance and usefulness of these analytical results should not be underrated, as they provide a much deeper understanding of the mechanisms at work than can be achieved numerically. Moreover, they constitute a benchmark for more complex models where no analytical solution is available. Our goal here is to provide such analytical results in the case of random homogeneous networks, which are characterized by their constant connectivity k. For any given value of k we obtain analytic expressions analogous to (and in some circumstances stronger than) the ones existing for the SIR model (1); when $k = 2$ or 3 we obtain simple explicit expressions, while in the limit $k \to \infty$ we recover the basic SIR, leading to some new physical insights as well as some useful approximations of this well-known model.

The article is organized as follows. In Sec. II, we present the SIR model on a random homogeneous network with k neighbors, called the SIR-k model, and its dynamic equations. In Sec. III, we derive the (implicit) analytical solution of these equations. We then study the impact of our results on the epidemic threshold, and the case of a small number of neighbors, which provides more explicit expressions. In Sec. IV, we focus on the limiting case $k \to \infty$ to derive the exact solution of the SIR model. We then derive some significant approximations with simpler expressions and study the consequences of our results on the epidemic's peak time. Finally, concluding remarks are gathered in Sec. V.

II. SIR MODEL ON A RANDOM HOMOGENEOUS NETWORK WITH k NEIGHBORS

We consider a population of N individuals who can be in one of the three possible states (susceptible, infected, recovered). Each agent is in contact with k fixed neighbors only. These neighbors are chosen randomly among the population. The standard SIR model, where everyone is in contact with everyone, corresponds to the large-k limit of this model. The population can be represented by a random homogeneous network with fixed connectivity k, where each node corresponds to an individual and edges connect neighboring individuals. Associated with each of these edges is a probability λdt that an infected individual will infect a (susceptible) neighbor during the time interval $[t, t+dt[$. As in the basic SIR model, infected individuals may also recover from the disease during that time interval with a probability γdt. The epidemic then spreads through the network following a standard Markovian process (see [33] for a detailed procedure), and dynamic quantities are averaged over realizations of the network and of the Markovian process.

The time evolution of the average fractions $S(t)$, $I(t)$, and $R(t)$ of susceptible, infected, and recovered individuals requires taking into account correlations between the states of two neighbors, which are very strong in a network. For a SIR model on a k-homogeneous network we obtain the system of equations

$$\dot{S} = -\lambda k G^{si} S, \tag{2a}$$

$$\dot{I} = \lambda k G^{si} S - \gamma I, \tag{2b}$$

$$\dot{R} = \gamma I, \tag{2c}$$

with $S(t)+I(t)+R(t)=1$. Here, $G^{si}(t)$ corresponds to the probability that a neighbor of a given susceptible individual is itself infected; thus $kG^{si}(t)$ is the average number of infected individuals in the neighborhood of a susceptible individual. Introducing $G^{ss}(t)$ and $G^{sr}(t)$ in a similar way, with $G^{ss}(t)+G^{si}(t)+G^{sr}(t)=1$, the time dependence of these two-point correlators is given by

$$[\dot{SG^{ss}}] = -2SG^{ss}(k-1)G^{si}\lambda, \tag{3a}$$

$$[\dot{SG^{si}}] = SG^{ss}(k-1)G^{si}\lambda, -SG^{si}[(k-1)G^{si}+1]\lambda - \gamma SG^{si} \tag{3b}$$

$$[\dot{SG^{sr}}] = \gamma SG^{si} - SG^{sr}(k-1)G^{si}\lambda. \tag{3c}$$

To derive (3) we made the degree pairwise approximation [34], that is, we neglected three-point correlations (and beyond) which should appear in the evolution of G^{si}. Within this approximation, the derivation can be sketched as follows. We note first that $XG^{xy}(t)$ corresponds to the probability for a given edge (here, considered oriented, with the starting vertex being in state x and the arrival vertex being in state y) to be in the state x—y at t. Consider first the case $x=y=s$ and a given edge s—s. For an agent located at one end of this edge to be infected, it is necessary that one of its $(k-1)$ other neighbors be infected and transmit the disease. If we neglect the three-point correlations (between the initial node, its neighbor, and the second neighbors), each of the other neighbors has a probability G^{si} to be infected, and in that case, a probability λdt to transmit the disease. Thus, the time evolution of SG^{ss} is given, at order dt, by Eq. (3a) (the factor 2 accounts for the two ends of edge s—s). Equation (3b) can be explained in a similar way; SG^{si} corresponds now to the number of edges, starting from a susceptible node to an infected one. See [35] for a more detailed derivation. This approximation has been for example used in [31] to derive equations for the SI model on a generic network.

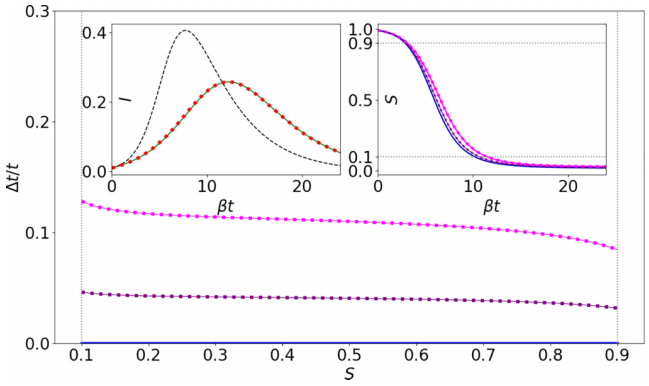

FIG. 1. Main panel: Time delay $\Delta t = t(S) - t_{\mathrm{SIR}}(S)$ with t_{SIR} obtained by numerically solving (1). Solid thick dark blue: analytical expression (26), corresponding to the limit case SIR-∞, yielding 0 as expected. Purple ($k=50$) and magenta ($k=20$) plots: numerical resolution of the SIR-k model (2) (solid lines) and corresponding analytical solution (11) (dots). Right inset: proportion of susceptible $S(t)$ for the same configurations. The gray horizontal dotted lines indicate the range of S values taken for the main panel. Left inset: proportion of infected $I(t)$ for $k=5$. Red dotted line: numerical resolution of the SIR-5 model Eqs. (2) and (3); green solid line: average over 100 realizations of the Markovian process of an epidemic on a large homogeneous network of degree $k=5$, with $N=3000$ nodes (with random initial infected nodes); black dashed line: basic SIR model with $\beta=\lambda k$. Parameters are $\mu=0.25$, $S_0=0.99$.

In the case of homogeneous networks with a large number of nodes $N\to\infty$, as we consider here, the fraction of loops with arbitrary finite size vanishes [36–38]. Therefore, the correlations beyond two-point ones can be neglected and the degree pairwise approximation becomes exact in this limit [39]. Equations (2) and (3) form what we will call the "SIR-k model" in the following. In Fig. 1 (left inset), we demonstrate the accuracy of our approximation by comparing a numerical solution of Eqs. (2) and (3) with a Markovian evolution of a population according to the same dynamics. The parameters of our problem are S_0 the initial proportion of susceptible agents, k the number of neighbors, $\beta=\lambda k$ the contagiousness and γ the recovery rate, which leads to a dimensionless quantity $\mu=\gamma/\beta$ driving the epidemic, while β only changes the time scale (see for example [10]).

III. ANALYTICAL SOLUTION OF THE SIR-k EQUATIONS

A. General expression

From Eqs. (2) and (3), we can obtain an ordinary differential equation involving only $S(t)$. Inserting $G^{si}=-\dot{S}/(\beta S)$, which we get from Eq. (2a), into Eq. (3a), we have

$$\frac{[\dot{SG^{ss}}]}{SG^{ss}} = 2\frac{k-1}{k}\frac{\dot{S}}{S}. \tag{4}$$

At $t = 0$, $S(0) = S_0 = G^{ss}(0)$ if we assume that there are no correlations at time 0 (i.e., the neighborhood of infected and susceptible individuals is the same), then Eq. (4) can be integrated as $G^{ss} = S_0^{\frac{2}{k}} S^{1-\frac{2}{k}}$. Using Eq. (2a) and this expression for G^{ss}, Eq. (3b) yields

$$\ddot{S} = \lambda S_0^{\frac{2}{k}} S^{1-\frac{2}{k}}(k-1)\dot{S} + \frac{k-1}{k}\frac{\dot{S}}{S} - (\gamma+\lambda)\dot{S}. \tag{5}$$

This is a second-order differential equation in S that we need to integrate twice. A first integration is obtained by dividing (5) by $\dot{S}$ and introducing $\varphi(S) = \dot{S}$, which verifies

$$\frac{d\varphi(S)}{dS} = \lambda S_0^{\frac{2}{k}} S^{1-\frac{2}{k}}(k-1) + \frac{k-1}{k}\frac{\varphi(S)}{S} - (\gamma+\lambda). \tag{6}$$

Equation (6) can be integrated as an equation in the variable S to give

$$\varphi(S) = kS_0^{2/k}\lambda S^{2(1-\frac{1}{k})} - k(\lambda+\gamma)S + C_1 S^{1-\frac{1}{k}}, \tag{7}$$

where C_1 is given by the initial conditions: $C_1 = \dot{S}(0)S_0^{-1+1/k} - \lambda k S_0^{1+1/k} + k(\lambda+\gamma)S_0^{1/k}$. Using $\dot{S}(0) = -\lambda k S_0(1-S_0)$, this constant reduces to $C_1 = k\gamma S_0^{1/k}$. Changing to the variable $z \equiv (S/S_0)^{\frac{1}{k}}$, and using $\mu = \gamma/\beta$, we obtain

$$\dot{z} = \lambda P(z), \quad P(z) = S_0 z^{k-1} - (k\mu+1)z + k\mu. \tag{8}$$

Separating the variables z and t and using the partial fraction decomposition of $1/P(z)$ in terms of the roots z_j ($j = 0, \ldots, k-2$) of $P(z)$, the integral of Eq. (8) becomes

$$\int_1^z \frac{dz'}{P(z')} = \sum_{j=0}^{k-2}\int_1^z \frac{A_j}{z'-z_j}dz' = \lambda t, \tag{9}$$

with

$$A_j = \frac{1}{P'(z_j)} = \frac{1}{\prod_{l\neq j}(z_j - z_l)}. \tag{10}$$

Equation (9) readily gives an explicit expression for t as a function of S as

$$t(S) = \frac{1}{\lambda}\sum_{j=0}^{k-2} A_j \ln\left(\frac{(S/S_0)^{1/k} - z_j}{1-z_j}\right). \tag{11}$$

Note that the complex roots z_j are pairwise complex conjugate so that the whole sum is real, as it should be. One then gets a parametric solution for the number of infected individuals under the form $(t(S), I(S))$ by integrating Eq. (2b). Indeed, since $S(t)$ is monotonous, Eq. (2b) can be rewritten as

$$\frac{dI}{dS} = -1 - \gamma I\frac{dt}{dS}, \tag{12}$$

which upon integration yields

$$I(S) = \left(1 - S_0 - \int_{S_0}^{S} e^{\gamma t(s')}ds'\right)e^{-\gamma t(S)}. \tag{13}$$

The maximum of I corresponds to the value of S where $dI/dS = 0$, that is,

$$I(S)\frac{dt}{dS} = -\frac{1}{\gamma}, \tag{14}$$

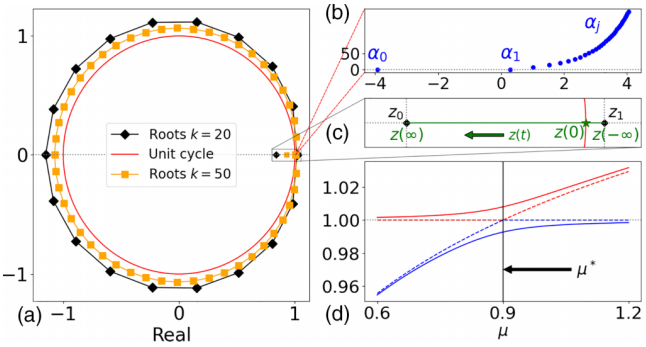

FIG. 2. (a) Orange squares (resp. black diamonds): location, in the complex plane, of the roots of the polynomial $P(z)$ Eq. (8) for $k = 50$ (resp. $k = 20$) with $S_0 = 0.8$ and $\mu = 0.25$. (b) Blow-up showing, in the complex plane, the limit as $k \to \infty$ of the α_j defined by $z_j = 1 + \alpha_j/k$. The complex z_j (and thus the complex α_j) come in conjugate pairs. (c) Zoom on the complex plane close to 1 with $z(t) = (S(t)/S_0)^{1/k}$ traveling the green line from $z_1 = z(-\infty)$ to $z_0 = z(\infty)$ and passing through $z(0) = 1$. (d) Blue line (resp. red line): illustration, for $k = 20$, of the variation with μ of the roots $z_0(\mu)$ (resp. $z_1(\mu)$) for $S_0 = 0.99$ (solid line) and $S_0 = 1$ (dashed line). The value μ_k^* such that $z_0(\mu_k^*) = z_1(\mu_k^*) = 1$ is the epidemic threshold.

with $t(S)$ explicitly given by (11), while the calculation of $I(S)$ involves a single numerical integral over S.

We checked for many different values of the parameters (S_0, μ, k) that the analytical solution (11) perfectly reproduces the numerical resolution of (2) and (3), and we illustrate it for one example in Fig. 1. Note that a similar approach allows us to address the SI model, which corresponds to the limit $\mu \to 0$; in that case we get

$$S(t) = S_0^{-\frac{2}{k-2}}\left(\frac{1-S_0}{S_0}e^{\lambda(k-2)t} + 1\right)^{-\frac{k}{k-2}}, \tag{15}$$

which in the limit $k \to \infty$ coincides with the known solution of the SI model [7].

B. Epidemic threshold

We now comment on the consequences of Eq. (11). Polynomials such as $P(z)$ in Eq. (8) have a long history, dating back to Lambert [40,41] and Euler [42]. In particular, one can explicitly express all the roots z_j as an infinite series (see [43,44]). As illustrated in Fig. 2(a), for $k > 2$ there are two real positive roots, $z_0 \in [0, 1]$ and $z_1 \in [1, \infty[$. Since $S/S_0 \in [0, 1]$, the only possible divergence of t in (11) corresponds to the root z_0, and we thus get that $S_\infty \equiv \lim_{t\to\infty} S(t) = S_0 z_0^k$. A useful quantity for public agencies in charge of controlling the epidemic (see [8] for the basic SIR model) is the fraction of the population that will be infected during the course of the epidemic; it can be expressed as $\mathcal{I}_{\text{tot}}^{(k)} = S_0 - S_\infty = S_0(1 - z_0^k)$. The second positive real root z_1 can then be interpreted as the nonphysical limit to which S would tend if one follows the SIR-k equations for negative times, $S_{-\infty} \equiv \lim_{t\to-\infty} S(t) = S_0 z_1^k > 1$. As illustrated in Fig. 2(c), the associated quantity $z(t) = (S(t)/S_0)^{1/k}$ decreases from 1 to z_0 for $t \in [0, +\infty[$, and from z_1 to 1 for the non-physical part $t \in]-\infty, 0]$.

Whatever the value of μ and k, $P(1) = S_0 - 1$. Thus, as illustrated in Fig. 2(d), $z = 1$ cannot be a root of $P(z)$ for $S_0 < 1$, but always is for $S_0 = 1$. In the latter case, two situations can occur. The first one would be that $z_1 = 1$ and $z_0 < 1$, in which case an epidemic starting with $S_0 = 1$ (i.e., with an infinitesimal fraction of infected individuals) would eventually propagate into the network and infect a finite fraction of the population. Introducing the time t_0 corresponding to the constant term in Eq. (11), namely

$$t_0 = -\frac{1}{\lambda}\sum_{j=0}^{k-2} A_j \ln|z_j - 1| \underset{S_0\to 1}{\sim} \frac{\ln(1-S_0)}{\lambda(2+k(\mu-1))}, \quad (16)$$

we see that $\lim_{S_0\to 1} t_0 = \infty$. This expresses the fact that the beginning of the epidemic takes an infinite amount of time as the initial proportion of infected individuals goes to zero. The other possibility, $z_0 = 1$ and $z_1 \geqslant 1$, corresponds to $S_\infty = 1$: an epidemic starting with $S_0 = 1$ does not propagate. The value μ_k^* of the parameter μ corresponding to the transition between these two regimes is the threshold beyond which, for $S_0 = 1$, the epidemic does not spread. At the threshold, $z = 1$ is a double root of $P(z)$ and thus $\mu_k^* = (k-2)/k$.[1] As $k \to \infty$ we get $\mu_k^* \to 1$, which coincides with the result of Kermack and McKendrick [3] for the original SIR model.

C. Small number of neighbors

It is possible to invert the expression (11) for $k = 2$ and 3. First, consider the case $k = 2$. A random network of size N then corresponds to a set of disconnected loops of different sizes. In the $N \to \infty$ limit, however, all but a negligible proportion of agents would belong to a large loop, and the average quantities we consider here, for example in Eqs. (2) and (3), behave in the same way within a random network or within a single connected loop. Furthermore, there is only one root $z_0 = 2\mu/(I_0 + 2\mu)$, with $I_0 = 1 - S_0$ the initial fraction of infected individuals. We can therefore write (11) as

$$t(S) = \frac{1}{\lambda} A_0 \ln\left(\frac{(S/S_0)^{1/2} - z_0}{1 - z_0}\right), \quad (17)$$

with $A_0 = -1/(I_0 + 2\mu) < 0$. Inverting Eq. (17) we get

$$S(t) = S_0\left[1 + \frac{I_0(e^{-t/\tau} - 1)}{I_0 + 2\mu}\right]^2, \quad \tau = \frac{1}{\lambda(2\mu + I_0)}. \quad (18)$$

$S(t)$ thus follows an exponential decay with rate τ and converges to $S_\infty = S_0 z_0^2$, as expected. We get $\mathcal{I}_{\text{tot}}^{(2)} = S_0(1 - (1 - I_0/(2\mu))^{-2})$, which varies from S_0 for strong epidemic $I_0/\mu \gg 1$ to 0 with $I_0/\mu \ll 1$. In particular, $\lim_{S_0\to 1} \mathcal{I}_{\text{tot}}^{(2)} = 0$ for any positive value of μ, which can also be seen from the fact that $\mu_2^* = (k-2)/k = 0$. This is unique to the $k = 2$ case because of its essentially 1d geometry, which implies that the number of infected agents caused by a single patient zero is necessarily finite.

For the case $k = 3$, we get $P(z) = S_0 z^2 - (3\mu + 1)z + 3\mu$, which has two (real positive) roots,

$$z_{0,1} = \frac{1}{2S_0}[(3\mu + 1) \pm \sqrt{(3\mu+1)^2 - 12\mu S_0}], \quad (19)$$

yielding

$$t(S) = \frac{A_0}{\lambda} \ln\left[\frac{((S/S_0)^{1/3} - z_0)(1 - z_1)}{((S/S_0)^{1/3} - z_1)(1 - z_0)}\right], \quad (20)$$

where we have used that $A_1 = -A_0 = 1/(z_1 - z_0)$. We can invert Eq. (20) to get

$$S(t) = S_0\left(\frac{z_0 - z_1 B e^{\lambda(z_0 - z_1)t}}{1 - B e^{\lambda(z_0 - z_1)t}}\right)^3, \quad B = \frac{1 - z_0}{1 - z_1}. \quad (21)$$

As expected, this expression verifies that $S(0) = S_0$ and $S_\infty = S_0 z_0^3$. The explicit expression for $\mathcal{I}_{\text{tot}}^{(3)}$ is $S_0 - \frac{1}{8S_0^2}[(3\mu + 1) + \sqrt{(3\mu+1)^2 - 12\mu S_0}]^3$. For $S_0 = 1$, the roots simplify to $z_0 = \min(1, 3\mu)$, $z_1 = \max(1, 3\mu)$, and we recover $\mu_3^* = \frac{1}{3}$; for $\mu < \mu_3^*$, $\mathcal{I}_{\text{tot}}^{(3)} = 1 - (3\mu)^3$, while for $\mu \geqslant \mu_3^*$ the epidemic does not propagate as $S_\infty = 1$.

Finally, we consider the case $k = 4$, but limiting ourselves for simplicity to the limit $S_0 \to 1$ and the regime $\mu < \mu_4^* = 1/2$. In that case, $P(z)$ has three roots, which, introducing $\kappa = \sqrt{1/4 + 4\mu}$, can be written as $z_0 = \kappa - \frac{1}{2}$, $z_1 = 1$, $z_2 = -\kappa - \frac{1}{2}$ with furthermore $A_0 = [\kappa(2\kappa + 3)]^{-1}$, $A_1 = [2 - 4\mu]^{-1}$, $A_2 = [\kappa(2\kappa - 3)]^{-1}$. The epidemics propagate only if $z_0 < 1$, that is if $\mu < \mu_4^* = 1/2$, in which case, scaling out the time t_0 introduced in Eq. (16), the dynamics is described by

$$t - t_0 = \frac{1}{\kappa\lambda}\sum_{\epsilon=\pm 1}\left(\frac{1}{2\kappa + 3\epsilon} \ln\left|\frac{S^{1/k} + \epsilon\kappa + \frac{1}{2}}{S^{1/k} - 1}\right|\right), \quad (22)$$

and $\mathcal{I}_{\text{tot}}^{(4)} = (-16\mu^2 - 8\mu + 1/2) + (1 + 8\mu)\sqrt{4\mu + 1/4}$ (which is indeed such that $\mathcal{I}_{\text{tot}}^{(4)}(\mu_4^*) = 0$).

IV. LARGE $-$ k LIMIT OF THE SIR $-$ k MODEL

A. Exact expression

Another interesting limit of the SIR-k model is $k \to \infty$, through which we recover the original SIR model, but with a new point of view. As illustrated in Fig. 2, z_0 and z_1 converge to 1 (from below and from above, respectively) and all the other roots converge to the unit circle in the complex plane. This can be understood from their series expansion in [43,44]. Using that z_j is a root of $P(z)$, we can write the factor A_j defined in Eq. (10) as

$$A_j = \left[(k-1)k\mu\frac{z_j - 1}{z_j} - k(\mu - 1) - 2\right]^{-1}. \quad (23)$$

For most roots of $P(z)$, $z_j - 1 = O(k^0)$ (we refer to them as "far from one") and thus $A_j = O(k^{-2})$. It is only for the roots close to one, and more precisely such that $z_j - 1 = O(k^{-1})$, that $A_j = O(k^{-1})$. In the same way, the logarithm factors are $O(k^{-1})$ for the roots far from one and $O(k^0)$ for the roots close to one. In Eq. (11), noting that $\lambda^{-1} = k\beta^{-1}$, we see that the sum over roots far from one involves $O(k)$ terms of order $O(k^{-2})$ and has therefore a negligible $O(k^{-1})$ contribution,

[1] This expression for the threshold can be derived also from the results in Sec. III C of [28]

whereas each root close to one has an $O(k^0)$ contribution. We can thus write all relevant roots as $z_j = 1 + \alpha_j/k$ where α_j reaches a constant value as $k \to \infty$. Writing that z_j is a root of $P(z)$ thus reads

$$S_0\Big(1+\frac{\alpha_j}{k}\Big)^{k-1} = k\mu\left[\left(1+\frac{1}{k\mu}\right)\left(1+\frac{\alpha_j}{k}\right)-1\right], \quad (24)$$

which, taking the limit $k \to \infty$ on both sides (with α_j now corresponding to that limit), gives $\exp(\alpha_j) = (\mu/S_0)(1/\mu + \alpha_j)$. Defining now $\gamma_j = \alpha_j + 1/\mu$ and $\chi = (S_0/\mu)e^{-1/\mu}$, we get

$$\chi = \gamma_j \exp(-\gamma_j). \quad (25)$$

Equation (25) can be rewritten in terms of the Euler T function (see [41] for mathematical details) as $\gamma_j = T(\chi)$. The T function has two real branches T_0 and T_{-1} which correspond to the two positive real roots of $P(z)$, and an infinite number of complex branches corresponding to the complex numbers γ_j. In particular, we get for the first root $\lim_{k\to\infty} S_\infty = \mu T_0(\chi)$, which is equivalent to the well-known self-consistent equation $S_\infty = 1 + \mu \ln(S_\infty/S_0)$ given, for instance, in [4]. Taking the large-k limit in Eqs. (23) and (11), together with $\beta = \lambda k$ and the expression of the relevant $z_j = 1 + \frac{\alpha_j}{k}$, leads to

$$\beta\, t(S) = \frac{1}{\mu}\sum_{j=-\infty}^{\infty} \frac{1}{\alpha_j + 1/\mu - 1} \ln\left(1+\frac{\ln(S_0/S)}{\alpha_j}\right),$$
$$\alpha_j = T_{-j}(\chi) - 1/\mu, \quad (26)$$

where the complex quantities α_j are pairwise complex conjugate (T_{-2} is conjugate with T_1, T_{-3} with T_2, etc.) so that the whole sum is real. In Fig. 1, we check the accuracy of this expression.

B. Approximate expression for $t(S)$

An implicit analytical solution $t(S)$ for the SIR model (1) is known in the literature and takes the form of an integral (see, for instance, [9]). Our formula (26) is an alternative expression for $t(S)$ and comes with interesting new insights, as it depends on quantities α_j, which have an explicit expression. In Fig. 2, we show the first terms of the sequence. We see that $\alpha_0 < 0$ and $\alpha_1 > 0$ are indeed the two unique real values, while the subsequent α_j are purely complex; the latter are well approximated by $\alpha_j \simeq 2\pi i j$ for large (possibly negative) j as the roots z_j converge to the unit circle $\exp(\frac{2\pi i j}{k-2})$. Therefore, for m sufficiently large, the contributions of the terms $j \geqslant m$ of Eq. (26) can be approximated by

$$\frac{2}{\mu}\Re\left[\sum_{j=m}^{\infty}\frac{\ln\left(1-\frac{1}{\alpha_j}\ln(S/S_0)\right)}{\alpha_j+1/\mu-1}\right]$$
$$\simeq -\frac{2\ln(S/S_0)}{(2\pi)^2\mu}\int_m^\infty \frac{1}{\alpha_j^2}dj \simeq \frac{2\ln(S/S_0)}{(2\pi)^2\mu}\frac{1}{m}, \quad (27)$$

in which we use that $\alpha_j + 1/\mu - 1 \simeq \alpha_j$ which is valid as long as $2\pi j \gg 1/\mu$, and which becomes quickly negligible as m increases if μ is not too small.

Further understanding of the qualitative behavior of the sum Eq. (26) can be obtained, noting that the effective reproduction number $R_{\text{eff}} = S/\mu$ has to be larger than 1 for the epidemic to propagate. One can therefore assume $\mu \in [0, 1]$ and S_0 in the interval $[\mu, 1]$. Thus, for μ not too far from 1 and using $\delta\mu = (1-\mu)$ as a small parameter, we can in any case assume $\delta S_0 = (1 - S_0) < \delta\mu$. In practice, however, we think of the initial time $t = 0$ as a situation where most agents are susceptible, only a very small fraction is infected, and nobody has recovered yet. In most of the concrete cases, and for essentially all the illustrations, we shall consider below $\delta S_0 \ll \delta\mu$, and we shall assume that at worse $\delta S_0 = O(\delta\mu^2)$. In that case, one can show (see Appendix A 3) that at all times $\delta S = (1 - S) = O(\delta\mu)$, implying also that $\ln(S_0/S) = O(\delta\mu)$.

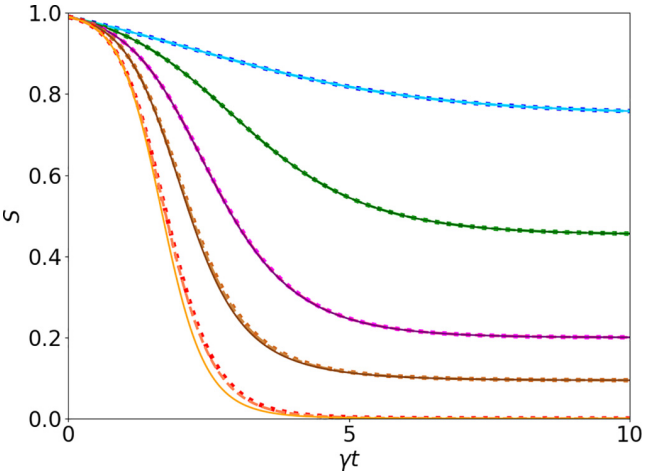

FIG. 3. Comparison of exact S (solid lines) with approximation Eq. (28) at first and second order in $\delta\mu = (1-\mu)$ (dotted and dashed lines respectively). $S_0 = 0.99$ is fixed and μ evolve from 0.1 to 0.9 : ($\mu = 0.1$, red), ($\mu = 0.3$, brown), ($\mu = 0.5$, magenta), ($\mu = 0.7$, green), ($\mu = 0.9$, blue). Although Eq. (28) is formally an expansion near $\mu = 1$, we see that its validity extends in practice in the whole range of μ, except in the neighborhood of 0.

Noting (cf. Appendix A) that at $\alpha_0(\mu=1) = \alpha_1(\mu=1) = 0$, when for $j \geqslant 2$ $\alpha_j^0 := \alpha_j(\mu=1) \neq 0$, this means that the contribution of the two first terms $j = 0, 1$ are $O(\delta\mu^0)$, when all the higher j contributions are $O(\delta\mu)$. We thus have

$$\beta t(S) = \frac{1}{\mu}\left[\sum_{j=0,1}\frac{\ln\left(1+\frac{1}{\alpha_j}\ln(S_0/S)\right)}{\alpha_j+1/\mu-1} - 2\mathcal{K}^{(0)}\ln(S_0/S) + O(\delta\mu^2)\right], \quad (28)$$

with $\mathcal{K}^{(0)} := \Re(\sum_{j=2}^{\infty}(\alpha_j^0)^{-2}) \simeq -0.028$ a, fairly small, pure number. As illustrated in Fig. 3, the approximation Eq. (28) is actually very accurate on a significant portion of the range $[0, 1]$, and this range can be even further extended by computing the $O(\delta\mu^2)$ correction to Eq. (28) (cf. Appendix A).

C. Epidemic peak time

As mentioned, an important quantity in the context of an epidemic breakout is the epidemic peak time, which, using the fact that, for SIR, the epidemic peak $dI/dt = 0$ implies

$S = \mu$, can be obtained as $t_{\rm peak} = t(S = \mu)$, and for which even a leading order approximation is presumably useful.

For μ sufficiently close to 1, this can be obtained starting from Eq. (28), neglecting the $-2\mathcal{K}^{(0)} \ln(S_0/S)$ correction, and evaluating α_0 and α_1 to leading order in $\delta\mu$. This calculation is performed in Appendix B, leading to Eq. (B1). From this we get

$$\beta t_{\rm peak} \simeq \frac{1}{p}\left[\ln\left(1 - \frac{\ln(S_0/\mu)}{\delta\mu - p}\right) - \ln\left(1 - \frac{\ln(S_0/\mu)}{\delta\mu + p}\right)\right], \tag{29}$$

with $p = \sqrt{2\delta S_0 + \delta\mu^2}$, valid for $\delta\mu = (1-\mu)$ small ($\delta S_0 = (1 - S_0) < \delta\mu$, and possibly $\ll \delta\mu$).

For μ a bit further away from 1, where this approximation starts to degrade, it turns out that a better approximation of $t_{\rm peak}$ can be obtained following the same approach but using the $\mu \to 0$ expansion of α_0 and α_1. We get (see Appendix B2)

$$\beta t_{\rm peak} \simeq \frac{1}{\mu}\left[\frac{\ln\left(1 - \frac{\ln(\mu/S_0)}{\chi + \chi^2 - 1/\mu}\right)}{\chi + \chi^2 - 1} + \frac{\ln\left(1 - \frac{\ln(\mu/S_0)}{(1-S_0)/(S_0-\mu)}\right)}{(1-S_0)/(S_0-\mu) + 1/\mu - 1}\right],$$
$$\chi = (S_0/\mu)e^{-1/\mu}. \tag{30}$$

An expansion for $\mu \ll 1$ can finally be obtained from the integral form of $t(S)$ given in [9], and leads to (cf. Appendix B1)

$$\beta t_{\rm peak} \simeq \ln\left(\frac{S_0}{1-S_0}\right) - \ln\mu - \mu\left(1 + \ln(1-S_0) - \frac{1}{2}\ln^2\frac{S_0}{\mu} - {\rm Li}_2(S_0)\right), \tag{31}$$

with Li_n the polylogarithm function.

In Fig. 4, we compare the predictions in Eqs. (29), (30), and (31) with the exact $\beta t_{\rm peak}$, demonstrating that, with $S_0 \geqslant 0.999$, the full range of $\mu \in [0, 1]$ is covered with these three regimes.

Equations (29), (30), and (31), corresponding respectively to large, intermediate, and small μ, provide explicit expressions and physical indications of how one can delay the epidemic peak in practice. Let us assume that the parameter γ which characterizes the rate of recovery from the illness is given by biological factors, and thus fixed, but that the transmission rate β can be modified by nonpharmaceutical interventions such as wearing masks or limiting contact between people. We thus assume that μ can be modified, but that this is done with $\beta\mu = \gamma$ constant.

First, we see in Fig. 4 that the curve $\beta t_{\rm peak}(\mu)$ is rather flat in the range $\mu \in [0.05, 0.5]$, implying that $t_{\rm peak}$ is essentially proportional to $1/\beta$ for $\mu < 0.5$. Then, different kinds of corrections appear in the different regimes. The most useful formula is presumably Eq. (30), which provides a compact and explicit analytical result (with only two terms), in a regime that corresponds to most of the practical use ($2 \leqslant R_0 \leqslant 5$).

As a practical example, starting with $S_0 = 0.99$ and applying restrictive measures to change $\mu = 0.25$ to $\mu = 0.5$ (which means changing R_0 from 4 to 2) would allow reducing $t_{\rm peak}$ by a factor of 2.25 according to Eq. (30), while the exact reduction factor is 2.18, with very similar absolute values. For $S_0 = 0.9$, this factor is only 1.61, according to Eq. (30), while the exact value is 1.57. We therefore have a precise indication about $t_{\rm peak}$ from a very simple expression, which does not require any knowledge of the Lambert function and does not involve the computation of an integral. This makes it possible to analyze qualitatively why early detection of the epidemic is important, as restrictive measures to delay the peak will be significantly less efficient for an epidemic that has already spread significantly in the population.

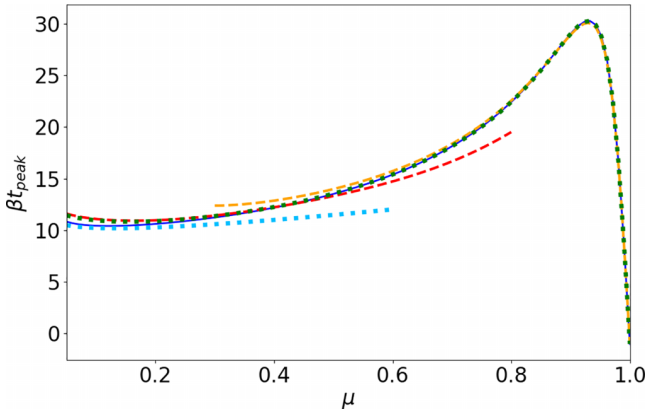

FIG. 4. Comparison of the exact $\beta t_{\rm peak}(\mu)$ (blue solid line) with different approximations, for a fixed $S_0 = 0.999$ and $\mu \in [0.05, 1]$. Cyan dotted line: approx. (31) which works at small μ. Red dashed line: approx. (30) which is rather valid for small and intermediate μ. Orange dashed line: approx. (29) for μ close to 1 and also for intermediate μ. Dotted green line: approximation obtained from Eq. (28) with $S = \mu$, which match the exact $t_{\rm peak}(\mu)$ extremely well except for very small μ's. The regimes of validity of the different approximations improve as $S_0 \to 1$, and would somewhat degrade as δS_0 increases.

V. CONCLUSION

In this work, we have derived Eqs. (2) and (3) for the SIR-k model, and obtained an exact implicit expression of $t(S)$ (11), valid for arbitrary k, as a finite sum over the roots z_j of the polynomial $P(z)$ (8).

It turns out that the main qualitative properties of the epidemic dynamics are governed by its two positive real roots (z_0, z_1). In particular, the proportion of agents infected during the total duration of the epidemic is given by $\mathcal{I}_{\rm tot}^{(k)} = S_0(1 - z_0^k)$, for which we have an explicit formula both for small and very large k. Taking $S_0 = 1$, i.e., assuming a negligibly small initial proportion of infected agents (for easier reading), we got $\mathcal{I}_{\rm tot}^{(3)} = 1 - (3\mu)^3$ for $k = 3$, while for the SIR model limit, we obtained $\mathcal{I}_{\rm tot}^{(\infty)} = 1 - \mu T_0(\chi) \simeq 1 - \mu\chi = 1 - e^{-1/\mu}$. Thus, for small μ (contagious diseases), the larger k, the more virulent the epidemic, as $\mathcal{I}_{\rm tot}^{(\infty)}$ will converge faster to 0 with $\mu \to 0$ than $\mathcal{I}_{\rm tot}^{(k)}$.

The values of the real roots (z_0, z_1) also affect the threshold value of μ for which, even for an infinitely small initial proportion of infected individuals, an epidemic starts to propagate

and affect a finite proportion of the agents. This threshold is given by the condition $z_0(\mu_k^*) = z_1(\mu_k^*) = 1$, leading to $\mu_k^* = (k-2)/k$. This value is lower than its counterpart for the basic SIR model $\mu_{\rm SIR}^* = \mu_\infty^* = 1$, which indicates that the propagation of epidemics is more difficult in the SIR-k model than in the basic SIR one, in agreement with the final epidemic size, which is also lower for the SIR-k model. This is in contrast with heterogeneous networks, for which an epidemic spreads more easily than in the SIR model.

In the cases $k = 2$ and $k = 3$ we got exact explicit expressions for $S(t)$. In the limit $k \to \infty$, we obtained new exact expressions for the original SIR model, which provides a new point a view, together with useful approximate results for this well-known problem. In particular, Eq. (28) and Fig. 3 demonstrate that for all values of μ except near 0, keeping only the contributions of the real α_j's, i.e., $j = 0, 1$, provide an excellent approximation of $t(S)$. Further approximation for the epidemic peak time Eqs. (29), (30), and (31) are shown in Fig. 4 to work extremely well numerically.

The SIR-k model on homogeneous networks presumably provides a good balance between an increase in complexity and an increase in effectiveness. It is characterized by only three parameters (S_0, μ, k) which, compared with the basic SIR, only adds the parameter k corresponding to the average number of possible contacts of individuals, a relatively accessible quantity in practice. Our SIR-k model is almost as simple as the basic SIR model. Indeed, it benefits from a simpler exact solution than the SIR, while numerical resolution remains fast and tractable (six equations instead of three). We therefore hope that our work will encourage institutions to consider using the SIR-k model in practice, instead of the basic SIR, especially as the two produce significantly different results when the number of neighbors is low, as shown in Fig. 1. Our results pave the way for the analytical study of more realistic social networks, such as heterogeneous networks with the small-world property [21,45].

APPENDIX A: THE $\mu \to 1$ REGIME FOR $t(S)$

We start by rewriting Eq. (26) as

$$\beta\, t(S) = \frac{1}{\mu}\sum_{j=0,1}\frac{1}{\alpha_j + 1/\mu - 1}\ln\left(1+\frac{\ln(S_0/S)}{\alpha_j}\right) + 2\Re\left[\frac{1}{\mu}\sum_{j=2}^{\infty}\frac{1}{\alpha_j + 1/\mu - 1}\ln\left(1+\frac{\ln(S_0/S)}{\alpha_j}\right)\right]. \tag{A1}$$

1. Contribution of the $j \geqslant 2$ to Eq. (A1)

Noting $\delta\mu = (1-\mu) \ll 1$ and $\delta S_0 = (1 - S_0) < \delta\mu$, one can show that for $j \geqslant 2$,

$$\alpha_j = -1 + \tau_j + \frac{\tau_j}{\tau_j - 1}\delta S_0 - \delta\mu + O(\delta\mu^2), \tag{A2}$$

with $\tau_j := T_{-j}(1/e) \neq 1, \forall j \geqslant 2$.

Therefore, for $j \geqslant 2$, $\ln(S_0/S)/\alpha_j = O(\delta\mu)$, and in Eq. (A1), we can expand the log as

$$\ln\left[1+\frac{\ln(S_0/S)}{\alpha_j}\right] = \frac{\ln(S_0/S)}{\alpha_j} - \frac{1}{2}\frac{\ln(S_0/S)^2}{\alpha_j^2}.$$

Together with Eq. (A2), this leads, for the contribution of the $j \geqslant 2$ to Eq. (A1), to

$$\frac{2}{\mu}\Re\sum_{j=2}^{\infty}\frac{1}{\alpha_j + 1/\mu - 1}\ln\left(1+\frac{\ln(S_0/S)}{\alpha_j}\right) = \frac{2\ln(S_0/S)}{\mu}[\mathcal{K}^0 + \delta\mu\mathcal{K}^\mu - \delta S_0\mathcal{K}^{S_0} - \ln(S_0/S)\mathcal{K}^{\ln} + O(\delta\mu^3)], \tag{A3}$$

with

$$\mathcal{K}^0 = \Re\sum_{j\geqslant 2}\frac{1}{(\tau_j-1)^2} \simeq -2.8\times 10^{-3}, \tag{A4}$$

$$\mathcal{K}^\mu = \Re\sum_{j\geqslant 2}\left[\frac{1}{(\tau_j-1)^2} + \frac{1}{(\tau_j-1)^3}\right] \simeq -3.0\times 10^{-3}, \tag{A5}$$

$$\mathcal{K}^{S_0} = \Re\sum_{j\geqslant 2}\frac{2\tau_j}{(\tau_j-1)^4} \simeq -3.8\times 10^{-3}, \tag{A6}$$

$$\mathcal{K}^{\ln} = \Re\sum_{j\geqslant 2}\frac{1}{2(\tau_j-1)^4} \simeq 7.7\times 10^{-5}. \tag{A7}$$

These dimensionless numbers are actually rather small, which explains the quality of the approximation (28) in a large range of $\delta\mu$. This is illustrated in Fig. 5.

2. Expansion for α_0 and α_1

For $z \to 1$, we have [41]

$$T_0(z) = 1 - p + O(p^2), \tag{A8}$$

$$T_{-1}(z) = 1 + p + O(p^2), \tag{A9}$$

with $p := \sqrt{2(1-ez)}$ and $z < 1/e$. With $z = \chi = (S_0/\mu)\exp(-1/\mu)$ (implying $z < 1/e$ since $S_0 < 1$ and the function $\frac{1}{\mu}e^{-1/\mu}$ increases over $[0, 1]$ from 0 to $1/e$), we have $ez \simeq 1 - \delta S_0 - \delta\mu^2/2$, and thus

$$p \simeq \sqrt{2\delta S_0 + \delta\mu^2}. \tag{A10}$$

With $\alpha_{0,1} = T_{0,-1}(\chi) - 1/\mu$, we eventually obtain

$$\alpha_0 = -p - \delta\mu, \quad \alpha_1 = +p - \delta\mu. \tag{A11}$$

3. Range of variation of $S(t)$

As t goes from O to ∞, S decreases monotonously from S_0 to $S_\infty = \mu T_0(\chi)$, which following the same reasoning as above, behaves for μ close to one as

$$S_\infty \simeq 1 - p - \delta\mu. \tag{A12}$$

If δS_0 and $\delta\mu$ are of similar magnitude, i.e., if $\delta S_0 = O(\delta\mu)$, this implies $\delta S_\infty = O(\sqrt{\delta\mu})$, which makes the discussion of the size of the neglected terms in Eqs. (28) and (29) somewhat more involved, without changing the main qualitative content

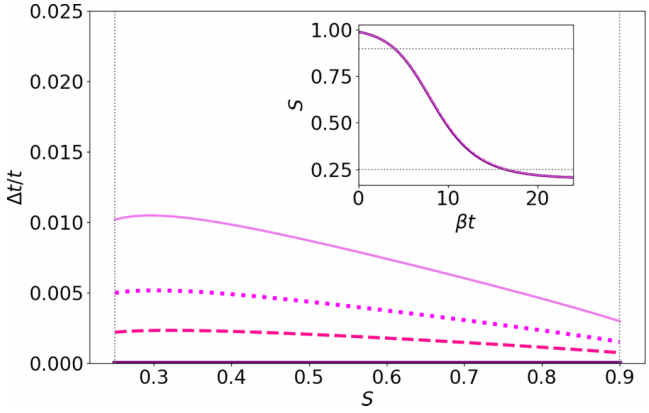

FIG. 5. Main panel: Time delay $\Delta t = t(S) - t_{\rm SIR}(S)$ with $t_{\rm SIR}$ obtained through analytical expression (26) which has been shown to be exact. Purple solid line: exact expression (26) as a reference. Magenta (Resp. pink) dotted (Resp. dashed) lines: first (Resp. second) order of Eq. (28). Violet solid line: expression (26) with the exact expression of the two real roots only. The gap between this last curve to the first (Resp. second) order curve shows the corresponding correction of these orders. Inset: proportion of susceptible S for the same configurations. The gray horizontal dotted lines indicate the range of S values taken for the main panel comparison (with corresponding vertical lines). Parameters are $\mu = 0.5$, $S_0 = 0.99$, corresponding to the third value of Fig. 3 which is near the standard values ($R_0 \simeq 2$). The discrepancy between the exact curve and the approximation (28) is at most of 0.5%, much lower than the uncertainty that one can expect from μ in practice.

of these equations. On the other hand, if one assumes, as is most of the time the case in practice, δS_0 significantly smaller than $\delta\mu$, and more specifically $\delta S_0 \leqslant O(\delta\mu^2)$, Eq. (A12) implies that $\delta S_\infty = O(\delta\mu)$, and thus $\ln(S_0/S) = O(\delta\mu)$ for all times. We have worked under this assumption in Secs. IV B and IV C and in the Appendixes A1 and B1.

APPENDIX B: EXPLICIT EXPRESSIONS FOR $t(S)$

1. Expansion near $\mu = 1$

With Eq. (A11), the leading order contribution to $t(S)$ as $\mu \to 1$ reads

$$\beta t(S) = \frac{1}{p}\left[\ln\left(1 - \frac{\ln(S_0/S)}{\delta\mu - p}\right) - \ln\left(1 - \frac{\ln(S_0/S)}{\delta\mu + p}\right)\right]. \tag{B1}$$

2. Expansion for intermediate μ

From Fig. 3, and from the discussion in Appendix A1, we see that even if this is formally justified from an expansion near $\mu = 1$, neglecting the contributions of the complex α_js ($j \geqslant 2$) is actually a rather accurate approximation in the whole range of μ except in a small neighborhood of 0. For reasonably small μ, the contribution of the two (remaining) real roots is then rather well described using the Taylor expansion of $T_0(\chi)$ (valid for $\chi \to 0$, thus $\mu \to 0$) given in [41]. We obtain $\alpha_0 \simeq \chi + \chi^2 - 1/\mu$ and $\alpha_1 \simeq (1 - S_0)/(S_0 - \mu)$, from which we get an explicit approximation of $t(S)$

$$\begin{aligned}\beta t(S) \simeq \frac{1}{\mu}\Bigg[&\frac{\ln\left(1 - \frac{\ln(S/S_0)}{\chi + \chi^2 - 1/\mu}\right)}{\chi + \chi^2 - 1} \\ &+ \frac{\ln\left(1 - \frac{\ln(S/S_0)}{(1-S_0)/(S_0-\mu)}\right)}{(1 - S_0)/(S_0 - \mu) + 1/\mu - 1}\Bigg], \\ \chi = (S_0/\mu)e^{-1/\mu}.&\end{aligned} \tag{B2}$$

Equation (B2), which has been derived assuming μ small (once the contribution of the α_j, $j \geqslant 2$ are neglected), is numerically accurate even for larger values of μ, as illustrated in Fig. 4 for $S_0 = 0.999$ and $\mu \in [0.2, 0.55]$.

3. Small μ expansion

For completeness, we provide here also the small μ expansion of $t_{\rm peak}$. Starting from the expression in [10], Eq. (10.22), the time $t_{\rm peak}$ for SIR is given (see the discussion below Eq. (10.37) and the one about time rescaling below Eq. (10.6)) by

$$t_{\rm peak} = \frac{\mu}{\gamma}\int_0^{\ln \mu/S_0} \frac{du}{S_0 e^u - \mu u - 1}. \tag{B3}$$

Changing variables to $v = e^u/\mu$ and expanding the integral gives

$$\begin{aligned} t_{\rm peak} &= \frac{\mu}{\gamma}\int_1^{\mu/S_0} \frac{dv}{v}\frac{1}{S_0 v - 1 - \mu \ln v} \\ &= \frac{\mu}{\gamma}\int_1^{\mu/S_0} \frac{dv}{v}\left(\frac{1}{S_0 v - 1} + \frac{\mu \ln v}{(S_0 v - 1)^2} + O(\mu^2)\right), \end{aligned} \tag{B4}$$

which upon integration gives at lowest order

$$\begin{aligned}\beta t_{\rm peak} = \Bigg[&\ln\left(\frac{S_0}{1 - S_0}\right) - \ln \mu \\ &- \mu\left(1 + \ln(1 - S_0) - \frac{1}{2}\ln^2\frac{S_0}{\mu} - {\rm Li}_2(S_0)\right)\Bigg],\end{aligned} \tag{B5}$$

with ${\rm Li}_n$ the polylogarithm function.

[1] A. A. Toda, Susceptible-infected-recovered (SIR) dynamics of Covid-19 and economic impact, Covid Economics(1), 43 (2020).

[2] J. D. Osofsky, H. J. Osofsky, and L. Y. Mamon, Psychological and social impact of Covid-19, Psychol. Trauma: Theory Res. Pract. Policy **12**, 468 (2020).

[3] W. O. Kermack and A. G. McKendrick, A contribution to the mathematical theory of epidemics, Proc. R. Soc. Lond. A **115**, 700 (1927).

[4] H. W. Hethcote, The mathematics of infectious diseases, SIAM Rev. **42**, 599 (2000).

[5] R. M. Anderson and R. M. May, *Infectious Diseases of Humans: Dynamics and Control* (Oxford University Press, Oxford, 1991).

[6] H. Salje, C. Tran Kiem, N. Lefrancq, N. Courtejoie, P. Bosetti, J. Paireau, A. Andronico, N. Hozé, J. Richet, C.-L. Dubost,

Estimating the burden of SARS-CoV-2 in France, Science **369**, 208 (2020).

[7] N. T. Bailey, *The Mathematical Theory of Infectious Diseases and its Applications* (Charles Griffin & Company Ltd, 5a Crendon Street, High Wycombe, Bucks HP13 6LE, 1975).

[8] D. G. Kendall, Deterministic and stochastic epidemics in closed populations, in *Proceedings of the Third Berkeley Symposium on Mathematical Statistics and Probability* (University of California Press, Berkeley, 1956), Vol. 4, pp. 149–165.

[9] T. Harko, F. S. Lobo, and M. Mak, Exact analytical solutions of the susceptible-infected-recovered (SIR) epidemic model and of the SIR model with equal death and birth rates, Appl. Math. Comput. **236**, 184 (2014).

[10] D. Prodanov, Analytical solutions and parameter estimation of the SIR epidemic model, Mathematical Analysis of Infectious Diseases 163 (2022).

[11] A. M. Carvalho and S. Gonçalves, An analytical solution for the Kermack–McKendrick model, Physica A **566**, 125659 (2021).

[12] H. Li and S. Guo, Dynamics of a SIRC epidemiological model, Electr. J. Differ. Equ. **2017**, 1 (2017).

[13] M. Y. Li, H. L. Smith, and L. Wang, Global dynamics of an SEIR epidemic model with vertical transmission, SIAM J. Appl. Math. **62**, 58 (2001).

[14] D. Sen and D. Sen, Use of a modified SIRD model to analyze Covid-19 data, Ind. Eng. Chem. Res. **60**, 4251 (2021).

[15] S. Gao, Z. Teng, J. J. Nieto, A. Torres, Analysis of an SIR epidemic model with pulse vaccination and distributed time delay, J. Biomed. Biotechnol. **2007**, 64870 (2007).

[16] G. Kozyreff, Asymptotic solutions of the SIR and SEIR models well above the epidemic threshold, IMA J. Appl. Math. **87**, 521 (2022).

[17] L. Fumanelli, M. Ajelli, P. Manfredi, A. Vespignani, and S. Merler, Inferring the structure of social contacts from demographic data in the analysis of infectious diseases spread, PLoS Comput. Biol. **8**, e1002673 (2012).

[18] D. Mistry, M. Litvinova, A. Pastore y Piontti, M. Chinazzi, L. Fumanelli, M. F. Gomes, S. A. Haque, Q.-H. Liu, K. Mu, X. Xiong, Inferring high-resolution human mixing patterns for disease modeling, Nat. Commun. **12**, 323 (2021).

[19] N. Ferguson, D. Laydon, G. Nedjati Gilani, N. Imai, K. Ainslie, M. Baguelin, S. Bhatia, A. Boonyasiri, Z. Cucunuba, G. Cuomo-Dannenburg *et al.*, Report 9: Impact of non-pharmaceutical interventions (NPIs) to reduce Covid-19 mortality and healthcare demand, Imperial College London COVID-19 (2020).

[20] L. Bremaud and D. Ullmo, Social structure description of epidemic propagation with a mean-field game paradigm, Phys. Rev. E **106**, L062301 (2022).

[21] D. J. Watts and S. H. Strogatz, Collective dynamics of 'small-world'networks, Nature (London) **393**, 440 (1998).

[22] F. C. Santos, J. F. Rodrigues, and J. M. Pacheco, Epidemic spreading and cooperation dynamics on homogeneous small-world networks, Phys. Rev. E **72**, 056128 (2005).

[23] D. H. Silva, F. A. Rodrigues, and S. C. Ferreira, High prevalence regimes in the pair-quenched mean-field theory for the susceptible-infected-susceptible model on networks, Phys. Rev. E **102**, 012313 (2020).

[24] S. Mizutaka, K. Mori, and T. Hasegawa, Synergistic epidemic spreading in correlated networks, Phys. Rev. E **106**, 034305 (2022).

[25] M. Barthélemy, A. Barrat, R. Pastor-Satorras, and A. Vespignani, Dynamical patterns of epidemic outbreaks in complex heterogeneous networks, J. Theor. Biol. **235**, 275 (2005).

[26] Y. Hu, L. Min, and Y. Kuang, Modeling the dynamics of epidemic spreading on homogenous and heterogeneous networks, Applicable Analysis **94**, 2308 (2015).

[27] F. D. Sahneh and C. Scoglio, Epidemic spread in human networks, in *2011 50th IEEE Conference on Decision and Control and European Control Conference* (IEEE, Orlando, FL, USA, 2011), pp. 3008–3013.

[28] M. E. Newman, Spread of epidemic disease on networks, Phys. Rev. E **66**, 016128 (2002).

[29] L. Di Domenico, Data-driven modeling of COVID-19 spread in France to inform pandemic response, Ph.D. thesis, Sorbonne Université, 2022.

[30] R. Pastor-Satorras, C. Castellano, P. Van Mieghem, and A. Vespignani, Epidemic processes in complex networks, Rev. Mod. Phys. **87**, 925 (2015).

[31] W. Wang, M. Tang, H. E. Stanley, and L. A. Braunstein, Unification of theoretical approaches for epidemic spreading on complex networks, Rep. Prog. Phys. **80**, 036603 (2017).

[32] Web of science citation report for the query "epidemic on networks", https://www-webofscience-com.inp.bib.cnrs.fr/wos/woscc/citation-report/e9511ae6-cc49-4efe-bd8d-41fc80a2ab17-caa9b524 (2024).

[33] L. J. Allen, An introduction to stochastic epidemic models, *Mathematical Epidemiology* (Springer, 2008), pp. 81–130.

[34] P. L. Simon and I. Z. Kiss, Super compact pairwise model for SIS epidemic on heterogeneous networks, J. Complex Netw. **4**, 187 (2016).

[35] M. J. Keeling, The effects of local spatial structure on epidemiological invasions, Proc. R. Soc. London B **266**, 859 (1999).

[36] N. C. Wormald, The asymptotic connectivity of labelled regular graphs, J. Comb. Theory, Ser. B **31**, 156 (1981).

[37] S. N. Dorogovtsev, A. V. Goltsev, J. F. Mendes, and A. N. Samukhin, Spectra of complex networks, Phys. Rev. E **68**, 046109 (2003).

[38] F. Goirand, B. Georgeot, O. Giraud, and S. Lorthois, Network community structure and resilience to localized damage: Application to brain microcirculation, Brain Multiphysics **2**, 100028 (2021).

[39] I. Z. Kiss, E. Kenah, and G. A. Rempała, Necessary and sufficient conditions for exact closures of epidemic equations on configuration model networks, J. Math. Biol. **87**, 36 (2023).

[40] J. H. Lambert, Observationes variae in mathesin puram, Acta Helvetica **3**, 128 (1758).

[41] R. M. Corless, G. H. Gonnet, D. E. Hare, D. J. Jeffrey, and D. E. Knuth, On the Lambert W function, Adv. Comput. Math. **5**, 329 (1996).

[42] L. Euler, De serie Lambertina plurimisque eius insignibus proprietatibus, Acta Academiae scientiarum imperialis petropolitanae 29 (1783).

[43] D. Belkić, All the trinomial roots, their powers and logarithms from the Lambert series, Bell polynomials and Fox-Wright function: Illustration for genome multiplicity in survival of irradiated cells, J. Math. Chem. **57**, 59 (2019).

[44] M. Glasser, Hypergeometric functions and the trinomial equation, J. Comput. Appl. Math. **118**, 169 (2000).

[45] A.-L. Barabási and R. Albert, Emergence of scaling in random networks, Science **286**, 509 (1999).

F - Mean-field game approach to epidemic propagation on networks

Mean-field game approach to epidemic propagation on networks

Louis Bremaud,[1] Olivier Giraud,[1,2,3] and Denis Ullmo[1]

[1] *Université Paris-Saclay, CNRS, LPTMS, 91405, Orsay, France*
[2] *MajuLab, CNRS–UCA-SU-NUS-NTU International Joint Research Laboratory, 17543 Singapore*
[3] *Centre for Quantum Technologies, National University of Singapore, 17543 Singapore, Singapore*

(Dated: January 27, 2025)

We investigate an SIR model of epidemic propagation on networks in the context of mean-field games. In a real epidemic, individuals adjust their behavior depending on the epidemic level and the impact it might have on them in the future. These individual behaviors in turn affect the epidemic dynamics. Mean-field games are a framework in which these retroaction effects can be captured. We derive dynamical equations for the epidemic quantities in terms of individual contact rates, and via mean-field approximations we obtain the Nash equilibrium associated with the minimization of a certain cost function. We first consider homogeneous networks, where all individuals have the same number of neighbors, and discuss how the individual behaviors are modified when that number is varied. We then investigate the case of a realistic heterogeneous network based on real data from a social contact network. Our results allow to assess the potential of such an approach for epidemic mitigation in real-world implementations.

Introduction

The lack of integration of dynamic human behavior into epidemic modeling remains a major limitation of contemporary epidemiological models [1–3] . Indeed, individual behavior creates a time-dependent feedback on the transmission rate that is often out of reach for epidemiologists. Relevant human behavioral dynamics can be separated into two primary categories. The first corresponds to behaviors independent of epidemics, driven by routine patterns such as day/night cycles, weekdays versus weekends, holidays, and other habitual activities. The second category includes adaptive responses triggered by the epidemic itself, where individuals adopt precautionary behaviors such as using masks, avoiding handshakes, or reducing contact to lower infection risks [4]. These adaptive behaviors may arise spontaneously or be prompted by specific non-pharmaceutical interventions, creating a feedback loop that can significantly influence the epidemic's trajectory. Despite evidence of its importance [5, 6], particularly highlighted by the Covid-19 pandemic [7], this "human-in-the-loop" factor is often not considered in predictive models, where the dynamics of human behavior is treated instead as an external parameter [2, 8] acting on the transmission rate.

To address this limitation, theoretical approaches have been developed, including models that incorporate parallel information spread [9, 10] or utilize payoff-based frameworks, as in Poletti's work [11]. In this study, we will focus on a recent and impactful approach: the Mean Field Game (MFG) paradigm. In short, MFGs are tools derived from game theory that enable to incorporate strategic interactions within systems involving a large number of agents. This game-theoretic framework makes it possible to account for anticipation effects arising from individuals optimizing intertemporal costs, and to describe "free-rider" behaviors, where individual optimization deviates from the collective societal optimum [4]. The solution associated with the MFG is referred to as a Nash equilibrium, meaning that no individual would benefit from modifying her strategy — that is, her behavior over the course of the epidemic — if the strategies of others remain unchanged. For a comprehensive mathematical introduction to MFG, see [12], and for applications of MFG to epidemiological modeling, see [13], and [8] for a recent review.

In this Letter we consider the propagation of an epidemic where contacts between individuals can be described by a network. In such an instance, the structure of the underlying contact network, including factors such as contact heterogeneity, correlations, clustering, and other forms of network organization, has been demonstrated to have an important influence on epidemic dynamics [14–19]. For instance, heterogeneity is known to significantly reduce the epidemic threshold on networks and to increase the propagation of the virus compared to a homogeneous network of the same average degree [16, 20]. Correlations between degrees, reflected by the assortativity [21] of the network and the clustering level [22], have also been shown to play a significant role in the propagation of epidemics.

On top of this network structure we implement a MFG framework. In the MFG approach, individuals are grouped into relevant classes to facilitate a mean-field treatment, requiring the identification of key factors driving individual behavioral responses. For instance in [23] the age-based social structure is considered, along with the contact location (e.g. schools, households, workplaces), recognizing that age significantly influences the risk of infection in many diseases, while different locations lead to distinct contact patterns. For epidemics on networks, we will make the basic assumption that individuals with the same number of neighbors behave in the same way.

The objective of this paper is to examine how individuals' spontaneous behavioral responses are shaped by network structure within a Susceptible-Infected-Recovered (SIR) model on networks. We begin by presenting a model that is grounded in the MFG approach. We then analyze the impact of network degree by examining Nash equilibrium outcomes on homogeneous networks. Finally, we demonstrate how heterogeneity and network correlations give rise to specific effects on realistic networks.

The MFG framework on networks

We consider a population of N individuals (N large), represented by nodes of a network. The possible contacts of an individual are the neighboring nodes on the network. The number of these contacts is called the degree of the individual, denoted k. The degree distribution is denoted by $P(k)$, and the two-point degree correlation matrix is represented by $G_{kk'} = P(k'|k)$, which is the conditional probability for a given node of degree k of having a neighbor of degree k'. Here we consider Markovian networks, defined by the fact that they are fully characterized by $P(k)$ and $G_{kk'}$ [24].

Each individual, or node of the network, can be in one of three possible states $x = s, i, r$ for, respectively, susceptible, infected and recovered. Contamination occurs via edges connecting a susceptible individual to an infected individual. The dynamics follows a standard Markov process : during the time interval $[t, t+dt[$, an edge between a susceptible and an infected individual transmits the disease with probability $\lambda(t)dt$. As in the basic SIR model, infected individuals recover from the disease during that time interval with probability γdt. In view of the mean-field treatment of the problem, we assume that nodes of a given degree and state are equivalent, which allows us to characterize the dynamics by the average quantities S_k, I_k, R_k giving the relative proportion of individuals of degree k in the state susceptible, infected or recovered at time t. Moreover, we make the degree pairwise approximation [25, 26], which posits that only correlations of degree and state between nearest neighbors on the network play a role in the dynamics. We thus introduce the conditional probability $G^{xy}_{kk'}$ for a given node to be of state y and degree k', knowing that this node has a neighbor of state x and degree k, a quantity which accounts for all pairwise correlations inside the network.

On top of the above SIR model, we implement a MFG setting in which individuals control their own contact rate via a control variable $n(t)$ which they can adjust. We assume that the transmission rate between individuals a and b is symmetric and given by $\lambda^{(0)} n_a(t) n_b(t)$, where $\lambda^{(0)}$ represents the baseline rate in the absence of an epidemic. We make the assumption (see [23] for discussion) that those infected individuals who are responsible for contamination are asymptomatic (otherwise they would isolate themselves after becoming ill), and therefore behave as susceptible. Therefore, only the control variable of susceptible (or infected asymptomatic) individuals matters, since the others are taken out of the game. Physically, $n_a(t)$, which we call the "effort parameter", represents the willingness of individual a to engage in risky interactions with her neighbors. In the absence of effort we have $n_a(t) = 1$, while the maximum effort corresponds to some fixed value $n_a(t) = \mathfrak{n}_{\min}$. In our mean-field framework, at the Nash equilibrium, the behavior of the agents only depends on their degree k, and one defines one control variable $n_k(t)$ for each degree. The effective transmission rate between individuals of degree k and k' is then given by $\lambda^{(0)} n_k(t) n_{k'}(t)$. Note that n_k is assumed to be independent of the neighbor's degree k'. While this assumption may overlook some practical circumstances, it simplifies both the analytical and numerical resolution of the model.

Epidemic dynamics. Considering now the dynamical equations describing our system, we introduce the following transition rates. We denote by $T^k_{x\to z} dt$ the probability for the state x of a node of degree k to change to state z in the time interval dt, and by $T^{kk'}_{(x,y)\to(x',y')} dt$ the probability for an edge of type (x, y) and degrees (k, k') to become of type (x', y'). As shown in the Supplemental Material [27], the only non-zero rates are

$$T^k_{i\to r} = \gamma \tag{1a}$$

$$T^k_{s\to i} = \lambda^{(0)} n_k(t)\, k \sum_{k'} n_{k'}(t) G^{si}_{kk'}(t) \tag{1b}$$

$$T^{kk'}_{(s,x)\to(i,x)} \simeq \lambda^{(0)} n_k(t) \Big[n_{k'}(t)\delta_{x,i} + (k-1) \sum_{k''} n_{k''}(t) G^{si}_{kk''}(t) \Big], \tag{1c}$$

where in Eq. (1c) we have used the pairwise approximation [25, 26]. The two terms in Eq. (1c) reflect the fact that contamination of a susceptible node along a susceptible-infected edge can come from the infected neighbor (Kronecker delta) or from the $(k-1)$ other neighbors of the susceptible node.

With these notations, the SIR system for each degree can be expressed as

$$\dot{S}_k(t) = -S_k(t) T^k_{s\to i} \tag{2a}$$

$$\dot{I}_k(t) = S_k(t) T^k_{s\to i} - I_k(t) T^k_{i\to r} \tag{2b}$$

$$\dot{R}_k(t) = I_k(t) T^k_{i\to r}\,. \tag{2c}$$

Within the pairwise approximation [25, 26], that is, neglecting three-point correlations (and beyond) which should appear in its evolution, the dynamics of $G^{si}_{kk'}$ is given (see Supplemental Material [27]) by the coupled

equations

$$\frac{d}{dt}(X_k G^{xy}_{kk'}) = \sum_{x'y'} X'_k\, G^{x'y'}_{kk'}\, T^{kk'}_{(x',y')\to(x,y)} - X_k\, G^{xy}_{kk'} \sum_{x'y'} T^{kk'}_{(x,y)\to(x',y')}\ , \tag{3}$$

where X_k denotes the relative proportion of agents of state x in the class k. The pairwise approximation has been shown to be very accurate on Markovian networks [28].

The system (1)–(3) forms the Kolmogorov system of our MFG. Given the set $\mathcal{S} = \{n_k(\cdot)\}_k$ of all collective strategies of degree-k individuals at all times, this system describes the evolution of all epidemic rates.

Individual optimization In the MFG setting, the $n_k(t)$ are given as the result of individual optimization of agents and depend themselves on the epidemic rates. In order to obtain the $n_k(t)$, we assume that individuals of degree k are sensitive to an intertemporal mean-field cost between the time t at which the optimization is performed and the end of the game at time T (assumed large). At time t, a representative *susceptible* individual a of degree k wishes to optimize the average cost [23, 29]

$$\mathfrak{C}\left(n_a(\cdot), \mathcal{S}, t\right) = \int_t^T \left[\lambda_a(\tau)\ r_I + f_k\left(n_a(\tau)\right)\right] P_a(\tau|t) d\tau\ , \tag{4}$$

in which we have introduced the force of infection perceived by individual a,

$$\lambda_a(\tau) = \lambda^{(0)} n_a(\tau) k \sum_{k'} n_{k'}(\tau) G^{si}_{kk'}(\tau)\ , \tag{5}$$

obtained in the same way as Eq. (1b), and $P_a(\tau|t) \equiv \exp\left[-\int_t^\tau \lambda_a(u)du\right]$ the probability for individual a of still being susceptible at time $\tau > t$, knowing that she is susceptible at time t. In (4), the cost function is the sum of a cost r_I, incurred in case of an infection, and a social cost f_k. Here we make the assumption that the infection cost r_I is independent of k (all individuals are equally affected by the disease), while the social cost of being deprived of contacts is likely to depend on the degree and hence is a function of k.

From an individual's perspective, the best strategy at time t is to tune her effort parameter $n_a(\tau), \tau > t$, in order to minimize her own foreseeable cost (4). Introducing the value function

$$U_a(t) = \begin{cases} \min\limits_{n_a(\cdot)} \mathfrak{C}\left(n_a(\cdot), \mathcal{S}, t\right), & a \text{ susceptible at } t \\ 0, & a \text{ infected/recovered at } t, \end{cases} \tag{6}$$

one can show, following the same reasoning as in [23], that

$$-\frac{dU_a}{dt} = \min_{n_a(t)} \left[\lambda_a(t)\left(r_I - U_a(t)\right) + f_k(n_a(t))\right]\ . \tag{7}$$

$(S_0, I_0, R_0) = (0.995, 0.005, 0), \quad \gamma = 1, \quad \lambda^{(0)}\langle k\rangle = 4$
$r_I = 50, \quad \mathfrak{n}_{\min} = 0.1$

TABLE I. Table of parameters used in our simulations. $\lambda^{(0)} = 4/\langle k\rangle$ allows to compare appropriately epidemics on different networks by rescaling the infection rate and keep a constant infection probability $\lambda^{(0)}\langle k\rangle$ on average.

This is a differential equation for which the final condition $U_a(T) = 0$ is fixed; it is known as the Hamilton-Jacobi-Bellman equation of the game. Finally, the MFG setting requires a consistency condition to be at a Nash equilibrium, namely that the optimal strategy $n^*_a(t)$ which minimizes the right-hand side of (7) should be the same as the one entering into the Kolmogorov system of equations (1)–(3) for individuals with the same degree. For any individual a of degree k one thus has

$$n^*_a(t) = n_k(t)\ . \tag{8}$$

Equations (1)–(3), together with Eqs. (7) and (8), form the MFG system of our game. We solve it numerically using a gradient descent approach (for details see [30]).

For all our simulations, the parameters characterizing the epidemics are the ones given in Table I. For the social cost function, we chose the specific form

$$f^\epsilon_k(n(t)) = k^\epsilon \left(\frac{1}{n(t)} - 1\right)\ , \quad \epsilon = 0, 1\ , \tag{9}$$

which allows us to explore different regimes of social dependence to neighbors. Physically, the choice $\epsilon = 1$ implies that a constant social cost of $(\frac{1}{n_a(t)} - 1)$ is assigned to each neighbor, which means that for a fixed fraction of contacts lost, an individual with a higher number of neighbors is more impacted than an individual with fewer neighbors. In the case $\epsilon = 0$ the social cost is the same for all individuals, whatever their degree.

Homogeneous networks

We first consider the simplest case of homogeneous networks (or regular graphs), where each node has the same number k of neighbors. After numerically solving the system of equations discussed above and reaching a Nash equilibrium, we obtain the epidemic rates and associated effort parameters. They are displayed in Fig. 1 for the two different possibilities $f^{0,1}_k$. Several observations can be made.

First, we observe in Fig. 1 that while individuals reduce their contact rate predominantly during the epidemic peak, their maximal effort occurs slightly after the peak is reached (see, for instance, the case $k = 4$ on the first row), and they maintain their effort well beyond the peak. This suggests that individuals engage in a form of

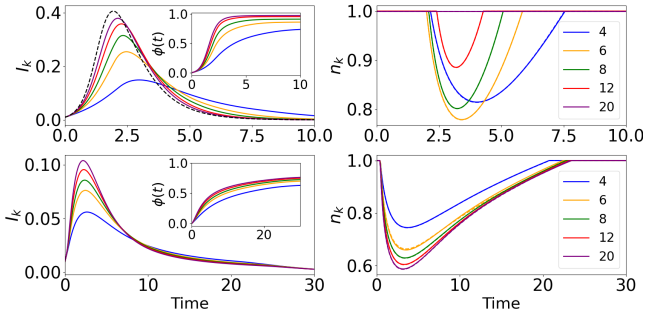

FIG. 1. Left column: Dynamics of infected individuals, corresponding to the Nash equilibrium, with the parameters of Table I for different homogeneous networks, with $k = 4$ (blue), 6 (orange), 8 (green), 12 (red), 20 (purple) and classical SIR model (black dashed); the social cost function is f_k^ϵ with $\epsilon = 1$ (top) and $\epsilon = 0$ (bottom). Inset: dynamics of the probability $\phi(t) = 1 - P(t|0)$ to be infected before t. Right column: Dynamics of the corresponding individual effort parameter, with the same parameters and color code as for the left column.

Intervals $[\tilde{k}_i, \tilde{k}_{i+1}[= [2,5[, [5,7[, [7,10[, [10,19[, [19,100]$					
Average $K_i = (3.2, 5.4, 7.8, 12.5, 31.2)$					
Distribution $\tilde{P}(K) = (0.26, 0.25, 0.22, 0.20, 0.07)$					
$G_{KK'} =$	0.76	0.03	0.04	0.06	0.11
	0.02	0.78	0.04	0.06	0.10
	0.02	0.03	0.79	0.06	0.10
	0.02	0.03	0.04	0.80	0.11
	0.03	0.06	0.07	0.11	0.72

TABLE II. Parameters characterizing the realistic heterogeneous network used for Fig. 2: the 5 batches $[\tilde{k}_i, \tilde{k}_{i+1}[$, the average degree K_i of the nodes in each interval, and the corresponding degree distribution $\tilde{P}(K)$ and correlation matrix $G_{KK'}$.

"reverse anticipation". More precisely, it is not the anticipation of the incoming epidemic that motivates their behavior, but the compound effect of the actual (present time) intensity of the epidemic and of the *anticipation of its end*. Indeed, at the onset of the epidemic, the prospect of maintaining a significant effort for the whole duration of the epidemic, while the latter is still growing slowly and individuals anticipate that collective immunity will not be reached anytime soon, appears more costly (with our choice of parameters) than paying the "one time" cost of infection. However, as collective immunity is in sight, shortly before the epidemic peak and for some time after, it becomes advantageous to make efforts to avoid infection, since the epidemic is still severe, and the remaining time before the epidemics is over is reasonably short. It then becomes advantageous for susceptible individuals to make significant efforts, as they have a good chance of avoiding infection forever if they protect themselves for a relatively short period.

While the mechanism described above is rather generic, the precise range and intensity at which it is at play of course depends on the choice of parameters. In particular, epidemics on random homogeneous networks progress faster and are more intense as k increases [29]. For constant f_k ($\epsilon = 0$, second row of Fig. 1), the ratios between social effort and infection cost remain essentially constant across degrees, and are fairly low for our choice of parameters. This leads to effort patterns that are similar across degrees, with individuals tending to protect themselves by "flattening" the infection curve $\phi(t)$, thereby minimizing their probability of infection. The only difference between classes is that individuals with higher degrees face more intense epidemics, requiring greater and more prolonged effort while maintaining the same overall pattern. On the other hand, when the social cost f_k increases with k ($\epsilon = 1$, first row of Fig. 1), this increasing social cost may compete with the one of the infection. As Fig. 1 shows, these two factors essentially balance each other around a critical value $k^* \simeq 6$, leading there to a significant intensity of efforts. However, below this threshold, the epidemic is not sufficiently virulent, and above k^* efforts becomes too costly to justify a strong reduction of social contact. As $k \to \infty$, individual behavior converges to the effortless parameter $n(t) = 1$, and the infection curve approaches that of the classical SIR model (see dashed curve in Fig. 1).

Heterogeneous networks

We now investigate the more realistic case of a heterogeneous network. SIR model on such networks is usually studied by considering a scale-free distribution $P(k)$ [20]. As the correlation matrix $G_{kk'}$ plays a crucial role in the MFG equations, we choose to investigate a realistic network constructed in the following way: We build $P(k)$ based on the work of Eubank *et al.* [31] and Béraud *et al.* [32]. We define it as a piecewise power-law distribution $P(k) \propto k^{\eta(k)}$ with $\eta(k) = 1$ for $k \in [2,5]$, -1.5 for $k \in [5,10]$, -3 for $k \in [10,100]$, which gives a maximum of around 5 contacts per day. We chose the above exponents $\eta(k)$ and intervals for k in such a way that the range of k, average, standard deviation and maximum of that distribution are consistent with [32]. In order to perform the numerical simulations in a reasonable time, we split our distribution $P(k)$ into batches containing approximately the same number of nodes. Namely, we consider that all nodes with degree $k \in [\tilde{k}_i, \tilde{k}_{i+1}[$ can be treated as nodes with degree K_i, with K_i the average degree of the nodes in that interval. Our choice for the batches is given in Table II. The quality of this approximation is demonstrated in Section II of the Supplemental Material [27].

For a given correlation matrix $G_{kk'}$, one can introduce an assortativity coefficient $r \in [-1,1]$, defined precisely in [21]. A positive r intuitively means that high-degree individuals will tend to have contacts with high-degree

individuals, and similarly for low-degree individuals. Social contact networks are known to be assortative, and here we choose r approximately equal to 0.3, compatible with the kind of networks described in [21]. Using the Newman rewiring algorithm [33], we obtain a matrix $G_{kk'}$ averaged over 10 networks of 20000 nodes with $r \simeq 0.3$.

The dynamics of the epidemics and the associated effort parameters at the Nash equilibrium are obtained by solving Eqs. (1)–(8). We assume that $G^{xy}_{kk'}(0) = X_k(0)G_{kk'}$, which indicates that there is no correlation between states and degrees at time $t = 0$. The results are displayed in Fig. 2 for the two different choices of f^ϵ_k. The specific impact of a realistic distribution, together with the interactions between classes (heterogeneity), can be captured. In all cases, we observe that, contrary to what might be expected, the spread, as a function of k, of the total number of infected at T (inset panel) increases compared to the homogeneous case. This is related to the collective immunity that is now achieved at the network level (and not for each degree class as in the homogeneous case). This essentially means that very high-degree individuals cannot really avoid the disease, since they are infected before all other classes. For them, applying a strong social distancing would only delay the infection peak, but would not lead to heard immunity. Then, the epidemic continues to spread in the network even though all high-degree individuals have been infected, since they represent a very small fraction of all nodes. On the other hand, low degree individuals take advantage of this situation and reach a collective immunity with a rate I_k below that required in the homogeneous case. In fact, more than the proportion of infected individuals among high-degree individuals, the average degree of the remaining susceptible nodes decreases rapidly, which helps achieve herd immunity.

Differences in infection rates result in infection curves that strongly depend on the degree. For $\epsilon = 1$ (Fig. 2, upper right panel), interactions between classes influence the competition between costs in a complex manner: the curve tails shorten with increasing degree, while effort levels decrease non-monotonically. In contrast, for $\epsilon = 0$ (Fig. 2, lower right panel), effort patterns become degree-specific in a more understandable way: high-degree individuals protect themselves, while low-degree individuals benefit from the collective immunity achieved by others more rapidly.

Conclusion

In the present Letter we studied the problem of epidemic propagation on networks from the point of view of mean-field games. This allowed us to analyze how individual behavior may affect the outcome of an epidemic when that behavior itself is modified at each time

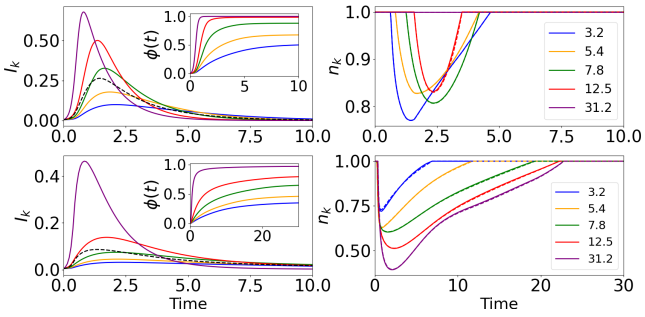

FIG. 2. Left panels: Dynamics of infected individuals at Nash equilibrium for different batches, with the parameters of Tables I and II. Inset: dynamics of the probability $\phi(t)$ to be infected before t. Right panels: Dynamics of the corresponding individual effort parameter. Colored solid lines corresponds to the dynamics (for infected and effort parameter) associated with each batch of the network: $K = 3.4$ (blue), 5.4 (orange), 7.8 (green), 12.5 (red), 31.2 (purple). Each row represents a specific choice of f^ϵ_k: $\epsilon = 1, 0$ for the first and second row, respectively.

by the epidemic. In our model, individuals can tune the intensity of the contacts they are willing to have with others (effort parameter) in order to optimize the cost that this choice will make them incur in the future. We showed that this interplay can be described by a Hamilton-Jacobi-Bellman system of equations for the individual costs and effort parameters, coupled with a set of Kolmogorov equations describing the epidemic dynamics.

Our MFG approach to networks highlights the "reverse anticipation" effect, where individuals adjust their behavior in anticipation of the end of the epidemic - a phenomenon likely to be observed in contexts other than networks. This anticipation can be brief, as in the case of increasing social costs with k, or have a long tail, as in the case of constant social costs, when efforts effectively reduce the probability of infection without being too costly. In the homogeneous case with $\epsilon = 1$, the model shows a balance between the increasing social cost with k and the higher epidemic costs experienced by individuals with high degrees, while a more homogeneous behavior is observed at $\epsilon = 0$. The introduction of heterogeneity and assortativity in a realistic network leads to differentiated collective immunity at the node level: low-degree individuals benefit from the fast spreading of the epidemic among high-degree individuals, which reduces the effective connectivity of the remaining susceptible network. Contrary to expectations, heterogeneity reduces costs for low-degree individuals, while positive assortativity weakens this protection, as it tends to reduce heterogeneity between classes.

In both cases, the role of the social cost f on the behavior of individuals is crucial, even though the only variations of f we considered were the ones associated with

its degree k. Our work underlines that a precise description of the behavior of f is a key element to go further in the practical implementation of MFG frameworks. This endeavor should benefit from the fact that the social cost properties should show little variation across epidemics, allowing large surveys to obtain the dependencies of f.

[1] A. Arenas, W. Cota, J. Gómez-Gardeñes, S. Gómez, C. Granell, J. T. Matamalas, D. Soriano-Paños, and B. Steinegger, Modeling the spatiotemporal epidemic spreading of covid-19 and the impact of mobility and social distancing interventions, Physical Review X **10**, 041055 (2020).

[2] H. Salje, C. Tran Kiem, N. Lefrancq, N. Courtejoie, P. Bosetti, J. Paireau, A. Andronico, N. Hozé, J. Richet, C.-L. Dubost, *et al.*, Estimating the burden of SARS-CoV-2 in France, Science **369** (2020).

[3] N. M. Ferguson, D. Laydon, G. Nedjati-Gilani, N. Imai, K. Ainslie, M. Baguelin, S. Bhatia, A. Boonyasiri, Z. Cucunubá, G. Cuomo-Dannenburg, *et al.*, *Report 9: Impact of non-pharmaceutical interventions (NPIs) to reduce COVID19 mortality and healthcare demand*, Vol. 16 (Imperial College London London, 2020).

[4] P. Poletti, *Human behavior in epidemic modelling*, Ph.D. thesis, University of Trento (2010).

[5] N. Ferguson, Capturing human behaviour, Nature **446**, 733 (2007).

[6] J. M. Epstein, Modelling to contain pandemics, Nature **460**, 687 (2009).

[7] B. Tang, W. Zhou, X. Wang, H. Wu, and Y. Xiao, Controlling multiple covid-19 epidemic waves: an insight from a multi-scale model linking the behaviour change dynamics to the disease transmission dynamics, Bulletin of Mathematical Biology **84**, 106 (2022).

[8] J. Guan, Y. Wei, Y. Zhao, and F. Chen, Modeling the transmission dynamics of Covid-19 epidemic: a systematic review, Journal of Biomedical Research **34** (2020).

[9] I. Z. Kiss, J. Cassell, M. Recker, and P. L. Simon, The impact of information transmission on epidemic outbreaks, Mathematical biosciences **225**, 1 (2010).

[10] X.-X. Zhan, C. Liu, G. Zhou, Z.-K. Zhang, G.-Q. Sun, J. J. Zhu, and Z. Jin, Coupling dynamics of epidemic spreading and information diffusion on complex networks, Applied Mathematics and Computation **332**, 437 (2018).

[11] P. Poletti, B. Caprile, M. Ajelli, A. Pugliese, and S. Merler, Spontaneous behavioural changes in response to epidemics, Journal of theoretical biology **260**, 31 (2009).

[12] J.-M. Lasry and P.-L. Lions, Mean field games, Japanese journal of mathematics **2** (2007).

[13] R. Elie, E. Hubert, and G. Turinici, Contact rate epidemic control of Covid-19: an equilibrium view, Mathematical Modelling of Natural Phenomena **15** (2020).

[14] D. J. Watts and S. H. Strogatz, Collective dynamics of 'small-world'networks, nature **393**, 440 (1998).

[15] F. C. Santos, J. F. Rodrigues, and J. M. Pacheco, Epidemic spreading and cooperation dynamics on homogeneous small-world networks, Phys. Rev. E **72**, 056128 (2005).

[16] M. Barthélemy, A. Barrat, R. Pastor-Satorras, and A. Vespignani, Dynamical patterns of epidemic outbreaks in complex heterogeneous networks, Journal of theoretical biology **235**, 275 (2005).

[17] Y. Hu, L. Min, and Y. Kuang, Modeling the dynamics of epidemic spreading on homogenous and heterogeneous networks, Applicable Analysis **94**, 2308 (2015).

[18] F. D. Sahneh and C. Scoglio, Epidemic spread in human networks, in *2011 50th IEEE Conference on Decision and Control and European Control Conference* (IEEE, 2011) pp. 3008–3013.

[19] M. E. Newman, Spread of epidemic disease on networks, Phys. Rev. E **66**, 016128 (2002).

[20] R. Pastor-Satorras, C. Castellano, P. Van Mieghem, and A. Vespignani, Epidemic processes in complex networks, Rev. Mod. Phys. **87**, 925 (2015).

[21] M. E. Newman, Mixing patterns in networks, Physical review E **67**, 026126 (2003).

[22] M. E. Newman, Random graphs with clustering, Physical review letters **103**, 058701 (2009).

[23] L. Bremaud, O. Giraud, and D. Ullmo, Mean-field-game approach to nonpharmaceutical interventions in a social-structure model of epidemics, Phys. Rev. E **110**, 064301 (2024).

[24] M. Boguná and R. Pastor-Satorras, Epidemic spreading in correlated complex networks, Physical Review E **66**, 047104 (2002).

[25] P. L. Simon and I. Z. Kiss, Super compact pairwise model for SIS epidemic on heterogeneous networks, J. Complex Netw. **4**, 187 (2016).

[26] M. J. Keeling, The effects of local spatial structure on epidemiological invasions, Proceedings of the Royal Society of London. Series B: Biological Sciences **266**, 859 (1999).

[27] See Supplemental Material at [URL will be inserted by publisher] for a derivation of the MFG equations and an assessment of the pairwise approximation.

[28] W. Wang, M. Tang, H. E. Stanley, and L. A. Braunstein, Unification of theoretical approaches for epidemic spreading on complex networks, Rep. Prog. Phys. **80**, 036603 (2017).

[29] L. Bremaud, O. Giraud, and D. Ullmo, Analytical solution of susceptible-infected-recovered models on homogeneous networks, Physical Review E **110**, 044307 (2024).

[30] L. Bremaud, *Mean Field Game description of virus propagation*, Ph.D. thesis, Université Paris-Saclay (2024).

[31] S. Eubank, H. Guclu, V. Anil Kumar, M. V. Marathe, A. Srinivasan, Z. Toroczkai, and N. Wang, Modelling disease outbreaks in realistic urban social networks, Nature **429**, 180 (2004).

[32] G. Béraud, S. Kazmercziak, P. Beutels, D. Levy-Bruhl, X. Lenne, N. Mielcarek, Y. Yazdanpanah, P.-Y. Boëlle, N. Hens, and B. Dervaux, The french connection: the first large population-based contact survey in france relevant for the spread of infectious diseases, PloS one **10**, e0133203 (2015).

[33] L. Di Lucchio and G. Modanese, Generation of scale-free assortative networks via newman rewiring for simulation of diffusion phenomena, Stats **7**, 220 (2024).

Supplemental Material: Mean-field game approach to epidemic propagation on networks

Louis Bremaud, Olivier Giraud, and Denis Ullmo

DERIVATION OF EQ. (1)-(3): DYNAMICS WITHIN THE PAIRWISE APPROXIMATION

Setting and definitions

In this Section, we provide a derivation of Eqs.(1)-(3) of the main text. Nodes are labeled with Greek letters $(\alpha, \beta, \cdots)$, and states $\{s, i, r\}$ with Roman letters $(x, y, x, \cdots)$. We denote by d_α the degree of node α, and by $A_{\alpha\beta}$ the adjacency matrix ($A_{\alpha\beta} = 1$ if there is an edge between α and β, and 0 otherwise). The state $x \in \{s, i, r\}$ of the node α at time t is denoted $c_t(\alpha)$; more generally $c_t(\alpha_1, \alpha_2, ...) = (x_1, x_2, ...)$ denotes the states x_i of nodes α_i at time t.

We introduce various sets characterizing the network:

Symbol	Definition	Description
$\mathbb{D}_k$	$\{\alpha \,/\, d_\alpha = k\}$	Nodes of degree k
$\mathbb{V}_\alpha$	$\{\beta \,/\, A_{\alpha\beta} = 1\}$	Neighbors of node α
$\mathbb{TD}_k$	$\{(\alpha,\beta) \,/\, \alpha \in \mathbb{D}_k \;\&\; \beta \in \mathbb{V}_\alpha\}$	Oriented edges starting from a node of degree k
$\mathbb{TD}_k^x$	$\{(\alpha,\beta) \,/\, \alpha \in \mathbb{D}_k \;\&\; \beta \in \mathbb{V}_\alpha\}$	Oriented edges starting from a node of degree k and state x
$\mathbb{E}_{kk'}$	$\{(\alpha,\beta) \,/\, \alpha \in \mathbb{D}_k \;\&\; \beta \in \mathbb{D}_{k'} \;\&\; A_{\alpha\beta} = 1\}$	Oriented edges between nodes of degree k and k'
$\mathbb{W}(k \overset{k'}{\underset{k''}{\rightrightarrows}})$	$\{(\alpha,\beta,\gamma) \in \mathbb{D}_k \times \mathbb{D}_{k'} \times \mathbb{D}_{k''} \,/\, \beta, \gamma \in V_\alpha\}$	Oriented wedges of degrees (k, k', k'')

Note that in the definition of $\mathbb{W}(k \overset{k'}{\underset{k''}{\rightrightarrows}})$, the two edges are oriented but also the wedge itself, i.e. the ordering of the two edges matters.

We furthermore introduce sets that characterize the epidemic status of nodes on the network:

Symbol	Definition	Description
$\mathbb{G}_k^x$	$\{\alpha \in \mathbb{D}_k \,/\, c_t(\alpha) = x\}$	Nodes of degree k and state x
$\mathbb{G}_{kk'}^{xy}$	$\{(\alpha,\beta) \in \mathbb{E}_{kk'} \,/\, c_t(\alpha,\beta) = (x,y)\}$	Oriented edges linking a node of degree k and state x to a node of degree k' and state y
$\mathbb{G}_{kk'k''}^{xyz}$	$\{(\alpha,\beta,\gamma) \in \mathbb{W}(k \overset{k'}{\underset{k''}{\rightrightarrows}}) \,/\, c_t(\alpha,\beta,\gamma) = (x,y,z)\}$	Wedges with given status and degree

The number of elements of a set $\mathbb{S}$ will be denoted by $\#\mathbb{S}$. In particular, we have $\#\mathbb{D}_k = N_k$, $\#\mathbb{TD}_k = kN_k$, and $\#\mathbb{TD}_k^x = kN_kX_k$.

Correlation matrices and transition rates

One-point, two-point and three-point correlators

With the above notation, the relative proportions $X_k = S_k, I_k, R_k$ of individuals of degree k in the state susceptible, infected or recovered is given by

$$X_k = \frac{\#\mathbb{G}_k^x}{N_k}, \tag{1}$$

which is a one-point correlator.

In the same way the two-point correlations between adjacent nodes are given by

$$G^{xy}_{kk'} \equiv \frac{\#\mathbb{G}^{xy}_{kk'}}{\#\mathbb{TD}^{x}_{k}} = \frac{\#\mathbb{G}^{xy}_{kk'}}{kN_kX_k} \, . \tag{2}$$

By symmetry $(\#\mathbb{G}^{xy}_{kk'}) = (\#\mathbb{G}^{yx}_{k'k})$, and thus we recover the detailed balance condition $kN_kX_kG^{xy}_{kk'} = k'N_{k'}Y_{k'}G^{yx}_{k'k}$.

Finally, the three points correlation matrix can be derived from the number of elements of the set $\mathbb{G}^{xyz}_{kk'k''}$, which we shall discuss in Section below.

Bare transition rates

The two processes that can lead to a transition between states on the network are processes transforming nodes and processes transforming edges. In the SIR model, during a time interval $[t, t+dt[$, a node has some probability to go from state i to r, and an edge connecting a node s and a node i has some probability to become an edge connecting i to i.

Consider a node α in the state x. We note $\Lambda^{x'}_{x}$ the rate of transformation of α at time t from state x to state x' *which is not due to any interaction with its neighbors.* For the SIR model, the only such bare process corresponds to the recovery process, where a node i transforms into r, and thus the only nonzero rate is

$$\Lambda^{r}_{i} = \gamma \, . \tag{3}$$

Similarly, consider an undirected edge between node α of state x and degree k and node β of state y and degree k'. We denote $\Lambda^{x'y'}_{xy}$ the rate of transformation at time t from state xy to state $x'y'$ which is due *only to the interaction between α and β.* For the SIR model, the only such bare process corresponds to an edge si transforming into ii. In the case of the SIR on networks considered in the main text, the only non-zero rate reads

$$\Lambda^{ii}_{si} = \lambda_{kk'}(t) = \lambda(0) n_k n_{k'} \, . \tag{4}$$

There is an important distinction to make between directed and undirected edges. The sets defined in Section count directed edges; this accounts for the fact that a node whose state is modified by the transformation of an edge can potentially sit at either ends of that edge. However, the above rates apply to undirected edges. Note also that the above rates depend on k and k'; to ease the reading we have omitted this dependency in the notation.

Dressed transition rate for the one-point correlators

In order to determine the time evolution of the correlators, we need to calculate their rate of change taking into account all possible processes (single-node events, events involving nearest neighbors, and so on), which we call *dressed* transition rates.

Let $\mathbb{T}^{k}_{(x;t)\to(x';t+dt)} = \{\alpha \in \mathbb{D}_k \, / \, c_t(\alpha)=(x) \,\&\, c_{t+dt}(\alpha)=(x')\}$ be the set of nodes of degree k that change their state from x to x' during the time interval $[t, t+dt[$. The corresponding transition rate $T^{k}_{x\to x'}$, defined by

$$\#\mathbb{T}^{k}_{(x;t)\to(x';t+dt)} = (\#\mathbb{G}^{x}_{k}) \, T^{k}_{x\to x'} dt \, , \tag{5}$$

gives the transition probability of a node of degree k from x to x' during dt. Neglecting contributions of order $(dt)^2$ (i.e. the probability of two independent events happening during the interval dt), a node is modified either by a single-node event (for SIR, the node transition $i \to r$), or by the transition of an indicent edge (for SIR, the edge transition $si \to ii$). Summing the corresponding probabilities, we have

$$\left(\#\mathbb{T}^{k}_{(x;t)\to(x';t+dt)}\right) = (\#\mathbb{G}^{x}_{k}) \, \Lambda^{x'}_{x} dt + \sum_{k';y,y'} (\#\mathbb{G}^{xy}_{kk'}) \, \Lambda^{x'y'}_{xy} dt \, , \tag{6}$$

Dividing both sides of (6) by $(\#\mathbb{G}^{x}_{k})dt$ and using Eq. (2), we get

$$T^{k}_{x\to x'} = \Lambda^{x'}_{x} + k \sum_{k';y,y'} G^{xy}_{kk'} \Lambda^{x'y'}_{xy} \, . \tag{7}$$

For our SIR model on networks, this reduces to $T^{k}_{i\to r} = \Lambda^{r}_{i} = \gamma$, and $T^{k}_{s\to i} = k \sum_{k'} \lambda_{kk'}(t) G^{si}_{kk'}$, which is exactly Eqs. (1a)–(1b) of the main text.

Dressed transition rates for the two-point correlator

To describe the time evolution of the $G^{xy}_{kk'}$, we need to additionally take into account the probability that an edge between two nodes α and β change due to processes that involves nodes other than α or β, but to which α or β are linked. We thus introduce the sets of directed edges going from state xy to state $x'y'$ between t and $t+dt$,

$$\mathbb{T}^{kk'}_{(x,y;t)\to(x',y';t+dt)} \equiv \{(\alpha,\beta)\in\mathbb{E}_{kk'} \;/\; c_t(\alpha,\beta)=(x,y)\,\&\,c_{t+dt}(\alpha,\beta)=(x',y')\} \tag{8}$$

and we define the corresponding dressed transition rates $T^{kk'}_{(x,y)\to(x',y')}$ as

$$\left(\#\mathbb{T}^{kk'}_{(x,y;t)\to(x',y';t+dt)}\right) = (\#\mathbb{G}^{xy}_{kk'})\,T^{kk'}_{(x,y)\to(x',y')}dt\;. \tag{9}$$

Neglecting again terms of order $(dt)^2$ (i.e. the probability of two independent simultaneous processes), we get the following contributions:

1. $(x\neq x')$ and $(y\neq y')$. The only process transforming two connected nodes is the process transforming the edge that connects them:

$$\left(\#\mathbb{T}^{kk'}_{(x,y;t)\to(x',y';t+dt)}\right) = (\#\mathbb{G}^{xy}_{kk'})\,\Lambda^{x'y'}_{xy}\,dt. \tag{10}$$

2. $(x\neq x')$ and $(y=y')$. The processes involved are the transformation of the edge $\alpha-\beta$ or of the node α alone, as well as the transformation of an edge connecting α with any of its other neighbors:

$$\left(\#\mathbb{T}^{kk'}_{(x,y;t)\to(x',y;t+dt)}\right) = (\#\mathbb{G}^{xy}_{kk'})\left[\Lambda^{x'y}_{xy}+\Lambda^{x'}_{x}\right]dt + \sum_{k''zz'}(\#\mathbb{G}^{xyz}_{kk'k''})\,\Lambda^{x'z'}_{xz}\,dt \tag{11}$$

3. $(x=x')$ and $(y\neq y')$. Symmetrically, as in (11) we have

$$\left(\#\mathbb{T}^{kk'}_{(x,y;t)\to(x,y';t+dt)}\right) = (\#\mathbb{G}^{xy}_{kk'})\left[\Lambda^{xy'}_{xy}+\Lambda^{y'}_{y}\right]dt + \sum_{k''zz'}(\#\mathbb{G}^{yxz}_{k'kk''})\,\Lambda^{y'z'}_{yz}\,dt\;. \tag{12}$$

Summing up all these contributions, we get

$$T^{kk'}_{(x,y)\to(x',y')} = \Lambda^{x'y'}_{xy} + \delta_{yy'}\left[\Lambda^{x'}_{x} + \sum_{k''zz'}\frac{(\#\mathbb{G}^{xyz}_{kk'k''})}{(\#\mathbb{G}^{xy}_{kk'})}\Lambda^{x'z'}_{xz}\right] + \delta_{xx'}\left[\Lambda^{y'}_{y} + \sum_{k''zz'}\frac{(\#\mathbb{G}^{yxz}_{k'kk''})}{(\#\mathbb{G}^{yx}_{k'k})}\Lambda^{y'z'}_{yz}\right]\;. \tag{13}$$

For our SIR model on networks, this leads for instance to

$$T^{kk'}_{(s,i)\to(i,i)} = \lambda_{kk'}(t) + \sum_{k''}\lambda_{kk''}(t)\frac{\left(\#\mathbb{G}^{sii}_{kk'k''}\right)}{\left(\#\mathbb{G}^{si}_{kk'}\right)}\;. \tag{14}$$

The Pairwise Approximation

As always, we need the $(\#\mathbb{G}^{xy}_{kk'})$ to compute the evolution of the $(\#\mathbb{G}^{x}_{k})$, but we need the $(\#\mathbb{G}^{xyz}_{kk'k''})$ to compute the evolution of the $(\#\mathbb{G}^{xy}_{kk'})$. We can move forward if we assume that the three-body correlations are negligible. For Markovian networks, loops are rare, in the sense that the probability that a given node α belongs to a loop of (fixed) finite length L goes to zero as the size of the network goes to infinity, and therefore this is a very good approximation. Within this (pairwise) approximation, given a node α, the degree and state of two of its neighbors β and γ are uncorrelated, so that the joint probability of having β of degree k' and state y and γ of degree k'' and state z is essentially the product of the two probabilities $G^{xy}_{kk'}$ and $G^{xz}_{kk''}$. More precisely, we get

$$(\#\mathbb{G}^{xyz}_{kk'k''}) \simeq \underbrace{N_kX_k}_{\#\mathbb{G}^{x}_{k}}\;\underbrace{k}_{\#\text{ of }\beta}\;\overbrace{G^{xy}_{kk'}}^{\text{conditional proba}}\;\underbrace{(k-1)}_{\#\text{ of }\gamma}\;\overbrace{G^{xz}_{kk''}}^{\text{conditional proba}}\;, \tag{15}$$

The coefficient $k(k-1)$ in (15) corresponds to the choice of the two neighbors of node α, taking into account the fact that not only the edges but also the wedges are oriented (see Section). From Eq. (2) we have $\#\mathbb{G}^{xy}_{kk'} = G^{xy}_{kk'} k N_k X_k = k' N_{k'} X_{k'} G^{yx}_{k'k}$, hence

$$T^{kk'}_{(x,y)\to(x',y')} = \Lambda^{x'y'}_{xy} + \delta_{yy'}\left[\Lambda^{x'}_{x} + \sum_{k''zz'}(k-1)G^{xz}_{kk''}\Lambda^{x'z'}_{xz}\right] + \delta_{xx'}\left[\Lambda^{y'}_{y} + \sum_{k''zz'}(k'-1)G^{yz}_{k'k''}\Lambda^{y'z'}_{yz}\right] . \tag{16}$$

For our SIR model on networks, this gives in particular

$$T^{kk'}_{(s,x)\to(i,x)} = \lambda_{kk'}\,\delta_{x,i} + (k-1)\sum_{k''}\lambda_{kk''}G^{si}_{kk''} , \tag{17}$$

which is Eq. (1c) of the main text.

Getting to Eqs. (2)–(3) of the main text

Equations (2) of the main text are a direct consequence of the definition of the one-point dressed rates $T^{k}_{x\to x'}$. Indeed,

$$(\#\mathbb{G}^{x}_{k})(t+dt) - (\#\mathbb{G}^{x}_{k})(t) = \sum_{x'\neq x}\mathbb{T}^{k}_{(x';t)\to(x;t+dt)} - \sum_{x'\neq x}\mathbb{T}^{k}_{(x;t)\to(x';t+dt)} , \tag{18}$$

which dividing both sides by $N_k dt$ gives

$$\dot{X}_k = \sum_{x'}\left(X'_k T^{k}_{x'\to x} - X_k T^{k}_{x\to x'}\right) . \tag{19}$$

Since for the SIR model the only non-zero one-point dressed rate are $T^{k}_{s\to i}$ and $T^{k}_{i\to r}$, this readily gives Eq. (2).

In the same way,

$$(\#\dot{\mathbb{G}}^{xy}_{kk'})dt = \sum_{(x'y')\neq(x,y)}\left(\#\mathbb{T}^{kk'}_{(x',y';t)\to(x,y;t+dt)} - \#\mathbb{T}^{kk'}_{(x,y;t)\to(x',y';t+dt)}\right)$$

and thus, removing the constant factor $kN_k dt$ which appears on both sides, we get

$$\frac{d}{dt}(X_k G^{xy}_{kk'}) = \sum_{(x'y')\neq(x,y)}\left(X'_k\, G^{x'y'}_{kk'}\, T^{kk'}_{(x',y')\to(x,y)} - X_k\, G^{xy}_{kk'} T^{kk'}_{(x,y)\to(x',y')}\right) , \tag{20}$$

which is Eq. (3) of the main text.

VALIDITY OF OUR BATCHING PROCEDURE WITH THE PAIRWISE APPROXIMATION

The pairwise approximation described above, combined with the batching procedure applied with 5 bins in the main text, provides a highly accurate representation of the network dynamics we aim to reproduce. This is illustrated in Fig. 1. The small discrepancies observed do not significantly affect the general observations or the conclusions drawn regarding the Nash equilibrium on such networks.

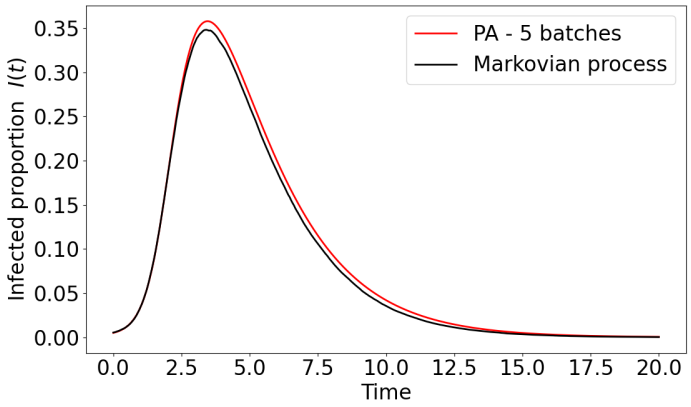

FIG. 1. Evolution of total infected proportion over time on a heterogeneous network. Red line: results provided by the pairwise approximation (PA) and batching procedure (5 batches) applied to the realistic heterogeneous network utilized in the second part of the main text. Black line: average Markovian process over $n_{\text{it}} = 10$ iterations, with $N = 15\,000$ nodes. Parameters of the epidemic are $\beta = 4, \gamma = 1, I_0 = 5.10^{-3}$.

G - Synthèse en Français

Le facteur humain est un paramètre significatif des propagations d'épidémie, à la fois à travers les réponses spontanées des individus face à l'épidémie et les mesures restrictives mises en place par les autorités. Ces effets comportementaux créent une boucle de rétroaction qui influence à son tour l'évolution de l'épidémie. Cependant, la plupart des modèles actuels utilisés pour les prévisions épidémiques ne prennent pas en compte ce facteur humain dans la boucle, le traitant plutôt comme un paramètre externe. Dans cette thèse, nous étudions le paradigme des jeux à champ moyen (Mean-Field Game, MFG), qui offre un cadre prometteur pour intégrer le comportement humain dans les modèles épidémiques. Notre objectif est de progressivement combler l'écart entre cette approche théorique et de potentielles utilisations pratiques. Concrètement, cela consiste en deux étapes : implémenter le cadre des MFG dans des modèles épidémiologiques utilisés aujourd'hui, et évaluer la pertinence d'une éventuelle application pratique : les comportements prédits par le modèle sont-ils cohérents avec ceux attendus ? Quels types de questions pouvons-nous adresser en pratique ? Quels sont les paramètres clés qu'il s'agira d'évaluer correctement ?

G.1 Introduction aux modèles épidémiologiques

Le Chapitre 1 présente une introduction aux modèles épidémiologiques. Nous commençons par construire pas à pas le célèbre modèle SIR (susceptible-infected-recover) pour susceptible-infecté-rétabli introduit par Kermack et McKendrick il y a environ 100 ans en 1927 [175]. Ce modèle intègre un nombre de paramètres minimal pour modéliser l'évolution temporelle des épidémies : les individus sont classés dans un des 3 états possibles mentionnés (S pour susceptible, I pour infecté, R pour rétabli). La transition de l'état susceptible à l'état infecté est donné par un taux de transmission, qui va correspondre phyiquement à la propention du virus à se propager rapidement entre les personnes, incluant donc la contagiosité de chaque contact et la fréquence de ces derniers, tandis que la transition de l'état infecté à l'état rétabli se fait via un taux de guérison. Ce modèle très simple a connu un grand succès au cours du 20ème sciècle et a permis de démontrer la notion de taux de reproduction R_0 de l'épidémie : l'épidémie s'accroît lorsque R_0 est supérieur à 1 et diminue sinon. Cependant, le modèle SIR adopte de nombreuses approximations qui limitent son utilisation en pratique. Les épidémiologistes actuels se sont donc dirigés vers des modèles plus complexes. Trois grandes familles de modèles ont émergé : les modèles compartimentaux, similaires au modèle SIR, qui intègrent à présent tout une structure sociale : les individus sont catégorisés selon leur âge et éventuellement leur ville de résidence, et leur état est caractérisé de façon bien plus précise avec de nombreux compartiments (vaccinés, asymptomatiques, etc). Ces modèles utilisent les bases de données actuelles sur les populations pour fournir des prédictions les plus précises possibles. Le modèle spatio-temporel d'Alex Arenas *et al.* [40] pour le Covid-19 en Espagne est présenté en illustration. Le second type de modèle concerne les modèles sur réseaux qui décrivent les individus au niveau individuel en les modélisant comme des noeuds du réseau, tandis que les liens correspondent aux contacts possibles. Différents type de réseaux ont été introduits, d'abord homogènes avec les réseaux d'Erdos-Rényi [63] en 1960, puis hétérogènes avec les réseaux dits sans échelle (scale-free) de Albert et Barabsi [67] et les "petits-mondes" (small-worlds) par Watts et Strogatz [42]. Ces réseaux sont de plus en plus utilisés et étudiés avec l'arrivée de large base de données, notamment dans l'objectif de prédire en pratique l'évolution des

épidémies, alors qu'ils ont longtemps été principalement l'objet d'études théoriques. Enfin, les modèles dits à "base agent" permettent de simuler au niveau microscopique une population synthétique composée d'un grand nombre d'agents. Les actions et les contacts de ces derniers sont modélisés par des règles simples, et le calcul de leur état à chaque instant permet de faire émerger l'épidémie au niveau de la société. Ces modèles à base agent ont connu un fort essort récemment avec l'arrivée d'ordinateurs plus puissants permettant des simulations plus importantes, ils ont notamment été utilisés pendant le Covid-19 par Ferguson et son équipe en Angleterre [17].

Cependant, ces différents types de modèles prennent rarement en compte l'évolution du comportement humain en dans leurs simulations. Plus précisément, ce dernier influence l'épidémie de deux façons différentes. Premièrement, une partie de cette évolution est prévisible et est dû aux variations temporelles habituelles (semaine versus week-end, vacances), elle a été très étudiée et est parfois prise en compte. La seconde concerne la réaction des individus à l'épidémie, c'est à dire le fait qu'ils vont adapter leur comportement si celle-ci présente un danger : réduire certaines activités, ne plus se serrer la main, porter le masque, appliquer la distanciation sociale ou encore se faire vacciner. Si une partie de ce comportement peut être induit par les authorités, il s'agit aussi surtout d'actions personnelles que chacun appliquera plus ou moins, alors que cela peut avoir une importance significative sur l'épidémie [93, 94, 102]. Plusieurs modèles différents ont été proposé récemment pour inclure ces comportements dans les modèles épidémiques [98, 108, 115], avec comme objectif de rendre ce facteur humain *intrinsèque* au modèle : l'idée est que ce comportement (dépendant de l'épidémie et donc du temps) puisse être estimé théoriquement à partir de paramètres fixes comme le risque associé à une infection. Cela permet d'éviter d'avoir à utiliser ou à estimer des paramètres comme celui-ci de façon *extrinsèque* au modèle à partir de base de données réelles. Il est en effet très difficile d'estimer des paramètres qui sont dépendants du temps comme le taux de transmission sans réaliser une anticipation particulière sur l'épidemie ou le comportement des individus.

Dans cette thèse, nous nous concentrerons sur un type de modélisation permettant de prendre en compte le facteur humain : les jeux à champ moyen (Mean-Field Games, MFG). Par rapport aux autres, les MFG permettent aux individus de réaliser leur propre optimisation à partir du coût qu'ils considèrent par rapport à l'épidémie (risque d'infection versus coût de réduction des contacts). Cette optimisation sera différente selon les individus et permettra de faire émerger une dynamique globale. En particulier, les MFG permettent de prendre en compte l'anticipation des individus, qui optimisent leur coût sur le long terme (l'anticipation peut être modulée). Les MFG permettent surtout de faire apparaître la différence intrinsèque entre optimisation individuelle et collective : si tous les individus restent chez eux, alors n'importe quel individu aura intérêt à sortir de chez lui, étant donné qu'il n'y aura plus de risque lié à l'infection. Ce phénomène que l'on retrouve dans de nombreux aspects de notre société est particulièrement à l'oeuvre ici et explique pourquoi des contraintes collectives sont parfois nécessaires pour venir à bout de l'épidemie.

G.2 Introduction aux jeux à champ moyen

Le Chapitre 2 est dédié à la mise en place du cadre mathématique de la théorie des jeux puis des jeux à champ moyen. Nous utilisons l'exemple connu du dilemme du prisonnier pour illustrer le type de comportement que nous souhaitons modéliser, cette situation ce décrit de la façon suivante. Deux individus A et B sont poursuivis pour avoir commis un délit. Ils sont intérrogés séparémments et ont le choix de trahir leur collègue ou de rester silencieux. Suivant les choix effectués par A et B, différentes issues du jeu sont possibles, elles sont présentées dans la figure G.1. Le raisonnement tenu par A est le suivant : si B

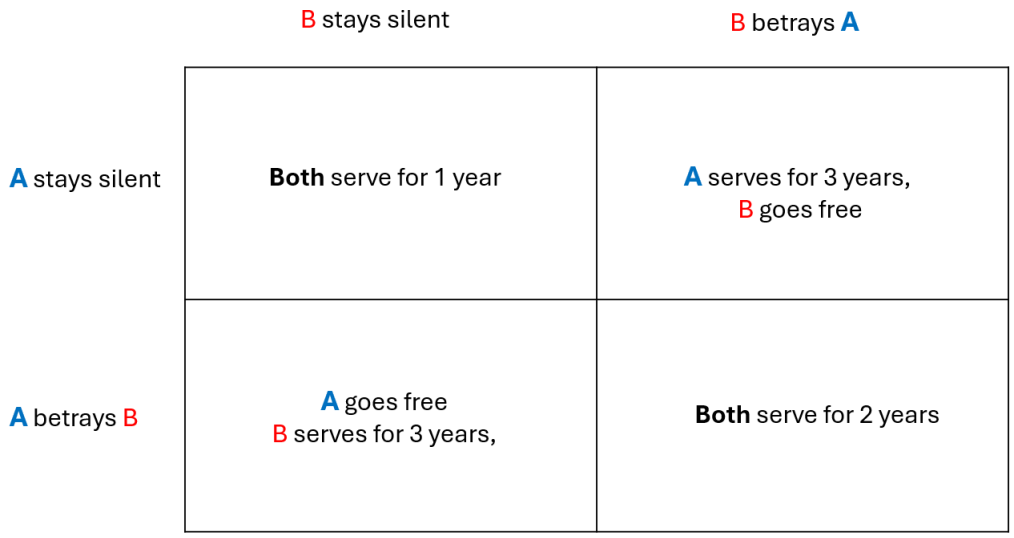

Figure G.1: Issues possibles du dilemme du prisonnier. Chaque individu à deux choix : trahir (betray) ou rester silencieux (stay silent). La situation est symmétique pour A et B et ils ne peuvent pas communiquer ou connaître le choix de l'autre avant de prendre leur décision.

choisi de me trahir, alors j'ai intérêt à trahir également pour limiter ma peine à 2 ans (au lieu d'en avoir 3 en restant silencieux). Si B choisi de rester silencieux, alors j'ai également intérêt à trahir, et cette fois je serai directement libre, plutôt que d'avoir une peine d'un an. Quelque soit le choix de B, A a intérêt à trahir B s'il agit pour son propre intérêt, et B arrive à la même conclusion de façon symmétrique. Ainsi, l'équilibre de Nash résultant du jeu est une situation où les deux joueurs trahissent l'autre. Cet équilibre est dit "de Nash" si aucun des joueurs n'a intérêt à changer de stratégie une fois qu'il connaît la stratégie des autres joueurs (c'est pourquoi nous parlons d'équilibre), et c'est le cas ici. Cette situation peut paraître contre-intuitive, car les deux joueurs auraient visiblement un intérêt personnel à rester silencieux tous les deux, ce qui permettrait de réduire leur peine par deux. Cette stratégie qui optimise le coût payé par l'ensemble des joueurs est appelée "optimum sociétal". Ici, ce sont les mécanismes liés à l'optimisation individuelle (et égoïste) qui empêche d'arriver à une solution qui serait pourtant souhaitable pour tous.

Une fois introduit de façon heuristique, les concepts d'équilibre de Nash et d'optimum sociétal sont décrits mathématiquement, puis les jeux à champ moyen (MFG) sont présentés. Cette méthode développée notamment par les mathématiciens JM Lasy et PL Lion il y a une vingtaine d'années [140, 142] permet de résoudre le problème d'optimisation des individus lorsque leur nombre devient très élevé. L'idée est de dire que chaque individu sera sensible au comportement moyen des autres, et non au comportement individuel de chacun, comme l'individu A peut l'être par rapport à celui de B dans le dilemme du Prisonnier. Cette hypothèse, en réalité assez naturelle dans le contexte des épidémies (cela revient à considérer que les individus sont sensibles au nombre total d'infectés dans la population), permet de considérablement réduire le nombre d'équations complées à résoudre et d'obtenir un système numériquement résoluble composée de deux équations couplées : l'équation d'Hamilton Jacobi Bellaman (HJB) décrivant l'optimisation des individus, et l'équation dite de Fokker-Plank qui décrit l'évolution du système. Pour terminer ce chapitre, nous présentons l'application des MFG au modèle SIR qui a été proposée par Elie *et al.* [19] récemment. Leur idée est que chaque agent considère deux coûts : un coût fixe lorsque celui-ci est infecté, et un coût variable dépendant de son taux d'effort pour réduire son taux de transmission, et donc sa probabilité d'être infecté. Toutefois, si ce modèle des MFG sur le modèle SIR permet de faire une preuve de concept au niveau théorique, il ne

permet pas encore d'envisager des applications pratiques.

G.3 Une approche basée sur les jeux à champ moyen pour évaluer et construire les interventions non pharmaceutiques dans un modèle SIR muni d'une structure sociale.

Pour évaluer la possibilité d'appliquer en pratique les MFG, nous étendons ce travail à un modèle compartimental plus structuré et bien plus proche des modèles utilisés actuellement dans le Chapitre 3. La structure sociale que nous utilisons est présenté dans la figure G.2 : nous considérons différentes classes d'âges (nous en prenons 3 pour l'exemple étudié) et les individus ont des contacts qui vont différer selon les lieux de contact : à l'école les enfants auront des contacts entre eux, au travail les adultes seront entre eux, tandis qu'il y aura plus de mixité entre les différentes classes d'âge au sein des foyers ou lors d'activités sociales. De plus, nous proposons une certaine façon de modéliser le contact entre les individus, présentée dans la figure G.3. Celle-ci est basée sur l'idée que le contact doit être symmétrique et dépendre de la "volonté de contact" de chaque individu. Cette volonté, propre à chaque individu, permet de moduler les contacts entre les classes d'âges qui seront décrits à la base (sans épidémie) par une matrice de contacts (décrivant les fréquences de contacts de chaque classe dans chaque lieu). Ainsi lors de l'épidémie les volontés de contacts (comprises entre 0 et 1) sont ajoutées en facteur de cette matrice. La première partie de ce chapitre se conclut par l'implémentation mathématique de la partie MFG qui est ajoutée en sur la structure sociale : chaque individu va pouvoir choisir son taux de contact dans chaque lieu. A l'équilibre, nous aurons besoin de considérer que les individus de chaque classe se comporteront de façon très similaire, d'où l'importance d'avoir différentes classes pour tenir compte de l'hétérogénité des comportements au sein de la population. En effet, notamment parce que toutes les catégories sociales n'ont pas les mêmes contacts mais surtout parce qu'elles n'ont pas le même coût associé à une infection (nous augmentons ce coût avec l'âge ici), les individus de chaque classe vont réaliser une optimisation différente.

Dans la seconde partie du chapitre, nous réalisons une expérience numérique pour

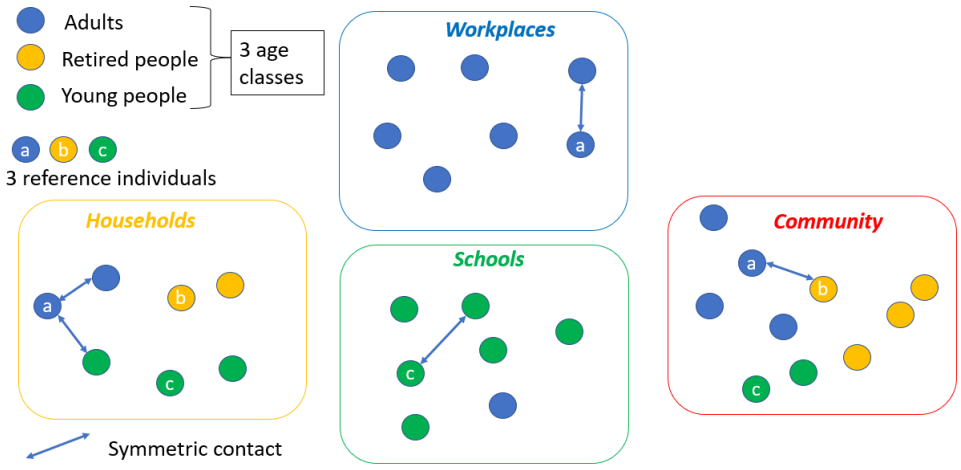

Figure G.2: Illustration de la structure sociale implémentée. Un individu de réfééerence pour chaque classe d'âge est pris (a, b et c), ils ont des contacts symmétriques dans chacun de slieux possibles avec différents type de contact à chaque fois (contacts entre adultes sur les lieux de travail, entre enfants à l'école, etc).

observer le comportement de notre modèle. Les paramètres liés à la structure sociale (population dans chaque classe, nombre de contacts,...) ou à la biologie de l'épidémie (contagiosité, taux de guérison,...) sont déterminés à partir de plusieurs travaux [17, 40, 41] afin de les rendre réalistes. Les paramètres liés à la fonction de coût optimisée par les individus sont eux choisis de façon plus intuitive et seront modifiés au cours de nos simulations pour observeur leurs effets sur les comportements des individus. L'idée de cette approche est d'observer les comportements qui pourraient être prédits par le modèle dans une application pratique, afin de vérifier leur cohérence. Cela permet également de pouvoir travailler sur les différents équilibres résultants en addressant des questions qui ne seront pas spécifiques à un cas particulier du modèle mais qui auront une portée plus générale et propre au cadre proposé. Nous étudions ainsi différents scénarios : la situation où personne ne fait d'effort, l'équipe de Nash libre, l'optimum sociétal mais également un équilibre de Nash contraint. Avec ce dernier, nous expliquons comment des interventions non pharmaceutiques (NPIs), c'est à dire des contraintes sur les taux de contacts des individus, peuvent être construites et imposées à la population pour obtenir une meilleure solution sociétale que l'équilibre de Nash libre qui résulte de l'optimisation égoïste des individus. Ainsi, nous proposons un modèle pour ces contraintes, composé de 3 paramètres, que nous optimisons pour arriver à un nouvel équilibre de Nash, illustré sur la figure G.4, dont le coût sociétal sera plus bas (mais toujours plus élevé que l'optimum sociétal). Sur cette figure, nous observons que les contraintes (lignes droites) sont respectées par les jeunes mais que les adultes et surtout les personnes agées sont parfois amenées à faire plus d'efforts que ceux qui sont requis. Nous comparons cette solution à l'optimum sociétal qui est obtenu lorsque tous les individus sont coordonnés par une entité dont le but est d'optimiser le coût sociétal, qui correspond ici à la somme des coût individuels. Cet optimum sociétal nous permet de nous rendre compte de la coopération qui apparaît entre les classes, avec des jeunes qui font des efforts pendant le pic épidémique, afin de réduire le risque pour les personnes âgées, alors qu'eux n'ont pas d'intérêt à le faire. Ce scénario

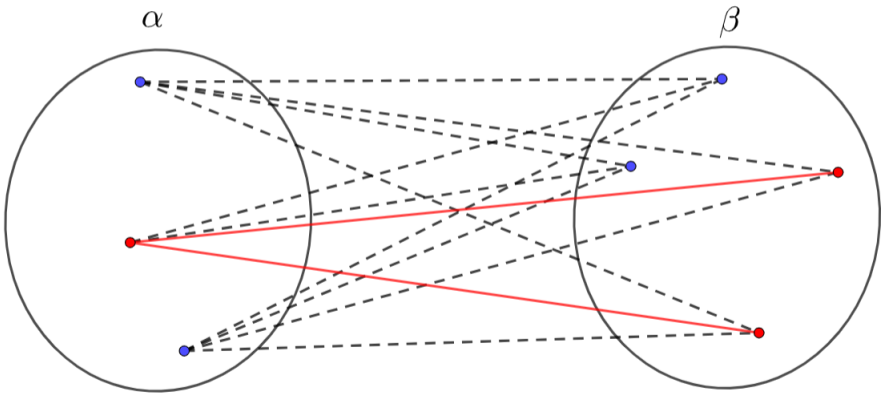

Figure G.3: Illustration des interactions au sein de notre modèle. Deux classes d'âge α et β sont reprentées avec respectivement 3 et 4 individus. Chaque individu (ou noeud) est actif (en rouge) s'il souhaite avoir des contacts avec l'autre classe. Ce souhait correspondra en fait à la volonté de contact de l'individu : si sa volonté est au maximum (1), alors il sera toujours activé, mais si celle-ci est de 0.5 il sera activié la moitié du temps. Les individus en bleus sont inactifs. Tous les contacts possibles sont indiquées par les traits en pointillés, mais les seuls contacts effectifs se font entre les pairs d'individus actifs, où les traits sont marqués en traint plein rouge. Ici, nous avons un individu actif de la classe α et 2 de la classe β, ce qui conduit à 2 contacts parmi les 12 possibles. Cette modélisation permet ensuite d'obtenir facilement les bonnes quantités dont nous aurons besoin dans nos équations.

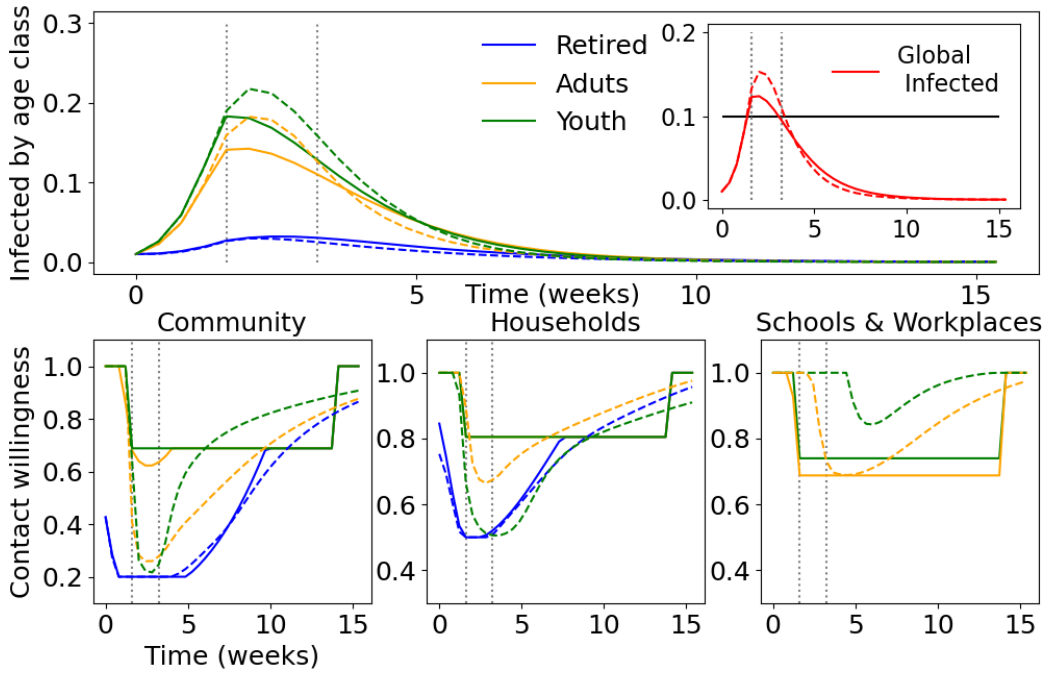

Figure G.4: Evolution des quantités épidémiques et des volontés de contact pour l'optimum sociétal (ligne pointillée) et l'équilibre de Nash avec des contraintes optimales (ligne en trait plein). Panel haut : évolution de la proportion d'infectés par classe d'age (panel principal) et en moyenne (insert). Panels du bas de gauche à droite : évolution de la volonté de contact pour chacune des classes d'âge dans la communauté, les foyers, dans les écoles et les lieux de travail. Les lignes pointillées correspondent à la période où les services sanitaires sont saturés ce qui fait augmenter le coût lié à l'épidémie.

correspond à une situation idéaliste qui ne peut pas être atteinte en pratique, car elle ne donne aucune liberté aux individus, mais elle permet de comprendre comment construire les contraintes pour s'en rapprocher.

Dans la dernière partie de ce chapitre, nous étendons l'étude de la stratégie collective à la possibilité pour une autorité (typiquement étatique) d'avoir recours à d'autres stratégies collectives gloables que celle étudiée jusqu'ici où la population n'avait pas d'autre choix que d'atteindre l'immunité collective pour sortir de l'épidémie. Cette immunité collective correspond au point où la population n'a plus assez d'individus "sains", susceptbiles d'être infectés, pour que l'épidémie puisse se propager. Ainsi, les stratégies qui consistent à contenir ou à éradiquer l'épidemie n'étaient pas envisageables, nous les intègrons ici dans notre discussion. Nous montrons sur la figure G.5 que différents régimes apparaissent entre ces différentes stratégies collectives, avec en réalité des transition discountinues (dites du premier ordre) concernant les comportements optimaux suivis par les individus. Ces différents régimes dépendent du temps d'optimisation choisi, c'est à dire de la fin attendue de l'épidémie et du coût lié à l'infection. Ce temps final ancitipé a un effet très important que nous pouvons comprendre intuitivement : si une épidémie virulente apparaît mais que des vaccins seront disponibles après 6 mois de façon quasi certaine (ou qu'il s'agit d'un virus saisonnier), alors il peut devenir intéressant de contenir l'épidémie pendant cette période, plutôt que de la laisser atteindre une large partie de la population. La stratégie d'éradication, quant à elle, demande des efforts bien plus importants et demande un déclenchement des contraintes tôt dans l'épidémie pour que ces efforts ne durent pas trop longtemps avant que l'épidémie ne disparaisse. Elle devient intéressante lorsque l'épidémie est à la fois dangereuse et qu'aucune fin à court terme ne semble envisageable. Ainsi, l'approche que nous proposons permet de quantifier ces différents aspects. De plus,

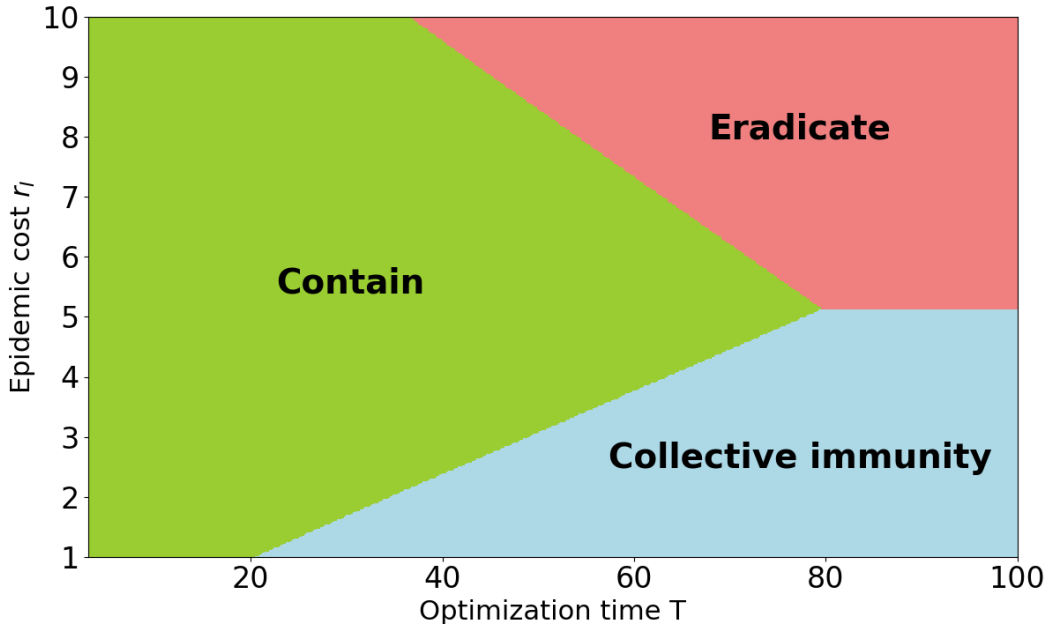

Figure G.5: Diagramme de phase montrant le meilleur choix de stratégie collective parmi : "atteindre l'immunité collective" (en bleu), "contenir l'épidémie" (en vert), et "éradiquer l'épidémie" (en rouge) avec les paramètres des tables 3.2-3.3 ainsi que ceux défini dans la figure originale 3.14.

l'équilibre de Nash proposé semble être une stratégie pertinente pour évaluer le coût réel associé à l'immunité collective, là où le coût lié à l'épidémie serait sûrestimé en gardant la stratégie "de ne pas faire d'effort" et sous estimé avec l'optimum sociétal. Cette dernière partie conclut ce premier projet qui a conduit à la publication d'une lettre (article court) dans PRE et à la rédaction d'un article plus long (soumis).

G.4 Propagation des épidémies sur réseaux avec une approche de jeux à champ moyen

Après avoir exploré l'implémentation des MFG dans un modèle compartimental avec une structure sociale, nous nous intéressons dans le Chapitre 4 à l'implémentation de ces derniers dans les modèles sur réseaux. Nous nous intéressons à des réseaux qui peuvent être hétérogènes (et plus précisément sans-échelle), c'est à dire qu'un certain nombre d'individus auront beaucoup plus de contacts que les autres, permettant ainsi l'apparition de "super-contaminateurs" qui accélèrent la propagation sur le réseau. Sur ce dernier, l'épidémie est simulée à l'aide d'un processus de Markov, c'est à dire que chaque individu a une certaine probabilité d'être infecté qui dépend de l'état de ses voisins. Hors, pour des réseaux de grande taille et dont on ne connait pas la stucture exacte, il devient rapidement très difficile de réaliser de telles simulations de l'épidémie, d'autant plus si nous souhaitons implémenter le paradigme des MFG qui nécessitera des calculs supplémentaires. Ainsi, la première partie du chapitre est dédiée aux différentes approximations que l'on peut faire sur les réseaux, en se basant sur la littérature existante [72]. Nous partons de l'approximation de champ moyen "pur", correspondant au modèle SIR, puis nous levons progressivement certaines hypothèses. Ainsi, le champ moyen "hétérogène" est proposé, en classant les noeuds du réseau suivant leur degré, c'est à dire leur nombre de voisins. Nous arrivons à l'approximation dite "par paire", dont nous dérivons les équations d'évolution associées à l'aide d'une autre approche que celle traditionnellement utilisée dans la littérature [196,

194]. Cette approximation prend en compte les correlations existantes entre deux voisins sur le réseau. Par corrélation, on entend ici le fait que la probabilité pour un individu d'avoir un voisin infecté va dépendre à la fois de son nombre de voisins (son degré), mais également de son état (susceptible ou infecté). De façon plus intuitive, et c'est ce que prend en compte cette approximation par rapport aux autres, la probabilité d'avoir un voisin infecté pour un individu susceptible à un instant donné sera plus faible que la moyenne, car cela signifiera que ce voisin ne doit pas lui avoir transmis la maladie jusqu'à cet instant. A l'inverse, si l'individu est infecté, cette probabilité sera plus élevé car ce voisin aura une plus grande probabilité d'avoir soit transmis la maladie à l'individu infecté, soit d'avoir été lui même infecté par l'individu en question. Ces correlations affectent la dynamique de l'épidémie sur le réseau et doivent être prises en compte dans les calculs permettant d'évaluer l'évolution du nombre total d'infectés sur le réseau. Les simulations

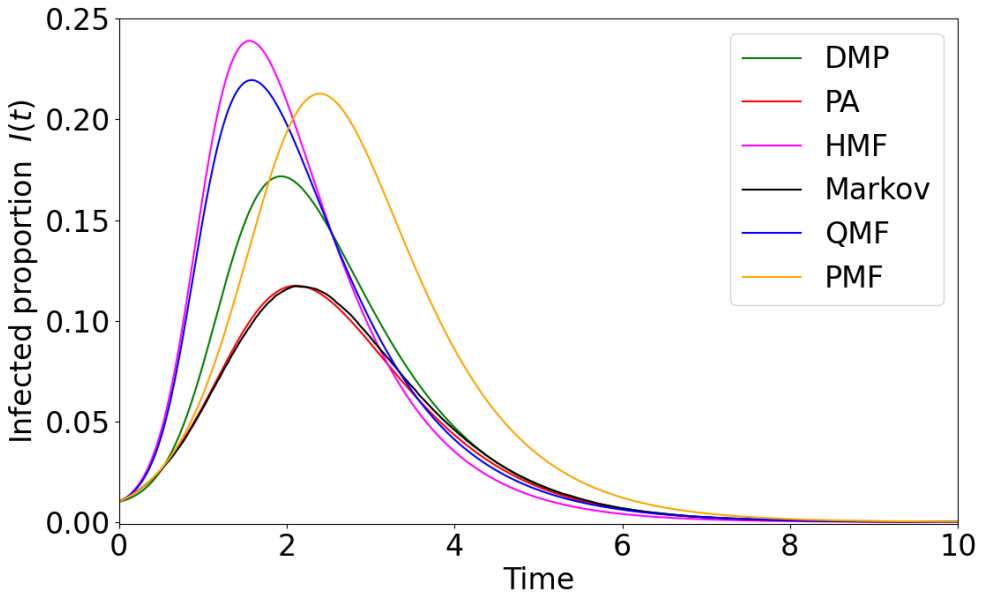

Figure G.6: Comparaison des différentes approximations avec la "vraie" courbe simulée (ligne noire) à l'aide d'un processus de Markov sur un réseau hétérogène aléatoire, avec une moyenne sur de nombreuses réalisations de l'épidémie. Nous avons pris un réseau de 3000 noeuds et 200 itérations différentes pour faire la simulation. Les approches PMF (Pure Mean Field), QMF (Quench Mean Field) et HMF (Heterogeneous Mean Field) respectivement en orange bleu et violet surestiment clairement le nombre d'infectés, car elles considèrent qu'un voisin d'un individu susecptible a une probabilité $I(t)$ d'être infecté (la moyenne), alors qu'elle est en réalité plus faible à cause des corrélations. L'approche DMP (Dynamical Message Passing) en vert permet d'avoir une meilleure approximation car elle prend en compte que l'individu susceptible ne peut pas avoir infecté son propre voisin. Finalement la Pairwise Approximation (apprximation par paires, PA) a une très bonne précision. Les autres paramètres utilisés sont précisés dans la figure 4.3.

de ces différentes approximations sur un réseau sans échelle hétérogène sont présentées sur la figure G.6, où l'approximation par paire (notée PA, courbe rouge) est clairement celle qui est la plus proche des observations simulées (courbe noire).

Dans une seconde partie, nous implémentons la méthode des MFG en proposant une approche possible sur réseau, avec une fonction coût et une description des contacts similaires au Chapitre 3. En revanche ici nous allons faire varier le coût lié à la réduction des contacts plutôt que le coût lié à l'infection, pour observer les comportements induits par ce type de modèle. Nous réalisons nos simulations à l'aide d'un réseau de contacts hétérogène réaliste, inspiré d'études récentes [181, 197].

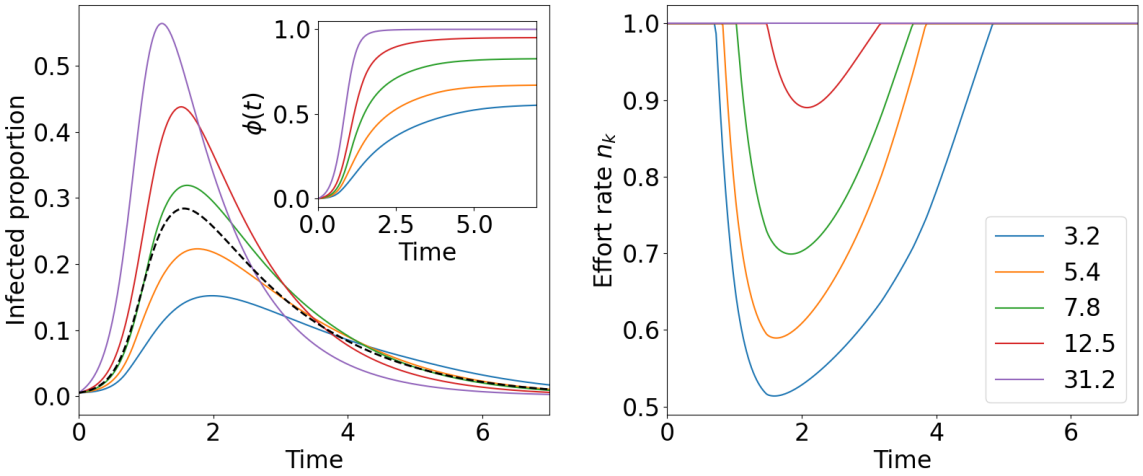

Figure G.7: Figure de gauche : évolution de la proportion d'infectés à l'équilibre de Nash solution du jeu à champ moyen. Figure insérée : évolution de la probabilitié cumulée d'être infecté avant l'instant considéré. Figure de droite : taux d'efforts correspondant des individus, avec un coût lié à la réduction des contacts qui augmente avec le nombre de contacts k. La ligne noire en pointillée (à gauche) montre l'évolution globale de la proportion d'individus infectés sur le réseau, tandis que les lignes colorées correspondent aux dynamiques (des infectés et des taux d'efforts) associées à des classes regroupant les degrés du réseau. La légende précise est idniquée sur la figure. Par exmple, $K = 5.4$ correspond aux individus dont le nombre de contacts k se situe entre 4 et 6. Une description plus détaillée de la figure est donnée sous la figure **??**, avec les tables des paramèters utilisés pour réaliser ces simulations.

Nous montrons sur la figure G.7 un exemple de ce que nous pouvons obtenir, avec à gauche l'évolution de l'épidémie et à droite l'évolution des taux d'efforts des différentes classes d'individus. Ici, nous avons regroupé les individus de différents degrés des classes plus larges (ainsi $K = 12.5$ correspondra aux individus dont le degré se situe typiquement entre 11 et 14 par exemple, en nombre de contacts par jour), afin d'améliorer la lisibilité et surtout pour permettre la réalisation des simulations numériques en un temps raisonnable. Dans la figure G.7, les efforts nécessaires à un individu pour réduire son taux de contact sont linéaires avec son nombre de contacts : cela correspond à la situation où un contact se vaut, quelque soit notre nombre total de contacts. Dit autrement, cela concerne les personnes très attachées à leurs contacts sociaux et pour qui une réduction de ces derniers demandera un effort important. Bien sûr, en réalité et contrairement à notre modélisation, l'effort demandé variera beaucoup suivant le type de contact à réduire (s'il s'agit d'un membre de sa famille ou d'un collègue de travail que l'on apprécie moyennement). Les individus avec un degré élevé sont donc moins enclins à faire des efforts et préfèrent accepter le risque, bien que l'épidémie soit plus virulente chez eux. De l'autre côté, les individus avec un degré faible ont peu de risque lié à l'épidémie et sont donc moins enclins aux efforts, mais comme ces derniers sont bien moins coûteux et plus rentables en termes de protection. C'est pour cela qu'ils apparaissent comme étant ceux qui se protègent le plus, alors que c'est l'inverse dès lors que la réduction du taux de contact devient constante et indépendante du nombre de voisins : les individus avec un faible degré sont moins exposés et ont donc moins d'intérêt à se protéger que les individus ayant un degré elevé. Ainsi, dans ce chapitre, nous avons étudié comment le degré, c'est à dire le nombre de contacts d'un individu pouvait influencer son comportement : à la fois car cela modifie son risque associé à l'infection, mais également par la forme du coût lié à la réduction des contacts qui l'incitera ou non à se protéger. Un phénomène intéressant révélé par notre analyse est que lorsque les individus décident de se protéger pour une courte période, ils le font

généralement un peu après le pic épidémique, lorsque l'épidémie présente encore des risques importants mais que la fin de celle-ci est proche. Cela permet aux individus qui ont eu la chance de ne pas avoir été infecté d'avoir une bonne probabilité de ne pas l'être avant la fin de l'épidémie, car l'immunité collective a été atteinte. Cela conclut le 2e projet de cette thèse (le 3e chronologiquement).

G.5 Résultats analytiques sur les réseaux homogènes

Le 3e et dernier projet de cette thèse est présenté dans le Chapitre 5, il ne concerne pas les jeux à champ moyen mais la résolution analytique des équations du modèle SIR sur réseau. Plus précisément, nous nous intéressons aux equations de l'approximation par paires sur un réseau homogène aléatoire (degré constant). Nous dérivons une solution implicite, c'est à dire que nous trouvons l'expression du temps en fonction du nombre de susceptible, là où une expression explicite nous aurait fournit l'opposé. Une fois dérivée et vérifiée numériquement, nous analysons la forme et le comportement de la solution trouvée, en explorant les différents cas limites. Nous expliquons notamment pourquoi l'épidémie se propage moins vite sur un réseau homogène (que sur un réseau hétérogène) et que ceci est d'autant plus vrai à mesure que le nombre de voisins diminue, même lorsque la fréquence des contacts est constante. Nous démontrons notamment que le seuil épidémique au deça duquel l'épidémie ne peut se déclencher est plus faible que dans les modèles hétérogènes ou le modèle SIR.

Dans la figure G.8, nous nous intéressons plus particulièrement à la nature et à l'expression des racines qui décrivent notre solution implicite. Ces dernières sont complexes et convergent vers le cercle unité d'une façon particulière que nous décrivons précisément. Cela nous permet ensuite de passer à la limite d'un nombre infini de voisins, correspondant au modèle SIR, et de dériver une nouvelle forme analytique implicite à l'aide de ces racines, alors que celle existante dans la littérature reposait sur un calcul d'intégrale. Cette nouvelle formule nous permet d'établir un certain nombre de nouvelles approximations permettant d'obtenir des expressions plus simples et intuitives, notamment pour l'instant du pic épidémique. Ces résultats permettent d'étendre le champ des connaissances sur les résultats analytiques des épidémies sur réseau, qui sont souvent limités en ce qui concerne l'épidémie à large échelle (et pas seulement au déclenchement de celle-ci). Bien qu'ayant une portée pratique limitée ici étant donné qu'il s'agit de réseaux homogènes, cela permet d'envisager des résolutions de modèles plus complexes, éventuellement hétérogènes, avec des méthodes analogues. De plus, les résultats analytiques permettent bien souvent de comprendre des concepts sur les modèles étudiés que ne permettront pas, ou dans une moindre mesure, les simulations numériques (comme la dépendance explicite des solutions dans certains paramètres du problème). Ce travail a conduit à la publication d'un article qui a été accepté récemment (PRE).

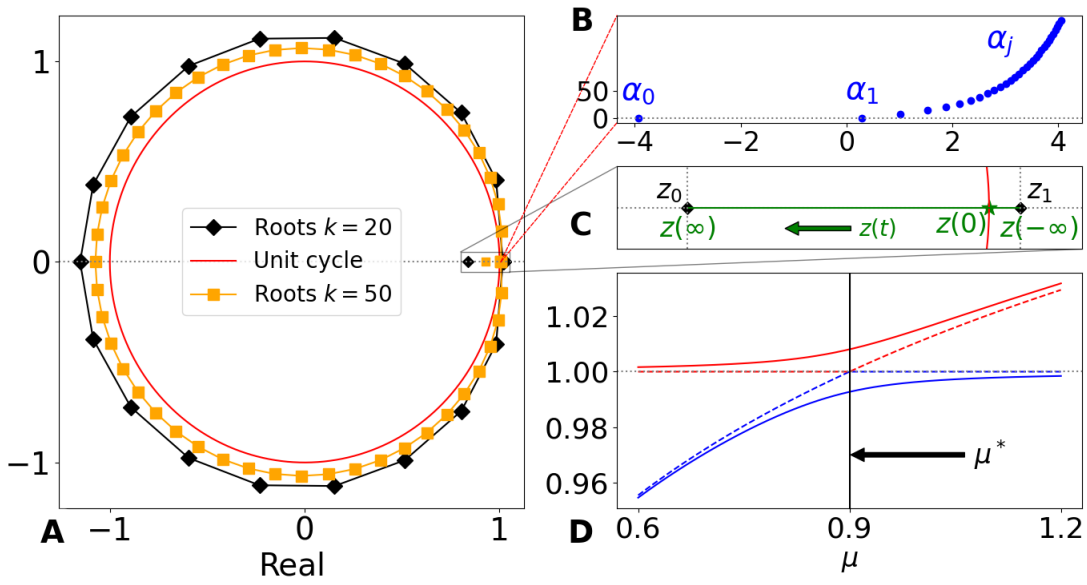

Figure G.8: **A**. Carrés oranges (respectivement. losanges noirs) : localisation dans le plan complexes des racines de notre solution pour un réseau de homogène de degrés 50 et 20 respectivement.**B** Vue éclatée dans le plan complexe de la manière dont les racines convergent vers le cercle unité, elle adopte une structure particulière autour de l'axe des réels positifs, suivant la fonction T de Lambert, nous le montrons dans le chapitre. **C** Zoom sur le plan complexe proche de 1 montrant comment le nombre de susceptible renoarmlisé passe de la racine Z1 en moins l'infini (après une continuation analytique) à la racine Z0 en plus l'infini. **D** Ligne bleue (respectivement rouge) : illustration pour un réseau homogène de degré 20 de la variation de la racine réelle inférieure à 1 notée Z0 (respectivement réelle supérieure à 1 notée Z1). Le paramètre mu correspond à l'inverse du taux de reproduction de l'épidémie. La valeur indiquée μ_k^* correspond au seuil épidémique pour ce réseau qui se trouve être inférieur à 1 : cela signifie qu'il faut que le R0 soit supérieur à l'inverse de 0.9 pour que l'épidémie puisse se propager sur le réseau. Les paramètres non indiqués ici le sont dans la figure 5.2.

G.6 Techniques numériques

Le Chapitre 6 est quant à lui consacré aux techniques numériques qui ont été utilisées tout au long de cette thèse. Nous présentons tout d'abord les librairies et méthodes générales utilisées, avant de détailler les algorihmes qui ont servi à résoudre l'équilibre de Nash ainsi que l'optimum sociétal. Pour l'équilibre de Nash, nous présentons une première méthode basée sur une suite récurrente qui s'avère très efficace dans les cas où cette dernière converge. Nous l'utilisons en complément d'une méthode plus classique qui repose sur une descente de gradient pour nous permettre de nous assurer que nous avons bien atteint l'équilibre de Nash quand nous pensons l'avoir atteint (pour confirmer la convergence de l'algorithme). La résolution de l'optimum sociétal repose également sur une descente de gradient, un peu plus sophistiquée car impliquant plus de termes. Nous présentons comment ces méthodes générales ont été appliquées au cas concret du Chapitre 3. Dans une seconde partie de ce chapitre, nous évoquons la complexité (temps de calcul) des algorithmes utilisés, et la dépendance de ces temps dans les paramètres clés des problèmes étudiés. Il apparaît que le calcul de l'optimum sociétal est le plus contraignant avec une complexité cubique dans le nombre de points de discrétisations utilisés et le nombre de classes de notre jeu à champ moyens. Enfin, une dernière partie de ce chapitre est consacrée à la présentation de deux méthodes prometteuses qui ont été étudiées mais peu ou partiellement implementées pendant cette thèse : la principe du maximum de Pontryagin

pour la résolution de l'optimum sociétal et l'utilisation d'algorithmes génétique pour la résolution de l'équilibre de Nash.

G.7 Conclusion

Nous concluons ce travail dans le Chapitre 7 où nous reprenons les différents points clés de nos objectifs et notre démarche. Nous décrivons les principaux enseignements de ce travail de recherche. Sur le plan théorique, les modèles MFG enrichissent les modèles épidémiologiques existants en tenant compte des comportements individuels de différentes classes d'agents (par âge, par type d'interaction, etc.). La modélisation du contact permettant l'implémentation des MFG doit se faire de façon attentive et normalement symmétrique, cela peut avoir une influence sur les résultats obtenus. Du point de vue physique, les simulations montrent que les individus réduisent leurs contacts lorsqu'ils perçoivent un risque élevé d'infection, concentrant leurs efforts autour du pic de l'épidémie. L'effet du à l'optimisation égoïste révèlent des écarts entre l'optimisation individuelle et collective, permettant ainsi d'imaginer la mise en place et l'optimisation d'interventions extérieures pour rapprocher ces deux optima. Concernant les paramètres clés, il semble essentiel de bien choisir l'horizon temporel de l'épidémie, car cela affecte les stratégies collectives (éradication, immunité de groupe, etc.). Les coûts liés à l'infection et à la réduction des contacts sociaux doivent également être soigneusement calibrés car ils vont beaucoup influer sur le comportement des individus. En termes de perspectives pratiques, trois axes ont été identifiés et mériteront d'être développés dans des recherches ultérieures : premièrement informer les individus de l'équilibre de Nash pour guider leurs comportements, car nous ne pouvons pas attendre d'eux qu'ils réalisent ce calcul d'optimisation. Cette information pourrait être transmise via une application mobile par exemple. Deuxièmement, concevoir des interventions non pharmaceutiques (NPIs) plus efficaces et plus adpatées aux populations concernées. Troisièmement, améliorer les prévisions épidémiologiques en tenant compte des comportements anticipés. Enfin, des collaborations interdisciplinaires seront nécessaires pour des applications concrètes des MFG, afin d'affiner la modélisation des coûts et des comportements. Du point de vue théorique, l'exploration de jeux de Stackelberg, qui analysent les interactions entre les autorités et les individus, semble une piste prometteuse.

J'espère que cette thèse permettra d'ouvrir la voie vers des applications concrètes intégrant les comportements humains dans les modélisations d'épidemies.

Bibliography

[1] John Horgan. Antonine plague. *Ancient History Encyclopedia*, 2019.

[2] Lee Mordechai, Merle Eisenberg, Timothy P Newfield, Adam Izdebski, Janet E Kay, and Hendrik Poinar. The justinianic plague: an inconsequential pandemic? *Proceedings of the National Academy of Sciences*, 116(51):25546–25554, 2019.

[3] Gabriel-Viorel Gardan. "the justinianic plague": the effects of a pandemic in late antiquity and the early middle ages. *Romanian Journal of Artistic Creativity*, 8(4):3–18, 2020.

[4] John M Barry. *The great influenza: The story of the deadliest pandemic in history*. Penguin Uk, 2020.

[5] Patrice Debré. *Louis Pasteur*. JHU Press, 2000.

[6] Jean-Marc Cavaillon and Sandra Legout. Louis pasteur: between myth and reality. *Biomolecules*, 12(4):596, 2022.

[7] Francis E Andre, Robert Booy, Hans L Bock, John Clemens, Sibnarayan K Datta, Thekkekara J John, Bee W Lee, S Lolekha, Heikki Peltola, TA Ruff, et al. Vaccination greatly reduces disease, disability, death and inequity worldwide. *Bulletin of the World health organization*, 86:140–146, 2008.

[8] William Ogilvy Kermack and Anderson G McKendrick. A contribution to the mathematical theory of epidemics. *Proceedings of the royal society of london. Series A, Containing papers of a mathematical and physical character*, 115(772), 1927.

[9] World Health Organization et al. Who report on global surveillance of epidemic-prone infectious diseases. Technical report, World Health Organization, 2000.

[10] Peter Daszak, Andrew A Cunningham, and Alex D Hyatt. Emerging infectious diseases of wildlife–threats to biodiversity and human health. *science*, 287(5452):443–449, 2000.

[11] Jiabao Xu, Shizhe Zhao, Tieshan Teng, Abualgasim Elgaili Abdalla, Wan Zhu, Longxiang Xie, Yunlong Wang, and Xiangqian Guo. Systematic comparison of two animal-to-human transmitted human coronaviruses: Sars-cov-2 and sars-cov. *Viruses*, 12(2):244, 2020.

[12] Peter Daszak, Andrew A Cunningham, and Alex D Hyatt. Anthropogenic environmental change and the emergence of infectious diseases in wildlife. *Acta tropica*, 78(2):103–116, 2001.

[13] Michael P Muehlenbein. Human-wildlife contact and emerging infectious diseases. *Human-environment interactions: Current and future directions*, pages 79–94, 2013.

[14] Camille Parmesan, Mike D Morecroft, and Yongyut Trisurat. *Climate change 2022: Impacts, adaptation and vulnerability*. PhD thesis, GIEC, 2022.

[15] Shlomo Angel, Jason Parent, Daniel L Civco, Alexander Blei, and David Potere. The dimensions of global urban expansion: Estimates and projections for all countries, 2000–2050. *Progress in planning*, 75(2):53–107, 2011.

[16] Jinxing Guan, Yongyue Wei, Yang Zhao, and Feng Chen. Modeling the transmission dynamics of Covid-19 epidemic: a systematic review. *Journal of Biomedical Research*, 34(6), 2020.

[17] Neil M Ferguson, Daniel Laydon, Gemma Nedjati-Gilani, Natsuko Imai, Kylie Ainslie, Marc Baguelin, Sangeeta Bhatia, Adhiratha Boonyasiri, Zulma Cucunubá, Gina Cuomo-Dannenburg, et al. *Report 9: Impact of non-pharmaceutical interventions (NPIs) to reduce COVID19 mortality and healthcare demand*, volume 16. Imperial College London London, 2020.

[18] Mario Coccia. Sources, diffusion and prediction in covid-19 pandemic: lessons learned to face next health emergency. *AIMS Public Health*, 10(1):145, 2023.

[19] Romuald Elie, Emma Hubert, and Gabriel Turinici. Contact rate epidemic control of Covid-19: an equilibrium view. *Mathematical Modelling of Natural Phenomena*, 15, 2020.

[20] Samuel Cho. Mean-field game analysis of SIR model with social distancing, 2020.

[21] Oluwatobiloba Ige. *Markov chain epidemic models and parameter estimation.* Marshall University, 2020.

[22] Lorenzo Rosso. *Dissipative Ytterbium gases.* PhD thesis, Université Paris-Saclay, 2023.

[23] Lasko Basnarkov, Igor Tomovski, Trifce Sandev, and Ljupco Kocarev. Non-markovian sir epidemic spreading model of covid-19. *Chaos, Solitons & Fractals*, 160:112286, 2022.

[24] Neil Sherborne, Joel C Miller, Konstantin B Blyuss, and Istvan Z Kiss. Mean-field models for non-markovian epidemics on networks. *Journal of mathematical biology*, 76:755–778, 2018.

[25] Norman TJ Bailey. *The mathematical theory of infectious diseases and its applications.* Number 2nd ediition. Charles Griffin and Company limited, 1975.

[26] Tiberiu Harko, Francisco SN Lobo, and MK3197716 Mak. Exact analytical solutions of the susceptible-infected-recovered (SIR) epidemic model and of the SIR model with equal death and birth rates. *Applied Mathematics and Computation*, 236:184–194, 2014.

[27] Thomas Stocker. *Climate change 2013: the physical science basis: Working Group I contribution to the Fifth assessment report of the Intergovernmental Panel on Climate Change.* Cambridge university press, 2014.

[28] Oliver Nelles. *Model Complexity Optimization*, pages 175–231. Springer International Publishing, Cham, 2020.

[29] David Adam. What covid pandemic forecasters can learn from climate models. *Nature*, 587(7835):533–534, 2020.

[30] D Adam. The simulations driving the world's response to covid-19. *Nature, April*, 2, 2020.

[31] Michael Y Li, Hal L Smith, and Liancheng Wang. Global dynamics of an SEIR epidemic model with vertical transmission. *SIAM Journal on Applied Mathematics*, 62(1), 2001.

[32] Devosmita Sen and Debasis Sen. Use of a modified SIRD model to analyze Covid-19 data. *Industrial & Engineering Chemistry Research*, 60(11), 2021.

[33] Shujing Gao, Zhidong Teng, Juan J Nieto, Angela Torres, et al. Analysis of an SIR epidemic model with pulse vaccination and distributed time delay. *BioMed Research International*, 2017, 2007.

[34] Herbert W Hethcote. The mathematics of infectious diseases. *SIAM review*, 42(4), 2000.

[35] Haijiao Li and Shangjiang Guo. Dynamics of a SIRC epidemiological model. *Electronic Journal of Differential Equations*, 2017, 05 2017.

[36] Stephen Eubank, Hasan Guclu, VS Anil Kumar, Madhav V Marathe, Aravind Srinivasan, Zoltan Toroczkai, and Nan Wang. Modelling disease outbreaks in realistic urban social networks. *Nature*, 429(6988):180–184, 2004.

[37] Dina Mistry, Maria Litvinova, Ana Pastore y Piontti, Matteo Chinazzi, Laura Fumanelli, Marcelo FC Gomes, Syed A Haque, Quan-Hui Liu, Kunpeng Mu, Xinyue Xiong, et al. Inferring high-resolution human mixing patterns for disease modeling. *Nature communications*, 12(1), 2021.

[38] Laura Fumanelli, Marco Ajelli, Piero Manfredi, Alessandro Vespignani, and Stefano Merler. Inferring the structure of social contacts from demographic data in the analysis of infectious diseases spread. *PLoS Computational Biology*, 8, 2012.

[39] Yue Xiang, Yonghong Jia, Linlin Chen, Lei Guo, Bizhen Shu, and Enshen Long. Covid-19 epidemic prediction and the impact of public health interventions: A review of covid-19 epidemic models. *Infectious Disease Modelling*, 6:324–342, 2021.

[40] Alex Arenas, Wesley Cota, Jesús Gómez-Gardeñes, Sergio Gómez, Clara Granell, Joan T Matamalas, David Soriano-Paños, and Benjamin Steinegger. Modeling the spatiotemporal epidemic spreading of covid-19 and the impact of mobility and social distancing interventions. *Physical Review X*, 10(4):041055, 2020.

[41] Laura Di Domenico. *Data-driven modeling of COVID-19 spread in France to inform pandemic response*. PhD thesis, Sorbonne Université, 2022.

[42] Duncan J Watts and Steven H Strogatz. Collective dynamics of 'small-world'networks. *nature*, 393(6684):440–442, 1998.

[43] Francisco C Santos, João F Rodrigues, and Jorge M Pacheco. Epidemic spreading and cooperation dynamics on homogeneous small-world networks. *Phys. Rev. E*, 72(5):056128, 2005.

[44] Diogo H Silva, Francisco A Rodrigues, and Silvio C Ferreira. High prevalence regimes in the pair-quenched mean-field theory for the susceptible-infected-susceptible model on networks. *Phys. Rev. E*, 102(1):012313, 2020.

[45] Shogo Mizutaka, Kizashi Mori, and Takehisa Hasegawa. Synergistic epidemic spreading in correlated networks. *Phys. Rev. E*, 106(3):034305, 2022.

[46] Marc Barthélemy, Alain Barrat, Romualdo Pastor-Satorras, and Alessandro Vespignani. Dynamical patterns of epidemic outbreaks in complex heterogeneous networks. *Journal of theoretical biology*, 235(2):275–288, 2005.

[47] Yao Hu, Lequan Min, and Yang Kuang. Modeling the dynamics of epidemic spreading on homogenous and heterogeneous networks. *Applicable Analysis*, 94(11):2308–2330, 2015.

[48] Gregory Kozyreff. Asymptotic solutions of the SIR and SEIR models well above the epidemic threshold. *IMA Journal of Applied Mathematics*, 87(4):521–536, 2022.

[49] Faryad Darabi Sahneh and Caterina Scoglio. Epidemic spread in human networks. In *2011 50th IEEE Conference on Decision and Control and European Control Conference*, pages 3008–3013. IEEE, 2011.

[50] Mark EJ Newman. Spread of epidemic disease on networks. *Phys. Rev. E*, 66(1):016128, 2002.

[51] Stefano Boccaletti, Vito Latora, Yamir Moreno, Martin Chavez, and D-U Hwang. Complex networks: Structure and dynamics. *Physics reports*, 424(4-5):175–308, 2006.

[52] Romualdo Pastor-Satorras, Claudio Castellano, Piet Van Mieghem, and Alessandro Vespignani. Epidemic processes in complex networks. *Rev. Mod. Phys.*, 87(3):925, 2015.

[53] Simon R Broadbent and John M Hammersley. Percolation processes: I. crystals and mazes. In *Mathematical proceedings of the Cambridge philosophical society*, volume 53, pages 629–641. Cambridge University Press, 1957.

[54] Pol Colomer-de Simón and Marián Boguñá. Double percolation phase transition in clustered complex networks. *Physical Review X*, 4(4):041020, 2014.

[55] John M Beggs and Dietmar Plenz. Neuronal avalanches in neocortical circuits. *Journal of neuroscience*, 23(35):11167–11177, 2003.

[56] Bryce Ryan and Neal C Gross. The diffusion of hybrid seed corn in two iowa communities. *Rural sociology*, 8(1):15, 1943.

[57] Denis Mollison. *Epidemic models: their structure and relation to data*. Number 5. Cambridge University Press, 1995.

[58] Erik Volz and Lauren Ancel Meyers. Epidemic thresholds in dynamic contact networks. *Journal of the Royal Society Interface*, 6(32):233–241, 2009.

[59] Deepayan Chakrabarti, Yang Wang, Chenxi Wang, Jurij Leskovec, and Christos Faloutsos. Epidemic thresholds in real networks. *ACM Transactions on Information and System Security (TISSEC)*, 10(4):1–26, 2008.

[60] Angélica S Mata and Silvio C Ferreira. Pair quenched mean-field theory for the susceptible-infected-susceptible model on complex networks. *Europhysics Letters*, 103(4):48003, 2013.

[61] Réka Albert, Hawoong Jeong, and Albert-László Barabási. Error and attack tolerance of complex networks. *nature*, 406(6794):378–382, 2000.

[62] Oriol Artime, Marco Grassia, Manlio De Domenico, James P Gleeson, Hernán A Makse, Giuseppe Mangioni, Matjaž Perc, and Filippo Radicchi. Robustness and resilience of complex networks. *Nature Reviews Physics*, 6(2):114–131, 2024.

[63] Paul Erdos, Alfréd Rényi, et al. On the evolution of random graphs. *Publ. math. inst. hung. acad. sci*, 5(1):17–60, 1960.

[64] Jingyi Lin and Yifang Ban. The evolving network structure of us airline system during 1990–2010. *Physica A: Statistical Mechanics and its Applications*, 410:302–312, 2014.

[65] Lada A Adamic and Bernardo A Huberman. Power-law distribution of the world wide web. *science*, 287(5461):2115–2115, 2000.

[66] Giulia De Masi, Giulia Iori, and Guido Caldarelli. Fitness model for the italian interbank money market. *Physical Review E—Statistical, Nonlinear, and Soft Matter Physics*, 74(6):066112, 2006.

[67] Albert-László Barabási and Réka Albert. Emergence of scaling in random networks. *science*, 286(5439):509–512, 1999.

[68] Jeffrey Travers and Stanley Milgram. An experimental study of the small world problem. In *Social networks*, pages 179–197. Elsevier, 1977.

[69] Jose M Montoya and Ricard V Solé. Small world patterns in food webs. *Journal of theoretical biology*, 214(3):405–412, 2002.

[70] Luıs A Nunes Amaral, Antonio Scala, Marc Barthelemy, and H Eugene Stanley. Classes of small-world networks. *Proceedings of the national academy of sciences*, 97(21):11149–11152, 2000.

[71] Danielle Smith Bassett and ED Bullmore. Small-world brain networks. *The neuroscientist*, 12(6):512–523, 2006.

[72] Wei Wang, Ming Tang, H Eugene Stanley, and Lidia A Braunstein. Unification of theoretical approaches for epidemic spreading on complex networks. *Rep. Prog. Phys.*, 80(3):036603, 2017.

[73] Xiang Wan, Jiming Liu, William K Cheung, and Tiejun Tong. Inferring epidemic network topology from surveillance data. *PLoS One*, 9(6):e100661, 2014.

[74] Francesco Di Lauro, J-C Croix, Masoumeh Dashti, Luc Berthouze, and IZ Kiss. Network inference from population-level observation of epidemics. *Scientific Reports*, 10(1):18779, 2020.

[75] Bisakha Ray, Elodie Ghedin, and Rumi Chunara. Network inference from multimodal data: a review of approaches from infectious disease transmission. *Journal of biomedical informatics*, 64:44–54, 2016.

[76] David Welch, Shweta Bansal, and David R Hunter. Statistical inference to advance network models in epidemiology. *Epidemics*, 3(1):38–45, 2011.

[77] Leon Danon, Ashley P Ford, Thomas House, Chris P Jewell, Matt J Keeling, Gareth O Roberts, Joshua V Ross, and Matthew C Vernon. Networks and the epidemiology of infectious disease. *Interdisciplinary perspectives on infectious diseases*, 2011(1):284909, 2011.

[78] Xiaoqian Sun, Sebastian Wandelt, and Anming Zhang. How did covid-19 impact air transportation? a first peek through the lens of complex networks. *Journal of Air Transport Management*, 89:101928, 2020.

[79] Josh A Firth, Joel Hellewell, Petra Klepac, Stephen Kissler, Adam J Kucharski, and Lewis G Spurgin. Using a real-world network to model localized covid-19 control strategies. *Nature medicine*, 26(10):1616–1622, 2020.

[80] Steven F Railsback and Volker Grimm. *Agent-based and individual-based modeling: a practical introduction*. Princeton university press, 2019.

[81] Fabian Lorig, Emil Johansson, and Paul Davidsson. Agent-based social simulation of the covid-19 pandemic: A systematic review. *Journal of Artificial Societies and Social Simulation*, 24(3), 2021.

[82] István Z Reguly, Dávid Csercsik, János Juhász, Kálmán Tornai, Zsófia Bujtár, Gergely Horváth, Bence Keömley-Horváth, Tamás Kós, György Cserey, Kristóf Iván, et al. Microsimulation based quantitative analysis of covid-19 management strategies. *PLoS computational biology*, 18(1):e1009693, 2022.

[83] Neil M Ferguson, Derek AT Cummings, Christophe Fraser, James C Cajka, Philip C Cooley, and Donald S Burke. Strategies for mitigating an influenza pandemic. *Nature*, 442(7101):448–452, 2006.

[84] Kari Lancaster, Tim Rhodes, and Marsha Rosengarten. Making evidence and policy in public health emergencies: lessons from covid-19 for adaptive evidence-making and intervention. *Evidence & policy*, 16(3):477–490, 2020.

[85] Joshua M Epstein. Agent-based computational models and generative social science. *Complexity*, 4(5):41–60, 1999.

[86] Charles M Macal and Michael J North. Tutorial on agent-based modeling and simulation. In *Proceedings of the Winter Simulation Conference, 2005.*, pages 14–pp. IEEE, 2005.

[87] Brandon G Aaby, Kalyan S Perumalla, and Sudip K Seal. Efficient simulation of agent-based models on multi-gpu and multi-core clusters. In *3rd International ICST Conference on Simulation Tools and Techniques*, 2010.

[88] Steven F Railsback, Steven L Lytinen, and Stephen K Jackson. Agent-based simulation platforms: Review and development recommendations. *Simulation*, 82(9):609–623, 2006.

[89] R Anderson. *Infectious diseases of humans: dynamics and control*. Cambridge Univer-sity Press, 1991.

[90] Benjamin D Dalziel, Babak Pourbohloul, and Stephen P Ellner. Human mobility patterns predict divergent epidemic dynamics among cities. *Proceedings of the Royal Society B: Biological Sciences*, 280(1766):20130763, 2013.

[91] Srikanta Sannigrahi, Francesco Pilla, Bidroha Basu, Arunima Sarkar Basu, and Anna Molter. Examining the association between socio-demographic composition and covid-19 fatalities in the european region using spatial regression approach. *Sustainable cities and society*, 62:102418, 2020.

[92] Kadir Amasyali and Nora M El-Gohary. A review of data-driven building energy consumption prediction studies. *Renewable and Sustainable Energy Reviews*, 81:1192–1205, 2018.

[93] Neil Ferguson. Capturing human behaviour. *Nature*, 446(7137):733–733, 2007.

[94] Joshua M Epstein. Modelling to contain pandemics. *Nature*, 460(7256):687–687, 2009.

[95] James Holland Jones and Marcel Salathé. Early assessment of anxiety and behavioral response to novel swine-origin influenza a (h1n1). *PLoS one*, 4(12):e8032, 2009.

[96] Joseph TF Lau, Hiyi Tsui, Mason Lau, and Xilin Yang. Sars transmission, risk factors, and prevention in hong kong. *Emerging infectious diseases*, 10(4):587, 2004.

[97] Bruno Buonomo, Alberto d'Onofrio, and Deborah Lacitignola. Global stability of an sir epidemic model with information dependent vaccination. *Mathematical biosciences*, 216(1):9–16, 2008.

[98] Piero Poletti, Bruno Caprile, Marco Ajelli, Andrea Pugliese, and Stefano Merler. Spontaneous behavioural changes in response to epidemics. *Journal of theoretical biology*, 260(1):31–40, 2009.

[99] Timothy C Reluga. Game theory of social distancing in response to an epidemic. *PLoS Computational Biology*, 6(5), 2010.

[100] Sebastian Funk, E Gilad, and Vincent AA Jansen. Endemic disease, awareness, and local behavioural response. *Journal of theoretical biology*, 264(2):501–509, 2010.

[101] Zhen Wang, Michael A Andrews, Zhi-Xi Wu, Lin Wang, and Chris T Bauch. Coupled disease–behavior dynamics on complex networks: A review. *Physics of life reviews*, 15:1–29, 2015.

[102] Piero Poletti. *Human behavior in epidemic modelling.* PhD thesis, University of Trento, 2010.

[103] Simiao Chen, Qiushi Chen, Weizhong Yang, Lan Xue, Yuanli Liu, Juntao Yang, Chen Wang, and Till Baernighausen. Buying time for an effective epidemic response: the impact of a public holiday for outbreak control on covid-19 epidemic spread. *Engineering*, 6(10):1108–1114, 2020.

[104] Biao Tang, Weike Zhou, Xia Wang, Hulin Wu, and Yanni Xiao. Controlling multiple covid-19 epidemic waves: an insight from a multi-scale model linking the behaviour change dynamics to the disease transmission dynamics. *Bulletin of Mathematical Biology*, 84(10):106, 2022.

[105] Zhen Wang, Chris T Bauch, Samit Bhattacharyya, Alberto d'Onofrio, Piero Manfredi, Matjaž Perc, Nicola Perra, Marcel Salathé, and Dawei Zhao. Statistical physics of vaccination. *Physics Reports*, 664:1–113, 2016.

[106] Vincenzo Capasso and Gabriella Serio. A generalization of the kermack-mckendrick deterministic epidemic model. *Mathematical biosciences*, 42(1-2):43–61, 1978.

[107] Wei-min Liu, Herbert W Hethcote, and Simon A Levin. Dynamical behavior of epidemiological models with nonlinear incidence rates. *Journal of mathematical biology*, 25:359–380, 1987.

[108] Mark M Tanaka, Jochen Kumm, and Marcus W Feldman. Coevolution of pathogens and cultural practices: a new look at behavioral heterogeneity in epidemics. *Theoretical population biology*, 62(2):111–119, 2002.

[109] Thilo Gross, Carlos J Dommar D'Lima, and Bernd Blasius. Epidemic dynamics on an adaptive network. *Physical review letters*, 96(20):208701, 2006.

[110] Leah B Shaw and Ira B Schwartz. Fluctuating epidemics on adaptive networks. *Physical Review E—Statistical, Nonlinear, and Soft Matter Physics*, 77(6):066101, 2008.

[111] Sebastian Funk, Erez Gilad, Chris Watkins, and Vincent AA Jansen. The spread of awareness and its impact on epidemic outbreaks. *Proceedings of the National Academy of Sciences*, 106(16):6872–6877, 2009.

[112] Sara Del Valle, Herbert Hethcote, James M Hyman, and Carlos Castillo-Chavez. Effects of behavioral changes in a smallpox attack model. *Mathematical biosciences*, 195(2):228–251, 2005.

[113] Joshua M Epstein, Jon Parker, Derek Cummings, and Ross A Hammond. Coupled contagion dynamics of fear and disease: mathematical and computational explorations. *PloS one*, 3(12):e3955, 2008.

[114] Istvan Z Kiss, Jackie Cassell, Mario Recker, and Péter L Simon. The impact of information transmission on epidemic outbreaks. *Mathematical biosciences*, 225(1):1–10, 2010.

[115] Xiu-Xiu Zhan, Chuang Liu, Ge Zhou, Zi-Ke Zhang, Gui-Quan Sun, Jonathan JH Zhu, and Zhen Jin. Coupling dynamics of epidemic spreading and information diffusion on complex networks. *Applied Mathematics and Computation*, 332:437–448, 2018.

[116] Douglas Guilbeault, Joshua Becker, and Damon Centola. Complex contagions: A decade in review. *Complex spreading phenomena in social systems: Influence and contagion in real-world social networks*, pages 3–25, 2018.

[117] Damon Centola and Michael Macy. Complex contagions and the weakness of long ties. *American journal of Sociology*, 113(3):702–734, 2007.

[118] Giulio Burgio, Sergio Gómez, and Alex Arenas. Triadic approximation reveals the role of interaction overlap on the spread of complex contagions on higher-order networks. *Physical Review Letters*, 132(7):077401, 2024.

[119] Josef Hofbauer and Karl Sigmund. *Evolutionary games and population dynamics*. Cambridge university press, 1998.

[120] John Von Neumann and Oskar Morgenstern. *Theory of games and economic behavior, 2nd rev.* Princeton university press, 1947.

[121] Robert Gibbons. *Game theory for applied economists*. Princeton University Press, 1992.

[122] Larry Samuelson. Game theory in economics and beyond. *Journal of Economic Perspectives*, 30(4):107–130, 2016.

[123] Peter Hammerstein and Reinhard Selten. Game theory and evolutionary biology. *Handbook of game theory with economic applications*, 2:929–993, 1994.

[124] Hocine Benseghir, Mohd Fadzil Mohd Idris, Muhammad Nomani Kabir, and Abdullah Bin Ibrahim. Survey on pedestrian-dynamics models for evacuation process based on game theory. In *2018 International Seminar on Application for Technology of Information and Communication*, pages 539–544. IEEE, 2018.

[125] Yunhan Huang and Quanyan Zhu. Game-theoretic frameworks for epidemic spreading and human decision-making: A review. *Dynamic Games and Applications*, 12(1), 2022.

[126] Owen Chen and Moshe Ben-Akiva. Game-theoretic formulations of interaction between dynamic traffic control and dynamic traffic assignment. *Transportation Research Record*, 1617(1):179–188, 1998.

[127] Amir-Hamed Mohsenian-Rad, Vincent WS Wong, Juri Jatskevich, Robert Schober, and Alberto Leon-Garcia. Autonomous demand-side management based on game-theoretic energy consumption scheduling for the future smart grid. *IEEE transactions on Smart Grid*, 1(3):320–331, 2010.

[128] William Poundstone. *Prisoner's dilemma*. Anchor, 2011.

[129] Martin A Nowak and Karl Sigmund. The alternating prisoner's dilemma. *Journal of theoretical Biology*, 168(2):219–226, 1994.

[130] Thibault Bonnemain. *Jeux en Champ Moyen Quadratique avec Coordination Négative*. PhD thesis, CY Cergy Paris Université, 2020. Thèse de doctorat dirigée par Gobron, Thierry et Ullmo, Denis Physique - ED EM2PSI CY Cergy Paris Université 2020.

[131] Denis Ullmo, Igor Swiecicki, and Thierry Gobron. Quadratic mean field games. *Physics Reports*, 799, 2019.

[132] J Ben Rosen. Existence and uniqueness of equilibrium points for concave n-person games. *Econometrica: Journal of the Econometric Society*, pages 520–534, 1965.

[133] Dinh The Luc. Pareto optimality. *Pareto optimality, game theory and equilibria*, pages 481–515, 2008.

[134] Thomas C Schelling. Dynamic models of segregation. *Journal of mathematical sociology*, 1(2):143–186, 1971.

[135] Andrew M Colman. Cooperation, psychological game theory, and limitations of rationality in social interaction. *Behavioral and brain sciences*, 26(2):139–153, 2003.

[136] David H Wolpert. Information theory—the bridge connecting bounded rational game theory and statistical physics. In *Complex Engineered Systems: Science meets technology*, pages 262–290. Springer, 2006.

[137] KM Ariful Kabir, Kazuki Kuga, and Jun Tanimoto. The impact of information spreading on epidemic vaccination game dynamics in a heterogeneous complex network-a theoretical approach. *Chaos, Solitons & Fractals*, 132:109548, 2020.

[138] Nichola J Raihani and Redouan Bshary. Resolving the iterated prisoner's dilemma: theory and reality. *Journal of Evolutionary Biology*, 24(8):1628–1639, 2011.

[139] Matteo Butano, Cécile Appert-Rolland, and Denis Ullmo. Discounted Mean-Field Game model of a dense static crowd with variable information crossed by an intruder. *SciPost Phys.*, 16:104, 2024.

[140] Jean-Michel Lasry and Pierre-Louis Lions. Mean field games. *Japanese journal of mathematics*, 2(1), 2007.

[141] Jean-Michel Lasry and Pierre-Louis Lions. Jeux à champ moyen. ii–horizon fini et contrôle optimal. *Comptes Rendus Mathématique*, 343(10), 2006.

[142] Jean-Michel Lasry and Pierre-Louis Lions. Jeux à champ moyen. i–le cas stationnaire. *Comptes Rendus Mathématique*, 343(9), 2006.

[143] Minyi Huang, Roland Malhame, and Peter Caines. Large population stochastic dynamic games: Closed-loop McKean-Vlasov systems and the Nash certainty equivalence principle. *Commun. Inf. Syst.*, 6, 01 2006.

[144] Peter E Caines. Mean field games. In *Encyclopedia of systems and control*. Springer, 2021.

[145] Diogo A Gomes, Joana Mohr, and Rafael Rigao Souza. Continuous time finite state mean field games. *Applied Mathematics & Optimization*, 68(1), 2013.

[146] René Carmona, François Delarue, et al. *Probabilistic theory of mean field games with applications I-II*. Springer, 2018.

[147] Igor Swiecicki, Thierry Gobron, and Denis Ullmo. Schrödinger approach to mean field games. *Phys. Rev. Lett*, 116(12):128701, 2016.

[148] Areski Cousin, Stéphane Crépey, Olivier Guéant, David Hobson, Monique Jeanblanc, Jean-Michel Lasry, Jean-Paul Laurent, Pierre-Louis Lions, Peter Tankov, Olivier Guéant, et al. Mean field games and applications. *Paris-Princeton lectures on mathematical finance 2010*, 2011.

[149] Patrick Chan and Ronnie Sircar. Bertrand and Cournot mean field games. *Applied Mathematics & Optimization*, 71(3), 2015.

[150] Thibault Bonnemain, Matteo Butano, Théophile Bonnet, Iñaki Echeverría-Huarte, Antoine Seguin, Alexandre Nicolas, Cécile Appert-Rolland, and Denis Ullmo. Pedestrians in static crowds are not grains, but game players. *Phys. Rev. E*, 107(2):024612, 2023.

[151] Dario Bauso, Raffaele Pesenti, and Marco Tolotti. Opinion dynamics and stubbornness via multi-population mean-field games. *Journal of optimization theory and applications*, 170, 2016.

[152] Laetitia Laguzet, Gabriel Turinici, and Ghozlane Yahiaoui. Equilibrium in an individual-societal SIR vaccination model in presence of discounting and finite vaccination capacity. In *New trends in differential equations, control theory and optimization: proceedings of the 8th congress of Romanian mathematicians*. World Scientific, 2016.

[153] Emma Hubert and Gabriel Turinici. Nash-MFG equilibrium in a SIR model with time dependent newborn vaccination. *Ricerche di matematica*, 67, 2018.

[154] Francesco Salvarani and Gabriel Turinici. Optimal individual strategies for influenza vaccines with imperfect efficacy and durability of protection. *Mathematical Biosciences and Engineering*, 15(3), 2018.

[155] S Yagiz Olmez, Shubham Aggarwal, Jin Won Kim, Erik Miehling, Tamer Başar, Matthew West, and Prashant G Mehta. Modeling presymptomatic spread in epidemics via mean-field games. In *2022 American Control Conference (ACC)*. IEEE, 2022.

[156] S Yagiz Olmez, Shubham Aggarwal, Jin Won Kim, Erik Miehling, Tamer Başar, Matthew West, and Prashant G Mehta. How does a rational agent act in an epidemic? In *2022 IEEE 61st Conference on Decision and Control (CDC)*. IEEE, 2022.

[157] Amal Roy, Chandramani Singh, and Y Narahari. Recent advances in modeling and control of epidemics using a mean field approach. *Sādhanā*, 48(4), 2023.

[158] Kenneth H Wickwire. Optimal isolation policies for deterministic and stochastic epidemics. *Mathematical biosciences*, 26(3-4), 1975.

[159] Richard Morton and Kenneth H Wickwire. On the optimal control of a deterministic epidemic. *Advances in Applied Probability*, 6(4), 1974.

[160] JM Tchuenche, SA Khamis, FB Agusto, and SC Mpeshe. Optimal control and sensitivity analysis of an influenza model with treatment and vaccination. *Acta biotheoretica*, 59, 2011.

[161] Dimitri Bertsekas. *Dynamic programming and optimal control: Volume I*, volume 4. Athena scientific, 2012.

[162] Andris Abakuks. An optimal isolation policy for an epidemic. *Journal of Applied Probability*, 10(2), 1973.

[163] Andris Abakuks. Optimal immunisation policies for epidemics. *Advances in Applied Probability*, 6(3), 1974.

[164] Markus Kantner and Thomas Koprucki. Beyond just "flattening the curve": Optimal control of epidemics with purely non-pharmaceutical interventions. *Journal of Mathematics in Industry*, 10(1), 2020.

[165] Thomas Kruse and Philipp Strack. Optimal control of an epidemic through social distancing. *SSRN*, 2020.

[166] MHR Khouzani, Saswati Sarkar, and Eitan Altman. Optimal control of epidemic evolution. In *2011 Proceedings IEEE INFOCOM*. IEEE, 2011.

[167] Franco Sassi. Calculating qalys, comparing qaly and daly calculations. *Health policy and planning*, 21(5):402–408, 2006.

[168] Grant MA Wyper, Eilidh Fletcher, Ian Grant, Gerry McCartney, Colin Fischbacher, Oliver Harding, Hannah Jones, Maria Teresa de Haro Moro, Niko Speybroeck, Brecht Devleesschauwer, et al. Measuring disability-adjusted life years (dalys) due to covid-19 in scotland, 2020. *Archives of Public Health*, 80(1):105, 2022.

[169] Linda Thunström, Stephen C Newbold, David Finnoff, Madison Ashworth, and Jason F Shogren. The benefits and costs of using social distancing to flatten the curve for covid-19. *Journal of Benefit-Cost Analysis*, 11(2):179–195, 2020.

[170] Viktoriya Petrakova and Olga Krivorotko. Mean field game for modeling of covid-19 spread. *Journal of Mathematical Analysis and Applications*, 514(1):126271, 2022.

[171] Emma Hubert, Thibaut Mastrolia, Dylan Possamaï, and Xavier Warin. Incentives, lockdown, and testing: from Thucydides' analysis to the Covid-19 pandemic. *Journal of mathematical biology*, 84(5), 2022.

[172] Alexander Aurell, Rene Carmona, Gokce Dayanikli, and Mathieu Lauriere. Optimal incentives to mitigate epidemics: a Stackelberg mean field game approach. *SIAM Journal on Control and Optimization*, 60(2), 2022.

[173] Wonjun Lee, Siting Liu, Wuchen Li, and Stanley Osher. Mean field control problems for vaccine distribution. *Research in the Mathematical Sciences*, 9(3):51, 2022.

[174] Boualem Djehiche, Alain Tcheukam, and Hamidou Tembine. A mean-field game of evacuation in multilevel building. *IEEE Transactions on Automatic Control*, 62(10):5154–5169, 2017.

[175] William Ogilvy Kermack and Anderson G McKendrick. A contribution to the mathematical theory of epidemics. *Proceedings of the royal society of london. Series A, Containing papers of a mathematical and physical character*, 115(772):700–721, 1927.

[176] Louis Bremaud and Denis Ullmo. Social structure description of epidemic propagation with a mean-field game paradigm. *Phys. Rev. E*, 106:L062301, Dec 2022.

[177] Louis Bremaud, Olivier Giraud, and Denis Ullmo. Mean field game approach to non-pharmaceutical interventions in a social structure model of epidemics. *arXiv preprint arXiv:2404.08758*, 2024.

[178] Louis Bremaud, Olivier Giraud, and Denis Ullmo. Epidemic models on homogeneous networks: some analytical results. *arXiv preprint arXiv:2312.11321*, 2023.

[179] Neil Ferguson, Daniel Laydon, Gemma Nedjati Gilani, Natsuko Imai, Kylie Ainslie, Marc Baguelin, Sangeeta Bhatia, Adhiratha Boonyasiri, ZULMA Cucunuba Perez, Gina Cuomo-Dannenburg, et al. Report 9: Impact of non-pharmaceutical interventions (NPIs) to reduce Covid19 mortality and healthcare demand. *Imperial College London COVID-19*, 2020.

[180] Sara Y Del Valle, James M Hyman, Herbert W Hethcote, and Stephen G Eubank. Mixing patterns between age groups in social networks. *Social Networks*, 29(4):539–554, 2007.

[181] Guillaume Béraud, Sabine Kazmercziak, Philippe Beutels, Daniel Levy-Bruhl, Xavier Lenne, Nathalie Mielcarek, Yazdan Yazdanpanah, Pierre-Yves Boëlle, Niel Hens, and Benoit Dervaux. The french connection: the first large population-based contact survey in france relevant for the spread of infectious diseases. *PloS one*, 10(7):e0133203, 2015.

[182] Laura Di Domenico, Giulia Pullano, Chiara E Sabbatini, Pierre-Yves Boëlle, and Vittoria Colizza. Impact of lockdown on covid-19 epidemic in île-de-france and possible exit strategies. *BMC medicine*, 18:1–13, 2020.

[183] Odo Diekmann, Johan Andre Peter Heesterbeek, and Johan Anton Jacob Metz. On the definition and the computation of the basic reproduction ratio R0 in models for infectious diseases in heterogeneous populations. *Journal of mathematical biology*, 28, 1990.

[184] Marián Boguná and Romualdo Pastor-Satorras. Epidemic spreading in correlated complex networks. *Physical Review E*, 66(4):047104, 2002.

[185] Mark EJ Newman. Mixing patterns in networks. *Physical review E*, 67(2):026126, 2003.

[186] Michelle Girvan and Mark EJ Newman. Community structure in social and biological networks. *Proceedings of the national academy of sciences*, 99(12):7821–7826, 2002.

[187] Pablo Barberá, Ning Wang, Richard Bonneau, John T Jost, Jonathan Nagler, Joshua Tucker, and Sandra González-Bailón. The critical periphery in the growth of social protests. *PloS one*, 10(11):e0143611, 2015.

[188] Mark Granovetter. Threshold models of collective behavior. *American journal of sociology*, 83(6):1420–1443, 1978.

[189] Fariba Karimi and Petter Holme. Threshold model of cascades in empirical temporal networks. *Physica A: Statistical Mechanics and its Applications*, 392(16):3476–3483, 2013.

[190] Romualdo Pastor-Satorras and Alessandro Vespignani. Epidemic spreading in scale-free networks. *Physical review letters*, 86(14):3200, 2001.

[191] Brian Karrer and Mark EJ Newman. Message passing approach for general epidemic models. *Physical Review E—Statistical, Nonlinear, and Soft Matter Physics*, 82(1):016101, 2010.

[192] DA Rand. Correlation equations and pair approximations for spatial ecologies. *Advanced ecological theory: principles and applications*, pages 100–142, 1999.

[193] Péter L Simon and Istvan Z Kiss. Super compact pairwise model for sis epidemic on heterogeneous networks. *Journal of Complex Networks*, 4(2):187–200, 2016.

[194] Ken T D Eames and Matt J Keeling. Modeling dynamic and network heterogeneities in the spread of sexually transmitted diseases. *Proc Natl Acad Sci U S A*, 99(20):13330–13335, September 2002.

[195] Matthew J Keeling. The effects of local spatial structure on epidemiological invasions. *Proceedings of the Royal Society of London. Series B: Biological Sciences*, 266(1421):859–867, 1999.

[196] Péter L Simon and Istvan Z Kiss. Super compact pairwise model for SIS epidemic on heterogeneous networks. *J. Complex Netw.*, 4(2):187–200, 2016.

[197] Zoltán Toroczkai and Hasan Guclu. Proximity networks and epidemics. *Physica A: Statistical Mechanics and its Applications*, 378(1):68–75, 2007.

[198] Nicholas C Wormald. The asymptotic connectivity of labelled regular graphs. *J. Comb. Theory. Ser. B*, 31(2):156–167, 1981.

[199] Sergey N Dorogovtsev, Alexander V Goltsev, José FF Mendes, and Alexander N Samukhin. Spectra of complex networks. *Phys. Rev. E*, 68(4):046109, 2003.

[200] Florian Goirand, Bertrand Georgeot, Olivier Giraud, and Sylvie Lorthois. Network community structure and resilience to localized damage: application to brain microcirculation. *Brain Multiphysics*, 2:100028, 2021.

[201] István Z Kiss, Eben Kenah, and Grzegorz A Rempała. Necessary and sufficient conditions for exact closures of epidemic equations on configuration model networks. *Journal of Mathematical Biology*, 87(2):36, 2023.

[202] Dimiter Prodanov. Analytical solutions and parameter estimation of the SIR epidemic model. *Mathematical Analysis of Infectious Diseases*, pages 163–189, 2022.

[203] Norman TJ Bailey et al. *The mathematical theory of infectious diseases and its applications*. Charles Griffin & Company Ltd, 5a Crendon Street, High Wycombe, Bucks HP13 6LE., 1975.

[204] Johann Heinrich Lambert. Observationes variae in mathesin puram. *Acta Helvetica*, 3(1):128–168, 1758.

[205] Robert M Corless, Gaston H Gonnet, David EG Hare, David J Jeffrey, and Donald E Knuth. On the Lambert W function. *Adv. Comput. Math.*, 5:329–359, 1996.

[206] Leonhard Euler. De serie lambertina plurimisque eius insignibus proprietatibus. *Acta Academiae scientiarum imperialis petropolitanae*, pages 29–51, 1783.

[207] Dževad Belkić. All the trinomial roots, their powers and logarithms from the Lambert series, bell polynomials and Fox-Wright function: Illustration for genome multiplicity in survival of irradiated cells. *Journal of Mathematical Chemistry*, 57:59–106, 2019.

[208] ML Glasser. Hypergeometric functions and the trinomial equation. *J. Comput. Appl. Math.*, 118(1-2):169–173, 2000.

[209] David G Kendall. Deterministic and stochastic epidemics in closed populations. In *Proceedings of the third Berkeley symposium on mathematical statistics and probability*, volume 4, pages 149–165. University of California Press Berkeley, 1956.

[210] Aric Hagberg and Drew Conway. Networkx: Network analysis with python. *URL: https://networkx. github. io*, 2020.

[211] Mohsen Bayati, Jeong Han Kim, and Amin Saberi. A sequential algorithm for generating random graphs. *Algorithmica*, 58:860–910, 2010.

[212] Jean-Pierre Bourguignon. *Calcul variationnel*, page 328. Éditions de l'École Polytechnique, 2008.

[213] Olivier Martin, Steve W Otto, and Edward W Felten. *Large-step Markov chains for the traveling salesman problem*. Citeseer, 1991.

[214] Robert E Schapire. The boosting approach to machine learning: An overview. *Nonlinear estimation and classification*, pages 149–171, 2003.

[215] Hector J Sussmann and Jan C Willems. 300 years of optimal control: from the brachystochrone to the maximum principle. *IEEE Control Systems Magazine*, 17(3):32–44, 1997.

[216] Agoston E Eiben and James E Smith. *Introduction to evolutionary computing*. Springer, 2015.

[217] Lars Ruthotto, Stanley J Osher, Wuchen Li, Levon Nurbekyan, and Samy Wu Fung. A machine learning framework for solving high-dimensional mean field game and mean field control problems. *Proceedings of the National Academy of Sciences*, 117(17):9183–9193, 2020.